

Utah State University

DigitalCommons@USU

---

All Graduate Theses and Dissertations

Graduate Studies

---

12-2017

## Reliability Underseepage Assessment of Levees Incorporating Geomorphic Features and Length Effects

Lourdes Polanco Boulware  
*Utah State University*

Follow this and additional works at: <https://digitalcommons.usu.edu/etd>



Part of the [Civil and Environmental Engineering Commons](#)

---

### Recommended Citation

Boulware, Lourdes Polanco, "Reliability Underseepage Assessment of Levees Incorporating Geomorphic Features and Length Effects" (2017). *All Graduate Theses and Dissertations*. 6826.  
<https://digitalcommons.usu.edu/etd/6826>

This Dissertation is brought to you for free and open access by the Graduate Studies at DigitalCommons@USU. It has been accepted for inclusion in All Graduate Theses and Dissertations by an authorized administrator of DigitalCommons@USU. For more information, please contact [digitalcommons@usu.edu](mailto:digitalcommons@usu.edu).



RELIABILITY UNDERSEEPAGE ASSESSMENT OF LEVEES INCORPORATING  
GEOMORPHIC FEATURES AND LENGTH EFFECTS

by

Lourdes Polanco Boulware

A dissertation submitted in partial fulfillment  
of the requirements for the degree

of

DOCTOR OF PHILOSOPHY

in

Civil and Environmental Engineering

Approved:

---

John Rice, Ph.D  
Major Professor

---

David Bowles, Ph.D  
Committee Member

---

Gilberto Urroz, Ph.D  
Committee Member

---

James Bay, Ph.D  
Committee Member

---

Thomas Lachmar, Ph.D  
Committee Member

---

Mark R. McLellan, Ph.D  
Vice President for Research and  
Dean of the School of Graduate Studies

UTAH STATE UNIVERSITY  
Logan, Utah

2017

Copyright © Lourdes Polanco Boulware

All Rights Reserved

## ABSTRACT

Reliability Underseepage Assessment of Levees Incorporating Geomorphic Features and  
Length Effects

by

Lourdes Polanco Boulware

Utah State University, 2017

Major Professor: Dr. John Rice  
Department: Civil and Environmental Engineering

Levees are structures built to protect land from flooding and their foundations are characterized by the enduring changes the (protected meandering) river went through over time. Two main characteristics are imposed by the river in a levee system: the length, since it runs parallel to the river and, the variable foundation they are built on, shaped by geomorphic features. Underseepage is an internal erosion mechanism that involves seepage flow under a structure and it is evaluated to assess the safety of a levee. Present methods for assessing the potential for unsatisfactory levee performance due to underseepage consist of deterministic seepage analyses and simplified reliability methods. The most common simplified reliability approach currently being used applies the first-order second-moment Taylor series method, utilizing the U.S. Army Corps of Engineers blanket theory equations as the performance functions. In many cases, these methods do not realistically reflect the geometry of the levee's foundation soils or the uncertainty associated with their performance and don't incorporate the effects of levee curvature. This study proposes a new application that allows modeling the initiation of erosion process with more accurate

failure mechanisms, incorporation of geomorphic features, and adjustment for levee curvature. The response surface–Monte Carlo simulation method uses finite-element analyses to develop a series of equations that define the relationship between key (soil and geometric) input parameters and the conditional probability of initiation of erosion of reaching critical hydraulic conditions (uplift pressures or hydraulic exit gradients) given a loading condition. Comparison of the two methods is presented to evaluate the effectiveness of the first-order second-moment Taylor series method and show the advantages of the response surface–Monte Carlo simulation method. Within the comparison, it is shown that the foundation’s geometry has a statistically significant effect on the computed conditional probability. Based on the assumption that geomorphic features impose the greatest effect on levee underseepage, two models present an innovative technique to address reliability underseepage. One model assesses the effect due to crevasse splays and the other due to high conductivity channels. Finally, it is shown that, where applicable, geomorphic underseepage reliability analysis results are easily adjusted for curvature with a multiplier method.

(402 pages)

## PUBLIC ABSTRACT

### Reliability Underseepage Assessment of Levees Incorporating Geomorphic Features and Length Effects

by

Lourdes Polanco Boulware

It has been estimated that approximately fifty percent of the United States' population lives behind levees. Because these earth structures are typically long, subjected to seasonal changes and spatial variability, it is logical to analyze them in an uncertainty-based approach. This research is focused on assessing the potential of internal erosion related failure due to underseepage with the general objective of assessing the failure potential of individual geomorphic features while considering length effects. The project team was granted \$204,000 from the National Science Foundation and \$10,000 from the United States Society on Dams which resulted in research collaboration within graduate students and University of Delaware faculty as well as several presentations in prestigious conferences (in the U.S and Europe) and publication of journal papers. Findings from this research should be easily transferrable to other linear earth structures (such as dams, construction excavations, detention ponds, road embankments, etc.), and should significantly enhance reliability analysis across a wide array of structure types and geologic settings allowing a broad impact on future research, as well as geotechnical engineering practice.

## ACKNOWLEDGMENTS

First, I honor God for providing the means and environment to allow me to balance a family and pursue a post-secondary education; to You the glory. To my parents, Lourdes Portalatín and José Polanco, who raised me in an environment where my brothers and I were always the priority. The sacrifices that you made taught me how to be strong yet caring and as time goes by I have realized how blessed I have been to have you as my parents. Your hard working loving dedication has paid off, this Doctor of Philosophy degree is for you.

To my husband, Jeffrey Boulware, for the constant reminder that I am more than I could have ever imagined, for pushing my boundaries, for your endless support on tired nights, for dealing with my frustrations when I was not able to solve things as fast as I would have liked, for being the best father figure to our kids and for always making me smile when I needed it the most, this is for you.

To my adviser, Dr. John Rice, for your guidance, for allowing me to pursue this degree under your wings, for your comprehension and flexibility when I needed time off to take care of my family, this is also for you.

To my committee members, thank you for your constant input on this long journey. To the faculty and staff of the Civil and Environmental Engineering department, it has been a privilege to be a part of this family.

Last and not least, to my wonderful children, Benjamin, Luna and Kai, this is to show you that it is possible to conquer anything in life as long as you are surrounded by the right people and have the strength to always persist while being humble and never

forgetting where you come from. Thank you for putting up with me not being a traditional mom and still giving me your lovely smiles that brighten my life every single day.

It took a village to get me where I am, I could have not been able to do it without all of you.

Lourdes Polanco Boulware



## CONTENTS

ABSTRACT.....	iii
PUBLIC ABSTRACT .....	v
ACKNOWLEDGMENTS .....	vi
LIST OF TABLES.....	xi
LIST OF FIGURES .....	xviii
CHAPTER	
1. INTRODUCTION.....	1
References .....	11
2. RELIABILITY-BASED UNDERSEEPAGE ANALYSIS IN LEVEES USING A RESPONSE SURFACE–MONTE CARLO SIMULATION METHOD.....	13
Abstract.....	13
2.1. Introduction.....	14
2.2. Present Analysis Methods.....	15
2.3. Benefits and Limitations of Present Methods.....	17
2.4. Proposed New Application: The RSMC Method .....	19
2.5. Analysis of Variables.....	40
2.6. Summary and Conclusions .....	41
2.7. Notation .....	43
References .....	44
3. A RELIABILITY-BASED EVALUATION OF THE EFFECTS OF GEOMETRY ON LEVEE UNDERSEEPAGE POTENTIAL .....	47
Abstract.....	47
3.1. Introduction.....	48
3.2. Analysis of internal erosion .....	49
3.3. FOSM-BT Method.....	52
3.4. RSMC Method.....	53
3.5. Purpose and Scope .....	54
3.6. General Procedure.....	56
3.7. Methodology.....	58
3.8. Description of Case Studies .....	62
3.9. Results.....	70
3.10. Conclusions.....	76
References .....	77
4. RELIABILITY-BASED THREE-DIMENSIONAL ASSESSMENT OF INTERNAL EROSION POTENTIAL DUE TO CREVASSE SPLAYS.....	82

Abstract.....	82
4.1. Introduction.....	83
4.2. Application Example—Crevasse Splay Geomorphic Feature.....	92
4.3. Discussion.....	115
4.4. Conclusion.....	116
4.5. Acknowledgments.....	118
4.6. Supplemental Data.....	118
References.....	127
<b>5. THREE DIMENSIONAL UNDERSEEPAGE ASSESSMENT OF HIGH CONDUCTIVITY CHANNELS WITHIN A LEVEE SYSTEM.....</b>	<b>132</b>
Abstract.....	132
5.1. Introduction.....	133
5.2. Typical levee subsurface characteristics.....	135
5.3. Geomorphology of high conductivity channels.....	136
5.4. Deterministic and probabilistic underseepage analysis methods.....	139
5.5. Response Surface Monte Carlo simulation (RSMC) method.....	142
5.6. Reliability assessment of high conductivity channels.....	144
5.7. Summary and Conclusions.....	167
5.8. Acknowledgement.....	168
5.9. Supplemental Data.....	169
References.....	175
<b>6. COMBINED EFFECTS OF GEOMORPHIC FEATURES AND LEVEE CURVATURE ON UNDERSEEPAGE ANALYSIS RELIABILITY.....</b>	<b>180</b>
Abstract.....	180
6.1. Introduction.....	181
6.2. Levee underseepage modeling characteristics and shortcomings.....	183
6.3. Combined effect of geomorphic features and levee curvature.....	195
6.4. Research case study.....	206
6.5. Summary and Conclusions.....	212
6.6. Acknowledgement.....	213
6.7. Supplemental data.....	214
References.....	225
<b>7. SUMMARY, CONCLUSIONS AND RECOMMENDATIONS.....</b>	<b>230</b>
7.1. Summary and Conclusions.....	230
7.2. Recommendations.....	233
APPENDICES.....	236
APPENDIX A.....	237
APPENDIX B.....	255
APPENDIX C.....	290
APPENDIX D.....	312

APPENDIX E .....	358
CURRICULUM VITAE.....	367
PERMISSIONS.....	372

## LIST OF TABLES

Table	Page
2.1. Input Variables for Proposed Method .....	26
2.2. Conditional Probability of unsatisfactory performance vs. PDF shape for Geometric Variable $A$ .....	35
2.3. Probability distribution variables for Uncertain Location of an Old Channel input variables .....	39
2.4. Summary of regression analyses ( $t$ Stat values for geometric variables in bold type) .....	42
3.1. Input Variables for Proposed Method .....	66
3.2. Summary of $P_{upS}$ and most significant parameters .....	71
3.3. Variation of $P_{up}$ results for different PDF shape assumptions using the RSMC Method .....	76
4.1. Range of values used for the parametric analyses of the crevasse-splay model .....	101
4.2. Results of one simplified flow model using MLVs .....	101
4.3. Results of parametric analysis to assess the validity of the simplified flow model for crevasse-splay response surface .....	104
4.4. PDFs for the 10 input parameters used to develop the CADFs shown in Figures 4.6 and 4.7. ....	107
S4.1. Parameters used to develop response surface .....	125
S4.2. Fit-equations' coefficients and corresponding goodness of fit for FCs with respect to each $C_{channel}$ used.....	126
5.1. Range of values used for the parametric analyses of the general model.....	147
5.2. Results of one simplified flow model using MLVs .....	153
5.3. Results of parametric analysis to assess the validity of the simplified flow model for the high conductivity channel response surface .....	155

Table	Page
5.4. Parameters used for development of the high conductivity channel response surface .....	156
5.5. Input parameters for the PDFs used to develop the CADFs for the abandoned channel .....	159
S5.1. Fit-equations' coefficients and corresponding goodness of fit for family of curves with respect to each $\lambda_m$ used.....	173
6.1. Values used for the curvature-channel model presented in Figure 6.8 .....	205
6.2. Input parameters for the PDFs used to develop the CADFs for the meander scrolls feature presented in Figure 6.10.....	207
6.3. Results for the conditional probabilities with respect to $i_{blanket}$ and $F_{heave}$ with and without curvature adjustment for the meander scroll feature presented in Figure 6.10 .....	209
6.4. Summary of results for sensitivity analyses showing the three most statistical significant parameter .....	211
S6.1. Parameters used for parametric analysis as presented in Figure 6.4.....	214
S6.2. Parameters used for parametric analysis as presented in Figure 6.6.....	215
S6.3. Parameters and results for the curvature model with $D_c = 90^\circ$ and $\alpha = 45^\circ$ .....	216
S6.4. Parameters and results for the curvature model with $D_c = 150^\circ$ and $\alpha = 90^\circ$ .....	218
S6.5. Parameters and results for the curvature model with $D_c = 150^\circ$ and $\alpha = 45^\circ$ .....	220
A.1. Hydraulic exit gradient ( $i_e$ ) as a function of $A$ , $K_{sb}$ and $K_{hv}$ used for Example 2.1 in Chapter 2. These values correspond to Figures A1.1 to A1.5 .....	238
A.2. Uplift pressure at the base of the blanket ( $u_{bl}$ ) as a function of $A$ , $K_{sb}$ and $K_{hv}$ used for Example 2.1 in Chapter 2. These values correspond to Figures A1.6 to A1.10 .....	239
A.3. Fit-equations' coefficients and corresponding goodness of fit for family of curves for the computation of $i_e$ with respect to each $K_{hv}$ used for Example 2.1 in Chapter 2. These values correspond to Figures A1.1 to A1.5 .....	245

Table	Page
A.4. Fit-equations' coefficients and corresponding goodness of fit for family of curves for the computation of $u_{bl}$ with respect to each $K_{hv}$ used for Example 2.1 in Chapter 2. These values correspond to Figures A1.6 to A1.10.....	246
A.5. Uplift pressure at the base of the blanket (above channel) ( $u_{bl}$ ) as a function of $h$ , $K_{sb}$ , $d_c$ , and $K_{hv} = 0.25$ used for Example 2.2 in Chapter 2. These values correspond to Figures A.11 to A.17 .....	247
A.6. Fit-equations' coefficients and corresponding goodness of fit for family of curves for the computation of $u_{bl}$ with respect to each $K_{sb}$ used for Example 2.2 in Chapter 2. These values correspond to Figures A.11 to A.17 .....	253
B.1. Input values used for comparative analyses. Supporting data for Table 3.1 .....	256
B.2. FOSM calculation for Case 1 as depicted in Figure 3.3 in Chapter 3. Supporting data for Table 3.2.....	257
B.3. Hydraulic exit gradient ( $i_e$ ) as a function of $h$ , $K_{sb}$ and $K_{hv} = 0.25$ used for Case 1 as depicted in Figure 3.3 in Chapter 3. These values correspond to Figure A2.1 .....	258
B.4. Fit-equations' coefficients and corresponding goodness of fit for family of curves for the computation of $i_e$ with respect to $K_{sb}$ used for Case 1. These values correspond to Figure B.1. ....	259
B.5. FOSM calculation for Case 2 as depicted in Figure 3.3 in Chapter 3. Supporting data for Table 3.2.....	260
B.6. Hydraulic exit gradient ( $i_e$ ) as a function of $Z_{bl}$ , $K_{sb}$ and $K_{hv} = 0.25$ used for Case 2 as depicted in Figure 3.3 in Chapter 3. These values correspond to Figure B.2.....	261
B.7. Fit-equations' coefficients and corresponding goodness of fit for family of curves for the computation of $i_e$ with respect to $K_{sb}$ used for Case 2. These values correspond to Figure B.2. ....	262
B.8. FOSM calculation for Case 3a as depicted in Figure 3.4 in Chapter 3. Supporting data for Table 3.2.....	263
B.9. Uplift pressure at the base of the blanket (above seepage block) ( $u_{bl}$ ) as a function of $d_b$ , $K_{sb}$ , $Z_{bl}$ and $K_{hv} = 1.0$ used for Case 3a as depicted in Figure 3.4 in Chapter 3. These values correspond to Figure B.3 through B.6 .....	264

Table	Page
B.10. Fit-equations' coefficients and corresponding goodness of fit for family of curves for the computation of $u_{bl}$ with respect to $K_{sb}$ used for Case 3a. These values correspond to Figures B.3 through B.6.....	268
B.11. FOSM calculation for Case 3b as depicted in Figure 3.5 in Chapter 3. Supporting data for Table 3.2.....	270
B.12. Uplift pressure at the base of the blanket (above seepage block) ( $u_{bl}$ ) as a function of $d_b$ , $K_{sb}$ , $Z_{bl}$ and $K_{hv} = 0.10$ used for Case 3b as depicted in Figure 3.5 in Chapter 3. These values correspond to Figure B.7 through B.10 .....	271
B.13. Fit-equations' coefficients and corresponding goodness of fit for family of curves for the computation of $u_{bl}$ with respect to $K_{sb}$ used for Case 3b. These values correspond to Figures B.7 through B.10. ....	275
B.14. FOSM calculation for Cases 4a and 4b as depicted in Figures 3.6 and 3.7, respectively, in Chapter 3. Supporting data for Table 3.2.....	277
B.15. Uplift pressure at the base of the blanket (above seepage block) ( $u_{bl}$ ) as a function of $d_e$ , $K_{sb}$ , $Z_{bl}$ and $K_{hv} = 1.0$ used for Case 4a as depicted in Figure 3.6 in Chapter 3. These values correspond to Figure B.11 through B.14 .....	278
B.16. Fit-equations' coefficients and corresponding goodness of fit for family of curves for the computation of $u_{bl}$ with respect to $K_{sb}$ used for Case 4a. These values correspond to Figures B.11 through B.14.....	282
B.17. Uplift pressure at the base of the blanket (above seepage block) ( $u_{bl}$ ) as a function of $d_e$ , $K_{sb}$ , $Z_{bl}$ and $K_{hv} = 0.10$ used for Case 4b as depicted in Figure 3.7 in Chapter 3. These values correspond to Figures B.14 through B.17 .....	284
B.18. Fit-equations' coefficients and corresponding goodness of fit for family of curves for the computation of $u_{bl}$ with respect to $K_{sb}$ used for Case 4b. These values correspond to Figures B.14 through B.17. ....	288
C.1. Results of parametric analysis to assess the validity of the simplified flow model for crevasse-splay response surface .....	290
C.2. Parametric analysis 1 corresponding to the combined parameter $T_{splay}$ .....	291
C.3. Parametric analysis 2 corresponding to the combined parameter $T_{splay}$ .....	293

Table	Page
C.4. Parametric analysis 3 corresponding to the combined parameter $C_{blanket}$ .....	295
C.5. Parametric analysis 4 corresponding to the combined parameter $C_{blanket}$ .....	296
C.6. Parametric analysis 5 corresponding to the combined parameter $C_{blanket}$ .....	297
C.7. Parametric analysis 6 corresponding to the combined parameter $C_{blanket}$ .....	298
C.8. Parametric analysis 7 corresponding to the combined parameter $C_{blanket}$ .....	299
C.9. Parametric analysis 8 corresponding to the combined parameter $C_{blanket}$ .....	300
C.10. Parametric analysis 9 corresponding to the combined parameter $C_{channel}$ .....	301
C.11. Parametric analysis 10 corresponding to the combined parameter $C_{channel}$ .....	302
C.12. Parametric analysis 11 corresponding to the combined parameter $C_{channel}$ .....	304
C.13. Parametric analysis 12 corresponding to the combined parameter $C_{channel}$ .....	306
C.14. Parametric analysis 13 corresponding to the combined parameter $C_{channel}$ .....	308
C.15. Parametric analysis 14 corresponding to the combined parameter $C_{channel}$ .....	309
C.16. Parametric analysis 15 corresponding to the combined parameter $C_{channel}$ .....	310
C.17. Parametric analysis 16 corresponding to the combined parameter $C_{channel}$ .....	311
D.1. Results of parametric analysis to assess the validity of the simplified flow model for the high conductivity channel response surface .....	313
D.2. Parametric analysis 1 corresponding to the combined parameter $T_{ch}$ .....	314
D.3. Parametric analysis 2 corresponding to the combined parameter $T_{ch}$ .....	316
D.4. Parametric analysis 3 corresponding to the combined parameter $T_{ch}$ .....	318



Table	Page
D.5. Parametric analysis 4 corresponding to the combined parameter $T_{ch}$ .....	320
D.6. Parametric analysis 5 corresponding to the combined parameter $T_{ch}$ .....	322
D.7. Parametric analysis 6 corresponding to the combined parameter $T_{ch}$ .....	324
D.8. Parametric analysis 7 corresponding to the combined parameter $T_{ch}$ .....	326
D.9. Parametric analysis 8 corresponding to the combined parameter $T_{ch}$ .....	328
D.10. Parametric analysis 9 corresponding to the combined parameter $T_{ch}$ .....	330
D.11. Parametric analysis 10 corresponding to the combined parameter $\lambda_m$ .....	332
D.12. Parametric analysis 11 corresponding to the combined parameter $\lambda_m$ .....	334
D.13. Parametric analysis 12 corresponding to the combined parameter $\lambda_m$ .....	336
D.14. Parametric analysis 13 corresponding to the combined parameter $\lambda_m$ .....	338
D.15. Parametric analysis 14 corresponding to the combined parameter $\lambda_m$ .....	340
D.16. Parametric analysis 15 corresponding to the combined parameter $\lambda_m$ .....	342
D.17. Parametric analysis 16 corresponding to the combined parameter $\lambda_m$ .....	344
D.18. Parametric analysis 17 corresponding to the combined parameter $\lambda_m$ .....	346
D.19. Parametric analysis 18 corresponding to the combined parameter $\lambda_m$ .....	348
D.20. Parametric analysis 19 corresponding to the combined parameter $\lambda_m$ .....	350
D.21. Parametric analysis 20 corresponding to the combined parameter $\lambda_m$ .....	352
D.22. Parametric analysis 21 corresponding to the combined parameter $\lambda_m$ .....	354
D.23. Parametric analysis 22 corresponding to the combined parameter $\lambda_m$ .....	356
E.1. Parameters and results for the curvature model with $D_c = 30^\circ$ and $\alpha = 45^\circ$ .....	360
E.2. Parameters and results for the curvature model with $D_c = 30^\circ$ and $\alpha = 90^\circ$ .....	362

Table	Page
E.3. Parameters and results for the curvature model with $D_c = 60^\circ$ and $\alpha = 45^\circ$ .....	364
E.4. Parameters and results for the curvature model with $D_c = 60^\circ$ and $\alpha = 90^\circ$ .....	366

## LIST OF FIGURES

Figure	Page
1.1. General components of a levee. ....	1
1.2. General failure mechanism that a levee can.....	2
1.3. Illustration of heave and backward erosion piping mechanisms.....	4
1.4. Sacramento River Levee system in California showing a clip of a geological map with most common geomorphic features.....	5
2.1. Simplified levee profile showing the zone in which the blanket could end. ....	23
2.2. Failure mechanisms based on the levee geometry. ....	23
2.3. PDF for geometric variable $A$ .....	24
2.4. Finite-element levee profile used in Example 2.1.....	29
2.5. Family of curves representing relationship between $K_{sb}$ , $A$ , and $i_e$ , for $K_{hv} = 0.25$ . ....	30
2.6. Family of curves representing relationship between $K_{sb}$ , $A$ , and $u_{bl}$ for $K_{hv} = 0.25$ . ....	30
2.7. Cumulative ascending distribution function for Example 2.1.....	34
2.8. Calculation convergence for $FS$ for Examples 2.1 and 2.2.....	34
2.9. Finite-element levee profile used in Example 2.2 showing geometric variables $h$ and $d_c$ .....	38
2.10. Cumulative ascending distribution for Example 2.2.....	39
3.1. General finite-element model showing boundary conditions .....	57
3.2. General blanket theory model corresponding to the finite-element model in Figure 3.1. ....	57
3.3. Cases 1 and 2 showing geometric parameter $Z_{bl}$ .....	64
3.4. Case 3a showing geometric parameter $Z_{bl}$ and $d_b$ . ....	64

Figure	Page
3.5. Case 3b showing geometric parameter $Z_{bl}$ and $d_b$ .	64
3.6. Case 4a showing geometric parameter $Z_{bl}$ and $d_e$ .	65
3.7. Case 4b showing geometric parameter $Z_{bl}$ and $d_e$ .	65
3.8. Case 5 showing geometric parameter $A$ .	65
3.9. Case 6 showing geometric parameter $h$ and $d_c$ .	66
3.10. Landside effect on the computed $FS$ with $K_{sb} = 10$ for Cases 3a and 3b.	72
3.11. Landside effects on the computed $FS$ for $d_c = 185'$ based on different $Z_{bl}$ and $K_{sb} = 10$ and 1000.	75
4.1. Common geomorphic features within the meandering river environment.	88
4.2. Schematic illustration of a crevasse-splay deposit.	94
4.3. Three-dimensional finite-element model of a crevasse-splay deposit.	98
4.4. Combination of parameters for a crevasse splay model.	101
4.5. Family of curves for the crevasse splay model for one constant $C_{channel}$ and different ranges of $T_{splay}$ and $C_{blanket}$ .	105
4.6. CADF for hydraulic exit gradient through the blanket, $i_{blanket}$ .	109
4.7. CADF for factor of safety against heave, $F_{heave}$ .	110
4.8. Example of one parametric analysis for the crevasse splay based on different flood levels while maintaining all parameters constant except the $C_{channel}$ .	112
4.9. Fragility curve for a crevasse splay model.	112
4.10. Sensitivity tornado graph for mean of $h_{max}$ .	114
4.11. Sensitivity tornado graph for mean of $i_{blanket}$ .	114
4.12. Sensitivity tornado graph for mean of $F_{heave}$ .	115

Figure	Page
4.13. Steps for calculating reliability of levee reaches and length effects with respect to underseepage.....	117
S4.1. Typical simplified subsurface cross section of a meandering river depositional environment. ....	119
S4.2. Sample of geomorphic features mapping along the Sacramento River in California.....	120
S4.3 Family of curves for the crevasse-splay model for $C_{channel} = 4.4E-04$ $m^2/s$ and different ranges of $T_{splay}$ and $C_{blanket}$ . ....	121
S4.4. Family of curves for the crevasse-splay model for $C_{channel} = 2.4E-04$ $m^2/s$ and different ranges of $T_{splay}$ and $C_{blanket}$ . ....	122
S4.5. Family of curves for the crevasse-splay model for $C_{channel} = 4.4E-05$ $m^2/s$ and different ranges of $T_{splay}$ and $C_{blanket}$ . ....	123
S4.6. Family of curves for the crevasse-splay model for $C_{channel} = 2.4E-05$ $m^2/s$ and different ranges of $T_{splay}$ and $C_{blanket}$ . ....	124
S4.7. Family of curves for the crevasse-splay model for $C_{channel} = 4.4E-06$ $m^2/s$ and different ranges of $T_{splay}$ and $C_{blanket}$ . ....	125
5.1. Different types of high-conductivity channels found around a meandering river environment. ....	138
5.2. Major high conductivity channels that intercept the Sacramento River (east side) levee system showing a close up of the location of an abandoned (cross) channel.....	145
5.3. Models used to analyze high conductivity channels. ....	147
5.4. Combination of parameters for a high conductivity channel. ....	151
5.5. Family of curves for the high conductivity channel model for one constant $\lambda_m$ and different ranges of $RL$ and $T_{ch}$ . ....	157
5.6. CADF for hydraulic exit gradient through the blanket, $i_{blanket}$ . ....	161
5.7. CADF for factor of safety against heave, $F_{heave}$ . ....	161

Figure	Page
5.8. Example of one parametric analysis based on different flood levels for the abandoned channel presented in Figure 5.4 with different RL while maintaining constant $T_{ch}$ and $\lambda_m$ . .....	163
5.9. Fragility curve for the abandoned channel presented in Figure 5.4. ....	164
5.10. Sensitivity tornado graph for mean of $h_{max}$ . ....	165
5.11. Sensitivity tornado graph for mean of $i_{blanket}$ . ....	166
5.12. Sensitivity tornado graph for mean of $F_{heave}$ . ....	166
S5.1. Family of curves for the high conductivity channel model for $\lambda_{m1} = 115$ m and different ranges of $T_{ch}$ and $RL$ . ....	169
S5.2. Family of curves for the high conductivity channel model for $\lambda_{m2} = 162$ m and different ranges of $T_{ch}$ and $RL$ . ....	170
S5.3. Family of curves for the high conductivity channel model for $\lambda_{m3} = 256$ m and different ranges of $T_{ch}$ and $RL$ . ....	170
S5.4. Family of curves for the high conductivity channel model for $\lambda_{m4} = 303$ m and different ranges of $T_{ch}$ and $RL$ . ....	171
S5.5. Family of curves for the high conductivity channel model for $\lambda_{m5} = 397$ m and different ranges of $T_{ch}$ and $RL$ . ....	171
S5.6. Family of curves for the high conductivity channel model for $\lambda_{m6} = 444$ m and different ranges of $T_{ch}$ and $RL$ . ....	172
S5.7. Family of curves for the high conductivity channel model for $\lambda_{m7} = 513$ m and different ranges of $T_{ch}$ and $RL$ . ....	172
6.1. General geomorphology found in meandering river systems. ....	186
6.2. General blanket theory cross-section corresponding to case 7c referred as seepage opening. ....	194
6.3. Normalized pressure head versus normalized longitudinal distance along the landside levee toe for BT case 7c. ....	194
6.4. Parameters used for a crevasse splay underseepage model together with flow equations. ....	198

Figure	Page
6.5. Family of curves for a crevasse splay with respect to the hydraulic conductivity of the foundation layer with constant $C_{channel}$ , $T_{splay}$ and $t_f$ and a range of $C_{blanket}$ . .....	199
6.6. Parameters used for a high conductivity channel underseepage model together with flow equations. ....	200
6.7. Family of curves for a high conductivity model with respect to the hydraulic conductivity of the foundation layer with constant $\lambda_m$ and $T_{ch}$ (where applicable) and a range of river lengths ( $RL$ ). ....	201
6.8. Schematic top view of the curvature model used for $D_c = 90^\circ$ and $\alpha = 90^\circ$ showing channel features at $ND = -4, 0, +1 +3$ . ....	203
6.9. Results for the curvature model presented in Figure 6.8. ....	204
6.10. Meander scroll feature located along the Little Pocket in Sacramento, CA. ....	207
6.11. CADF for factor of safety against heave, $F_{heave}$ with no curvature adjustment for the meander scroll feature presented in Figure 6.10. ....	209
6.12. Historical map showing locations of boils and seepage along the Little Pocket in Sacramento, CA. ....	210
6.13. Sensitivity tornado graph for mean of $h_{max}$ with no curvature adjustment. ....	211
S6.1. Schematic top view of the curvature model used for $D_c = 90^\circ$ and $\alpha = 45^\circ$ showing channel features at $ND = -4, 0, +1 +3$ . ....	215
S6.2. Results for the curvature model with $D_c = 90^\circ$ and $\alpha = 45^\circ$ . ....	217
S6.3. Schematic top view of the curvature model used for $D_c = 150^\circ$ and $\alpha = 90^\circ$ showing channel features at $ND = -3, -1, 0 +2$ . ....	217
S6.4. Results for the curvature model with $D_c = 150^\circ$ and $\alpha = 90^\circ$ . ....	219
S6.5. Schematic top view of the curvature model used for $D_c = 150^\circ$ and $\alpha = 45^\circ$ showing channel features at $ND = -3, -1, 0, +2$ . ....	219
S6.6. Results for the curvature model with $D_c = 150^\circ$ and $\alpha = 45^\circ$ . ....	221

Figure	Page
S6.7. CADF for factor of safety against heave, $F_{heave}$ with curvature adjustment. ....	221
S6.8. CADF for hydraulic exit gradient through the blanket, $i_{blanket}$ with no curvature adjustment. ....	222
S6.9. CADF for hydraulic exit gradient through the blanket, $i_{blanket}$ with curvature adjustment. ....	222
S6.10. CADF for hydraulic exit gradient through the blanket, $i_{blanket}$ , with no curvature adjustment. ....	223
S6.11. CADF for hydraulic exit gradient through the blanket, $i_{blanket}$ , with curvature adjustment. ....	223
S6.12. CADF for hydraulic exit gradient through the blanket, $F_{heave}$ , with no curvature adjustment. ....	224
S6.13. CADF for hydraulic exit gradient through the blanket, $F_{heave}$ , with curvature adjustment. ....	224
A.1. Family of curves representing relationship between $K_{sb}$ , $A$ , and $i_e$ for $K_{hv} = 0.50$ . ....	240
A.2. Family of curves representing relationship between $K_{sb}$ , $A$ , and $i_e$ for $K_{hv} = 0.25$ . ....	240
A.3. Family of curves representing relationship between $K_{sb}$ , $A$ , and $i_e$ for $K_{hv} = 0.15$ . ....	241
A.4. Family of curves representing relationship between $K_{sb}$ , $A$ , and $i_e$ for $K_{hv} = 0.05$ . ....	241
A.5. Family of curves representing relationship between $K_{sb}$ , $A$ , and $i_e$ for $K_{hv} = 0.005$ . ....	242
A.6. Family of curves representing relationship between $K_{sb}$ , $A$ , and $\mu_{bl}$ for $K_{hv} = 0.50$ . ....	242
A.7. Family of curves representing relationship between $K_{sb}$ , $A$ , and $\mu_{bl}$ for $K_{hv} = 0.25$ . ....	243
A.8. Family of curves representing relationship between $K_{sb}$ , $A$ , and $\mu_{bl}$ for $K_{hv} = 0.15$ . ....	243



Figure	Page
A.9. Family of curves representing relationship between $K_{sb}$ , $A$ , and $\mu_{bl}$ for $K_{hv} = 0.05$ . .....	244
A.10. Family of curves representing relationship between $K_{sb}$ , $A$ , and $\mu_{bl}$ for $K_{hv} = 0.005$ . .....	244
A.11. Family of curves representing relationship between $K_{sb}$ , $h$ , and $\mu_{bl}$ for $K_{hv} = 0.25$ and $d_c = 175$ ft. ....	249
A.12. Family of curves representing relationship between $K_{sb}$ , $h$ , and $\mu_{bl}$ for $K_{hv} = 0.25$ and $d_c = 150$ ft. ....	249
A.13. Family of curves representing relationship between $K_{sb}$ , $h$ , and $\mu_{bl}$ for $K_{hv} = 0.25$ and $d_c = 125$ ft. ....	250
A.14. Family of curves representing relationship between $K_{sb}$ , $h$ , and $\mu_{bl}$ for $K_{hv} = 0.25$ and $d_c = 100$ ft. ....	250
A.15. Family of curves representing relationship between $K_{sb}$ , $h$ , and $\mu_{bl}$ for $K_{hv} = 0.25$ and $d_c = 75$ ft. ....	251
A.16. Family of curves representing relationship between $K_{sb}$ , $h$ , and $\mu_{bl}$ for $K_{hv} = 0.25$ and $d_c = 50$ ft. ....	251
A.17. Family of curves representing relationship between $K_{sb}$ , $h$ , and $\mu_{bl}$ for $K_{hv} = 0.25$ and $d_c = 25$ ft. ....	252
B.1. Family of curves representing relationship between $Z_{bl}$ , $K_{sb}$ , and $i_e$ for $K_{hv} = 0.25$ for Case 1. ....	259
B.2. Family of curves representing relationship between $Z_{bl}$ , $K_{sb}$ , and $i_e$ for $K_{hv} = 0.25$ for Case 2. ....	262
B.3. Family of curves representing relationship between $d_b$ , $K_{sb}$ , and $u_{bl}$ for $K_{hv} = 1.0$ and $Z_{bl} = 5$ ft for Case 3a. ....	266
B.4. Family of curves representing relationship between $d_b$ , $K_{sb}$ , and $u_{bl}$ for $K_{hv} = 1.0$ and $Z_{bl} = 10$ ft for Case 3a. ....	266
B.5. Family of curves representing relationship between $d_b$ , $K_{sb}$ , and $u_{bl}$ for $K_{hv} = 1.0$ and $Z_{bl} = 15$ ft for Case 3a. ....	267
B.6. Family of curves representing relationship between $d_b$ , $K_{sb}$ , and $u_{bl}$ for $K_{hv} = 1.0$ and $Z_{bl} = 20$ ft for Case 3a. ....	267

Figure	Page
B.7. Family of curves representing relationship between $d_b$ , $K_{sb}$ , and $u_{bl}$ for $K_{hv} = 0.10$ and $Z_{bl} = 5$ ft for Case 3b. ....	273
B.8. Family of curves representing relationship between $d_b$ , $K_{sb}$ , and $u_{bl}$ for $K_{hv} = 0.10$ and $Z_{bl} = 10$ ft for Case 3b. ....	273
B.9. Family of curves representing relationship between $d_b$ , $K_{sb}$ , and $u_{bl}$ for $K_{hv} = 0.10$ and $Z_{bl} = 15$ ft for Case 3b. ....	274
B.10. Family of curves representing relationship between $d_b$ , $K_{sb}$ , and $u_{bl}$ for $K_{hv} = 0.10$ and $Z_{bl} = 20$ ft for Case 3b. ....	274
B.11. Family of curves representing relationship between $d_{be}$ , $K_{sb}$ , and $u_{bl}$ for $K_{hv} = 1.0$ and $Z_{bl} = 5$ ft for Case 4a. ....	280
B.12. Family of curves representing relationship between $d_e$ , $K_{sb}$ , and $u_{bl}$ for $K_{hv} = 1.0$ and $Z_{bl} = 10$ ft for Case 4a. ....	280
B.13. Family of curves representing relationship between $d_e$ , $K_{sb}$ , and $u_{bl}$ for $K_{hv} = 1.0$ and $Z_{bl} = 15$ ft for Case 4a. ....	281
B.14. Family of curves representing relationship between $d_e$ , $K_{sb}$ , and $u_{bl}$ for $K_{hv} = 1.0$ and $Z_{bl} = 20$ ft for Case 4a. ....	281
B.15. Family of curves representing relationship between $d_e$ , $K_{sb}$ , and $u_{bl}$ for $K_{hv} = 0.10$ and $Z_{bl} = 5$ ft for Case 4b. ....	286
B.16. Family of curves representing relationship between $d_e$ , $K_{sb}$ , and $u_{bl}$ for $K_{hv} = 0.10$ and $Z_{bl} = 10$ ft for Case 4b. ....	286
B.17. Family of curves representing relationship between $d_e$ , $K_{sb}$ , and $u_{bl}$ for $K_{hv} = 0.10$ and $Z_{bl} = 15$ ft for Case 4b. ....	287
B.18. Family of curves representing relationship between $d_e$ , $K_{sb}$ , and $u_{bl}$ for $K_{hv} = 0.10$ and $Z_{bl} = 20$ ft for Case 4b. ....	287
C.1. Results from parametric analysis 1 corresponding to the combined parameter $T_{splay}$ . ....	292
C.2. Results from parametric analysis 2 corresponding to the combined parameter $T_{splay}$ . ....	294
C.3. Results from parametric analysis 3 corresponding to the combined parameter $C_{blanket}$ . ....	295

Figure	Page
C.4. Results from parametric analysis 4 corresponding to the combined parameter $C_{blanket}$ .....	296
C.5. Results from parametric analysis 5 corresponding to the combined parameter $C_{blanket}$ .....	297
C.6. Results from parametric analysis 6 corresponding to the combined parameter $C_{blanket}$ .....	298
C.7. Results from parametric analysis 7 corresponding to the combined parameter $C_{blanket}$ .....	299
C.8. Results from parametric analysis 8 corresponding to the combined parameter $C_{blanket}$ .....	300
C.9. Results from parametric analysis 9 corresponding to the combined parameter $C_{channel}$ .....	301
C.10. Results from parametric analysis 10 corresponding to the combined parameter $C_{channel}$ .....	303
C.11. Results from parametric analysis 11 corresponding to the combined parameter $C_{channel}$ .....	305
C.12. Results from parametric analysis 12 corresponding to the combined parameter $C_{channel}$ .....	307
C.13. Results from parametric analysis 13 corresponding to the combined parameter $C_{channel}$ .....	308
C.14. Results from parametric analysis 14 corresponding to the combined parameter $C_{channel}$ .....	309
C.15. Results from parametric analysis 15 corresponding to the combined parameter $C_{channel}$ .....	310
C.16. Results from parametric analysis 16 corresponding to the combined parameter $C_{channel}$ .....	311
D.1. Results from parametric analysis 1 corresponding to the combined parameter $T_{ch}$ .....	315
D.2. Results from parametric analysis 2 corresponding to the combined parameter $T_{ch}$ .....	317

Figure	Page
D.3. Results from parametric analysis 3 corresponding to the combined parameter $T_{ch}$ .....	319
D.4. Results from parametric analysis 4 corresponding to the combined parameter $T_{ch}$ .....	321
D.5. Results from parametric analysis 5 corresponding to the combined parameter $T_{ch}$ .....	323
D.6. Results from parametric analysis 6 corresponding to the combined parameter $T_{ch}$ .....	325
D.7. Results from parametric analysis 7 corresponding to the combined parameter $T_{ch}$ .....	327
D.8. Results from parametric analysis 8 corresponding to the combined parameter $T_{ch}$ .....	329
D.9. Results from parametric analysis 9 corresponding to the combined parameter $T_{ch}$ .....	331
D.10. Results from parametric analysis 10 corresponding to the combined parameter $\lambda_m$ .....	333
D.11. Results from parametric analysis 11 corresponding to the combined parameter $\lambda_m$ .....	335
D.12. Results from parametric analysis 12 corresponding to the combined parameter $\lambda_m$ .....	337
D.13. Results from parametric analysis 13 corresponding to the combined parameter $\lambda_m$ .....	339
D.14. Results from parametric analysis 14 corresponding to the combined parameter $\lambda_m$ .....	341
D.15. Results from parametric analysis 15 corresponding to the combined parameter $\lambda_m$ .....	343
D.16. Results from parametric analysis 16 corresponding to the combined parameter $\lambda_m$ .....	345
D.17. Results from parametric analysis 17 corresponding to the combined parameter $\lambda_m$ .....	347

Figure	Page
D.18. Results from parametric analysis 18 corresponding to the combined parameter $\lambda_m$ . .....	349
D.19. Results from parametric analysis 19 corresponding to the combined parameter $\lambda_m$ . .....	351
D.20. Results from parametric analysis 20 corresponding to the combined parameter $\lambda_m$ . .....	353
D.21. Results from parametric analysis 21 corresponding to the combined parameter $\lambda_m$ . .....	355
D.22. Results from parametric analysis 22 corresponding to the combined parameter $\lambda_m$ . .....	357
E.1. Schematic top view of the curvature model used for $D_c = 30^\circ$ and $\alpha = 45^\circ$ showing channel features at $ND = -8, -4, 0, +6$ . .....	359
E.2. Results for the curvature model with $D_c = 30^\circ$ and $\alpha = 45^\circ$ . .....	359
E.3. Schematic top view of the curvature model used for $D_c = 30^\circ$ and $\alpha = 90^\circ$ showing channel features at $ND = -5, -2, +1 +4$ . .....	361
E.4. Results for the curvature model with $D_c = 30^\circ$ and $\alpha = 90^\circ$ . .....	361
E.5. Schematic top view of the curvature model used for $D_c = 60^\circ$ and $\alpha = 45^\circ$ showing channel features at $ND = -5, -1, +3 +7$ . .....	363
E.6. Results for the curvature model with $D_c = 60^\circ$ and $\alpha = 45^\circ$ . .....	363
E.7. Schematic top view of the curvature model used for $D_c = 60^\circ$ and $\alpha = 90^\circ$ showing channel features at $ND = -5, -2, +3 +5$ . .....	365
E.8. Results for the curvature model with $D_c = 60^\circ$ and $\alpha = 90^\circ$ . .....	365

# CHAPTER 1

## INTRODUCTION

Levees are long earth structures that protect land by preventing flooding from a river. Since a vast portion of the United States' population lives behind miles of levees (ASCE 2009, Schleifstein 2010), it is important that the structure operates well under day by day and extreme conditions. Unfortunately, like any structure, levees have weaknesses that are inherent from early (non-engineered) construction and a geomorphologic environment. As a consequence, levees are subjected to different types of failure mechanisms.

As shown in Figure 1.1, in general, levees are composed of an embankment, a crest or crown, foundation soils, a landside, a river or water side, and a landside and riverside toe. Based on the overall ability of levee components, levees can fail by overtopping, slope instability, through seepage, and underseepage (Wolff 2008, ASCE 2009) as shown in Figure 1.2.

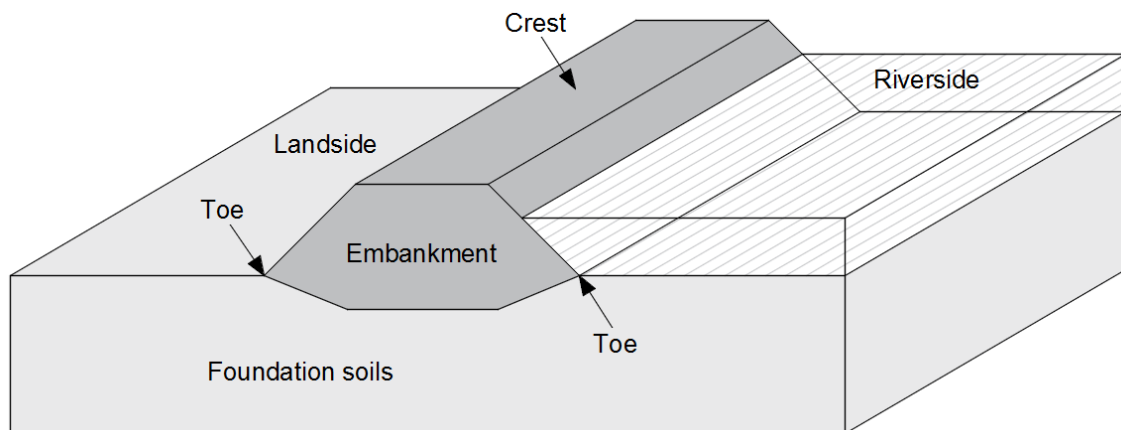


Figure 1.1. General components of a levee.

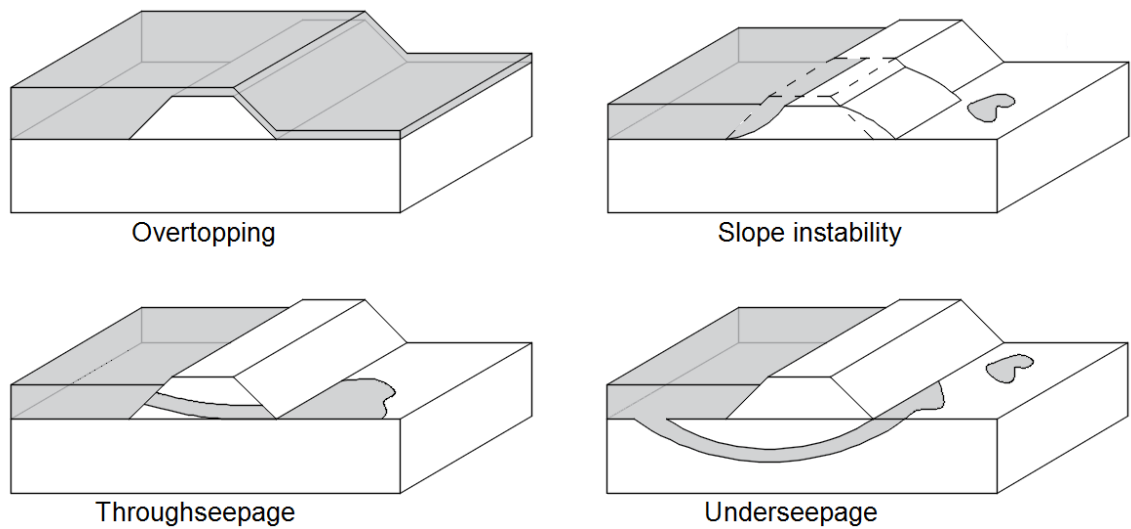


Figure 1.2. General failure mechanism that a levee can

Overtopping is the simplest failure where the flood stage exceeds the crest of the levee. Slope instability involves the sliding of the embankment due to surcharge and seepage pressures from flood waters. Through seepage refers to the case where flood waters erode material pertinent to the embankment forming a path for erosion. Underseepage occurs when seeping water, driven by a differential hydraulic head, erodes the foundation soils, forming a path for erosion.

A technical concept used to describe the dislodgment of particles relevant to levee failure is internal erosion. The term internal erosion has been accepted as a generic term to describe erosion of particles by water passing through a body of soil or rock (ICOLD 2015). Terminology describing the various mechanisms of internal erosion has evolved over recent years, as our understanding of the mechanisms of erosion has developed. Since terminology continues to be inconsistent in practice and in available technical literature, this research has adopted the nomenclature suggested by the International Committee on Large Dams (ICOLD).

This research has been conducted in the context of assessing the potential of internal erosion related failure due to underseepage since the study of the geomorphologic environment levees are built on (aka foundation soils) is of interest. Internal erosion processes that occur in foundation soils are referred to as backward erosion (ICOLD 2015). There are two kinds of backward erosion: backward erosion piping (BEP) and global backward erosion (GBE). BEP mainly occurs in the foundation soils (although it may also occur in the embankment), and GBE occurs in the core of an embankment. Therefore, BEP is the failure mechanism of interest. BEP describes the erosion that initiates when particles of soil are dislodged from the soil matrix at an unprotected seepage exit point. As BEP continues, a pathway, or pipe, is formed by progressive erosion at the upstream end of the erosion void. The “pipe” progresses against the hydraulic gradient and flow, thus the term backward erosion piping. As described by Vrouwenvelder et al. (2010) and shown in Figure 1.3, the authors believe BEP is often preceded by the heave mechanism. Heave is the uplift movement of a mass of soil due to underlying hydraulic pressure or seepage forces (Terzaghi and Peck 1968). Heave can occur due to seepage forces exceeding the buoyant unit weight of the soil layer (zero effective stress) or where hydraulic pressures below a low-permeability layer exceed the weight of the layer (McCook 2004, 2007; ICOLD 2015). Heave usually occurs within the unprotected seepage exit area, lifting and cracking the soil layer (mass of soil) providing the unprotected exit point for BEP to occur. Both heave and BEP mechanisms can contribute to the potential for internal erosion beneath a levee; therefore, both mechanisms are included in the assessments presented herein.



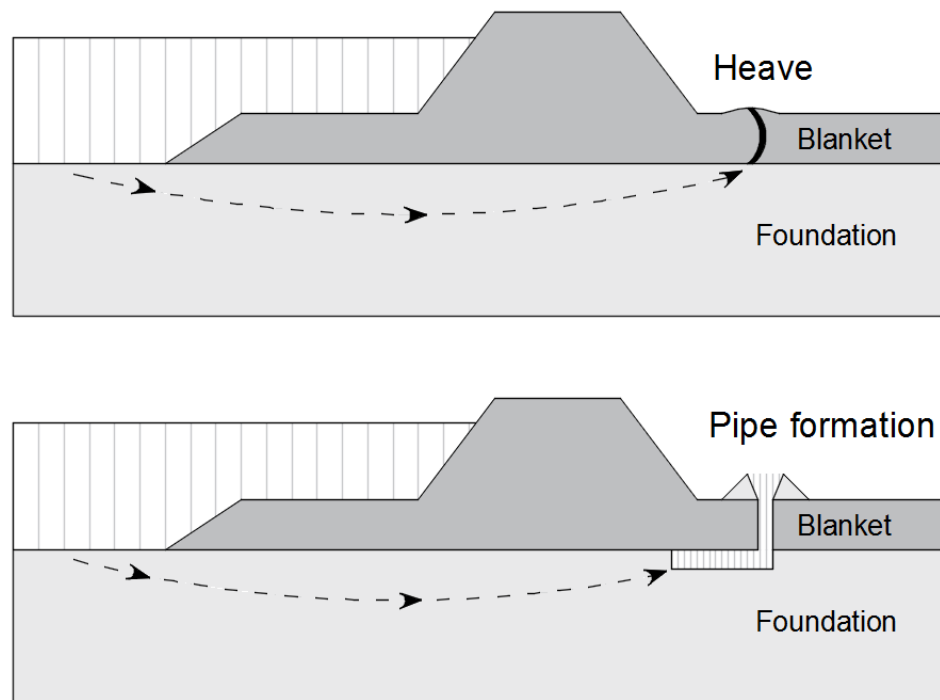


Figure 1.3. Illustration of heave and backward erosion piping mechanisms.

Underseepage analysis results vary considerably based on soil parameters and geologic conditions. Nevertheless, for simplicity of such complex analysis, levee sections' geometry and soil profile are simplified in a manner that underseepage analyses may not represent the true state of nature of the levee itself. Since levee structures are long and subjected to variable foundation conditions, it is logical to analyze them in an uncertainty-based approach but, for the same reason, reliability analyses tend to be simple as well. The incorporation of soil parameters in the analysis is broader than the consideration of the levee's geometric structure.

While the findings of this research can be applied to a number of geomorphic settings, it will be underlain by meandering river sediments since most of the levee structures encountered in the United States are found within this type of environment. The

Sacramento River Levee system in California will be used as a case study. A small sample of the surficial geologic map of the Sacramento River levee system is shown as Figure 1.4.

Underseepage vulnerability along a levee's alignment is usually associated with localized geomorphic features (Glynn and Kuszmaul 2010) that shape the meandering river floodplains. Therefore, the integration of such features in levee's underseepage analyses (in the context of both reliability and deterministic analyses) should be considered. The most common geomorphic features encountered to intercept the alignment of a levee are abandoned channels, point bars, meander scrolls and, crevasse splays as can be seen from Figure 1.4 (William Lettis & Associates 2008). In common levee underseepage analyses, the typical subsurface geometry is depicted by two layers as seen in Figure 1.3.

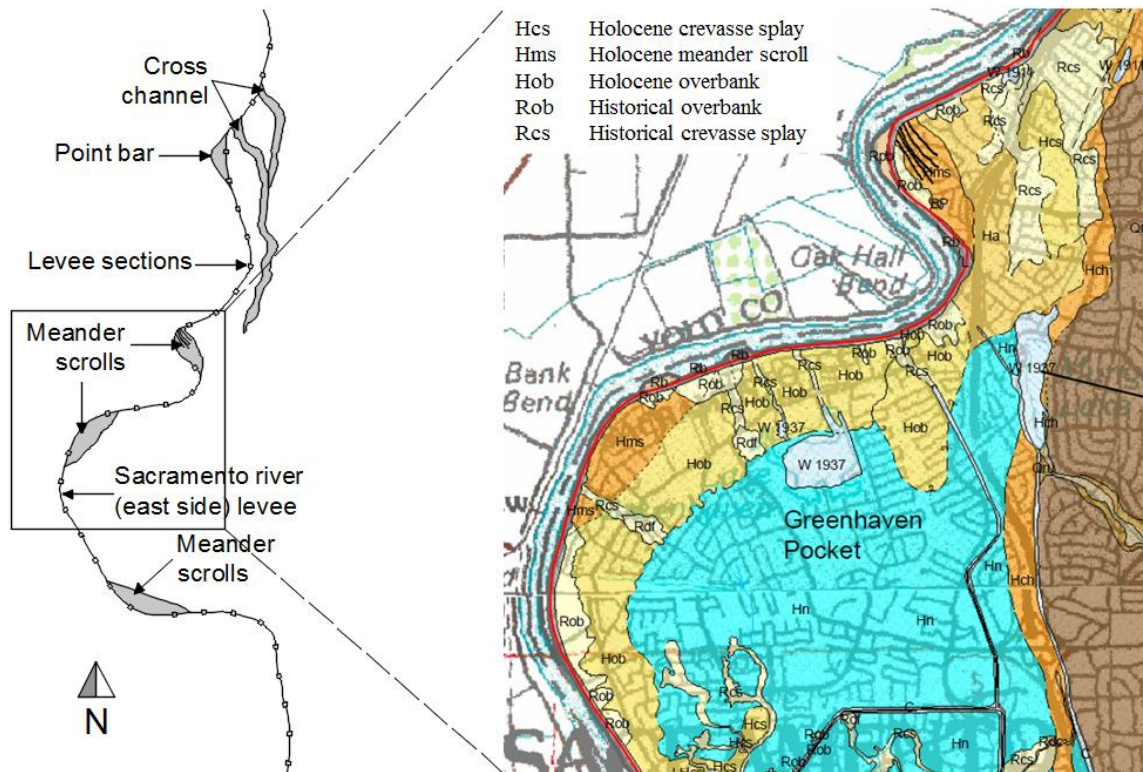


Figure 1.4. Sacramento River Levee system in California showing a clip of a geological map with most common geomorphic features.

The top layer, usually characterized by low hydraulic conductivity, is called the blanket layer. The bottom layer, referred to as the foundation layer, typically is composed of high hydraulic conductivity soils on the contrary to the blanket layer. As a clarification, the term ‘foundation’ is used interchangeably in the geotechnical engineering community to refer to the foundation layer and the foundation as a whole. Within the context of this manuscript, the term ‘foundation soils’ describes the combination of the blanket and foundation layers.

Based on the simple two layer configuration, the U.S. Army Corps of Engineers (USACE) developed theoretical relationships for the computation of seepage flow beneath levees referred to as the blanket theory (BT) equations (USACE 1956). The computation of hydraulic heads within the seepage regime by means of the BT equations is easily achieved for either a piping or heave mechanism in a short period of time and, therefore, is a very popular method among the levee engineering community. Despite the BT method’s attractive easiness, the simplification of the foundation soils serves as the core and main limitation of the method since, in many cases, it doesn’t represent a realistic state of nature of the levee section. In the cases where a levee section may be represented by two homogeneous soil layers the method is quite accurate. But, unfortunately, due to the nature of the foundation soils, more complex levee subsurface arrangements are encountered where the BT method does not accurately handle the complexity of the correspondent analysis. Usually, the complexity of the analysis is a consequence of the interception of geomorphic features on the levee alignment.

In an effort to analyze levee underseepage uncertainty, probabilistic methods are used together with deterministic methods such as the BT method. The most common probabilistic method used, also proposed by the USACE, is the simplified form of the Taylor's series method. The first-order second-moment (FOSM) Taylor series method only requires the expected value and standard deviation of the random parameters in order to analyze the associated underseepage uncertainty within a levee section. The method is limited by the requirement of modeling the random parameters as normal or lognormal distributions. This assumption might not be accurate for modeling complex levee geometries. Nevertheless, the coupling of the BT and FOSM methods is popularly used due to their ease of application.

On the other hand, although geomorphic features tend to provide much of the uncertainty in underseepage reliability analyses, the levee reach's length tends to increase the probability of failure, a phenomenon often called length effects (Vrouwenvelder et al. 2010; Bowles et al. 2012; Kanning 2012). In other words, as the length of the levee increases, the probability of encountering unfavorable subsurface conditions increases, thus, the probability of unsatisfactory performance or failure increases. It is the author's hypothesis that by identifying and analyzing the geomorphic features along the alignment of a levee structure, the vast majority of the underseepage length effect hazard can be evaluated.

Based on the limitations of the FOSM-BT method and on the concept that discrete subsurface geomorphic features provide vulnerable locations for hydraulic pressure buildup and/or concentration of seepage flow, a method is presented where the interactive

hydraulic behavior between the geomorphic features, the levee structure, and the surrounding characteristic subsurface profile is characteristically three-dimensional. The methodology, called the Response Surface–Monte Carlo (RSMC) simulation method, uses multiple finite element analyses to develop a relationship (i.e. the response surface) between key input parameters (hydraulic properties and subsurface geometry of the soil layers) and the conditional probability of reaching critical hydraulic conditions (uplift pressures or hydraulic exit gradients). The response surface (Xu and Low 2006; Low 2008), is used to perform a Monte Carlo simulation that results in a cumulative ascending distribution function (CADF). The range and probability distribution for each soil or geometric input parameter are represented using a probability density function (PDF) that describes the relative likelihood for this parameter to take on a given value. Since the analyses is conditional on the river reaching a certain level, the result is considered as a conditional probability of initiation of erosion and not failure of the levee structure. To assess failure, an event tree analysis is needed as stated by ICOLD (2015).

In addition, as it can be observed in Figure 1.4, levee systems may be represented either by straight or curved sections. Nonetheless, the vast majority of underseepage analyses are based on the analysis of straight levee sections. Since some geomorphic features are naturally inherent to the curvature of a levee system, it is counterintuitive that curvature should have an effect on the underseepage flow regime. Also, even without the presence of a major geomorphic feature, the effect of curvature by itself could negatively affect the underseepage reliability of a levee system. Therefore, the effect of curvature on levee underseepage reliability is studied and incorporated in the RSMC methodology.

In summary, this research focuses on the assessment of levee internal erosion potential due to underseepage with the following objectives:

1. Developing the reliability assessment of initiation of erosion by means of a response-surface Monte Carlo simulation method
2. Assessing the feasibility and accuracy of the most common U.S. Army Corps of Engineers underseepage method (Blanket Theory) on handling complex levee sections
3. The study and incorporation of geomorphic features into seepage analyses in a meandering river levee environment
4. The study of the combined effect of levee curvature and geomorphic features on underseepage reliability

Chapter 2 introduces the application of the two-dimensional RSMC methodology. The chapter states the limitations of USACE's FOSM-BT method especially the lack of incorporating key geometric parameters. By means of two hypothetical case studies, steps for the application of the RSMC method are presented. Due to the complexity of the hypothetical levee sections, a direct comparison with the FOSM-BT method is not feasible and, therefore, advances of the RSMC method over the FOSM-BT method are delineated. Multiple regression analyses are performed to assess the relative effect that changes in the various input variables have on the outcome for the various analyses.

Chapter 3 evaluates the capability of the USACE's FOSM-BT methodology compared to the two-dimensional RSMC methodology with the purposes of: 1) investigating the effects of levee subsurface geometry on the probability of initiation of

internal erosion due to underseepage, and 2) assessing the capability of the FOSM-BT method in analyzing internal erosion potential in increasingly complex foundation conditions. Eight levee cross sections were analyzed. All cross-sections were analyzed by means of the RSMC methodology. Cross-sections that are simple enough to be analyzed by FOSM-BT method were compared to the RSMC methodology. For all of the cases, an analysis of the relative importance of the input parameters is performed (multivariate regression with analysis of variance) to assess which parameters (soil parameters or geometric parameters) have the greatest effect on the potential for underseepage internal erosion.

Chapter 4 introduces the three-dimensional reliability (RSMC) assessment of underseepage due to the interception of geomorphic features on the alignment of a levee system. Based on the assumption that the preponderance of the underseepage risk to a levee reach is due to the geomorphic features along that reach, the RSMC methodology was expanded using three-dimensional finite element analyses to account for the three-dimensional seepage aspects of the individual geomorphic features. As an application example, the analysis of a historical crevasse splay deposit is presented. The underseepage flow regime of a crevasse spay feature is hypothesized by three parameters: 1) the conductance of the crevasse channel, 2) the transmissivity of the splay, and 3) the conductance of the blanket overlying the splay.

Chapter 5 demonstrates the flexibility of the three-dimensional RSMC methodology in adapting to the needs of particular geomorphic features. The methodology is adapted to abandoned channels as it was performed on crevasse splay features from

Chapter 4. The underseepage flow regime of an abandoned channel is also hypothesized to be controlled by three combined parameters: the “blanket layer river length”, the “tongue effect” and the “modified leakage factor”.

Chapter 6 expands the application of the three-dimensional RSMC methodology by incorporating the effect of curvature on levee systems. It is discussed in which situations the analysis of geomorphic features might need curvature adjustment (or not) based on natural geological formation location and/or key parameters. In particular, the study of convex curvature is of interest.

## References

- ASCE (American Society of Civil Engineers) (2009). So, you live behind a levee. *ASCE Publications, Technology & Engineering* - 28 pages.
- Bowles, D. S., Chauhan, S. S., Anderson, L. R., and Grove, R. C. (2012). “Baseline risk assessment for Herbert Hoover dike.” *Proc., ANCOLD Conf. on Dams*, Australian National Committee on Large Dams (ANCOLD), Hobart, Tasmania, Australia, 1–20.
- ICOLD (International Commission on Large Dams). (2015). “Internal erosion of existing dams, levees, and dikes, and their foundations.” *Internal erosion processes and engineering assessment*, Vol. 1, Paris, France.
- Kanning, W. (2012). “The weakest link.” Ph.D. dissertation, Delft Technical Univ., Delft, Netherlands.
- McCook, Danny (2004). A Comprehensive Discussion of Piping and Internal Erosion Failure mechanisms, *ASDSO National Conference*, Phoenix, AZ.
- McCook, Danny (2007). A discussion of uplift computations for embankments and levees. *Journal of Dam Safety*, 5(1), 1-9.
- Schleifstein, Mark (2010, January 2). Levee statistics point up their importance to nation's economy. *The Times-Picayune's*, p. 1. Retrieved from [http://www.nola.com/hurricane/index.ssf/2010/01/levee\\_statistics\\_point\\_up\\_thei.html](http://www.nola.com/hurricane/index.ssf/2010/01/levee_statistics_point_up_thei.html)



- Terzaghi, Karl and Ralph Peck (1968). *Soil Mechanics in Engineering Practice*, 2nd Edition. John Wiley and Sons.
- USACE. (1956). "Investigation of underseepage and its control." *Technical Memorandum No. 3-424*, U.S. Army Engineer Waterways Experiment Station, Vicksburg, MS.
- Vrouwenvelder ACWM, Van Mierlo MCLM, Calle EOF, Markus AA, Schweckendiek T, Courage WMG (2010) Risk analysis for flood protection systems. Deltares, Main Report, The Netherlands
- William Lettis & Associates, Inc. (2008) Surficial geologic map and initial geomorphic assessment, Sacramento River (east side), Sacramento County, California. Unpublished consultant report prepared for URS Corporation
- Wolff, D. (2008). "Reliability of levee systems." *Reliability-based design in geotechnical engineering*, K.-K. Phoon, ed., Taylor and Francis Group, New York, 448–496.

## CHAPTER 2

RELIABILITY-BASED UNDERSEEPAGE ANALYSIS IN LEVEES USING A  
RESPONSE SURFACE–MONTE CARLO SIMULATION METHOD**Abstract**

Present methods for assessing the potential for unsatisfactory levee performance because of underseepage consist of deterministic seepage analyses and simplified reliability methods. Deterministic methods consist of calculating factors of safety based on the ratio of the critical gradients of the soil and hydraulic exit gradients without taking into account high levels of uncertainty in soil properties and subsurface geometry that are inherent to many levee analyses. The most common simplified reliability approaches currently being used to analyze levees against underseepage apply the first-order second-moment Taylor series method, using the U.S. Army Corps of Engineers blanket theory equations as the performance functions. In many cases, these methods do not realistically reflect the geometry of the levee's foundation soils and the uncertainty associated with their performance. This study proposes a new application for the response surface method that allows modeling the initiation of erosion process with more accurate failure mechanisms and more complex subsurface geometry. The response surface–Monte Carlo (RSMC) simulation method uses finite-element analyses to develop a series of equations that define the relationship between the variables and the factor of safety ( $FS$ ). Using these equations, probability density functions (PDF) for variables, and the computer program @Risk, a Monte Carlo simulation is performed to calculate the conditional probability of

unsatisfactory performance ( $P_{up}$ ) because of underseepage for a given river flood level. Two examples are presented to illustrate the proposed procedure. Multiple regression analyses are performed to assess the relative effect that changes in the input variables have on the  $FS$  for the various analyses. The results suggest that uncertainty in the levee geometry has the greatest effect on the variation of the  $FS$  for the cases studied.

## 2.1. Introduction

Levee underseepage occurs when water retained by the levee imposes a hydraulic gradient across the foundation soils resulting in seepage flow through the foundation toward the landside of the levee. If the imposed gradient is low, the water may seep out gently, resulting in wet conditions but causing no soil erosion. However, if the imposed hydraulic gradient is large enough, the underseepage may result in erosion of the foundation soils that, if left unchecked, may act to destabilize the levee and could eventually lead to a levee breach. Soil erosion caused by underseepage can occur because of several mechanisms. First, where the hydraulic gradient at the location where the seepage exits the soil (exit gradient) is larger than the gradient required to cause erosion of the soil at this location (critical gradient), the soil particles will be eroded from the exit location. Continued erosion will result in the formation of a conduit or “pipe” leading back toward the source of the seepage. This mechanism is commonly referred to as backward erosion piping (BEP).

A second mechanism may occur when high-hydraulic conductivity soils on the landside of the levee are overlain by a soil layer having significantly lower hydraulic

conductivity (often termed the “blanket” layer). Because of the lower hydraulic conductivity, water pressure builds up at the base of the blanket layer. If the water pressure becomes great enough, it may lift the blanket layer upward; a mechanism generally referred to as “heave.” In cases where the underlying hydraulic conductivity is very high, heave may result in a catastrophic failure or “blowout.” In other cases, the blanket layer may crack, resulting in a pathway for BEP of the underlying sand to develop through (sand boil formation).

## **2.2. Present Analysis Methods**

Both deterministic and probabilistic methods are presently used to analyze the potential for subsurface erosion because of underseepage. Deterministic methods consist of calculating factors of safety based on either (1) the ratio of critical gradients of the soil and hydraulic exit gradients calculated using the finite-element method or other seepage analyses, or (2) the ratio of the hydraulic pressure beneath the blanket layer and the weight of the blanket. Some of the earliest work in deterministic underseepage analysis was performed by Bligh (1910, 1913) who developed an empirical relationship between piping potential and the shortest flow path length beneath a water-retaining structure. Lane (1934) later recognized a distinction between flow along the base of the structure, vertical flow along vertical barriers, and flow through a granular media and modified Bligh’s work to develop the weighted creep ratio method. Lane’s empirical method also took into account the varied erosion resistance of different soil types.

Later efforts by the U.S. Army Corps of Engineers (USACE) developed theoretical relationships for the computation of seepage flow beneath levees (USACE 1956). These relationships provided the basis for the “blanket theory” equations presented in the *USACE Engineering Manual EM 1110-2-1913 “Design and Construction of Levees”* (USACE 2000). The equations usually assume two soil layers in the levee foundation with constant thickness and horizontal boundaries; the top layer is considered a semi pervious soil consisting of silt and/or clay (the blanket), and the layer below is considered pervious (sand and gravel) (USACE 2005). Flow is assumed to be horizontal (and therefore the horizontal hydraulic conductivity is used) for the pervious layer and vertical for the blanket layer. The blanket theory equations calculate the head at the base of the blanket layer that can be used to calculate either a gradient through the blanket or an uplift pressure beneath the blanket. Thus, the factor of safety ( $FS$ ) can be calculated for either piping or heave.

The main limitation of the “blanket theory” equations is that the subsurface geometry is restricted to two homogenous layers of constant thickness. This limitation was partially resolved by the finite difference computer program LEVEEMSU (Wolff 1989; Gabr et al. 1995) that numerically solves the blanket theory equations to allow for nonuniform thickness of layers and varied soil hydraulic conductivity. The development of the finite-element seepage analysis program CSEEP by the USACE (Knowles 1992; Tracy 1994) has greatly increased engineers’ ability to model complex subsurface geometries. Numerous commercial finite-element seepage analyses programs have become available since the development of CSEEP. Probabilistic methods for assessing underseepage have been developed by coupling the deterministic methods discussed above with probability

models such as the Taylor' series method, point estimate method, or the method of perturbations (Harr 1987; Duncan 2000; Baecher and Christian 2003; Sleep and Duncan 2008; USACE 2004). One common approach that is well documented by the USACE consists of using the "blanket theory" equations as the performance function and the first-order second-moment (FOSM) Taylor series method as the probability model (Wolff 1994; Wolff et al. 1996; Crum 1996; and Wolff 2008). The FOSM method used in the USACE method is a simplified form of the Taylor's series method that uses only the expected value and standard deviation of the random variables. Thus, the method works well for variables modeled with normal or lognormal distributions of the random variables and linear performance functions (USACE 2004). For more complex performance functions, the Hasofer and Lind (1974) method may be used at the expense of needing multiple iterations for a solution convergence.

Fell et al. (2004) estimated the probability of failure of embankment dams by internal erosion and piping by historic performance and event tree methods. Also, Calle et al. (1989), developed a probabilistic procedure for analyzing the likelihood of piping beneath sea dikes and river levees considering the dynamic equilibrium necessary to accelerate or terminate erosion and material movement once piping has initiated.

## **2.3. Benefits and Limitations of Present Methods**

### **2.3.1. Deterministic Methods**

The main benefit of deterministic analyses is the flexibility of finite element seepage analyses. The numerous finite-element seepage analysis programs available easily

allow analyses to model multiple soil layers and complex subsurface configurations. The finite element method also gives the analyst flexibility to model a mechanism resembling the anticipated mode of failure. The primary limitation of deterministic methods is that they do not take into account the uncertainty and variability of the input variables. As Duncan (2000) points out, engineers will often use the same *FS*, applying it to conditions that involve a wide range of uncertainty. This approach is not reasonable as the same *FS* may represent different levels of reliability because of the varying levels of uncertainty in the analysis and input variable values. As discussed above, underseepage erosion may initiate by one of several mechanisms. It is unreasonable to assume that the equivalent *F* for different failure mechanisms represent the same level of reliability.

### 2.3.2. FOSM Blanket Theory Method

Due to its ease of application, the commonly used form of the FOSM blanket theory method documented in USACE manuals (USACE 2000) is often used as a first approach for underseepage reliability analyses in levees. The blanket theory equations that are commonly used with the FOSM method are limited in the complexity of the subsurface geometry and failure mechanism modeled because of the requirement that the layers be of constant thickness. The blanket theory equations calculate an exit gradient through the blanket layer and compare this with the weight of the blanket or the critical gradient of the silt to calculate the *FS*. This assumes the mechanism of failure is BEP in the blanket layer or heave and cracking of the blanket (Wolff et al. 1996; Crum 1996). However, because the blanket layer generally consists of cohesive soils, backward erosion is rarely the failure mechanism. A more likely mode of failure would be heave of the blanket and/or piping of

the underlying soil through a crack or defect in the blanket (sand boil formation). Because of the inflexibility of the blanket theory equations, modifications to account for differing failure mechanisms are not possible.

The form of the FOSM method typically used in underseepage analyses (USACE 1999, Wolff 1994) also has its limitations. First, while it is possible to apply the FOSM to other distributions, the form commonly used in underseepage analyses requires the variability of all variables be modeled with a normally or lognormally distributed probability density function (PDF). Often this is unrealistic, especially for the geometric variables as will be discussed subsequently in this paper. Secondly, the FOSM method assumes a linear relationship between the variable and the *FS*. When these relationships are nearly linear, this assumption introduces a small amount of error to the calculation. However, many of the geometric variables are not linear and in some cases the relationships are closer to parabolic than linear. In these cases the error introduced can be significant.

In some cases the mode of failure will change as the subsurface geometry varies (an example is provided in this paper). Because the FOSM method requires that a single performance function be used, it does not have the flexibility to deal with this situation.

#### **2.4. Proposed New Application: The RSMC Method**

To address the previously discussed limitations of currently used reliability-based underseepage assessment methods, a response surface–Monte Carlo simulation method (RSMC) is proposed. The RSMC method involves developing a relationship between the significant variables and the performance of the levee system with regards to underseepage



and the initiation of piping or heave (i.e., the “response surface”) and using this relationship in a Monte Carlo simulation to assess the probability of a specified level of performance. In the examples presented herein, the *FS* against piping initiation or heave (both described generally as the ratio of the forces resisting soil movement to the forces tending to cause soil movement) is used as the performance function and a *FS* below 1.0 is deemed to be unsatisfactory performance. The RSMC method could also be applied using other values as the performance function (i.e., the exit gradient); however, because the *FS* incorporated both the hydraulic conditions (gradient or pressure) and the soil properties (unit weight), its use incorporates more aspects of the failure mechanisms into the analysis. Furthermore, when multiple failure mechanisms are incorporated into the analysis, the key parameter for each mechanism may be different. By using the *FS* as the performance function, the effects of both mechanisms can be combined in one analysis.

The response surface is created using a series of finite-element seepage analyses where each of the significant parameters affecting the *FS* are sequentially varied—in essence a multivariable parametric analysis. While in some RSMC analyses the response surface may be represented by an equation fitted to the results of the analysis, in the examples presented subsequently the response surface is represented by series of plots where each plot contains a series of curves. Each of the curves can then be represented by a polynomial equation fit to the analysis results that relates a variable and either the exit gradient or the uplift pressure. Each set of curves (on a plot) represents the relationship between two variables and the exit gradient or uplift pressure at a fixed value of a third variable represented by that plot. By interpolating between the curves and then the plots,

the exit gradient or uplift pressure can be quickly calculated for any combination of values for the significant variables. The *FS* is then calculated using simple equations that complete the response surface relationship (as described in detail below). Thus, by programming the equations and interpolations into an Excel spreadsheet and linking the spreadsheet with the program @Risk, a Monte Carlo simulation is performed. The result of the simulations is a probability of the *FS* being below a given value. While *FS* equal to 1.0 was used as the criteria for unsatisfactory performance in the examples below, other values of *FS* could be assessed.

The use of the series of plots and curves in the examples below has two advantages. First, the curves give the analyst a visual perspective of the relationship between the variables and the *FS*; a perspective difficult to achieve using a multivariable equation. Second, by limiting the number of variables in the polynomial equations, a better correlation is often achieved than with a multiple variable equation and, as a result, less error is introduced in the analysis. It is also possible to incorporate two different mutually exclusive failure mechanisms by developing a set of curves and plots for each failure mechanism and incorporating a logic statement identifying when each mechanism is to be used into the Excel spreadsheet. Examples of use of the RSMC method and the features described above are detailed in the following sections.

#### 2.4.1. Example 2.1: Pinching Out of Blanket Layer

A representative version of a profile levee in the Natomas Basin area north of Sacramento, CA, is presented in Figure 2.1. This levee profile is more complex than profiles that could be analyzed using the blanket theory equations. Simplified versions of

three of the borings used to define the subsurface are shown on the profile. Note that borings B-2 and B-3 indicate that a 15-to 20-foot thick clay/silt blanket exists above the sand layer. However, in boring B-1 the blanket layer is not observed beneath the levee. Thus, the blanket appears to pinch out somewhere between borings B-1 and B-2, ending either at the ground surface beyond the levee toe or beneath the landside of the levee.

The location where the blanket pinches out not only affects the seepage regime in the levee foundation (hydraulic gradients and pressures) but also affects the mechanism responsible for the initiation of subsurface erosion. If the blanket were to pinch out at the ground surface exposing the underlying sand, the most likely mechanism for initiating seepage-related erosion would be backward erosion piping of the sand because of high exit gradients. However, if the blanket were to pinch out beneath the levee, the failure mechanism would either be heave of the blanket or piping of the underlying sand through a defect in the blanket layer (sand boil formation). A combination of these two mechanisms is also possible where the heave results in cracking of the blanket, thus providing a defect through which erosion of the underlying sand can occur. Because the failure mode changes depending on the geometry of the profile, a realistic assessment of the probability of erosion initiation must be flexible enough to account for this change.

To model the uncertainty of subsurface geometry, “geometric variables” must first be defined. For the geometric variability of the profile described above, the geometric variable (denoted as  $A$ ) is defined as the horizontal coordinate of the location where the blanket pinches out, measured from the center of the levee crown as illustrated in Figure 2.2.

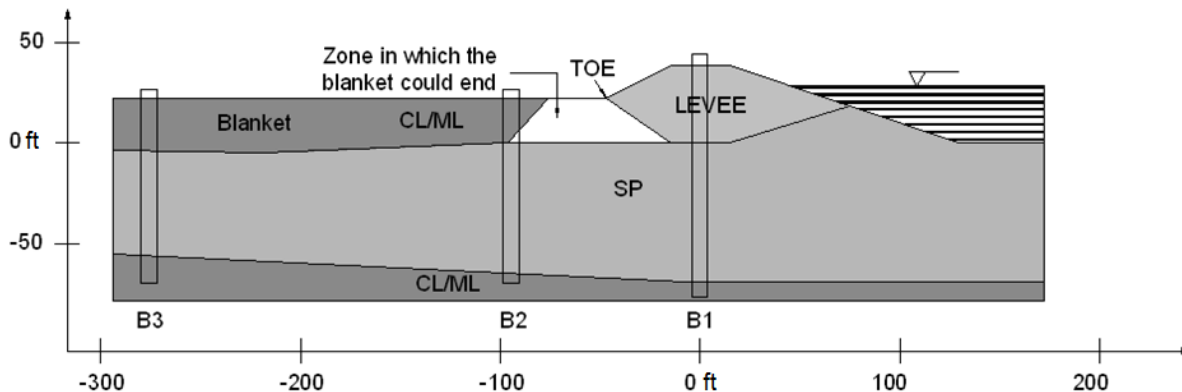


Figure 2.1. Simplified levee profile showing the zone in which the blanket could end.

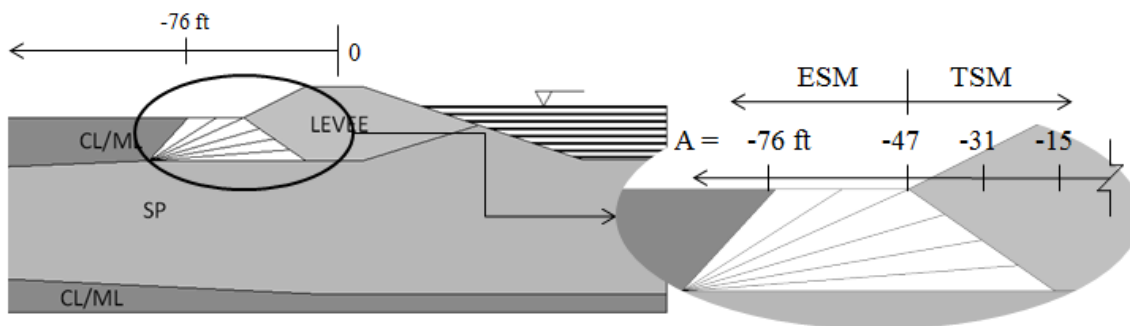


Figure 2.2. Failure mechanisms based on the levee geometry.

A PDF is developed to define the relative probabilities of  $A$  being located at the range of locations between borings B1 and B2. The trapezoidal probability density function presented in Figure 2.3 is selected to define this PDF based on judgment and consideration of the geologic processes that likely resulted in the pinching out of the blanket. As shown in Figure 2.3, the probability of the blanket layer pinching out at either boring B1 or B2 is defined as zero, the probability increases linearly toward the center of the area between the two borings, and is considered constant in the central portion of this area.

Because the selection of the PDF is subject to much uncertainty, the sensitivity of the analysis to the assumed PDF shape is assessed by performing the analysis with other PDF distribution shapes.

The results of these analyses are discussed along with the results of this example. In addition to the geometric variable, the variation of some soil variables are considered to significantly affect the probability for initiation of erosion and, as such, the uncertainty of these variables are included in the analysis.

As is typical of many geotechnical analyses, there is insufficient data to develop site-specific PDFs for the variables using statistical analysis. As such, PDFs for these variables are estimated based on (1) a limited number of laboratory tests, and (2) published guidance on probability distributions for similar soil types (Harr 1987; Sleep and Duncan 2008).

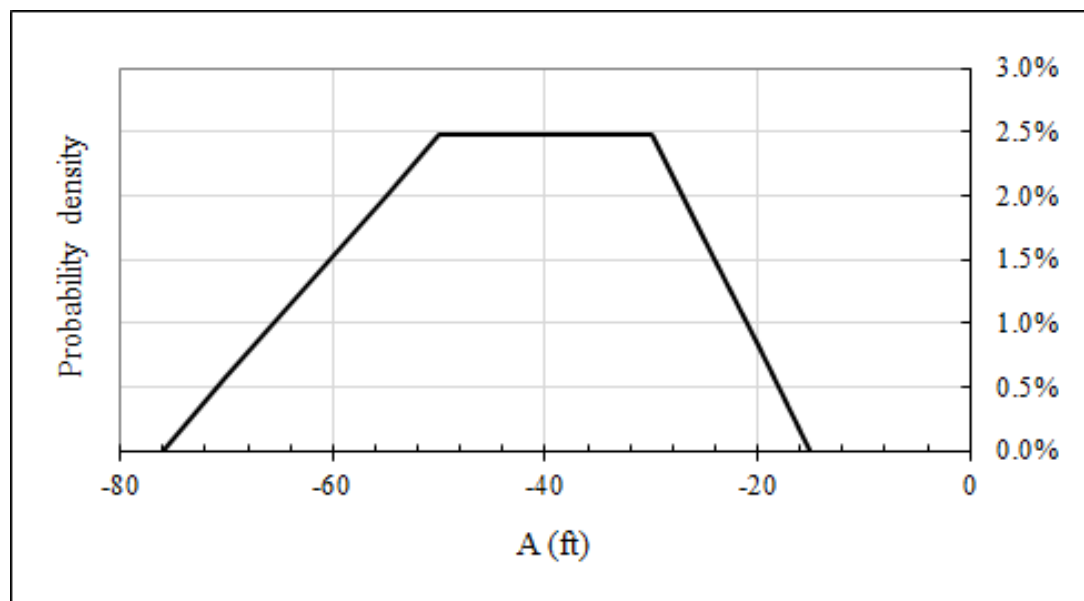


Figure 2.3. PDF for geometric variable A.

The variability of the horizontal hydraulic conductivity of the sand,  $K_s$ , the vertical hydraulic conductivity of the blanket layer,  $K_b$ , and the anisotropy ratio (ratio of the horizontal hydraulic conductivity to the vertical hydraulic conductivity) of the sand,  $K_{hv}$ , are assumed to be represented by lognormal distributions. In the actual analyses, the probability density functions for the hydraulic conductivity variables are determined for the log of the actual values, resulting in normal distributions. The antilogs of the values from the normal distributions are then taken to be used in the calculations. The variability of the total unit weights of the blanket soils,  $\gamma_{blkt}$ , and the underlying sand,  $\gamma_{sand}$ , are modeled with normal distributions. Data describing the assumed probability density functions for the significant variables in this analysis are presented in Table 2.1. The maximum and minimum values provided in Table 2.1 are used to truncate the normal and lognormal distributions to avoid numerical errors and unrealistic values.

It is assumed that the variables used in the analysis are independent. While it could be argued that some correlation between variables may exist (i.e., a relationship between unit weight and hydraulic conductivity), the limited amount of soil parameter data available for this study does not allow for developing a meaningful dependence relationship. Furthermore, the authors are unaware of any published guidance for assessing dependence between the variables used in the analyses.

#### 2.4.2. Relationship between Variables and Factor of Safety (Response Surface)

Finite-element seepage analyses are used to develop a relationship that, given the geometric variable, the hydraulic conductivities of the sand and blanket, and the anisotropy

ratio of the sand, calculates either a hydraulic exit gradient or an uplift pressure for the model, depending on the failure mode.

This relationship can be represented by a multidimensional surface or “response surface.” For the previously described profile, the finite-element analyses are used to calculate a hydraulic exit gradient,  $i_e$ , where the sand exists at the ground surface ( $A < -47$  ft). Alternatively, where the blanket pinches out below the levee ( $A > -47$  ft) an intact blanket overlies the sand and an uplift pressure at the base of the blanket,  $u_{bl}$ , is calculated. Using the resulting gradient or uplift pressure along with the unit weight of the affected soil, the  $FS$  against initiation of erosion is calculated as described below.

Table 2.1. Input Variables for Proposed Method

Variable	Type of PDF distribution	Most Likely Value	Standard Deviation	Truncated Maximum Value	Truncated Minimum Value
Geometric Variable ( $A$ ), ft	Trapezoidal	-47	-	-15	-76
Log of Blanket Hydraulic Conductivity ( $\log K_b$ ), log(ft/s)	Normal	-6.00	0.67	-5.10	-7.00
Log of Sand Hydraulic Conductivity ( $\log K_s$ ), log(ft/s)	Normal	-3.00	0.67	-2.00	-3.80
Log of Sand, Anisotropy Ratio ( $\log[K_h/K_v]_s$ )	Normal	-0.60	0.163	-0.30	-2.30
Saturated Unit Weight of Blanket Soils ( $\gamma_{blkt}$ ), lb/ft <sup>3</sup>	Normal	120	5.0	130	110
Saturated Unit Weight of Underlying Sand ( $\gamma_{sand}$ ), lb/ft <sup>3</sup>	Normal	130	5.0	140	120

In the first failure mechanism case (exit gradient in sand at the ground surface), the  $FS$  against backward erosion piping,  $F_{bep}$ , is calculated using the following equation:

$$F_{bep} = \frac{i_c}{i_e} \quad (1)$$

where  $i_e$  = exit gradient calculated at the ground surface in the finite-element analyses; and  $i_c$  = critical gradient of the eroding soil (the sand in this case). The exit gradient is calculated using hydraulic head data from the top two to three rows of elements below the ground surface. The critical gradient of the soil is calculated as the ratio of the buoyant unit weight of the soil ( $\gamma_{buoy}$ ) to the unit weight of water ( $\gamma_w$ ) or

$$i_c = \frac{\gamma_{buoy}}{\gamma_w} = \frac{\gamma_{sand} - \gamma_w}{\gamma_w} \quad (2)$$

where  $\gamma_{sand}$  = total unit weight of the sand

In the second failure mechanism case (heave of the blanket), the  $FS$  against heave,  $F_{heave}$ , is calculated directly from the uplift pressure and the unit weight of the blanket soils using the following equation:

$$F_{heave} = \frac{H\gamma_{blkt}}{u_{bl}} \quad (3)$$

where  $H$  = thickness of overlying soil blanket,  $\gamma_{blkt}$  = saturated unit weight of overlying blanket,  $u_{bl}$  = water pressure at the base of the blanket.

The model assumes the two failure modes are independent. Where the blanket pinches out before the toe of the levee, the water pressure will not be trapped beneath the blanket and, thus, the heave mechanism will not occur. Where the blanket extends below



the levee, the blanket must heave to initiate the erosion process and, thus, the mechanism to initiate seepage erosion is heave. As such, there is no overlap between the two mechanisms.

The response surface development consists of a parametric analysis involving each of the uncertain input variables. The PDF distributions for each variable are discretized into 5 or 6 values that represent the range of values in the PDFs. Finite element seepage analyses are then run for every combination of values for each variable using the finite-element model presented in Figure 2.4. The model consists of a silt/clay blanket layer overlying sand in the levee foundation and consists of 1,733 six-noded triangular elements. The downstream and upstream ends are modeled with constant head boundary conditions equal to downstream ground elevation or the river water level elevation, respectively. The downstream ground surface is modeled with an exit face boundary condition. By building several potential boundary locations in the region where the end of the blanket is uncertain (see the highlighted region of Figure 2.4), the location of the boundary between the blanket and the sand (and thus the end of the blanket) can be changed by reassigning the material type to the small triangular regions. By doing so, the end of blanket can be changed without changing the finite-element grid of the model and thus changes in results because of changes in the element configurations are eliminated.

If four variables are considered in the above analysis with the potential range of each represented by 5 discretized values, the total number of finite-element analyses run will be  $5^4$  or 625; a daunting number of runs. However, it has been shown by others (USACE 1956), and confirmed by analyses performed for this study, that the exit gradients

and uplift pressures are functions of the ratio of the hydraulic conductivities of the sand and blanket as much as the individual values for the soils (this is generally the case with seepage analyses involving a blanket layer). This allows for the combining of the  $K_b$  and  $K_s$  variables into the hydraulic conductivity ratio,  $K_{sb}$ . Doing so reduces the number of variables to relate to hydraulic gradient or uplift pressure from four to three and thus reduces the number of finite-element analyses to be run to a reasonable number (i.e., around  $5^3$  or 125). It should be noted that the finite-element analyses are relatively quickly run once the base model has been developed by simply changing a variable or redefining a material boundary.

The results of the finite-element analyses are plotted to develop curves or surfaces describing the relationship between the variables and the exit gradient and the uplift pressure. Examples of such curves are presented in Figures 2.5 and 2.6. Figure 2.5 represents the relationship between the geometric variable  $A$  and the hydraulic conductivity ratio,  $K_{sb}$ , with the calculated exit gradient in the sand,  $i_e$ , for a given value of anisotropy ratio,  $K_{hv}$  (equal to 0.25 in this case).

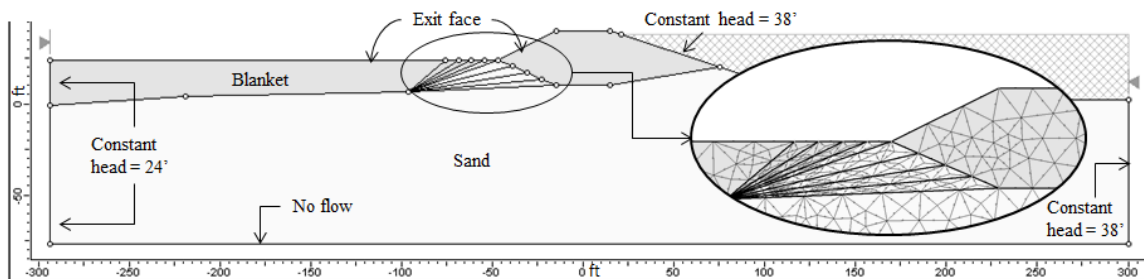


Figure 2.4. Finite-element levee profile used in Example 2.1.

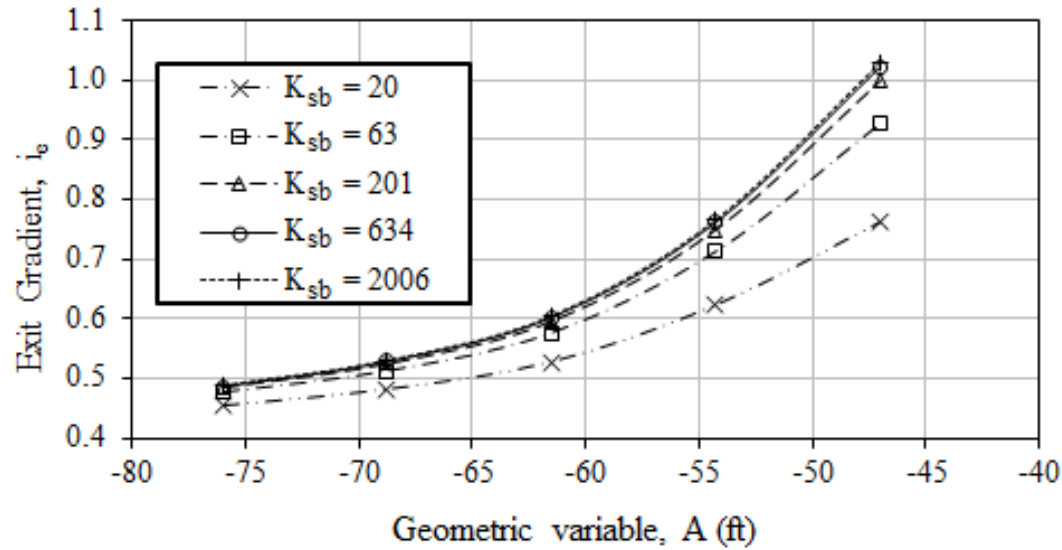


Figure 2.5. Family of curves representing relationship between  $K_{sb}$ ,  $A$ , and  $i_e$ , for  $K_{hv} = 0.25$ .

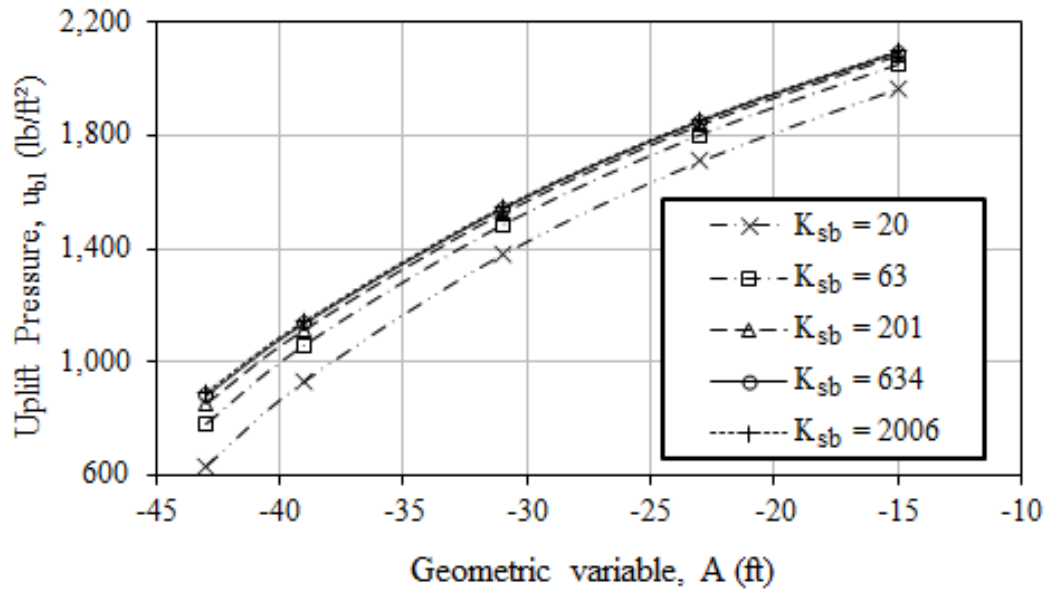


Figure 2.6. Family of curves representing relationship between  $K_{sb}$ ,  $A$ , and  $u_{bl}$  for  $K_{hv} = 0.25$ .

Figure 2.6 represents the relationship between the geometric variable  $A$  and the hydraulic conductivity ratio,  $K_{sb}$ , with the calculated uplift pressure at the base of the blanket  $u_{bl}$  for a single value anisotropy ratio,  $K_{hv}$  (equal to 0.25 in this case). Each curve in Figures 2.5 and 2.6 represents a relationship between the geometric variable and either the gradient or uplift pressure for a specific value of  $K_{sb}$  at the  $K_{hv}$  value (0.25) represented by the figure.

To represent the variation over the full range of  $K_{hv}$ , a series of plots similar to those shown in Figures 2.5 and 2.6, each containing a set of curves representing the range of  $K_{sb}$  values, must be developed for each discrete value of  $K_{hv}$ . Connecting the curves for respective values of  $K_{sb}$  would produce surfaces describing the relationship between  $A$ ,  $K_{hv}$ ,  $K_{sb}$ , and either the gradient or the uplift pressure ( $i_e$  or  $u_{bl}$ ). The resulting four-dimensional relationships are termed a response surface.

The response surface derived from the results of the finite element analyses is incorporated into an Excel spreadsheet that, given a set of values of the variables ( $A$ ,  $K_{sb}$ ,  $K_{hv}$ ,  $\gamma_{sand}$ , and  $\gamma_{blkt}$ ), produces a  $FS$  against unsatisfactory performance. The curves, similar to those in Figures 2.5 and 2.6, are incorporated into the spreadsheet using equations derived using polynomial regression fitting of the finite-element results. The applicable failure mechanism to be analyzed is assessed in the spreadsheet using a logic statement and the geometric variable,  $A$ .

If  $A$  indicates the blanket pinches out before the levee toe, the backward erosion piping mode is assumed and the curves for calculating an exit gradient are used. Alternatively, if  $A$  indicates the blanket pinches out beneath the levee, the heave

mechanism is assumed and the curves for calculating the uplift pressure are used. As stated previously, the model assumes the two failure modes are independent, thus where the piping failure mechanism is assumed to occur the probability of heave is zero and vice versa.

Two levels of linear interpolation are performed to assess the exit gradient or uplift pressure. First, values of exit gradient or uplift pressure are interpolated between curves of constant  $K_{sb}$  on plots similar to Figures 2.5 and 2.6. These interpolations are performed on the sets of curves representing  $K_{hv}$  values directly above and below the given  $K_{hv}$  value. A second interpolation is performed between the values obtained in the first interpolations to calculate values representative of the appropriate  $K_{hv}$  value. Once the values of exit gradient or uplift pressure are calculated from the curves, the factor of safety,  $F_{bep}$  or  $F_{heave}$ , is calculated using Equations (1) and (3) for the piping or heave mechanism, respectively.

#### 2.4.3. Monte Carlo Simulation

A Monte Carlo simulation is performed by linking the @Risk program to the Excel spreadsheet. Data describing the PDFs of the variables are input into @Risk, which then produces random sets of variable values based on the PDFs using the “Mersenne Twister” random number generator with a clock-dependent seed. The spreadsheet calculates a value of  $F_{bep}$  or  $F_{heave}$  (as described above) and returns the value to @Risk. This process is repeated a large number of times (5,000 iterations are used in this analysis) and the factors of safety are assembled into a cumulative ascending distribution function (CADF) as

shown in Figure 2.7. The CADF is a plot of the probability of the  $FS$  being below a given value (the “performance probability”).

The performance probability presented on the CADF represents the probability of either the  $F_{bep}$  or  $F_{heave}$  being below 1.0. With a defined  $FS$  of 1.0 as the criteria for unsatisfactory performance, the probability for unsatisfactory performance for this example is 70.4%. The probabilities presented on the CADF are conditional probabilities of unsatisfactory performance given the 100-year flood level is reached.

Analyses are performed to assess an appropriate number of iterations needed to produce probability of unsatisfactory performance results with less than 2% error. The Monte Carlo simulations described above are performed using a wide range in the number of iterations in the simulation. At each iteration level, 10 simulations are performed, and the range of resulting values are noted (maximum probability minus the minimum probability). The results of these analyses are presented in Figure 2.8 and indicate that the range of results where 5,000 iterations are performed is approximately 1% for both this example and the following Example 2.2.

Analyses are also performed to assess the sensitivity of the result to the selection of the PDF shape for the geometric variable  $A$ . The Monte Carlo simulations described above are repeated assuming a variety of PDF distributions for the geometric variable  $A$ . The results of these analyses are presented in Table 2.2, which shows that the selected distribution of the PDF for  $A$  has a considerable effect on the conditional probability of unsatisfactory performance.

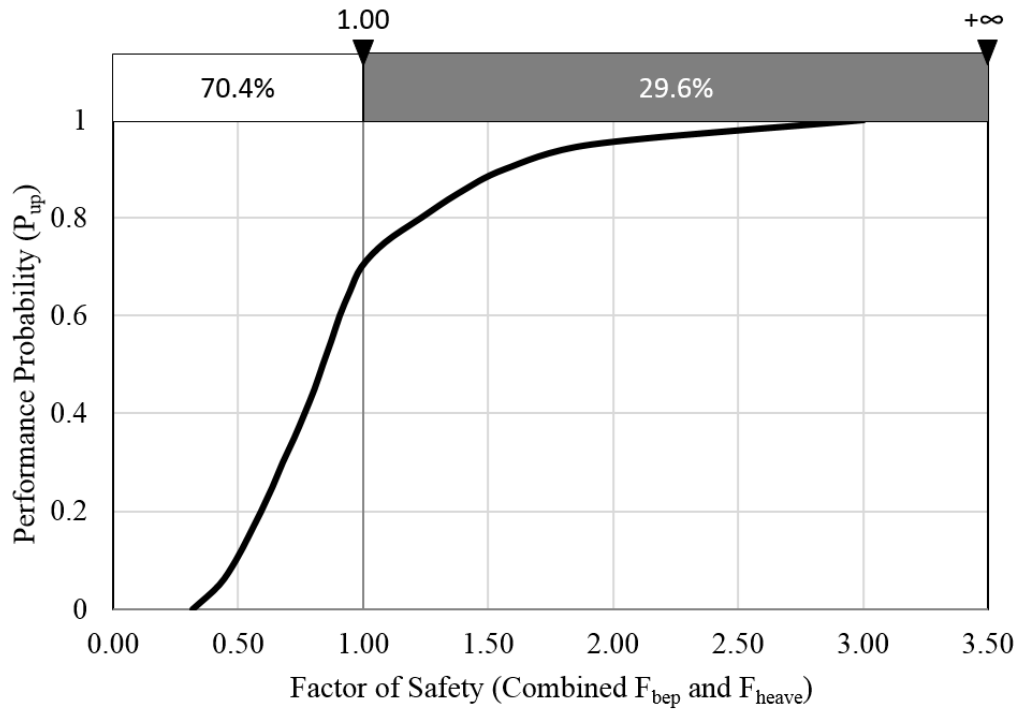


Figure 2.7. Cumulative ascending distribution function for Example 2.1.

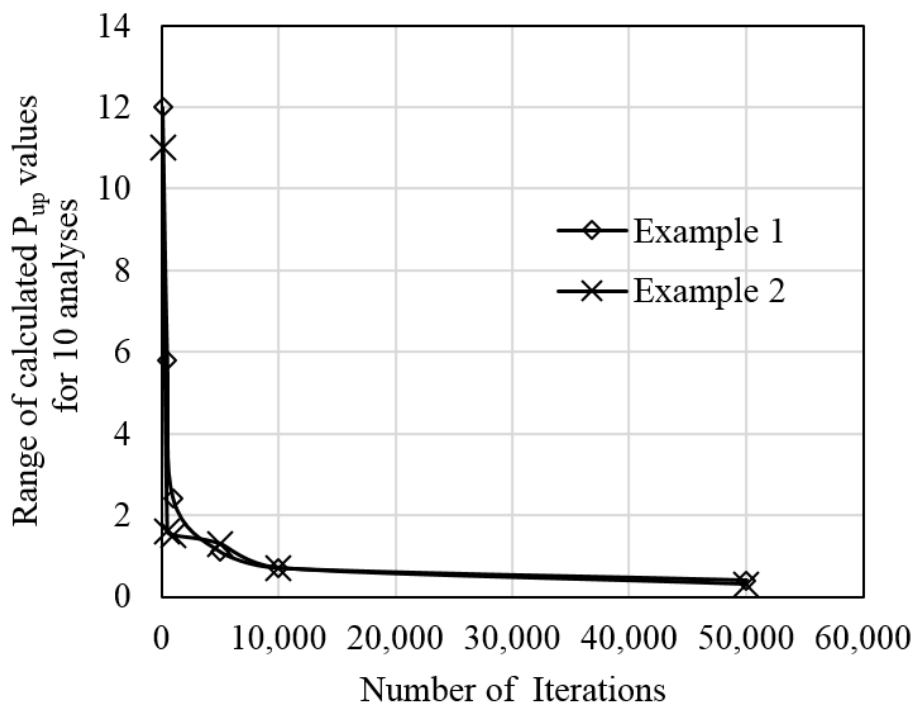


Figure 2.8. Calculation convergence for  $FS$  for Examples 2.1 and 2.2.

#### 2.4.4. Comments and Discussion of Results

The calculated conditional probability of unsatisfactory performance discussed previously represents the conditional probability of initiating a piping or heave failure, given the water level rises to the 100-year flood level, against the levee. Three points should be noted with regard to this result. First, the conditional probability represents the initiation of the erosion process and not failure of the levee. The potential for continuation and progression of the erosion process needs to be assessed, either numerically or by judgment, and the probabilities of these events considered in a risk assessment. Such assessment should consider factors that are not included in the above analyses such as erodibility of the eroding soil and the ability of the erosion pipe to remain open without collapse. Second, the calculated probability is conditional on the 100-year river level being reached. To calculate the annual probability of failure, additional analyses need to be performed at different river levels and a “fragility curve” of probability versus flood level developed. The fragility curve can then be compared with the exceedance probability of the river levels to assess the annual probability of unsatisfactory performance.

Table 2.2. Conditional Probability of unsatisfactory performance vs. PDF shape for Geometric Variable *A*

<b>PDF shapes for geometric variable <i>A</i></b>	<b><math>P_{up}, FS \leq 1.0</math></b>
Trapezoidal	70.40%
Uniform	54.90%
Normal	98.20%
Triangular	66.60%



Third, the analysis assumes a two-dimensional model representing a finite length of levee in a levee system and thus does not take into account the effects of levee length or necessary changes to the model to account for the known variation of the levee profile within the system. For instance, the longer a levee reach is, the higher the probability of failure will be, even if the same two-dimensional model is applicable to the full length. Therefore, to assess the reliability of the levee system, the system needs to be divided into reaches having lengths such that the two-dimensional models adequately model the probability of unsatisfactory performance for each reach (even if this means modeling several adjacent reaches with the same two-dimensional model). The probability of unsatisfactory performance of the system is then calculated by considering combined probabilities for all of the reaches in the system.

The calculated conditional probability of unsatisfactory performance for this levee profile is quite high (70.4%). This probability may seem unreasonable until one considers two points: (1) this reach is selected as one having a low deterministic *FS* and thus would be expected to have a high probability of unsatisfactory performance, and (2) the probability of unsatisfactory performance is only the first step toward levee failure (initiation of erosion). To assess the probability of levee failure, the probabilities of other factors related to the continuation and propagation of the failure mechanisms need to be assessed.

It is not possible to assess the profile from this example using the FOSM blanket theory method because of the geometric complexity of the profile and, hence, a comparison of the two methods is not possible for this example. Polanco and Rice (2011) performed

such a comparison on a simplified profile that is within the capabilities of the FOSM blanket theory method and obtained similar results. The details of this analysis have been omitted from this paper because of length restrictions.

#### 2.4.5. Example 2.2: Uncertain Location of an Old Channel

This case presents a hypothetical levee profile based loosely on conditions observed within the Natomas Basin. The analysis is designed to model a buried channel or point bar within the blanket. The location of the channel with respect to the levee and the depth of the channel below the ground surface are both considered uncertain. The conditional probability of unsatisfactory performance given the river rises to the 100-year flood level is analyzed using the proposed RSMC method. The finite-element model used in this analysis is shown in Figure 2.9. The model consists of a silt/clay blanket layer overlying sand in the levee foundation and consists of 2,230 six-noded triangular elements. The downstream and upstream ends are modeled with constant head boundary conditions equal to downstream ground elevation or the river water level elevation, respectively. The downstream ground surface is modeled with an exit face boundary condition. Similar to Example 2.1, by subdividing the potential channel region into rectangles (see the highlighted region of Figure 2.9), the location and depth of the channel can be changed by reassigning the material type to the small rectangular regions without changing the finite-element grid.

Two geometric variables are used to define the geometric variation of the profile: (1) the thickness of the silty soil cover above the channel,  $h$ , and (2) the distance of the channel,  $d_c$ , taken from the landside of the channel to a fixed point beneath the levee (from

left to right) as shown in Figure 2.9. The PDFs for these variables are assumed uniform, indicating equal potential for all depths and locations of the channel within the range of possible values. The soil variables are the hydraulic conductivity ratio,  $K_{sb}$ , and the total unit weight of the blanket,  $\gamma_{blkt}$ . The PDFs for the soil variables are the same as used in the analysis of Example 2.1. Details of the variable PDFs are presented in Table 2.3. The failure mechanism considered is uplift of the blanket layer using the total stress method.

Analyses are performed in a fashion similar to that presented in the first example. The conditional probability of unsatisfactory performance (that the  $FS$  is less than 1.0) is calculated to be 56.7% (see cumulative ascending distribution in Figure 2.10). A proof of the convergence similar to that performed for Example 2.1 is shown in Figure 2.8. This example demonstrates the flexibility of the proposed RSMC method in modeling a variety of complex geometries. The RSMC method is flexible enough to allow more than one geometric variable to be modeled. This analysis can represent uncertainty in the height of the channel or where it might be situated with respect to the levee toe.

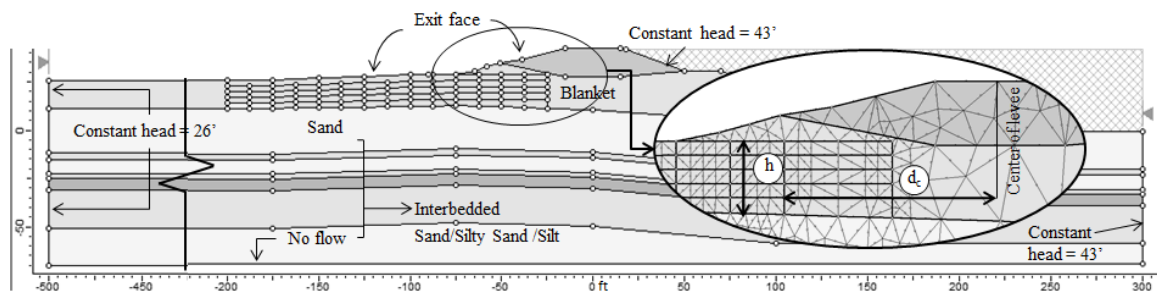


Figure 2.9. Finite-element levee profile used in Example 2.2 showing geometric variables  $h$  and  $d_c$ .

Table 2.3. Probability distribution variables for Uncertain Location of an Old Channel input variables

Variable	MLV	$\sigma$	MIN	MAX	Type of distribution
$\log(K_b)$	-6.00	0.67	-7.00	-5.10	Normal
$\log(K_s)$	-3.00	0.67	-3.80	-2.00	Normal
$\gamma_{blkt}$	120	4.800	110	130	Normal
$d_c$	-	-	25	175	Uniform
$h$	-	-	0	12	Uniform

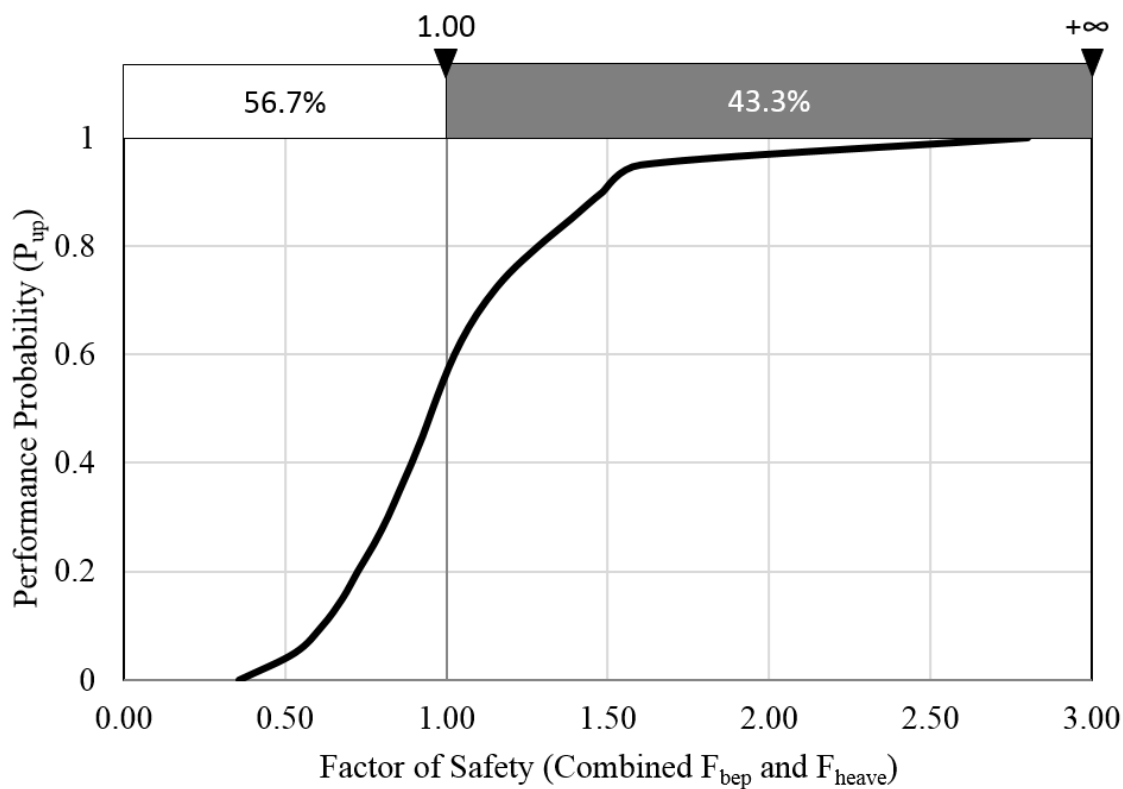


Figure 2.10. Cumulative ascending distribution for Example 2.2.

## 2.5. Analysis of Variables

To illustrate the importance of including the geometric variables in the reliability analyses, analyses of variables (ANOVA) are performed for both examples presented above to assess the relative effects that the significant variables have on the variation of the performance of the levee (i.e.,  $FS$ ). This process has two parts: (1) develop a functional form equation, and (2) use multiple regression analyses to calculate the coefficients giving the best-fit for the functional form equation to the data from the Monte Carlo analyses. Assessing the resulting coefficients for the variables gives an indication of the effect variation of the variable has on the  $FS$ . Again, the  $FS$  represents the combined effects of both the  $F_{bep}$  and  $F_{heave}$ . The functional form equation for Example 2.1 is as follows:

$$FS = \beta_0 + \beta_1 * A^2 + \beta_2 * K_b + \beta_3 * K_s + \beta_4 * K_{hv} + \beta_5 * \gamma_{blkt} + \beta_6 * \gamma + \varepsilon_i \quad (4)$$

where  $\beta_0$  = the F intercept value in the equation;  $\beta_1$  through  $\beta_6$  = coefficients that describe the magnitude effects of the variables  $A^2$ ,  $K_b$ ,  $K_s$ ,  $K_{hv}$ ,  $\gamma_{blkt}$ , and  $\gamma_{sand}$  have on the  $FS$ ; and  $\varepsilon_i$  is the error term called the regression residual. It should be noted that the geometric variable  $A$  is squared in Eq. (4) because the plot of  $A$  values versus  $FS$  is more closely approximated with a parabola than a straight line like the other variables. The values of the coefficients indicate how much the  $FS$  is expected to either increase or decrease when the respective variables increase or decrease by a value of one while holding the other variables constant.

Similar multiple regression analyses are performed for Example 2.2 using the following functional form equation:

$$FS = \beta_0 + \beta_1 * d_c + \beta_2 * h + \beta_3 * \gamma_{blkt} + \beta_4 * K_b + \beta_5 * K_s + \varepsilon_i \quad (5)$$

Summary outputs for both analyses are presented as Table 2.4. A relative indicator of the importance of a variable's variation is the “*t* Stat,” the ratio between the coefficient and its standard error. Because the standard error is a measure of the variation of the coefficient that results from variation of the variable, it can be considered analogous to the standard deviation of a variable. Thus, the “*t* Stat” values calculated in Excel are a good relative indicator of how much effect the potential variation of a variable has on the variation of the *FS*.

The “*t* Stat” values for the geometric variables (*A* for Example 2.1, *d* and *h* for Example 2.2) are in bold type for emphasis. Based on the “*t* Stat” values, the results of the regression analyses suggest that the geometric variables (*A*, *d<sub>c</sub>*, and *h*) have a greater effect in the variation of the *FS* for the two examples. The “*t* Stat” values for the geometric variables (*A*, *d<sub>c</sub>*, and *h*) are greater than the values for other variables, therefore indicating that the geometric variables have the largest effect on the *FS* and thus the conditional probability of underseepage related failure.

## 2.6. Summary and Conclusions

This study proposes an application of the RSMC simulation method for assessing the potential for unsatisfactory performance of a levee because of underseepage erosion that addresses some of the limitations of simplified analyses such as FOSM Taylor series based methods.

Table 2.4. Summary of regression analyses (*t* Stat values for geometric variables in bold type)

Analysis 1				Analysis 2			
Variable	Coefficients	Standard Error	<i>t</i> Stat	Variable	Coefficients	Standard Error	<i>t</i> Stat
Intercept	-1.009	0.173	-5.846	Intercept	0.627	0.083	7.514
$A^2$	2.38E-04	4.07E-06	<b>58.483</b>	$d_c$	-0.005	7.63E-05	<b>-59.555</b>
$K_b$	9198.69	2800.02	3.290	$h$	-0.043	0.001	<b>-44.739</b>
$K_s$	-10.627	2.337	-4.547	$\gamma_{blkt}$	0.009	0.001	12.830
$K_{hv}$	0.895	0.055	16.202	$K_b$	6.86E+04	1922.701	35.655
$\gamma_{blkt}$	0.002	0.001	1.905	$K_s$	-37.852	1.605	-23.585
$\gamma_{sand}$	0.008	0.001	8.147	-	-	-	-

The application combines the results of multiple finite-element analyses to develop a response surface that is then coded into an excel spreadsheet. The spreadsheet is then linked to the computer program @Risk to perform a Monte-Carlo simulation and calculate the probability of unsatisfactory performance.

The RSMC method has several advantages over the FOSM blanket theory that is commonly used to assess levee reliability with respect to underseepage. First, the RSMC method allows flexibility in the erosion failure mechanism that is modeled as well as considering multiple failure mechanisms in a single analysis.

The RSMC method also allows the incorporation of complex variation of subsurface geometry, a feature that is significantly limited in the FOSM blanket theory method. Finally, the RSMC method allows for flexibility in defining the PDFs for the variables (soil variables and geometric variation).

This study presents two examples where the condition for unsatisfactory performance is defined as a  $FS$  of less than 1.0 against either the initiation of piping or heave. First, a levee profile is modeled where there is uncertainty as to where a low-hydraulic conductivity landside blanket ends. This example considers two different failure mechanisms that can occur and are controlled by the geometric variation of the profile. The second example considers the uncertainty in the location of a buried channel or point bar in the subsurface soils and incorporated two geometric variables to define the location and depth of the buried feature.

Multiple regression analyses performed to assess the relative effects that changes in the input variables have on the  $FS$  for the two analyses indicate that the geometric variables ( $A$ ,  $d_c$ , and  $h$ ) have the greatest effect on the variation of the  $FS$  and thus, on the probability of unsatisfactory performance.

## 2.7. Notation

The following symbols are used in this paper:

$A$  = geometric variable representing the location where the blanket layer pinches out;

$d_c$  = geometric variable representing distance from the channel to a fixed point beneath the levee;

$FS$  = factor of safety;

$F_{bep}$  = factor of safety against backward erosion piping;

$F_{heave}$  = factor of safety against heave;

$h$  = geometric variable representing thickness of the soil cover above a channel;



$i_c$  = critical gradient of the eroding soil;

$i_e$  = hydraulic exit gradient;

$K_b$  = hydraulic conductivity of the blanket;

$K_h$  = horizontal hydraulic conductivity in sand;

$K_s$  = hydraulic conductivity of the sand;

$K_v$  = vertical hydraulic conductivity in sand;

$K_{hv}$  = anisotropy ratio ( $K_h/K_v$ );

$K_{sb}$  = hydraulic conductivity ratio ( $K_s/K_b$ );

$P_{up}$  = conditional probability of unsatisfactory performance;

$\beta_0$  = factor of safety intercept value;

$\beta_x$  = coefficients that describe the magnitude effects of the variables  $A^2$ ,  $K_b$ ,  $K_s$ ,  $K_{hv}$ ,  $\gamma_{blkt}$ ,

$\gamma_{sand}$ ,  $h$ , and  $d_c$  have on the  $FS$ ;

$\varepsilon_i$  = error term (regression residual);

$\gamma_{buoy}$  = buoyant unit weight of the soil;

$\gamma_{sand}$  = total unit weight of sand;

$\gamma_w$  = unit weight of water;

$\gamma_{blkt}$  = saturated unit weight of overlying blanket; and

$u_{bl}$  = uplift pressure at the base of the blanket.

## References

Baecher, G. B., and Christian, J. T. (2003). *Reliability and statistics in geotechnical engineering*, Wiley, Chichester, England.

- Bligh, W. G. (1910). "Dams, barrages, and weirs on porous foundations." *Eng. News-Rec.*, 64(26), 708–710.
- Bligh, W. G. (1913). "Lessons from the failure of a weir and sluices on porous foundations." *Eng. News-Rec.*, 69(6), 266–270.
- Calle, E. O. F., Best, H., Sellmeijer, J. B., and Weijers, J. (1989). "Probabilistic analysis of piping underneath water retaining structures." *Proc., 12th Int. Conf. Soil Mech. Foundation Eng.*, Rio de Janeiro, Brazil, Vol. 2, 819–822.
- Crum, D. A. (1996). "Reliability applied to levee seepage analysis." *Probabilistic Mechanics and Structural Reliability: ASCE Proc. 7th Specialty Conf.*, Worcester, MA, 1, 946–949.
- Duncan, M. J. (2000). "Factors of safety and reliability in geotechnical engineering." *J. Geotech. Geoenviron. Eng.*, 126(4), 307–316.
- Fell, R., Wan, C., and Foster, M. (2004). "Methods for estimating the probability of failure of embankment dams by internal erosion and piping through the embankment." *Rep. Prepared for University of New South Wales*, Sydney, Australia.
- Gabr, M. A., Taylor, H. M. Jr., Brizendine, A. L., and Wolff, T. F. (1995). "LEVEEMSU: Analysis software for levee underseepage and rehabilitation." *Technical Rep. GL-95-9*, U.S. Army Engineer Waterways Experiment Station, Vicksburg, MS.
- Harr, M. E. (1987). *Reliability-based design in civil engineering*, McGraw-Hill, New York.
- Hasofer, A. M., and Lind, N. C. (1974). "An exact and invariant first-order reliability format." *J. Eng. Mech. Div.*, 100(1), 111–121.
- Knowles, V. R. (1992). "Applications of the finite element seepage analysis Corps program CSEEP (X8202)." *Technical Rep. ITL-92-6*, U.S. Army Engineer Waterways Experiment Station, Vicksburg, MS.
- Lane, E. W. (1934). "Security from under-seepage: Masonry dams on earth foundation." *Proceedings, ASCE*, 60, 1235–1272.
- Polanco, L., and Rice, J. (2011). "Reliability based underseepage analysis in levees using Monte Carlo simulation." *2011 GeoFrontiers Proc.*, Paper #2978.
- @Risk 5.5. [Computer software] Palisade Corporation, Ithaca, NY.
- Sleep, M., and Duncan, M. J. (2008). "Manual for geotechnical engineering reliability." *Rep. by Virginia Tech Center for Geotechnical Practice and Research*, Blacksburg, VA.

- Tracy, F. T. (1994). "Seepage Package." *CSEEP Micro Version*, X8202, U.S. Army Engineer Waterways Experiment Station, Vicksburg, MS.
- USACE. (1956). "Investigation of underseepage and its control." *Technical Memorandum No. 3-424*, U.S. Army Engineer Waterways Experiment Station, Vicksburg, MS.
- USACE. (1999). "Evaluating the reliability of existing levees." *ETL 1110-2-556*, App. B, U.S. Army Core of Engineers, Washington, DC.
- USACE. (2000). "Design and construction of levees." *Engineering Manual EM 1110-2-1913*, U.S. Army Core of Engineers, Washington, DC.
- USACE. (2004). "Geotechnical reliability of dam and levee embankments." *ERDC/GSL CR-04-1*, Geotechnical and Structural Laboratory, U.S. Army Core of Engineers, Washington, DC.
- USACE. (2005). "Engineering and design: Design guidance for levee underseepage." *ETL 1110-2-569*, U.S. Army Core of Engineers, Washington, DC.
- Wolff, D. (2008). "Reliability of levee systems." Chapter 12, *Reliability based design in geotechnical engineering*, Taylor & Francis, New York, 448–496.
- Wolff, T. F. (1989). "LEVEEMSU: A software package designed for levee underseepage analysis." *Technical Report GL-89-13*, U.S. Army Engineer Waterways Experiment Station, Vicksburg, MS.
- Wolff, T. F. (1994). "Evaluating the reliability of existing levees." *Research Rep. Prepared for U.S. Army Engineer Waterways Experiment Station*, Michigan State University, East Lansing MI.
- Wolff, T. F., Demsky, E. C., Schauer, J., and Perry, E. (1996). "Reliability assessment of dike and levee embankments." *ASCE Geotechnical Special Publication*, 1, 636–650.

## CHAPTER 3

A RELIABILITY-BASED EVALUATION OF THE EFFECTS OF GEOMETRY ON  
LEVEE UNDERSEEPAGE POTENTIAL**Abstract**

Levee foundations along meandering rivers are often modeled in seepage analyses with simplified models consisting of two layers having uniform thickness and soil properties. While this may simplify the analysis and allow for use of simplified reliability methods, it is important to realize the limitations of these simplifying assumptions. Due to the complex geomorphic regime that is often encountered in the fluvial environment, levee foundation geometry can range from simple to very complex. Variations in layer thickness and continuity affect the pore pressure and seepage regime and, consequently, affect the potential for internal erosion of the foundation soils. A study has been performed to assess the effects of complex subsurface geometry on the susceptibility of levees to underseepage related internal erosion. Reliability-based internal erosion analyses have been performed on eight hypothetical levee profiles using two analytical methods. The first-order second-moment-blanket theory (FOSM-BT) method applies a simplified reliability assessment technique to the US Army Corps of Engineers “Blanket Theory” equations. This method requires that the analysis profile be simplified to meet the requirements of the equations and places limitations on how the uncertainty of the various input parameters is modeled. The more complex response surface-Monte Carlo simulation method is capable of modeling more complex geometries and multiple failure modes and is flexible in how

uncertainty of the various input parameters are modeled. The results of the two methods are compared to evaluate the effectiveness of the FOSM-BT in evaluating internal erosion potential in increasingly complex levee foundation conditions.

### **3.1. Introduction**

Underseepage is the flow of water through a levee's foundation soils due to a differential head across the levee. Internal erosion is the general term to describe the erosion of soil due to subsurface water flow (ICOLD 2012). Specific mechanisms of internal erosion include: piping, concentrated leak erosion, heave, contact erosion, and suffusion (ICOLD 2012). In this paper we will be assessing the potential for initiation of two of these mechanisms: (1) heave—where a low permeability layer is uplifted due to pressure buildup in an underlying permeable layer, and (2) piping—where individual particles of soil are dislodged by forces from water seeping through the soil structure.

To make underseepage modeling more manageable, the geomorphology along a meandering river is often simplified into two layers: a deeper layer consisting of predominantly granular soils deposited in the main river channel, and a surficial layer of finer overbank deposits that were deposited during flood events as sediment laden water overtops the river banks and predominantly silty and clay soils settle out as the water loses energy (USACE 1956, 2000, 2003, 2005). A simple levee foundation in this environment is often modeled having these two layers. The top layer is generally characterized by fine grained materials and is commonly referred to as the “blanket layer” and the bottom layer, commonly referred to as the “foundation layer” tends to be granular (Walling et al. 1997,

2004; USACE 2000, 2003, 2005; Filgueira-Rivera et al. 2007; Smith and Pérez-Arlucea 2008; Ritter et al. 2011). Due to the low permeability of the blanket layer there is potential for buildup of large pore water pressures beneath the blanket. These excess pressures can lead to heave and cracking of the blanket followed by piping of the foundation sands through the defect.

However, the geology along a meandering river is often more complex than the two-layer system described above, including features such as point bars, abandoned cross channels from tributaries, and other erosional and depositional features (Saucier 1994; William Lettis & Associates 2008). In these cases, the levee foundation may be much more complex, characterized by thinning or discontinuity of the basic layers. Such complexity often results in seepage blockages or open seepage exits that considerably alter the pore pressure and seepage regimes that result from underseepage (Bridge 2003; Brierley and Fryirs 2005; Fryirs and Brierley 2013; Glynn and Kuszmaul 2010). In such cases, the foundation configuration beneath a levee has a significant effect on the underseepage behavior and potential for internal erosion; resulting in a significantly higher potential for high hydraulic gradients and pressures leading to the initiation of internal erosion (Glynn and Kuszmaul 2010).

## **3.2. Analysis of internal erosion**

### **3.2.1. Deterministic Analysis**

The analysis of internal erosion due to underseepage in dams and levees has focused on comparing the imposed forces due to seepage to the soils ability to resist erosion. Bligh

(1910, 1913, 1915) performed some of the earliest work with respect to underseepage analysis presenting an empirical relationship between piping potential and the shortest flow path length beneath a water-retaining structure. Lane (1935) modified Bligh's work to develop the weighted creep ratio method, which recognized a distinction between flow along the base of the structure, vertical flow along vertical barriers, and flow through a granular media. Sellmeijer (1988) carried out physical model tests and proposed an analytical equation that simulates the progression of a pipe based on groundwater flow, flow of the eroded soils and soil equilibrium. Sellmeijer's model is based on simple levee geometry (Weijers and Sellmeijer 1993). These methods are typically used in the Netherlands with the latter used the most (Steenbergen et al. 2004; Vrouwenvelder 2006; Möllmann and Vermeer 2007; Lopez de la Cruz et al. 2011; Vrouwenvelder et al. 2010; Kanning 2012; Van Beek et al. 2012).

Common deterministic methods to analyze the potential of internal erosion due to underseepage in levees generally consist of calculating factors of safety based for either the piping mechanism or the heave mechanism. The factor of safety against the backward erosion piping mechanism,  $F_{bep}$ , is often calculated as the ratio of critical hydraulic gradient,  $i_c$ , of the soils to the exit gradient,  $i_e$ . In early work on this problem, Terzaghi derived an evaluation procedure for assessing the potential for soil to heave due to seepage forces from vertical seepage flow (Terzaghi 1922; Terzaghi and Ralph 1948). Terzaghi's work compared the exit hydraulic gradient to the critical gradient,  $i_c$ , needed to initiate piping in the affected soil. In this case the critical gradient is a function of soil buoyant unit weight,  $\gamma_{buoy}$ , through the following equation,

$$i_c = \frac{\gamma_{buoy}}{\gamma_w} \quad (1)$$

where  $\gamma_w$  is the unit weight of water. The factor of safety against the heave mechanism,  $F_{heave}$ , is often calculated as the ratio of hydraulic pressures to the weight of the overlying soil layer, or,

$$F_{heave} = \frac{H\gamma}{u} \quad (2)$$

where  $H$  = thickness of overlying soil (often the thickness of the blanket,  $Z_{bl}$ ),  $\gamma$  = saturated unit weight of overlying soil (often related to the blanket layer,  $\gamma_{blkt}$ ),  $u$  = water pressure at the base of the soil (often related to the blanket layer,  $u_{bl}$ ).

At a factor of safety ( $FS$ ) of 1.0, the equations discussed above represent the theoretical condition at which internal erosion will initiate. Several points need to be clarified regarding what this represents. First, the initiation of erosion does not represent failure of the levee. The erosion that initiates may progress to failure or it may cease due to human intervention or natural causes such as recession of the flood waters or clogging of the piping channel. For this reason we will refer to the initiation of erosion as “unsatisfactory performance”. Secondly, empirical data from case studies [for example the Mississippi River Study (USACE 1956, 2003)] often indicates that piping may initiate at  $FS < 1.0$ . Thus, because the reliability analyses described below will use the factors of safety as performance functions, judgment may be warranted in selecting the appropriate factor of safety for the conditions analyzed. For the purposes of this paper a  $FS = 1.0$  is assumed to represent “unsatisfactory performance”. The analyses could also be performed



assuming different criteria such as higher factors of safety, a limit-state critical gradient, or limit state uplift pressure.

### 3.2.2. Reliability Analyses

The deterministic analyses described above require the assumption of values for parameters describing the subsurface conditions; either material properties or the geometric configuration of the subsurface. Often in levee underseepage analyses there is much uncertainty in the values of the material and geometric parameters making it difficult to ascertain the level of reliability that a certain value of factor of safety represents. In order to incorporate this uncertainty into the analyses, reliability analyses which take into account the uncertainty of these parameters are used. The two reliability methods used in this study are described below. For each method a probability of unsatisfactory performance,  $P_{up}$ , will be calculated based on the probability of the factor of safety ( $F_{bep}$  or  $F_{heave}$ ) being  $<1.0$ .

### 3.3. FOSM-BT Method

A common approach for reliability assessments of underseepage related internal erosion in levee foundations is using the U.S. Army Corps of Engineers (USACE) “blanket theory” (BT) equations as the safety design criteria and the first-order second-moment (FOSM) Taylor Series method as the reliability evaluation methodology (USACE 2000). The BT equations are closed-form equations based on design procedures from the Lower Mississippi River levees (USACE 1956, 2000). The equations usually require the assumption of two soil layers in the levee foundation with homogeneous properties, constant thickness, and horizontal boundaries (USACE 2005); thus limiting the complexity

of levee subsurface geometry and failure mechanism that are modeled. The blanket layer is considered either impervious or semi-pervious soil (either silt or clay), and the foundation layer is considered pervious (sand and gravel) (USACE 2005). The levee is assumed to be impervious. Wolff (2008), Brandon et al. (2013) and Meehan and Benjasupattananan (2012) give good explanations of the BT equations along with examples of its use.

The FOSM method is a simplified form of the Taylor's series method that uses only the expected value and standard deviation of the relevant input parameters in the reliability calculation. FOSM works well for parameters modeled with normal or lognormal probability density functions (PDFs) and nearly-linear performance functions (USACE 2004). When using the FOSM method,  $2n + 1$  calculations of the factor of safety are required, where  $n$  is the number of relevant parameters. Since few calculations are required, it provides a quick assessment of probability of unsatisfactory performance based on the uncertainty of the parameters. For details of the FOSM method refer to Harr (1987), Duncan (2000), Baecher and Christian (2003), USACE (2003), Sleep and Duncan (2008) and Wolff (1994, 1997, 2008).

### **3.4. RSMC Method**

A response surface-Monte Carlo (RSMC) simulation method that analyzes underseepage reliability in levees has been developed by Polanco and Rice (2010, 2011) and Rice and Polanco (2012). Finite element underseepage analyses are used to develop a relationship between key input parameters (such as hydraulic conductivity, unit weight,

anisotropy ratio, and parameters describing the geometry of the soil layers) and computed uplift pressures or hydraulic exit gradients. This relationship is known as the “response surface” (Xu and Low 2006; Low 2008) and is represented in the analysis by a series of equations derived from the finite element analysis results. The variability of key parameters is represented by PDFs describing the likelihood of the parameter being equal to a given value within the range of possible values. Using the response surface and PDFs, a Monte Carlo simulation is performed using the program @Risk (Palisade Corporation 2013). The resulting  $P_{up}$  due to underseepage (conditional on the water surface reaching a certain level) can be represented either by a limit state uplift pressure ( $u$ ), a hydraulic exit gradient ( $i_e$ ), or a factor of safety ( $FS$ ). This conditional probability represents the initiation of erosion and not the probability of a levee breach (total probability of failure). In order to assess failure an event tree analysis is needed with similar computations or judgments to assess the probabilities assigned to the remaining event tree nodes. The conditional probability of unsatisfactory performance is one single node of the event tree.

### **3.5. Purpose and Scope**

Based on the above discussion, it is clear that the FOSM-BT method is a much more efficient tool for performing reliability-based underseepage analyses, provided that the subsurface geometry can be adequately described within the limitations of the method. However, in many cases, especially those involving complex subsurface geometry, the simplifying assumptions that are required for the FOSM-BT method may result in results that are not representative of the actual conditions. In such cases, the RSMC method will

likely provide more representative results; but at the expense of considerably more computational time. Therefore, it is important to understand when the limitations of the FOSM significantly affect the outcome of the reliability analysis and when it is necessary to use a more complex analysis approach such as the RSMC method.

The purposes of this paper are to (1) investigate the effects of levee foundation geometry on the probability of developing conditions where internal erosion may initiate due to underseepage and (2) to assess when the FOSM-BT method is capable of accurately analyzing internal erosion potential in increasingly complex foundation conditions and when a more complex analysis method is necessary. Underseepage related internal erosion potential for eight levee cross sections has been analyzed using the FOSM-BT and RSMC methods. The first six cross-sections represent foundation geometries that are generally considered to be within the capabilities of the blanket theory equations. These six cases are analyzed using both methods, the results are compared, and differences in results are resolved. The final two cases represent foundation geometries that are beyond the capabilities of the blanket theory equations due to the complexity of their foundations. In these cases, only the RSMC methodology is applied. For all of the cases, an analysis of the relative importance of the input parameters is performed (multivariate regression with analysis of variance or ANOVA) to assess which parameters (soil parameters or geometric parameters) have the greatest effect on the potential for underseepage-related internal erosion.

### 3.6. General Procedure

The comparisons of the results from the FOSM-BT and RSMC methods for each case study are performed by analyzing models that are as similar as possible considering the differences in the two methods. Each model consists of a generalized profile within which certain parameters describing the subsurface geometry (geometric parameter) can be modified. A general finite-element model of a simple levee cross section is presented in Figure 3.1 showing the boundary conditions used in the RSMC analyses for all of the cases. Alternatively, Figure 3.2 shows the BT model that is used in the FOSM-BT analysis for this profile. It should be mentioned that for Cases 1 and 2 the model in Figure 3.1 extends 3,000 feet landward to better match the BT equations that assume an infinite landside layer. In essence, the difference between the two analyses is that the RSMC models two dimensional flow while the FOSM-BT models one dimensional flow in the foundation (horizontal) and blanket (vertical) layers.

Reliability analyses are performed using both models using the same parameter PDF distributions in both analyses. Because the FOSM-BT method generally assumes normal or lognormal distributions of the PDFs for all uncertain parameters (soil property and geometric parameters), these distributions are also used for both analyses. However, because the RSMC can easily accommodate essentially any PDF distribution, additional RSMC analyses are performed using a variety of PDF distributions for the geometric parameters to compare the effects of these distributions. This comparison may show the effect the PDF shape limitation may have on the accuracy of the FOSM-BT method should distributions other than normal and lognormal be deemed appropriate. The  $P_{up}$  is calculated

using both the FOSM-BT and RSMC methods with  $FS = 1.0$  being the performance criteria. As noted above, the analyses could also be performed using a different value of  $FS$ , such as a  $FS$  based on a limit-state critical gradient ( $i_c$ ) or a limit-state uplift pressure ( $u$ ).

Once the analyses have been performed, analyses are performed to assess which parameters in the analyses have the greatest effect on the probability of unsatisfactory performance. These analyses are described later in this paper.

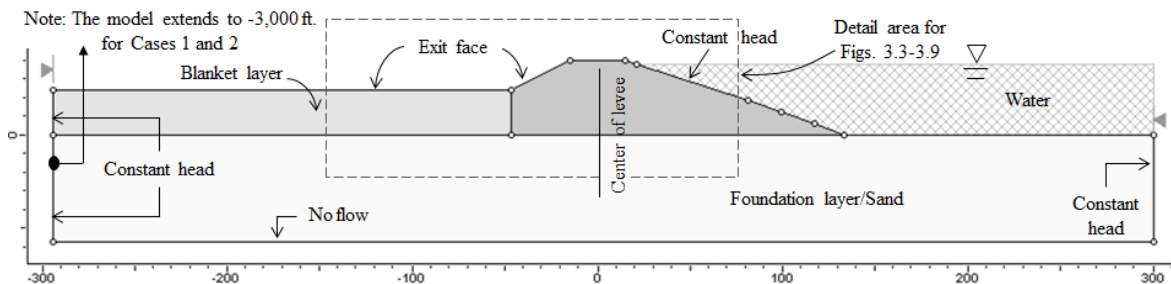


Figure 3.1. General finite-element model showing boundary conditions

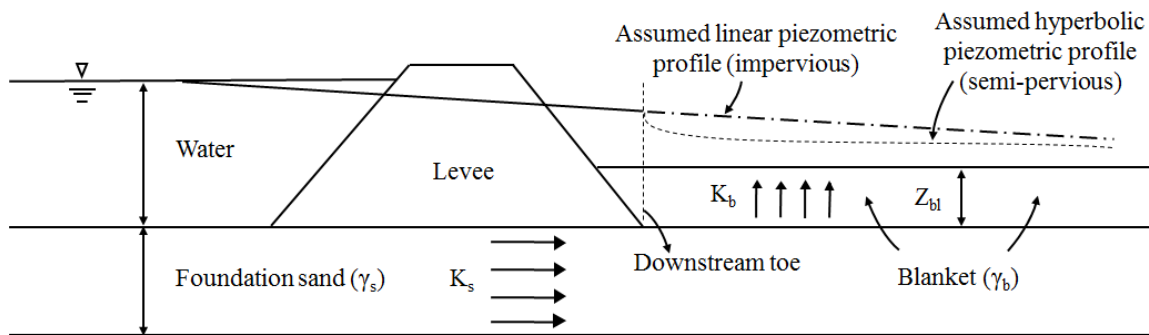


Figure 3.2. General blanket theory model corresponding to the finite-element model in Figure 3.1.

### 3.7. Methodology

A brief explanation of the methodology used for all cases is presented herein. For the six simple cross-section's, the first step is to analyze the profile by means of FOSM-BT method, then by the RSMC method and finally perform the multivariate regression/ANOVA analysis. For the two complex cross-sections, the analysis is only done using the RSMC method followed by the multivariate regression/ANOVA analysis.

#### 3.7.1. Step 1: FOSM-BT

Brief steps to compute the  $P_{up}$  using the FOSM-BT method are as follows:

1. Set up a table including the relevant parameters, i.e. those that are assumed to significantly affect the probability for initiation of erosion (see Table 3.1).
2. Estimate the most likely value (MLV) and standard deviation ( $\sigma$ ) for the normal probability distributions of each parameter.
3. Compute the  $FS$  using the MLVs of all of the relevant parameters,  $F_{MLV}$ , using the BT-equation appropriate for the subsurface conditions.
4. For each parameter, compute the  $FS$  based on the  $MLV \pm \sigma$  while holding the other parameters constant at their MLVs. This is part of the Taylor Series method. Recall that  $2n + 1$  calculations of the  $FS$  are required, where  $n$  is the number of relevant parameters.
5. Using the Taylor Series method (Duncan 2000; Sleep and Duncan 2008; Wolff 1994, 1997, 2008) estimate the standard deviation ( $\sigma_F$ ) and the coefficient of variation (COVF) of the  $FS$  using the formulas  $\sigma_F = \sqrt{\sum_{i=1}^n (\Delta F_n / 2)^2}$  and  $COV_F =$

$\sigma_F/F_{MLV}$ , where  $\Delta F_n = F_n^{MLV+\sigma} - F_n^{MLV-\sigma}$ .  $F_n^{MLV+\sigma}$  is the *FS* computed with the value of one of the parameters increased by one  $\sigma$  from its MLV and  $F_n^{MLV-\sigma}$  is the *FS* computed with the value of the same parameter decreased by one  $\sigma$  from its MLV, and  $n$  is the number of relevant parameters in the analysis.

6. Using the  $F_{MLV}$  and the  $\sigma_F$ , calculate the reliability index ( $\beta$ ) of the *FS* as  $\beta = (F_{MLV} - 1)/\sigma_F$ . This is assuming that the *FS* follows a normal PDF.
7. Finally, using  $\beta$ , calculate the  $P_{up}$  by means of a normal (or lognormal) distribution table as shown in Duncan (2000) or using the *NORMSDIST* function in Excel as  $P_{up} = 1 - \text{NORMSDIST}(\beta)$ .

### 3.7.2. Step 2: RSMC

Brief steps to compute the  $P_{up}$  using the RSMC method are as follows (details of this procedure are presented in Rice and Polanco 2012):

1. Set up the finite-element model in a way that allows changing the geometric parameters without altering the mesh (see Rice and Polanco 2012).
2. While varying soil and geometric parameters, analyze the levee finite-element profile and record the design criteria results (hydraulic exit gradient or uplift pressure) on an Excel table format based on the soil and geometric parameters.
3. Create the response surface by generating a series of plots (containing a series of curves) that represent the relationship between the soil and geometric parameters and the design criteria. Each set of curves (on a plot) represents the relationship



between two parameters and the design criteria at a fixed value of a third parameter represented by that plot.

4. Fit polynomial equations to the series of curves.
5. Create an input spreadsheet and write a macro in Excel setting up interpolation between the curves and the plots so that the design criteria and the resulting  $F$  can be easily calculated for any combination of values for the significant parameters.
6. Link the input spreadsheet with the program @Risk by adding PDFs to the significant parameters. Since PDFs for the hydraulic conductivities were assumed to be represented by lognormal distribution, the macro code is programmed to take the anti-log of the values from the lognormal distributions resulting in normal distributions.
7. Perform a Monte Carlo simulation by starting the simulation in @Risk that will result in a  $P_{up}$ . The design criterion for unsatisfactory performance is defined as a  $FS = 1.0$  provided a 100-year flood level. The RSMC result is based on 5 simulations each of 10,000 runs respectively but setting can be changed. Analyses were performed to assess an appropriate number of iterations needed to produce results with less than one percent variance between multiple runs having identical input parameters. Results for these analyses are presented in Rice and Polanco (2012) showing that 10,000 runs provide an error of less than one percent and increasing the number of iterations beyond 10,000 produces only small decreases in potential error.

### 3.7.3. Step 3: Regression and DF Analyses

Multivariate regression analyses were performed to assess the relative effect that changes in the input parameters have on the *FS* for the various cases. The program @Risk provides the simulation data used to compute the  $P_{up}$  (i.e. one set of parameter values and a calculated *FS* for each of the 10,000 runs of the Monte Carlo simulation) and this data is used to perform the multivariate analysis in an excel spreadsheet. Brief steps to perform the analysis in Excel are as follow:

1. Fit the data into a characteristic curve that will provide the best correlation ( $R^2$ ) (Armitage et al. 2008; Chatterjee and Simonoff 2013).
2. Perform a multiple regression analysis on the data to calculate the respective equation coefficients,  $\beta_n$  (Cameron 2009).
3. From the summary output check which parameters have the highest and second highest *t-stat*.

The statistical significance of the characteristic equation's coefficients is provided by the t-statistic (*t-stat*). The *t-stat* is the ratio between a coefficient,  $\beta_n$ , and its standard error. The coefficient is estimated based on the mean and standard deviation of the respective parameter and the standard error is the standard deviation of the coefficient. Thus, the t-stat values are a good relative indicator of how much effect the potential variation of a parameter has on the variation of the *FS*. The “goodness of fit” of the regression model is provided by the R-Squared ( $R^2$ ). The closer  $R^2$  is to 1.0, the stronger the fit/correlation. A log–log characteristic regression equation (Eq. 3) provided the

strongest  $R^2$  values for Cases 1 through 4 and 6. Case 5 was analyzed based on the two failure mechanisms considered and, a linear equation (Eq. 4) provided the strongest  $R^2$  for the heave mechanism data while a log–log equation (Eq. 3) provided the strongest  $R^2$  for the piping mechanism data. For both equations  $\beta_0$  = the intercept value of the equation,  $\beta_n$  = estimated coefficients that describe the magnitude effects of the parameters, and  $x_n$  = significant geometric and soil parameters within each case as  $Z_{bl}$ ,  $h$ ,  $d$ ,  $A$ ,  $K_b$ ,  $K_s$ ,  $Kh_v$ ,  $\gamma_{blkt}$ , and  $\gamma_{sand}$ .

$$\log(F) = \beta_0 + \sum_{i=1}^n \beta_n \log(x_n) \quad (3)$$

$$F = \beta_0 + \sum_{i=1}^n \beta_n x_n \quad (4)$$

A regression analysis is not performed for the FOSM-BT method; instead the significance of the parameters can be related to the difference of the computed  $\Delta F_n$  (significant difference,  $\Delta F$ ) with respect to the standard deviation ( $\sigma$ ). The  $\Delta F_n$  values are calculated in the FOSM-BT reliability analysis described in Step 1.

### 3.8. Description of Case Studies

The levee cross section shown in Figure 3.1 is the most basic of the cases analyzed and it is used to show the general settings of the finite-element models used in the RSMC analyses. The landside and riverside ends of the profile are modeled with constant head boundary conditions equal to landside ground surface elevation or the river water level elevation, respectively. The landside ground surface is modeled with an exit face boundary condition.

Details of the rectangular area around the levee toe in Figure 3.1 are presented in Figures 3.3, 3.4, 3.5, 3.6, 3.7, 3.8 and 3.9 to show the details of the general subsurface geometry of the eight cases along with the geometric parameters used in the respective reliability analyses. Brief descriptions of each of the levees' cross-sections, assumed failure mechanisms, and relevant parameters are presented below. An extended explanation is provided for Case 1 to serve as the basis for understanding the terminology, parameters, and computations for all cases. Soil and geometric parameters are chosen based on the assumption that they significantly affect the probability for initiation of internal erosion. Table 3.1 presents a summary of the soil and geometric parameters considered in the reliability analyses for each case.

Case 1 is a simple levee profile composed of two homogeneous, constant thickness layers (blanket and foundation) (see Figure 3.3). The blanket is assumed to be impervious, consisting of silty clay, and it is only encountered on the landside of the levee. The foundation layer consists of sand. This case is equivalent to the USACE's "Case 4—Impervious landside top stratum and no riverside top stratum" (USACE 2000). Due to the levee's geometric simplicity, the thickness of the blanket layer ( $Z_{bl}$ ) is the only geometric parameter considered. The thickness of the foundation layer could also be considered as a geometric parameter but experience and preliminary parametric analyses have shown it does not represent a significant effect on the computed  $P_{up}$  unless it is very thin.

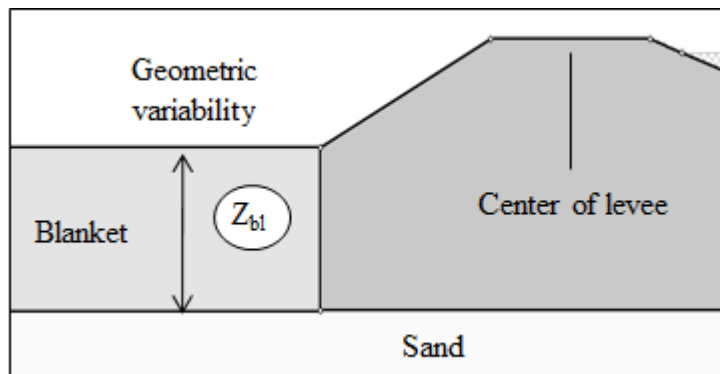


Figure 3.3. Cases 1 and 2 showing geometric parameter  $Z_{bl}$ .

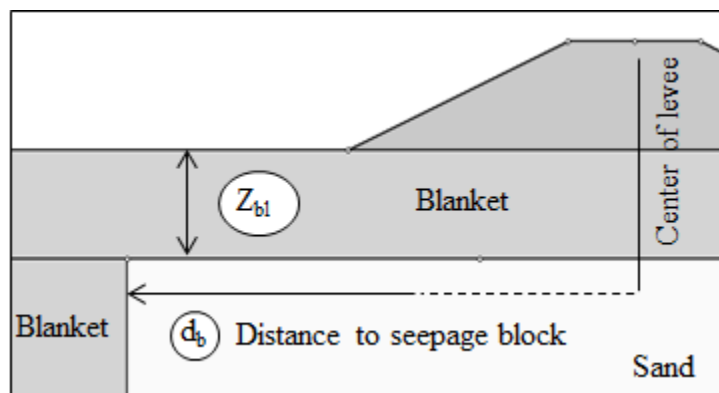


Figure 3.4. Case 3a showing geometric parameter  $Z_{bl}$  and  $d_b$ .

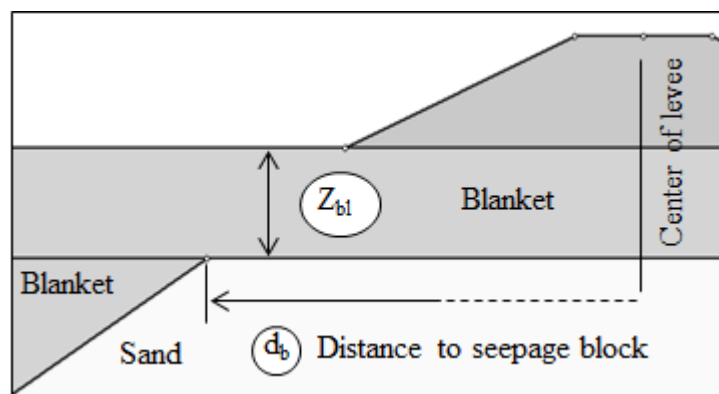


Figure 3.5. Case 3b showing geometric parameter  $Z_{bl}$  and  $d_b$ .

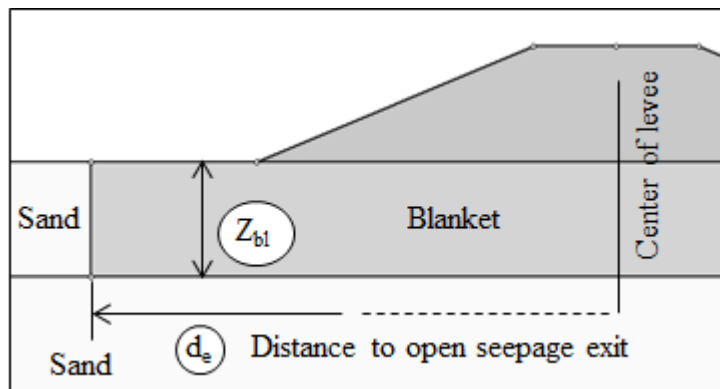


Figure 3.6. Case 4a showing geometric parameter  $Z_{bl}$  and  $d_e$ .

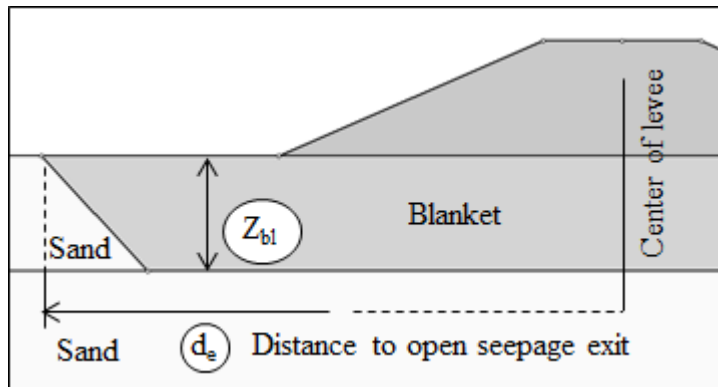


Figure 3.7. Case 4b showing geometric parameter  $Z_{bl}$  and  $d_e$ .

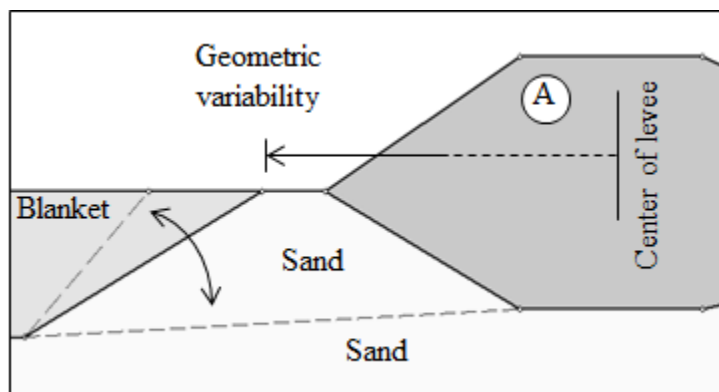


Figure 3.8. Case 5 showing geometric parameter A.

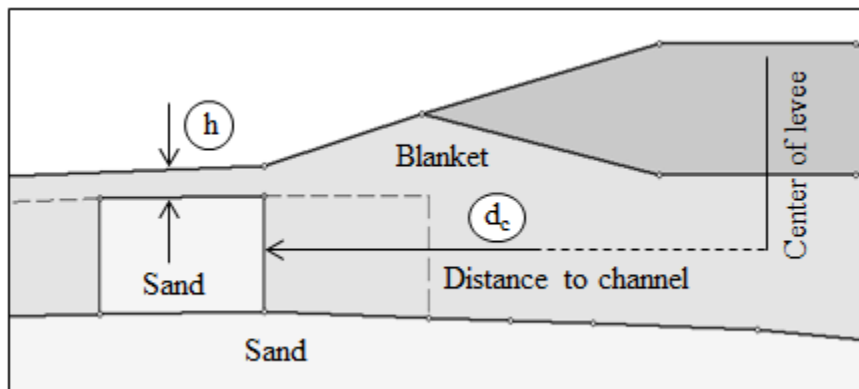


Figure 3.9. Case 6 showing geometric parameter  $h$  and  $d_c$ .

Table 3.1. Input Variables for Proposed Method

Case	Soil parameters considered in reliability analysis	Geometric parameters considered in reliability analysis
1	$\gamma_{blkt}, K_s, K_b$	$Z_{bl}$
2	$\gamma_{blkt}, K_s, K_b$	$Z_{bl}$
3a	$\gamma_{blkt}, K_s, K_b$	$Z_{bl}, d_b$
3b	$\gamma_{blkt}, K_s, K_b$	$Z_{bl}, d_b$
4a	$\gamma_{blkt}, K_s, K_b$	$Z_{bl}, d_e$
4b	$\gamma_{blkt}, K_s, K_b$	$Z_{bl}, d_e$
5	$\gamma_{blkt}, \gamma_{sand}, K_s, K_b, K_{hv}$	$A$
6	$\gamma_{blkt}, K_s, K_b$	$h, d_c$

The unit weight of the blanket ( $\gamma_{blkt}$ ), horizontal hydraulic conductivity of the foundation layer ( $K_s$ ), and vertical hydraulic conductivity of the blanket layer ( $K_b$ ) are the soil parameters considered in the reliability analysis. However, it has been shown by USACE (1956) that the variation in the hydraulic regime (hydraulic uplift pressures and gradients) can be represented as a function of the ratio of the hydraulic conductivities ( $K_s$  and  $K_b$ ) in lieu of their individual values, the hydraulic conductivities are combined into a

single parameter, the hydraulic conductivity ratio,  $K_{sb}$ . The anisotropy ratio of the sand (ratio of the horizontal to vertical hydraulic conductivities,  $K_{hv}$ ) is considered to be 1.0 to allow for a direct comparison between the FOSM-BT and RSMC analysis methods. The failure mechanism is assumed to be heave/piping of the blanket layer. The PDFs of the hydraulic conductivities are assumed to be represented by lognormal distributions and the rest of the parameters are represented by normal distributions.

Case 2 is very similar to Case 1 but differs in that the blanket layer is considered semi-pervious instead of impervious as in Case 1. The USACE refers to this scenario as “Case 6A—Semi-pervious landside top stratum and no riverside top stratum—landside blanket infinite” (USACE 2000). It is also a simple levee section with uncertainty in the thickness of the blanket layer ( $Z_{bl}$ ). The finite-element profile, soil parameters (except the hydraulic conductivity of the blanket layer) and failure mechanism are exactly the same as Case 1 (Figure 3.3).

Two similar levee profiles are presented as Cases 3a and 3b (Figures 3.4 and 3.5). Both profiles represent the abrupt cut-off of the foundation layer by the blanket layer. The difference between them is the angle in which the foundation is blocked by the blanket layer ( $90^\circ$  or perpendicular to the blanket in Case 3a and at  $45^\circ$  counterclockwise from the foundation layer for Case 3b) and the assumed  $K_{hv}$  (1.0 for Case 3a and 0.1 for Case 3b). The USACE refers to this scenario as “Case 7B—Semi-pervious top strata both riverside and landside—landside blanket is finite to a seepage block” (USACE 2000). The blanket layer, together with the seepage block, is composed of silty clay and the foundation layer of sand. The thickness of the blanket and the distance from the levee centerline to the



seepage block are considered as geometric parameters  $Z_{bl}$  and  $d_b$ , respectively. Soil parameters are  $K_s$ ,  $K_b$  and  $\gamma_{blkt}$ . Similar to Case 1, all parameters are assumed to be normal or lognormal PDFs. The failure mechanism considered is heave of the blanket layer at the levee toe.

Cases 4a and 4b represent the abrupt discontinuation of the blanket layer by the foundation layer (Figures 3.6 and 3.7). Once again, the difference between them is the angle in which the blanket/foundation layer opening occurs ( $90^\circ$  or perpendicular to the blanket in Case 4a and at  $45^\circ$  clockwise from the foundation layer for Case 4b) and the assumed  $K_{hv}$  (1.0 for Case 4a and 0.1 for Case 4b). The USACE refers to this scenario as “CASE 7C—Semi-pervious top strata both riverside and landside—landside blanket is finite to an open seepage exit” (USACE 2000). This case is analyzed with no riverside blanket. The geometric parameters are the distance from center of the levee to the end of the blanket,  $d_e$ , and the thickness of the blanket,  $Z_{bl}$ . The soil parameters considered are  $K_s$ ,  $K_b$  and  $\gamma_{blkt}$ . All the parameters are assumed to follow normal and lognormal PDFs as in Case 1. The failure mechanism considered is heave of the blanket layer at the levee toe using the factor of safety against heave.

Case 5 models the discontinuation of the blanket layer near the levee toe (Figure 3.8). This profile is more complex than profiles that can reasonably be analyzed using the FOSM-BT method. The levee section has two layers (blanket and foundation) but there is uncertainty as to where the blanket layer ends in the area of the levee toe as shown in Figure 3.8. This uncertainty is treated as geometric parameter  $A$ , defined as the location where the edge of the blanket intercepts the ground surface or the base of the levee. A trapezoidal

PDF is used to describe the likelihood of the blanket ending at any one location. If the blanket pinches out at the ground surface exposing the underlying sand, it is likely to encounter high exit gradients resulting in the backward erosion piping of the sand mechanism. On the other hand, if the blanket pinches out beneath the levee, high pressures beneath the blanket would result in heave of the blanket and subsequent piping of the underlying sand through a defect in the blanket layer (sand boil formation). Both mechanisms are analyzed with the RSMC method in the same analysis. Soil parameters considered in the analysis are  $K_s$ ,  $K_b$ ,  $K_{hv}$ ,  $\gamma_{blkt}$  and the unit weight of the sand ( $\gamma_{sand}$ ). The hydraulic conductivities and anisotropy ratio are represented by lognormal distributions and the unit weights by normal distributions.

Case 6 analyzes the chance of encountering a buried abandoned channel or point bar near the levee within the blanket layer (Figure 3.9). The location of the channel with respect to the levee and the depth of the channel below the ground surface are both considered uncertain. Two geometric parameters are used to define the geometric variation of the profile: (1) the thickness of the silty soil cover above the channel,  $h$ , and (2) the distance of the channel from the levee,  $d_c$ . The PDFs for these parameters are assumed to be uniform, indicating equal potential for all depths and locations of the channel within the range of possible values. Soil parameters are  $K_s$ ,  $K_b$  and  $\gamma_{blkt}$  and have the same PDFs as Case 1. A constant value of  $K_{hv} = 0.25$  was used for finite-element computations. The failure mechanism considered is heave of the blanket layer in the area where the abandoned channel is encountered.

### 3.9. Results

A summary table presenting the  $P_{ups}$  and most significant parameters based on the RSMC and FOSM-BT methods is presented as Table 3.2. Where applicable the difference between the  $P_{ups}$  is computed showing that in most cases, the difference between methods is minor but generally tends to increase with increasing model complexity.

The RSMC method provides a slightly higher  $P_{up}$  than the FOSM-BT method for Case 1. This could be due to the fact that the FOSM-BT does not consider the hydraulic conductivities in the calculation of the leakage coefficient used to compute the head at the toe of the levee, assuming (since it's impervious) that there is no leakage (seepage through the blanket layer). Nevertheless, results are very close and it can be concluded that methods essentially agree for this scenario.

Results for Case 2 are not as close as Case 1 but they are still very close. The difference is due to computed values of the hydraulic exit gradient with respect to both methods and the assumed  $K_{sb}$  ratio. The BT equation assumes linearity between computed exit gradients whereas the RSMC finite-element computation follows a non-linear relationship. According to regression and DF analyses, the thickness of the blanket layer,  $Z_{bt}$ , provides the greatest effect on the F for Cases 1 and 2.

The difference between the results of the two methods in Case 3 is small and is likely due to the way the BT equation handles the length of the levee landside with respect to the location of the seepage block.

Table 3.2. Summary of  $P_{up}$ s and most significant parameters

Case	Description	$P_{up}$			Significant parameters			
					RSMC regression analysis		FOSM-BT $\Delta F$ analysis	
		FOSM-BT (%)	RSMC (%)	Differ. (%)	Most significant	Second-most significant	Most significant	Second-most significant
1	Impervious blanket layer/ Case 4	24.87	25.70	-0.83	$Z_{bl}$	$K_b$	$Z_{bl}$	$\gamma_{blkt}$
2	Semi-pervious blanket layer/ Case 6a	36.87	33.55	3.32	$Z_{bl}$	$K_b$	$Z_{bl}$	$K_s$
3a	Perp. seepage block, $K_{hv} = 1.0$ / Case 7b	65.80	61.25	4.55	$K_b$	$Z_{bl}$	$\gamma_{blkt}$	$Z_{bl}$
3b	Angled seepage block, $K_{hv} = 0.10$ / Case 7b	65.80	64.05	1.75	$Z_{bl}$	$K_b$	$\gamma_{blkt}$	$Z_{bl}$
4a	Perp. open exit, $K_{hv} = 1.0$ / Case 7c	23.26	17.50	5.76	$Z_{bl}$	$d_e$	$Z_{bl}$	$d_e$
4b	Angled open exit, $K_{hv} = 0.10$ / Case 7c	23.26	13.65	9.61	$Z_{bl}$	$K_b$	$Z_{bl}$	$d_e$
5	Blanket pinching out	N/A	67.55 %	N/A	heave mechanism $A$	$K_b$	N/A	N/A
6	Abandoned channel	N/A	35.60 %	N/A	heave mechanism $A$	$K_{hv}$	N/A	N/A
					pipng mechanism $K_b$	$d_c$		

Since the BT equation considers the landside edge of the model to end at the location of the seepage block, the total heads at the seepage block are considered to be equal to the landside boundary condition, resulting in higher heads below the landside portion of the blanket than the finite-element analyses results. As a consequence, the computed  $FS$ s are lower, thus producing a higher  $P_{up}$ . Notice that the finite-element profile

for the RSMC method (shown in Figures 3.4 and 3.5) continues beyond the seepage block which consequently produces lower total heads, higher  $F_s$  and a lower  $P_{up}$ . The landside effect for both methods is shown on Figure 3.10. The results in Figure 3.10 are based on a  $K_{sb} = 10$  with the location of the seepage block being 75' and 165' from the center of the levee. It can be seen from the figure that as the location of the seepage block gets farther away from the levee, the landside boundary condition effect described above decreases. A secondary effect of the higher heads is more upward seepage through the blanket, an effect that tends to increase the computed  $F_s$ s. Thus, when the seepage block is near the levee, the effect of the increased heads causes the FOSM-BT  $F_s$  values to be lower, but when the seepage block is far away from the levee, the increased leakage effect becomes more significant as shown in Figure 3.10.

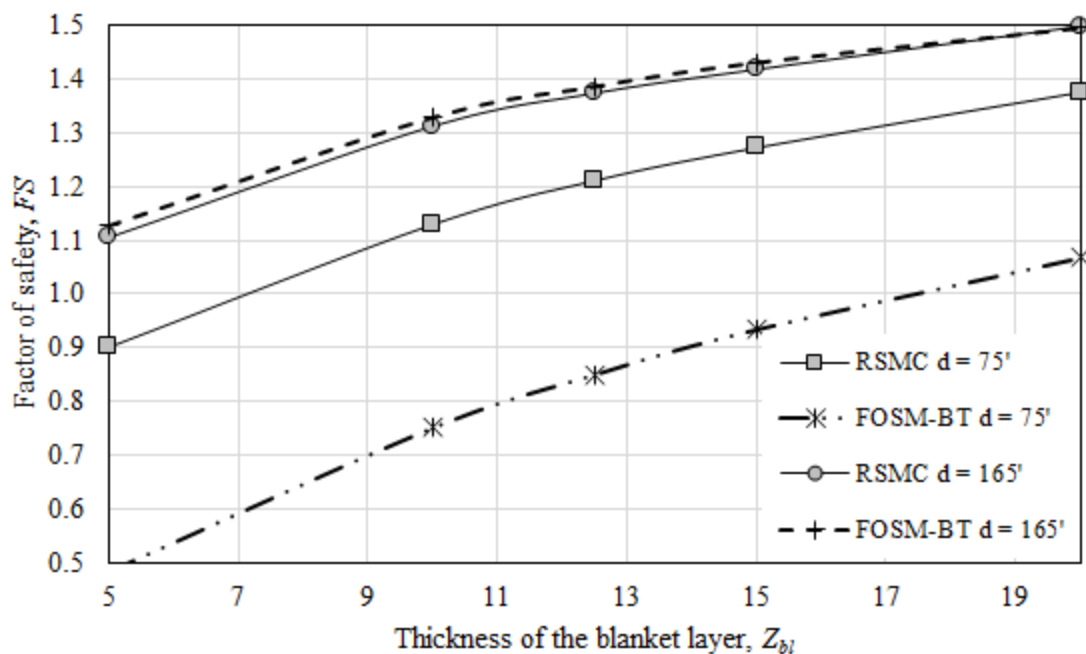


Figure 3.10. Landside effect on the computed  $F_s$  with  $K_{sb} = 10$  for Cases 3a and 3b.

Case 3a has a higher  $P_{up}$  than Case 3b likely due to the perpendicular angle of the block and  $K_{hv} = 1.0$ . The  $P_{up}$  for Case 3b is much closer to the FOSM-BT result. The  $\Delta F$  computations show that the unit weight of the blanket ( $\gamma_{bkt}$ ) is the most significant parameter in the FOSM-BT analysis (for both cases). However, the regression analyses show that for Case 3a the hydraulic conductivity of the blanket ( $K_b$ ) is most significant parameter, followed by the thickness of the blanket ( $Z_{bl}$ ), while for Case 3b the thickness of the blanket ( $Z_{bl}$ ) has the greatest effect on the  $FS$ .

The difference between the results of the two methods for Case 4 is still small but slightly higher than with the other cases. The difference relies on two different effects that depend on the  $K_{sb}$  ratio and the geometric parameter  $d_e$ . In the RSMC finite-element model the landside length continues beyond the seepage opening whereas the BT equations consider the landside to end at the seepage opening exit. When the  $K_{sb}$  ratio is low, higher seepage (leakage) is allowed to flow from the foundation layer to the blanket layer which should result in lower total heads near the levee toe. Under these circumstances the RSMC method, or specifically, the finite-element analysis, computes lower total heads resulting in higher  $FS$ s compared to the BT method. This suggests that the distance from the center of the levee to the seepage opening is negligible and that computations depend on the  $K_{sb}$  ratio when the  $K_{sb}$  ratio is low. Alternatively, when the  $K_{sb}$  ratio is high, not much leakage is allowed and higher pressures develop underneath the blanket. Under these conditions the BT equation provides slightly lower total heads with higher factors of safety compared to the finite-element analysis. Since the difference between methods is so small the effect of the  $K_{sb}$  ratio can be considered negligible while computations depend on the location of the

seepage opening exit. The finite-element analysis can handle the complexity of the flow of the levee profile more accurately providing precise equipotential lines whereas the BT equations only compute the total heads beneath the blanket layer assuming that the equipotential lines are vertical in the sand layer. An example of the combined effects of these phenomena on the computed  $FS$  is presented on Figure 3.11 for given values of  $d_e = 185'$ ,  $K_{sb}$  of 10 and 1,000, and different values of  $Z_{bl}$ .

For this scenario, Case 4b provided a lower  $P_{up}$  than Case 4a. Regression and  $\Delta F$  analyses for Case 4a agree that the geometric parameters ( $Z_{bl}$ ) and  $d_e$  provide the greatest effect on the  $FS$ . The thickness of the blanket layer ( $Z_{bl}$ ) is also the most significant parameter in Case 4b but based on the regression analysis the second most significant is the hydraulic conductivity of the blanket ( $K_b$ ) and based on the  $\Delta F$  analysis is the geometric parameter  $d_e$ .

Since Cases 5 and 6 are complex geometry levee profiles, only the RSMC method was used to analyze underseepage reliability. Both cases show the advantage of the RSMC method over the FOSM-BT method. Case 5 shows the flexibility of handling two failure mechanisms in the same analysis whereas Case 6 shows the flexibility of handling two different geometric parameters. Regression analysis for Case 5 indicates that the geometric parameters have the strongest effect on the  $FS$  regardless of the failure mechanism. Computation of correlation coefficients for Case 6 shows that the hydraulic conductivity of the blanket ( $K_b$ ), followed by the geometric parameter ( $d_c$ ), have the greatest effect on the  $FS$ .

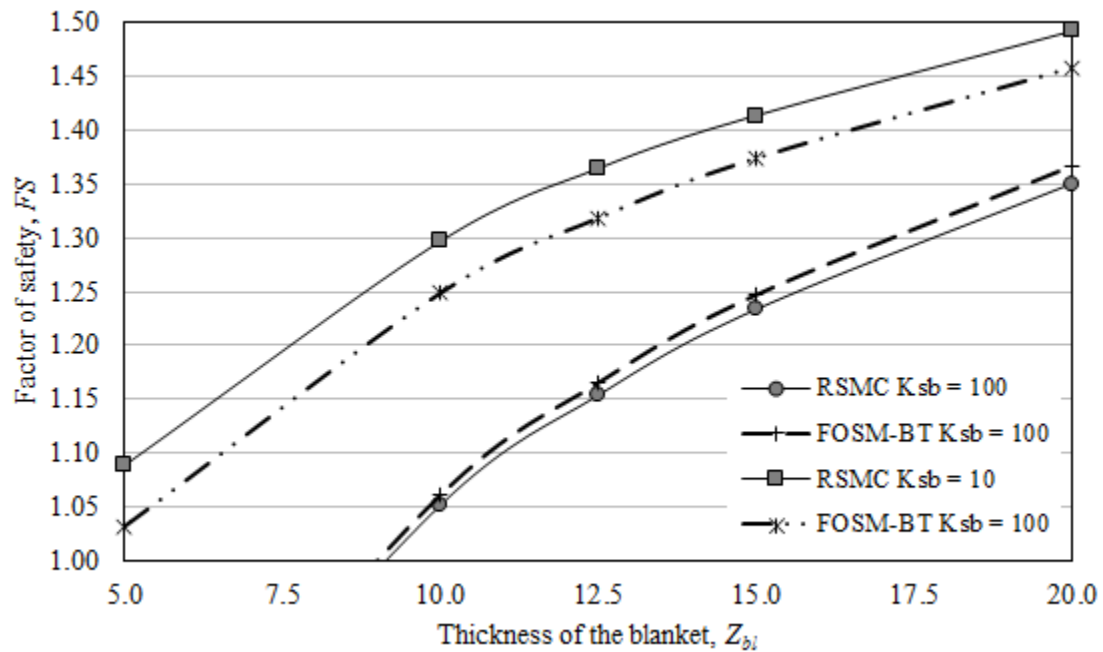


Figure 3.11. Landside effects on the computed  $FS$  for  $d_c = 185'$  based on different  $Z_{bl}$  and  $K_{sb} = 10$  and 1000.

Table 3.3 presents the results of the analyses investigating the sensitivity of the reliability analyses to the shape of the PDF functions for the geometric parameters using the RSMC method. The values in bold type represent the PDF shapes used in the comparative analysis presented in Table 3.2. As can be seen in Table 3.3, variation of the assumed PDF shapes can result variation of the  $P_{up}$  of up to 15.5 %. Thus, because the FOSM-BT method only allows for normal or lognormal PDF distributions, the variations presented in Table 3.3 represent additional error that could occur if a different PDF shape is deemed appropriate.



Table 3.3. Variation of  $P_{up}$  results for different PDF shape assumptions using the RSMC Method

Case	Key geometric parameter	$P_{up}$ for key parameter PDF distributions (%)				Range of Variation (%)
		Normal	Uniform	Trapezoidal	Triangular	
1	$Z_{bl}$	<b>25.7</b>	29.7	25.0	22.2	7.5
2	$Z_{bl}$	<b>33.5</b>	36.6	33.0	30.1	5.1
3a	$Z_{bl}$ and $d_b$	<b>61.2</b>	46.8	59.4	60.4	14.4
3b	$Z_{bl}$ and $d_b$	<b>64.0</b>	51.6	62.3	63.3	12.4
4a	$Z_{bl}$ and $d_e$	<b>17.5</b>	22.7	20.4	18.1	5.2
4b	$Z_{bl}$ and $d_e$	<b>13.6</b>	19.6	13.3	11.1	8.5
5	$A$	67.5	66.7	<b>52.0</b>	63.8	15.5
6	$h$ and $d_c$	35.6	<b>42.3</b>	39.1	40.5	6.7

### 3.10. Conclusions

This paper presents results of eight case studies investigating the effects of levee foundation geometry on the probability of internal erosion due to underseepage. A comparison of the RSMC methodology was performed versus the USACE's FOSM-BT method. Where applicable the difference between the  $P_{ups}$  is computed showing that in most cases, the difference between methods is minor.

Six case studies investigate foundation geometries that are analyzable using both the FOSM-BT and RSMC methods. While there are minor differences between the results of the two analysis methods, it was found that the FOSM-BT method was reasonably accurate for these analyses. The differences can be attributed to more complex pore

pressure and flow regime modeled by the finite element analyses of the RSMC. With the exception of two scenarios for each of the RSMC and FOSM-BT methods, the geometric parameters have the greatest effect on the *FS*. In the cases where the geometric parameters are not the most significant parameters, they are the second most significant parameters.

Two case studies investigated complex foundation geometries by the RSMC method that were beyond the capabilities of the FOSM-BT method. In both these case studies the geometric parameters were found to be the most significant parameters in the analyses, thus illustrating the limitations of FOSM-BT in analyzing complex foundation geometry.

## References

- Armitage P, Berry G, Matthews JNS (2008) Statistical methods in medical research. Wiley, Chichester
- Baecher GB, Christian JT (2003) Reliability and statistics in geotechnical engineering. Wiley, Chichester
- Bligh WG (1910) Dams, barrages, and weirs on porous foundations. Eng News 64(26):708–710
- Bligh WG (1913) Lessons from the failure of a weir and sluices on porous foundations. Eng News 69(6):266–270
- Bligh WG (1915) Submerged weirs founded on sand. In: Bligh WG (ed) Dams and weirs. American Technical Society, Chicago, pp 151–179
- Brandon TL, Batool A, Jimenez M, Vroman ND (2013) Draft: levee seepage analysis using blanket theory and finite element analysis. Report submitted to the US Army Corps of Engineers, Vicksburg District, by the Department of Civil and Environment Engineering Virginia Tech
- Bridge J (2003) Rivers and floodplains: forms, processes, and sedimentary record. lackwell Publishing, Oxford

- Brierley GJ, Fryirs KA (2005) *Geomorphology and river management: applications of the river styles framework*. Blackwell Publishing, Oxford
- Cameron AC (2009) EXCEL 2007: multiple regression, handout. Department of Economics, University of California UCDAVIS. <http://cameron.econ.ucdavis.edu/excel/ex61multipleregression.html>. Accessed 7 Jan 2014
- Chatterjee S, Simonoff JS (2013) *Handbook of regression analysis*. Somerset, Wiley
- Duncan MJ (2000) Factors of safety and reliability in geotechnical engineering. *J Geotech Geoenviron Eng ASCE* 1264:307–316
- Filgueira-Rivera M, Smith ND, Slingerland RL (2007) Controls on natural levee development in the Columbia River. *Sedimentology* 54:905–919
- Fryirs KA, Brierley GJ (2013) *Geomorphic analysis of river systems*. Wiley-Blackwell, Oxford
- Glynn ME, Kuzmaul J (2010) Prediction of piping erosion along middle Mississippi River levees: an empirical model. USACE, Technologies and Operational Innovations for Urban Watershed Networks Research Program, ERDC/GSL TR-04-12. Originally published in 2004 and revised in 2010
- Harr ME (1987) *Reliability-based design in civil engineering*. McGraw-Hill, New York
- ICOLD (2012) Internal erosion of existing dams, levees, and dikes, and their foundations—international glossary. *CIGB-ICOLD Bulletin*, 1
- Kanning W (2012) *The weakest link*. Dissertation, Delft Technical University. <http://repository.tudelft.nl/search/ir/?q=isbn%3A%229789461860880%22> Accessed 7 Jan 2014
- Lane EW (1935) Security from under-seepage: masonry dams on earth foundation. *Trans ASCE* 100(1):1235–1272
- Lopez de la Cruz J, Calle EOF, Schweckendiek T (2011) Calibration of piping assessment models in the Netherlands. Paper presented at the ISGSR 2011: 3rd international symposium on geotechnical safety and risk, Munich, Germany, 2–3 June 2011. ISBN 978-3-939230-01-4
- Low BK (2008) Reliability of levee systems. In: Phoon K-K (ed) *Reliability-based design in geotechnical engineering*. Taylor & Francis Group, New York, pp 134–168
- Meehan CL, Benjasupattananan S (2012) An analytical approach for levee underseepage analysis. *J Hydrol Elsevier* 470–471:201–211. doi:10.1016/j.jhydrol.2012.08.050

- Möllmann AFD, Vermeer PA (2007) Reliability analysis of a dike failure. Paper presented at the 18th European Young Geotechnical Engineers' Conference EYGEC, Ancona, Italy, June 2007
- Palisade Corporation (2013) @Risk 6.1. Integrated Excel program that performs risk analysis using Monte Carlo simulation
- Polanco L, Rice J (2010) Reliability based underseepage analysis in levees using Monte Carlo simulation. Paper presented at the 2010 ASDSO Conference, concurrent session IV: engineering solutions for levees, 19–23 Sept 2010
- Polanco L, Rice J (2011) Reliability based underseepage analysis in levees using Monte Carlo simulation. Paper presented at the 2011 ASCE GeoFrontiers Conference, Paper #2978, 13–16 March 2011
- Rice J, Polanco L (2012) Reliability-based underseepage analysis in levees using a response surface-Monte Carlo simulation method. *J Geotech Geoenviron Eng ASCE* 138(7):821–830
- Ritter DF, Kochel RC, Miller JR (2011) *Process geomorphology*, 5th edn. Waveland Press, Illinois
- Saucier RT (1994) *Geomorphology and quaternary geologic history of the lower Mississippi valley*. U.S. Army Engineer Waterways Experiment Station, Vicksburg, Mississippi, vol 1, p 414
- Sellmeijer JBA (1988) *On the mechanism of piping under impervious structures*. Dissertation, Delft Technical University, Delft, The Netherlands. <http://repository.tudelft.nl/view/ir/uuid%3A7f3c5919-1b37-4de9-a552-1f6e900eeaad/> Accessed 7 Jan 2014
- Sleep M, Duncan MJ (2008) *Manual for geotechnical engineering reliability*. Report by Virginia Tech Center for Geotechnical Practice and Research, Blacksburg
- Smith ND, Pe´rez-Arlucea M (2008) Natural levee deposition during the 2005 flood of the Saskatchewan River. *Geomorphology* 101:583–594
- Steenbergen HMGM, Lassing B, Vrouwenvelder ACWM, Waarts PH (2004) Reliability analysis of flood defence systems. *Heron* 49(1):51–73
- Terzaghi K (1922) *Der Grundbruch an Stauwerken and seine Verhiltung* (Includes English translation: *Piping in Dams and Its Prevention*). *Die Wasserkraft* 1724:445–449
- Terzaghi K, Ralph P (1948) *Soil mechanics in engineering practice*. Wiley, New York

- USACE (1956) Investigation of underseepage and its control. TM No. 3-424, U.S. Army Engineer Waterways Experiment Station, Vicksburg, MS
- USACE (2000) Design and construction of levees. Engineering Manual EM 1110-2-1913, U.S. Army Core of Engineers, Washington, DC
- USACE (2003) Design and construction of levees. Risk-based analysis in geotechnical engineering for support of planning studies. ETL 1110-2-556, Appendix B: evaluating the reliability of existing levees, U.S. Army Core of Engineers, Washington, DC
- USACE (2004) Geotechnical reliability of dam and levee embankments. ERDC/GSL CR-04-1, Geotechnical and Structural Laboratory, U.S. Army Core of Engineers, Washington, DC
- USACE (2005) Engineering and design: design guidance for levee underseepage. ETL 1110-2-569, U.S. Army Corps of Engineers, Washington, DC
- Van Beek V, Yao Q, Van M, Barends F (2012) Validation of Sellmeijer's model for backward piping under dikes on multiple sand layers. Presented at the ICSE6: sixth international conference on Scour and Erosion, Paris, 27–31 August 2012
- Vrouwenvelder T (2006) Spatial effects in reliability analysis of flood protection systems. Presented at the 2nd international forum on engineering decision making, Lake Louise, Canada, 26–29 April 2006
- Vrouwenvelder ACWM, Van Mierlo MCLM, Calle EOF, Markus AA, Schweckendiek T, Courage WMG (2010) Risk analysis for flood protection systems. Deltares, Main Report, The Netherlands
- Walling DE, Owens PN, Leeks GJL (1997) The characteristics of overbank deposits associated with a major flood event in the catchment of the River Ouse, Yorkshire UK. *Catena* 31(2):53–75
- Walling DE, Fang D, Nicholas AP, Sweet RJ (2004) The grain size characteristics of overbank deposits on the floodplains of British lowland rivers. Paper presented at Sediment Transfer through the Fluvial System: Proceedings of the International Symposium, Moscow, 288: 226–234, 2–6 Aug 2004
- Weijers JBA, Sellmeijer JB (1993) A new model to deal with the piping mechanism. In: Brauns J, Heilbaum M, Schuler U (eds) *Filters in geotechnical and hydraulic engineering: proceedings of the first international conference*. Balkema, Rotterdam, pp 349–355

- William Lettis & Associates, Inc. (2008) Surficial geologic map and initial geomorphic assessment, Sacramento River (east side), Sacramento County, California. Unpublished consultant report prepared for URS Corporation
- Wolff TF (1994) Evaluating the reliability of existing levees. Research report prepared for U.S. Army engineer waterways experiment station, Michigan State University, East Lansing MI. This is also appendix B to U.S. Army Corps of Engineers ETL 1110-2-556, Risk-based analysis in geotechnical engineering for support of planning studies, 28 May 1999
- Wolff TF (1997) Geotechnical reliability of levees. Paper presented at the USACE hydrology and hydraulics workshop on risk-based analysis for flood damage reduction studies, SP-28, Paper No. 6, 67–84
- Wolff D (2008) Reliability of levee systems. In: Phoon K-K (ed) Reliability-based design in geotechnical engineering. Taylor & Francis Group, New York, pp 448–496
- Xu B, Low BK (2006) Probabilistic stability analyses of embankments based on finite-element method. *J Geotech Geoenviron Eng ASCE* 132(11):1444–1454

## CHAPTER 4

RELIABILITY-BASED THREE-DIMENSIONAL ASSESSMENT OF INTERNAL  
EROSION POTENTIAL DUE TO CREVASSE SPLAYS**Abstract**

Geomorphic features in the soil layers underlying a structure often have a significant effect on the underseepage behavior and the potential for initiating internal erosion. Based on the assumption that the preponderance of the underseepage risk to a levee reach is due to the geomorphic features along that reach, methodology has been developed to perform a stochastic assessment of the properties of the seepage regime with the intention of assessing the probability of internal erosion initiation. The methodology consists of a response surface-Monte Carlo analysis that takes into account the uncertainty in the subsurface geometry and soil properties in assessing the seepage regime associated with the feature. Three-dimensional finite-element seepage analyses are used to develop the response surface to take into account the inherent three-dimensional aspects of the feature. As a result of the analysis, probability distribution functions with respect to hydraulic gradient and factor of safety against heave are developed. The methodology can be adapted to any type of geomorphic feature and, as an example, a crevasse splay deposit is presented.

#### 4.1. Introduction

Reliability assessments of dams and levees (either by means of a factor of safety or probabilistic methods) founded on variable geologic conditions have often struggled with quantifying the probability of unsatisfactory performance or failure due to localized adverse foundation conditions (Terzaghi 1929). With levees, a failure at any one location along the perimeter of a protected basin often leads to failure of the entire system. The analogy of a weak link in a chain is often used to illustrate this situation (Steenbergen et al. 2004; Vrouwenvelder 2006; Vrouwenvelder et al. 2010). Natural geologic variation along the alignment of a levee affects the overall reliability of the system and in some cases can even affect the critical mode of failure (Shannon and Wilson 2011; Kanning 2012). As the length of levee protecting a basin increases, the probability of encountering unfavorable subsurface conditions increases, and thus, the probability of unsatisfactory performance or failure increases. This phenomenon has often been referred to as length effects (Bernitt and Lynett 2010; Vrouwenvelder et al. 2010; Shannon and Wilson 2011; Bowles et al. 2012; Kanning 2012).

Many levee foundations are underlain by alluvial foundation deposits (geomorphic features) that are commonly encountered in a meandering river flood plain. Adverse foundation conditions along a levee's alignment are often associated with localized geomorphic features. For instance, existence of an abandoned, sand filled creek channel crossing beneath the levee may concentrate seepage and result in an increased probability of a piping failure and may even change the critical mechanism of internal erosion for that levee reach. In many cases, the locations of highest hazard along a structure's alignment



can be tied to the occurrence of one or more problematic geomorphic features. By quantifying the hazard to the levee due to the individual geomorphic features and combining those risks for the entire length of the levee, the total probability of unsatisfactory performance for the levee can be quantitatively assessed.

Of course, not all geomorphic features of the same type will represent the same level of risk. Variation in geometric configuration and soil properties will lead to different probabilities of internal erosion due to underseepage. Thus, the models for each feature must have flexibility to account for variations in geometry, soil properties, depth, and other relevant parameters as well as account for varying levels of uncertainty in these parameters. Furthermore, features that are situated close to each other may be interdependent and affect the seepage regime of each other. Finally, the alignment of the levee itself may affect the hydraulic pressure and flow regime on a feature. The goal of this research is to develop steady-state methodology for assessing the reliability with respect to internal erosion in a system of levees protecting a basin. The related hazard is due to underseepage through geomorphic features encountered along the levee alignment.

#### 4.1.1. Internal Erosion and Underseepage

Terminology describing the various mechanisms of internal erosion has evolved over recent years as our understanding of the mechanisms of erosion has developed. Nomenclature for these mechanisms has been and continues to be inconsistent in practice and in available technical literature on the subject. In a recent publication, the International Committee on Large Dams (ICOLD 2015) presents a system of nomenclature describing

the various mechanisms of internal erosion. This paper has adopted the ICOLD nomenclature. The term internal erosion has been accepted as a generic term to describe erosion of particles by water passing through a body of soil or rock. The term underseepage is used to describe seepage flow under a structure and, therefore, some internal erosion mechanisms are initiated by underseepage (CIRIA 2013). Underseepage occurs when a differential hydraulic head forces water through the foundation soils or bedrock beneath a structure, such as a dam or levee.

According to ICOLD (2015), internal erosion can be triggered by means of four mechanisms: concentrated leak erosion, backward erosion, contact erosion, or suffusion. Since this research study is interested in analyzing the geometry of the foundation of levee sections and due to the specific typical soil layering arrangement of the foundation (Figures 4.1 and S4.1), the failure mechanism considered is backward erosion. There are two kinds of backward erosion: backward erosion piping (BEP) and global backward erosion (GBE). BEP mainly occurs in the foundation (although it may also occur in the embankment), and GBE occurs in the core of an embankment. Therefore, BEP is the failure mechanism of interest. BEP describes the erosion of soil due to underseepage flow through a soil mass that initiates when particles of soil are dislodged from the soil matrix at an unprotected seepage exit point. As BEP continues, a pathway or pipe is formed by progressive erosion at the upstream end of the erosion void. As described by Vrouwenvelder et al. (2010), the authors believe BEP is often preceded by the heave mechanism. Heave is the movement of mass of soil due to underlying hydraulic pressure or seepage forces. Heave usually occurs within the unprotected seepage exit area lifting and cracking the soil layer (mass of soil)

providing the unprotected exit point for BEP to occur. Both heave and BEP mechanisms can contribute to the potential for internal erosion beneath a levee; therefore, both mechanisms are included in the assessments presented herein.

#### 4.1.2. General Meandering River Levee Foundation Conditions

The term meandering river relates to a river that has a sinuous plan view (Leopold and Wolman 1957). The typical (general) depositional environment of a meandering river is characterized by river channel deposits and flood (overbank) deposits (Leopold and Wolman 1957; Brierley and Fryirs 2005). Channel deposits in an active river channel are typically granular and tend to become finer in the upward direction, although exceptions can be found due to uncommon circumstances (Walling et al. 1997, 2004; Filgueira-Rivera et al. 2007; Smith and Pérez-Arlucea 2008; Ritter et al. 2011). Overbank deposits are typically located above the channel deposits and are deposited when floodwaters exit the river channel and deposit the finer grained materials due to decreasing flow velocity (Walling et al. 2004; Ritter et al. 2011). The thickness of overbank deposits is generally greatest adjacent to the river bank, resulting in low ridges adjacent to the active channel known as natural levees (Brierley et al. 1997; Cazanacli and Smith 1998; Ferguson and Brierley 1999; Hudson and Heitmuller 2003; Adams et al. 2004; Temmermana et al. 2004; Smith and Pérez-Arlucea 2008; Hudson 2011; Ritter et al. 2011). Channel deposits are often referred to as the foundation layer, and the overbank deposits are often referred to as the blanket layer (USACE 1956, 2000).

Figure S4.1 illustrates the simplified meandering river stratigraphy described above (this can also be seen in Figure 4.1). This pattern of deposition has a significant effect on the underseepage behavior and associated internal erosion mechanisms. Due to the high hydraulic conductivity of the foundation and low hydraulic conductivity of the blanket, only a small percentage of the total head loss occurs in the foundation. This results in large pressures beneath the blanket that can lead to heave and cracking of the blanket. In some cases, heave may result in a catastrophic failure (blowout), but more commonly, the blanket cracking leads to a concentrated flow through the blanket, high gradients, and the initiation of BEP in the foundation. This process initially results in sand boils but can progress to full piping failures of the structures (USACE 1956; Glynn and Kuszmaul 2010; Rice and Polanco 2012).

In addition to the general meandering river geomorphic profile described above, a number of local geomorphic features are common within the meandering river environment including: abandoned channels, point bars, meander scrolls, and crevasse splays. These features are shown schematically on Figure 4.1 (adapted from Allen 1970). Where these features intercept the alignment of an artificial levee, flow concentration or localized blanket thinning may occur, resulting in a significantly higher potential for internal erosion than in the surrounding areas (Glynn and Kuszmaul 2010).

Abandoned channels (paleo channels) are river or tributary channels that were once active. They are often infilled by overbank deposits, but in some cases (i.e., chute and neck cutoffs and tributary channels) they may be partially infilled with coarse-grained soil (Bridge 2003; Brierley and Fryirs 2005; Fryirs and Brierley 2013).

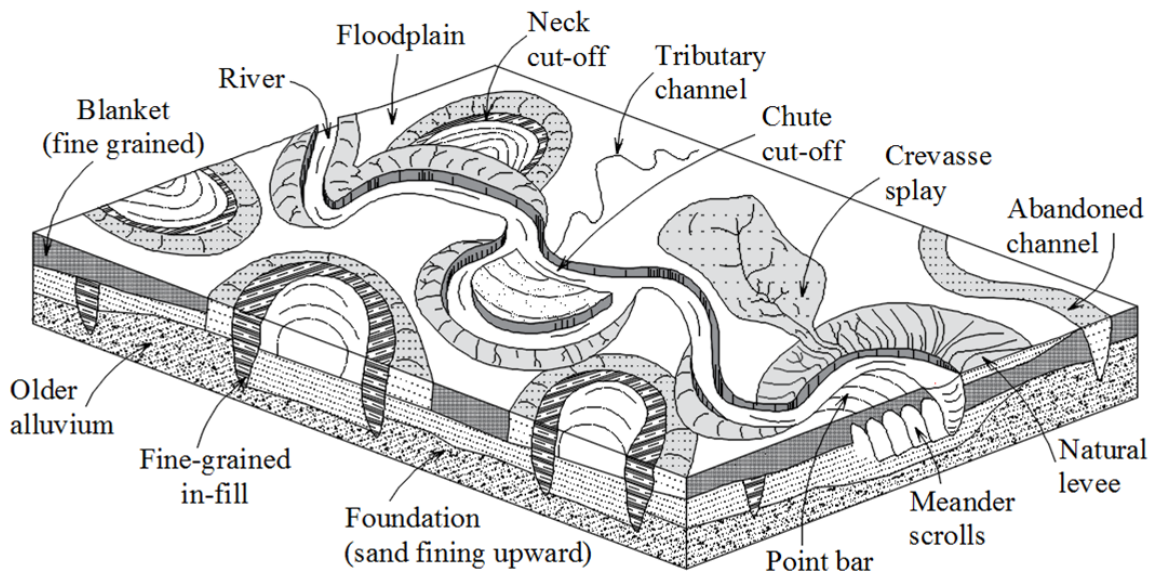


Figure 4.1. Common geomorphic features within the meandering river environment.

These layers may represent a point of concentrated seepage flow or local blanket thinning that locally increases the potential for internal erosion. Point bars consist of sand and gravel bars that commonly form on the inner (convex) meandering bank of a river (Nanson 1980; Brierley and Fryirs 2005; Ritter et al. 2011). They can represent both concentrated flow due to their granular makeup and localized thinning of the blanket layer. Meander scrolls are a complex depositional feature associated with successive point bar formation and infilling between point-bar ridges with fine-grained soils (Nanson 1981; Saucier 1994; Woolfe and Purdon 1996; Brierley and Fryirs 2005; William Lettis and Associates 2008; Glynn and Kuszmaul 2010). The low hydraulic conductivity of the fine-grained infilling has the potential to block or concentrate seepage into the point bars resulting in higher hydraulic gradient than surrounding areas. Crevasse splays form in association with the natural levee. During paleo flood events, floodwaters breach the natural levee forming a crevasse through it (Bristow et al. 1999; Bridge 2003; Brierley and

Fryirs 2005; Ritter et al. 2011). As the water passes through the crevasse, it splays out on the landside of the natural levee and deposits coarse-grained sediment. The crevasse splay deposit represents a concentrated pathway to a layer of sand within the blanket, resulting in elevated potential for the heave and piping mechanisms.

#### 4.1.3. Current Methods for Analysis of Internal Erosion

Some of the earliest work in deterministic underseepage analysis was performed by Bligh (1910, 1913, 1916) who developed an empirical relationship between piping potential and the shortest flow path length beneath a water-retaining structure. Lane (1935) later recognized a distinction between flow along the base of the structure, vertical flow along vertical barriers, and flow through a granular media and modified Bligh's work to develop the weighted creep ratio method. Lane's empirical method also took into account the varied erosion resistance of different soil types (i.e., average gradient versus concentrated flow).

Efforts by the U.S. Army Corps of Engineers (USACE) led to steady-state theoretical relationships for the computation of seepage flow beneath levees (USACE 1956). These relationships provided the basis for the blanket theory (BT) equations that are presented in the USACE Engineering Manual "Design and Construction of Levees" (USACE 2000). The blanket theory equations calculate the head at the base of the blanket layer that can be used to calculate either a gradient through the blanket or an uplift pressure beneath the blanket. Thus, the factor of safety can be calculated for either piping or heave.

Due to the nature of the geology encountered in the levee stratigraphy, the blanket layer is usually composed of different types of soils and, for simplicity of the blanket theory model, these different layers are transformed to an equivalent single layer corresponding to an equivalent hydraulic conductivity (USACE 2000). The main limitation of the blanket theory equations is that the subsurface geometry is restricted to two homogenous layers of constant thickness (the blanket and foundation layers as shown in Figures 4.1 and S4.1). This limitation was partially resolved by the finite difference computer program LEVEEMSU (Wolff 1989; Gabr et al. 1995) that numerically solves the two-dimensional blanket theory equations to allow for nonuniform thickness of layers and varied soil hydraulic conductivity. Finite-element analyses have enabled the modeling of complex subsurface geometries where converging and diverging seepage flows can affect the magnitude of exit gradients. An additional benefit of finite-element analyses is it can calculate fluid velocities, pore pressures, and gradients internal to the blanket layer.

In an attempt to quantify the effects of uncertainty in the subsurface geometry and soil parameters, probabilistic methods for assessing underseepage in levees have been developed. One common approach is using the blanket theory equations developed by the USACE as the performance function and the first-order second-moment (FOSM) Taylor series method as the probability model (Wolff 1994; Crum 1996; Wolff et al. 1996; Wolff 2008). This methodology is subject to the same limitations as the blanket theory; that is, it works well for simple profiles but is characteristically a two-dimensional analysis and cannot model the complex subsurface conditions and three-dimensional aspects often associated with the fluvial depositional environment.

Based on the hypothesis that the majority of the underseepage hazard along a levee comes from discrete subsurface geomorphic features that interrupt the characteristic profile, Rice and Polanco (2012) and Polanco and Rice (2014) have developed steady-state two-dimensional models for assessing hydraulic conditions in geometrically complex levee profiles using what they call the response surface-Monte Carlo (RSMC) method. The steady-state RSMC methodology uses multiple finite-element analyses to develop a relationship between the key input parameters (hydraulic conductivity and unit weight of the soil layers and subsurface geometry of the soil layers) and the probability of reaching critical hydraulic conditions (uplift pressures or hydraulic exit gradients) given a loading condition (such as the water level associated with a flood with an annual exceedance probability of 1% or the 100-year-flood level). This relationship, generally called a response surface (Xu and Low 2006; Low 2008), is used to perform a Monte Carlo simulation that results in a cumulative ascending distribution function (CADF)—a plot of increasing values of a key parameter versus the probability of the parameter being less than that value—of the key hydraulic parameters controlling the potential for initiation of internal erosion, that is hydraulic pressure beneath a clay blanket or hydraulic exit gradient.

The range and probability distribution for each soil or geometric input parameters is represented using a probability density function (PDF) that describes the relative likelihood for this parameter to take on a given value. Comparison analyses within the FOSM-BT and RSMC methods are presented in Rice and Polanco (2012) and Polanco and Rice (2014). Rice and Polanco (2012) describe the differences within methods and present detailed steps of the RSMC method by means of the analysis of two hypothetical complex



levee profiles. Polanco and Rice (2014) present the comparison of eight hypothetical levee profiles where six of these studies are analyzable using both the FOSM-BT and RSMC methods, and the other two are beyond the capabilities of the FOSM-BT method and are only analyzed with the RSMC method [as presented in Rice and Polanco (2012)]. Where applicable, the difference between methods is minor but generally tends to increase with increasing model complexity. In both papers, regression analyses are performed to assess the relative effects that changes in the input parameters have on the results with the conclusion that, in most cases, geometric parameters have the greatest effect on the results.

The effect geomorphic features have on the flow regime is characteristically three-dimensional and requires more complexity than those provided by the close-form equations by USACE. Therefore, for this study, the steady-state RSMC methodology has been expanded, using three-dimensional finite-element analyses to account for the three-dimensional seepage aspects of individual geomorphic features. Although rodent burrows, roots, tension cracks, and utilities have their role in the uncertainty of a levee's underseepage performance, they are not considered in the RSMC model but are considered in a separate background hazard analysis. Refer to the "Discussion" section for further information.

#### **4.2. Application Example—Crevasse Splay Geomorphic Feature**

The application example presented herein to illustrate the methodology is based on an analysis of a crevasse splay feature located along the Sacramento River Levee System in California. The first step in analyzing a levee system consists of identifying the locations

of crevasse splays (along with other geomorphic features) along the levee reach being analyzed. In this case, this task was accomplished using existing geologic information, such as maps prepared along the Sacramento River Levee System (Pearce et al. 2009; William Lettis and Associates 2008). A small sample of these maps is presented as Figure S4.2.

#### 4.2.1. The Crevasse-Splay Geomorphic Feature

Crevasse splays (Figure 4.2) are geomorphic features that formed with the break of a natural levee during paleo flood events. Floodwaters breach the natural levee forming a crevasse for water to pass through (Bristow et al. 1999; Bridge 2003; Brierley and Fryirs 2005; Ritter et al. 2011). The sediment-laden water splays out on the landside of the crevasse and deposits coarse-grained sediment through a distributary channel and the landside splay (Mjos et al. 1993). The resulting configuration is a lobate (sinuous tongue) or fan-shaped splay area (Allen 1965; Mjos et al. 1993; Saucier 1994; Brierley et al. 1997; Bridge 2003). The splay can thin gradually with the thickest part connected to the natural levee by means of the crevasse channel or end abruptly (Mjos et al. 1993; Bridge 2003). Thickness ranges from a few centimeters to several meters and the length can be up to kilometers long (Allen 1965; Farrell 1987; Bridge 2003). Usually, clayey or silty overbank material overlies the coarse-grained crevasse splay deposits (Farrell 1987; Saucier 1994), and as a consequence of the thin clayey deposit overlying the crevasse splay, sand boils form on the ground surface above the splay during hydraulic loading (Bristow et al. 1999). The crevasse splay deposit represents a concentrated pathway (the distributary channel) to

a layer of sand within the blanket (the splay), resulting in elevated potential for the heave and piping internal erosion mechanisms.

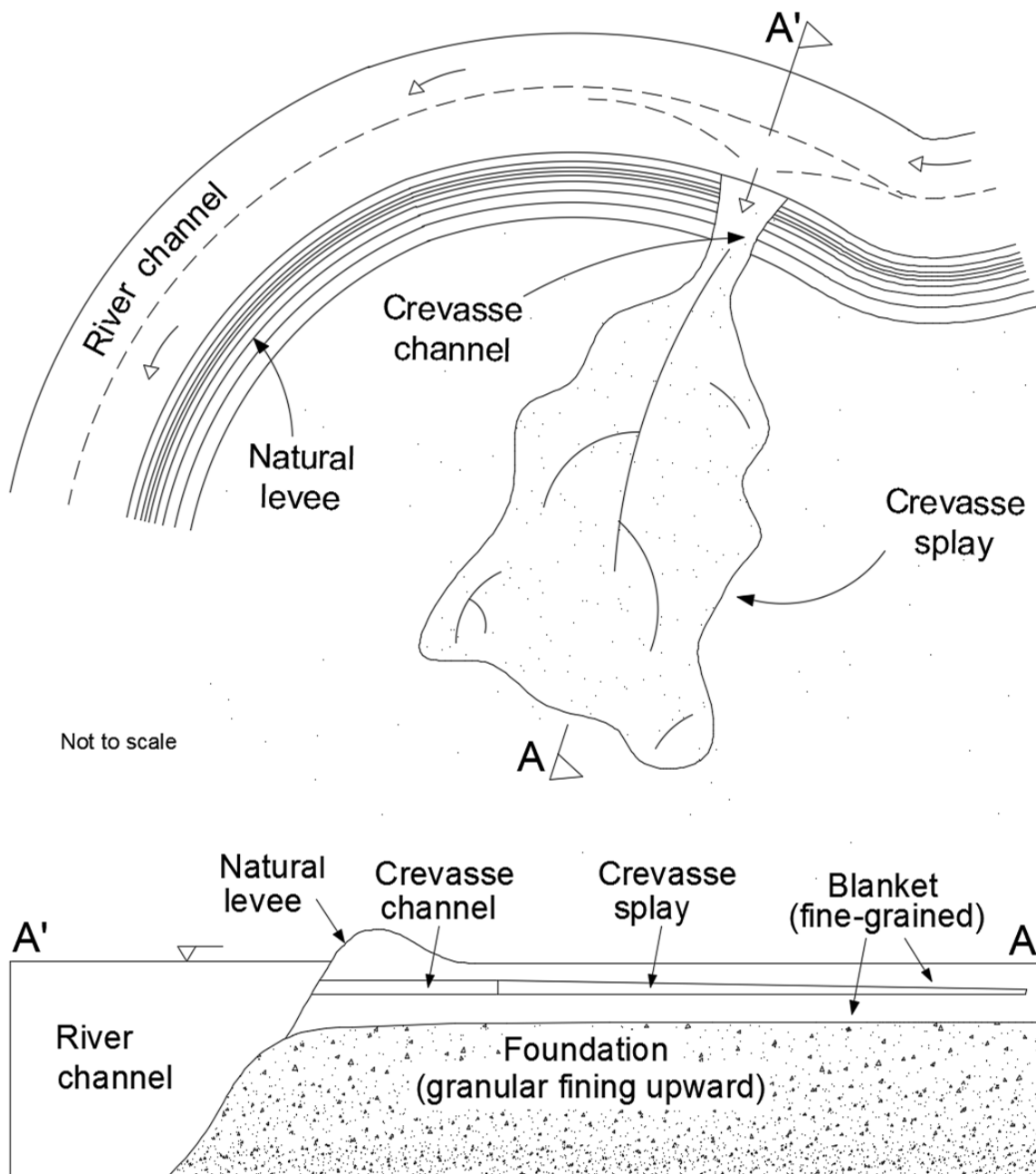


Figure 4.2. Schematic illustration of a crevasse-splay deposit.

#### 4.2.2. Methodology

The assessment of the hazard that a crevasse splay poses to the levee system can be quantified by developing a CADF for values representing the critical hydraulic condition, either the exit gradient or uplift pressure. The probability of exceeding a limit value of the exit gradient or uplift pressure can be obtained directly from the CADF. Depending on the failure mechanism (i.e., piping, heave) either the exit gradient or the uplift pressure on the landside of the levee will be the key parameter dictating the likelihood of initiating internal erosion. It is important to note, the probabilities of exceeding these values are not the probabilities of levee failure because other factors will need to be considered in the assessment of the probability of the internal erosion progressing to a levee failure. That said, this computed probability is considered as a conditional probability of initiation of erosion. To assess failure an event tree analysis is needed with similar computations or judgments to assess the probabilities assigned to the remaining event tree nodes corresponding to the potential for continuation of erosion, progression to form a pipe, and formation of a breach/failure as stated by ICOLD (2015).

The RSMC analyses will produce a CADF of key hydraulic parameters (i.e., uplift pressure or exit gradient) for a crevasse splay mapped along the levee alignment. To accomplish this, a general response surface will be developed that describes the relationship between the key hydraulic parameters (uplift pressure or exit gradient) and key soil and geometry parameters describing the crevasse splay feature. Then, using PDFs representing uncertainty in key hydraulic, geometric, and soil parameters as input for the response surface, a Monte Carlo simulation is performed that results in a CADF for either

uplift pressure or exit gradient. Because the response surface has been developed to model the general hydraulic behavior of a crevasse splay configuration, it can be used beyond the context of the current application example and applied to crevasse splay deposits in other levee reaches and other river systems. For example, along the Sacramento River valley there are very nonplastic silt material deposits from hydraulic gold mining in the Sierras. This fact should be taken into consideration when defining the PDFs for the hydraulic conductivity of the various elements of the model around this area. Also, the following steps showing how to develop the response surface and eventually the RSMC can be applied to other geomorphic features such as point bars, cut-off channels or paleo channels.

The response surface is developed using the following steps:

1. A general three-dimensional model is developed, and key soil and geometry input parameters are identified;
2. The general model is simplified to reduce the number of input parameters in the response surface;
3. The simplified model is verified for consistency with the general model;
4. Multiple three-dimensional finite-element analyses are performed using the simplified model to develop the response surface; and
5. A macro program is written within an Excel spreadsheet to randomly select values of key parameters from input PDFs and apply the response surface to produce the output CADFs.

Once the response surface and macro program have been developed, the RSMC analysis is performed using input PDFs of all of the key soil and geometry parameters as

mentioned. The input PDFs are specific to the crevasse splay being analyzed and represent the range of values of each parameter and the level of uncertainty associated with the crevasse splay being modeled; therefore, the analyst should use judgement or data for each specific model. Once the RSMC analysis has been performed, an analysis of parameters can be performed to assess which input parameters are responsible for the uncertainty in the resulting CADFs.

#### 4.2.3. Model Development and Identification of Parameters

To characterize some of the geometric parameters (physical characteristics) of the crevasse splays, measurements within the east side of the Sacramento River Levee System map were done recording width and length of the crevasse channels and splays with the purpose of acquiring data to develop PDFs and boundary conditions for the three-dimensional model. In addition, the measurements were assisted by studies where crevasse splays have been well characterized, such as William Lettis and Associates (2008) and Pearce et al. (2009, 2010) along the Sacramento River levees in California, USACE's TM 3-242 (USACE 1956), Saucier (1994), and Farrell (1987) along the Mississippi River levees, and Bristow et al. (1999) along the Niobrara River in Nebraska, among others. Identification of the soil parameters (seepage characteristics) were also assisted by the same studies and also estimated based on published guidance on probability distributions for similar soil types (Harr 1987; Baecher and Christian 2003; Sleep and Duncan 2014).

A three-dimensional finite-element seepage model of the crevasse splay model geomorphic feature is presented in Figure 4.3. It consists of (1) a crevasse channel directly

hydraulically connected to the river and leading from the river water to the splay on the landside of the levee, (2) a splay area on the landside of the levee, and (3) a low permeability blanket on top of the splay. The geometric parameters for the model include the width, length, and thickness of the crevasse channel ( $W_{ch}$ ,  $L_{ch}$ , and  $t_{ch}$  respectively); the width, length, and thickness of the splay ( $W_s$ ,  $L_s$ , and  $t_s$  respectively) as well as the thinning of the splay distal to the levee ( $L_{ts}$ ); the depth that the splay deposit is buried in the blanket ( $t_b$ ), and thickness of the foundation ( $t_f$ ). Soil parameters include the hydraulic conductivities of the channel ( $K_{ch}$ ), splay ( $K_{sp}$ ), blanket ( $K_b$ ), and underlying foundation deposits ( $K_f$ ) as well as the unit weight of the blanket soils ( $\gamma_{blkt}$ ). Also, the decreasing hydraulic conductivity of the splay ( $K_{ds}$ ) distal to the levee can be considered. Thus, a total of 15 geometric and soil parameters comprise the crevasse splay model.

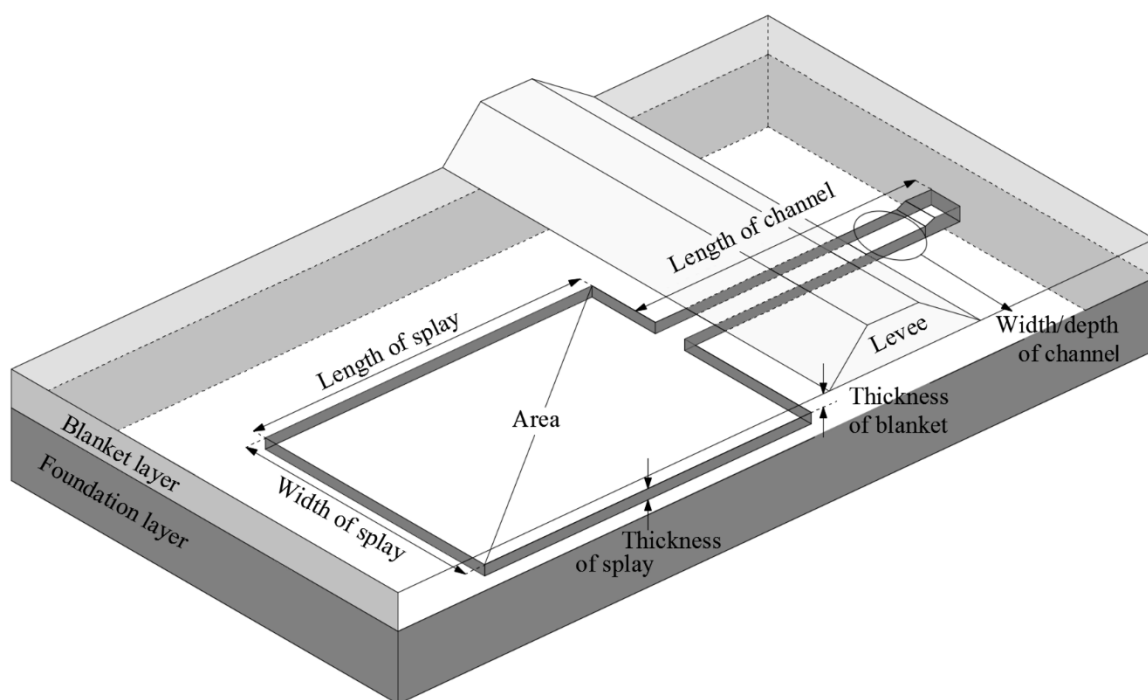


Figure 4.3. Three-dimensional finite-element model of a crevasse-splay deposit.

The behavior of each parameter is represented by a PDF discretized by 5 or more values. If 15 parameters are considered in the above analysis and the potential range of each is represented by 5 discretized values, the total number of finite-element analyses run will be at least  $5^{15}$  or more than 30 billion runs, an impossible number to complete. Therefore, it is necessary to reduce the number of parameters in the finite-element analyses by identifying parameters that have insignificant effect on the outcome of the analysis and combining some of the remaining parameters.

Parametric analyses were performed to eliminate the parameters from the response surface that have an insignificant effect on the analysis outcome. Five parameters were eliminated: the thinning on the splay distal to the levee ( $L_{ts}$ ), the decreasing hydraulic conductivity of the splay ( $K_{ds}$ ) distal to the levee, the foundation's thickness ( $t_f$ ), the foundation's hydraulic conductivity ( $K_f$ ), and the unit weight of the blanket soils ( $\gamma_{blkt}$ ). These parameters are not eliminated from the computation but are not varied during the modeling to define the response surface. To produce a response surface, a most likely value is assigned to each respective eliminated parameter. The  $\gamma_{blkt}$  is the only eliminated parameter that is incorporated later in the computations of the factor of safety with respect to heave.

Thus, the number of parameters is decreased from 15 to 10 by eliminating parameters that have insignificant effect on the outcome. These 10 parameters are presented in Table 4.1 together with the range of values used for the parametric analysis. However, 10 parameters are still too many to develop a reasonable response surface. Therefore, a simplified model is developed that combines the 10 parameters into three



parameters that describe the seepage flow behavior in the crevasse splay deposit: the conductance of the crevasse channel, the transmissivity of the splay, and the conductance of the blanket overlying the splay. The theory being that the total hydraulic head in the splay is controlled by the flow capacity of the three elements. The conductance of the crevasse channel,  $C_{channel}$ , describes the resistance to flow from the river to the splay. The transmissivity of the splay,  $T_{splay}$ , describes how easily the flow reaching the splay is distributed throughout the splay. The conductance of the blanket,  $C_{blanket}$ , defines the ease at which the pressures in the splay can be dissipated through the blanket. The combined parameters are calculated as presented in the following equations and schematically illustrated in Figure 4.4:

$$C_{channel} = \frac{K_{ch}W_{ch}t_{ch}}{L_{ch}} \quad (1)$$

$$T_{splay} = K_s t_s \quad (2)$$

$$C_{blanket} = \frac{K_b W_s L_s}{t_b} \quad (3)$$

The combination of parameters describes a specific flow in one direction through each respective component of the feature; therefore, the corresponding transverse flow is of little consequence to the model outcome. Therefore, hydraulic conductivity is considered as horizontal for the crevasse channel and splay and vertical for the blanket layer. Table 4.2 shows results of one simplified model using most likely values (MLVs).

Table 4.1. Range of values used for the parametric analyses of the crevasse-splay model

Parameter	Description	Units	Values	
			Min	Max
$t_s$	Thickness of the crevasse splay	m	0.3	3.0
$t_{ch}$	Thickness of the crevasse channel	m	0.3	3.0
$t_b$	Thickness of blanket above the splay	m	0.6	6.1
$W_s$	Width of the crevasse splay area	m	45.7	91.4
$W_{ch}$	Width of the crevasse channel	m	22.9	91.4
$L_s$	Length of the crevasse splay area	m	213.4	457.2
$L_{ch}$	Length of the crevasse channel	m	29.0	57.9
$K_{ch}$	Horizontal hydraulic conductivity of the crevasse channel	cm/s	3.0E-05	3.0E-01
$K_{sp}$	Horizontal hydraulic conductivity of the crevasse splay area	cm/s	3.0E-05	3.0E-02
$K_b$	Vertical hydraulic conductivity of the blanket above the splay	cm/s	3.0E-08	3.0E-06

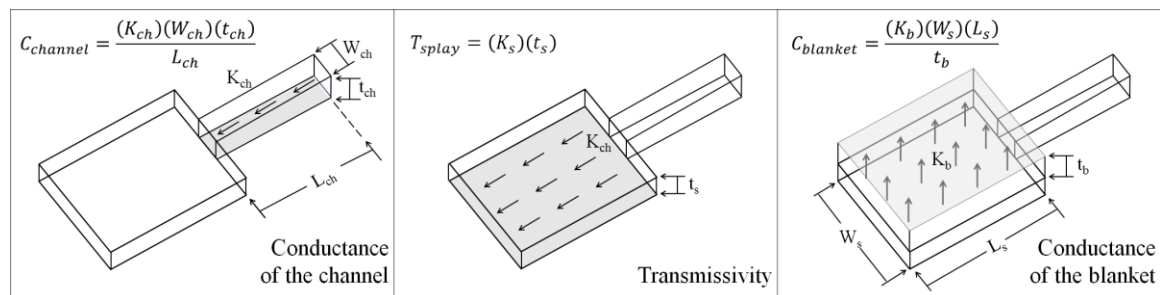


Figure 4.4. Combination of parameters for a crevasse splay model.

Table 4.2. Results of one simplified flow model using MLVs

Description	Parameter	Result
Resulting combined parameter from flow model	$C_{channel}$ (m <sup>2</sup> /s)	4.4E-06
	$T_{splay}$ (m <sup>2</sup> /s)	5.6E-08
	$C_{blanket}$ (m <sup>2</sup> /s)	8.7E-04
Flow model results @ levee toe	Head @ top of splay (m)	6.25
	$i_{blanket}$	1.37
	$F_{heave}$	0.81

Note: MLVs for these computations are shown in Table 4.4.

#### 4.2.4. Validation of Simplified Mode

For the simplified model to be considered valid, it should provide results that are reasonably close to those resulting from the original model for the expected ranges of all 10 original parameters. The simplified model presented above was validated by performing comparative parametric analyses in which individual parameters are varied independently of the remaining parameters and the results compared with those of the original model, that is, the differences between the analyses results using all the true parameter values and the results using the simplified model (combination of parameters). The PDF distributions for each parameter are discretized into 5 or 6 values (or more if needed) that provide sufficient points in the results so that intermediate values can be interpolated.

Table 4.3 presents the results of the comparative parametric analyses performed using a model with 6.71 m (22 ft) of differential head across the levee. For all the analyses performed, the maximum total head was always observed at the bottom of the blanket layer specifically at the interception between the crevasse channel and splay (which is, in turn, the top of crevasse channel and splay). For ease of computation, the zero head datum is set as the landside ground surface elevation. The combined parameters that make up the simplified models are presented in the first column. The second column presents the dependent parameters (those that are constituents of the respective combined parameter) that are held constant during the respective parametric analyses. The third column presents the independent parameters (those that are not constituents of the respective combined parameter) that are held constant during the analysis. Columns 4 and 5 respectively present the dependent and independent parameters that are varied in the respective parametric

analysis. Finally, the maximum amount of variation resulting from each analysis is presented in the final column. The numbers in the final column represent the largest variation that occurs with variation of the parameters listed in Columns 4 and 5. Thus, if the simplified model perfectly matched the model with all parameters used, the values in the final column would all be zero.

As can be observed from Table 4.3, the maximum variation resulting from using the simplified model is less than 0.30 m (1 ft) of total head for all but three parameters. Furthermore, most of the variation that is observed occurs when using values at the ends of PDF distributions where the probability of occurrence is very low relative to the values in the center of the distribution.

Therefore, it can be concluded that the simplified model reasonably approximates the general model. The analyses performed for the table represent the full range of values we deemed reasonable for each parameter based on reviews of literature and crevasse features located at geologic maps and, therefore, represent a reasonable range for all crevasse splays in a meandering river environment.

#### 4.2.5. Developing the Response Surface

Using the simplified model and the combined parameters identified above ( $T_{splay}$ ,  $C_{blanket}$ , and  $C_{channel}$ ), the response surface was generated for the crevasse splay geomorphic feature using multiple runs of a three-dimensional finite-element analysis. The ranges of values for the three combined parameters represent the ranges of the possible values resulting from variation of the original parameters of the model.

Table 4.3. Results of parametric analysis to assess the validity of the simplified flow model for crevasse-splay response surface

Combined Parameter for Response Surface	Constant Parameters		Varied Parameters		Max. variation in $h_{max}$	
	Dependent	Independent	Dependent	Independent	Diff. (m)	Percentage (%)
Transmissivity of Splay, $T_{splay}$	N/A	$W_s, L_s, W_{ch}, L_{ch}, t_b, K_b$	$K_{sp}, t_s$	$t_{ch}, K_{ch}$	0.24	3.54
		$W_s, L_s, W_{ch}, L_{ch}$		$K_{ch}, t_{ch}, K_b, t_b$	0.02	0.27
Conductance of Blanket, $C_{blanket}$	$W_s, L_s$	$W_{ch}, L_{ch}, t_s, t_{ch}, K_{sp}$	$K_b, t_b$	$K_{ch}$	0.08	1.14
	$W_s, L_s$		$K_b, t_b$		0.21	3.13
	$t_b, L_s$		$K_b, W_s$		0.13	1.86
	$t_b, W_s$	$W_{ch}, L_{ch}, t_s, t_{ch}, K_{ch}$	$K_b, L_s$	$K_{sp}$	0.26	3.91
	$K_b, L_s$		$t_b, W_s$		0.07	1.00
	$K_b, W_s$		$t_b, L_s$		0.04	0.55
	$K_b, t_b$		$W_s, L_s$		0.02	0.36
Conductance of Channel, $C_{channel}$	$W_{ch}, L_{ch}$		$t_{ch}, K_{ch}$		0.15	2.27
	$K_{ch}, L_{ch}$	$W_s, L_s, t_b, K_b$	$t_{ch}, W_{ch}$	$K_{sp}, t_s$	0.17	2.50
	$K_{ch}, W_{ch}$		$t_{ch}, L_{ch}$		0.49	7.27
	$t_{ch}, L_{ch}$		$K_{ch}, W_{ch}$		0.08	1.14
	$t_{ch}, W_{ch}$	$W_s, L_s, t_s, t_b, K_b$	$K_{ch}, L_{ch}$	$K_{sp}$	0.32	4.82
	$K_{ch}, t_{ch}$		$W_{ch}, L_{ch}$		0.32	4.77
	$W_{ch}, L_{ch}$	$W_s, L_s, t_b$	$K_{ch}, t_{ch}$	$K_{sp}, t_s, K_b$	0.02	0.27

Note: Maximum variation percentage based on 6.71 m of differential head as stated in the main body of the paper.

This range of values is shown in Table 4.1. The possible range of each combined parameter was discretized into 5 to 6 values to represent the variation of the parameter. Finite-element analyses were then performed on every possible combination of the discretized values for each combined parameter using a three dimensional finite-element model (for instance —SVFlux). The results of the analyses were plotted on a family of curves that together represent a four-dimensional surface that defines the relationship between the three combined parameters and the maximum total head in the splay. One of the family of curves is presented in Figure 4.5. The full family of curves (response surface)

with its corresponding equations can be found in the “Supplemental Data” section (Figures S4.3–S4.7 and Tables S4.1 and S4.2) and, as mentioned, can be used beyond the context of the current application example and applied to crevasse splay deposits in other levee reaches and other river systems.

Thus given values of each of the combined parameters, the value of the maximum total head in the splay can be calculated, resulting in a response surface. Equations were developed through regression analysis to fit the curves of the response surfaces to facilitate computer coding the response surface into a spreadsheet linked with the computer program @Risk (Palisade 2013), which runs the Monte Carlo simulation.

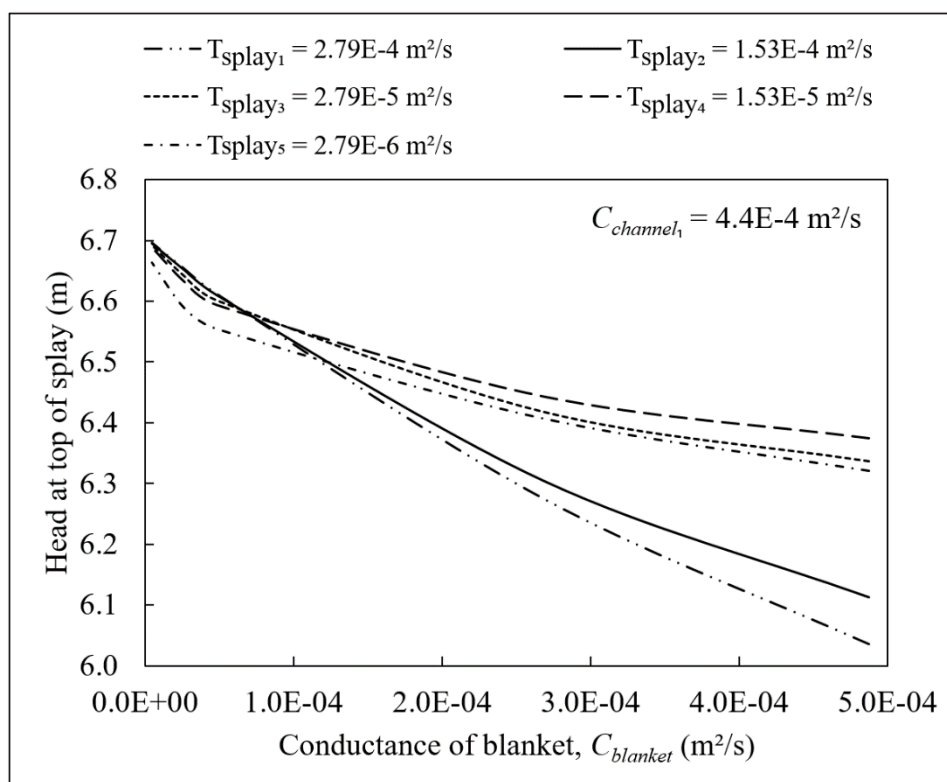


Figure 4.5. Family of curves for the crevasse splay model for one constant  $C_{channel}$  and different ranges of  $T_{splay}$  and  $C_{blanket}$ .

#### 4.2.6. RSMC Analysis

Rice and Polanco (2012) provide a more detailed explanation involved in the steps of the RSMC analysis. A Monte Carlo analysis was performed using a program written in an Excel spreadsheet and linked with the computer program *@Risk*. The Monte Carlo analysis is performed with *@Risk* due to the ease of use and many options available within the program. *@Risk* is very flexible in defining the type of distribution for the parameters from its vast selection of distributions. Output cells are easy to define, which after running a simulation provide an output distribution together with data (Excel reports) that can be manipulated for the desired purpose. Multiple simulations can be performed within iterations, and an error within simulation can be inferred. Sensitivity analyses are also available within simulations. Although a Monte Carlo analysis can be performed in Excel using the random number generator, it does not allow directly to define a specific distribution and it does not provide the convenience of the output data. It can definitely be done, but programming would be needed. PDFs for each of the 10 original model parameters plus one additional parameter (the unit weight of the blanket,  $\gamma_{blk}$ ) are input into the program. Details of the PDFs are presented in Table 4.4. PDFs for these parameters are estimated based on (1) a limited number of laboratory tests and (2) published guidance on probability distributions for similar soil types (Harr 1987; Sleep and Duncan 2014). The precision of the values selected for the PDFs will vary depending on the amount of data available for each geomorphic feature. The variability of the hydraulic conductivities of the crevasse channel and blanket layer are assumed to be represented by lognormal distributions.

Table 4.4. PDFs for the 10 input parameters used to develop the CADFs shown in Figures 4.6 and 4.7.

Parameter	Units	Type of PDF distribution	Most likely value	Standard deviation	Truncated value	
					Min	Max
Thickness of the splay ( $t_s$ )	m	Normal	0.9	0.6	0.3	3.0
Thickness of the channel ( $t_{ch}$ )	m	Normal	0.9	0.3	0.3	3.0
Thickness of the blanket ( $t_b$ )	m	Normal	4.6	0.6	0.6	6.1
Width of the splay ( $W_s$ )	m	Normal	61.0	26.2	15.2	91.4
Width of the channel ( $W_{ch}$ )	m	Normal	45.7	26.2	22.9	91.4
Length of splay ( $L_s$ )	m	Normal	213.4	105.8	213.4	457.2
Length of channel ( $L_{ch}$ )	m	Normal	29.0	0.9	29.0	32.0
Log of channel hydraulic conductivity ( $\log K_{ch}$ )	log(cm/s)	Normal	-3.5	2.5	-4.5	-2.5
Hyd. cond. of channel to splay ratio ( $K_{ch}/K_{sp}$ )	-	Lognormal	50	100	1	1000
Log of blanket hydraulic conductivity ( $\log K_b$ )	log(cm/s)	Normal	-6.5	2.5	-7.5	-5.5
Unit weight of the blanket ( $\gamma_{blk}$ )	KN/m <sup>3</sup>	Normal	18.85	1.57	17.28	20.42

In the actual analyses, the probability density functions for the hydraulic conductivity parameters are estimated for the log of the actual values, resulting in normal distributions. The antilogs of the values from the normal distributions are then taken to be used in the calculations. Due to the natural deposition of this particular geomorphic feature, the splay should have a hydraulic conductivity less than or equal to the channel's hydraulic conductivity.

Therefore, the hydraulic conductivity of the splay is estimated based on the ratio of the channel to splay hydraulic conductivities. This ratio is represented by a lognormal distribution as shown in Table 4.4. In the actual analysis, the random generated value for the hydraulic conductivity of the channel is divided by the hydraulic conductivity ratio, which provides a hydraulic conductivity of the splay that satisfies the natural geologic



assumption. All the other parameters are modeled with normal distributions. The maximum and minimum values provided in Table 4.4 are used to truncate the normal and lognormal distributions to avoid numerical errors and unrealistic values outside the response surface. Although most of the PDFs are modeled with normal or lognormal distributions, it is important to mention that the program *@Risk* is very flexible in defining the type of distribution for the parameters from its vast selection of distributions. For each iteration of the Monte Carlo analysis, the gradient through the blanket,  $i_{blanket}$ , and the factor of safety against heave,  $F_{heave}$ , are calculated using the following sequence:

1. Values of each of the 10 parameters are randomly selected based on the PDF distributions;
2. These parameter values are then combined into the three combined parameters using Equations (1)–(3);
3. The three combined parameters are then used with the response surface to calculate the maximum total head in the splay  $h_{max}$  (the zero head datum is set as the landside ground surface elevation); and
4. Using the maximum head value, the key hydraulic parameters: gradient through the blanket,  $i_{blanket}$ , and the factor of safety against heave,  $F_{heave}$ , are calculated using Equations (4) and (5):

$$i_{blanket} = \frac{\Delta h}{t_b} = \frac{h_{max}}{t_b} \quad (4)$$

$$F_{heave} = \frac{t_b(\gamma_{blkt})}{u_{splay}} = \frac{t_b(\gamma_{blkt})}{(h_{max}+t_b)\gamma_w} \quad (5)$$

The sequence above was repeated for 10,000 iterations to produce CADFs representing the conditional probability of the key hydraulic parameters,  $i_{blanket}$  and  $F_{heave}$  (Figures 4.6 and 4.7). The y-axes in Figure 4.6 represent the conditional probability of the  $i_{blanket}$  being less than or equal to a specific cumulative frequency of a computed  $i_{blanket}$ . Similarly, the y-axes in Figure 4.7 represent the conditional probability of the  $F_{heave}$  being less than or equal to a specific cumulative frequency of a computed  $F_{heave}$ .

The conditional probability of exceeding an exit gradient of 1.0 and the conditional probability of not exceeding a factor of safety of 1.0 against heave are indicated in Figures 4.6 and 4.7 and are specifically shown on the top of the figures as  $P(i_{blanket} \geq 1.0) = 85.1\%$  and  $P(F_{heave} \leq 1.0) = 91.7\%$ .

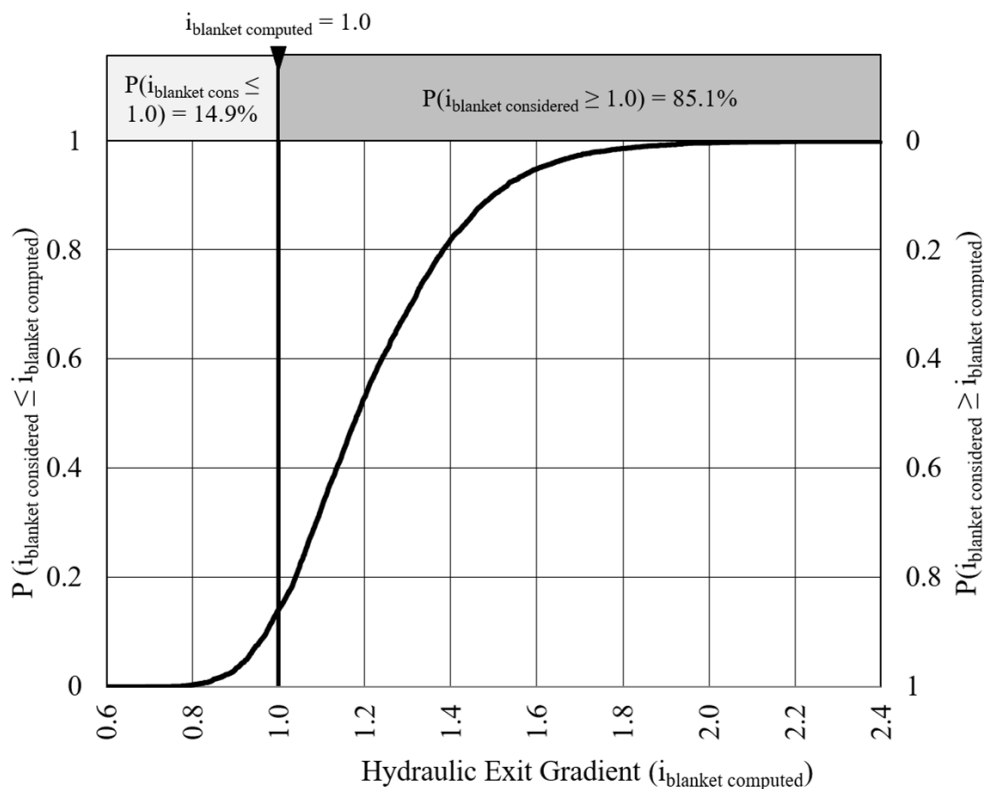


Figure 4.6. CADF for hydraulic exit gradient through the blanket,  $i_{blanket}$ .

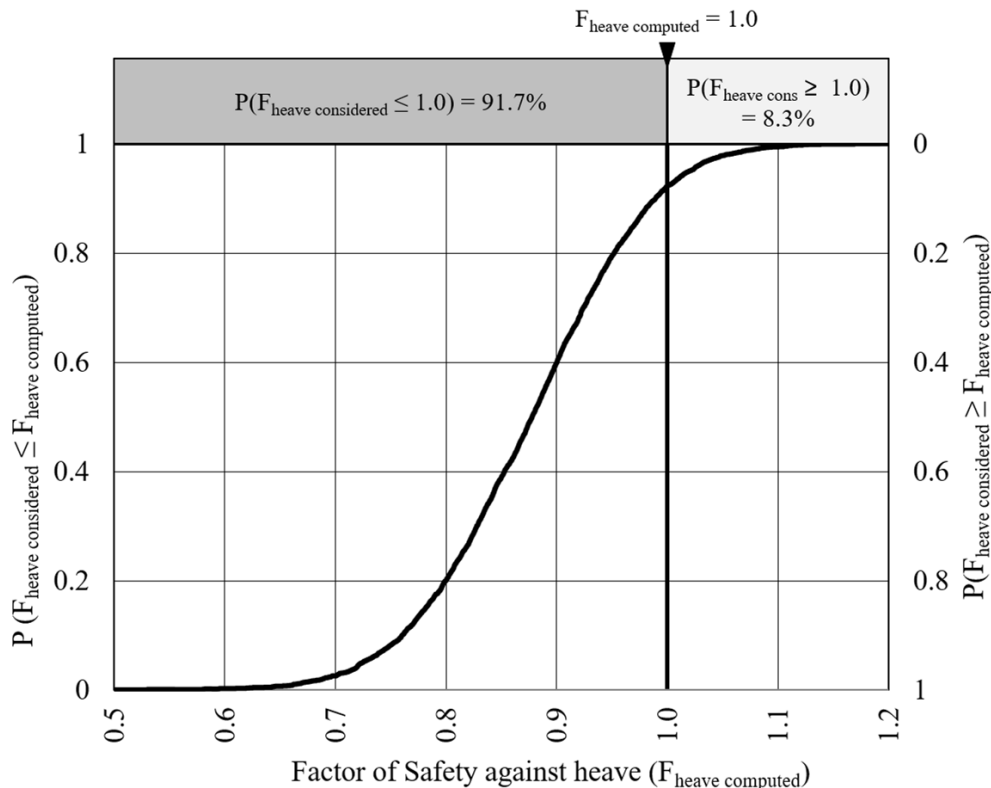


Figure 4.7. CDF for factor of safety against heave,  $F_{heave}$ .

It should be noted that Figure 4.6 presents the performance probability of the  $i_{blanket}$  being greater than 1.0 on the right side, and Figure 4.7 presents the performance probability of the  $F_{heave}$  being less than 1.0 on the left side. The figures can also be used to calculate the probabilities of exceeding lesser or greater values of these parameters that may indicate greater or lesser conditional probabilities of initiating internal erosion.

The hydraulic exit gradients and pore pressures calculated for this crevasse splay model are generally higher than those computed by a two-dimensional or blanket theory model. For comparison, a gradient calculated using an open-seepage-exit blanket-theory scenario model (Case 7c, USACE 2000) using MLVs and a blanket thickness equal to 3.35 m (11 ft) is about 1.0. In the actual levee model, the differential head is 6.71 m (22 ft) with

blanket thicknesses as low as 0.61 m (2 ft) and as high as 6.10 m (20 ft) and, consequently, gradients greater than 1.0 are expected. That said, these results illustrate to some extent the three-dimensional concentration effect that this geomorphic feature has on the seepage flow. It is also important to note that these results represent a condition that may initiate internal erosion and that the probability of failure would require further assessment through an event-tree analysis that are the subject of further research and development.

Since this crevasse splay model is conditional on the river reaching a flood with an annual exceedance probability of 1% or the 100-year-flood level, parametric analyses were also performed with respect to other flood levels to determine a way to compute the probability of erosion initiation based on different flood stages. Results from these parametric analyses are consistent and illustrate a linear relationship of differential flood level versus head at splay (see Figure 4.8 for an example). Based on these results, the crevasse splay model can compute the maximum total head at the splay with respect to various flood stages by a simple linear interpolation centered on the 100-year-flood model. Results for different flood levels are presented in Figure 4.9 resulting in a fragility curve (Shannon and Wilson 2011) for the initiation of internal erosion.

#### 4.2.7. Analysis of Parameter Influences

By means of the program *@Risk*, an advanced sensitivity analysis was performed to illustrate the relative effect that input (soil and geometric) parameters have on the output (design criteria results) and, therefore, determine which parameters are the most statistically significant.

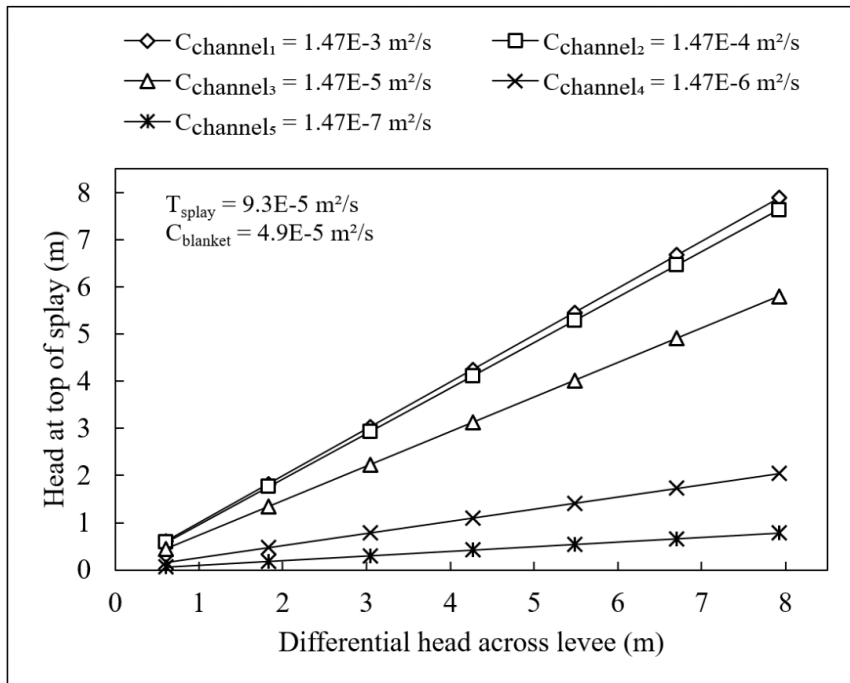


Figure 4.8. Example of one parametric analysis for the crevasse splay based on different flood levels while maintaining all parameters constant except the  $C_{channel}$ .

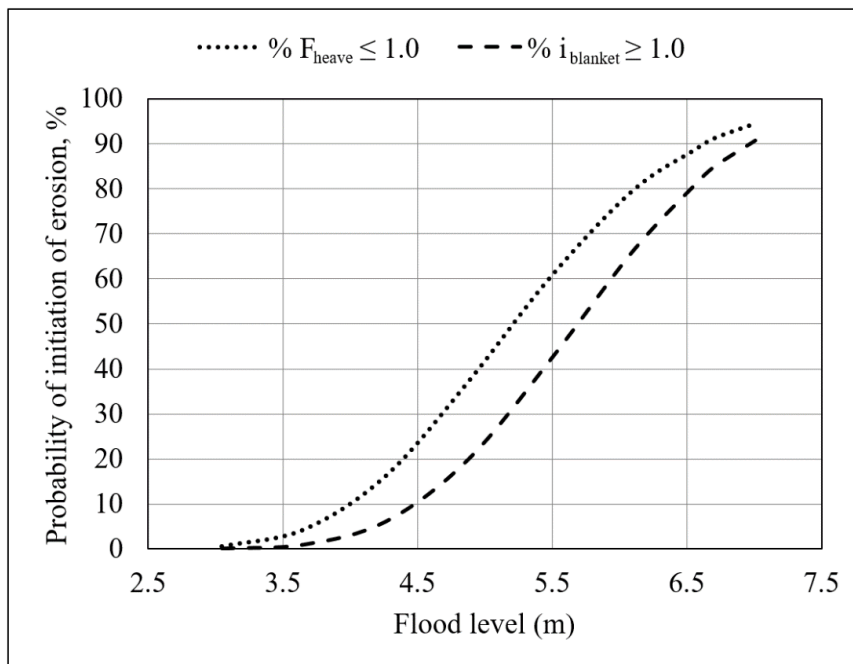


Figure 4.9. Fragility curve for a crevasse splay model.

Although multiple regression analyses could also be performed, the advanced sensitivity analysis was chosen due to its ease of understanding while presenting a tornado graph as a result (Eschenbach 1992). The tornado graph is a bar plot where the data is presented as horizontal bars organized from largest to smallest as in the shape of a tornado. The sensitivity analysis is performed directly by @Risk where an output cell can be monitored by tracking one of its many statistics (like the mean, mode, median, standard deviation, variance, minimum value, or maximum value) while simulating the model. For the purpose of this paper, a sensitivity analysis has been done while tracking the mean of  $h_{max}$ ,  $i_{blanket}$ , and  $F_{heave}$ . Resulting tornado graphs are presented as Figures 4.10-4.12. Tornado results for  $h_{max}$  show that the hydraulic conductivities of the blanket and the crevasse channel together with the thickness of the blanket are the three most statistically significant parameters for this computation. Based on the result of the mean of  $i_{blanket}$ , the three most statistically significant parameters are the thickness of the blanket and the hydraulic conductivities of the blanket and crevasse channel soils. With respect to the  $F_{heave}$ , the three most statistically significant parameters are the thickness of the blanket and the unit weight and hydraulic conductivity of the blanket. Results suggest that the thickness of the blanket ( $t_b$ ) and the hydraulic conductivity of the blanket ( $K_b$ ) are the most significant parameters that provide the greater effect in the variation of the  $h_{max}$ ,  $i_{blanket}$ , and  $F_{heave}$ . These results are dependent on the set of input parameters presented in Table 4.4. Different distributions, parameters, and differential head might lead to different conclusions.

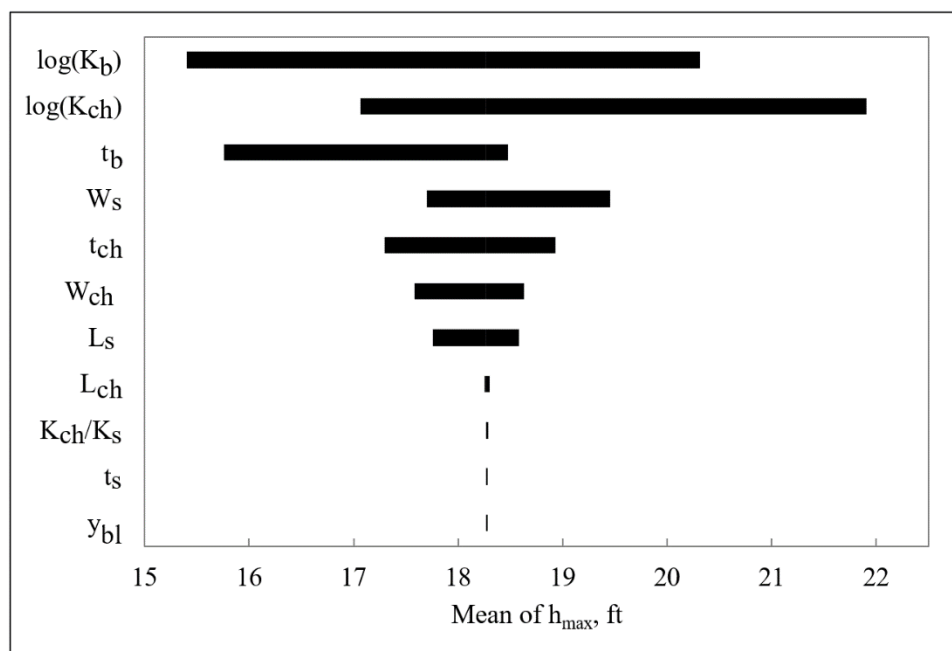


Figure 4.10. Sensitivity tornado graph for mean of  $h_{max}$ .

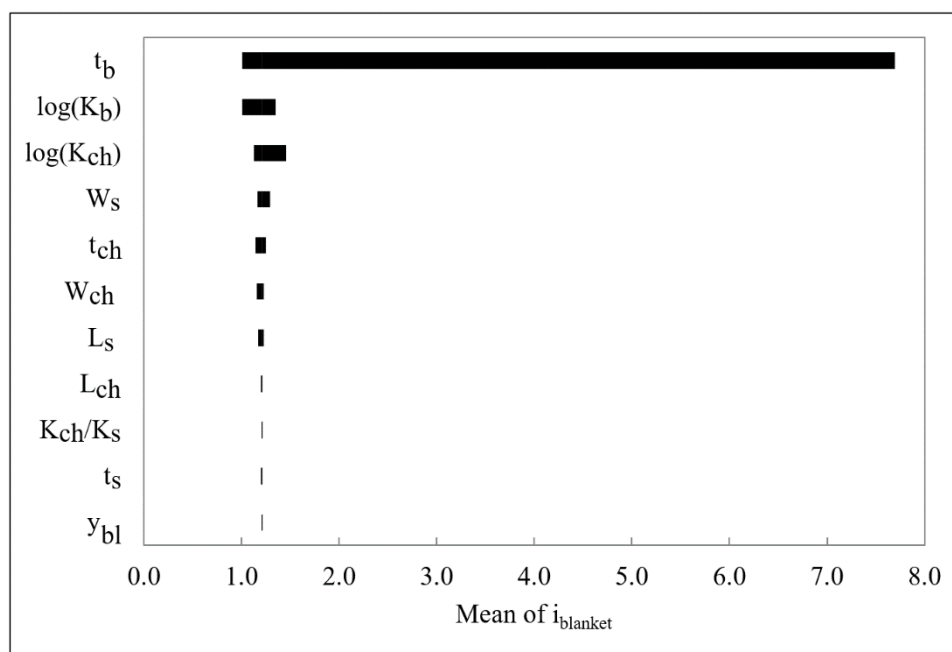


Figure 4.11. Sensitivity tornado graph for mean of  $i_{blanket}$ .

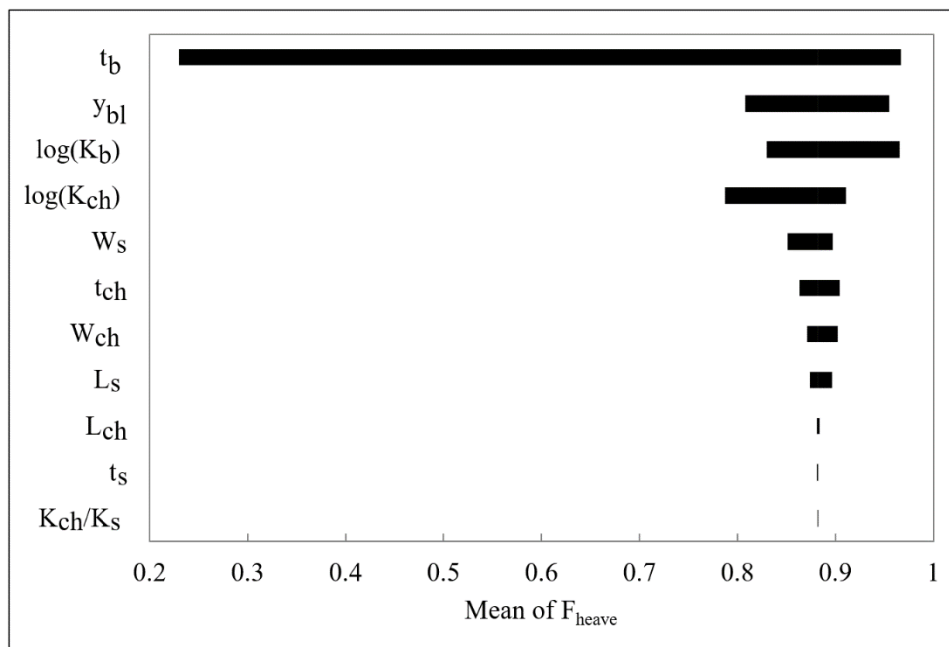


Figure 4.12. Sensitivity tornado graph for mean of  $F_{heave}$ .

### 4.3. Discussion

The methodology presented in this paper is based on the concept that the majority of the underseepage hazard along a levee comes not from the background hazard due to a characteristic subsurface profile but from discrete geomorphic features that interrupt the characteristic profile, providing locations for concentration of seepage flow and/or buildup of hydraulic pressure. The features can be taken from a previously prepared map (if one exists) or assumed at a frequency that is judged appropriate for the river being analyzed. The interactive hydraulic behavior between these features, the structure, and the surrounding characteristic subsurface profile is definitely three-dimensional, concentrating seepage flow into the geomorphic feature and decreasing flow in the surrounding area (or vice versa if the feature represents a seepage block). Thus, by identifying and analyzing



the geomorphic features (such as a crevasse splay) along the alignment of a structure, the vast majority of the underseepage hazard can be evaluated. This is not to say that the remaining portion of the characteristic subsurface profile does not contribute to the overall hazard. In fact, numerous substructures within the characteristic profile that cannot feasibly be identified by normal means of exploration pose a level of background hazard that will still need to be considered.

Besides computing the initiation of erosion of a geomorphic feature, the main purpose of this methodology is to develop CADFs that may be used in conjunction with event tree analyses to assess the likelihood of levee failure due to an individual geomorphic feature along the alignment. A similar procedure could be repeated for all of the geomorphic features (of various types) located along the levee alignment and the probabilities of failure for each feature combined to produce the total probability of failure for the entire levee.

The series of steps for calculating the total failure probability of a levee-protected basin using the proposed methodology are outlined in Figure 4.13. Details of Steps 1 and 2 are presented in this paper while the remaining steps are the subject of further research and implementation.

#### **4.4. Conclusion**

The paper presents steady-state methodology for calculating the probability of initiation of erosion due to underseepage that a historical crevasse splay imposes on a levee section. The paper outlines the procedure needed to identify and characterize a crevasse

splay to develop CADFs that represent the conditional probability of heave or BEP initiation. The crevasse splay model is flexible enough to account for variations in geometric and soil properties parameters as well as flood stages. Due to the vast amount of parameters involved in the development of the crevasse splay response surface, a simplified model is used.

The simplified model consists of combining the most significant parameters into three parameters that adequately describe the flow regime in the crevasse splay deposit. With the hypothesis that the total hydraulic head in the splay is controlled by the flow capacity of the three combined elements, the combined parameters are the conductance of the crevasse channel, the transmissivity of the splay, and the conductance of the blanket overlying the splay. Parametric analyses involving the uncertain input parameters were performed to assess the effects the simplification has on the results concluding that it imposes insignificant errors to the results.

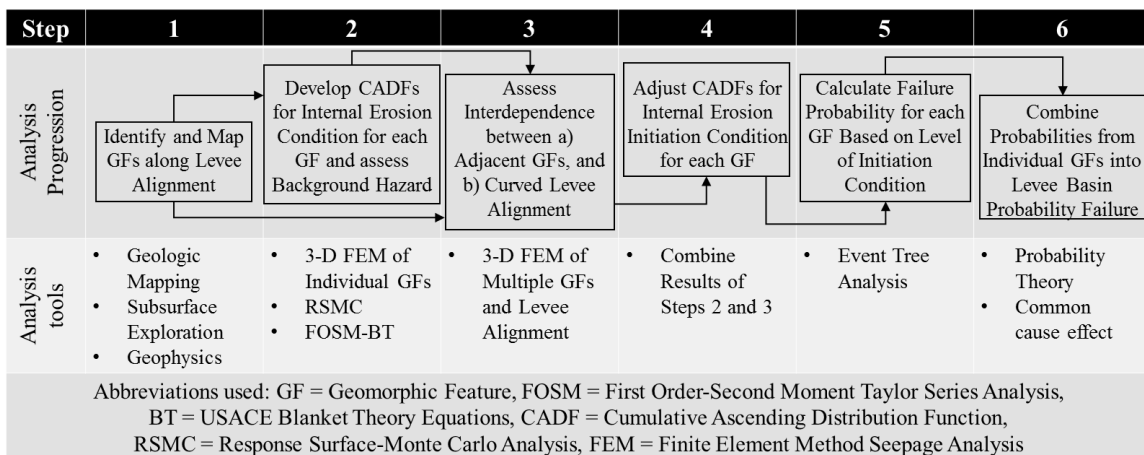


Figure 4.13. Steps for calculating reliability of levee reaches and length effects with respect to underseepage.

The probabilities of exceeding an exit gradient of 1.0 or not exceeding a factor of safety of 1.0 against heave are presented together with a fragility curve describing the initiation of internal erosion with respect to different flood levels. Based on advanced sensitivity analyses, the thickness of the blanket above the splay is the most significant parameter in the computation of the hydraulic exit gradient and factor of safety against heave. This result is likely due to the influence of the thickness of the blanket in the computation of the hydraulic exit gradient and the factor of safety against heave. Sensitivity analysis for the maximum total head at the top of the crevasse splay shows lower dependence on the thickness of the blanket, indicating most of the influence is in calculating gradients and factors of safety rather than its effect on the pore pressure regime. Procedures for the remaining steps to compute the probability of failure of the levee reach are currently under development with ongoing research.

#### **4.5. Acknowledgments**

This material is based upon work supported by the National Science Foundation (NSF) under Grant CMMI 1400640 and the United States Society on Dams (USSD) 2015 Scholarship. Any opinions, findings, and conclusions or recommendations expressed in this material are those of the authors and not necessarily the views of NSF and USSD.

#### **4.6. Supplemental Data**

Figure S4.1 illustrates the typical simplified levee cross section stratigraphy within a meandering river environment. The depositional environment of a meandering river is

characterized by blanket and foundation layers. A small sample of the Surficial Geologic Map of the Sacramento River Levee System is presented as Figure S4.2. These maps provide the geomorphic features beneath and adjacent to the levee alignment and were performed with the assistance of 1937 aerial photos, subsurface exploration data, and the results of a Helicopter-Borne Electromagnetic (HEM) Survey (Fugro 2009, Fugro-WLA 2010, URS 2011). The base map is a USGS 7.5-minute topographic map from West Sacramento published in 1948 and revised in 1992. The map area shows several crevasse splays deposits (as well as other geomorphic features like channel and overbank deposits, and point bars defining meander scroll bars) that make up the complex configuration of the landside of the levee. The full family of curves (FCs) (response surface) is presented as Figures S4.3 through S4.7. Its corresponding equations are presented in Table S4.2. Please refer to ‘Model Development and identification of parameters’ section for corresponding equations to compute the combined parameters.

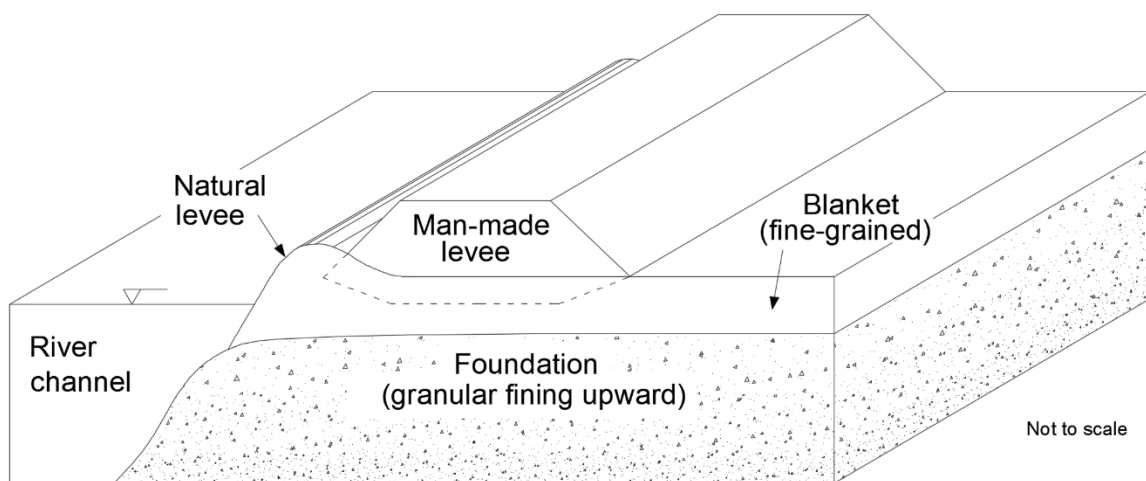


Figure S4.1. Typical simplified subsurface cross section of a meandering river depositional environment.

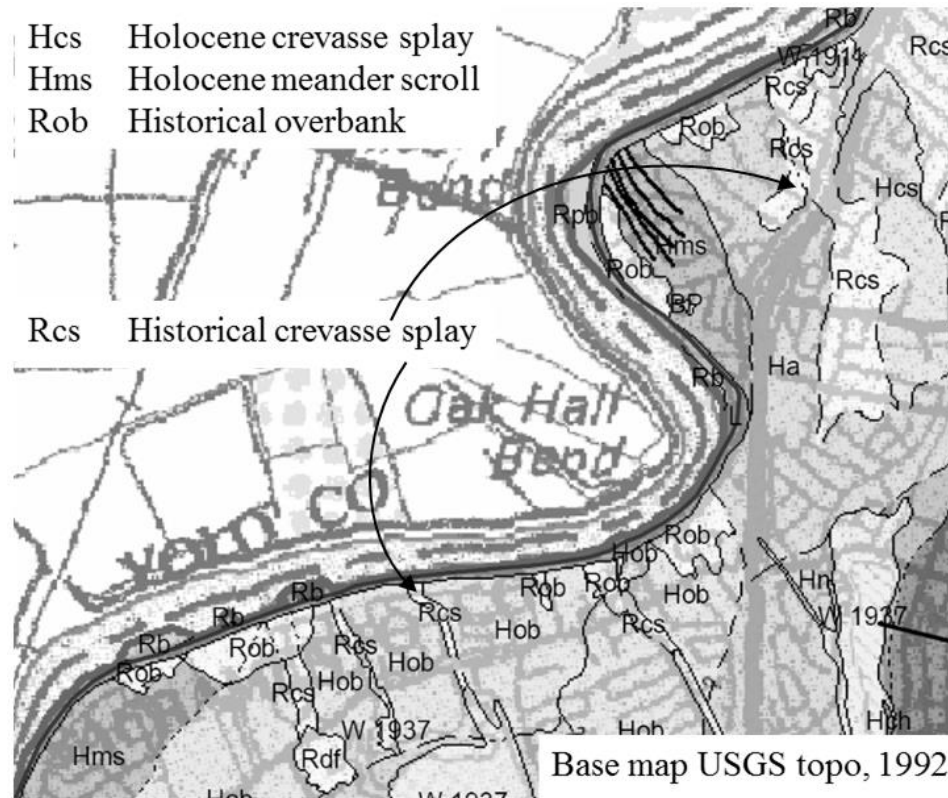


Figure S4.2. Sample of geomorphic features mapping along the Sacramento River in California.

As mentioned in the main body of the paper, this response surface can be used beyond the context of the current application example. It can be applied to crevasse splay deposits in other levee reaches and other meandering river systems provided the parameter values are within the ranges used in the parametric analyses (Table 4.3) and to develop the response surface. Values for the parameters used to develop the family of curves are presented in Table S4.1. Based on the parametric analyses' results one simplified model was used where the geometric parameters were assigned a constant value and the soil parameters were varied. Equations describing the family of curves were developed through a polynomial curve fitting method in Excel.

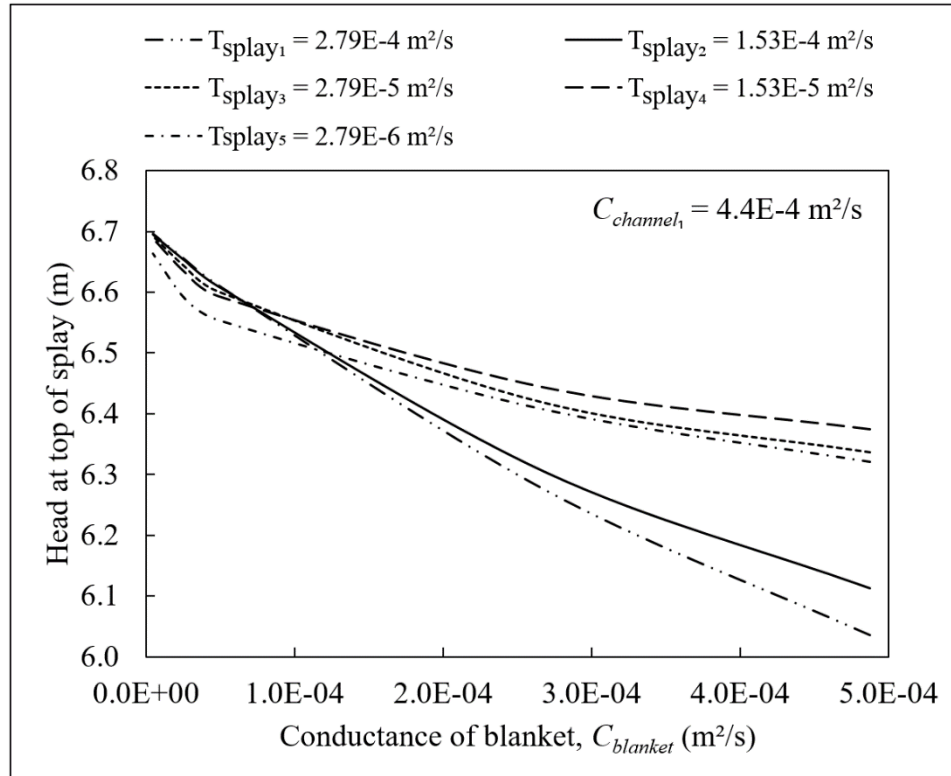


Figure S4.3 Family of curves for the crevasse-splay model for  $C_{channel} = 4.4E-04 \text{ m}^2/\text{s}$  and different ranges of  $T_{splay}$  and  $C_{blanket}$ .

The equations are up to a third order polynomial curve fitting determined by the “least squares” method by means of linear regression analysis. The “goodness of fit” of the regression model is provided by the R-Squared ( $R^2$ ) (Armitage et al. 2001, Chatterjee and Simonoff 2013). The general form of the equations is  $h_{max} = a_3 * Cb^3 + a_2 * Cb^2 + a_1 * Cb^1 + a_0$ , where  $a_3$ ,  $a_2$ ,  $a_1$ , and  $a_0$  are the coefficients determined by the regression analysis and  $C_{blanket}$  is the varied conductance of the blanket depending on each varied transmissivity of the splay ( $T_{splay}$ ) and conductance of the channel ( $C_{channel}$ ). As explained, due to the natural deposition of the crevasse splay, the splay should have a hydraulic conductivity less than or equal to the channel’s hydraulic conductivity. Using these

equations, and interpolation/extrapolation between them,  $h_{max}$  can be calculated and used to calculate the  $i_{blanket}$  and  $F_{heave}$  for the profile given any combination of parameters within the defined ranges shown in Table 4.1.

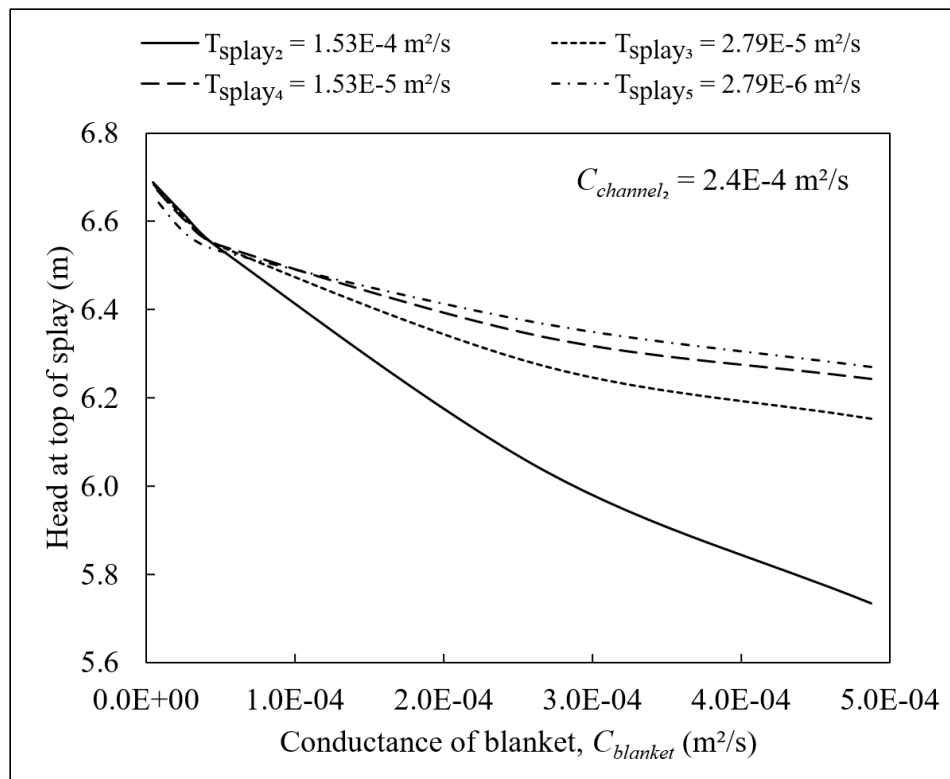


Figure S4.4. Family of curves for the crevasse-splay model for  $C_{channel} = 2.4E-04$  m<sup>2</sup>/s and different ranges of  $T_{splay}$  and  $C_{blanket}$ .

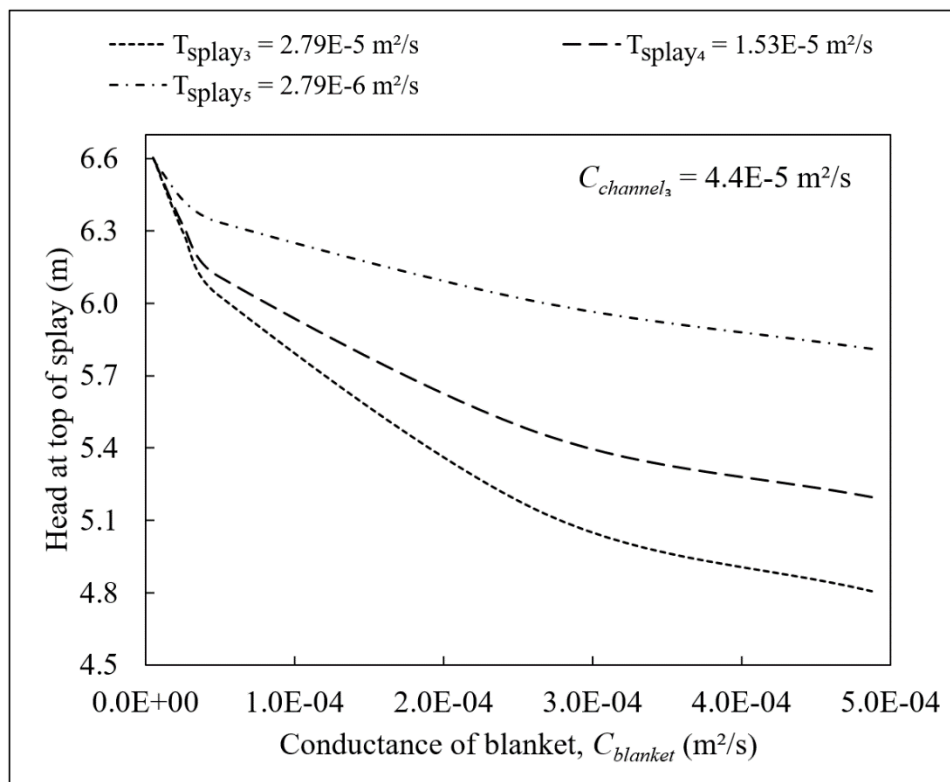


Figure S4.5. Family of curves for the crevasse-splay model for  $C_{channel} = 4.4E-05$  m<sup>2</sup>/s and different ranges of  $T_{splay}$  and  $C_{blanket}$ .



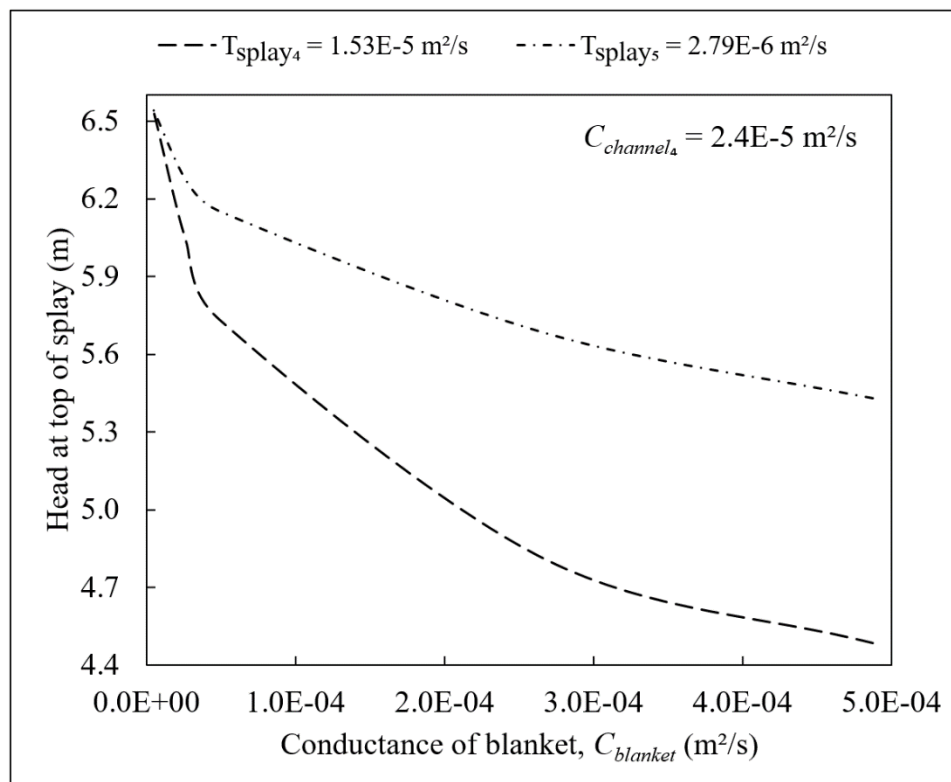


Figure S4.6. Family of curves for the crevasse-splay model for  $C_{channel} = 2.4E-05$  m²/s and different ranges of  $T_{splay}$  and  $C_{blanket}$ .

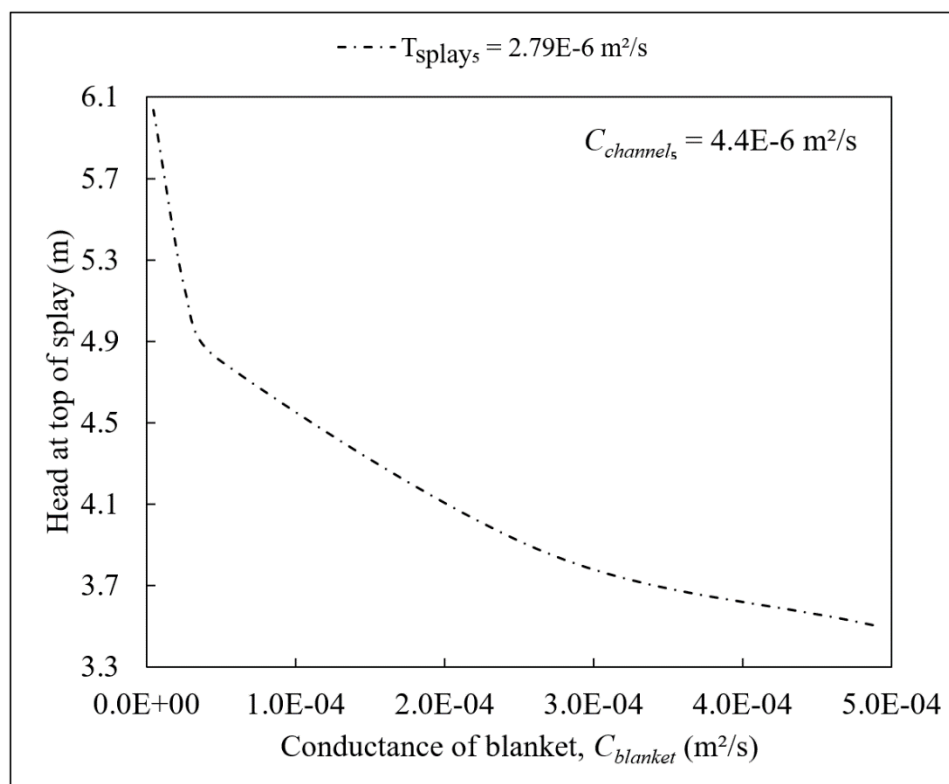


Figure S4.7. Family of curves for the crevasse-splay model for  $C_{channel} = 4.4E-06 \text{ m}^2/\text{s}$  and different ranges of  $T_{splay}$  and  $C_{blanket}$ .

Table S4.1. Parameters used to develop response surface

Constant		Varied		Combined	
Parameter	Value	Parameter	Value	Parameter	Value
$W_s$ (m)	91.44		3.05E-06		4.88E-04
$L_s$ (m)	213.36		1.68E-06		2.68E-04
$t_b$ (m)	1.2192	$K_b$ (cm/s)	3.05E-07	$C_{blanket}$ ( $\text{m}^2/\text{s}$ )	4.88E-05
$t_s$ (m)	0.9144		1.68E-07		2.68E-05
$W_{ch}$ (m)	45.72		3.05E-08		4.88E-06
$L_{ch}$ (m)	28.956		3.05E-02		2.79E-04
$t_{ch}$ (m)	0.9144		1.68E-02		1.53E-04
<b>Not in Response Surface</b>		$K_{sp}$ (cm/s)	3.05E-03	$T_{splay}$ ( $\text{m}^2/\text{s}$ )	2.79E-05
$t_f$ (m)	19.81		1.68E-03		1.53E-05
$K_f$ (cm/s)	3.05E-04		3.05E-04		2.79E-06

Note:  $t_r$  and  $K_r$  were not used for the development of the family of curves but were needed for the development of the model as explained in the main body of the paper.

Table S4.2. Fit-equations' coefficients and corresponding goodness of fit for FCs with respect to each  $C_{channel}$  used.

$T_{splay}$ (m <sup>2</sup> /s)	$h_{max} = a_3 * Cb^3 + a_2 * Cb^2 + a_1 * Cb + a_0$				$R^2$
	$a_3$	$a_2$	$a_1$	$a_0$	
Using $K_{ch1} = 3.05E-02$ cm/s to compute $C_{channel1} = 4.4E-04$ m <sup>2</sup> /s					
2.79E-04	-1.074E+09	1.864E+06	-2.029E+03	6.706E+00	0.99
1.53E-04	-1.944E+09	2.735E+06	-2.087E+03	6.705E+00	0.99
2.79E-05	-	1.379E+06	-1.375E+03	6.682E+00	0.99
1.53E-05	-	1.265E+06	-1.221E+03	6.672E+00	0.98
2.79E-06	-	1.167E+06	-1.208E+03	6.636E+00	0.97
Using $K_{ch2} = 1.68E-02$ cm/s to compute $C_{channel2} = 2.4E-04$ m <sup>2</sup> /s					
2.79E-04	N/A				
1.53E-04	-4.039E+09	5.377E+06	-3.651E+03	6.705E+00	0.99
2.79E-05	-	2.116E+06	-2.083E+03	6.668E+00	0.99
1.53E-05	-	1.796E+06	-1.719E+03	6.657E+00	0.98
2.79E-06	-	1.323E+06	-1.368E+03	6.626E+00	0.97
Using $K_{ch3} = 3.05E-03$ cm/s to compute $C_{channel3} = 4.4E-05$ m <sup>2</sup> /s					
2.79E-04	N/A				
1.53E-04	N/A				
2.79E-05	-	8.579E+06	-7.661E+03	6.516E+00	0.98
1.53E-05	-	6.581E+06	-5.864E+03	6.505E+00	0.97
2.79E-06	-	2.847E+06	-2.850E+03	6.533E+00	0.97
Using $K_{ch4} = 1.68E-03$ cm/s to compute $C_{channel4} = 2.4E-05$ m <sup>2</sup> /s					
2.79E-04	N/A				
1.53E-04	N/A				
2.79E-05	N/A				
1.53E-05	-	1.043E+07	-8.862E+03	6.350E+00	0.96
2.79E-06	-	4.279E+06	-4.134E+03	6.440E+00	0.96
Using $K_{ch5} = 3.05E-04$ cm/s to compute $C_{channel5} = 4.4E-06$ m <sup>2</sup> /s					
2.79E-04	N/A				
1.53E-04	N/A				
2.79E-05	N/A				
1.53E-05	N/A				
2.79E-06	-	1.316E+07	-1.069E+04	5.634E+00	0.90

Note: Not applicable (N/A) corresponds to situations where  $K_{sp} \geq K_{ch}$  and does not satisfy the assumption of the model as explained in the main body of the paper.

## References

- Adams, P. N., Slingerland, R. L., and Smith, N. D. (2004). "Variations in natural levee morphology in anastomosed channel flood plain complexes." *Geomorphology*, 61(1–2), 127–142.
- Allen, J. R. (1965). "A review of the origin and characteristics of recent alluvial sediments." *Sedimentology*, 5(2), 89–191.
- Allen, J. R. (1970). *Physical processes of sedimentation*, George Allen and Unwin, London.
- Baecher, G. B., and Christian, J. T. (2003). *Reliability and statistics in geotechnical engineering*, Wiley, Chichester, U.K.
- Bernitt, L., and Lynett, P. (2010). "Breaching of sea dikes." *Proc. Coastal Eng.*, 1(32), 1–10.
- Bligh, W. G. (1910). "Dams, barrages, and weirs on porous foundations." *Eng. News-Rec.*, 64(26), 708–710.
- Bligh, W. G. (1913). "Lessons from the failure of a weir and sluices on porous foundations." *Eng. News-Rec.*, 69(6), 266–270.
- Bligh, W. G. (1916). "Submerged weirs founded on sand." *Dams and weirs*, American Technical Society, Chicago, 151–179.
- Bowles, D. S., Chauhan, S. S., Anderson, L. R., and Grove, R. C. (2012). "Baseline risk assessment for Herbert Hoover dike." *Proc., ANCOLD Conf. on Dams*, Australian National Committee on Large Dams (ANCOLD), Hobart, Tasmania, Australia, 1–20.
- Bridge, J. (2003). *Rivers and floodplains: Forms, processes, and sedimentary record*, Blackwell, Oxford, U.K.
- Brierley, G. J., Ferguson, R. J., and Woolfe, K. J. (1997). "What is a fluvial levee?" *Sediment. Geol.*, 114(1–4), 1–9.
- Brierley, G. J., and Fryirs, K. A. (2005). *Geomorphology and river management: Applications of the river styles framework*, Blackwell, Oxford, U.K.
- Bristow, C. S., Skelly, R. L., and Ethridge, F. G. (1999). "Crevasse splays from the rapidly aggrading, sand-bed, braided Niobrara River, Nebraska: Effect of base-level rise." *Sedimentology*, 46(6), 1029–1047.

- Cazanacli, D., and Smith, N. D. (1998). "A study of morphology and texture of natural levees—Cumberland Marshes, Saskatchewan, Canada." *Geomorphology*, 25(1–2), 43–55.
- CIRIA (Construction Industry Research and Information Association). (2013). *The international levee handbook*, London.
- Crum, D. A. (1996). "Reliability applied to levee seepage analysis." *Proc., 7th Specialty Conf. on Probabilistic Mechanics and Structural Reliability*, Vol. 1, Worcester, MA, 946–949.
- Eschenbach, T. G. (1992). "Spiderplots versus Tornado diagrams for sensitivity analysis." *Interfaces*, 22(6), 40–46.
- Farrell, K. M. (1987). "Sedimentology and facies architecture of overbank deposits of the Mississippi River, False River region, Louisiana." *Recent developments in fluvial sedimentology*, F. G. Ethridge, R. M. Flores, and M. D. Harvey, eds., Vol. 39, Society of Economic Paleontologists and Mineralogists, Fort Collins, CO, 111–120.
- Ferguson, R. J., and Brierley, G. J. (1999). "Levee morphology and sedimentology along the lower Tuross River, south-eastern Australia." *Sedimentology*, 46(4), 627–648.
- Filgueira-Rivera, M., Smith, N. D., and Slingerland, R. L. (2007). "Controls on natural levee development in the Columbia River, British Columbia, Canada." *Sedimentology*, 54(4), 905–919.
- Fryirs, K. A., and Brierley, G. J. (2013). *Geomorphic analysis of river systems: An approach to reading the landscape*, Wiley, Chichester, U.K.
- Gabr, M. A., Taylor Jr., H. M., Brizendine, A. L., and Wolff, T. F. (1995). "LEVEEMSU: Analysis software for levee underseepage and rehabilitation." *Technical Rep. GL-95-9*, U.S. Army Engineer Waterways Experiment Station, Vicksburg, MS.
- Glynn, M. E., and Kuszmaul, J. (2010). "Prediction of piping erosion along middle Mississippi river levees—An empirical model." *Technical Rep. ERDC/GSL TR-04-12*, USACE, Vicksburg, MS.
- Harr, M. E. (1987). *Reliability-based design in civil engineering*, McGraw-Hill, New York.
- Hudson, P. F. (2011). "Natural levees." *Encyclopedia of water science*, 2nd Ed., S. W. Trimble, ed., Taylor and Francis Group, Boca Raton, FL, 763–767.
- Hudson, P. F., and Heitmuller, F. T. (2003). "Local and watershed scale controls on the spatial variability of natural levee deposits in a large fine-grained floodplain: Lower Pánuco Basin, Mexico." *Geomorphology*, 56(3–4), 255–269.

- ICOLD (International Commission on Large Dams). (2015). "Internal erosion of existing dams, levees, and dikes, and their foundations." *Internal erosion processes and engineering assessment*, Vol. 1, Paris, France.
- Kanning, W. (2012). "The weakest link." Ph.D. dissertation, Delft Technical Univ., Delft, Netherlands.
- Lane, E. W. (1935). "Security from under-seepage: Masonry dams on earth foundation." *Transactions*, 100, 1235–1272.
- Leopold, L. B., and Wolman, M. G. (1957). "River channel patterns: Braided, meandering and straight." U.S. Geological Survey, Washington, DC, 39–84.
- Low, B. K. (2008). "Reliability of levee systems." *Reliability-based design in geotechnical engineering*, K.-K. Phoon, ed., Taylor and Francis Group, New York, 134–168.
- Mjøs, R., Walderhaug, O., and Prestholm, E. (1993). "Crevasse splay sandstone geometries in the Middle Jurassic Ravenscar group of Yorkshire, U.K." *Alluvial sedimentation*, M. Marzo and C. Puigdefabregas, eds., Blackwell Scientific, Oxford, U.K., 167–184.
- Nanson, Gerald C. (1980). "Point bar and floodplain formation of the meandering Beatton River, northeastern British Columbia, Canada." *Sedimentology*, 27, 3–29.
- Nanson, Gerald C. (1981). "New evidence of scroll-bar formation on the Beatton River." *Sedimentology*, 28(6), 889–891.
- Palisade Corporation. (2013). "Integrated excel program that performs risk analysis using Monte Carlo simulation." Ithaca, New York.
- Pearce, J. T., Marlow, D., Avila, C., and Selvamohan, S. (2009). "Use of geomorphic and airborne geophysical data for analysis of levees and floodplain processes for levee evaluations in California." *ASFPM Annual Conf.*, Association of State Floodplain Managers, Orlando, FL.
- Pearce, J. T., Sowers, J. M., Brossy, C., and Kelson, K. (2010). "Surficial geology of the northern Sacramento—San Joaquin Delta, recognizing deposits, landforms, and sedimentary environments and their relevance to science and engineering." *San Francisco (California) Bay-Delta Science Conf.*, San Francisco.
- Polanco, L., and Rice, J. D. (2014). "A reliability-based evaluation of the effects of geometry on levee underseepage potential." *Geotech. Geol. Eng.*, 32(4), 807–820.
- Rice, J. D., and Polanco, L. (2012). "Reliability-based underseepage analysis in levees using a response surface-Monte Carlo simulation method." *J. Geotech. Geoenviron. Eng.*, 10.1061/(ASCE)GT.1943-5606.0000650, 821–830.

- Ritter Dale, F., Kochel, R. C., and Miller, J. R. (2011). *Process geomorphology*, 5th Ed., Waveland Press, Long Grove, IL.
- Saucier, R. T. (1994). "Geomorphology and quaternary geologic history of the lower Mississippi Valley." U.S. Army Engineer Waterways Experiment Station, Vicksburg, MS.
- Shannon and Wilson. (2011). "Skagit river levee general investigation levee risk and reliability analysis." USACE, Washington, DC.
- Sleep, M., and Duncan, M. J. (2014). "Manual for geotechnical engineering reliability." *Rep. No. 76*, Virginia Tech Center for Geotechnical Practice and Research (CGPR), Blacksburg, VA.
- Smith, N. D., and Pérez-Arlucea, M. (2008). "Natural levee deposition during the 2005 flood of the Saskatchewan River." *Geomorphology*, 101(4), 583–594.
- Steenbergen, H. M. G. M., Lassing, B. L., Vrouwenvelder, A. C. W. M., and Waarts, P. H. (2004). "Reliability analysis of flood defence systems." *Heron*, 49(1), 51–73.
- SVFlux* [Computer software]. SoilVision Systems, Saskatoon, SK, Canada.
- Temmermana, S., Goversa, G., Meireb, P., and Wartel, S. (2004). "Simulating the long-term development of levee-basin topography on tidal marshes." *Geomorphology*, 63(1–2), 39–55.
- Terzaghi, K. (1929). "Effect of minor geologic details on the safety of dams." *Am. Inst. Min. Metall. Eng.*, 215, 31–46.
- USACE (U.S. Army Corps of Engineers). (1956). "Investigation of underseepage and its control." *Technical Memorandum No. 3-424*, U.S. Army Engineer Waterways Experiment Station, Vicksburg, MS.
- USACE (U.S. Army Corps of Engineers). (2000). "Design and construction of levees." *Engineering Manual EM 1110-2-1913*, Washington, DC.
- Vrouwenvelder, A. C. W. M., Van Mierlo, M. C. L. M., Calle, E. O. F., Markus, A. A., Schweckendiek, T., and Courage, W. M. G. (2010). "Risk analysis for flood protection systems." Deltares, Netherlands.
- Vrouwenvelder, T. (2006). "Spatial effects in reliability analysis of flood protection systems." *Proc., 2nd Int. Forum Engineering Decision Making*, Technical Univ. of Denmark, Lyngby, Denmark, 1–12.

- Walling, D. E., Fang, D., Nicholas, A. P., and Sweet, R. J. (2004). "The grain size characteristics of overbank deposits on the floodplains of British lowland rivers." *Proc., Int. Symp. Sediment Transfer through Fluvial System, International Association of Hydrological Sciences, U.K.*, 226–234.
- Walling, D. E., Owens, P. N., and Leeks, G. J. L. (1997). "The characteristics of overbank deposits associated with a major flood event in the catchment of the River Ouse, Yorkshire, UK." *Catena*, 31(1–2), 53–75.
- William Lettis and Associates, Inc. (2008). "Surficial geologic map and initial geomorphic assessment, Sacramento River (east side), Sacramento County, California." Sacramento, CA.
- Wolff, D. (2008). "Reliability of levee systems." *Reliability-based design in geotechnical engineering*, K.-K. Phoon, ed., Taylor and Francis Group, New York, 448–496.
- Wolff, T. F. (1989). "LEVEEMSU: A software package designed for levee underseepage analysis." *Technical Rep. GL-89-13*, U.S. Army Engineer Waterways Experiment Station, Vicksburg, MS.
- Wolff, T. F. (1994). "Evaluating the reliability of existing levees." U.S. Army Engineer Waterways Experiment Station, Michigan State Univ., East Lansing, MI.
- Wolff, T. F., Demsky, E. C., Schauer, J., and Perry, E. (1996). "Reliability assessment of dike and levee embankments." *Uncertainty in the geologic environment: From theory to practice*, ASCE, Reston, VA, 636–650.
- Woolfe, Ken J., and Purdon, Richard G. (1996). "Deposits of a rapidly eroding meandering river: terrace cut and fill in the Taupo Volcanic Zone." *N. Z. J. Geol. Geophys.*, 39(2), 243–249.
- Xu, B., and Low, B. K. (2006). "Probabilistic stability analyses of embankments based on finite-element method." *J. Geotech. Geoenviron. Eng.*, 10.1061/(ASCE)1090-0241(2006)132:11(1444), 1444–1454.



CHAPTER 5  
THREE DIMENSIONAL UNDERSEEPAGE ASSESSMENT OF HIGH  
CONDUCTIVITY CHANNELS WITHIN A LEVEE SYSTEM

**Abstract**

High-conductivity abandoned channels such as cross-channels and chute cut-offs are among the most common geomorphic features found in a meandering river geomorphic environment, and thus commonly intercept the alignments of a levee systems. Unfortunately, due to the complexity of a levee foundation's stratigraphic geometry and limitation of common analysis methods for assessing internal erosion safety, levee foundation stratigraphy is often simplified in order to accommodate the limitations of these methods. As a result, the effects of geomorphic features intercepting the levee alignment are often overlooked. Incorporating geomorphic features into underseepage analyses is important since they serve as preferred pathways for internal erosion initiation either by concentrating or blocking seepage flow. This paper presents a formulation for assessing the effects of high-conductivity channels crossing a levee alignment on the internal erosion hazard potential using a response surface–Monte Carlo (RSMC) simulation method. The RSMC method utilizes three-dimensional steady-state finite-element underseepage analyses to develop a response surface representing the relationship between soil properties and the three-dimensional levee foundation. The response surface then serves as the driving function for reliability analyses by means of Monte Carlo simulation analyses, resulting in cumulative probability functions for either hydraulic exit gradient or factor of safety

against heave. These computed probability functions represent an assessment of conditional probability of initiation of internal erosion. The analysis of an abandoned (cross) channel found in the Sacramento River (east side) levee system in California is presented as an application example.

### **5.1. Introduction**

Levee systems are unique structures usually built upon a foundation of soils deposited by a river that meandered across a flood plain. Levees are also unique in the sense that they are generally very long structures. Due to these unique characteristics, levee foundations can be highly variable as their alignments cross the various depositional features of the fluvial geology. Often the variation is due to identifiable geomorphic features laid down by the various fluvial processes of the meandering river system, including: point bars, meander scrolls, cross channels, tributary channels, crevasse splays, and infilled oxbows.

As water seeps through the foundation soils underlying a levee the geomorphic features encased in the foundation have an effect on the resulting seepage pressures and gradients. Geomorphic features with high permeability allow water to flow with less resistance under the levee, resulting in higher hydraulic pressures on the landside. Water seeping toward the path of least resistance will tend to flow toward the high-permeability feature, resulting in a three-dimensional seepage flow phenomenon. Conversely, low-permeability features can block seepage flow, preventing the dissipation of hydraulic

pressures in the foundation and forcing seepage flows to the ground surface. This too, is a three-dimensional phenomenon.

Because geomorphic features tend to increase hydraulic gradients and pressures as described above, it can be concluded that the preponderance of the underseepage and internal erosion risk along a levee reach is due to the combined risk associated with the geomorphic features encountered beneath the levee alignment. Also, levee systems are often broken up into basins (or pollards) that are protected by a finite length of levee and, a failure of any portion of the levee leads to failure of the entire basin. The resemblance of a weak link in a chain is frequently used to exemplify this situation (Steenbergen et al. 2004, Vrouwenvelder 2006, Vrouwenvelder et al. 2010). Therefore, it can also be surmised that as the length of levee protecting a basin increases, so does the number of geomorphic features it is likely to cross and, in general, as the length of a reach of levee increases, the likelihood of failure also increases; a phenomenon often referred to as a *length effect* (Bernitt and Lynett 2010, Vrouwenvelder et al. 2010, Shannon and Wilson 2011, Bowles et al. 2012, Kanning 2012).

Addressing the hazard that these individual geomorphic features impose on the internal erosion process of the levee is instrumental in assessing the length-effect phenomenon. The interactive hydraulic behavior between these features, the structure, and the surrounding characteristic subsurface profile is characteristically three-dimensional, concentrating seepage flow into the geomorphic feature and decreasing flow in the surrounding area (or vice versa if the feature represents a seepage block). Therefore, is the goal of this research to develop a three-dimensional, steady-state methodology for

assessing the reliability with respect to internal erosion in a system of levees protecting a basin underlain by geomorphic features. Even though the general methodology can be applied to a vast arrange of geomorphic features, this paper focuses on high-conductivity abandoned channels point bars and meander scrolls since their hydraulic behaviors are similar. It is also acknowledged that the curvature of the levee alignment may also have an effect on the resulting hydraulic pressure and flow regime, however, this phenomenon is discussed in a separate paper.

## **5.2. Typical levee subsurface characteristics**

Meandering rivers are characteristic of a sinuous plan view (Leopold and Wolman 1957). Usually, the depositional environment of meandering rivers is depicted by alluvial deposits and flood (overbank) deposits (Leopold and Wolman 1957, Brierley and Fryirs 2005). Alluvial deposits are typically granular and tend to become finer in the upward direction (Walling et al. 1997, Walling et al. 2004, Filgueira-Rivera et al. 2007, Smith and Pérez-Arlucea 2008, Ritter et al. 2011). Overbank deposits, consisting of finer grained materials deposited when flood waters exit the river channel usually overlay the alluvial deposits (Walling et al. 2004, Ritter et al. 2011). Natural levees are features near the river bank characterized by low ridges parallel to the river bank that gradually thin laterally (Brierley et al. 1997, Cazanacli and Smith 1998, Ferguson and Brierley 1999, Hudson and Heitmuller 2003, Adams et al. 2004, Temmermana 2004, Smith and Pérez-Arlucea 2008, Hudson 2011, Ritter et al. 2011). In the engineering community, overbank deposits are

usually called the “blanket” layer whereas alluvial deposits are usually called the “foundation” layer (USACE 1956, 2000).

This resulting stratigraphy has a significant effect on the underseepage behavior below a levee alignment and associated internal erosion mechanisms. Due to the large difference in hydraulic conductivities between the foundation and blanket layers, little total head loss occurs in the foundation beneath the levee. Therefore, large pressures develop beneath the blanket layer on the landside of the levee leading to high gradients and uplift pressures. In some cases these large pressures may result in uplift and cracking of the blanket, concentrating flow into the defect and developing high gradients that result in sand boils or in a tragic blowout. (USACE 1956, Glynn and Kuszmaul 2010, Rice and Polanco 2012). Along with the general depositional stratigraphy composed of the blanket and foundation layers, geomorphic features shape the flood plain and intercept the alignment of man-made levees.

### **5.3. Geomorphology of high conductivity channels**

Abandoned channels (also known as paleo-channels) are river or tributary channels that were once active (see Figure 5.1). Soil composition of abandoned channels are found to vary in the flood plain; some may be infilled by overbank deposits (such as neck cut-offs and oxbows) while others (such as chute cut-offs) are usually infilled with coarse-grained deposits (USACE 1956, Bridge 2003, Brierley and Fryirs 2005, Fryirs and Brierley 2013). Within this paper, abandoned channels that represent high-conductivity channels, like cross channels and chute cut-offs, are of interest while low-conductivity channels are

currently under ongoing research and their importance as potentially hazardous geomorphic features along a levee alignment will be presented in another paper. Chute channels are formed within the river system while trying to approach its need of efficiency by short-cutting the sinuous alignment with a relative straight channel (Brierley and Hickin 1992). With time, flow increases in the chute channel and due to the general cut and fill mechanism of the river, the end boundaries of the old curved channel plug and it is cut-off from the main river system (USACE 1956, Bridge 2003). This cut-off is referred to as a chute cut-off. It is also believed that chute cut-offs occur as an effect of meander scroll formation when the chute channel arcuates within its alignment forcing the old channel to become abandoned (McGowan and Gardner 1970, Brierley and Hickin 1992, Bridge 2003). The stratigraphic composition of chute cut-offs might also represent a point of concentrated seepage flow or local blanket thinning that locally increases the potential for internal erosion within the levee alignment.

Besides how the high conductivity channel's stratigraphy might concentrate or block seepage flow near the levee toe alignment, the location and/or orientation of the feature channel to the levee toe alignment might also be of relevance. USACE (1956) reports that among the Mississippi river levees, where high conductivity channels are encountered angled to the levee alignment, heavy underseepage and sand boils usually occurred along the respective levee reach. Glynn and Kuszmaul (2010) also state that the orientation at which high conductivity channels intercept the levee, might affect where internal erosion occurs. Kolb (1975) found that the most severe cases of internal erosion were present where high conductivity channels intercept the levee alignment at an acute

angle or parallel to the levee. Using a geotechnical GIS database related to piping and seepage analysis, Wilson (2003) and Glynn and Kuszmaul (2010) performed GIS analyses and confirmed that higher potential of internal erosion occur where high conductivity channels run parallel to the levee alignment due to the short distance among the feature and the levee toe.

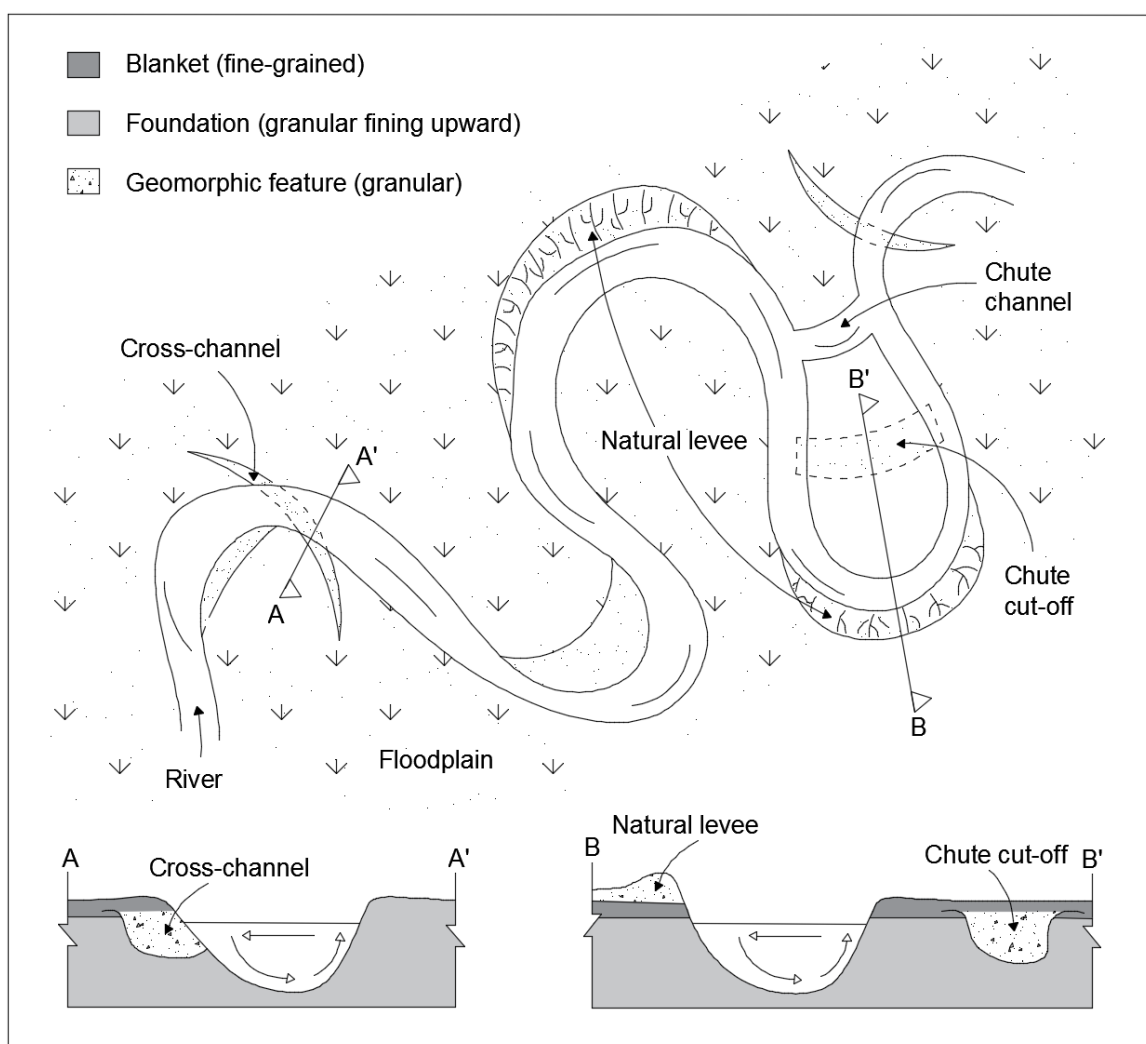


Figure 5.1. Different types of high-conductivity channels found around a meandering river environment.

#### 5.4. Deterministic and probabilistic underseepage analysis methods

The term internal erosion has been accepted as a generic term to describe erosion of particles by water passing through a body of soil or rock (ICOLD 2015). This paper has adopted the International Committee on Large Dams (ICOLD) nomenclature which describes the various mechanisms of internal erosion. Underseepage occurs when a differential hydraulic head forces water through the foundation soils or bedrock beneath a structure such as a dam or levee (CIRIA 2013). Since this research study is interested in analyzing the geometry of levee foundation due to the soil configuration in the foundation (see Figure 5.1), the failure mechanism considered is backward erosion piping (BEP). BEP describes the erosion of soil due to seepage flow through a soil mass that initiates when particles of soil are dislodged from the soil matrix at an unprotected seepage exit point (ICOLD 2015). As BEP continues, a pathway or “pipe” is formed by progressive erosion at the upstream end of the erosion void. As described by Vrouwenvelder et al. (2010), the authors believe BEP is often preceded in levee foundations by the heave mechanism, wherein the blanket layer is uplifted due to underlying hydraulic pressure or seepage forces. Heave results in a defect in the blanket (crack) that provides an unprotected seepage exit area for BEP to occur. Both heave and BEP mechanisms can contribute to the potential for internal erosion beneath a levee and therefore both mechanisms are included in the assessments presented herein.

In levees, the potential for BEP initiation is usually analyzed by comparing resisting forces to driving forces. These methods result in a ratios or factors of safety. The most common factors of safety against BEP are ( $F_{bep}$ ) and factor of safety against heave ( $F_{heave}$ ).



The resisting force relevant to the computation of the  $F_{bep}$  is called critical gradient (Terzaghi 1922). The critical gradient ( $i_c$ ) is computed based on the ratio of the buoyant unit weight of the soil to the unit weight of the water. The respective driving force is called the hydraulic exit gradient ( $i_{blanket}$ ) computed as shown in Eq. 1. With respect to the computation of the  $F_{heave}$ , the resisting force is based on the weight a layer of soil lays on another to counteract the driving force of the water trying to seep through it. The computation of the  $F_{heave}$  is presented as Eq. 2.

$$F_{bep} = \frac{i_c}{i_{blanket}} = \frac{\frac{\gamma_{buoy}}{\gamma_w}}{\frac{\Delta h}{t_b}} = \frac{\frac{(\gamma_{blkt} - \gamma_w)}{\gamma_w}}{\frac{h_{max}}{t_b}} \quad (1)$$

$$F_{heave} = \frac{t_b \gamma_{bl}}{u_{splay}} = \frac{t_b (\gamma_{blkt})}{(h_{max} + t_b) \gamma_w} \quad (2)$$

Usually, these factors of safety can be computed by assessing the hydraulic conditions using either empirical equations or finite-element analyses. The blanket theory (BT) equations are steady state theoretical relationships that compute seepage flow beneath levees (USACE 1956). They are commonly used in the United States and were developed by the U.S. Army Corps of Engineers (USACE) (USACE 2000). The blanket theory equations calculate the head at the base of the blanket layer that can be used to calculate either a gradient through the blanket or an uplift pressure beneath the blanket. Thus, the factor of safety can be calculated for either BEP or heave. Although the ease of assessing underseepage in levees using the BT equations is very reasonable, in many cases the simplifications needed to apply the BT equations results in an unrealistic oversimplification of the subsurface geology. In general, the levee subsurface is restricted to two homogenous

layers of constant thickness with no place for geomorphic features to be included except on the cases of seepage block or open seepage exit. Among finite-element analysis programs are LEVEEMSU (Wolff 1989, Gabr et al. 1995), CSEEP (Knowles 1992, Tracy 1994) and Slide (Rice and Polanco 2012, Polanco and Rice 2014) and SVFlux (Polanco-Boulware and Rice 2016). Finite-element analyses programs are powerful tools that have enabled the analysis of complex levee sections by allowing a more accurate representation of the geology encountered in the levee stratigraphy.

Since levees are prone to variable subsurface geometry and soil parameters, it is logical to analyze underseepage failure mechanism by means of a probabilistic approach. One common approach used in the United States is using the blanket theory equations as the performance function and the first-order second-moment (FOSM) Taylor series method as the probability model (Wolff 1994, Crum 1996, Wolff et al. 1996, Wolff 2008). This methodology is subject to the same limitations as the blanket theory; that is, it works well for simple profiles cannot model the complex subsurface conditions. Also, since it's a two-dimensional approach, it's not feasible to account for the three-dimensional aspects often associated with the interaction of the levee and surrounding geomorphic features.

Based on the hypothesis that the majority of the underseepage hazard along a levee comes from discrete subsurface geomorphic features that interrupt the characteristic profile, Rice and Polanco (2012) and Polanco and Rice (2014) have developed steady state two-dimensional models for assessing hydraulic conditions in geometrically complex levee profiles using what they call the Response Surface-Monte Carlo (RSMC) method. Rice and Polanco (2012) describe the differences within methods and present detailed steps of the

RSMC method by means of the analysis of two hypothetical complex levee profiles. Polanco and Rice (2014) presents the comparison of eight hypothetical levee profiles where six of these studies are analyzable using both the FOSM-BT and RSMC methods and the other two are beyond the capabilities of the FOSM-BT method and are only analyzed with the RSMC method (as presented in Rice and Polanco 2012). Where the BT is applicable, the difference between methods is minor but generally tends to increase with increasing model complexity. In both papers regression analyses are performed in order to assess the relative effects that changes in the input parameters have on the results with the conclusion that in most cases geometric parameters have the greatest effect on the results.

### **5.5. Response Surface Monte Carlo simulation (RSMC) method**

The steady state RSMC methodology uses multiple finite element analyses to develop a relationship between the key input parameters (hydraulic conductivity and unit weight of the soil layers and subsurface geometry of the soil layers) and the probability of reaching critical hydraulic conditions (uplift pressures or hydraulic exit gradients) given a loading condition (such as the water level associated with a flood with an annual exceedance probability of 1% or the 100-year flood level). This relationship, generally called a Response Surface (Xu and Low 2006, Low 2008), is used to perform a Monte Carlo simulation that results in a Cumulative Ascending Distribution Function (CADF - a plot of increasing values of a key parameter versus the probability of the parameter being less than that value) of the key hydraulic parameters controlling the potential for initiation of internal erosion; that is hydraulic pressure beneath a clay blanket or hydraulic exit

gradient. The range and probability distribution for each soil or geometric input parameters are represented using a probability density function (PDF).

Since Rice and Polanco (2012) and Polanco and Rice (2014) concluded that, in most cases, geometric parameters may have the greatest effect in the outcome of underseepage analysis, it was of interest to expand the methodology to account for the three dimensional seepage aspects of individual geomorphic features. Therefore, Polanco-Boulware and Rice (2016) present a steady state three-dimensional RSMC methodology applied to a crevasse splay geomorphic feature for calculating the probability of initiation of erosion due to underseepage. Crevasse splays form in association with the natural levee and represent a concentrated pathway to a layer of sand within the blanket, resulting in elevated potential for internal erosion. Since the methodology presented was developed to be used among any individual geomorphic feature (and not just for crevasse plays), it will be used herein to account for the underseepage reliability of high conductivity channels.

Steps for the RSMC are as follow:

1. Identify soil and geometric parameters with the aid of geological maps and published studies or reports,
2. Develop PDFs for soil and geometric parameters,
3. Develop a general three-dimensional model with the identified key soil and geometry input parameters,
4. Perform parametric analyses using the general three-dimensional model,

5. Simplify the general model to reduce the number of input parameters in the response surface based on the parametric analyses while using values of the developed PDFs,
6. Verify the simplified model for consistency with the general model with values of the developed PDFs by means of parametric analyses,
7. Develop response surface by means of multiple three-dimensional finite-element analyses using the simplified model,
8. Fit response surface to curves developed through regression analysis to facilitate computer coding,
9. Write an Excel spreadsheet to randomly select values of key parameters from input PDFs and apply the response surface to produce the output CADFs taking into account curvature of levee if present.

### **5.6. Reliability assessment of high conductivity channels**

For the purpose of this research study, the Sacramento River Levee system in California is used as an application example. A sample map of the east side of the Sacramento River Levee system showing a close-up of a historical abandoned (cross) channel is shown as Figure 5.2. Geometric data was collected based on geological maps and reports prepared along the east side of the Sacramento River Levee system (Knight 1955, Pearce et. al. 2009, William Lettis and Associates 2008). Furthermore, the measurements were assisted by studies from the Mississippi River levees (USACE 1956, Saucier 1994, Farrel 1987) that also present vast high-conductivity channels in its

meandering river environment. Soil data was also collected based on the same reports and with the aid of published work (Harr 1987, Baecher and Christian 2003, Sleep and Duncan 2014).

### 5.6.1. Identification of parameters and development of model

For ease of modeling, it could be generalized that abandoned channels can be represented by a four size polygon (i.e. a rectangle) within a finite-element model. Chutes and cross-channels usually intercept the levee alignment (no matter if it's curved or straight) in an angle and share similar geometric and soil characteristics. Therefore, a general three-dimensional model is used to represent these geomorphic features.

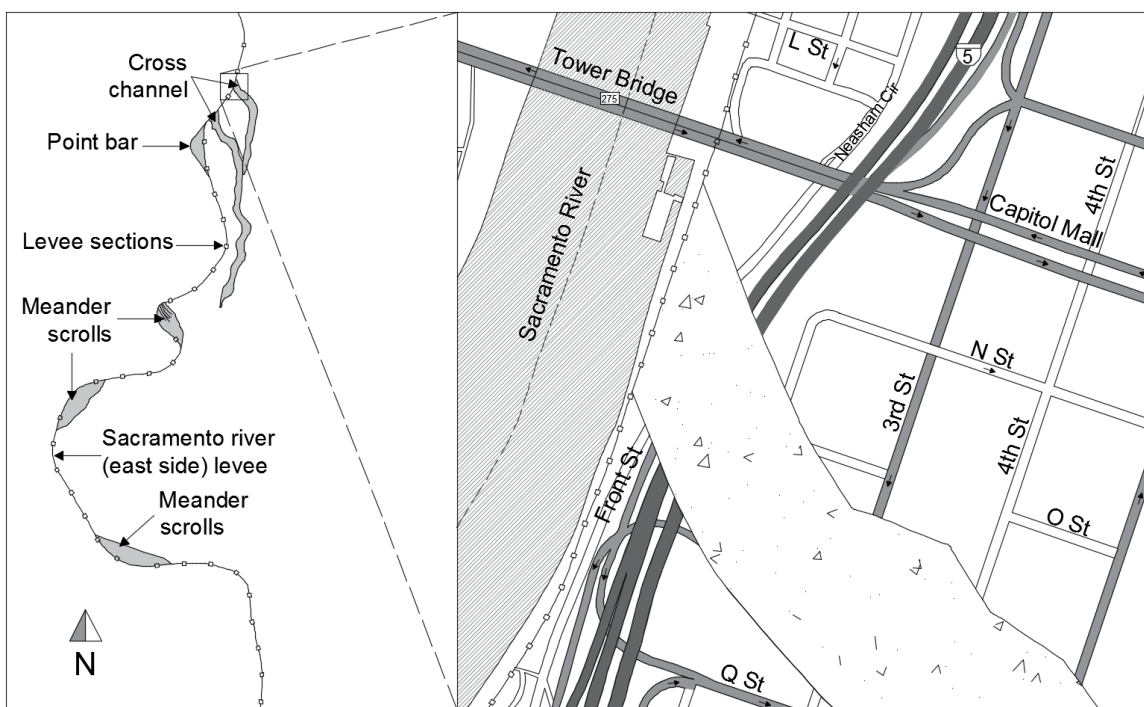


Figure 5.2. Major high conductivity channels that intercept the Sacramento River (east side) levee system showing a close up of the location of an abandoned (cross) channel.

Parametric analyses were performed on this model to understand the underseepage behavior based on the geometric and soil variability. Figure 5.3 presents the general model used to analyze high conductivity (abandoned) channels. Geometric parameters range from thickness ( $t_{ch}$ ), width ( $w_{ch}$ ), and angle of incision of the bar feature ( $\alpha$ ), thickness of the overlaying blanket and the foundation layers ( $t_b$  and  $t_f$ , respectively), and the length of the blanket layer on the riverside ( $RL$ ). Soil parameters are the hydraulic conductivity of the bar feature, the blanket and foundation layers ( $K_{ch}$ ,  $K_b$ ,  $K_f$ , respectively) and the anisotropy ratio of the bar (ratio of the horizontal to vertical hydraulic conductivities,  $K_{hv}$ ). Parametric analyses were performed to assess which parameters have a significant effect on the underseepage analysis outcome and which parameters could be eliminated based on having an insignificant effect.

Table 5.1 presents the range of values used for modeling and presents which parameters have a significant and insignificant effect on the outcome. The hydraulic head at the bottom of the blanket layer overlying the channel was considered as the critical output parameter of the analyses and was used for computing either the  $i_{blanket}$  or the  $F_{heave}$ . The width of the channel ( $w_{ch}$ ) was found to have little effect on the resulting hydraulic head and, thus was eliminated from the response surface model.

Unless the thickness of the foundation ( $t_f$ ) is modeled to be very thin, which is unlikely, it has an insignificant effect on the underseepage behavior and thus, was eliminated. In contrast, the angle of incision of the channel ( $\alpha$ ) was found to affect the underseepage analysis outcome. This is in agreement with Kolb (1975) who reported, acute angles were found to have a higher effect on the underseepage regime.

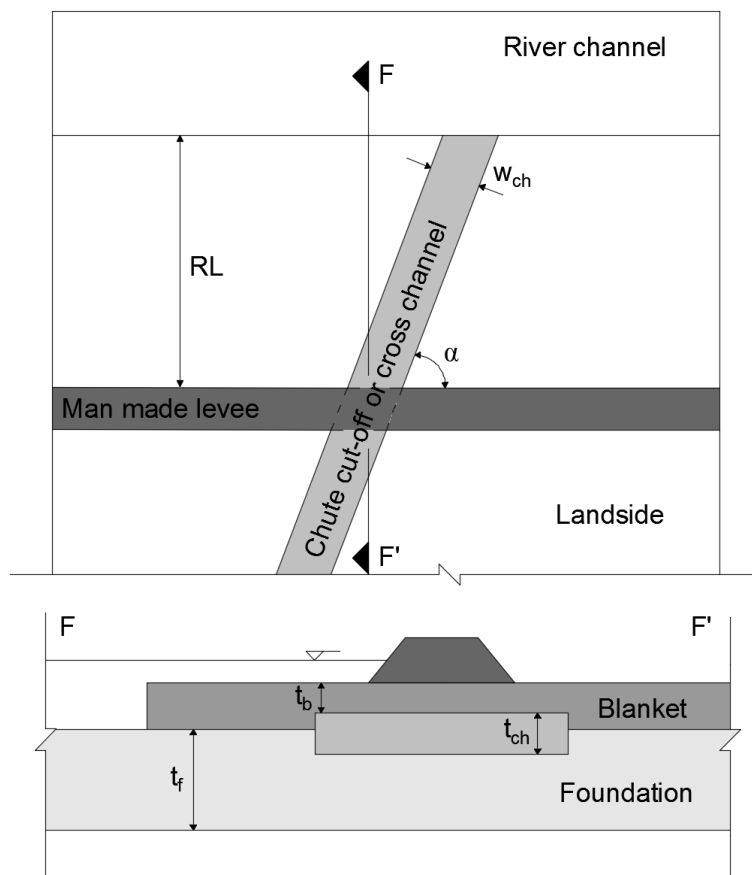


Figure 5.3. Models used to analyze high conductivity channels.

Table 5.1. Range of values used for the parametric analyses of the general model

Parameter	Units	Values		Effect on the outcome
		Min	Max	
Width of channel ( $w_{ch}$ )	m	9.1	15.2	No
Thickness of the foundation ( $t_f$ )	m	18.3	33.5	No
Angle of incision of channel ( $\alpha$ )	°	0	90	Yes
Thickness of channel ( $t_{ch}$ )	m	1.5	6	Yes
Thickness of overlaying blanket ( $t_b$ )	m	0.6	6	Yes
Blanket layer river length (RL)	m	0	2000	Yes
Anisotropy ratio ( $K_{hv}$ )	-	0.1	1.0	No
Horizontal hydraulic conductivity of channel ( $K_{ch}$ )	cm/s	$3.0 \times 10^{-5}$	$3.0 \times 10^{-1}$	Yes
Horizontal hydraulic conductivity of blanket ( $K_b$ )	cm/s	$3.0 \times 10^{-8}$	$3.0 \times 10^{-6}$	Yes
Vertical hydraulic conductivity of foundation ( $K_f$ )	cm/s	$3.0 \times 10^{-5}$	$3.0 \times 10^{-3}$	Yes



The thickness of the blanket layer ( $t_b$ ) has an effect on the computation of the  $F_{heave}$  (see Eq. 2) and, therefore, the thinner the blanket layer was the higher the resulting  $F_{heave}$  was. The thickness of the channel and blanket layer were found to affect the underseepage behavior. With respect to the thickness of the channel ( $t_{ch}$ ), the variation does not seem to significantly affect the outcome as long as the thickness is considerably greater than the overlaying thickness of the blanket layer. If a channel with a very small thickness is encountered, the effect is negligible and the levee system acts more like a simple two-dimensional flow system. This scenario should be considered as a very small meandering deposit and not as a channel feature per se. Lastly, parametric analyses revealed that shorter blanket layer river lengths ( $RL$ ) resulted in higher hydraulic heads; thus  $RL$  is considered to have a significant effect in the outcome.

The anisotropy ratio of the channel (ratio of the horizontal to vertical hydraulic conductivities,  $K_{hv}$ ) was considered to be insignificant since it is assumed that flow (seepage) occurs predominantly unidirectional (horizontally) along the channel and head loss occurs vertically through the blanket layer. Despite this assumption, parametric analyses were performed and, it was confirmed that  $K_{hv}$  has low significance in the underseepage outcome.

The hydraulic conductivity of the channel ( $K_{ch}$ ) together with the hydraulic conductivity of the blanket layer ( $K_b$ ) and foundation layer ( $K_f$ ) affect the underseepage outcome. As  $K_b$  increases, more leakage occurs through the blanket layer decreasing the hydraulic head at the top of the channel. On the contrary, as  $K_f$  increases, less leakage occurs through the blanket layer increasing the hydraulic head at the top of the channel.

The effect of the  $K_{ch}$  is similar to the one produced by the  $K_f$ . Despite their individual effect, it seems that the effect of the hydraulic regime is driven by the interaction of the blanket and foundation layers with the channel feature. USACE (1956) has shown that this interaction can be represented as a function of the ratio of the hydraulic conductivities instead of their individual values.

In total, the general model is defined by ten parameters. Based on parametric analysis three of these parameters were not included in the probabilistic analyses since they were found to have low significance in the underseepage outcome analysis: the width of the channel ( $w_{ch}$ ), the thickness of the foundation ( $t_f$ ) and, the anisotropy ratio ( $K_{hv}$ ). The most likely value (MLV) is assigned to these parameters in the simplified model and variation of these parameters is not used to define the response surface. The rest of the parameters are used to develop the simplified model and eventually the response surface. To develop a feasible response surface the seven significant parameters are combined into three parameters that define the seepage flow behavior in the channel deposit: 1) the blanket layer river length, 2) the tongue effect, and 3) the modified leakage factor. The hypothesis behind the combination of this parameters is that flow travels from the riverside to the landside by means of the channel and leakage dissipates through the blanket layer overlaying the channel feature. The blanket layer river length ( $RL$ ) (see Figure 5.4) is treated as is and it takes into account how far the flow has to travel from the riverside to the levee. The 'tongue effect' ( $T_{ch}$ ), describes the interaction between the channel and underlying foundation layer and the angle of incision at which the channel intercepts the levee alignment. Following the angle of incision, the hydraulic conductivity ratio between

the channel and the foundation layer allows the flow to advance under the levee (from the riverside to the landside) faster than in the foundation. The analogy of a tongue comes due to the fact that most of the flow is concentrated within the angled channel providing a tongue shape (see Figure 5.4). When the flow reaches the levee and eventually the landside, it encounters a head loss due to the interaction of the channel and blanket layer.

In its study of underseepage behavior in the Lower Mississippi River levees, USACE (1956) provides an equation called ‘leakage factor’ ( $\lambda$ ) that describes the flow between the blanket and foundation layers. This concept can be applied to aid with the description of how easily the pressures in the channel dissipate through the blanket layer. For the purpose of this research study, this relationship is called the *modified* leakage factor ( $\lambda_m$ ). The combined parameters are calculated as presented in the following equations and schematically illustrated in Figure 5.4:

$$T_{ch} = \frac{K_{ch}}{K_f} \sin(\alpha) \quad (3)$$

$$\lambda_m = \sqrt{\frac{K_{ch} t_{ch} t_b}{K_b}} \quad (4)$$

### 5.6.2. PDF Development

A PDF describes the relative likelihood that a parameter takes on a given value. Identifying the parameters for the development of the model goes hand to hand with the development of the PDFs.

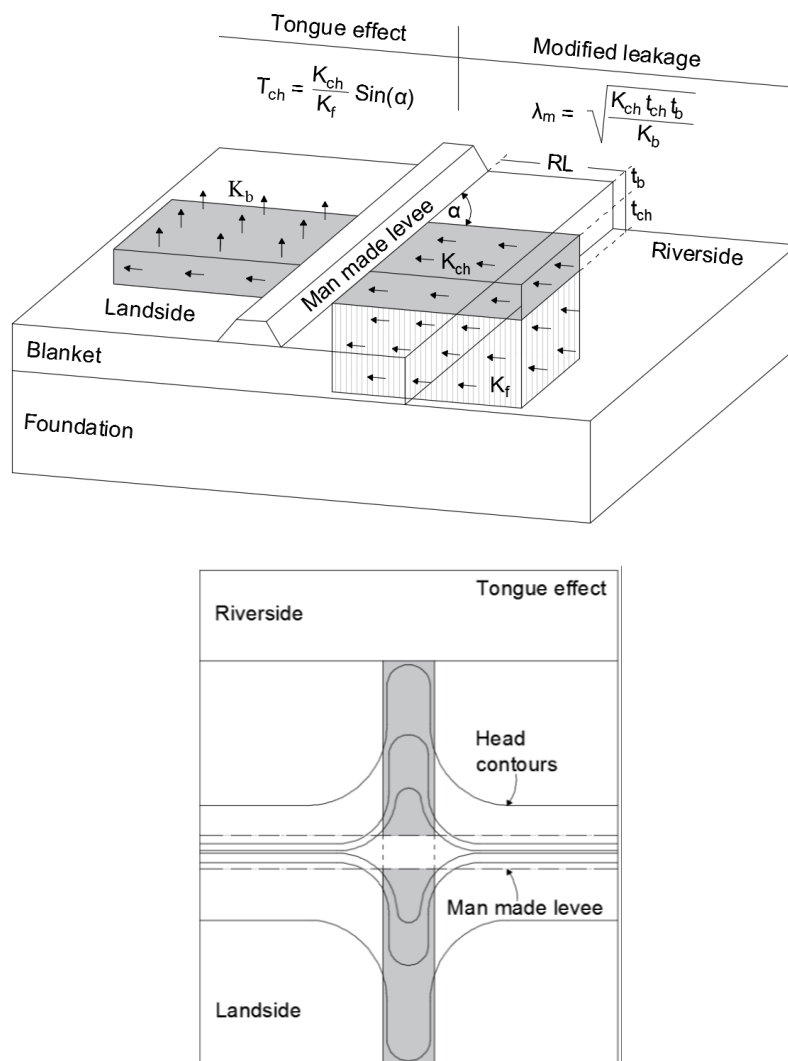


Figure 5.4. Combination of parameters for a high conductivity channel.

PDFs are estimated based on a limited number of laboratory tests, published guidance on probability distributions for similar soil types (Harr 1987, Sleep and Duncan 2014), and on geological maps as those mentioned above. The precision of the values selected for the PDFs will vary depending on the amount of data available for each geomorphic feature.

ArcMap (GIS) is a powerful tool that can be used to develop some geometric PDFs (parameters) of geomorphic features such as the angle of incision ( $\alpha$ ) and blanket layer river length ( $RL$ ). For the development of the  $RL$ , the levee alignment was divided into 500 m levee sections (as presented in Figure 5.2) with the purpose of acquiring enough data points (i.e. levee sections) that could be considered as statistically significant (greater than 30 data points). An attribute table (tabular information that allows visualization and analysis of data in GIS) that represents levee toe points with respective proximate river length points was created within each levee (data point) section. Nearest distance between points was calculated by means of a geoprocessing proximity tool. The resulting tabular data was fitted to a PDF distribution using a distribution fitting tool in @Risk (Palisade 2013).

@Risk is a program that interfaces with Excel where powerful statistical analysis can be performed in a very easy and flexible manner. @Risk provides simultaneous fittings allowing the user to choose the appropriate distribution for the purpose of the model. Based on the data, a lognormal distribution was determined to be the best fit for the  $RL$  parameter.

Alternatively, high conductivity channels that intercept the Sacramento River Levee System were identified for the development of the  $\alpha$  parameter PDF. A unique central data point was assigned to each channel to measure the angle between the feature and the levee alignment. Several angles per channel were measured and recorded as tabular data in GIS with the purpose of fitting the data as done for the  $RL$ . A normal distribution was determined to be the best fit for the  $\alpha$  parameter. Based on the data, @Risk provides

the parameters necessary to represent the fitted distributions (i.e. MLV and standard deviation).

### 5.6.3. Validation of simplified model

To verify the validity of the simplified model, results from the original model should be reasonably close to the general model results. Therefore, comparative parametric analyses were performed in which individual parameters in the simplified model are varied independently of the remaining parameters. The results from these parametric analyses are compared with those of the original model. Table 5.2 shows results of one simplified model using MLVs with 6.71m (22 ft) of differential head across the levee.

Table 5.3 presents the results of the comparative parametric analyses performed using a model with 6.71m (22 ft) of differential head across the levee. As mentioned, the hydraulic head at the bottom of the blanket layer overlying the channel was considered as the criteria of interest for all the parametric analyses. For ease of computation, the zero head datum is set as the landside ground surface elevation.

Table 5.2. Results of one simplified flow model using MLVs

<b>Description</b>	<b>Parameter</b>	<b>Result</b>
Resulting combined parameter from flow model	$RL$ (m)	15.5
	$T_{ch}$	39.1
	$\lambda_m$ (m)	373.4
Flow model results at levee toe	Head at top of the channel (m)	5.37
	$i_{blanket}$	1.17
	$F_{heave}$	0.88

The first column presents the combined parameters that make up the simplified models. The second column presents the dependent parameters (those that are constituents of the respective combined parameter) that are held constant during the respective parametric analyses. The third column presents the independent parameters (those that are not constituents of the respective combined parameter) that are held constant during the analysis. Columns 4 and 5 respectively present the dependent and independent parameters that are varied in the respective parametric analysis. Finally, the maximum amount of variation resulting from each analysis is presented in the final column. The numbers in the final column represent the largest variation that occurs with variation of the parameters listed in columns 4 and 5. Thus, if the simplified model perfectly matched the model with all parameters used the values in the final column would all be zero.

As can be observed from Table 5.3, the maximum variation resulting from using the simplified model is less than 0.30 m (1 ft) of total head for all but one parameter. Furthermore, most of the variation that is observed occurs when using values at the ends of PDF distributions where the probability of occurrence is very low relative to the values in the center of the distribution. Therefore, it can be concluded that the simplified model reasonably approximates the general model. The analyses performed for the table represent the full range of values we deemed reasonable for each parameter based on reviews of literature and high conductivity channel features located at geologic maps and therefore represent a reasonable range for all high conductivity channels in a meandering river environment.

Table 5.3. Results of parametric analysis to assess the validity of the simplified flow model for the high conductivity channel response surface

Combined Parameter for RS	Constant Parameters		Varied Parameters		Max. variation in resulting head (m)
	Dependent	Independent	Dependent	Independent	
Tongue effect, $T_{ch}$		$t_b, t_{ch}, RL$		$K_b$	0.00
		$t_{ch}, K_b, RL$		$t_b$	0.09
	$\alpha$	$t_b, RL$	$K_{ch}, K_f$	$K_b, t_{ch}$	0.00
		$K_b, RL$		$t_{ch}, t_b$	0.10
		$t_{ch}, t_b$		$RL, K_b$	0.00
	$K_{ch}$	$t_b, t_{ch}, RL$	$K_f, \alpha$	$K_b$	0.05
		$K_{ch}, K_b, t_{ch}, t_b$		$RL$	0.29
	$K_f$	$t_b, t_{ch}, RL$	$K_{ch}, \alpha$	$K_b$	0.28
		$t_{ch}, t_b$		$RL, K_b$	0.58
	Modified leakage factor, $\lambda_m$	$t_b, t_{ch}$	$\alpha, RL$	$K_{ch}, K_b$	$K_f$
		$\alpha$		$RL, K_f$	0.00
$t_b, K_b$		$\alpha, RL$	$t_{ch}, K_{ch}$	$K_f$	0.02
		$\alpha$		$RL, K_f$	0.22
$t_{ch}, K_b$		$\alpha, RL$	$t_b, K_{ch}$	$K_f$	0.02
		$\alpha$		$RL, K_f$	0.17
$t_b, K_{ch}$		$RL, K_f$	$t_{ch}, K_b$	$\alpha$	0.04
		$K_f, \alpha$		$RL$	0.07
$t_{ch}, K_{ch}$		$RL, K_f$	$t_b, K_b$	$\alpha$	0.02
		$K_f, \alpha$		$RL$	0.14
		$RL, K_f$		$\alpha$	0.03
$K_{ch}, K_b$		$K_f, \alpha$	$t_b, t_{ch}$	$RL$	0.15
	$K_f, RL$		$\alpha$	0.03	

#### 5.6.4. Development of response surface

Using the simplified model and the combined parameters identified above ( $T_{ch}$ ,  $\lambda_m$ ,  $RL$ ), the response surface was generated for the channel geomorphic feature using multiple



runs of a three-dimensional finite element analysis. The ranges of values for the three combined parameters represent the ranges of the possible values resulting from variation of the original parameters of the model over their respective PDFs. These range of values are shown in Table 5.4. The possible range of each combined parameter was discretized into 5 to 6 values to represent the variation of the parameter.

Finite element analyses were then performed on every possible combination of the discretized values for each combined parameter using a 3-D finite element model (SoilVision Systems Ltd.- SVFlux).

Table 5.4. Parameters used for development of the high conductivity channel response surface

Constant		Varied				Combined	
Parameter	Value	Parameter	Value	Parameter	Value	Parameter	Value
$\alpha$ (°)	45		4.31E-02		1.50		115
<b>Not in Response Surface</b>			3.05E-02		3.00		162
			2.42E-02		1.50		256
		$t_f$ (m)	25.00	$K_{ch}$ (cm/s)	1.71E-02	$t_{ch}$ (m)	3.00
$w_{ch}$ (m)	9		9.64E-03		3.00		397
$K_f$ (cm/s)	3.05E-04		3.05E-03		4.60		444
			9.64E-04		6.10		513
			3.05E-04		-		-
Note: $t_f$ , $w_{ch}$ and $K_f$ were not used for the development of the family of curves but were needed for the development of the model as explained in the manuscript			3.05E-06		0.60		100
			2.16E-06		0.60		71
			1.71E-06		3.00		56
			1.21E-06		2.10		40
			6.82E-07	$t_b$ (cm/s)	3.70	$T_{ch}$	22
			2.16E-07		3.00		7
			6.82E-08		3.00		2
	2.16E-08		-		1		

The results of the analyses were plotted on a “family of curves” that together represent a four-dimensional surface that defines the relationship between the three combined parameters and the maximum total head in the high conductivity channel. One of the family of curves is presented in Figure 5.5. Notice that in Figure 5.5, number subscripts are added for certain parameters to denote the different discretized values used along the corresponding PDFs. The full family of curves (response surface) with its corresponding equations can be found in the ‘Supplemental Data’ section and, as mentioned, can be used beyond the context of the current application example and applied to high conductivity channel deposits in other levee reaches and other river systems. Thus, given values of each of the combined parameters, the value of the maximum total head in the channel can be calculated using the response surface.

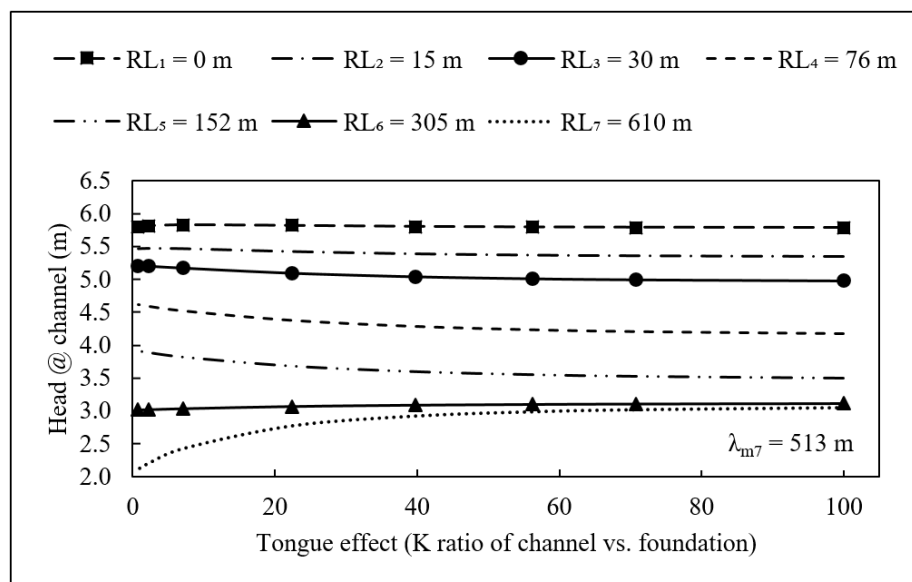


Figure 5.5. Family of curves for the high conductivity channel model for one constant  $\lambda_m$  and different ranges of  $RL$  and  $T_{ch}$ .

Equations were developed through regression analysis to fit the curves of the response surfaces to facilitate computer coding the response surface into a spreadsheet linked with the computer program @Risk which runs the Monte Carlo Simulation.

#### 5.6.5. RSMC analysis for high conductivity channel research case study

Figure 5.2 presents the interception of an abandoned (cross) channel to the Sacramento (east side) levee located near the Tower Bridge in the City of Sacramento. This geometric feature is used as a research case study to demonstrate the applicability of the RSMC methodology. PDFs that represent this geomorphic feature are presented in Table 5.5. These 7 parameters plus the unit weight of the blanket ( $\gamma_{blkt}$ ) are input parameters used in an Excel spreadsheet that is linked to the computer program @Risk which eventually performs a Monte Carlo analysis. @Risk is used since it does not require programing to perform a Monte Carlo analysis, it provides a wide range of distributions to choose as input, for the ease of sensitivity analysis and, for its flexibility handling the resulting data.

With respect to the PDFs, although the hydraulic conductivities of the channel and blanket layer are represented by normal distributions, in the actual analysis the antilog of the random normal values are taken for the calculations. Since the foundation layer should have a hydraulic conductivity less than or equal to the channel's hydraulic conductivity (due to the natural deposition of this particular geomorphic feature), the hydraulic conductivity of the foundation layer is estimated based on the ratio of the channel to foundation hydraulic conductivities. This ratio is represented by a normal distribution as shown in Table 5.5. In the actual analysis, the random generated value for the hydraulic

conductivity of the channel is divided by the hydraulic conductivity ratio of the foundation which provides a hydraulic conductivity of the foundation that satisfies the natural geologic assumption.

The maximum and minimum values provided in Table 5.5 are used to truncate the normal distributions to avoid numerical errors and unrealistic values outside the response surface. As similarly presented in Polanco-Boulware and Rice (2016), the sequence of iteration to compute the factor of safety against heave,  $F_{heave}$ , and the gradient through the blanket,  $i_{blanket}$ , are as follows:

1. Values of each of the 7 parameters (plus  $\gamma_{blanket}$ ) are randomly selected based on the PDF distributions.
2. These parameter values (except  $RL$  which is used as an independent parameter) are then combined into the two combined parameters using Equations 3 and 4.

Table 5.5. Input parameters for the PDFs used to develop the CADFs for the abandoned channel

Parameter	Units	Type of PDF distribution	Most likely value	Standard deviation	Truncated value	
					Min	Max
Thickness of the channel ( $t_{ch}$ )	m	Normal	3.0	0.6	1.5	6.1
Thickness of the blanket ( $t_b$ )	m	Normal	4.6	0.9	1.5	7.6
Angle of incision of channel ( $^\circ$ )	m	Normal	34	19.9	10.0	90
Blanket layer river length ( $RL$ )	m	Normal	18.0	27.4	4.0	392.0
Log of channel hyd. cond. ( $\log K_{ch}$ )	log(cm/s)	Normal	-2.5	2.5	-4.5	-2.5
Log of blanket hyd. cond. ( $\log K_b$ )	log(cm/s)	Normal	-6.5	2.5	-7.5	-5.5
Hydraulic conductivity channel to foundation ratio ( $K_{ch}/K_f$ )	-	Lognormal	70	30	1	140
Unit weight of the blanket ( $\gamma_{blanket}$ )	KN/m <sup>3</sup>	Normal	18.85	1.57	17.28	20.42

3. The two combined parameters ( $T_{ch}$  and  $\lambda_m$ ) and  $RL$  are then used with the response surface to calculate the maximum total head in the splay  $h_{max}$  (the zero head datum is set as the landside ground surface elevation).
4. Using the maximum head value, the key hydraulic parameters: gradient through the blanket,  $i_{blanket}$ , and the factor of safety against heave,  $F_{heave}$ , are calculated using Equations 1 and 2.

This sequence of 10,000 iterations results in the CADFs presented as Figures 5.6 and 5.7. For both CADFs, the conditional probability is presented in the y-axes whereas the x-axes present the randomly computed hydraulic criteria. The specific conditional probability of the hydraulic exit gradient exceeding the boundary value of 1.0 and the specific conditional probability of the factor of safety against heave not exceeding a boundary value of 1.0 are shown on the top of Figures 5.6 and 5.7 as  $P(i_{blanket} \geq 1.0) = 70.0\%$  and  $P(F_{heave} \leq 1.0) = 91.7\%$ , respectively. The condition of a value of 1.0 has been chosen as a critical criteria but other conditional probabilities can be calculated as desired using the same CADFs.

The hydraulic exit gradients and pore pressures calculated for this abandoned (cross) channel (using the RSMC methodology) are higher than those computed by a two dimensional or blanket theory model. A direct comparison with the BT equations is not plausible since these equations are two-dimensional and the case that could be considered as a comparison considers the channel (called an open-seepage-exit scenario) to be beyond the landside levee toe and not directly intercepting the landside levee toe as is with the case of the modeled abandoned channel herein.

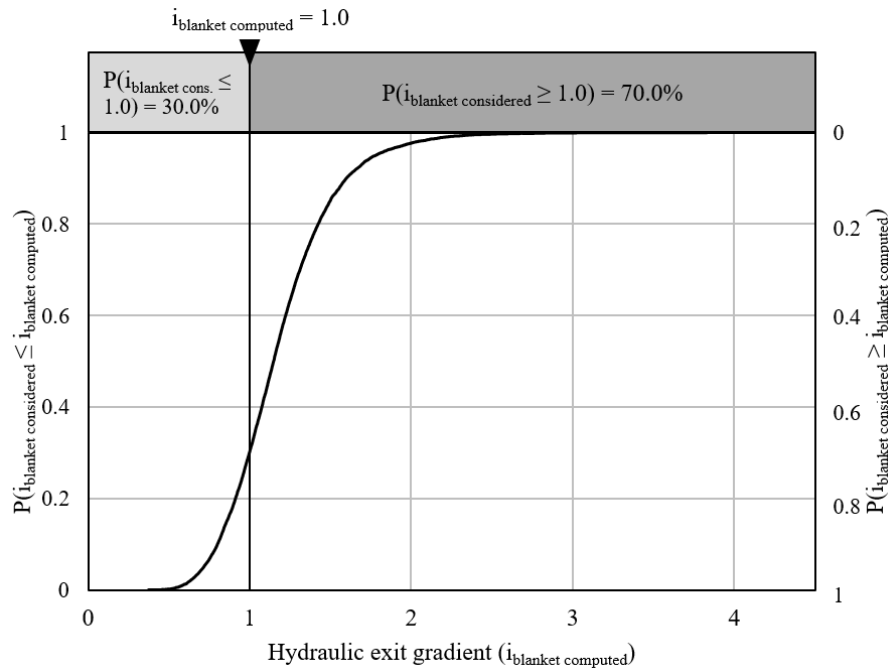


Figure 5.6. CADF for hydraulic exit gradient through the blanket,  $i_{blanket}$ .

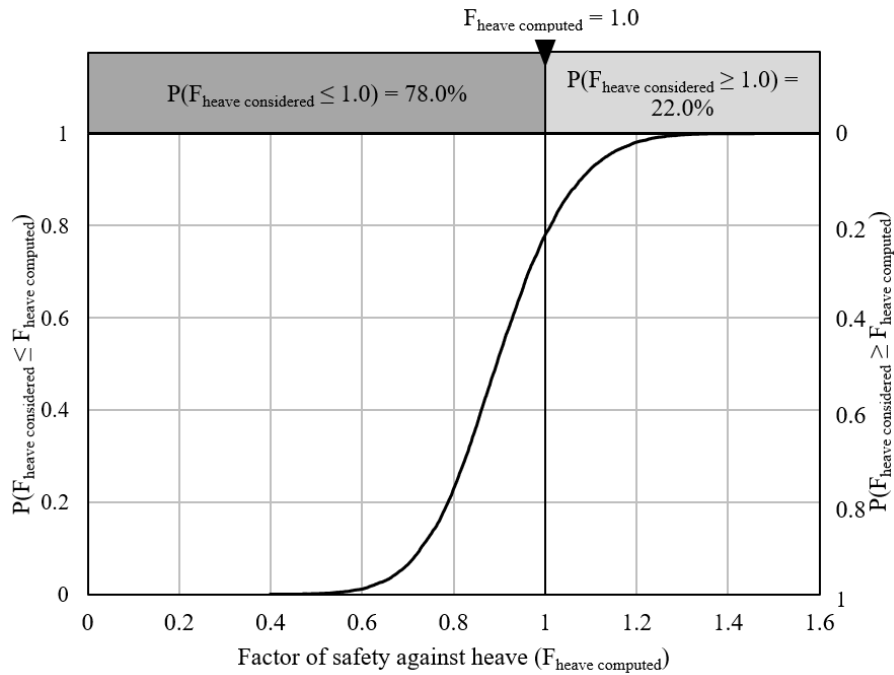


Figure 5.7. CADF for factor of safety against heave,  $F_{heave}$ .

Nevertheless, it is the intent of the authors to provide an idea of the results if this abandoned channel scenario were analyzed by BT equations to provide data proofing that the hydraulic exit gradients and pore pressures computed with the RSMC method are higher than those computed by a two dimensional model. The hydraulic exit gradient reaches a value of 1.0 when computed with the BT equations from Case 7C (USACE 2000) while using MLVs and a blanket thickness of 5.5 m (18 ft). Recall from Table 5.5 that the blanket thickness ranges as low as 1.5 m (5 ft) to 7.6 m (25 ft) and, as a result, the computation of higher hydraulic exit gradients are expected. As reported in the crevasse splay model from Polanco-Boulware and Rice (2016), these results exemplify the three-dimensional effect that geomorphic features have on levee's seepage flow.

On the other hand, parametric analyses centered on flood levels were performed on this abandoned channel model since the results presented in Figures 5.6 and 5.7 are conditional to the 100-year-flood level (annual exceedance probability of 1%). As with the crevasse splay model (Polanco-Boulware and Rice 2016), results for this abandoned channel model (an example is shown as Figure 5.8) indicate a consistent linear relationship based on head at the bottom of the blanket intercepting the channel versus differential flood levels and, consequently, the analysis of the channel with respect to other flood levels can be computed by means of a simple linear iteration. The relationship of increasing flood levels versus probability of occurrence (in this case conditional probability of initiation of erosion) is referred to as a fragility curve (Shannon and Wilson 2011) and is presented as Figure 5.9.

### 5.6.6. Sensitivity of parameters

It is usually of interest when a reliability analysis is performed to determine, by sensitivity analysis, which parameters affect the outcome the most. An advanced sensitivity analysis was performed by means of @Risk due to its ease of use and comprehensible presentation of the results. A tornado graph (Eschenbach 1992) is a plot shaped like a tornado where horizontal bars present the variation of input parameters while tracking a specific outcome.

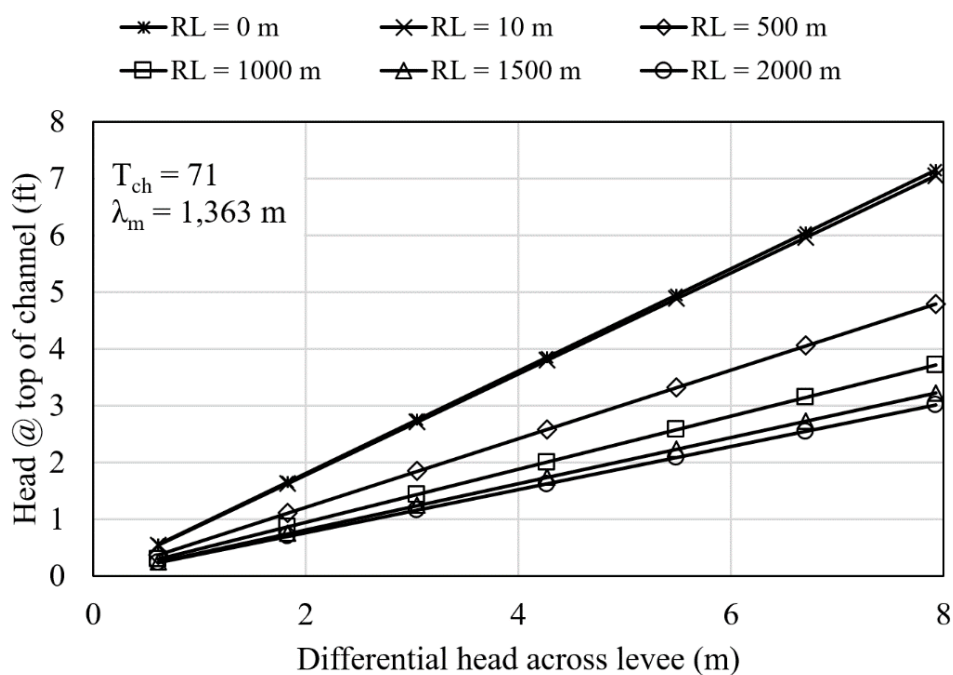


Figure 5.8. Example of one parametric analysis based on different flood levels for the abandoned channel presented in Figure 5.4 with different RL while maintaining constant  $T_{ch}$  and  $\lambda_m$ .



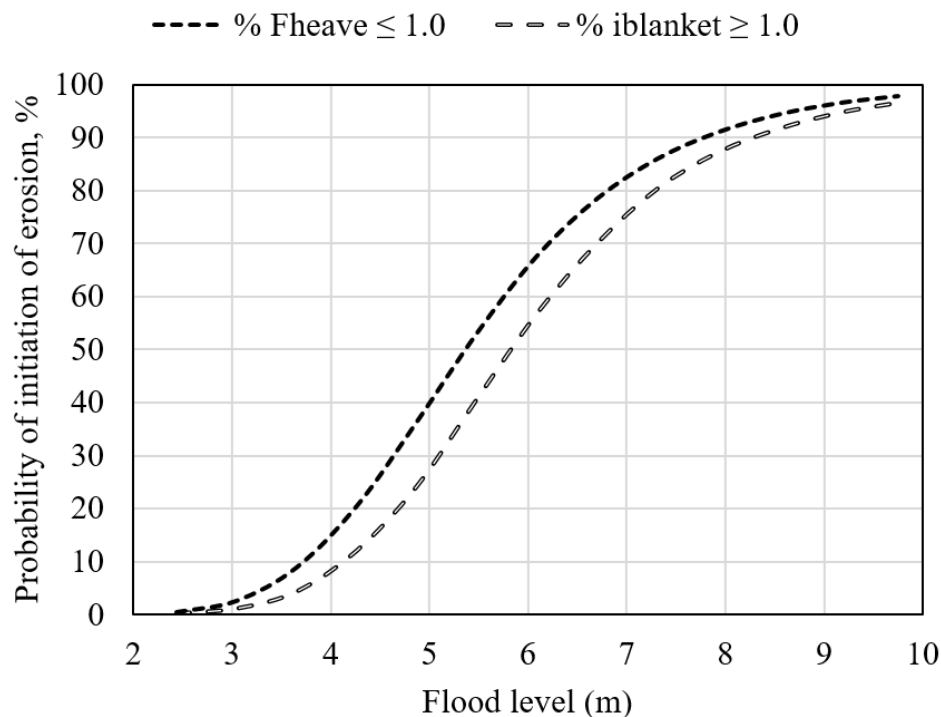


Figure 5.9. Fragility curve for the abandoned channel presented in Figure 5.4.

The largest bars in a tornado graph represent the parameters that affect the outcome the most and the smallest bars represent the least variation. @Risk has the flexibility of tracking different statistics for the sensitivity analysis such as the mean, mode, median, standard deviation, variance, minimum or maximum value of the outcome. The statistical function considered for this research case study was the mean and the resulting tornado graphs are presented as Figures 5.10, 5.11 and 5.12, respectively. Since  $i_{blanket}$  (Figure 5.10) and  $F_{heave}$  (Figure 5.11) are subjected to certain input parameters for their computation, it was of interest to track the sensitivity of the  $h_{max}$  since it depends on mostly all the input parameters. Sensitivity analysis for  $h_{max}$  show that the ratio of the hydraulic conductivity of the channel ( $K_{ch}$ ) with respect to the blanket layer ( $K_b$ ) and the  $RL$  are the most statistically significant parameters. With respect to the sensitivity analysis on the  $i_{blanket}$  and

$F_{heave}$  as expected, the thickness of the blanket overlapping the high conductivity channel ( $t_b$ ) is the most statistically significant parameter following the hydraulic conductivity ratio of the channel ( $K_{ch}$ ) with respect to the blanket layer ( $K_b$ ). Results could infer that the modified leakage is the most statistically significant combined parameter for the representation of underseepage flow on the landside while the  $RL$  acts as the length that flow has to travel from the riverside to the landside levee toe in order to reach an unsatisfactory performance. Smaller values of  $RL$  result in higher  $h_{max}$  at the bottom of the blanket layer intercepting the high conductivity channel (see Figure 5.8) and, hence, the more vulnerable the landside levee toe according to the hydraulic conductivity ratio of the channel to the blanket layer.

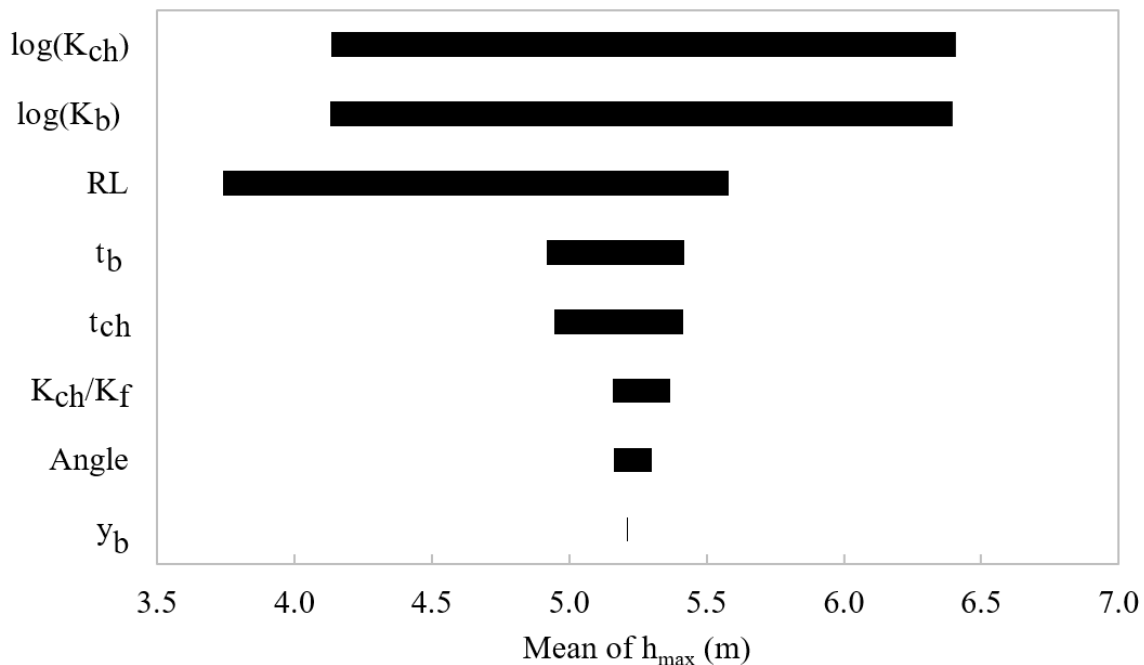


Figure 5.10. Sensitivity tornado graph for mean of  $h_{max}$ .

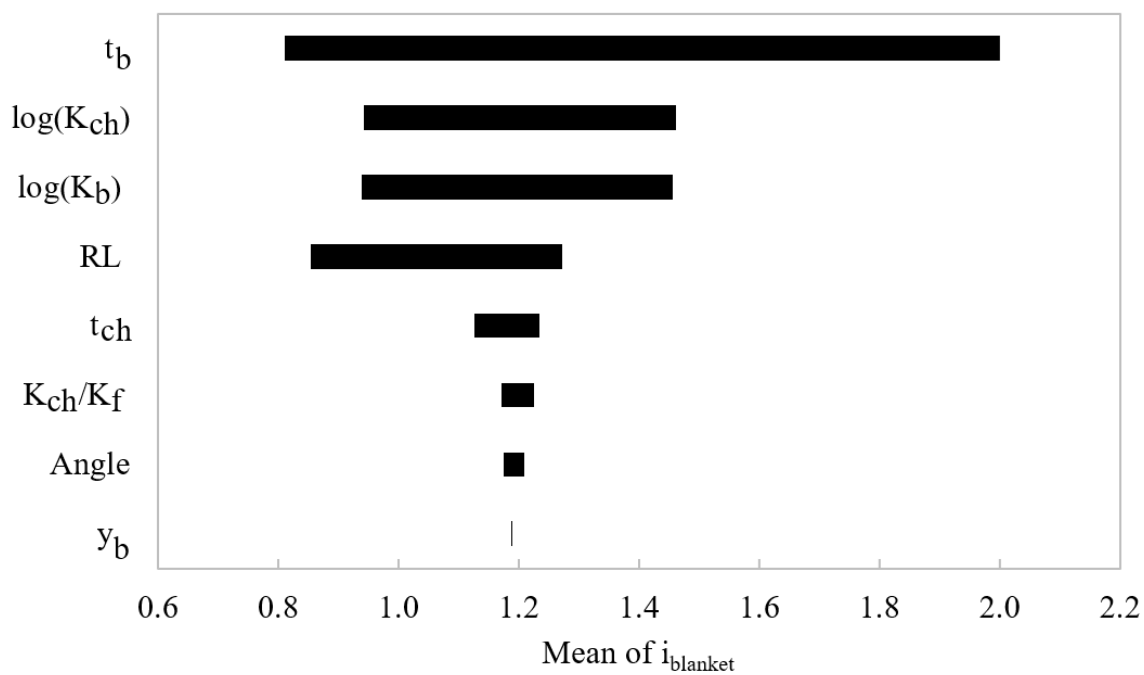


Figure 5.11. Sensitivity tornado graph for mean of  $i_{blanket}$ .

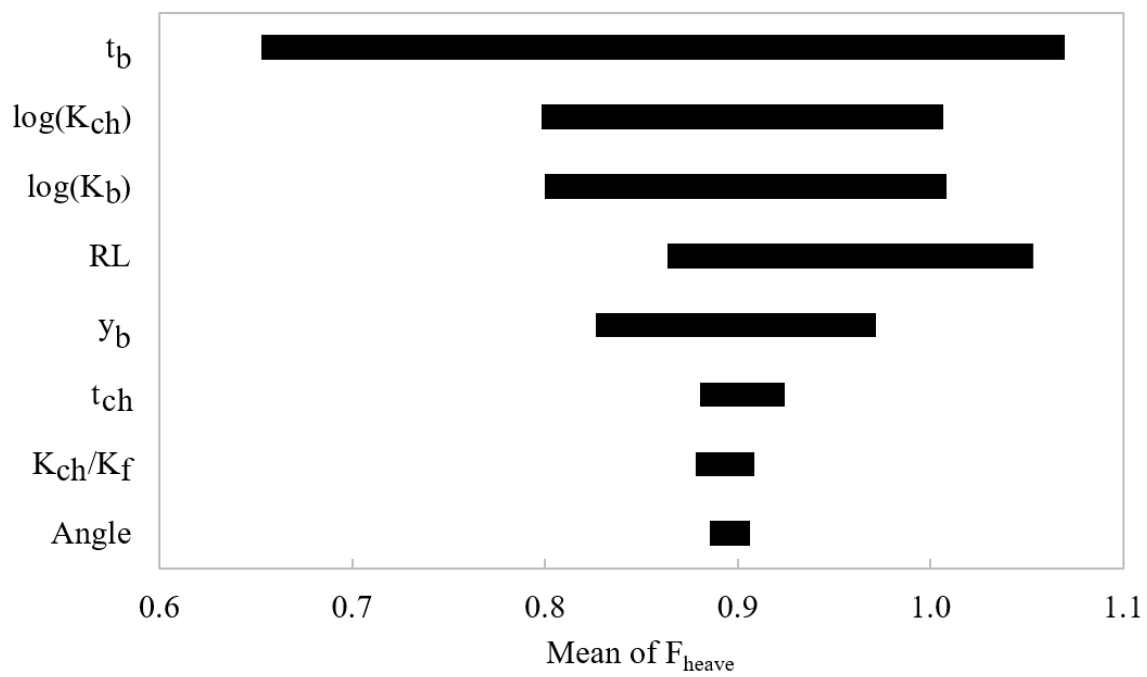


Figure 5.12. Sensitivity tornado graph for mean of  $F_{heave}$ .

## 5.7. Summary and Conclusions

This paper presents the reliability of internal erosion assessment of a historical abandoned (cross) channel that intercepts the levee alignment located on the east side of the Sacramento River levee system south to the intersection with the American River system in California. An innovative method, called the response-surface Monte Carlo simulation method, is used to analyze the underseepage hazard that the high conductivity channel imposes on the levee section. In summary, soil and geometric levee parameters are used to produce probability density functions and generate a three-dimensional finite-element model to perform parametric underseepage analyses with the purpose of simplifying the general model. After validating the simplified method, family of curves (response surface) are developed that represent a relationship between key soil and geometric parameters and the hydraulic design criteria. By means of the program @Risk, the developed probability density functions are used as random input parameters on the family of curves resulting in cumulative ascending density functions that represent the conditional probability of initiation of erosion.

The simplification of the general model uses state-of the-art methodology on the flow regime depiction of high conductivity channels. Key parameters are combined into two parameters with the hypothesis that seepage flow advances horizontally along the high conductivity channel from the riverside to the landside (tongue effect) while head dissipation occurs vertically through the blanket layer (modified leakage) on the landside.

The outcome of the Monte Carlo analysis, the cumulative ascending distribution functions with respect to the hydraulic exit gradient and the factor of safety against heave,

can be used to assess a desired conditional probability of initiation of erosion. In the case of this research study paper, values for the probabilities of exceeding a hydraulic exit gradient of 1.0 or not exceeding a factor of safety of 1.0 against heave are presented.

Parametric analyses on the abandoned channel model also indicate a consistent linear relationship between the head at the top of the channel and differential flood levels. As a consequence, a fragility curve describing the initiation of internal erosion with respect to different flood levels is presented and can be easily developed by a simple linear iteration. The sensitivity of the parameters is presented by means of tornado graphs, due to its ease of understanding, to statistically show the impact of the key input parameters on the outcome. Sensitivity analysis for  $h_{max}$  show that the ratio of the hydraulic conductivity of the channel ( $K_{ch}$ ) with respect to the blanket layer ( $K_b$ ) and the  $RL$  are the most statistically significant parameters. With respect to the sensitivity analysis on the  $i_{blanket}$  and  $F_{heave}$  as it would be expected, the thickness of the blanket overlapping the high conductivity channel ( $t_b$ ) is the most statistically significant parameter following the hydraulic conductivity ratio of the channel ( $K_{ch}$ ) with respect to the blanket layer ( $K_b$ ).

## **5.8. Acknowledgement**

This material is based upon work supported by the National Science Foundation (NSF) under Grant CMMI 1400640 and the United States Society on Dams (USSD) 2015 Scholarship. Any opinions, findings, and conclusions or recommendations expressed in this material are those of the authors and not necessarily the views of NSF and USSD.

### 5.9. Supplemental Data

Figures S5.1 through S5.5 show the response surface used to develop the CADFs shown in Figures 5.6 and 5.7. Its corresponding equations are presented in Table S5.1. In order to compute the combined parameters presented in Table S5.1, please refer to the equations presented in section ‘Identification of parameters and development of model’.

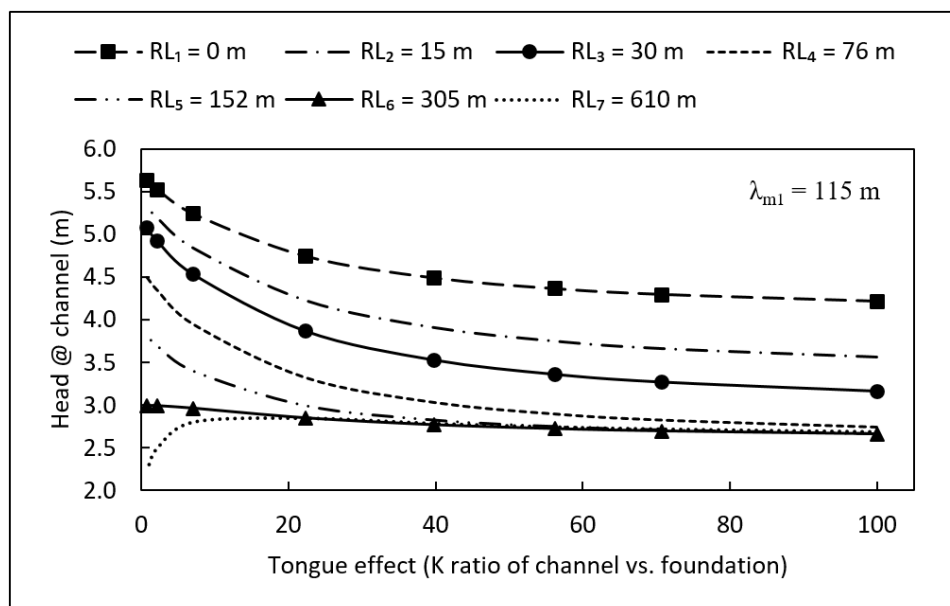


Figure S5.1. Family of curves for the high conductivity channel model for  $\lambda_{m1} = 115$  m and different ranges of  $T_{ch}$  and  $RL$ .

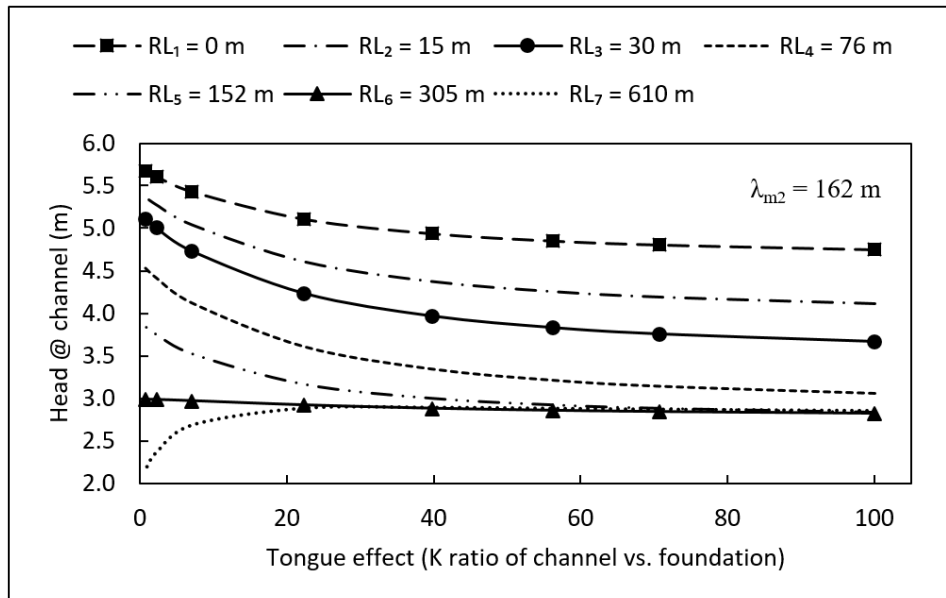


Figure S5.2. Family of curves for the high conductivity channel model for  $\lambda_{m2} = 162$  m and different ranges of  $T_{ch}$  and  $RL$ .

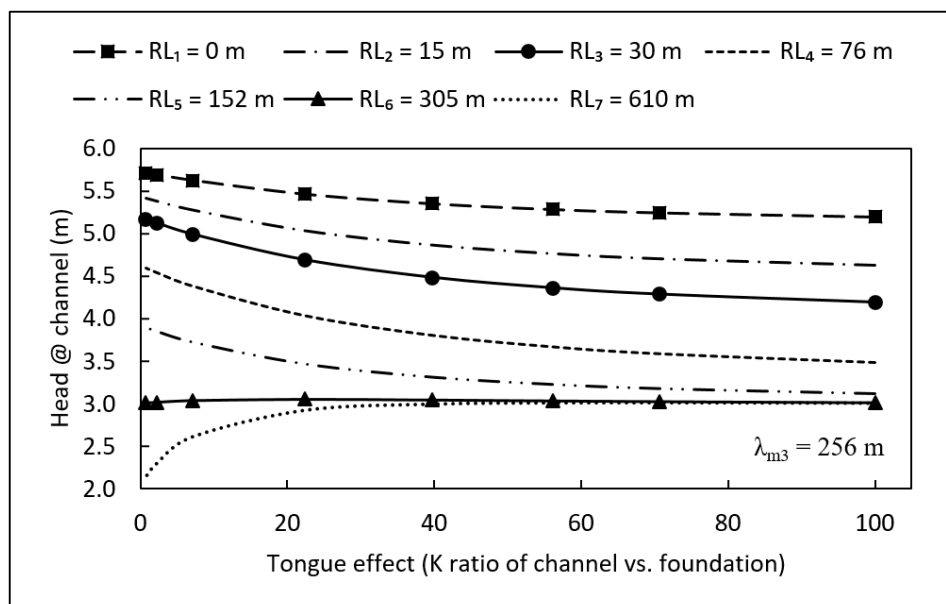


Figure S5.3. Family of curves for the high conductivity channel model for  $\lambda_{m3} = 256$  m and different ranges of  $T_{ch}$  and  $RL$ .

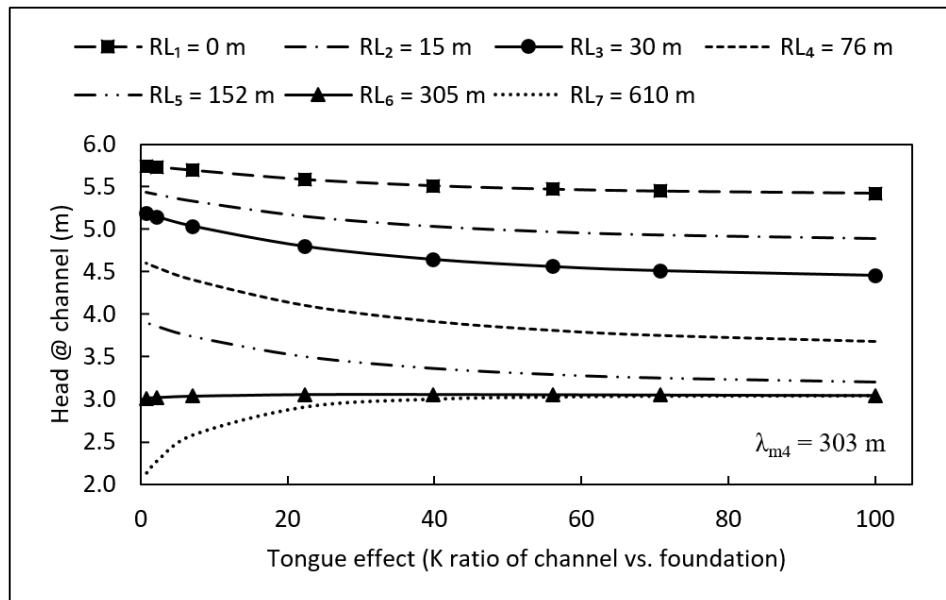


Figure S5.4. Family of curves for the high conductivity channel model for  $\lambda_{m4} = 303$  m and different ranges of  $T_{ch}$  and  $RL$ .

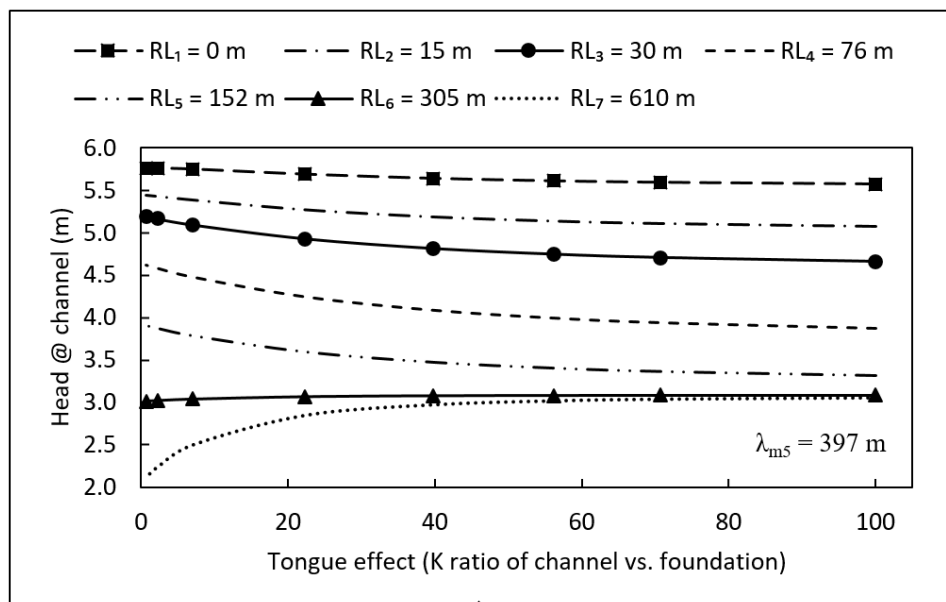


Figure S5.5. Family of curves for the high conductivity channel model for  $\lambda_{m5} = 397$  m and different ranges of  $T_{ch}$  and  $RL$ .



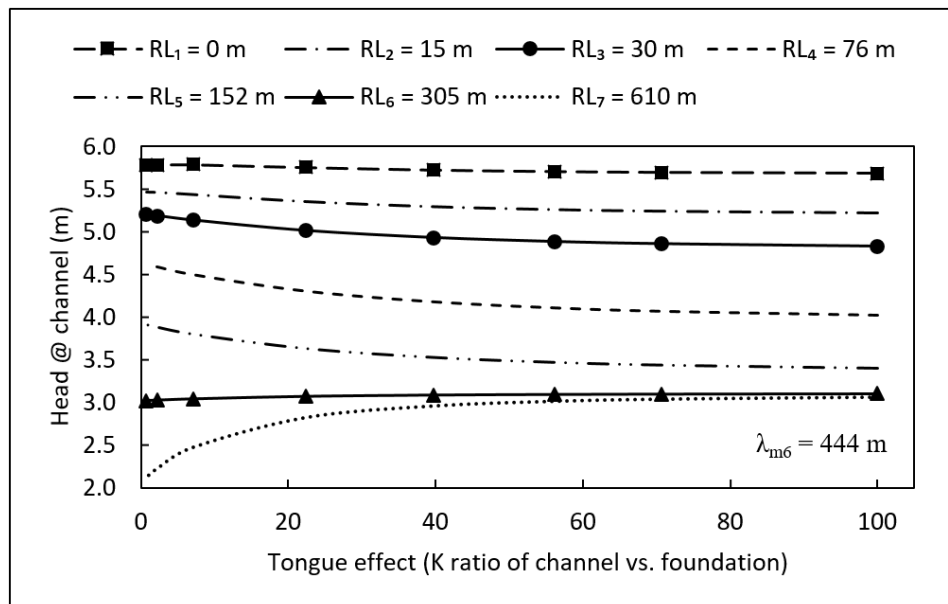


Figure S5.6. Family of curves for the high conductivity channel model for  $\lambda_{m6} = 444$  m and different ranges of  $T_{ch}$  and  $RL$ .

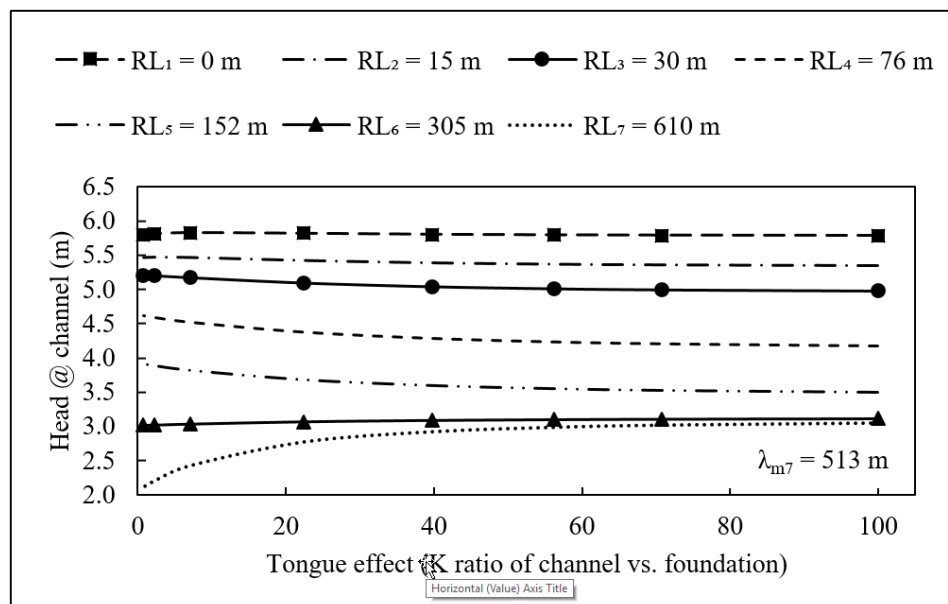


Figure S5.7. Family of curves for the high conductivity channel model for  $\lambda_{m7} = 513$  m and different ranges of  $T_{ch}$  and  $RL$ .

Table S5.1. Fit-equations' coefficients and corresponding goodness of fit for family of curves with respect to each  $\lambda_m$  used.

RL (m)	$h_{max} = \mathbf{a}_4 * T_{ch}^4 + \mathbf{a}_3 * T_{ch}^3 + \mathbf{a}_2 * T_{ch}^2 + \mathbf{a}_1 * T_{ch}^1 + \mathbf{a}_0$					R <sup>2</sup>	
	$\mathbf{a}_4$	$\mathbf{a}_3$	$\mathbf{a}_2$	$\mathbf{a}_1$	$\mathbf{a}_0$		
Using $t_{ch} = 1.5$ m and $t_b = 0.6$ m to compute $\lambda_{m1} = 115$ m							
0	6.45E-08	-1.63E-05	1.52E-03	-6.88E-02	5.67E+00	0.99	
15	-	-4.47E-06	9.44E-04	-6.75E-02	5.33E+00	0.99	
30	-	-4.99E-06	1.05E-03	-7.39E-02	5.07E+00	0.99	
76	-	-5.28E-06	1.08E-03	-7.30E-02	4.50E+00	0.99	
152	-	-3.99E-06	7.97E-04	-5.13E-02	3.80E+00	0.99	
305	-	-2.43E-07	7.49E-05	-8.49E-03	3.01E+00	0.99	
610	$T_{ch} \leq 7$	-	-	-1.81E-02	2.30E-01	0.99	
	$T_{ch} \geq 7$	-3.20E-08	7.45E-06	-5.78E-04	1.49E-02	2.72E+00	0.99
Using $t_{ch} = 3.0$ m and $t_b = 0.6$ m to compute $\lambda_{m2} = 162$ m							
0	3.83E-08	-9.75E-06	9.29E-04	-4.32E-02	5.70E+00	0.99	
15	-	-2.98E-06	6.35E-04	-4.64E-02	5.37E+00	0.99	
30	-	-3.44E-06	7.33E-04	-5.35E-02	5.12E+00	0.99	
76	-	-3.81E-06	8.00E-04	-5.68E-02	4.54E+00	0.99	
152	-	-3.03E-06	6.19E-04	-4.17E-02	3.84E+00	0.99	
305	-	-9.32E-08	3.08E-05	-3.85E-03	2.99E+00	0.99	
610	$T_{ch} \leq 7$	-	1.80E-06	-3.46E-04	1.93E-02	2.58E+00	0.94
	$T_{ch} \geq 7$	-	-	-	7.79E-02	2.15E+00	0.97
Using $t_{ch} = 1.5$ m and $t_b = 3.0$ m to compute $\lambda_{m3} = 256$ m							
0	4.30E-09	-1.47E-06	2.08E-04	-1.57E-02	5.73E+00	0.99	
15	-	-9.91E-07	2.43E-04	-2.23E-02	5.43E+00	0.99	
30	-	-1.29E-06	3.10E-04	-2.81E-02	5.18E+00	0.99	
76	-	-1.61E-06	3.78E-04	-3.30E-02	4.61E+00	0.99	
152	-	-1.44E-06	3.21E-04	-2.56E-02	3.90E+00	0.99	
305	-	3.78E-07	-6.86E-05	3.09E-03	3.01E+00	0.99	
610	-1.24E-07	2.86E-05	-2.30E-03	7.59E-02	2.13E+00	0.99	

RL (m)	$h_{max} = \mathbf{a}_4 * T_{ch}^4 + \mathbf{a}_3 * T_{ch}^3 + \mathbf{a}_2 * T_{ch}^2 + \mathbf{a}_1 * T_{ch}^1 + \mathbf{a}_0$					$R^2$
	$\mathbf{a}_4$	$\mathbf{a}_3$	$\mathbf{a}_2$	$\mathbf{a}_1$	$\mathbf{a}_0$	
Using $t_{ch} = 3.0$ m and $t_b = 2.1$ m to compute $\lambda_{m4} = 303$ m						
0	3.00E-10	-4.65E-07	1.07E-04	-9.66E-03	5.75E+00	0.99
15	-	-8.29E-07	1.98E-04	-1.71E-02	5.45E+00	0.99
30	-	-1.20E-06	2.79E-04	-2.32E-02	5.20E+00	0.99
76	-	-1.60E-06	3.65E-04	-2.99E-02	4.62E+00	0.99
152	-	-1.41E-06	3.10E-04	-2.40E-02	3.91E+00	0.99
305	-	2.84E-07	-5.41E-05	2.88E-03	3.02E+00	0.97
610	-	4.30E-06	-8.24E-04	4.82E-02	2.18E+00	0.97
Using $t_{ch} = 3.0$ m and $t_b = 3.7$ m to compute $\lambda_{m5} = 397$ m						
0	-6.20E-09	1.17E-06	-4.77E-05	-2.72E-03	5.76E+00	0.99
15	-	-3.72E-07	1.00E-04	-1.01E-02	5.45E+00	0.99
30	-	-6.87E-07	1.69E-04	-1.54E-02	5.20E+00	0.99
76	-	-1.04E-06	2.49E-04	-2.21E-02	4.62E+00	0.99
152	-	-9.53E-07	2.20E-04	-1.85E-02	3.91E+00	0.99
305	-	2.55E-07	-5.21E-05	3.35E-03	3.01E+00	0.99
610	-8.54E-08	2.04E-05	-1.73E-03	6.42E-02	2.09E+00	0.99
Using $t_{ch} = 4.6$ m and $t_b = 3.0$ m to compute $\lambda_{m6} = 444$ m						
0	-9.80E-09	2.03E-06	-1.23E-04	8.61E-04	5.78E+00	0.99
15	-	-1.93E-07	5.89E-05	-6.44E-03	5.47E+00	0.99
30	-	-5.29E-07	1.29E-04	-1.15E-02	5.21E+00	0.99
76	-	-9.64E-07	2.24E-04	-1.89E-02	4.63E+00	0.99
152	-	-9.03E-07	2.06E-04	-1.67E-02	3.92E+00	0.99
305	-	2.00E-07	-4.33E-05	3.17E-03	3.02E+00	0.99
610	-7.51E-08	1.81E-05	-1.57E-03	6.02E-02	2.09E+00	0.99
Using $t_{ch} = 6.1$ m and $t_b = 3.0$ m to compute $\lambda_{m7} = 513$ m						
0	-1.30E-08	2.81E-06	-1.94E-04	4.11E-03	5.81E+00	0.90
15	-	2.65E-08	1.02E-05	-2.56E-03	5.48E+00	0.99
30	-	-2.79E-07	7.27E-05	-6.86E-03	5.22E+00	0.99
76	-	-7.60E-07	1.76E-04	-1.45E-02	4.63E+00	0.99
152	-	-7.63E-07	1.73E-04	-1.39E-02	3.92E+00	0.99
305	-	1.61E-07	-3.73E-05	3.10E-03	3.01E+00	0.99
610	-6.10E-08	1.50E-05	-1.33E-03	5.43E-02	2.08E+00	0.99

## References

- Adams, P. N., Slingerland, R. L. and Smith, N. D. (2004). "Variations in natural levee morphology in anastomosed channel flood plain complexes." *Geomorphology*, 61 (1-2), 127–142.
- Baecher, G. B., and Christian, J. T. (2003). *Reliability and statistics in geotechnical engineering*, Wiley, Chichester, England.
- Bernitt, L. and Lynett, P. (2010). Breaching of sea dikes. *Proc. 32nd Conf. Coastal Eng.*, 1(32), 1-10.
- Bligh, W. G. (1910). "Dams, barrages, and weirs on porous foundations." *Engineering News-Rec.*, 64(26), 708–710.
- Bligh, W. G. (1913). "Lessons from the failure of a weir and sluices on porous foundations". *Engineering News-Rec.*, 69(6), 266–270.
- Bligh, W. G. (1915). Submerged weirs founded on sand. In *Dams and weirs*, 151-179, American Technical Society, Chicago, US.
- Bowles, D. S., Chauhan, S. S., Anderson, L. R. and Grove, R. C. (2012). Baseline Risk Assessment for Herbert Hoover Dike. *Proc. ANCOLD Conf. Dams*, 1-20.
- Bridge, J. (2003). *Rivers and floodplains: Forms, processes, and sedimentary record*, Blackwell Publishing, Oxford, UK.
- Brierley, G. J. and Fryirs, K. A. (2005). *Geomorphology and river management: applications of the river styles framework*, Blackwell Publishing, Oxford, UK.
- Brierley, G. J. and Hickin, E. J. (1992). "Floodplain development based on selective preservation of sediments, Squamish River, British Columbia." *Geomorphology*, 4, 381-391.
- Brierley, G. J., Ferguson, R. J. and, Woolfe, K. J. (1997). "What is a fluvial levee?". *Sedimentary Geology*, 114, 1-9.
- Cazanacli, D. and Smith, N. D. (1998). "A study of morphology and texture of natural levees—Cumberland Marshes, Saskatchewan, Canada". *Geomorphology*, 25, 43–55.
- Construction Industry Research and Information Association (CIRIA). (2013). "*The International Levee Handbook*."

- Crum, D. A. (1996). "Reliability applied to levee seepage analysis". *Proc., ASCE 7th Specialty Conf. of the Prob. Mech. Str. Reliab.*, D. M. Frangopol and M. D. Grigoriu, eds., Vol. 1, Worcester, MA, 946–949.
- Eschenbach, T. G. (1992). "Spiderplots versus Tornado diagrams for sensitivity analysis." *Interfaces*, 22(6), 40-46.
- Farrell, K. M. (1987). "Sedimentology and facies architecture of overbank deposits of the Mississippi river, False River region, Louisiana". *Recent Developments in Fluvial Sedimentology*, F. G. Ethridge, R. M. Flores, and M. D. Harvey, eds., Vol. 39, Society of Economic Paleontologist and Mineralogists, Fort Collins, CO, 111-120.
- Ferguson, R. J. and Brierley, G. J. (1999). "Levee morphology and sedimentology along the lower Tuross River, south-eastern Australia." *Sedimentology*, 46, 627-648.
- Filgueira-Rivera, M., Smith, N. D. and Slingerland, R. L. (2007). "Controls on natural levee development in the Columbia River, British Columbia, Canada." *Sedimentology*, 54, 905–919.
- Fryirs, K.A. and Brierley, G.J. (2013). *Geomorphic analysis of river systems*, Blackwell Publishing, Oxford, UK.
- Gabr, M. A., Taylor, H. M. Jr., Brizendine, A. L., and Wolff, T. F. (1995). "LEVEEMSU: Analysis software for levee underseepage and rehabilitation." *Technical Rep. GL-95-9*, U.S. Army Engineer Waterways Experiment Station, Vicksburg, MS.
- Glynn, M. E. and Kuszmaul, J. (2010). "Prediction of piping erosion along middle Mississippi river levees-An empirical model." *Technical Rep. ERDC/GSL TR-04-12*. USACE, Vicksburg, MS.
- Harr, M.E. (1962). *Groundwater and Seepage*, McGraw-Hill, New York, U.S.
- Harr, M. E. (1987). *Reliability-based design in civil engineering*, McGraw-Hill, New York, US.
- Hudson, P. F. (2011). Natural levees. In Stanley W. Trimble (Ed.), *Encyclopedia of water science*, second edition, 763-767, Taylor & Francis Group, Boca Raton, FL, US.
- Hudson, P. F. and Heitmuller, F. T. (2003). "Local and watershed scale controls on the spatial variability of natural levee deposits in a large fine-grained floodplain: Lower Pánuco Basin, Mexico". *Geomorphology*, 56, 255–269.
- International Commission on Large Dams (ICOLD). (2015). "Internal erosion of existing dams, levees, and dikes, and their foundations." *Internal erosion processes and engineering assessment*, Vol. 1, Paris, France.

- Kanning, W. (2012). "The weakest link." Ph. D. dissertation, Delft Technical Univ., Delft, Netherlands.
- Knight, G. J., Durkee, F. B. and Edmonston, A. D. (1955). "Seepage condition in Sacramento Valley". *Report to the water project authority of the state of California*. Sacramento, CA.
- Knowles, V. R. (1992). Applications of the finite element seepage analysis Corps program CSEEP (X8202). *Technical Rep. ITL-92-6*, U.S. Army Engineer Waterways Experiment Station, Vicksburg, MS.
- Kolb, C. R. (1975). "Geologic control of sand boils along Mississippi River levees," Technical Report S-75-22, U. S. Army Engineer Waterways Experiment Station, Vicksburg, MS.
- Lane, E. W. (1935). "Security from under-seepage: Masonry dams on earth foundation." *Transactions*, 100, 1235-1272.
- Leopold, L. B. and Wolman, M. G. (1957). "River channel patterns: Braided, meandering and straight." U.S. Geological Survey, Washington, DC, 39-84.
- McGowen, J.H. and Garner, L.E., 1970. "Physiographic features and stratification types of coarse-grained point bars: modern and ancient examples." *Sedimentology*, 14, 77-111.
- Pearce, J.T., Marlow, D., Avila, C. and Selvamohan, S., (2009). "Use of geomorphic and airborne geophysical data for analysis of levees and floodplain processes for levee evaluations in California". *ASFPM Annual Conf.*, Association of State Floodplain Managers, Orlando, FL.
- Polanco, L. and Rice, J. D. (2014). "A reliability-based evaluation of the effects of geometry on levee underseepage potential." *Springer: Geotechnical and Geological Engineering*, 32(4), 807-820.
- Polanco-Boulware, L. and Rice, J. D. (2016). "Reliability-based three-dimensional assessment of internal erosion potential due to crevasses splays." *J. Geotech. Geoenviron. Eng.*, 10.1061/(ASCE)GT.1943-5606.0001596, ADD PAGES.
- Rice, J. D. and Polanco, L. (2012). "Reliability-based underseepage analysis in levees using a response surface–monte carlo simulation method." *J. Geotech. Geoenviron. Eng.*, 10.1061/(ASCE)GT.1943-5606.0000650, 821-830.
- Ritter Dale F., Kochel R. C. and Miller J. R. (2011). *Process geomorphology*, fifth edition, Waveland Press, Long Grove, IL, US.

- Saucier, R.T. (1994). "Geomorphology and quaternary geologic history of the lower Mississippi Valley." U.S. Army Engineer Waterways Experiment Station, Vicksburg, MS.
- Shannon & Wilson, Inc. (2011). "Skagit river levee general investigation - Levee risk and reliability analysis. USACE, Washington, USA.
- Smith, N. D. and Pérez-Arlucea, M. (2008). "Natural levee deposition during the 2005 flood of the Saskatchewan River." *Geomorphology*, 101, 583–594.
- Steenbergen H. M. G. M., Lassing B. L., Vrouwenvelder A. C. W. M., and Waarts P. H. (2004). "Reliability analysis of flood defence systems," *Heron*, 49 (1), 51–73.
- SVFlux [Computer software]. SoilVision Systems, Saskatoon, SK, Canada.
- Temmermana, S., Goversa, G., Meireb, P. and Wartel, S. (2004). "Simulating the long-term development of levee–basin topography on tidal marshes." *Geomorphology*, 63, 39–55.
- Terzaghi, K. (1922). "Der Grundbruch an Stauwerken und Seine Verhütung [The Failure of Dams and Its Prevention]." *Die Wasserkraft*, 17, 445-449.
- Terzaghi, K. (1929). "Effect of minor geologic details on the safety of dams". *Amer. Inst. Mining Metallurgical Eng.*, 215, 31–46.
- Tracy, F. T. (1994). Seepage Package. "CSEEP Micro Version, X8202," U.S. Army Engineer Waterways Experiment Station, Vicksburg, MS.
- U. S. Army Corps of Engineers (USACE) (1956). "Investigation of underseepage and its control. Technical Memorandum No. 3-424." *U.S. Army Engineer Waterways Experiment Station, Vicksburg, MS.*
- U. S. Army Corps of Engineers (USACE) (2000). "Design and construction of levees. Engineering Manual EM 1110-2-1913." Washington, DC.
- Vrouwenvelder, A. C. W. M, Van Mierlo, M. C. L. M., Calle, E. O. F., Markus, A.A., Schweckendiek, T. and Courage, W. M. G. (2010). "Risk analysis for flood protection systems." Deltares, Netherlands.
- Vrouwenvelder, T. (2006). "Spatial effects in reliability analysis of flood protection systems." *Int. Forum Eng. Decision Making*, Lake Louise, Canada.
- Walling, D. E., Fang, D., Nicholas, A. P. and Sweet, R. J. (2004). "The grain size characteristics of overbank deposits on the floodplains of British lowland rivers." *Proc., Int. Symp. Sediment Transfer through the Fluvial System*, V. Golosov, V. Belyaev and D. E. Walling, eds., Moscow, Russia, 288, 226–234.

- Walling, D. E., Owens, P. N. and Leeks, G. J. L. (1997). "The characteristics of overbank deposits associated with a major flood event in the catchment of the River Ouse, Yorkshire, UK." *Catena*, 31(1-2), 53-75.
- William Lettis and Associates, Inc. (2008). "Surficial Geologic Map and Initial Geomorphic Assessment, Sacramento River (East Side), Sacramento County, California." Sacramento, CA.
- Wilson, J. D. (2003). "Middle Mississippi River levee flood performance: assessing the occurrence of piping through empirical modeling." Thesis, Univ. Mississippi, MS, US.
- Wolff, D. (2008). "Reliability of levee systems." *Reliability-based design in geotechnical engineering*, K.-K. Phoon, ed., 448-496. Taylor and Francis Group, New York, 448-496.
- Wolff, T. F. (1989). "LEVEEMSU: A software package designed for levee underseepage analysis. *Technical Rep. GL-89-13.*" U.S. Army Engineer Waterways Experiment Station, Vicksburg, MS.
- Wolff, T. F. (1994). "Evaluating the reliability of existing levees." U.S. Army Engineer Waterways Experiment Station, Michigan State Univ., East Lansing MI.
- Wolff, T. F., Demsky, E. C., Schauer, J., and Perry, E. (1996). "Reliability assessment of dike and levee embankments." *Uncertainty in the geologic environment: From theory to practice*, ASCE Reston, VA, 636-650.
- Xu, B. and Low, B. K. (2006). "Probabilistic stability analyses of embankments based on finite-element method." *J. Geotech. Geoenviron. Eng.*, 10.1061/(ASCE)1090-0241(2006)132:11(1444), 1444-1454.



## CHAPTER 6

COMBINED EFFECTS OF GEOMORPHIC FEATURES AND LEVEE CURVATURE  
ON UNDERSEEPAGE ANALYSIS RELIABILITY**Abstract**

It has been reported that levee curvature has an effect on internal erosion mechanisms triggered by underseepage. Although the geotechnical engineering community has slowly started to incorporate the effects of levee curvature in underseepage assessment, most of the analyses are still performed by means of two-dimensional profiles with simplified subsurface geometry that can't handle the combined three-dimensional effects of levee curvature and complex geometry due to geomorphic features. Geomorphic features tend to interrupt the characteristic subsurface profile by either blocking or concentrating seepage flow which consequently result in the main hazard of unsatisfactory performance. A response surface Monte Carlo simulation model is presented that allows for the assessment of geomorphic features while adjusting the results for curvature effects. Parametric analyses based on a range of curvatures and geomorphic feature alignments with respect to different levels of significant soil parameters result in a response surface describing the hydraulic head at the top of the geomorphic feature along the longitudinal levee toe curvature alignment. A meander scroll feature located in the Little Pocket in Sacramento, CA is used to present an example application of the method.

## 6.1. Introduction

Natural levees are among some of the features that emerge due to geologic changes that floodplains experience by flooding rivers. Since civilizations have developed near rivers, experiencing recurrent flood events, man-made levees (referred to as levee for now on) have been built as a protection; sometimes on top of natural levees or near them. As a consequence, levees often follow the trajectory of the river which they intend to control. In most river systems where levees are present, some sections follow a series of meanders (curves) whereas others are relatively straight (linear) sections (Throne 1997). Also, due to geologic changes, the subsurface that serves as the levees' foundation varies from one point to another due to the occurrence of geomorphic features which tend to affect and concentrate underseepage flow.

Backward erosion piping (BEP) is an internal erosion mechanism that occurs by means of underseepage flow (ICOLD 2015). BEP describes the erosion that initiates when particles of soil are dislodged from the soil matrix at an unprotected seepage exit point. (ICOLD 2015). Heave is the uplift movement of a mass of soil due to underlying hydraulic pressure or seepage forces (Terzaghi and Peck 1968). BEP is commonly analyzed by the combination of the "blanket theory" (BT) equations developed by the USACE and the first-order second-moment (FOSM) Taylor series method (Wolff 1994; Crum 1996; Wolff et al. 1996; Wolff 2008). The BT equations are used as the performance underseepage function whereas the FOSM allows assessment of the effects of uncertainty of input parameters. This method is attractive due to its ease of application but, due to limitations, often requires oversimplifying the levee's subsurface geometry. While limiting the

probabilistic assessment and it does not consider the effect of curvature of the levee alignment.

Geomorphic features are depositional landforms formed as a result of a river meandering within its floodplain. Geomorphic features are usually either over simplified or not considered at all in underseepage analyses since most analyses are performed on two-dimensional (2D) sections of a generalized, characteristic profile that averages the geology over a length of levee. With respect to curvature, levee sections are regularly considered straight and it is argued that resulting analyses are conservative enough to incorporate the effect curvature would provide. However, it has been reported that underseepage in levees may be linked to the presence of confined geomorphic features (USACE 1956, Glynn and Kuszmaul 2010, Polanco-Boulware and Rice 2016) and curved levee alignment possibly has the potential of augmenting underseepage flow (Inci 2008, Merry and Du 2014, Jafari et al. (2016).

The methods presented in this paper assess both levee curvature and geomorphic features as parameters to assess the extent to which these naturally inherent features can affect the seepage flow beneath the levee toe. Therefore, it is the purpose of the authors to present a methodology whereby the effects of geomorphic features and levee curvature can be incorporated into underseepage analysis in order to characterize a closer representative state of the nature of the levee.

## 6.2. Levee underseepage modeling characteristics and shortcomings

Although there are many failure mechanisms that can contribute to a levee failure, this paper focuses in the context of assessing the potential of internal erosion related failure due to underseepage. Levee underseepage refers to the scenario where seepage flows under the structure. Internal erosion may occur where forces due to differential hydraulic head dislodge and transport subsurface soils (CIRIA 2013, ICOLD 2015). Historic performance has shown that internal erosion is one of the main causes of levee failure (McCook 2007). To analyze internal erosion potential due to underseepage, probabilistic methods have been developed utilizing the basic mechanics of long-standard deterministic methods. Deterministic methods focus on the computation of factors of safety based on the process of two erosion initiation conditions: (1) BEP mechanism (ratio of resisting to driving hydraulic gradient forces) and (2) heave mechanism (ratio of resisting weight of the layers) as shown in Eqs. (1) and (2) respectively (Terzaghi 1922, McCook 2007, CIRIA 2013).

$$F_{bep} = \frac{i_c}{i_{blanket}} = \frac{\frac{(\gamma_{buoy})}{\gamma_w}}{\frac{\Delta h}{t_b}} = \frac{\frac{(\gamma_{blkt} - \gamma_w)}{\gamma_w}}{\frac{h_{max}}{t_b}} \quad (1)$$

$$F_{heave} = \frac{t_b \gamma_{blkt}}{u_{GF}} = \frac{t_b (\gamma_{blkt})}{(h_{max} + t_b) \gamma_w} \quad (2)$$

Where,  $F_{bep}$  = factor of safety against gradient,  $i_c$  = critical gradient,  $i_{blanket}$  = hydraulic exit gradient through blanket layer,  $\gamma_{buoy}$  = buoyant unit weight of the soil,  $\gamma_w$  = unit weight of the water,  $\Delta h = h_{max}$  = difference in total hydraulic head through the levee measured on the bottom of the blanket layer, top of the geomorphic feature (datum of zero

is set on the landside levee toe for ease of computation),  $t_b$  = thickness of the blanket layer overlaying the geomorphic feature,  $\gamma_{blkt}$  = total unit weight of the blanket,  $F_{heave}$  = factor of safety against heave, and,  $u_{GF}$  = pore pressure of the geomorphic feature.

These factors of safety are usually calculated using finite-element methods such as Slide (Rocscience Inc.), SVFlux (SoilVision Systems), ABAQUS (Dassault Sytemes), CSEEP and LEVEEMSU (USACE) and SEEP/W (GEO-SLOPE International Ltd.) or other seepage analyses such as the BT equations (USACE 1956, 2000).

#### 6.2.1. FOSM-BT method

The most common reliability-based underseepage approaches apply the BT closed-form equations together with the FOSM Taylor series method (Wolff 1994; Crum 1996; Wolff et al. 1996; Wolff 2008). The BT equations were proposed by the USACE in 1956 (USACE 1956) and have been WIDELY used ever since. The equations model simplified subsurface conditions of 2D levee sections (assumed to be linear) where a hydraulic exit gradient or  $F_{heave}$  mechanism can be computed at the toe of the levee. The simplified subsurface conditions assumed in the BT equations is one of the biggest limitations of the method.

On the other hand, the FOSM Taylor series method is a simple reliability method that uses the most likely value and standard deviation of the parameters that are prone to provide uncertainty in the probabilistic assessment. When using the FOSM Taylor Series method,  $2n + 1$  calculations of the factor of safety are required, where N is the number of parameters. Also, the probability density functions (PDFs) of the parameters are limited to normal or lognormal distributions. Similar to the BT equations, the simplicity of the FOSM Taylor series method serves as its biggest limitation since, due to the fact that it only uses

the most likely value and standard deviation of the parameters, it is usually only accurate for small variability and non-linearity in the system response to the parameters's variation.

Despite these limitations, the FOSM-BT method is commonly used in the United States due to two main reasons: (1) the BT equations are an easy underseepage assessment tool and (2) the FOSM Taylor series method requires few calculations. Nevertheless, this method is limited to: (1) the modeling of 2D-straight levee sections that simplify the levee subsurface geometry as far as not having the capability of incorporating geomorphic features and, (2) the representation of uncertain parameters by normal or lognormal probability distributions with small variability and non-linearity (USACE 2004, Rice and Polanco 2012, Benjasupattananan 2013, Polanco and Rice 2014, 2016, 2017). Therefore, based on the limitations of the FOSM-BT method, an assessment on levee underseepage by the combined effect of geomorphic features and curved alignment may not be accurately achievable.

#### 6.2.2. Geomorphology surrounding levee system

The plan view pattern of rivers has been classified into braided, meandering and straight (Leopold and Wolman 1957). Meandering rivers are characterized by a sinuous alignment and, thus, its geomorphology has been widely studied due to the intriguing geomorphic formations that are encountered as part of their floodplains (Walling et al. 2004). Typical foundation profiles consist of soils deposited in the river channel that are typically granular whereas overbank deposits, those deposited when flood waters exceed the river banks, tend to be finer-grained (Walling et al. 2004, Ritter et al. 2011). The typical arrangement consists of overbank deposits overlying the channel deposits as seen on Figure 6.1. The terms that commonly describe these deposits among the engineering community

are blanket layer (overbank deposits) and foundation layer (channel deposits) (USACE 1956, 2000) as shown in Figure 6.1.

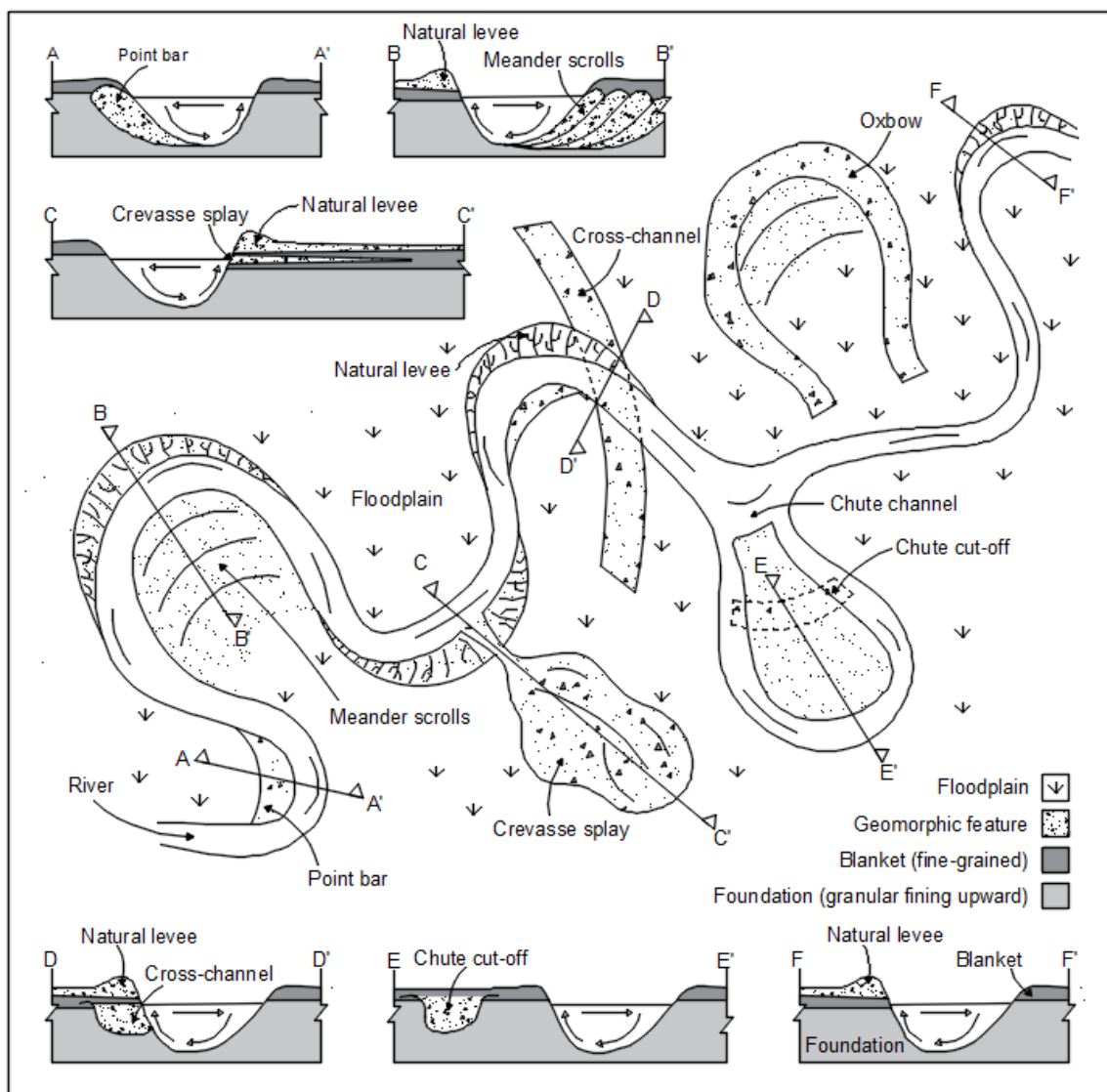


Figure 6.1. General geomorphology found in meandering river systems.

Figure 6.1 illustrates the most common geomorphic features encountered in a meandering river environment are high conductivity channels such as point bars, meander scrolls and abandoned channels; low conductivity channels such as neck cut-offs and

oxbows; and crevasse splays. Natural levees form adjacent to the river bank as a result of deposition when flood waters lose velocity when they escape the main channel. They are characterized by broad ridges that distally fade perpendicular to the river (see Figure 6.1, sections C-C', D-D', F-F') (Saucier 1994). Due to the deposition of natural levees, weak areas are present and erosion occurs when met with high flood stages. Eventually, with continuing erosion, a breach occurs forming a crevasse splay adjacent to the natural levee (Jacobson and Oberg 1997) as shown in Figure 6.1, section C-C'.

Point bars are accretionary alluvial deposits that generally develop along the convex bank of a meandering river (Nanson 1980, Brierley and Fryirs 2005, Ritter et al. 2011). As shown in Figure 6.1, they classically have an arcuate shape that imitate the curvature alignment of the river section adjacent to their formation (Brierley and Fryirs 2005). Likewise, meander scrolls (also known as scroll bars), form as an accumulation of successive point bars (Nanson 1981, Saucier 1994, Brierley and Fryirs 2005, Glynn and Kuszmaul 2010). They mirror activity of conflicting flow stages reflected as a complex ridge and swale feature (see Figure 6.1) (Brierley and Fryirs 2005, Wolman and Leopold 1957).

Paleo or abandoned channels consisting of cross channels and chute cut-offs, are generally characterized by granular deposits. Other channel deposits, like oxbows and neck cut-offs, consist of finer material (USACE 1956, Saucier 1994, Bridge 2003, Brierley and Fryirs 2005, Fryirs and Brierley 2013). In general, as shown in Figure 6.1, the authors consider a cross channel as an abandoned channel that intercepts the alignment of the river (and ultimately the levee). It is believed that chute cut-offs form either by successive



propagation of meandering scrolls or by river sediment transportation and erosion efficiency (USACE 1956, McGowen and Garner 1970, Brierley and Hickin 1992, Bridge 2003).

As the river channel migrates laterally, low-velocity flow tends to deposit finer sediment (overbank deposit) on top of the existing feature, creating the blanket layer that often underlay levees (Nanson 1980, Saucier 1994). This configuration does not allow enough total head loss to occur, increasing the probability of unsatisfactory performance near the landside levee toe. Crevasse splays and point bars both represent concentrated flow due to their granular makeup and confined reduction of the blanket layer thickness which pose a unique contribution on the internal erosion mechanism near the landside levee toe. The presence of the low hydraulic conductivity swale (scroll) may possibly block or concentrate seepage into the successive ridges, resulting in higher potential for internal erosion compared to the adjacent areas. Similar scenarios may be encountered with the presence of abandoned channels whether they are composed of granular or fine material.

Regardless of whether geomorphic features exist below the levee alignment, the typical arrangement of the overbank deposits (blanket) overlying the channel deposits (foundation) directly affects the internal erosion mechanism of a levee system due to the tendency for this configuration to result in high uplift pressure below the blanket. This phenomenon results in a background internal erosion hazard as well as interacting with the geomorphic features, should they exist.

### 6.2.3. RSMC analysis

Based on the limitations of the FOSM-BT method and on the hypothesis that levee underseepage susceptibility comes from localized subsurface geomorphic features that interrupt the characteristic profile, Rice and Polanco (2012) and Polanco and Rice (2014) have developed steady-state, 2D seepage models for assessing hydraulic conditions in geometrically complex levee profiles using what they call the Response Surface-Monte Carlo (RSMC) method. Rice and Polanco (2012) state the differences within methods and presents detailed steps for the RSMC method by means of analyzing two hypothetical complex levee profiles. Polanco and Rice (2014) presents the comparison of eight hypothetical levee profiles, where six of these studies are analyzable using both the FOSM-BT and RSMC methods. The other two levee profiles are beyond the capabilities of the FOSM-BT method and are only analyzed by means of the RSMC method (as presented in Rice and Polanco 2012). Where applicable, the difference between methods is minor but generally tends to increase with increasing model complexity. In both papers, regression analyses are performed in order to assess the relative effects that changes in the input parameters have on the results with the conclusion that, in most cases, geometric parameters have the greatest effect on the results.

Originally, the RSMC methodology was defined by 2D finite element (FEM) analysis with the flexibility of adjusting to any encountered levee scenario. The downfall of the method is that it can be time consuming since numerous FEM runs have to be done in order to develop the response surface (relationship between critical hydraulic conditions and uncertain input parameters) (Xu and Low 2006, Low 2008) that is used as the performance function for the Monte Carlo simulation analysis. Nevertheless, the RSMC

method builds on the limitations of the BT- FOSM method allowing for flexibility by: defining the underseepage failure mechanism (or critical hydraulic condition), (2) allowing more complex geologic foundation arrangement and, (3) defining the probabilistic state of the key input parameters.

In order to improve the methodology and focus on the effect of geomorphic features encountered along levee alignments, extensive research by Polanco-Boulware and Rice (2016, 2017) culminated in the expansion of the method by means of three-dimensional (3D) FEM computation and parametric analyses that help the method be less labor intensive. As mentioned, geomorphic features represent a concentrated pathway or blockage of flow that affect the internal erosion mechanism of a levee. Based on this hypothesis, Polanco-Boulware and Rice (2016, 2017) present the RSMC methodology applied to the underseepage effect of crevasse splays and high conductivity channels (such as point bars, meander scrolls, cross channels and chute cut-offs), respectively. The RSMC general steps that can be applied to geomorphic features are as follows:

1. Identify soil and geometric parameters with the aid of geological maps and published studies or reports,
2. Develop PDFs,
3. Develop a general 3D model with the identified key soil and geometry input parameters,
4. Perform parametric analyses using the general 3D model,

5. Simplify the general model to reduce the number of input parameters in the response surface based on the parametric analyses while using values of the developed PDFs,
6. Verify the simplified model for consistency with the general model with values of the developed PDFs by means of parametric analyses,
7. Develop response surface by means of multiple 3D finite-element analyses using the simplified model,
8. Fit response surface to curves developed through regression analysis to facilitate computer coding,
9. Write an Excel spreadsheet to randomly select values of key parameters from input PDFs and apply the response surface to produce cumulative ascending distribution functions (CADFs) taking into account curvature of levee if present and needed.

A CADF is a plot of increasing values of a key parameter versus the probability of the parameter being less than that value. It is important to mention that the resulting CADFs are a conditional (on a year flood level) probability of initiation of erosion assuming that the design flood level has been achieved. In order to compute the (total) probability of failure, similar analysis or judgement needs to be applied considering an event tree process as proposed by Foster et al. (2002) and Fell et al. (2003) of initiation, continuation and progression of erosion that leads to a failure or breach. Since the use of fragility curves, relationship of increasing flood loading versus conditional probability (Simm et al. 2008, USACE 2010), are useful and popular, Polanco-Boulware and Rice (2016, 2017) also demonstrate that fragility curves can be developed as a result of the RSMC's CADFs. In

addition, although the last RSMC step mentions the need for adjusting for levee curvature where applicable, it is a procedure that has never been presented in either of the papers and, for that reason, it is the main focus of this paper.

#### 6.2.4. Levee curvature

As mentioned, it is well known that levees may follow the meandering trajectory of the river aimed to protect from flooding. Nevertheless, one of the first simplifications (and limitation) that current methods use to analyze reliability of levees, is that of analyzing the levees as linear sections. In many analyses, the 3D effect of the levee curvature is likely counteracted by being more conservative, i.e. using higher factors of safety for the design calculations. However, the effect of levee curvature on the internal erosion potential of a site is undeniable. Inci (2008) and Merry and Du (2014) performed FEM analyses in the Natomas Basin levees in Sacramento, California and concluded that convex levee sections produce higher seepage gradients and consequently, lower factors of safety. Jafari et al. (2016) presented a 3D seepage model, using the Sherman Island levee system located at the confluence of the Sacramento and San Joaquin Rivers in Northern California as calibration, and also concluded that convex levee bends produce higher seepage gradients whereas concave bends produce lower seepage when compared to straight sections by means of 2D FEM seepage flow models.

Benjasupattananan (2013), Benjasupattananan and Meehan (2013) and, Meehan and Benjasupattananan (2014) expanded the blanket theory methodology and developed 2D closed-form equations that account for axisymmetric levee underseepage analysis. As

expected, it was reported that the concentration of seepage flow in convex levee sections is greater compared to straight sections and the opposite is expected on concave sections due to diffusive effects as reported by Jafari et al. (2016). Benjasupattananan (2013) also studied the 3D effect of curvature on levees with respect to different degrees of curvatures. Degree of curvature is the angle that the alignment changes over the length of the curve (Ghilani and Wolf 2014). Degrees of curvature were generally analyzed for two semi-pervious blanket cases: a limited region and, an extensive (or relatively infinite) region. Within the extensive semi pervious blanket theory cases, two scenarios were considered: a seepage block and a seepage opening, which correspond to cases 7b and 7c, respectively, as presented in USACE (1956, 2000). Based on boundary conditions (and not by the actual incorporation of a geomorphic feature), a seepage block can be considered as the modeling of a low conductivity channel and a seepage opening as a high conductivity channel for the BT cases mentioned above. A general blanket theory cross-section corresponding to case 7c related to a seepage opening is presented as Figure 6.2. For various degrees of curvature, results were reported as a function of pressure head at the landside levee toe versus arc length along the landside levee toe. In order for the results to be used within underseepage levee scenarios that fit the characterization of a seepage block or opening, pressure heads were normalized to their minimum value and longitudinal distances were normalized to half the arc length resulting in curves that can be used as enhancement coefficients for curvature adjustment. Figure 6.3 (adapted from Benjasupattananan, 2013), presents the normalized curves that embody a seepage opening (case 7c) for degrees of curvatures

ranging from  $30^\circ$  to  $180^\circ$  (semi-circle) with boundaries of  $0^\circ$  (straight) and  $360^\circ$  (axisymmetric) levee sections.

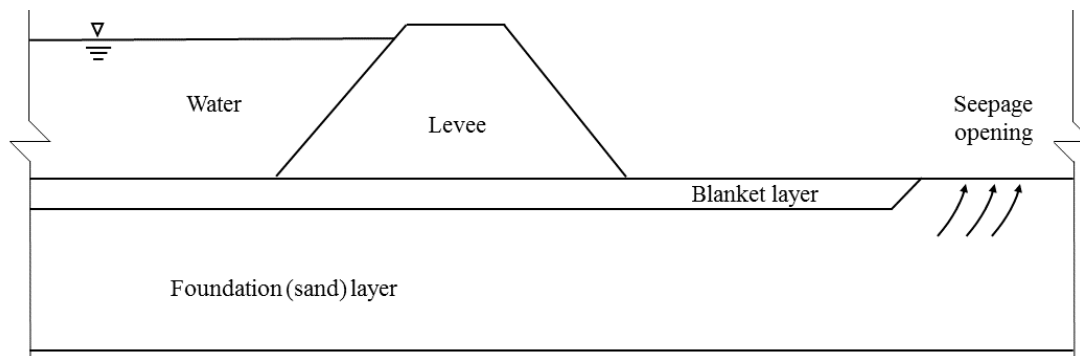


Figure 6.2. General blanket theory cross-section corresponding to case 7c referred as seepage opening.

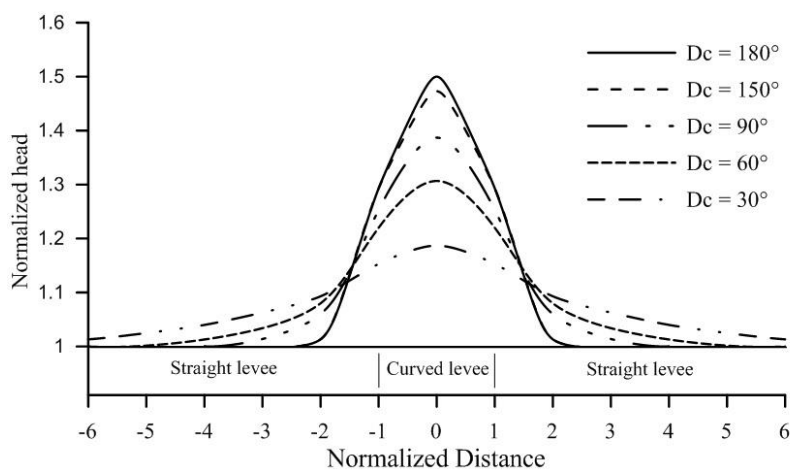


Figure 6.3. Normalized pressure head versus normalized longitudinal distance along the landside levee toe for BT case 7c.

Even though there has been great effort to account for levee curvature in underseepage analysis, an equivalent analysis that considers the effects that both geomorphic features and curvature alignment have on the internal erosion potential of the

levee reach does not currently exist. Therefore, the purpose of this paper is to describe a method that is easily understood and flexible enough to incorporate the effects of both geomorphic features and curvature in levee underseepage reliability. In particular, the effect of a seepage opening scenario (case 7c from BT equations) will be presented herein. With respect to geomorphic features, the interception of a point bar, meander scroll, or abandoned channels such as a cross channel or chute cut-offs can be considered as an open seepage scenario.

### **6.3. Combined effect of geomorphic features and levee curvature**

As it can be seen from Figure 6.1, geomorphic features form in association with river curvature and, thus, they are found to intersect the levee alignment. As mentioned, a great effort of research has focused on incorporating curvature as a levee underseepage parameter and it has shown that curvature has an important effect on levee underseepage performance (Inci 2008, Benjasupattananan 2013, Benjasupattananan and Meehan 2013, Meehan and Benjasupattananan 2014, Merry and Du 2014, Jafari et. al 2016). Nonetheless, the underseepage curvature levee scenario has not been studied in a geomorphic context.

Crevasse splays and high conductivity channels differ (for the most part) in where they form with respect to curvatures along the levee alignment and where they are found in the stratigraphic subsurface profile (refer to Figure 6.1). Usually, crevasse splays form between the “straight section” and concave bend of a curve in contrast with high conductivity channels that form on the convex bend (Allen 1965, Nanson 1980, Saucier 1994, Brierley and Fryirs 2005, USGS 2011). With respect to the subsurface profile,



crevasse splays are usually interbedded in the blanket layer (Farrell 1987, Saucier 1994) lacking a connection with the foundation layer while high conductivity channels are generally found to be in direct contact with the foundation. Based on the facts that some features are more prone to form on the concave alignment while others on the convex, and some features are connected to the foundation layer while others are not, it is reasonable to question if curvature influences the underseepage behavior of the levee and geomorphic feature relationship.

Recall that Inci (2008), Benjasupattananan (2013), Merry and Du (2014) and, Jafari et al. (2016) reported that analyses performed on concave bends resulted in lower hydraulic exit gradients as a consequence of seepage flow divergence whereas convex levee bends produced higher hydraulic exit gradients as a consequence of seepage flow concentration. Also, all of these analyses were performed on a simple two layer (blanket-foundation) model suggesting that the foundation to blanket layer connection provides most of the 3D curvature effects.

Polanco-Boulware and Rice (2016) proposed that the interconnection of the crevasse (channel and splay) to the blanket layer is what controls the underseepage behavior. Underseepage flow is described by the continuity of the conductance of the river flow to the channel ( $C_{channel}$ ), followed by the transmissivity of the splay ( $T_{splay}$ ) and dissipation by the conductance of the blanket ( $C_{blanket}$ ). Figure 6.4 presents a sketch of the model together with flow equations. This theory originated from parametric analyses where parameters that didn't provide significant changes to the outcome were not considered in the (simplified) flow model. That is the case of the hydraulic conductivity and thickness of

the foundation layer where it was found that modeling different ranges of these parameters while maintaining the others constant did not affect the flow outcome. Figure 6.5 presents results of these parametric analysis and the range of values used for each parameter are presented in the Supplemental Data section. Therefore, it can be implied, that underseepage analyses performed on the basis of crevasse splays along a levee may not need curvature adjustment.

On the other hand, Polanco-Boulware and Rice (2017) present a model for the underseepage analysis of high conductivity channels where seepage flow is controlled by the combination of a tongue effect ( $T_{ch}$ ) with respect to the (blanket layer) river length ( $RL$ ) that dissipates by means of a modified leakage ( $\lambda_m$ ). Figure 6.6 presents a sketch of the model together with flow equations.

As with the crevasse splay model, parametric analyses were performed to develop this theory. Parametric results based on the thickness ( $t_f$ ) and hydraulic conductivity ( $K_f$ ) of the foundation layer are shown as Figure 6.7 and the range of values used for each parameter are presented in the Supplemental Data section. Results for the variation of thickness of the foundation layer was found to not significantly affect the flow outcome contrary to the variation of the hydraulic conductivity of the foundation layer. Notice that for these parametric analyses values for the number of channel bars ( $N$ ), location of channel to levee ( $l_{ch}$ ), length of channel ( $L_{ch}$ ), landside blanket slope ( $m$ ), radius of curvature ( $R$ ) and, degree of curvature ( $Dc$ ) are not considered. The number of channel bars is only relative when meander scrolls are modeled and also by means of parametric analysis it was determined that it does not affect the seepage flow outcome. The location of channel to

levee, length of channel and landside blanket slope were also found to be insignificant. The radius and degree of curvature are only considered when curvature is modeled. Therefore, the model proposed by Polanco-Boulware and Rice (2017) can be applied to all high-hydraulic conductivity channels with the modification of curvature adjustment when needed.

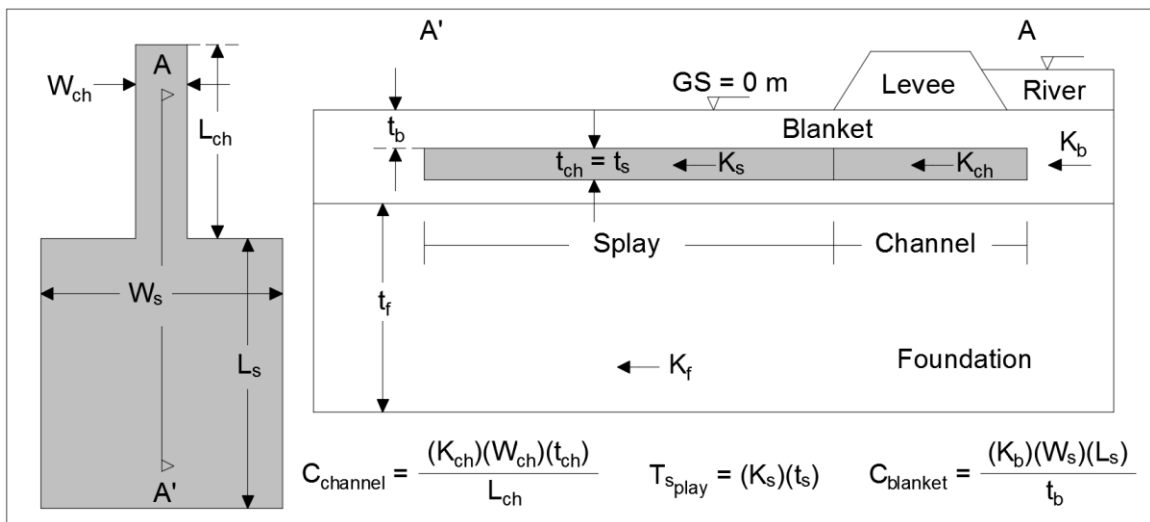


Figure 6.4. Parameters used for a crevasse splay underseepage model together with flow equations.

It is assumed that the high conductivity channel feature is hydraulically connected to the foundation layer.

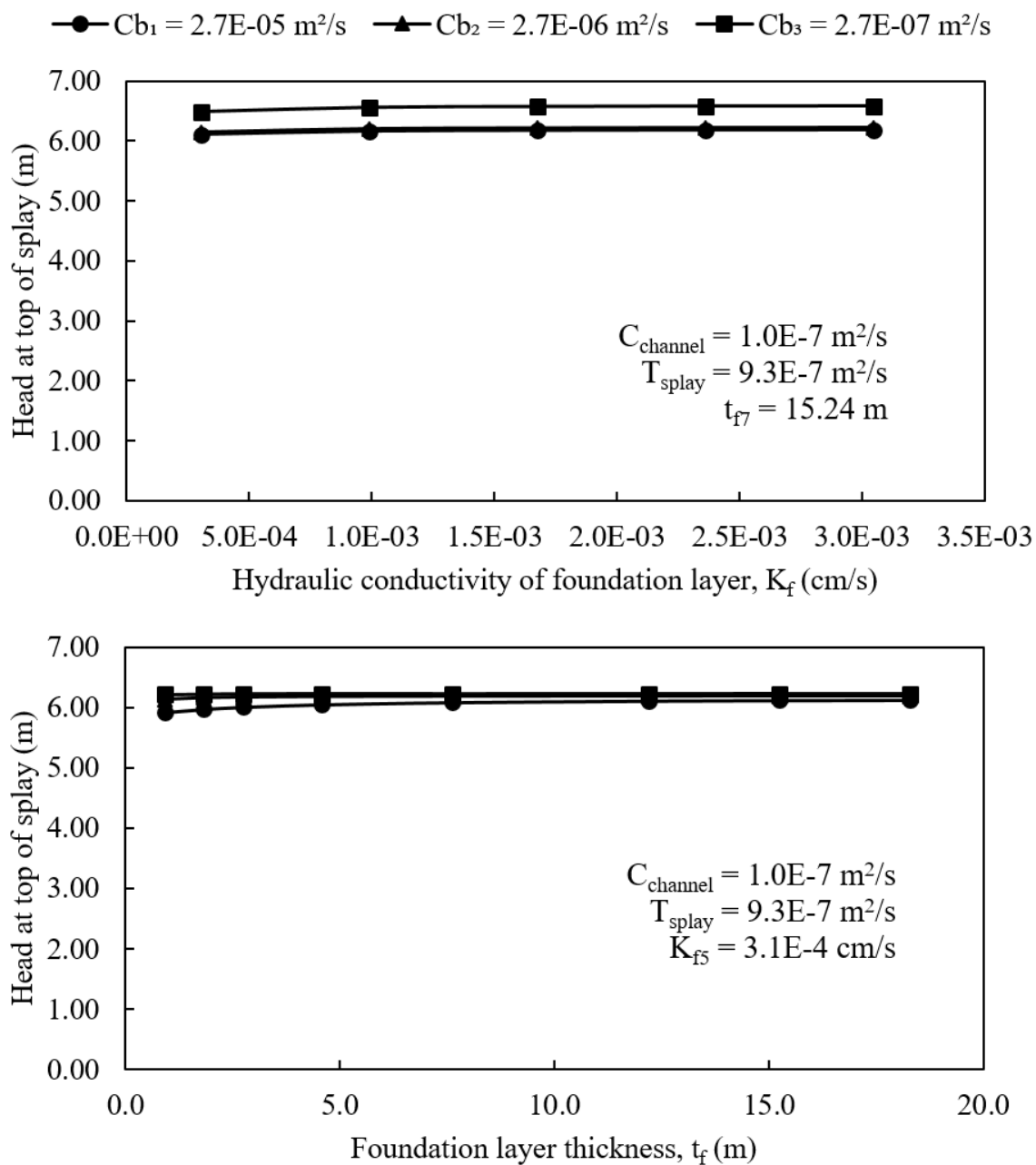


Figure 6.5. Family of curves for a crevasse splay with respect to the hydraulic conductivity of the foundation layer with constant  $C_{\text{channel}}$ ,  $T_{\text{splay}}$  and  $t_f$  and a range of  $C_{\text{blanket}}$ .

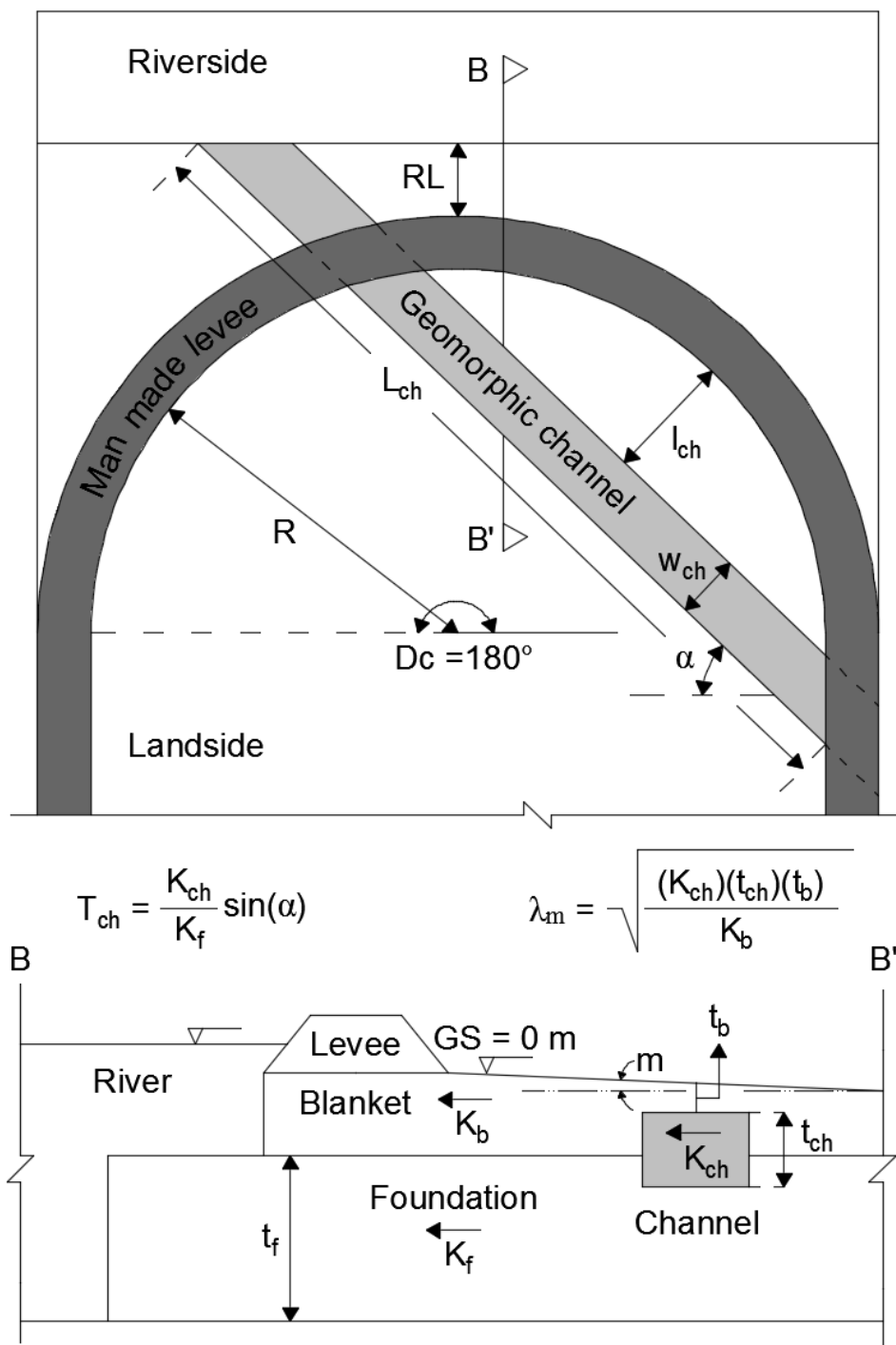


Figure 6.6. Parameters used for a high conductivity channel underseepage model together with flow equations.

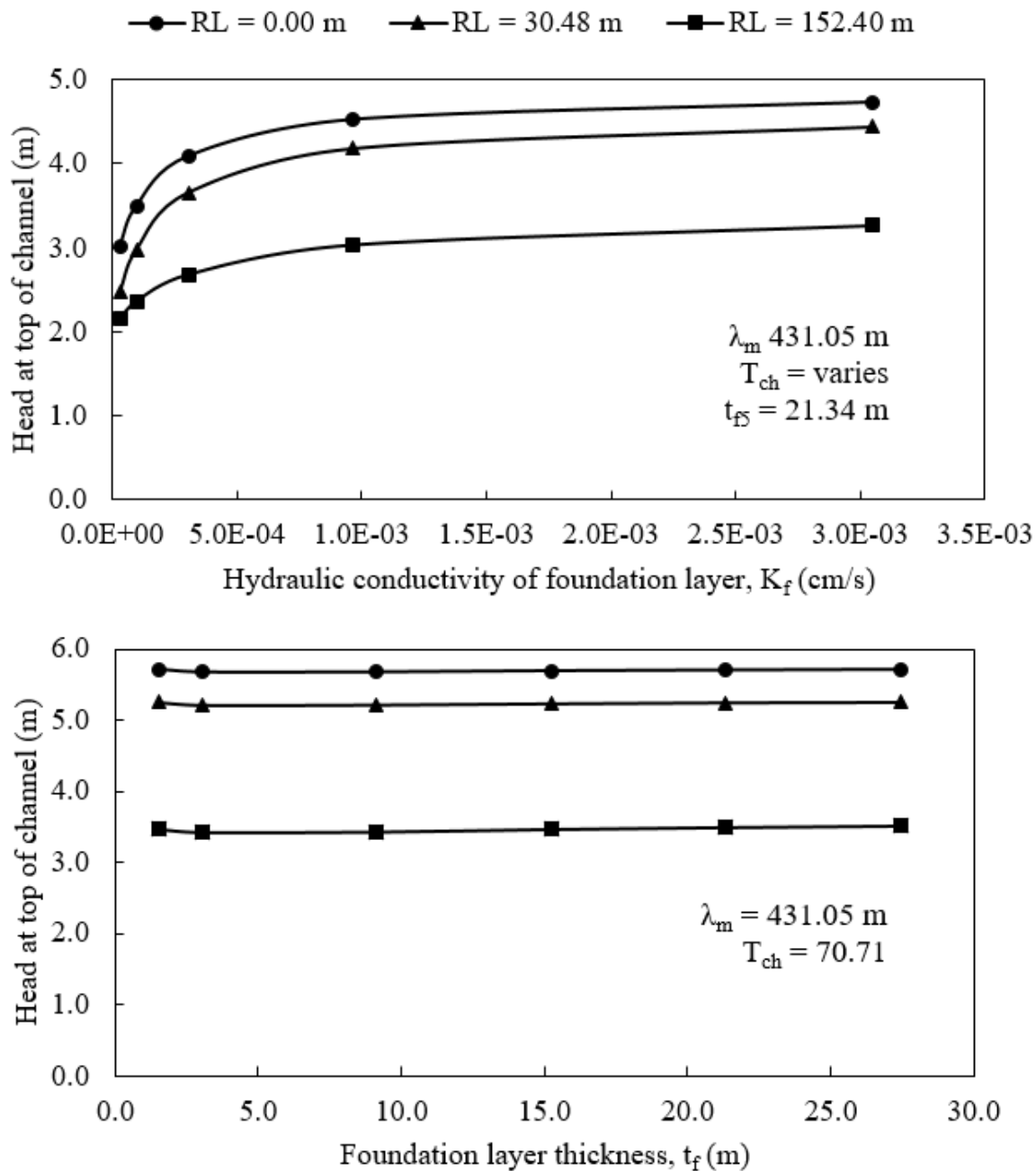


Figure 6.7. Family of curves for a high conductivity model with respect to the hydraulic conductivity of the foundation layer with constant  $\lambda_m$  and  $T_{ch}$  (where applicable) and a range of river lengths ( $RL$ ).

This assumption is supported by understanding of the depositional processes that create high conductivity channels (such as cross channels and point bars) (see Figure 6.1).

This hydraulic connection allows a three dimensional concentration of flow that occurs in the foundation layer due to the levee degree of curvature to be translated to the channel or point bar, thus affecting the flow in the geomorphic feature. This hydraulic connection between layers is similar to those presented by Inci (2008), Merry and Du (2014), Jafari et al. (2016) and specially Benjasupattananan (2013). Benjasupattananan (2013)'s curvature approach is reasonably straight forward, provides the analysis of an open seepage levee scenario for different degrees of curvature, and it is able to handle the incorporation of geomorphic features while performing parametric analysis. Therefore, Benjasupattananan (2013)'s degree of curvature approach is used to study the combined effects of high conductivity channels and degree of curvature.

### 6.3.1. Curvature-channel model description and results

The 3D-FEM models presented in this section follow the same geometry and boundary conditions as used by Benjasupattananan (2013), with the difference of the incorporation of a high conductivity channel feature. In order to compare results between different degrees of curvature, a constant radius of curvature was used while analyzing four degree of curvatures: 30°, 60°, 90° and 150°. For these degrees of curvature, a high conductivity channel was modeled based on the location of the feature with respect to the levee curvature alignment as to match the exact locations when normalized to half the arc length (this parameter is called normalized distance, *ND*). Forty-five degree and 90° angles of incision (angle at which the channel intercepts the levee alignment) were used to characterize the high conductivity channel's angularity. Figure 6.8 presents the curvature-

channel model used for a  $Dc = 90^\circ$  with a high conductivity channel angle of incision ( $\alpha$ ) equal to  $90^\circ$ .

The normalized curves represent a curvature response surface useful to adjust the analysis of high conductivity channels by means of a RSMC approach. Results for a  $Dc = 90^\circ$  with an  $\alpha = 90^\circ$  is presented as Figure 6.9. Values used for this curvature-channel model together with normalized results are provided in Table 6.1.

Results and parameters used for the other combinations of curvature and channel angularity are presented in the Supplemental Data section.

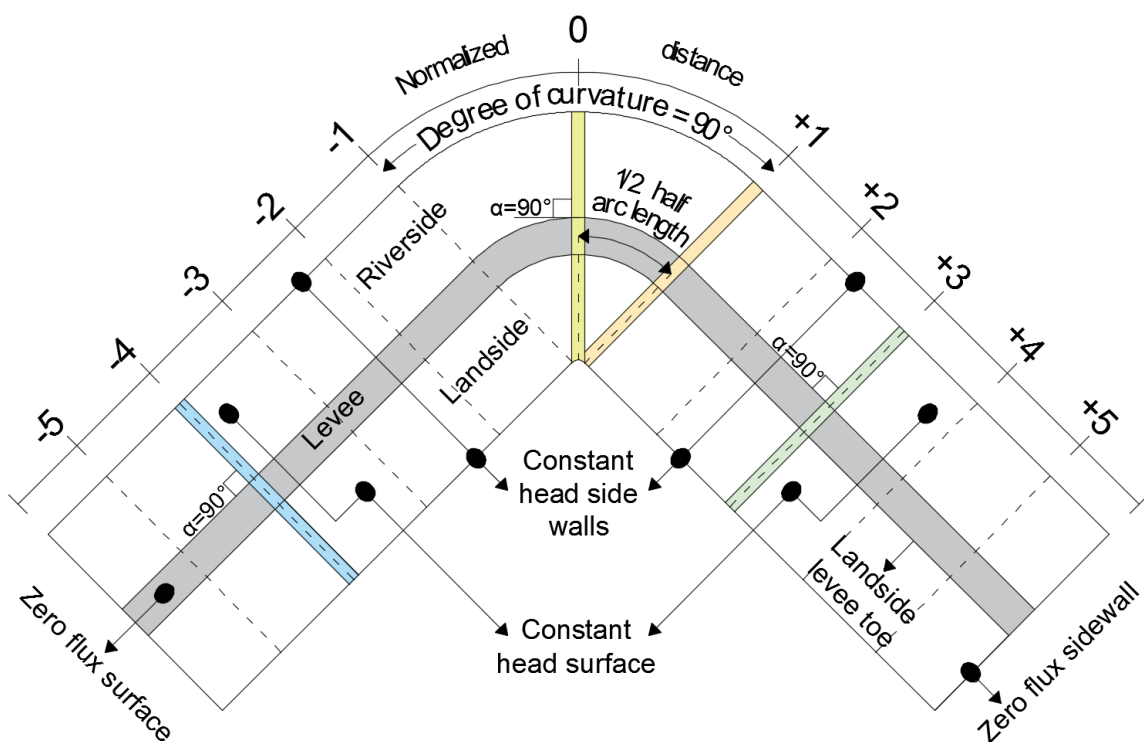


Figure 6.8. Schematic top view of the curvature model used for  $Dc = 90^\circ$  and  $\alpha = 90^\circ$  showing channel features at  $ND = -4, 0, +1 +3$ .



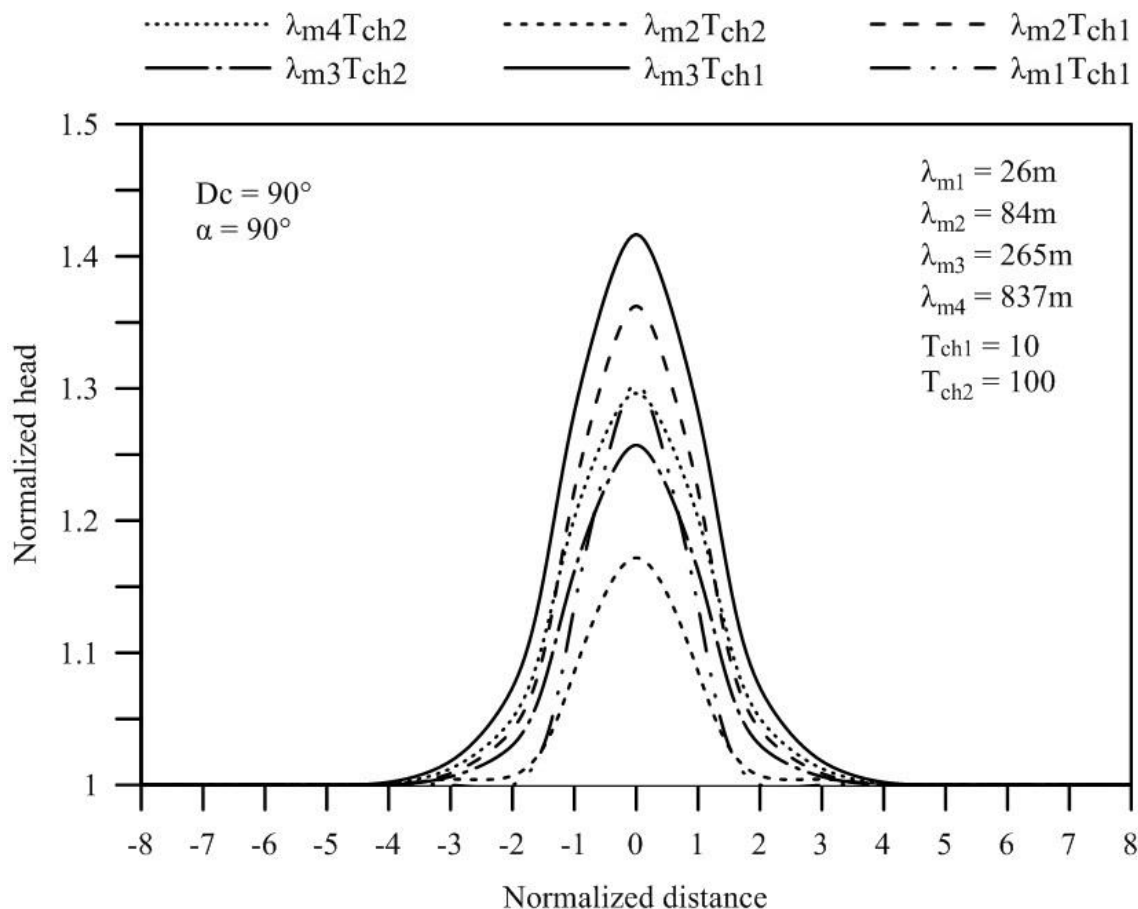


Figure 6.9. Results for the curvature model presented in Figure 6.8.

As seen on Figure 6.9, different sets of coefficients result from the combination of different levels of  $T_{ch}$  and  $\lambda_m$ .  $\lambda_m$  acts as an inhibitor coefficient since as it increases the head dissipation through the blanket layer decreases, and vice versa. With respect to  $T_{ch}$ , as  $T_{ch}$  increases the head dissipation will also increase and vice versa. Hence, the combination of a high  $\lambda_m$  (less dissipation through the blanket) and a low  $T_{ch}$  (less dissipation through the channel) provides the highest coefficient ( $\lambda_{m3}T_{ch1}$ ). The combination of an average (high) modified leakage with a high tongue ( $\lambda_{m2}T_{ch2}$ ) provides the smallest coefficient due to the fact that the leakage between the blanket and foundation

layer ( $\lambda$ ) is low allowing for more dissipation through the blanket, contrary to the previous scenario where  $\lambda \approx \lambda_m$ . Finally, the combination of a low  $\lambda_m$  and  $T_{ch}$  ( $\lambda_{m1}T_{ch1}$ ) provides an average coefficient where  $\lambda \approx \lambda_m$ . Contrary to what the authors' had originally hypothesized, the interception of a high conductivity channel diminishes the curvature effect by allowing more 3D dissipation as can be seen for the modeled scenarios where  $T_{ch} = T_{ch2}$  in Figure 6.9.

Table 6.1. Values used for the curvature-channel model presented in Figure 6.8

<b>Curvature multiplier for <math>Dc = 90^\circ</math> with <math>\alpha = 90^\circ</math></b>						
$K_f = 1E-05$ m/s, $t_b = 2$ m, $t_{ch} = 3.5$ m, $t_f = 32$ m, $w_{ch} = 10$ m, $RL = 200$ m						
Stage	$\lambda_{m1}T_{ch1}$	$\lambda_{m2}T_{ch1}$	$\lambda_{m3}T_{ch1}$	$\lambda_{m2}T_{ch2}$	$\lambda_{m3}T_{ch2}$	$\lambda_{m4}T_{ch2}$
$K_b$ (m/s)	1.00E-06	1.00E-07	1.00E-08	1.00E-06	1.00E-07	1.00E-08
$K_{ch}$ (m/s)	1.00E-04	1.00E-04	1.00E-04	1.00E-03	1.00E-03	1.00E-03
$\lambda_m$ (m)	26.5	83.7	264.6	83.7	264.6	836.7
$T_{ch}$	10	10	10	100	100	100
$\lambda$ (m)	25.3	80.0	253.0	25.3	80.0	253.0
Normalized distance	Head at top of channel (m)					
-8	1	1	1	1	1	1
-7	1	1	1	1	1	1
-6	1	1	1	1	1	1
-5	1	1	1	1	1	1
-4	1	1	1	1	1	1
-3	1.00	1.01	1.02	1.00	1.01	1.01
-2	1.00	1.04	1.07	1.01	1.03	1.05
-1	1.14	1.22	1.28	1.09	1.16	1.20
0	1.30	1.36	1.42	1.17	1.26	1.30
1	1.14	1.22	1.28	1.09	1.16	1.20
2	1.00	1.04	1.07	1.01	1.03	1.05
3	1.00	1.01	1.02	1.00	1.01	1.01
4	1	1	1	1	1	1
5	1	1	1	1	1	1
6	1	1	1	1	1	1
7	1	1	1	1	1	1
8	1	1	1	1	1	1

A similar trend can be seen for the curvature model where  $D_c = 90^\circ$  and  $\alpha = 45^\circ$ . A schematic figure of this model together with results and parameters are part of the Supplemental Data section. Two main differences can be observed: (1) the curves are not symmetrical and rather skewed due to the way the channel feature intercepts the levee and the location of the channel with respect to the landside toe of the levee in certain locations and, (2) the condition where  $\lambda_m$  and  $T_{ch}$  are the lowest ( $\lambda_m T_{chl}$ ) provide the highest curvature coefficient which might be either a consequence of angularity or that the channel is acting as a seepage block due to the low tongue effect. As with the  $D_c = 90^\circ$  and  $\alpha = 90^\circ$  model, results suggest that the presence of high conductivity channel diminishes the underseepage curvature effect.

#### **6.4. Research case study**

The developed curvature-channel response surface is used to assess a meander scroll feature that intercepts the Sacramento, California east side levee reach located along the Little Pocket as shown in Figure 6.10. The response surface presented by Polanco-Boulware and Rice (2017) is used with the input parameters as presented in Table 6.2. The maximum and minimum values provided in Table 6.2 are used to truncate the distributions to avoid numerical errors and unrealistic values outside the response surface. The sequence to compute the factor of safety against heave,  $F_{heave}$ , and the hydraulic exit gradient through the blanket,  $i_{blanket}$ , are presented in the RSMC section above. The analysis is based on 5.8m (19 ft) of differential head across the levee which corresponds to the 100-year flood level.

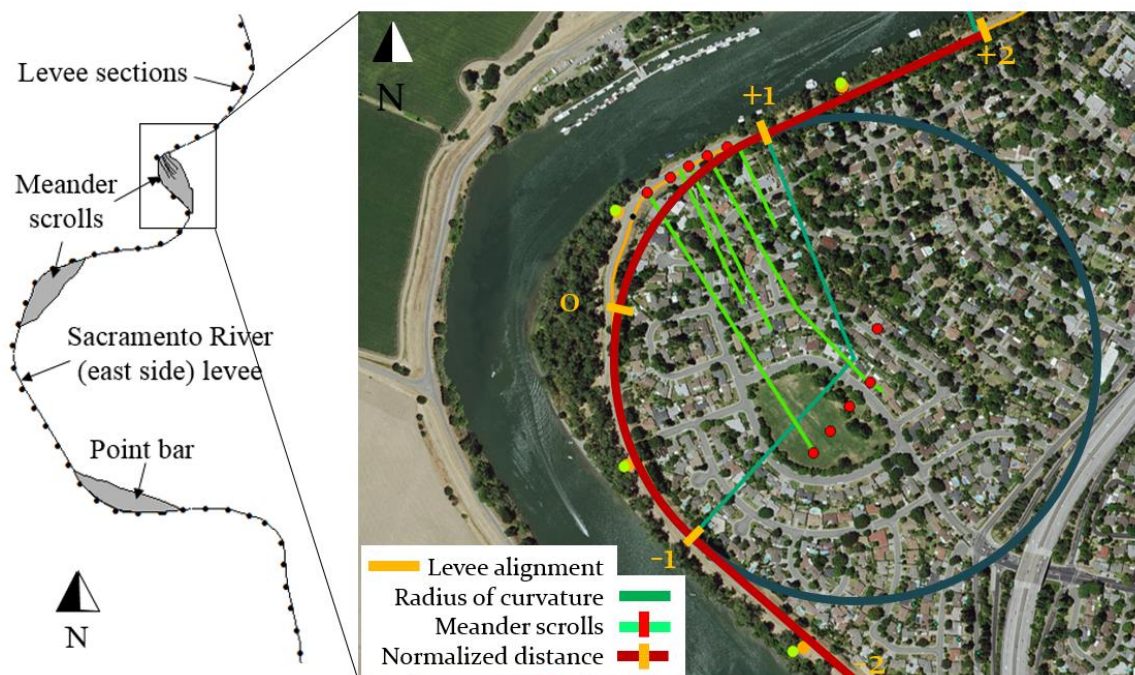


Figure 6.10. Meander scroll feature located along the Little Pocket in Sacramento, CA.

Table 6.2. Input parameters for the PDFs used to develop the CADFs for the meander scrolls feature presented in Figure 6.10

Parameter	Units	Type of PDF distribution	Most likely value	Standard deviation	Truncated value	
					Min	Max
Thickness of the channel ( $t_{ch}$ )	m	Normal	4.1	0.6	1.5	6.1
Thickness of the blanket ( $t_b$ )	m	Normal	3.7	0.9	0.6	6.1
Angle of incision of channel ( $\theta$ )	m	Normal	82	19.9	10	90
Blanket layer river length ( $RL$ )	m	Normal	5.5	27.4	4.0	392.0
Log of channel hyd. cond. ( $\log K_{ch}$ )	log(cm/s)	Normal	-2.0	2.5	-4.5	-2.5
Log of blanket hyd. cond. ( $\log K_b$ )	log(cm/s)	Normal	-6.5	2.5	-7.5	-5.5
Hydraulic conductivity channel to foundation ratio ( $K_{ch}/K_f$ )	-	Lognormal	50	100	1	1000
Unit weight of the blanket ( $\gamma_{blkt}$ )	KN/m <sup>3</sup>	Normal	18.85	1.57	17.28	20.42
Normalized distance ( $ND$ )	-	Normal	0.8	0.1	0	1.4
Degree of curvature ( $Dc$ )	°	Normal	106	3	96	116

The resulting conditional probabilities are presented as Table 6.3 and the CADF corresponding to  $F_{\text{heave}}$  with no curvature adjustment is presented as Figure 6.11 for illustration. The rest of the CADFs are presented in the Supplemental Data section. The condition of a value of 1.0 for the respective conditional probabilities has been chosen as a critical criteria but other conditional probabilities can be calculated as desired using the same CADFs.

At first glance, the resulting probability of failures presented in Table 6.3 for all the cases may seem high, however, this is mainly due to several reasons: (1) this is an assessment for a 100-year flood level, the annual probability will be about 1% of the value (2) a single analysis by using the MLVs simulates the condition were a high  $\lambda_m$  with a low  $T_{ch}$  and  $\lambda \approx \lambda_m$  are present which is the combination of parameters that provides the highest curvature coefficient (combination  $\lambda_{m3}T_{ch1}$  as presented in Figure 6.9), (3) the meander scrolls feature are located between NDs of 0 and +1 which also provide high coefficients of curvature adjustment, (4) the  $t_b$  near the center of the feature along the landside levee toe is as low as 6.6 m (2 ft) according to borings by URS (2008) and in situations like this, low FSs are expected and, (5) the RL near this area is significantly low which also provides higher hydraulic heads which result in lower FSs. Furthermore, historical data for the years 1986 and 1995 presented by URS (2008) confirm a vast presence of boil and seepage along the specific area of study as shown in Figure 6.12.

Table 6.3. Results for the conditional probabilities with respect to  $i_{blanket}$  and  $F_{heave}$  with and without curvature adjustment for the meander scroll feature presented in Figure 6.10

Conditional probability of initiation of erosion (%)	Curvature adjustment	
	No	Yes
$F_{heave}$ considered $\leq 1.0$	88.7	97.6
$i_{blanket}$ considered $\geq 1.0$	82.8	95.0

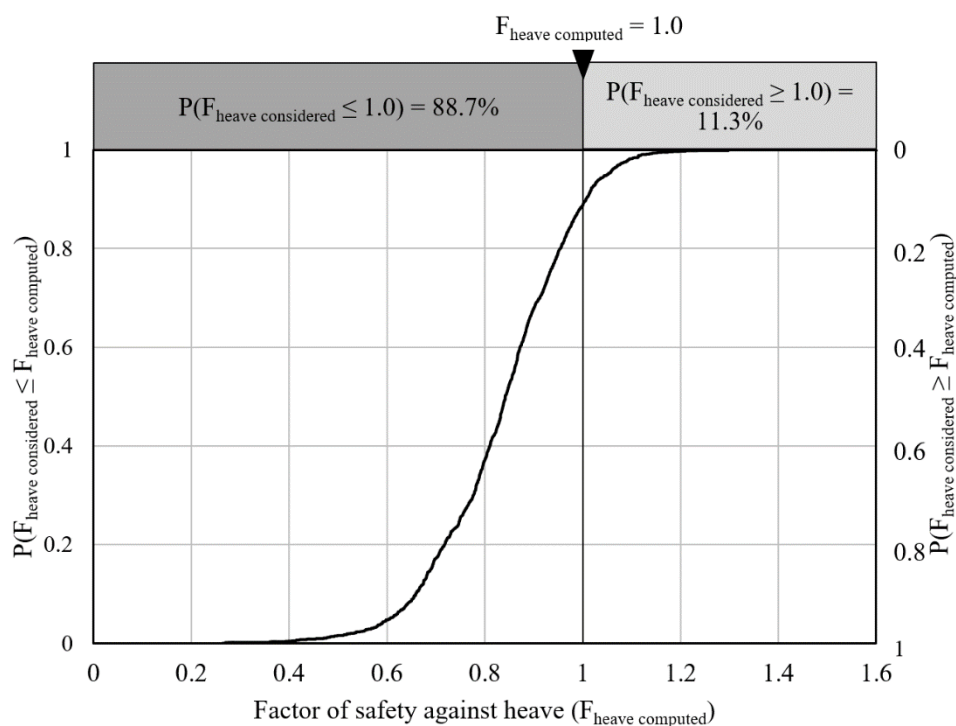


Figure 6.11. CADF for factor of safety against heave,  $F_{heave}$  with no curvature adjustment for the meander scroll feature presented in Figure 6.10.

Sensitivity analyses for the four conditional probabilistic scenarios considered were performed and are presented by means of tornado graphs as was done by Polanco-Boulware and Rice (2016, 2017).

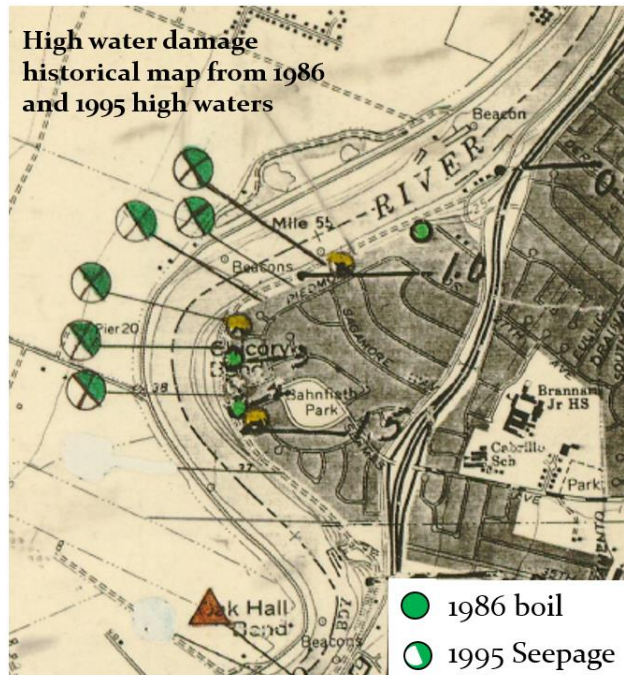


Figure 6.12. Historical map showing locations of boils and seepage along the Little Pocket in Sacramento, CA.

Since the computation for  $i_{blanket}$  and  $F_{heave}$  depend directly on certain parameters, sensitivity analysis with respect to  $h_{max}$  (at the top of the channel) at the landside levee toe was also performed due to its dependence to most of the input parameters. The statistical function considered for the development of the tornado graphs was the mean. A summary of the results is presented as Table 6.4. The tornado graph for  $h_{max}$  is presented as Figure 6.13 and the rest are available in the Supplemental Data section. Results suggest that the thickness of the blanket ( $t_b$ ) is the most significant parameter whether there is curvature adjustment or not for all scenarios. Also, in general, the hydraulic conductivity of the blanket ( $K_b$ ) and hydraulic conductivity of the channel feature ( $K_{ch}$ ) and blanket layer river length ( $RL$ ) tend to be among the most significant parameters. All of these parameters are involved in the computation of the combined parameters  $\lambda_m$  and  $T_{ch}$  and the independent

parameter  $RL$ . Taking this into consideration, it could be inferred that the response surface based on these combined parameters is a good depiction of the seepage flow in a high-hydraulic conductivity channel.

Table 6.4. Summary of results for sensitivity analyses showing the three most statistical significant parameter

Tracked parameter (mean)	Significant parameter					
	No curvature			With curvature		
	Most	Second	Third	Most	Second	Third
$h_{max}$	$t_b$	$RL$	$\log(K_{ch})$	N/A – $h_{max}$ not affected by curvature		
$i_{blanket}$	$t_b$	$\log(K_b)$	$\log(K_{ch})$	$t_b$	$\log(K_b)$	$\log(K_{ch})$
$F_{heave}$	$t_b$	$\log(K_{ch})$	$\log(K_b)$	$t_b$	$RL$	$\log(K_{ch})$

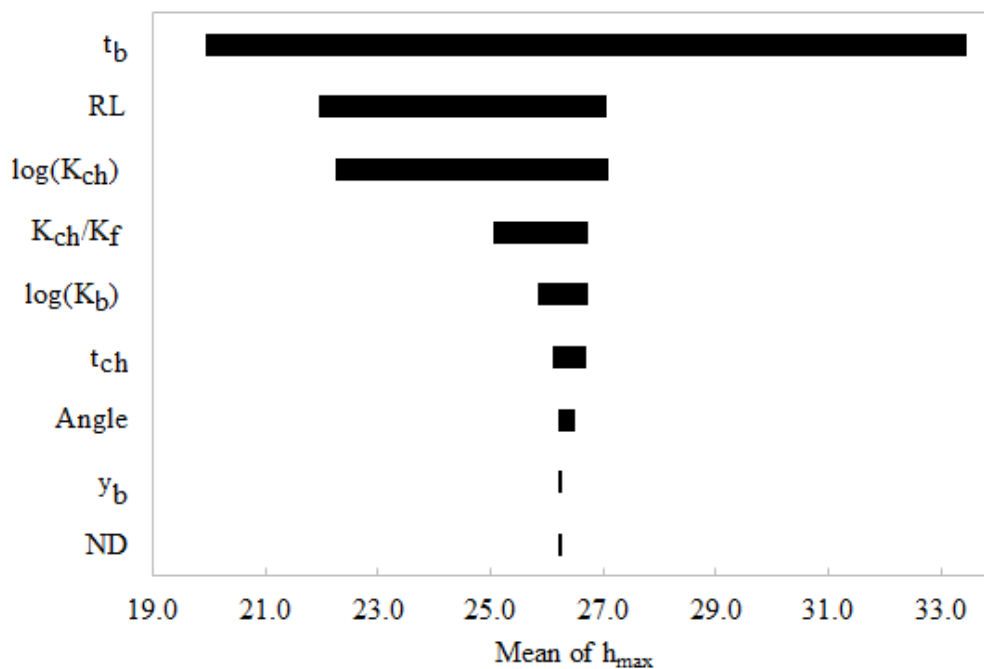


Figure 6.13. Sensitivity tornado graph for mean of  $h_{max}$  with no curvature adjustment.



## 6.5. Summary and Conclusions

This paper presents the combined effect that levee curvature and the interception of a geomorphic feature have on the backward erosion piping internal erosion levee mechanism due to underseepage. The three-dimensional curvature model is based on findings by Benjasupattananan (2013). Based on parametric analysis, a high hydraulic conductivity channel was determined to need curvature adjustment and is used as the main geomorphic feature of study. The combined curvature-feature effect was studied for degrees of curvature corresponding to 30°, 60°, 90° and 150° are with channel feature angularities of 90° and 45°. Three-dimensional parametric analyses performed with respect to these combinations and significant soil parameters result in a curvature-feature response surface that describes the total hydraulic head at the landside levee toe versus arc length along the landside levee toe.

Parametric results were normalized in order to make direct comparison between the various degrees of curvatures. Normalizing the results provide a curvature-feature response surface that act as enhancement coefficients for curvature adjustment. This curvature-feature response surface can be used together with a response surface Monte Carlo (RSMC) simulation method as presented by Polanco-Boulware and Rice (2017). Also, parametric results suggest that the interception of a high hydraulic conductivity channel on a curved levee alignment aids with seepage dissipation.

A meander scroll geomorphic feature located in the Little Pocket of the Sacramento River levee system is found to intercept the east side levee alignment and it is used as a research case study. Results are presented by means of cumulative ascending distribution

functions that represent the conditional probability of initiation of erosion with respect to a hydraulic exit gradient through the blanket layer ( $i_{blanket}$ ) or a factor of safety with respect to heave ( $F_{heave}$ ). Several reasons are found to produce unfavorable results: (1) the reliability analysis is performed for a 100-year flood, (2) simulation by means of MLVs provide the worst case scenario that produces high curvature enhancement coefficients, (3) the meander scroll is near the apex of the curvature alignment which also provides the highest enhancement coefficients, (4) thickness of the blanket ( $t_b$ ) near the center of the meander scroll feature have been found to be thin which is expected to produce low factors of safety ( $FS$ ) and, (5) the blanket layer river length ( $RL$ ) near this area is significantly low which also provides higher hydraulic heads which result in lower FSs.

Tornado graphs are presented to provide the statistical significance the input parameters used in the reliability assessment have on the computed  $i_{blanket}$  and  $F_{heave}$ . Sensitivity analysis for  $h_{max}$  were also performed since this outcome depends mostly on all the input parameters compared to the  $i_{blanket}$  and  $F_{heave}$  only depend on some specific ones respectively. Overall, the  $t_b$  is found to be the most significant parameter whether there is curvature adjustment or not followed by the  $K_{ch}$ ,  $K_b$  and the  $RL$ . This parameters are used to describe the seepage that controls a high conductivity channel and based on results are representative of the seepage behavior.

## 6.6. Acknowledgement

This material is based upon work supported by the National Science Foundation (NSF) under Grant CMMI 1400640 and the United States Society on Dams (USSD) 2015

Scholarship. Any opinions, findings, and conclusions or recommendations expressed in this material are those of the authors and not necessarily the views of NSF and USSD.

### **6.7. Supplemental data**

Tables S6.1 and S6.2 present the parameters used for the crevasse splay and high hydraulic conductivity models shown as Figures 6.4 and 6.6, respectively. Figure S6.1 presents the curvature-channel model used for a  $Dc = 90^\circ$  with a high conductivity channel with  $\alpha = 45^\circ$ ; the corresponding parameters and results for the curvature model are presented as Table S6.3 and Figure S6.2. Figure S6.3 presents the curvature-channel model used for a  $Dc = 150^\circ$  with a high conductivity channel with  $\alpha = 90^\circ$ ; the corresponding parameters and results for the curvature model are presented as Table S6.4 and Figure S6.4. Figure S6.5 presents the curvature-channel model used for a  $Dc = 150^\circ$  with a high conductivity channel with  $\alpha = 45^\circ$ ; the corresponding parameters and results for the curvature model are presented as Table S6.5 and Figure S6.6. Figures S6.7 through S6.9 provide the CADFs related to Table 6.3. Figures S6.10 through S6.13 present the sensitivity tornado graphs also related to the results of Table 6.3.

Table S6.1. Parameters used for parametric analysis as presented in Figure 6.4

$K_{ch} = K_{sp} = 3.05 \text{ E-4 cm/s}$	$K_{b1} = 2.7 \text{ E-5 cm/s}$	$t_{f1} = 0.91 \text{ m}$
$W_{ch} = 1.22 \text{ m}$	$K_{b2} = 2.7 \text{ E-6 cm/s}$	$t_{f2} = 1.83 \text{ m}$
$t_{ch} = t_s = 0.30 \text{ m}$	$K_{b3} = 2.7 \text{ E-7 cm/s}$	$t_{f3} = 2.74 \text{ m}$
$L_{ch} = 11.28 \text{ m}$	$K_{f1} = 3.1 \text{ E-3 cm/s}$	$t_{f4} = 4.57 \text{ m}$
$W_s = 15.24 \text{ m}$	$K_{f2} = 2.4 \text{ E-3 cm/s}$	$t_{f5} = 7.62 \text{ m}$
$L_s = 35.05 \text{ m}$	$K_{f3} = 1.7 \text{ E-3 cm/s}$	$t_{f6} = 12.19 \text{ m}$
$t_b = 0.61 \text{ m}$	$K_{f4} = 9.9 \text{ E-4 cm/s}$	$t_{f8} = 18.29 \text{ m}$

Table S6.2. Parameters used for parametric analysis as presented in Figure 6.6

$K_{ch} = 3.05 \text{ E-2 cm/s}$	$K_{f1} = 3.05 \text{ E-5 cm/s}$	$t_{f1} = 1.52 \text{ m}$
$K_b = 3.05 \text{ E-6 cm/s}$	$K_{f2} = 9.64 \text{ E-5 cm/s}$	$t_{f2} = 3.05 \text{ m}$
$W_{ch} = 9.14 \text{ m}$	$K_{f3} = 3.05 \text{ E-4 cm/s}$	$t_{f3} = 9.14 \text{ m}$
$t_{ch} = 6.10 \text{ m}$	$K_{f4} = 9.64 \text{ E-4 cm/s}$	$t_{f4} = 15.24 \text{ m}$
$t_b = 3.05 \text{ m}$	$K_{f5} = 3.05 \text{ E-3 cm/s}$	$t_{f5} = 21.34 \text{ m}$
$\alpha = 45^\circ$	$N = m = l_{ch} = L_{ch} = R = D = 0$	$t_{f6} = 27.43 \text{ m}$

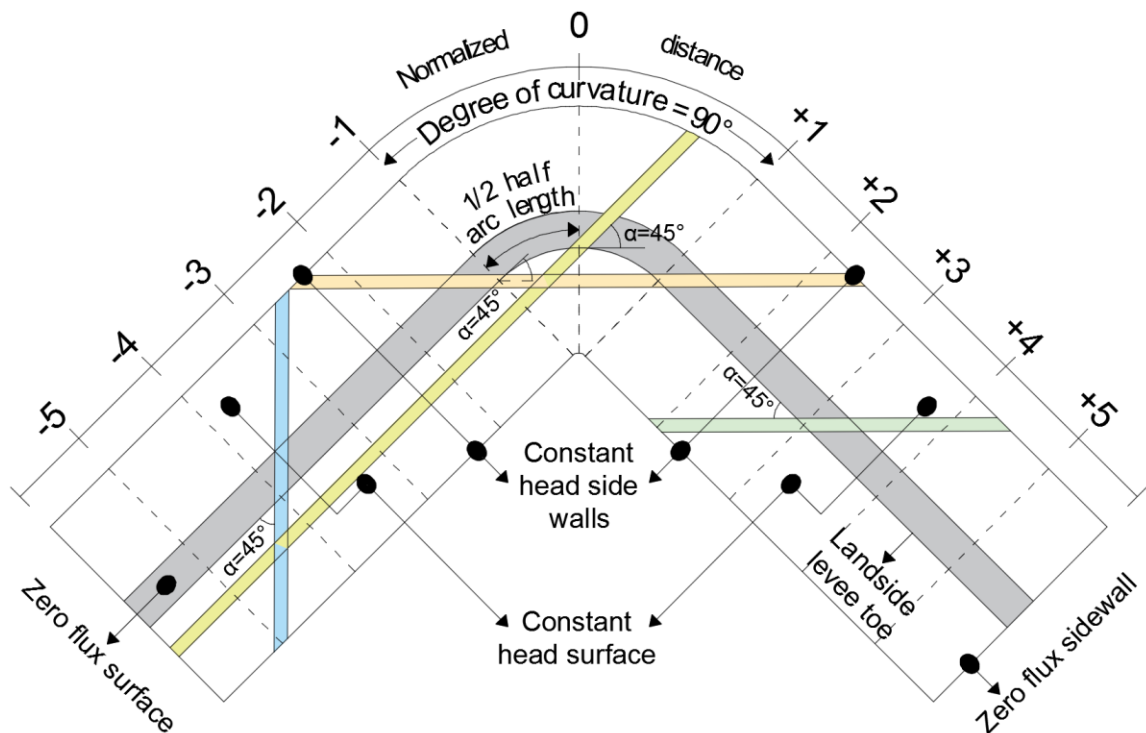
Figure S6.1. Schematic top view of the curvature model used for  $Dc = 90^\circ$  and  $\alpha = 45^\circ$  showing channel features at  $ND = -4, 0, +1 +3$ .

Table S6.3. Parameters and results for the curvature model with  $D_c = 90^\circ$  and  $\alpha = 45^\circ$ 

<b>Curvature multiplier for <math>D_c = 90^\circ</math> with <math>\alpha = 45^\circ</math></b>					
$K_f = 1\text{E-}05$ m/s, $t_b = 2$ m, $t_{ch} = 3.5$ m, $t_f = 32$ m, $w_{ch} = 10$ m, $RL = 200$ m					
Stage	$\lambda m_1 T_{ch_1}$	$\lambda m_2 T_{ch_1}$	$\lambda m_3 T_{ch_1}$	$\lambda m_2 T_{ch_2}$	$\lambda m_3 T_{ch_2}$
$K_b$ (m/s)	1.00E-06	1.00E-07	1.00E-08	1.00E-06	1.00E-07
$K_{ch}$ (m/s)	1.00E-04	1.00E-04	1.00E-04	1.00E-03	1.00E-03
$\lambda_m$ (m)	26.5	83.7	264.6	83.7	264.6
$T_{ch}$	10	10	10	100	100
$\lambda$ (m)	83	262	830	83	262
Normalized distance, ND	Normalized head at top of channel				
-8	1	1	1	1	1
-7	1	1	1	1	1
-6	1	1	1	1	1
-5	1	1	1	1	1
-4	1	1	1	1	1
-3	1.01	1.01	1.02	1.00	1.01
-2	1.07	1.21	1.29	1.08	1.23
-1	1.37	1.51	1.59	1.24	1.40
0	1.65	1.44	1.47	1.41	1.43
1	1.22	1.25	1.30	1.16	1.31
2	1.00	1.04	1.07	1.00	1.04
3	1.02	1.01	1.01	1.01	1.01
4	1	1	1	1	1
5	1	1	1	1	1
6	1	1	1	1	1
7	1	1	1	1	1
8	1	1	1	1	1

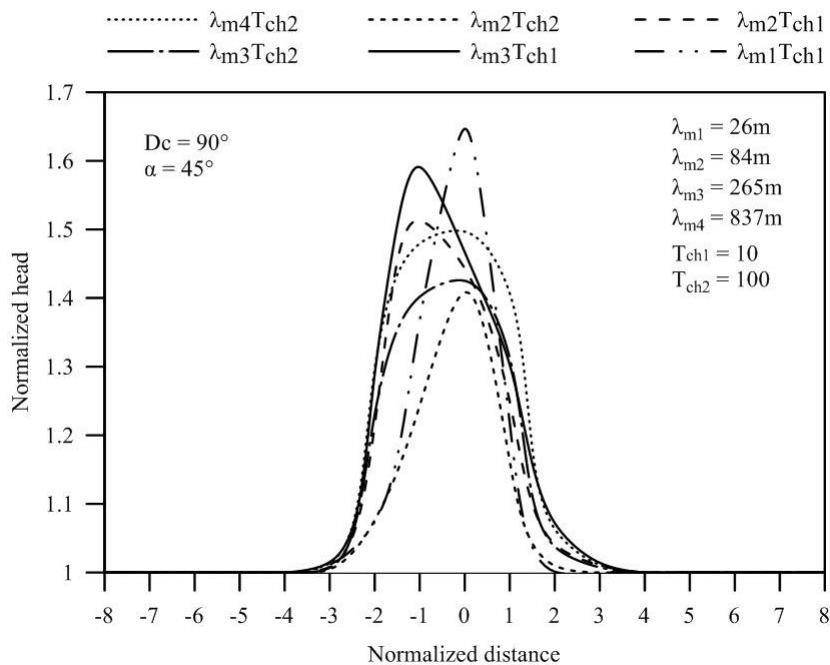


Figure S6.2. Results for the curvature model with  $D_c = 90^\circ$  and  $\alpha = 45^\circ$ .

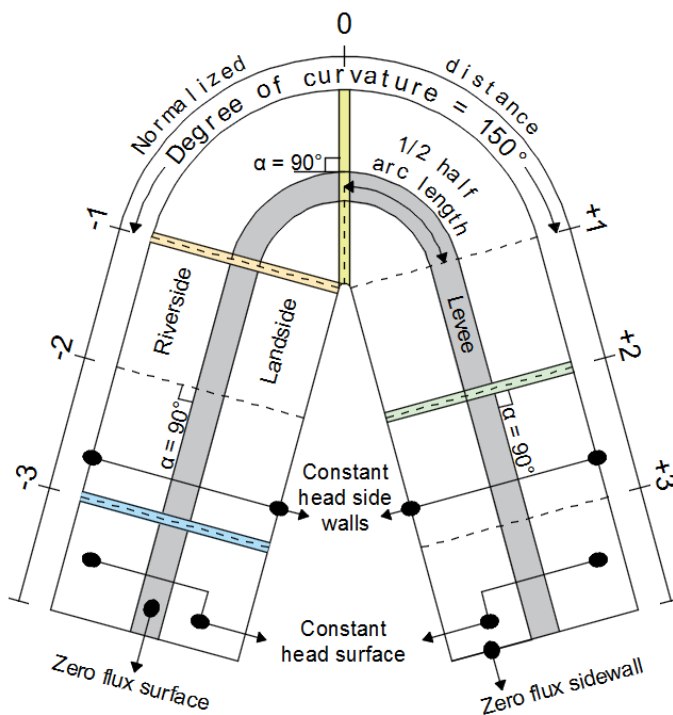


Figure S6.3. Schematic top view of the curvature model used for  $D_c = 150^\circ$  and  $\alpha = 90^\circ$  showing channel features at  $ND = -3, -1, 0 +2$ .

Table S6.4. Parameters and results for the curvature model with  $D_c = 150^\circ$  and  $\alpha = 90^\circ$ 

<b>Curvature multiplier for <math>D_c = 150^\circ</math> with <math>\alpha = 90^\circ</math></b>					
$K_f = 1\text{E-}05 \text{ m/s}, t_b = 2 \text{ m}, t_{ch} = 3.5 \text{ m}, t_f = 32 \text{ m}, w_{ch} = 10 \text{ m}, RL = 200 \text{ m}$					
Stage	$\lambda m_1 T_{ch_1}$	$\lambda m_2 T_{ch_1}$	$\lambda m_3 T_{ch_1}$	$\lambda m_2 T_{ch_2}$	$\lambda m_3 T_{ch_2}$
$K_b$ (m/s)	1.00E-06	1.00E-07	1.00E-08	1.00E-06	1.00E-07
$K_{ch}$ (m/s)	1.00E-04	1.00E-04	1.00E-04	1.00E-03	1.00E-03
$\lambda_m$ (m)	26.5	83.7	264.6	83.7	264.6
$T_{ch}$	10	10	10	100	100
$\lambda$ (m)	83	262	830	83	262
Normalized distance, ND	Head at top of channel (m)				
-8	1	1	1	1	1
-7	1	1	1	1	1
-6	1	1	1	1	1
-5	1	1	1	1	1
-4	1	1	1	1	1
-3	1.00	1.00	1.00	1.00	1.00
-2	1.00	1.01	1.03	1.00	1.01
-1	1.13	1.24	1.32	1.08	1.17
0	1.34	1.45	1.55	1.18	1.31
1	1.13	1.24	1.32	1.08	1.17
2	1.00	1.01	1.03	1.00	1.01
3	1.00	1.00	1.00	1.00	1.00
4	1	1	1	1	1
5	1	1	1	1	1
6	1	1	1	1	1
7	1	1	1	1	1
8	1	1	1	1	1

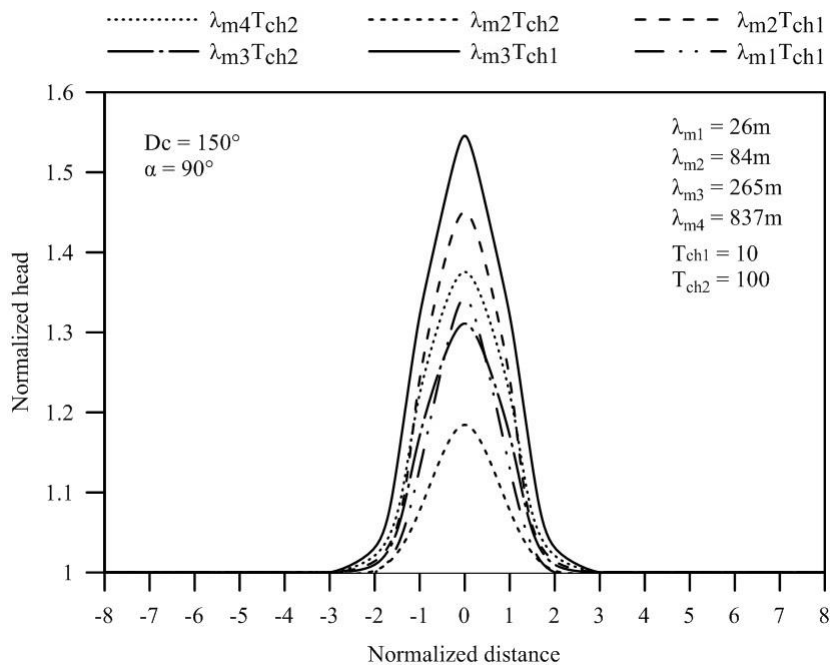


Figure S6.4. Results for the curvature model with  $D_c = 150^\circ$  and  $\alpha = 90^\circ$ .

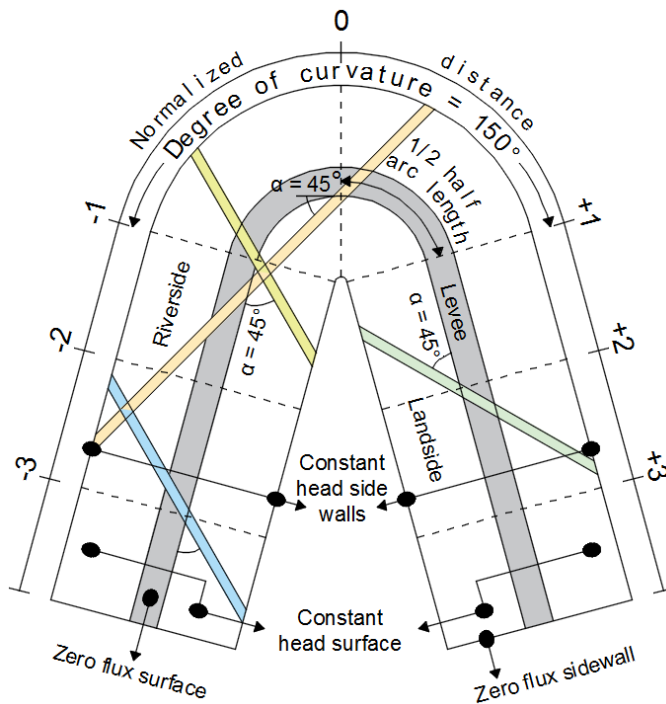


Figure S6.5. Schematic top view of the curvature model used for  $D_c = 150^\circ$  and  $\alpha = 45^\circ$  showing channel features at  $ND = -3, -1, 0, +2$ .



Table S6.5. Parameters and results for the curvature model with  $Dc = 150^\circ$  and  $\alpha = 45^\circ$ 

<b>Curvature multiplier for <math>Dc = 150^\circ</math> with <math>\alpha = 45^\circ</math></b>					
$K_f = 1E-05$ m/s, $t_b = 2$ m, $t_{ch} = 3.5$ m, $t_f = 32$ m, $w_{ch} = 10$ m, $RL = 200$ m					
Stage	$\lambda m_1 T_{ch_1}$	$\lambda m_2 T_{ch_1}$	$\lambda m_3 T_{ch_1}$	$\lambda m_2 T_{ch_2}$	$\lambda m_3 T_{ch_2}$
$K_b$ (m/s)	1.00E-06	1.00E-07	1.00E-08	1.00E-06	1.00E-07
$K_{ch}$ (m/s)	1.00E-04	1.00E-04	1.00E-04	1.00E-03	1.00E-03
$\lambda_m$ (m)	26.5	83.7	264.6	83.7	264.6
$T_{ch}$	10	10	10	100	100
$\lambda$ (m)	83	262	830	83	262
Normalized distance	Head at top of channel (m)				
-8	1	1	1	1	1
-7	1	1	1	1	1
-6	1	1	1	1	1
-5	1	1	1	1	1
-4	1	1	1	1	1
-3	1.00	1.00	1.00	1.00	1.00
-2	1.00	1.01	1.03	1.00	1.01
-1	1.24	1.27	1.33	1.16	1.22
0	1.72	1.56	1.64	1.48	1.56
1	1.21	1.27	1.35	1.15	1.35
2	1.10	1.11	1.05	1.04	1.08
3	1.05	1.08	1.01	1.02	1.04
4	1.05	1.08	1.01	1.02	1.04
5	1.05	1.08	1.01	1.02	1.04
6	1.05	1.08	1.01	1.02	1.04
7	1.05	1.08	1.01	1.02	1.04
8	1.05	1.08	1.01	1.02	1.04

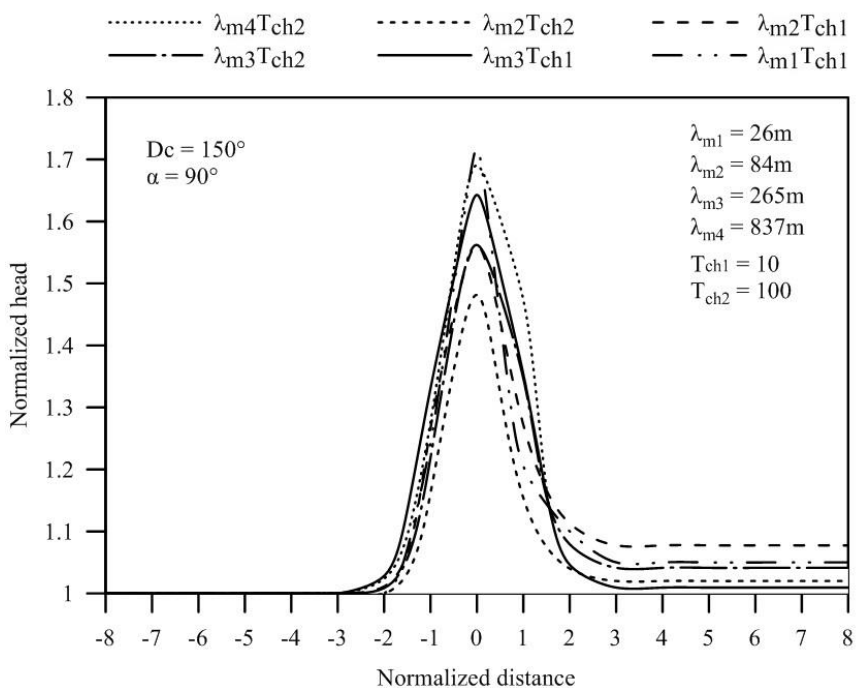


Figure S6.6. Results for the curvature model with  $D_c = 150^\circ$  and  $\alpha = 45^\circ$ .

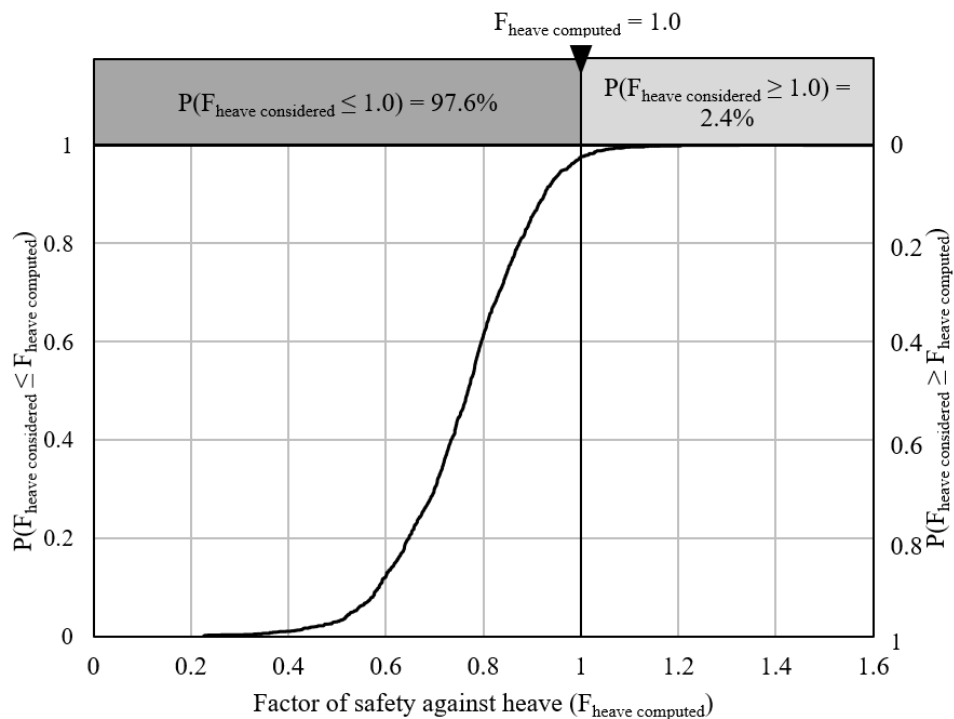


Figure S6.7. CDF for factor of safety against heave,  $F_{heave}$  with curvature adjustment.

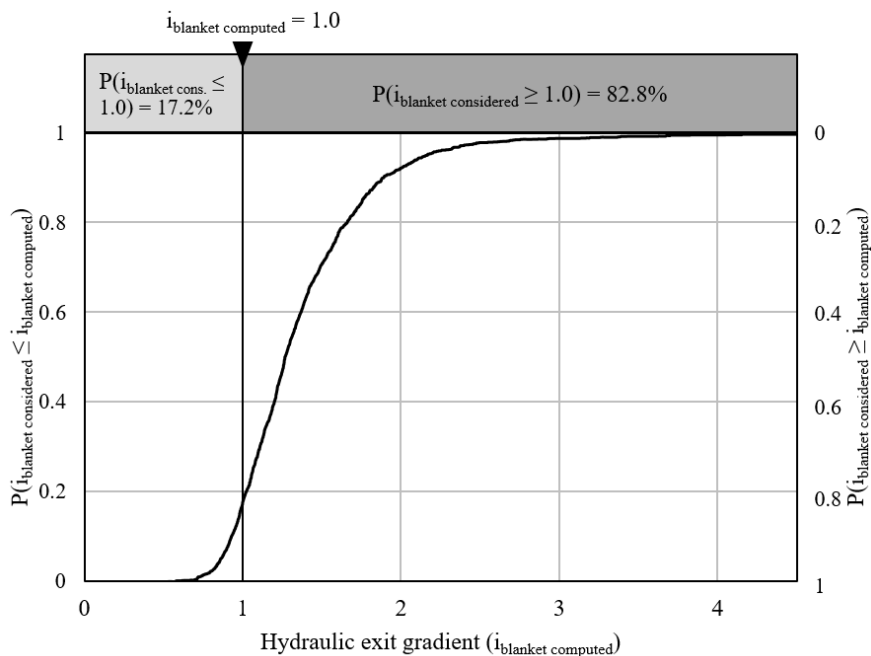


Figure S6.8. CDF for hydraulic exit gradient through the blanket,  $i_{blanket}$  with no curvature adjustment.

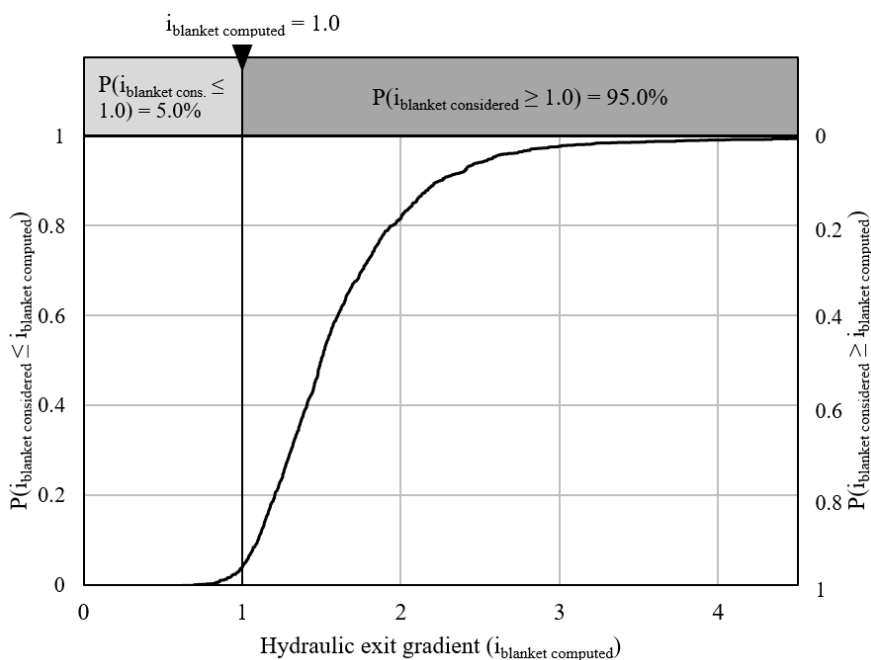


Figure S6.9. CDF for hydraulic exit gradient through the blanket,  $i_{blanket}$  with curvature adjustment.

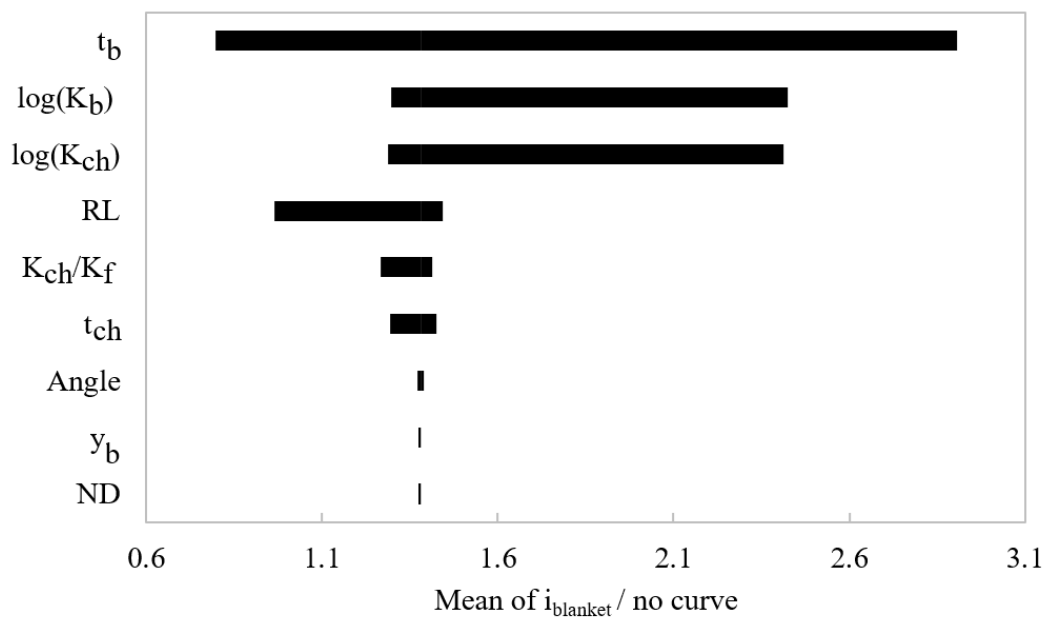


Figure S6.10. CDF for hydraulic exit gradient through the blanket,  $i_{blanket}$ , with no curvature adjustment.

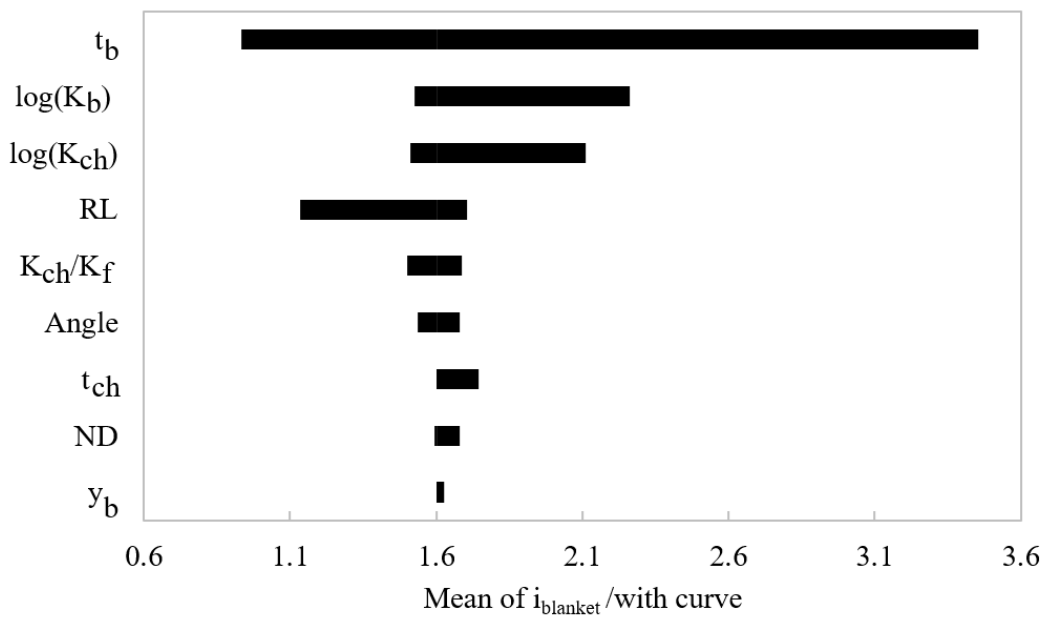


Figure S6.11. CDF for hydraulic exit gradient through the blanket,  $i_{blanket}$ , with curvature adjustment.

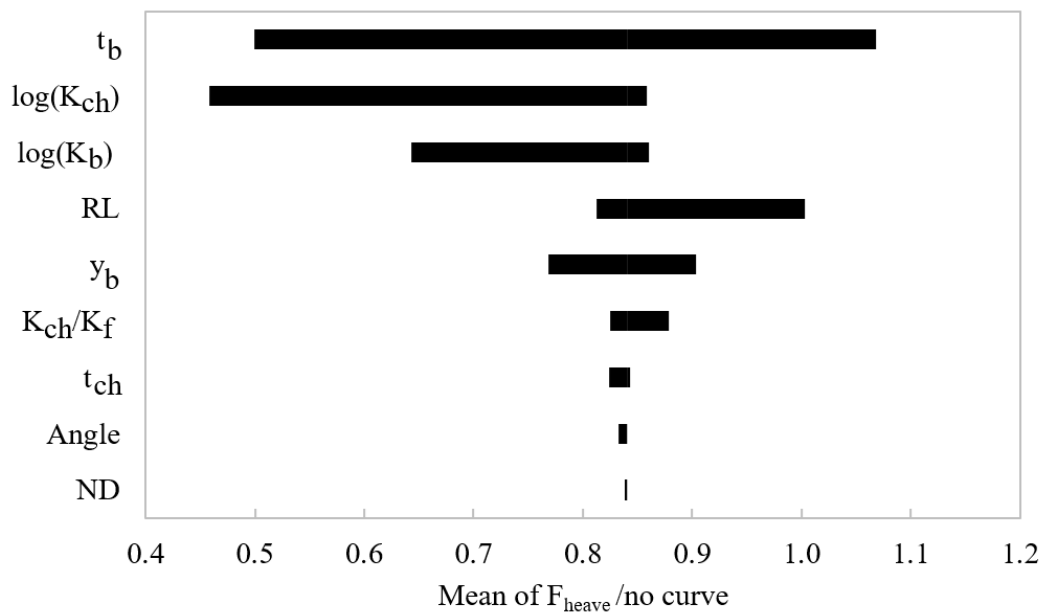


Figure S6.12. CDF for hydraulic exit gradient through the blanket,  $F_{heave}$ , with no curvature adjustment.

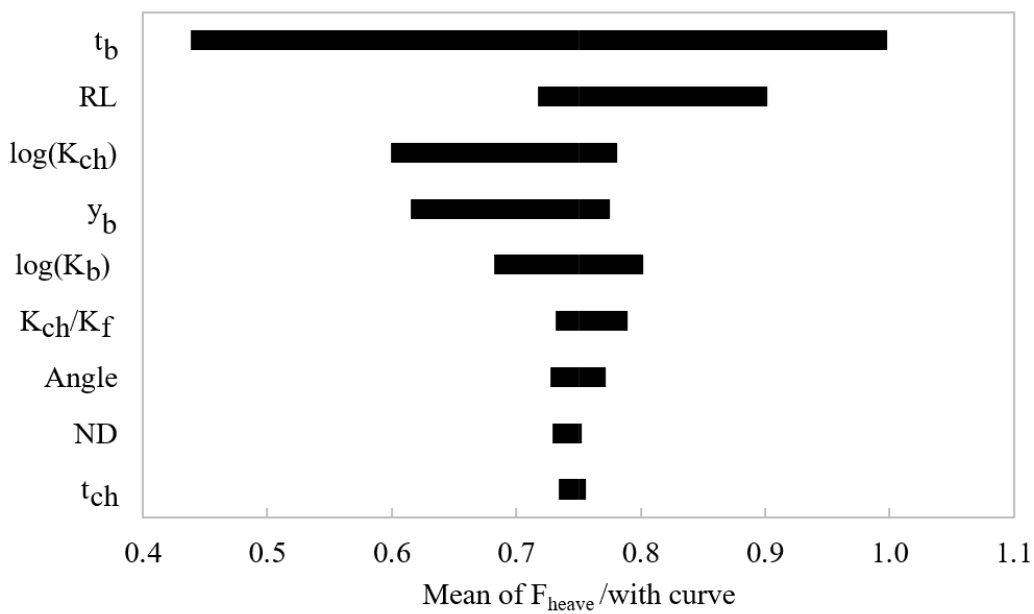


Figure S6.13. CDF for hydraulic exit gradient through the blanket,  $F_{heave}$ , with curvature adjustment.

## References

- ABAQUS* [Computer software]. Dassault Systemes, Waltham, MA, USA.
- Allen, J. R. (1965). "A review of the origin and characteristics of recent alluvial sediments." *Sedimentology*, 5(2), 89–191.
- Benjasupattananan, S. (2013). "Deterministic and probabilistic approaches for modelling levee underseepage." Ph.D. dissertation, Univ. Delaware, Newark, U.S.
- Benjasupattananan, S. and Meehan, C. (2013). "Analytical solutions for levee underseepage analysis: straight and curved levee sections with an infinite blanket." *Proceedings of 2013 ASCE GeoCongress Conference*. San Diego, California, March 3-7, 2013.
- Bridge, J. (2003). *Rivers and floodplains: Forms, processes, and sedimentary record*, Blackwell Publishing, Oxford, UK.
- Brierley, G. J. and Fryirs, K. A. (2005). *Geomorphology and river management: applications of the river styles framework*, Blackwell Publishing, Oxford, UK.
- Brierley, G. J. and Hickin, E. J. (1992). "Floodplain development based on selective preservation of sediments, Squamish River, British Columbia." *Geomorphology*, 4, 381-391.
- Construction Industry Research and Information Association (CIRIA). (2013). "*The International Levee Handbook*."
- Crum, D. A. (1996). "Reliability applied to levee seepage analysis". *Proc., ASCE 7th Specialty Conf. of the Prob. Mech. Str. Reliab.*, D. M. Frangopol and M. D. Grigoriu, eds., Vol. 1, Worcester, MA, 946–949.
- CSEEP* [Computer software]. U.S. Army Corps of Engineers (USACE), Washington, D.C., USA.
- Farrell, K. M. (1987). "Sedimentology and facies architecture of overbank deposits of the Mississippi river, False River region, Louisiana". *Recent Developments in Fluvial Sedimentology*, F. G. Ethridge, R. M. Flores, and M. D. Harvey, eds., Vol. 39, Society of Economic Paleontologist and Mineralogists, Fort Collins, CO, 111-120.
- Fell, R., Wan, C.F., Cyganiewicz, J. and Foster, M. (2003). "Time for development of internal erosion and piping in embankment dams", *J. Geotech. GeoEnviron. Eng.*, ASCE, 129(4), 307-314.

- Foster, M. A., Fell, R., Davidson, R., and Wan, C. F. (2002). "Estimation of the probability of failure of embankment dams by internal erosion and piping using event tree methods." *ANCOLD Bulletin 121*, Australian National Committee on Large Dams, Melbourne, Australia, 75–82.
- Fryirs, K.A. and Brierley, G.J. (2013). *Geomorphic analysis of river systems*, Blackwell Publishing, Oxford, UK.
- Ghilani, C. D. and Wolf, P. R. (2014). *Elementary surveying: An introduction to geomatics*, Pearson, New York, USA.
- Glynn, M. E. and Kuszmaul, J. (2010). "Prediction of piping erosion along middle Mississippi river levees-An empirical model." *Technical Rep. ERDC/GSL TR-04-12*. USACE, Vicksburg, MS.
- Inci, G. (2008). "3D effects on flood protection levees – plain strain versus axisymmetric modelling." *Proceedings of 2008 Int. Assoc. Comp. Methods Advances in Geomechanics (IACMAG) Conference*. Goa, India, October 1-6, 2008.
- International Commission on Large Dams (ICOLD). (2015). "Internal erosion of existing dams, levees, and dikes, and their foundations." *Internal erosion processes and engineering assessment*, Vol. 1, Paris, France.
- Jacobson, R. B. and Oberg, K. A. (1997). "Geomorphic changes on the Mississippi river flood plain at miller city, Illinois, as a result of the flood of 1993." *U.S. Geol Survey Circular 1120-J*.
- Jafari, N. H., Stark, T. D. Leopold, A. L. and Merry, S. M. (2016). "Three-dimensional levee and floodwall underseepage." *Can. Geotech. J.*, 53, 72–84  
dx.doi.org/10.1139/cgj-2014-0343
- Leopold, L. B. and Wolman, M. G. (1957). "River channel patterns: Braided, meandering and straight." U.S. Geological Survey, Washington, DC, 39-84.
- LEVEEMSU* [Computer software]. U.S. Army Corps of Engineers (USACE), Washington, D.C., USA.
- Low, B. K. (2008). "Reliability of levee systems." *Reliability-based design in geotechnical engineering*, K.-K. Phoon, ed., Taylor and Francis Group, New York, 134–168.
- McCook, Danny (2007). A discussion of uplift computations for embankments and levees. *J. Dam Safety*, 5(1), 1-9.
- McGowen, J.H. and Garner, L.E., 1970. "Physiographic features and stratification types of coarse-grained point bars: modern and ancient examples." *Sedimentology*, 14, 77-111.

- Meehan, C. and Benjasupattananan, S. (2014). “Analytical approach for modeling axisymmetric levee underseepage”. *J. Geotech. Geoenviron. Eng.* 10.1061/(ASCE)GT.1943-5606.0000952, ADD PAGES.
- Merry, S and Du, R. (2014). “Plane strain versus axisymmetric modeling of convex levees.” *J. Geotech. Geoenviron. Eng.*, 10.1061/(ASCE)GT.1943-5606.0001255, ADD PAGES.
- Nanson, Gerald C. (1980). “Point bar and floodplain formation of the meandering Beatton River, northeastern British Columbia, Canada.” *Sedimentology*, 27, 3–29.
- Nanson, Gerald C. (1981). “New evidence of scroll-bar formation on the Beatton River.” *Sedimentology*, 28(6), 889–891.
- Polanco, L. and Rice, J. D. (2014). “A reliability-based evaluation of the effects of geometry on levee underseepage potential.” *Springer: Geotech. Geological Eng.*, 32(4), 807-820.
- Polanco-Boulware, L. and Rice, J. D. (2017). “Reliability-based three-dimensional assessment of internal erosion potential due to crevasses splays.” *J. Geotech. Geoenviron. Eng.*, 143(4), 10.1061/(ASCE)GT.1943-5606.0001596
- Polanco-Boulware, L. and Rice, J. (2017). “Three dimensional underseepage assessment of high conductivity channels within a levee system”. Chapter 5. Submitted in the Canadian Geotechnical Journal.
- Rice, J. D. and Polanco, L. (2012). “Reliability-based underseepage analysis in levees using a response surface–monte carlo simulation method.” *J. Geotech. Geoenviron. Eng.*, 138 (7), 821-830, 10.1061/(ASCE)GT.1943-5606.0000650
- Ritter Dale F., Kochel R. C. and Miller J. R. (2011). *Process geomorphology*, fifth edition, Waveland Press, Long Grove, IL, US.
- Saucier, R.T. (1994). “Geomorphology and quaternary geologic history of the lower Mississippi Valley.” U.S. Army Engineer Waterways Experiment Station, Vicksburg, MS.
- SEEP/W* [Computer software]. GEO-SLOPE International Ltd., Calgary, AB, Canada.
- Simm, J., Gouldby, B., Sayers, P., Flikweert, J. J., Wersching, S. and Bramley, M. (2008). “Representing fragility of flood and coastal defences: getting into the detail.” *Proceedings of FLOODrisk 2008 Conference*, Oxford, UK, September 30<sup>th</sup> to October 2<sup>nd</sup>, 2008.
- Slide* [Computer software]. Rocscience Inc., Toronto, ON, Canada.



- SVFlux* [Computer software]. SoilVision Systems, Saskatoon, SK, Canada.
- Terzaghi, K. (1922). "Der Grundbruch an Stauwerken und Seine Verhütung [The Failure of Dams and Its Prevention]." *Die Wasserkraft*, 17, 445-449.
- Terzaghi, Karl and Ralph Peck (1968). *Soil Mechanics in Engineering Practice*, 2nd Edition. John Wiley and Sons.
- Thorne, C. R. (1997). Channel types and morphological classification. In: Thorne, C. R., Hey, R. D. and Newson, M. D. (eds) *Applied Fluvial Geomorphology in River Engineering Management*. John Wiley and Sons, 175-222.
- Wolff D (2008) Reliability of levee systems. In: Phoon K-K (ed) *Reliability-based design in geotechnical engineering*. Taylor & Francis Group, New York, pp 448-496
- URS Corporation (2008). High water damage historical map from 1986 and 1995. Sacramento County, California. Unpublished map used for consultant reports.
- U. S. Army Corps of Engineers (USACE) (1956). "Investigation of underseepage and its control. Technical Memorandum No. 3-424." *U.S. Army Engineer Waterways Experiment Station, Vicksburg, MS*.
- U. S. Army Corps of Engineers (USACE) (2000). "Design and construction of levees. Engineering Manual EM 1110-2-1913." Washington, DC.
- U. S. Army Corps of Engineers (USACE) (2004). "Geotechnical reliability of dam and levee embankments ERDC/GSL CR-04-1.", Geotechnical and Structural Laboratory, Washington, DC.
- U. S. Army Corps of Engineers (USACE) (2010). "Beyond the factor of safety: developing fragility curves to characterize system reliability." *Report ERDC SR-10-1*, Washington, DC.
- United States Geological Survey (USGS) (2011). "Characterization of geomorphic units in the alluvial valleys and channels of gulf coastal plain rivers in Texas, with examples from the Brazos, Sabine, and Trinity rivers, 2010." *Scientific Investigations Report 2011-5067*, Denver, CO.
- Walling, D. E., Fang, D., Nicholas, A. P. and Sweet, R. J. (2004). "The grain size characteristics of overbank deposits on the floodplains of British lowland rivers." *Proc., Int. Symp. Sediment Transfer through the Fluvial System*, V. Golosov, V. Belyaev and D. E. Walling, eds., Moscow, Russia, 288, 226-234.
- Wolff, D. (2008). "Reliability of levee systems." *Reliability-based design in geotechnical engineering*, K.-K. Phoon, ed., 448-496. Taylor and Francis Group, New York, 448-496.

- Wolff, T. F. (1994). "Evaluating the reliability of existing levees." U.S. Army Engineer Waterways Experiment Station, Michigan State Univ., East Lansing MI.
- Wolff, T. F., Demsky, E. C., Schauer, J., and Perry, E. (1996). "Reliability assessment of dike and levee embankments." *Uncertainty in the geologic environment: From theory to practice*, ASCE Reston, VA, 636–650.
- Wolman, M. G. and Leopold, L. B. (1957). "River flood plains: some observations on their formation." *Geological survey professional paper 282-C*. Washington, DC.
- Xu, B. and Low, B. K. (2006). "Probabilistic stability analyses of embankments based on finite-element method." *J. Geotech. Geoenviron. Eng.*, 10.1061/(ASCE)1090-0241(2006)132:11(1444), 1444-1454.

## CHAPTER 7

### SUMMARY, CONCLUSIONS AND RECOMMENDATIONS

#### **7.1. Summary and Conclusions**

Levee underseepage reliability has been limited to a simplified two-layered system with straight sections analyzed by means of two-dimensional deterministic methods. These limitations have been, in part, due to the general depositional characteristic where levees are built and due to the complexity of underseepage computation. Even though the general two-layered pattern found beneath a levee structure has a significant effect on the underseepage behavior and associated internal erosion mechanisms, the interception of geomorphic features with the levee alignment results in an even higher effect. The introduction of geotechnical finite-element analysis programs has helped to eradicate these limitations to some degree. But, despite the availability of powerful finite-element programs, levee underseepage reliability is still being analyzed, for the most part, with the omission of intercepted geomorphic features.

The most common underseepage reliability method used in the United States is by coupling the U.S. Army Corps of Engineers (USACE) blanket theory (BT) equations as the performance function and the first-order second-moment (FOSM) Taylor series method as the probability model. The most attractive characteristics of these methods is that few parameters are needed and the assessment is relatively quick to perform. Despite the ease of computation, the BT method limits the levee subsurface geometry and it is not flexible for the consideration of different failure mechanisms. The FOSM method (at least the

typical form used for underseepage reliability) requires the parameters to be modeled either with a normal or lognormal distribution and it assumes a linear relationship between the parameters and the design criteria outcome.

To address the limitations of the most common levee underseepage reliability method (FOSM-BT), a response surface–Monte Carlo simulation method (RSMC) is proposed. The RSMC method involves the use of geologic maps, engineering reports, finite-element analyses, and Monte Carlo simulation to assess a conditional probability of initiation of erosion. Geologic maps and engineering reports are used to determine the location of geomorphic features together with their most characteristic parameters. Finite-element analysis provides the flexibility to analyze the levee subsurface more accurately (individually and parametrically) while incorporating geomorphic features. Finally, Monte Carlo simulation allows for a probabilistic assessment where different types of distributions can be used to model more accurate failure mechanisms. The analysis outcome is presented by means of cumulative ascending distribution functions (CADFs) where several desired design criteria can be evaluated for different probabilities.

Chapter 2 outlines the most common methods used for underseepage reliability together with their benefits and limitations. The two-dimensional RSMC method is introduced by means of two hypothetical levee scenarios. A direct comparison with the FOSM-BT method is not feasible due to the complexity portrayed in the levees' subsurface. Statistical analysis was performed to determine which parameters have the most significant effect on the outcome and, for the most part, results suggest that geometric parameters have the highest effect.

In order to make direct comparisons with the FOSM-BT method, several levee scenarios (as of those found to be modeled by the BT equations) were analyzed in Chapter 3. Steps to perform underseepage reliability analysis under both methods are outlined. Results between methods show minor differences. Statistical analysis was performed as in Chapter 2 and results also suggest that geometric parameters, in most cases, have the highest effect.

Based on the findings (from Chapters 2 and 3) that geometric parameters contribute significantly to levee underseepage behavior, the RSMC methodology is expanded to three-dimensional finite-element analysis with the purpose of introducing geomorphic features. Chapters 4 and 5 provide steps for the methodology outlined based on the example of a historical crevasse splay and an abandoned (high-conductivity) channel, respectively. In Chapter 4, for ease of computation and reduction of computation time, a simplified crevasse splay model is proposed and validated where its seepage flow regime is described by the combination of critical parameters: the conductance of the crevasse channel, the transmissivity of the splay, and the conductance of the blanket overlying the splay.

Chapter 5 presents the analysis proposed for the abandoned channel. The simplified model that describes the seepage flow behavior for this case is by means of the combined parameters tongue effect and modified leakage. A third parameter called the blanket layer river length is also part of the response surface but it is treated as an individual parameter. CADFs for both models are presented based on the criteria of a hydraulic exit gradient and a factor of safety against heave. Fragility curves describing the initiation of internal erosion with respect to different flood levels are also presented for both models in Chapters 4 and

5. Finally, tornado graphs are used to show the impact that the critical input individual parameters have on the outcome.

Chapter 6 assesses the effect curvature has on levee underseepage by the presence of a geomorphic feature. Data shows how curvature (convex alignment) might affect some geomorphic features and how it might not affect others. Parametric analyses performed on point bar models (representing high-conductivity channel models) based on the location of the feature at different convex curvature alignments and different hydraulic conductivities provide several family of curves (a curvature response surface) that can be used together with the RSMC methodology when needed. The family of curves represent a simple coefficient method that adjusts the resulting outcomes based on straight underseepage levee section analyses.

## **7.2. Recommendations**

The usual approach to compute the probability of failure of a levee system based on different types of failure mechanisms (such as overtopping, slope instability, through seepage, and underseepage) is by dividing the levee system in sections or segments based on similar embankment and foundation soils characteristics together with the elevation of the crest and riverside. This configuration provides a general profile for each section of levee length (usually a two-dimensional cross-section) that allows for the computation of the conditional probability of failure which is eventually used to compute the probability of failure of the levee system.

By using this approach, levee length effects can be considered in the computation of the probability of failure. either by assuming correlation or independence between levee sections. Recall that it is the author's hypothesis that by identifying and analyzing the geomorphic features along the levee structure alignment, the vast majority of the underseepage length-effect hazard can be evaluated. Based on this hypothesis, a geologic map will enhance the accuracy of the evaluation of a meandering river levee system but not having one should not limit the assessment. Where geologic maps providing geomorphic data are not available, it is recommended to study similar and nearby meandering river levee systems in order to identify where prominent geomorphic features are likely to be located and assess the levee system in question based on the judgement of wherer similar formations could be found along levee alignment.

On the othere hand, due to the size of this research, there is still the need to assess the underseepage reliability that low-conductivity channels pose on a levee section. Neck cut-offs and oxbows are geomorphic features that can be considered as low-conductivity channels. The term low-conductivity channel comes from the fine-grained (overbank deposit) soil composition of these geomorphic features. Refer to Figure 4.1 that illustrates a neck cut-off as a common geomorphic feature within the meandering river environment. As with the crevasses splay and high-conductivity channel models, with the help of parametric analyses and the combination of significant parameters, a simplified response surface could be developed. As an initial and final remark, the theory would be that low-conductivity channels represent a blockage of flow that affect the internal erosion mechanism of a levee. The assessment would be very similar to the one done for the high-

conductivity channel where there is continuation of flow from the riverside to the landside. The hypothesis would be that flow horizontally concentrates by means of the angularity of the feature and by how far it travels from the riverside to the landside followed by a vertical concentration (or blockage) based on the anisotropy of the foundation layer and the thickness ratio between the feature and the foundation layer. Finally, a vertical leakage dissipation within the interaction of the blanket layer on top of the low-conductivity channel and the feature itself. The latter could be represented by the leakage factor presented by USACE (1956) and explained in Chapter 5.



APPENDICES

## APPENDIX A

Appendix A provides supporting data for the family of curves (response surface) presented in Chapter 2. The complete family of curves with respect to the hydraulic exit gradient ( $i_e$ ) and uplift pressure at the base of the blanket ( $u_{bl}$ ) are presented herein. Tables A1.1 and A1.2 provide the computed  $i_e$  and  $u_{bl}$ , respectively, corresponding to Example 2.1 depicted in Figure 2.1. The corresponding plots are presented as Figures A1.1 through A1.10. The fitted corresponding polynomial equations are presented as Tables A1.3 and A1.4. Likewise, Table A1.5 provides the computed  $u_{bl}$  corresponding to Example 2.2 depicted in Figure 2.4. The corresponding plots are presented as Figures A1.11 through A1.17. The fitted corresponding polynomial equations are presented as Table A1.6.

Table A.1. Hydraulic exit gradient ( $i_e$ ) as a function of  $A$ ,  $K_{sb}$  and  $K_{hv}$  used for Example 2.1 in Chapter 2. These values correspond to Figures A1.1 to A1.5

A (ft)	$i_e$				
	$K_{sb}$				
	20	65	200	1300	13000
Using $K_{hv} = 0.50$					
-76	0.419	0.439	0.453	0.462	0.463
-68.75	0.441	0.472	0.493	0.505	0.507
-61.5	0.479	0.532	0.566	0.585	0.588
-54.25	0.554	0.653	0.715	0.750	0.757
-47	0.844	1.246	1.517	1.679	1.709
Using $K_{hv} = 0.25$					
-76	0.519	0.560	0.592	0.611	0.614
-68.75	0.543	0.604	0.647	0.673	0.677
-61.5	0.584	0.679	0.744	0.782	0.790
-54.25	0.663	0.826	0.940	1.009	1.022
-47	0.856	1.319	1.673	1.901	1.945
Using $K_{hv} = 0.15$					
-76	0.582	0.643	0.693	0.724	0.730
-68.75	0.606	0.692	0.760	0.801	0.809
-61.5	0.645	0.779	0.876	0.937	0.949
-54.25	0.719	0.944	1.114	1.222	1.244
-47	0.841	1.354	1.792	2.092	2.152
Using $K_{hv} = 0.05$					
-76	0.667	0.769	0.874	0.947	0.962
-68.75	0.673	0.823	0.963	1.062	1.083
-61.5	0.684	0.914	1.115	1.264	1.295
-54.25	0.702	1.072	1.417	1.681	1.737
-47	0.768	1.256	1.897	2.442	2.564
Using $K_{hv} = 0.005$					
-76	0.644	0.728	0.960	1.231	1.308
-68.75	0.665	0.745	0.989	1.380	1.494
-61.5	0.685	0.763	1.029	1.613	1.797
-54.25	0.704	0.780	1.085	1.998	2.320
-47	0.723	0.798	1.065	2.327	2.864

Table A.2. Uplift pressure at the base of the blanket ( $u_{bl}$ ) as a function of  $A$ ,  $K_{sb}$  and  $K_{hv}$  used for Example 2.1 in Chapter 2. These values correspond to Figures A1.6 to A1.10

A (ft)	$u_{bl}$ (lb/ft <sup>2</sup> )				
	$K_{sb}$				
	20	65	200	1300	13000
Using $K_{hv} = 0.50$					
-39	707.80	920.00	1084.65	1194.30	1216.75
-31	1011.50	1210.00	1356.00	1450.80	1469.30
-23	1232.25	1422.80	1561.00	1650.00	1667.50
-15	1403.00	1588.80	1723.25	1809.25	1826.30
Using $K_{hv} = 0.25$					
-39	662.95	880.73	1061.50	1189.50	1216.00
-31	975.81	1180.50	1339.30	1447.50	1469.50
-23	1201.37	1397.50	1547.00	1646.90	1667.00
-15	1374.00	1565.30	1710.00	1806.50	1826.00
Using $K_{hv} = 0.15$					
-39	627.50	843.93	1038.83	1184.50	1215.30
-31	946.95	1153.60	1323.79	1444.09	1468.95
-23	1176.70	1375.65	1534.11	1644.10	1666.75
-15	1351.70	1545.25	1698.15	1803.94	1825.53
Using $K_{hv} = 0.05$					
-39	548.66	743.43	965.35	1166.25	1213.95
-31	880.77	1081.77	1276.30	1433.10	1467.81
-23	1121.93	1319.53	1497.87	1635.65	1665.65
-15	1302.13	1495.38	1666.00	1796.69	1824.25
Using $K_{hv} = 0.005$					
-39	428.31	511.98	678.98	1038.39	1196.60
-31	759.00	875.91	1076.80	1365.58	1459.41
-23	1013.84	1166.52	1366.78	1596.31	1661.17
-15	1204.15	1368.08	1559.02	1764.93	1821.11

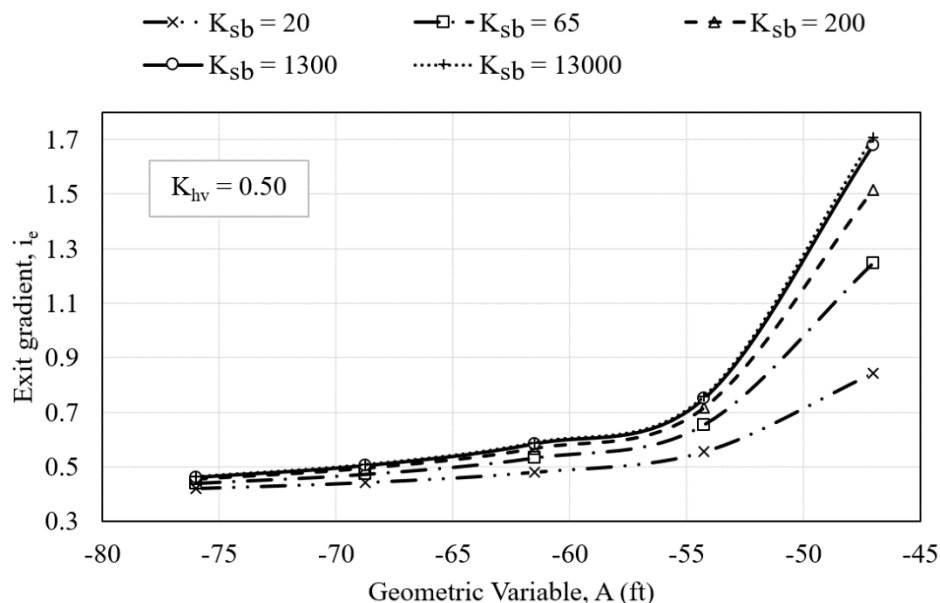


Figure A.1. Family of curves representing relationship between  $K_{sb}$ ,  $A$ , and  $i_e$  for  $K_{hv} = 0.50$ .

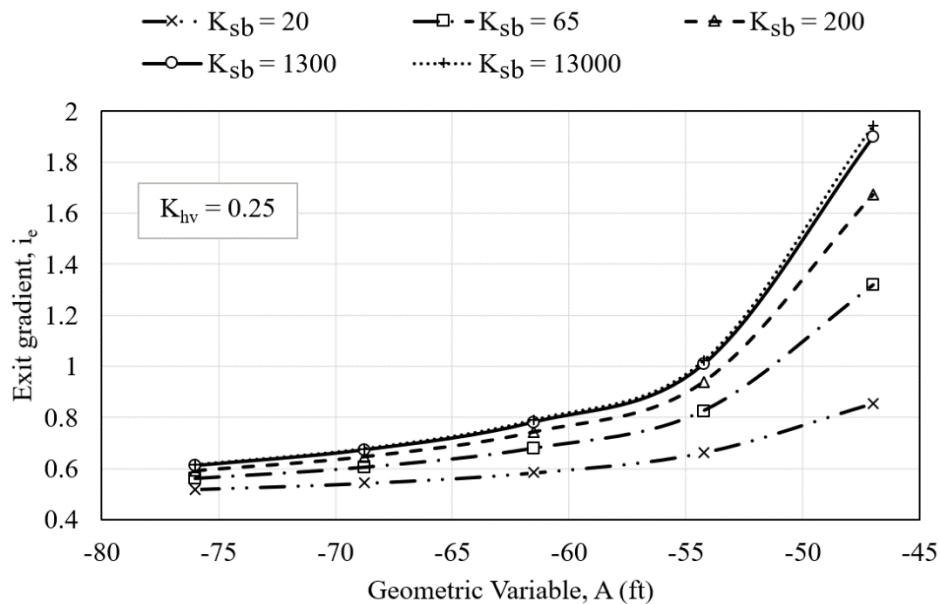


Figure A.2. Family of curves representing relationship between  $K_{sb}$ ,  $A$ , and  $i_e$  for  $K_{hv} = 0.25$ .

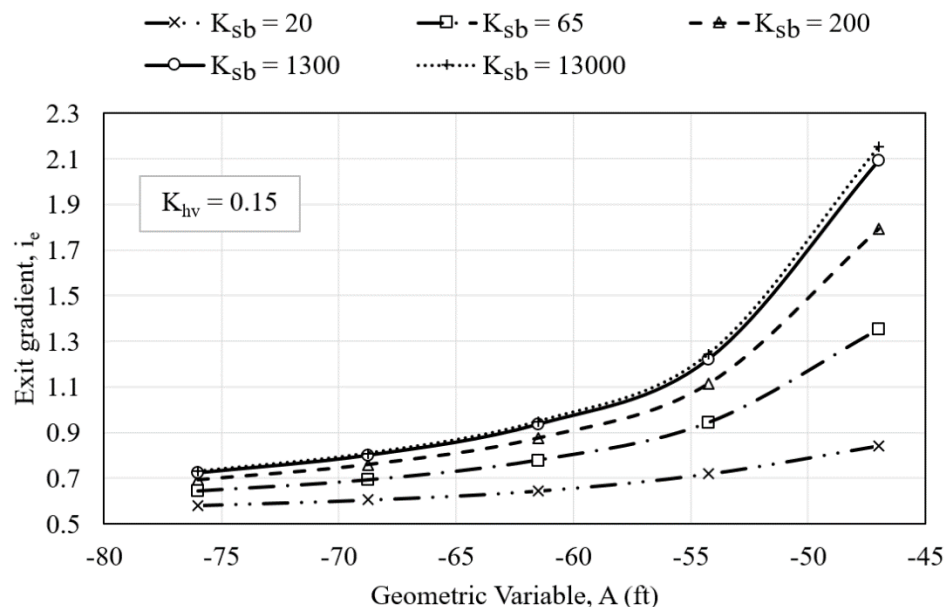


Figure A.3. Family of curves representing relationship between  $K_{sb}$ ,  $A$ , and  $i_e$  for  $K_{hv} = 0.15$ .

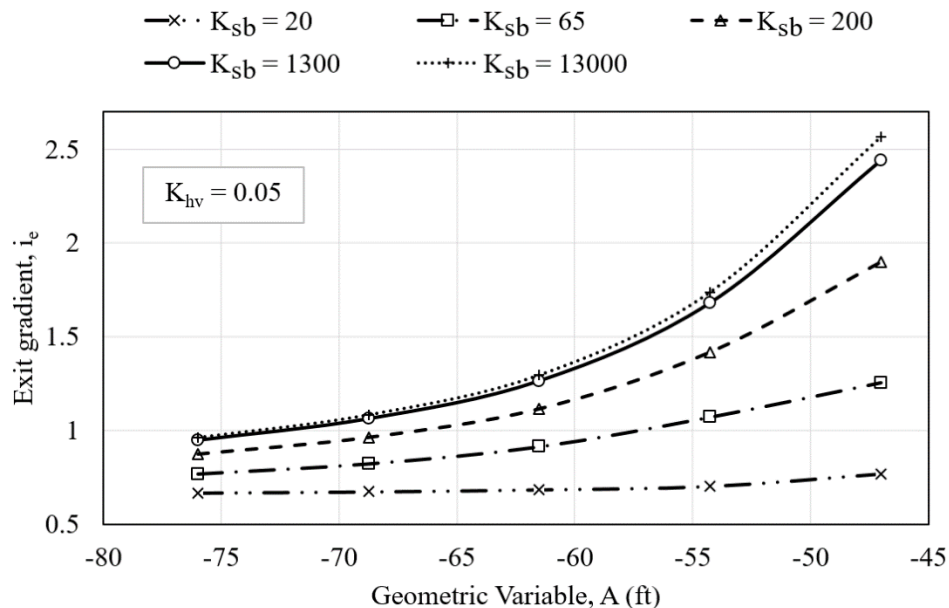


Figure A.4. Family of curves representing relationship between  $K_{sb}$ ,  $A$ , and  $i_e$  for  $K_{hv} = 0.05$ .

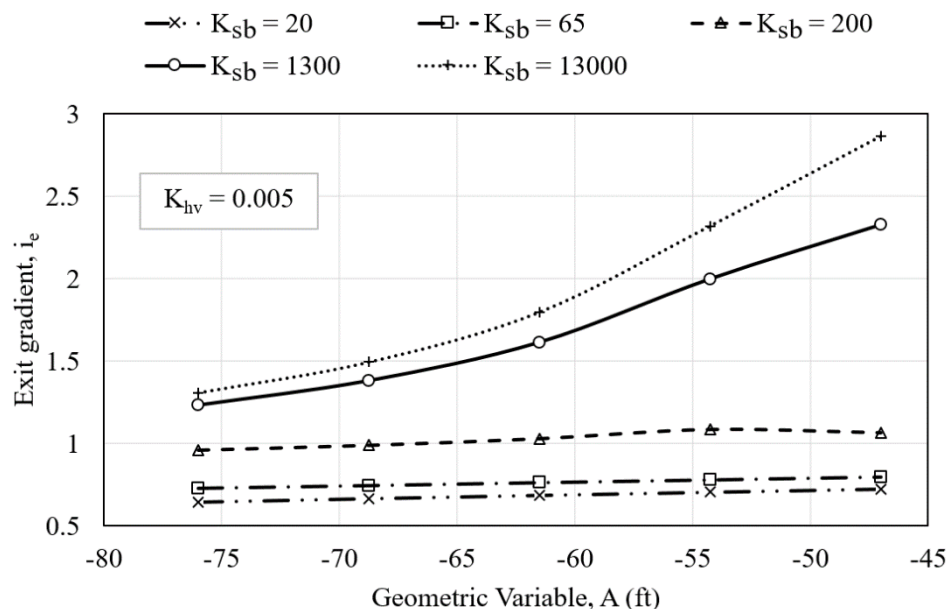


Figure A.5 .Family of curves representing relationship between  $K_{sb}$ ,  $A$ , and  $i_e$  for  $K_{hv} = 0.005$ .

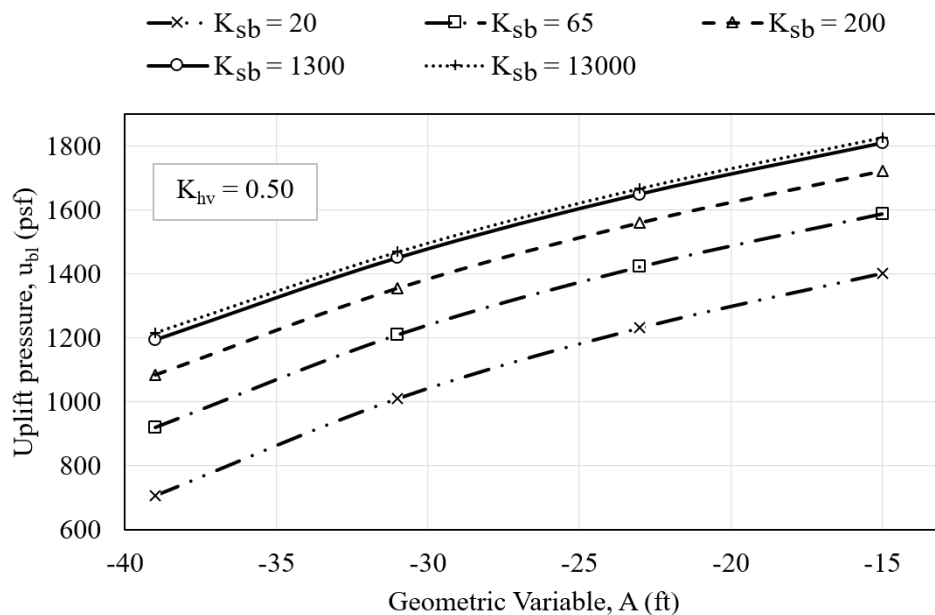


Figure A.6. Family of curves representing relationship between  $K_{sb}$ ,  $A$ , and  $\mu_{bl}$  for  $K_{hv} = 0.50$ .

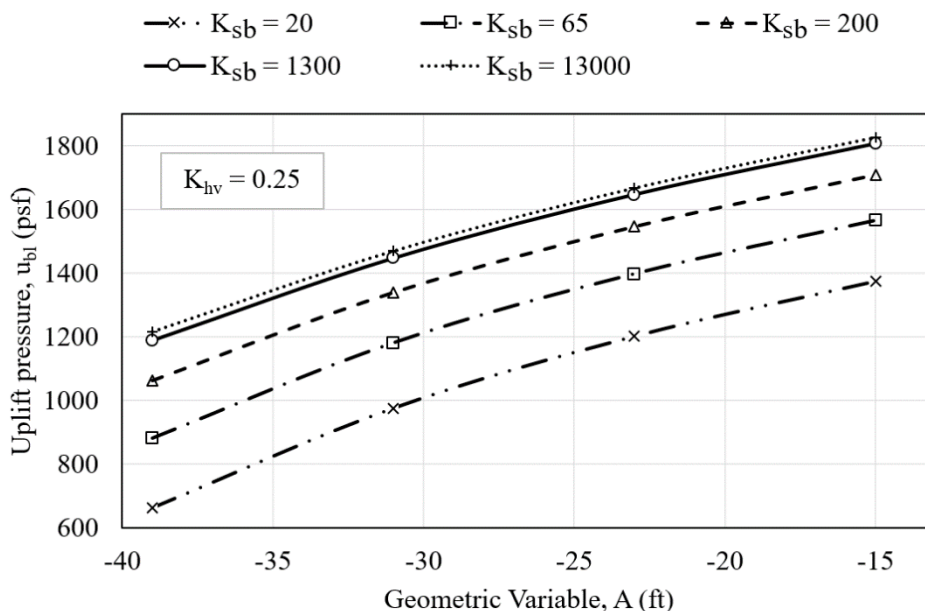


Figure A.7. Family of curves representing relationship between  $K_{sb}$ ,  $A$ , and  $\mu_{bl}$  for  $K_{hv} = 0.25$ .

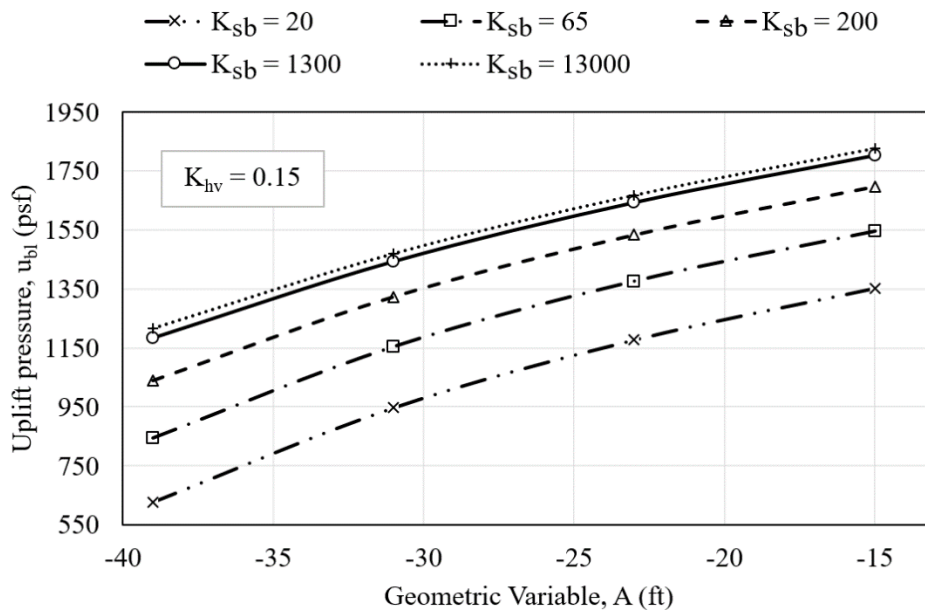


Figure A.8. Family of curves representing relationship between  $K_{sb}$ ,  $A$ , and  $\mu_{bl}$  for  $K_{hv} = 0.15$ .



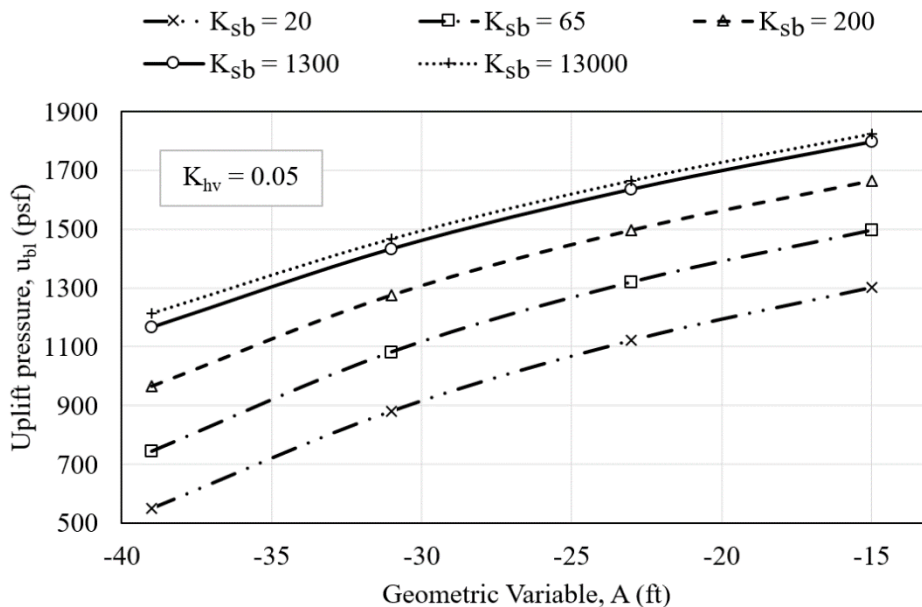


Figure A.9. Family of curves representing relationship between  $K_{sb}$ ,  $A$ , and  $\mu_{bl}$  for  $K_{hv} = 0.05$ .

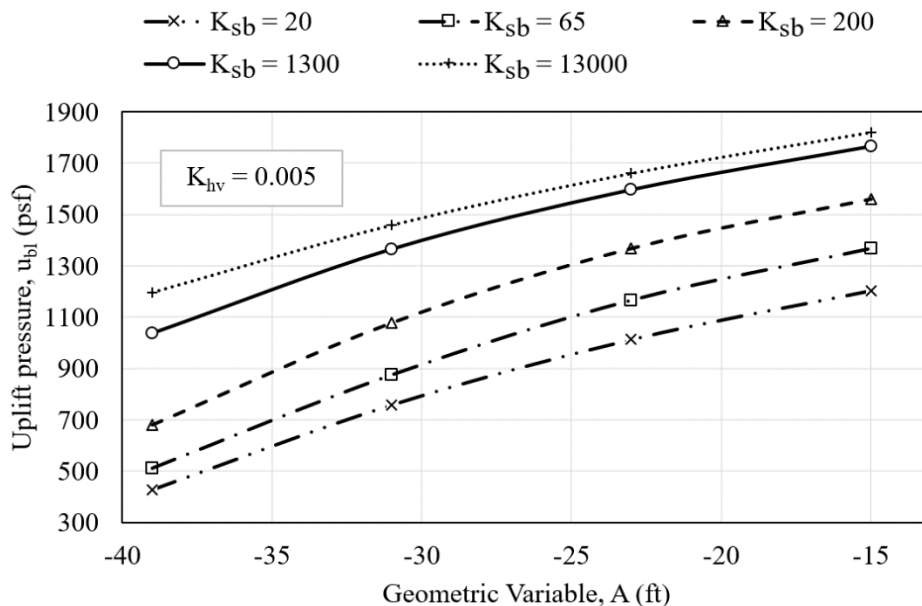


Figure A.10. Family of curves representing relationship between  $K_{sb}$ ,  $A$ , and  $\mu_{bl}$  for  $K_{hv} = 0.005$ .

Table A.3. Fit-equations' coefficients and corresponding goodness of fit for family of curves for the computation of  $i_e$  with respect to each  $K_{hv}$  used for Example 2.1 in Chapter 2. These values correspond to Figures A1.1 to A1.5

$K_{sb}$	$i_e = a_4*A^4 + a_3*A^3 + a_2*A^2 + a_1*A + a_0$					$R^2$
	$a_4$	$a_3$	$a_2$	$a_1$	$a_0$	
Using $K_{hv} = 0.50$						
20	2.37E-06	6.26E-04	6.20E-02	2.73E+00	4.57E+01	0.99
65	5.69E-06	1.50E-03	1.47E-01	6.44E+00	1.06E+02	0.99
200	8.05E-06	2.12E-03	2.08E-01	9.08E+00	1.49E+02	0.99
1300	9.52E-06	2.50E-03	2.46E-01	1.07E+01	1.75E+02	0.99
13000	9.71E-06	2.55E-03	2.51E-01	1.09E+01	1.79E+02	0.99
Using $K_{hv} = 0.25$						
20	8.30E-07	2.25E-04	2.31E-02	1.06E+00	1.90E+01	0.99
65	3.51E-06	9.33E-04	9.30E-02	4.12E+00	6.96E+01	0.99
200	5.75E-06	1.52E-03	1.51E-01	6.67E+00	1.11E+02	0.99
1300	7.18E-06	1.90E-03	1.89E-01	8.32E+00	1.39E+02	0.99
13000	7.59E-06	2.01E-03	1.99E-01	8.76E+00	1.46E+02	0.99
Using $K_{hv} = 0.15$						
20	-1.06E-07	-1.88E-05	-7.26E-04	3.27E-02	2.55E+00	0.99
65	1.92E-06	5.16E-04	5.25E-02	2.39E+00	4.21E+01	0.99
200	3.70E-06	9.94E-04	1.01E-01	4.55E+00	7.85E+01	0.99
1300	5.22E-06	1.40E-03	1.41E-01	6.32E+00	1.08E+02	0.99
13000	5.49E-06	1.47E-03	1.48E-01	6.65E+00	1.14E+02	0.99
Using $K_{hv} = 0.05$						
20	5.88E-07	1.54E-04	1.51E-02	6.60E-01	1.15E+01	0.99
65	-1.07E-06	-2.66E-04	-2.41E-02	-9.21E-01	-1.13E+01	0.99
200	-8.90E-07	-1.94E-04	-1.41E-02	-3.31E-01	1.65E+00	0.99
1300	1.51E-08	5.99E-05	1.28E-02	9.43E-01	2.47E+01	0.99
13000	2.41E-07	1.24E-04	1.95E-02	1.26E+00	3.05E+01	0.99
Using $K_{hv} = 0.005$						
20	1.51E-08	3.93E-06	3.72E-04	1.79E-02	1.08E+00	0.99
65	6.03E-08	1.48E-05	1.36E-03	5.70E-02	1.73E+00	0.99
200	-1.46E-06	-3.79E-04	-3.65E-02	-1.54E+00	-2.30E+01	0.99
1300	-4.16E-06	-1.06E-03	-9.84E-02	-3.97E+00	-5.60E+01	0.99
13000	-4.56E-06	-1.14E-03	-1.05E-01	-4.13E+00	-5.59E+01	0.99

Table A.4. Fit-equations' coefficients and corresponding goodness of fit for family of curves for the computation of  $u_{bl}$  with respect to each  $K_{hv}$  used for Example 2.1 in Chapter 2. These values correspond to Figures A1.6 to A1.10

$K_{sb}$	$u_{bl} = a_3*A^3 + a_2*A^2 + a_1*A + a_0$				$R^2$
	$a_3$	$a_2$	$a_1$	$a_0$	
Using $K_{hv} = 0.50$					
20	1.07E-02	3.50E-01	2.28E+01	1.70E+03	0.99
65	9.90E-03	3.17E-01	2.19E+01	1.88E+03	0.99
200	7.68E-03	1.96E-01	1.93E+01	1.99E+03	0.99
1300	5.65E-03	7.76E-02	1.67E+01	2.06E+03	0.99
13000	4.87E-03	2.80E-02	1.56E+01	2.07E+03	0.99
Using $K_{hv} = 0.25$					
20	1.12E-02	3.59E-01	2.29E+01	1.68E+03	0.99
65	1.09E-02	3.70E-01	2.30E+01	1.86E+03	0.99
200	8.27E-03	2.21E-01	1.97E+01	1.98E+03	0.99
1300	6.12E-03	1.11E-01	1.75E+01	2.06E+03	0.99
13000	5.70E-03	9.23E-02	1.71E+01	2.08E+03	0.99
Using $K_{hv} = 0.15$					
20	1.14E-02	3.57E-01	2.30E+01	1.65E+03	0.99
65	1.15E-02	3.80E-01	2.31E+01	1.84E+03	0.99
200	9.23E-03	2.76E-01	2.08E+01	1.98E+03	0.99
1300	6.31E-03	1.22E-01	1.77E+01	2.06E+03	0.99
13000	5.48E-03	7.30E-02	1.66E+01	2.08E+03	0.99
Using $K_{hv} = 0.05$					
20	9.76E-03	1.97E-01	1.93E+01	1.58E+03	0.99
65	1.26E-02	3.85E-01	2.28E+01	1.79E+03	0.99
200	1.17E-02	3.90E-01	2.30E+01	1.96E+03	0.99
1300	7.42E-03	1.88E-01	1.91E+01	2.07E+03	0.99
13000	5.46E-03	7.00E-02	1.65E+01	2.07E+03	0.99
Using $K_{hv} = 0.005$					
20	3.68E-03	-2.50E-01	1.02E+01	1.43E+03	0.99
65	-5.12E-03	-1.05E+00	-9.03E+00	1.45E+03	0.99
200	3.30E-03	-5.36E-01	3.58E-02	1.69E+03	0.99
1300	1.12E-02	2.86E-01	1.97E+01	2.03E+03	0.99
13000	6.27E-03	1.06E-01	1.71E+01	2.08E+03	0.99

Table A.5. Uplift pressure at the base of the blanket (above channel) ( $u_{bl}$ ) as a function of  $h$ ,  $K_{sb}$ ,  $d_c$ , and  $K_{hv} = 0.25$  used for Example 2.2 in Chapter 2. These values correspond to Figures A.11 to A.17

$h$ (ft)	$u_{bl}$ (lb/ft <sup>2</sup> )				
	$K_{sb}$				
	20	65	200	1300	13000
Using $d_c = 175'$					
0	1068.09	1195.56	1398.96	1627.45	1795.56
3	869.67	997.52	1202.75	1434.37	1605.46
6	666.89	793.07	1000.01	1236.52	1412.83
9	458.32	577.97	785.03	1029.18	1215.07
12	240.48	339.43	536.15	791.69	999.76
Using $d_c = 150'$					
0	1089.12	1213.43	1408.65	1626.04	1785.49
3	887.11	1012.20	1209.60	1430.20	1592.49
6	680.48	804.41	1004.10	1229.77	1397.09
9	467.84	585.92	786.67	1020.37	1196.93
12	245.64	343.84	536.10	782.36	980.48
Using $d_c = 125'$					
0	1112.53	1230.55	1415.45	1620.32	1770.32
3	904.74	1023.62	1210.77	1418.74	1571.31
6	692.55	810.43	1000.04	1212.93	1370.14
9	474.77	587.17	778.24	998.99	1164.72
12	248.21	341.78	525.67	759.13	944.83
Using $d_c = 100'$					
0	1142.31	1252.11	1424.94	1615.98	1755.74
3	928.33	1039.39	1214.65	1408.66	1550.74
6	709.94	820.59	998.63	1197.45	1343.76
9	486.07	592.15	772.31	978.88	1133.03
12	253.63	342.57	517.34	736.91	909.53

<i>h</i> (ft)	<i>u<sub>bl</sub></i> (lb/ft <sup>2</sup> )				
	<i>K<sub>sb</sub></i>				
	20	65	200	1300	13000
Using <i>d<sub>c</sub></i> =75'					
0	1178.14	1277.71	1436.81	1612.83	1741.67
3	960.31	1062.07	1223.97	1402.93	1533.89
6	737.80	840.69	1005.97	1189.62	1324.42
9	509.63	609.79	778.41	969.78	1111.69
12	271.60	357.77	524.19	729.23	888.02
Using <i>d<sub>c</sub></i> =50'					
0	1258.29	1342.25	1484.95	1644.60	1761.95
3	1022.49	1108.45	1252.86	1414.09	1532.69
6	806.62	894.11	1040.48	1204.05	1324.80
9	587.00	675.05	823.62	990.98	1115.39
12	359.96	444.85	595.28	769.66	901.80
15	95.71	115.15	149.18	179.31	191.99
Using <i>d<sub>c</sub></i> =25'					
0	1379.32	1445.73	1570.47	1712.27	1817.12
3	1104.08	1171.54	1296.94	1438.83	1543.86
6	896.35	964.50	1090.20	1231.99	1337.32
9	688.76	757.52	883.33	1024.77	1130.44
12	481.31	550.59	675.97	816.93	922.94
15	274.11	343.85	467.99	607.81	713.53

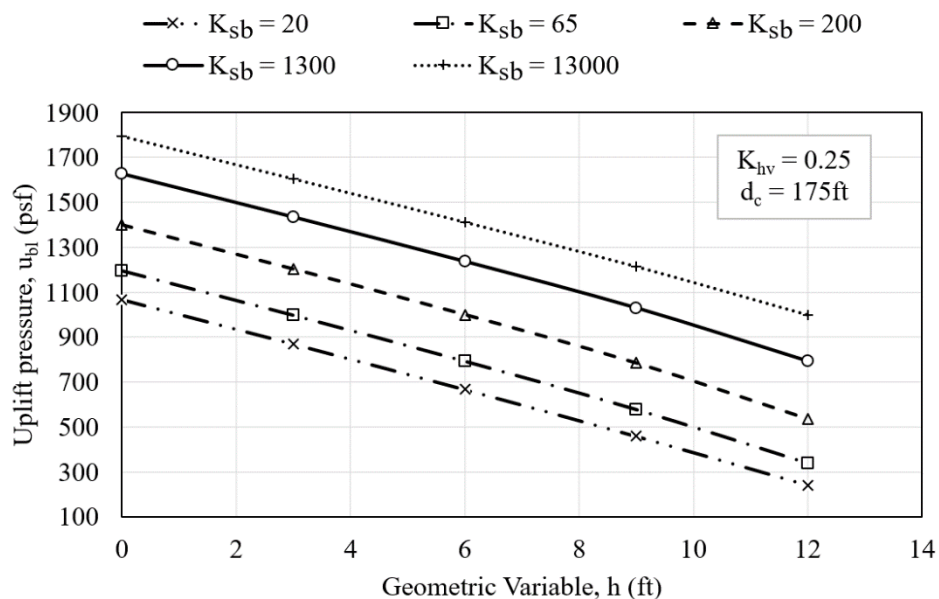


Figure A.11. Family of curves representing relationship between  $K_{sb}$ ,  $h$ , and  $\mu_{bl}$  for  $K_{hv} = 0.25$  and  $d_c = 175$  ft.

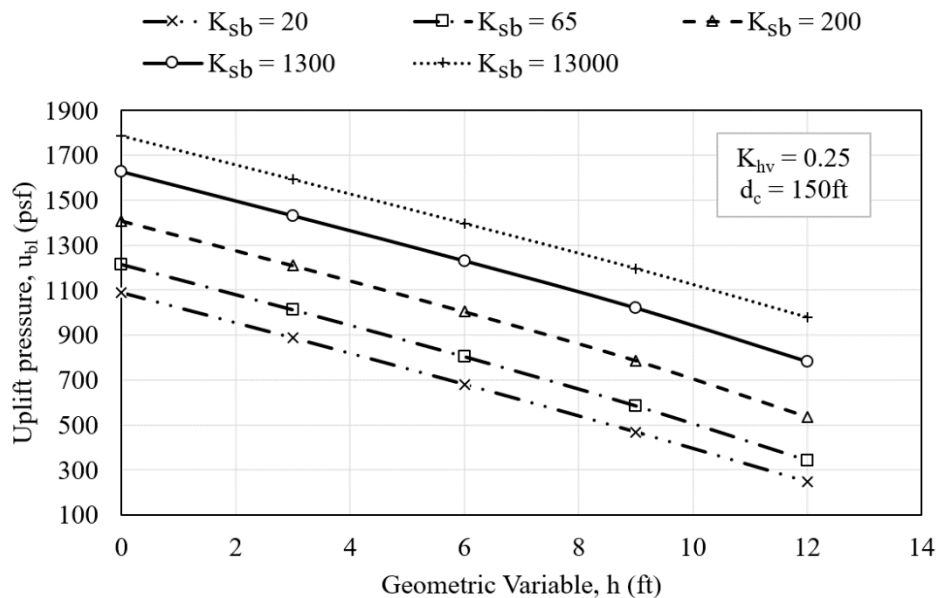


Figure A.12. Family of curves representing relationship between  $K_{sb}$ ,  $h$ , and  $\mu_{bl}$  for  $K_{hv} = 0.25$  and  $d_c = 150$  ft.

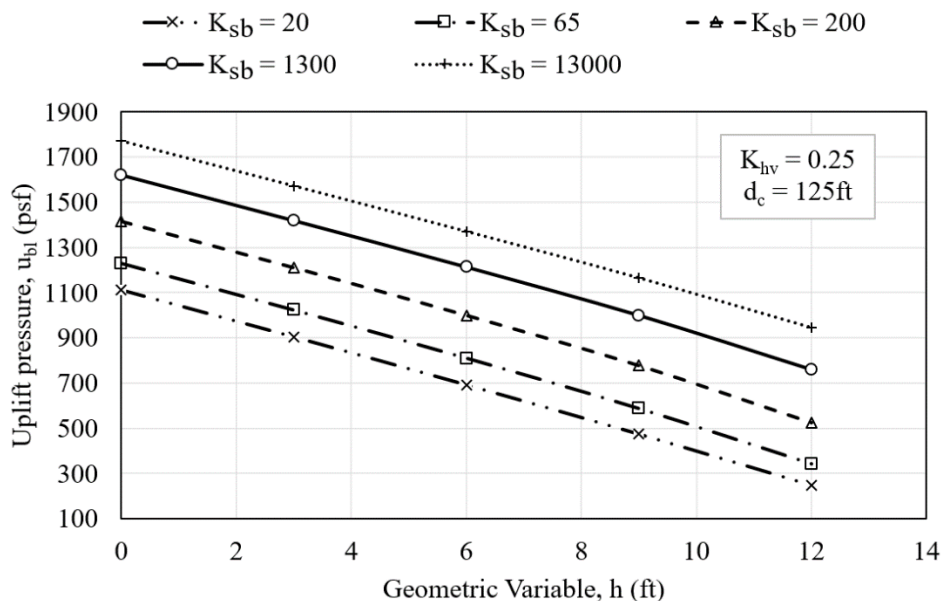


Figure A.13. Family of curves representing relationship between  $K_{sb}$ ,  $h$ , and  $\mu_{bl}$  for  $K_{hv} = 0.25$  and  $d_c = 125$  ft.

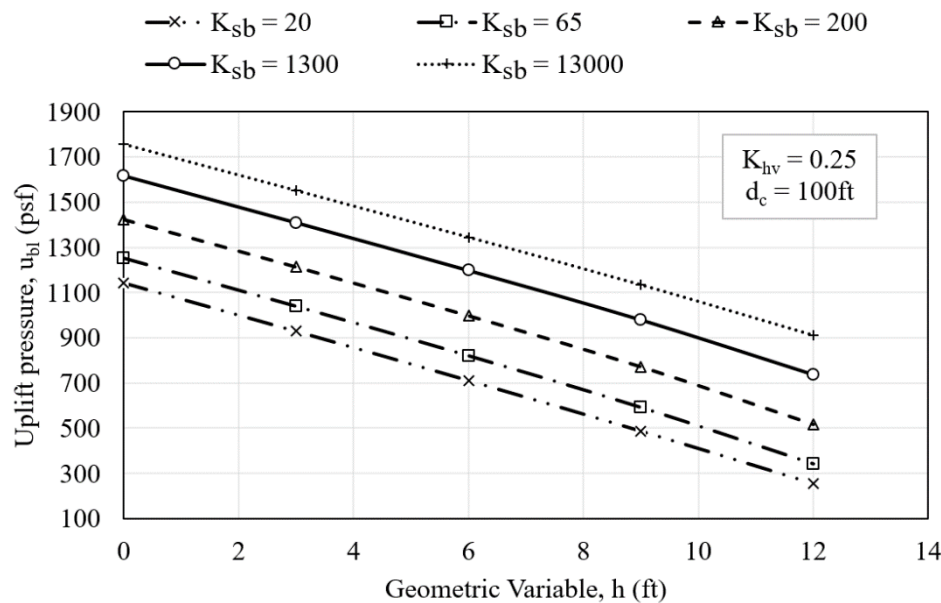


Figure A.14. Family of curves representing relationship between  $K_{sb}$ ,  $h$ , and  $\mu_{bl}$  for  $K_{hv} = 0.25$  and  $d_c = 100$  ft.

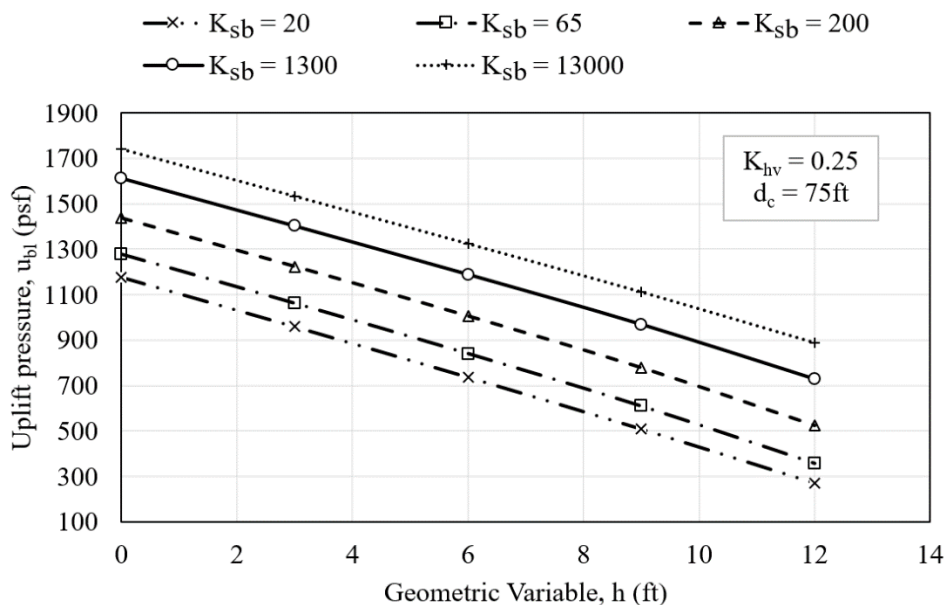


Figure A.15. Family of curves representing relationship between  $K_{sb}$ ,  $h$ , and  $\mu_{bl}$  for  $K_{hv} = 0.25$  and  $d_c = 75$  ft.

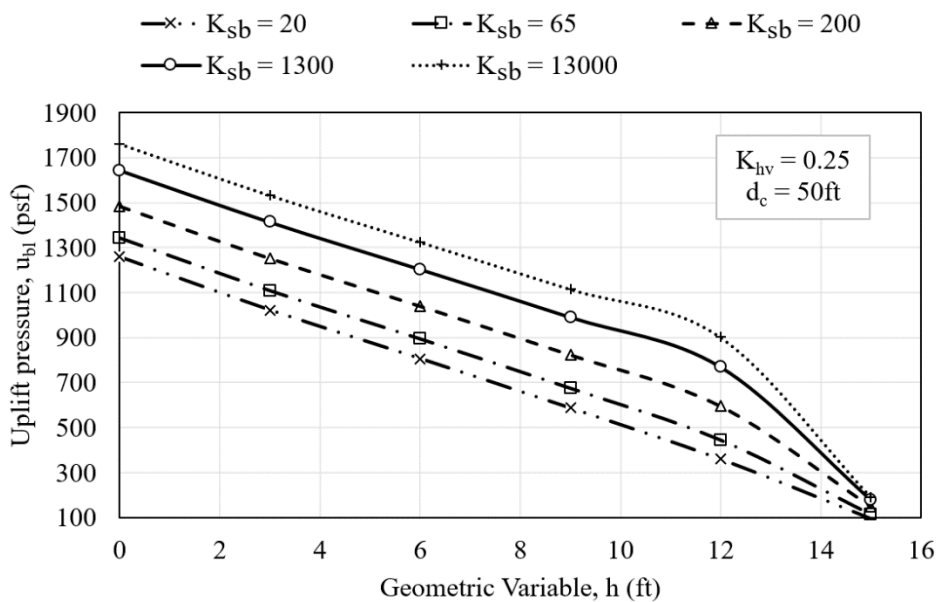


Figure A.16. Family of curves representing relationship between  $K_{sb}$ ,  $h$ , and  $\mu_{bl}$  for  $K_{hv} = 0.25$  and  $d_c = 50$  ft.



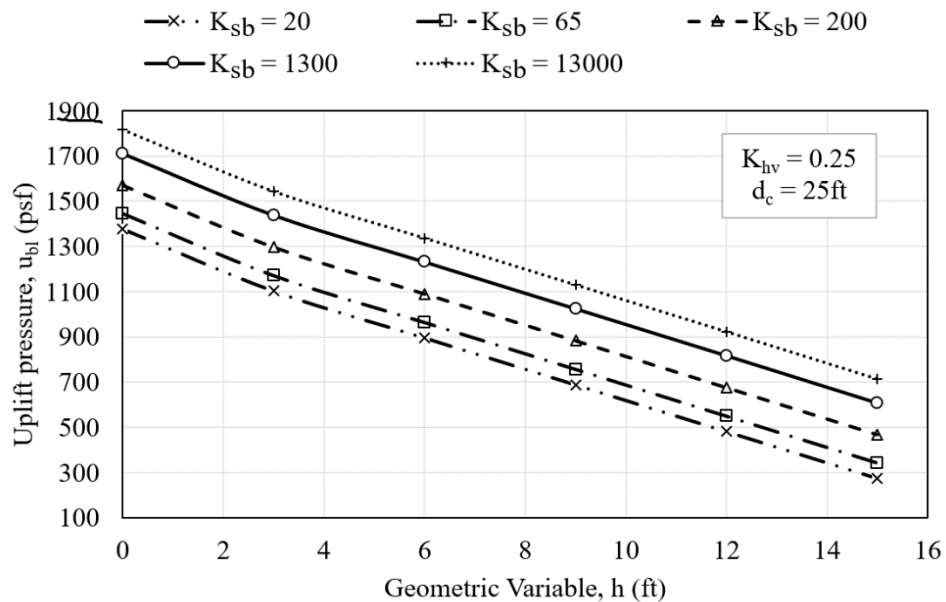


Figure A.17. Family of curves representing relationship between  $K_{sb}$ ,  $h$ , and  $\mu_{bl}$  for  $K_{hv} = 0.25$  and  $d_c = 25$  ft.

Table A.6. Fit-equations' coefficients and corresponding goodness of fit for family of curves for the computation of  $u_{bl}$  with respect to each  $K_{sb}$  used for Example 2.2 in Chapter 2. These values correspond to Figures A.11 to A.17

$K_{sb}$	$u_{bl} = H_4 * h^4 + H_3 * h^3 + H_2 * h^2 + H_1 * h + H_0$					$R^2$
	$H_4$	$H_3$	$H_2$	$H_1$	$H_0$	
Using $d_c = 175\text{ft}$						
20	-	-1.51E-02	-8.24E-02	-6.58E+01	1.07E+03	0.99
65	-	-5.25E-02	2.18E-01	-6.64E+01	1.20E+03	0.99
200	-	-8.45E-02	5.88E-01	-6.68E+01	1.40E+03	0.99
1300	-	-7.83E-02	6.30E-01	-6.59E+01	1.63E+03	0.99
13000	-	-4.64E-02	3.94E-01	-6.44E+01	1.80E+03	0.99
Using $d_c = 150\text{ft}$						
20	-	-1.53E-02	-9.32E-02	-6.70E+01	1.09E+03	0.99
65	-	-5.25E-02	2.12E-01	-6.75E+01	1.21E+03	0.99
200	-	-8.24E-02	5.71E-01	-6.77E+01	1.41E+03	0.99
1300	-	-7.41E-02	5.94E-01	-6.68E+01	1.63E+03	0.99
13000	-	-4.29E-02	3.63E-01	-6.53E+01	1.79E+03	0.99
Using $d_c = 125\text{ft}$						
20	-	-1.36E-02	-9.83E-02	-6.89E+01	1.11E+03	0.99
65	-	-4.90E-02	1.92E-01	-6.93E+01	1.23E+03	0.99
200	-	-7.63E-02	5.25E-01	-6.95E+01	1.42E+03	0.99
1300	-	-6.70E-02	5.33E-01	-6.85E+01	1.62E+03	0.99
13000	-	-3.80E-02	3.18E-01	-6.71E+01	1.77E+03	0.99
Using $d_c = 100\text{ft}$						
20	-	-1.28E-02	-1.06E-01	-7.09E+01	1.14E+03	0.99
65	-	-4.65E-02	1.75E-01	-7.12E+01	1.25E+03	0.99
200	-	-7.08E-02	4.83E-01	-7.12E+01	1.43E+03	0.99
1300	-	-6.02E-02	4.76E-01	-7.03E+01	1.62E+03	0.99
13000	-	-3.33E-02	2.76E-01	-6.90E+01	1.76E+03	0.99

$K_{sb}$	$u_{bl} = H_4 * h^4 + H_3 * h^3 + H_2 * h^2 + H_1 * h + H_0$					$R^2$
	$H_4$	$H_3$	$H_2$	$H_1$	$H_0$	
Using $d_c = 75\text{ft}$						
20	-	-1.59E-02	-7.85E-02	-7.23E+01	1.18E+03	0.99
65	-	-4.75E-02	2.02E-01	-7.22E+01	1.28E+03	0.99
200	-	-6.63E-02	4.62E-01	-7.20E+01	1.44E+03	0.99
1300	-	-5.34E-02	4.23E-01	-7.10E+01	1.61E+03	0.99
13000	-	-2.85E-02	2.35E-01	-6.99E+01	1.74E+03	0.99
Using $d_c = 50\text{ft}$						
20	-	-1.02E-01	1.92E+00	-8.34E+01	1.26E+03	0.99
65	-	-2.11E-01	3.66E+00	-8.93E+01	1.34E+03	0.99
200	-4.68E-02	9.91E-01	-5.87E+00	-6.57E+01	1.48E+03	0.99
1300	-8.68E-02	1.93E+00	-1.25E+01	-5.14E+01	1.64E+03	0.99
13000	-1.21E-01	2.73E+00	-1.81E+01	-3.93E+01	1.76E+03	0.99
Using $d_c = 25\text{ft}$						
20	-	-1.153E-01	3.272E+00	-9.678E+01	1.377E+03	0.99
65	-	-1.148E-01	3.254E+00	-9.639E+01	1.443E+03	0.99
200	-	-1.160E-01	3.255E+00	-9.619E+01	1.568E+03	0.99
1300	-	-1.167E-01	3.255E+00	-9.617E+01	1.710E+03	0.99
13000	-	-1.180E-01	3.280E+00	-9.620E+01	1.815E+03	0.99

## APPENDIX B

Appendix B provides supporting data for the comparative analyses presented in Chapter 3. Table B.1 presents the input parameters used for each analyzed case complementing Table 3.1. Tables B.2 through Table B.18 together with Figure B.1 through Figure B.18 correspond to supporting data for Table 3.2 for the analysis of Cases 1, 2, 3a, 3b, 4a and 4b with respect to the FOSM and RSMC methods. Supporting data for the RSMC analysis of Cases 5 and 6 are the same as presented in Appendix A

Table B.1. Input values used for comparative analyses. Supporting data for Table 3.1

Parameter	Type of PDF distribution	Most likely value (MLV)	Standard deviation ( $\sigma$ )	Truncated minimum value (MIN)	Truncated maximum value (MAX)
Cases 1 and 2					
$Z_{bl}$	Normal	14	8	2	26
$\log(K_b)$	Normal	-5.5	1	-7.0	-4.0
$\log(K_s)$	Normal	-3.0	1	-3.1	-2.9
$y_{blkt}$	Normal	120	5	110	130
Cases 3a and 3b					
$Z_{bl}$	Normal	12.5	5	5	20
$d_b$	Normal	165	50	3	315
$\log(K_b)$	Normal	-6.00	1	-7.00	-4.00
$\log(K_s)$	Normal	-3.00	1	-3.10	-2.95
$y_{blkt}$	Normal	120	5	110	130
Cases 4a and 4b					
$Z_{bl}$	Normal	12.5	5	5	20
$d_e$	Normal	185	50	65	365
$\log(K_b)$	Normal	-6.0	1	-7.0	-4.3
$\log(K_s)$	Normal	-3.0	1	-3.1	-2.8
$y_{blkt}$	Normal	120	5	110	130
Case 5					
$A$	Trapezoidal	-47	-	-15	-76
$\log(K_b)$	Normal	-6	1	-7	-4
$\log(K_s)$	Normal	-3.0	1	-3.2	-2.8
$\log(K_{hv})$	Normal	-0.6	0	-0.3	-2.3
$y_{blkt}$	Normal	120	5	130	110
$y_{sand}$	Normal	130	5	140	120
Case 6					
$d_c$	Uniform	-	-	25	175
$h$	Uniform	-	-	0	12
$\log(K_b)$	Normal	-6	1	-6	-4
$\log(K_s)$	Normal	-3.0	1	-3.1	-2.9
$y_{blkt}$	Normal	120	5	110	130

Table B.2. FOSM calculation for Case 1 as depicted in Figure 3.3 in Chapter 3.

Supporting data for Table 3.2.

Input Variables	MLV	$\sigma$	COV
Blanket thickness ( $Z_{bl}$ )	14	8	57%
Vertical permeability of top stratum (blanket) ( $k_b$ )	5.5E-06	5.0E-06	90%
Horizontal permeability of pervious substratum (sand) ( $K_f$ )	1.0E-03	9.0E-04	90%
Unit weight of top stratum material ( $\gamma_{blkt}$ )	120	5	4%

## FOSM calculations

Variable	Values	F.S.	$\Delta F$
Blanket thickness ( $Z_{bl}$ ) (ft)			
MLV + $\sigma$	22	F1+ 2.585	1.880
MLV - $\sigma$	6	F1+ 0.705	
Unit weight of top stratum material ( $\gamma_{blkt}$ ) (lb/ft <sup>3</sup> )			
MLV + $\sigma$	125	F2+ 1.788	0.286
MLV - $\sigma$	115	F2+ 1.502	
Vertical permeability of blanket ( $K_b$ ) (ft/s)			
MLV + $\sigma$	1.0E-05	F3+ 1.645	0.000
MLV - $\sigma$	5.5E-07	F3+ 1.645	
Horizontal permeability of sand ( $K_f$ ) (ft/s)			
MLV + $\sigma$	1.9E-03	F4+ 1.645	0.000
MLV - $\sigma$	1.0E-04	F4+ 1.645	
With all variables assigned their most likely values		F.S. =	1.65

$$\sigma_{FS} = 0.951$$

$$COV_{FS} = 58\%$$

$$\beta = 0.678$$

$$P_{up} = 24.87\%$$

Table B.3. Hydraulic exit gradient ( $i_e$ ) as a function of  $h$ ,  $K_{sb}$  and  $K_{hv} = 0.25$  used for Case 1 as depicted in Figure 3.3 in Chapter 3. These values correspond to Figure A2.1

$Z_{bl}$ (ft)	$i_e$				
	$K_{sb}$				
	20	63	201	634	2006
	Using $K_{hv} = 0.25$				
2	0.881	2.451	3.004	4.541	6.022
4	0.516	1.450	1.745	2.491	3.114
6	0.460	1.116	1.298	1.770	2.119
8	0.394	0.859	1.001	1.350	1.596
10	0.354	0.756	0.865	1.119	1.290
12	0.262	0.612	0.707	0.927	1.070
14	0.294	0.577	0.651	0.819	0.926
16	0.265	0.513	0.578	0.721	0.811
18	0.225	0.451	0.510	0.640	0.719
20	0.205	0.409	0.462	0.578	0.646
22	0.188	0.376	0.424	0.528	0.588
24	0.178	0.348	0.391	0.486	0.539
26	0.143	0.309	0.351	0.443	0.493

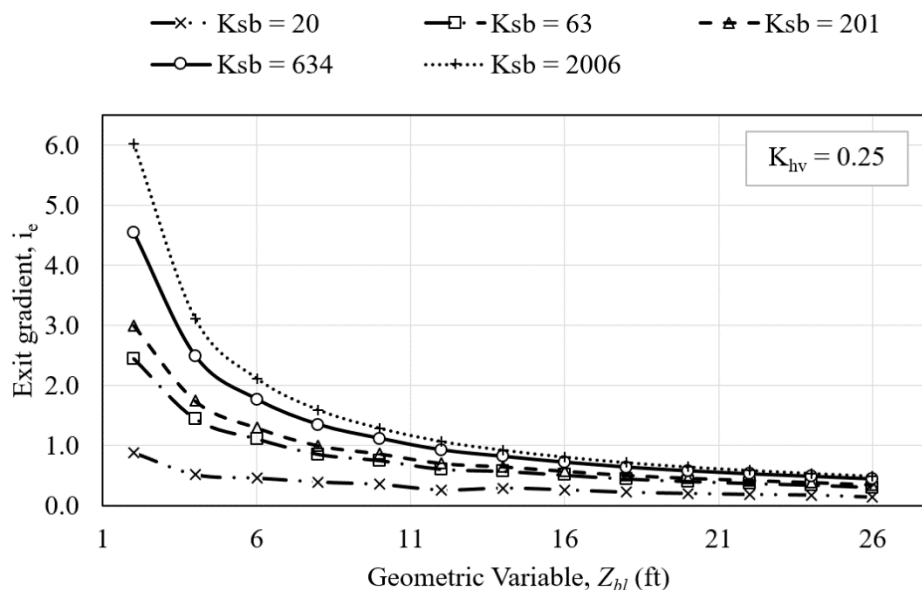


Figure B.1. Family of curves representing relationship between  $Z_{bl}$ ,  $K_{sb}$ , and  $i_e$  for  $K_{hv} = 0.25$  for Case 1.

Table B.4. Fit-equations' coefficients and corresponding goodness of fit for family of curves for the computation of  $i_e$  with respect to  $K_{sb}$  used for Case 1. These values correspond to Figure B.1.

$K_{sb}$	$i_e = a_6 * Z_{bl}^6 + a_5 * Z_{bl}^5 + a_4 * Z_{bl}^4 + a_3 * Z_{bl}^3 + a_2 * Z_{bl}^2 + a_1 * Z_{bl} + a_0$							$R^2$
	$a_6$	$a_5$	$a_4$	$a_3$	$a_2$	$a_1$	$a_0$	
Using $K_{hv} = 0.25$								
20	1.93E-07	-1.78E-05	6.53E-04	-1.21E-02	1.19E-01	-6.09E-01	1.70E+00	0.98
63	3.11E+00	-2.98E-05	1.14E-03	-2.25E-02	2.43E-01	-1.43E+00	4.49E+00	0.99
201	3.87E-07	-3.71E-05	1.43E-03	-2.84E-02	3.08E-01	-1.81E+00	5.60E+00	0.99
634	6.78E-07	-6.48E-05	2.49E-03	-4.90E-02	5.27E-01	-3.05E+00	8.88E+00	0.99
2006	6.78E-07	-9.64E-05	3.69E-03	-7.26E-02	7.77E-01	-4.44E+00	1.23E+00	0.99



Table B.5. FOSM calculation for Case 2 as depicted in Figure 3.3 in Chapter 3.

Supporting data for Table 3.2.

Input Variables	MLV	$\sigma$	COV
Blanket thickness ( $Z_{bl}$ )	14	8	57%
Vertical permeability of top stratum (blanket) ( $K_b$ )	5.5E-06	5.0E-06	90%
Horizontal permeability of pervious substratum (sand) ( $K_f$ )	1.0E-03	9.0E-04	90%
Unit weight of top stratum material ( $\gamma_{blkt}$ )	120	5	4%

## FOSM calculations

Variable	Values	F.S.	$\Delta F$
Blanket thickness ( $Z_{bl}$ ) (ft)			
MLV + $\sigma$	22	F1+ 1.876	1.258
MLV - $\sigma$	6	F1+ 0.618	
Unit weight of top stratum material ( $\gamma_{blkt}$ ) (lb/ft <sup>3</sup> )			
MLV + $\sigma$	125	F2+ 1.372	0.219
MLV - $\sigma$	115	F2+ 1.153	
Vertical permeability of blanket ( $K_b$ ) (ft/s)			
MLV + $\sigma$	1.0E-05	F3+ 1.390	0.360
MLV - $\sigma$	5.5E-07	F3+ 1.030	
Horizontal permeability of sand ( $K_f$ ) (ft/s)			
MLV + $\sigma$	1.9E-03	F4+ 1.169	-0.826
MLV - $\sigma$	1.0E-04	F4+ 1.995	
With all variables assigned their most likely values		F.S. =	1.26

$$\sigma_{FS} = 0.781$$

$$COV_{FS} = 62\%$$

$$\beta = 0.335$$

$$P_{up} = 36.87\%$$

Table B.6. Hydraulic exit gradient ( $i_e$ ) as a function of  $Z_{bl}$ ,  $K_{sb}$  and  $K_{hv} = 0.25$  used for Case 2 as depicted in Figure 3.3 in Chapter 3. These values correspond to Figure B.2

$Z_{bl}$ (ft)	$i_e$				
	$K_{sb}$				
	10	100	182	1000	10000
	Using $K_{hv} = 1.0$				
2	1.414	3.128	3.655	5.044	6.235
4	0.933	1.878	2.135	2.752	3.218
6	0.730	1.379	1.543	1.915	2.176
8	0.613	1.100	1.217	1.474	1.645
10	0.524	0.916	1.006	1.199	1.322
12	0.468	0.793	0.864	1.015	1.106
14	0.405	0.690	0.751	0.876	0.950
16	0.367	0.613	0.665	0.771	0.832
18	0.365	0.569	0.611	0.691	0.743
20	0.310	0.506	0.545	0.624	0.667
22	0.280	0.462	0.498	0.569	0.607
24	0.274	0.434	0.465	0.526	0.558
26	0.276	0.413	0.439	0.491	0.516

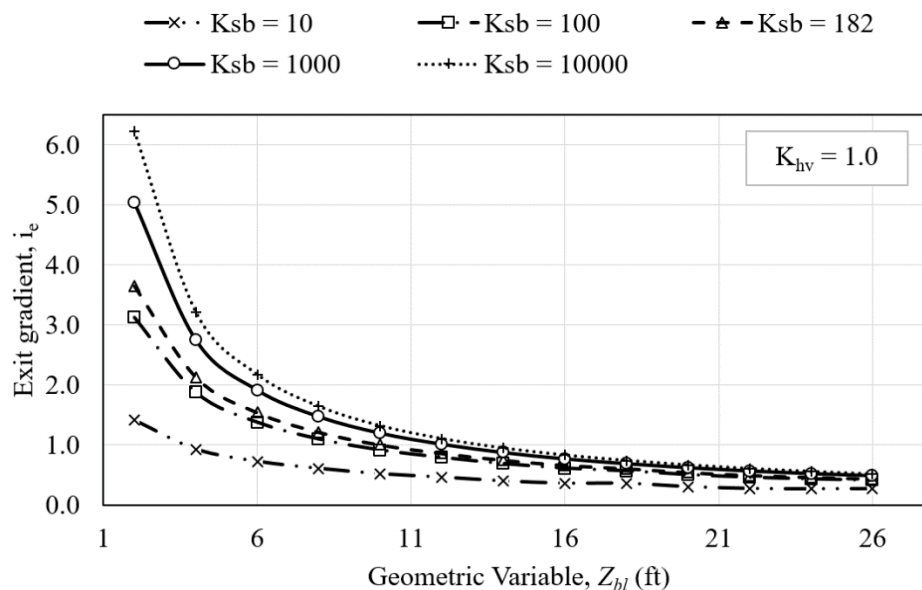


Figure B.2. Family of curves representing relationship between  $Z_{bl}$ ,  $K_{sb}$ , and  $i_e$  for  $K_{hv} = 0.25$  for Case 2.

Table B.7. Fit-equations' coefficients and corresponding goodness of fit for family of curves for the computation of  $i_e$  with respect to  $K_{sb}$  used for Case 2. These values correspond to Figure B.2.

$K_{sb}$	$i_e = a_6 * Z_{bl}^6 + a_5 * Z_{bl}^5 + a_4 * Z_{bl}^4 + a_3 * Z_{bl}^3 + a_2 * Z_{bl}^2 + a_1 * Z_{bl} + a_0$							$R^2$
	$a_6$	$a_5$	$a_4$	$a_3$	$a_2$	$a_1$	$a_0$	
Using $K_{hv} = 1.0$								
10	1.75E-07	-1.61E-05	5.95E-04	-1.13E-02	1.19E-01	-6.95E-01	2.41E+00	0.99
100	3.86E-07	-3.67E-05	1.41E-03	-2.78E-02	3.02E-01	-1.79E+00	5.71E+00	0.99
182	4.74E-07	-4.53E-05	1.74E-03	-3.43E-02	3.73E-01	-2.20E+00	6.81E+00	0.99
1000	7.52E-07	-7.20E-05	2.77E-03	-5.46E-02	5.89E-01	-3.42E+00	9.91E+00	0.99
10000	1.05E-06	-1.00E-04	3.84E-03	-7.54E-02	8.08E-01	-4.62E+00	1.28E+01	0.99

Table B.8. FOSM calculation for Case 3a as depicted in Figure 3.4 in Chapter 3.

Supporting data for Table 3.2.

Input Variables	MLV	$\sigma$	COV
Blanket thickness ( $Z_{bl}$ )	12.5	5	40%
Length of foundation and top stratum beyond landside levee toe ( $L_3$ )	1.0E+02	5.0E+01	50%
Vertical permeability of top stratum (blanket) ( $K_b$ )	1.0E-06	9.0E-07	90%
Horizontal permeability of pervious substratum (sand) ( $K_f$ )	0.001	0.0009	90%
Unit weight of top stratum material ( $\gamma_{blkt}$ )	120	5	4%

## FOSM calculations

Variable	Values	F.S.	$\Delta F$
Blanket thickness ( $Z_{bl}$ ) (ft)			
MLV + $\sigma$	18	F1+ 1.901	0.027
MLV - $\sigma$	8	F1+ 1.875	
Length of foundation and top stratum beyond landside levee toe ( $L_3$ ) (ft)			
MLV + $\sigma$	150	F2+ 1.897	0.008
MLV - $\sigma$	50	F2+ 1.888	
Unit weight of top stratum material ( $\gamma_{blkt}$ ) (lb/ft <sup>3</sup> )			
MLV + $\sigma$	1.3E+02	F3+ 1.972	0.158
MLV - $\sigma$	1.2E+02	F3+ 1.814	
Vertical permeability of blanket ( $K_b$ ) (ft/s)			
MLV + $\sigma$	1.9E-06	F4+ 1.894	0.002
MLV - $\sigma$	1.0E-07	F4+ 1.892	
Horizontal permeability of sand ( $K_f$ ) (ft/s)			
MLV + $\sigma$	1.9E-03	F5+ 1.893	-0.006
MLV - $\sigma$	1.0E-04	F5+ 1.899	
With all variables assigned their most likely values		F.S. =	0.97

$$\sigma_{FS} = 0.080$$

$$COV_{FS} = 8\%$$

$$\beta = -0.407$$

$$P_{up} = 65.80\%$$

Table B.9. Uplift pressure at the base of the blanket (above seepage block) ( $u_{bl}$ ) as a function of  $d_b$ ,  $K_{sb}$ ,  $Z_{bl}$  and  $K_{hv} = 1.0$  used for Case 3a as depicted in Figure 3.4 in Chapter 3. These values correspond to Figure B.3 through B.6

$d_b$ (ft)	$u_{bl}$				
	$K_{sb}$				
	20	65	200	1300	13000
Using $K_{hv} = 1.0$ , $Z_{bl} = 5$ ft					
3	420.295	426.903	428.357	429.399	429.711
15	427.802	438.341	439.377	440.906	441.717
35	448.119	472.256	475.126	479.419	480.711
55	508.098	610.884	625.747	648.835	655.886
75	665.933	1095.182	1177.636	1319.261	1366.685
95	602.834	1006.262	1103.856	1293.240	1363.502
115	569.818	935.438	1040.395	1267.403	1360.195
135	553.476	883.210	990.288	1243.882	1356.950
155	544.977	842.650	948.106	1221.355	1353.706
175	540.652	812.323	914.784	1201.075	1350.648
195	538.381	788.674	887.016	1181.856	1347.590
215	537.177	769.954	863.366	1163.323	1344.408
315	535.922	722.966	793.853	1087.819	1329.370
Using $K_{hv} = 1.0$ , $Z_{bl} = 10$ ft					
3	794.976	809.141	810.763	813.134	813.758
15	808.766	829.046	831.355	834.662	835.910
35	842.275	885.893	891.696	900.245	902.554
55	925.642	1071.096	1093.248	1126.819	1136.304
75	1062.485	1457.102	1529.362	1645.862	1680.557
95	998.587	1391.330	1478.318	1630.387	1678.747
115	959.774	1336.046	1432.330	1615.224	1677.000
135	936.936	1288.310	1391.021	1599.936	1675.128
155	924.019	1250.434	1356.139	1585.771	1673.318
175	916.531	1219.858	1326.312	1572.480	1671.571
195	912.038	1193.712	1299.792	1559.501	1669.824
215	909.355	1171.934	1276.205	1546.834	1668.077
315	905.798	1107.912	1196.770	1491.360	1659.403

$d_b$ (ft)	$u_{bl}$				
	$K_{sb}$				
	20	65	200	1300	13000
Using $K_{hv} = 1.0$ , $Z_{bl} = 15$ ft					
3	1145.789	1166.506	1169.002	1172.496	1173.120
15	1163.760	1192.589	1196.208	1201.325	1202.698
35	1204.445	1265.098	1274.021	1286.064	1289.184
55	1296.859	1466.712	1493.107	1532.232	1542.840
75	1414.546	1789.008	1857.336	1963.166	1993.181
95	1353.019	1734.845	1815.715	1951.498	1991.870
115	1313.645	1686.547	1777.838	1939.829	1990.498
135	1288.810	1644.302	1742.894	1928.222	1989.125
155	1273.646	1609.483	1712.443	1917.240	1987.814
175	1264.162	1578.970	1684.675	1906.445	1986.504
195	1258.234	1553.323	1660.027	1896.024	1985.131
215	1254.490	1531.171	1637.626	1885.728	1983.821
315	1248.811	1461.970	1558.378	1840.176	1977.331
Using $K_{hv} = 1.0$ , $Z_{bl} = 20$ ft					
3	1484.309	1509.331	1512.701	1517.318	1518.566
15	1503.278	1540.531	1545.336	1552.075	1553.885
35	1549.330	1623.648	1634.506	1650.168	1654.099
55	1642.618	1826.261	1856.088	1899.082	1910.563
75	1744.454	2109.058	2175.514	2277.288	2305.430
95	1687.296	2060.510	2139.134	2267.366	2304.307
115	1648.171	2016.893	2105.276	2257.382	2303.184
135	1622.525	1978.018	2073.864	2247.398	2302.061
155	1606.488	1945.445	2046.221	2237.976	2300.938
175	1596.130	1916.990	2020.824	2228.678	2299.014
195	1589.390	1892.530	1997.986	2219.755	2298.691
215	1585.085	1870.502	1977.206	2210.957	2297.568
315	1577.971	1799.054	1899.581	2170.459	2292.077

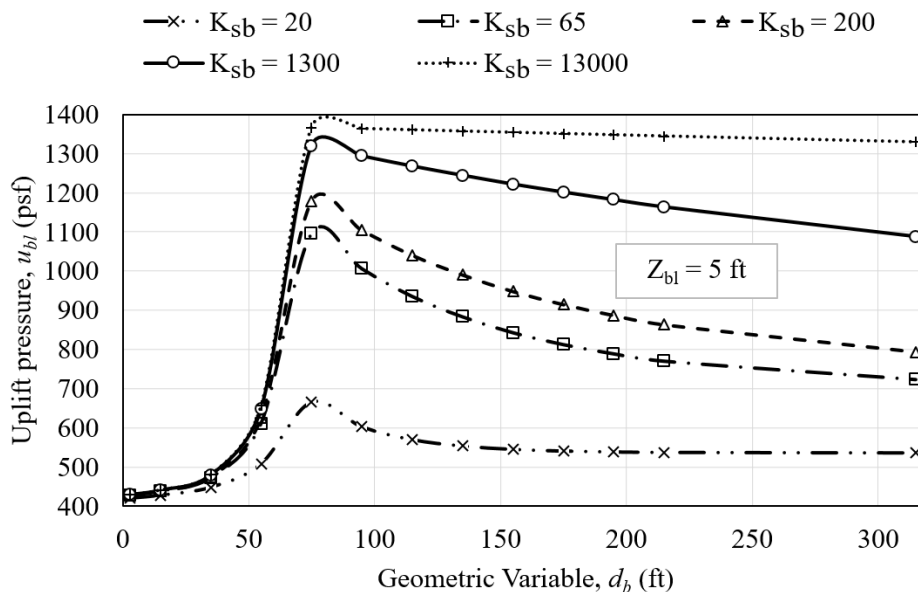


Figure B.3. Family of curves representing relationship between  $d_b$ ,  $K_{sb}$ , and  $u_{bl}$  for  $K_{hv} = 1.0$  and  $Z_{bl} = 5$  ft for Case 3a.

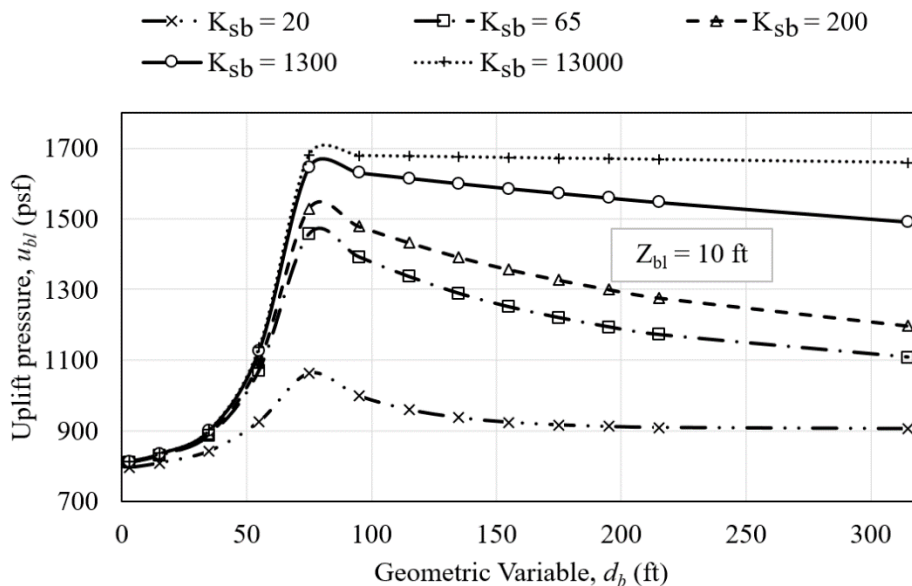


Figure B.4. Family of curves representing relationship between  $d_b$ ,  $K_{sb}$ , and  $u_{bl}$  for  $K_{hv} = 1.0$  and  $Z_{bl} = 10$  ft for Case 3a.

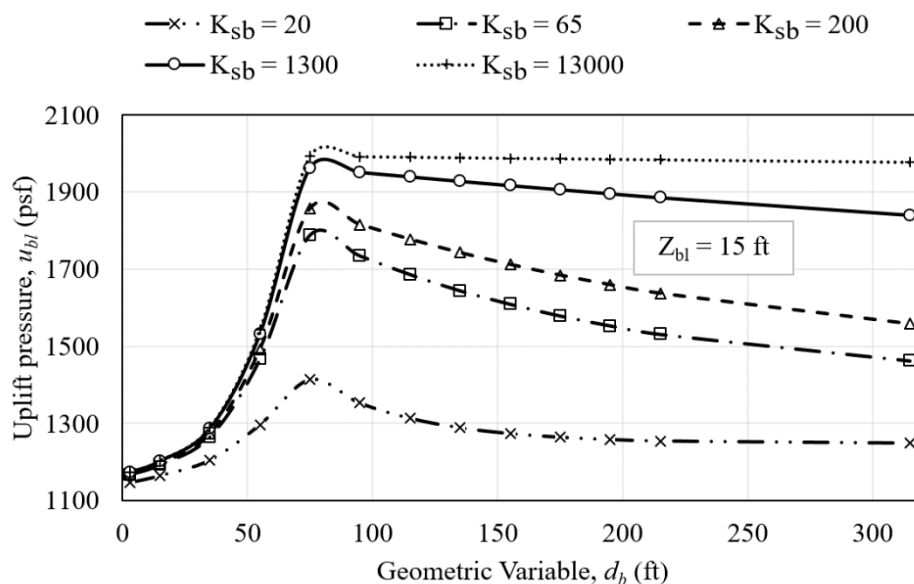


Figure B.5. Family of curves representing relationship between  $d_b$ ,  $K_{sb}$ , and  $u_{bl}$  for  $K_{hv} = 1.0$  and  $Z_{bl} = 15$  ft for Case 3a.

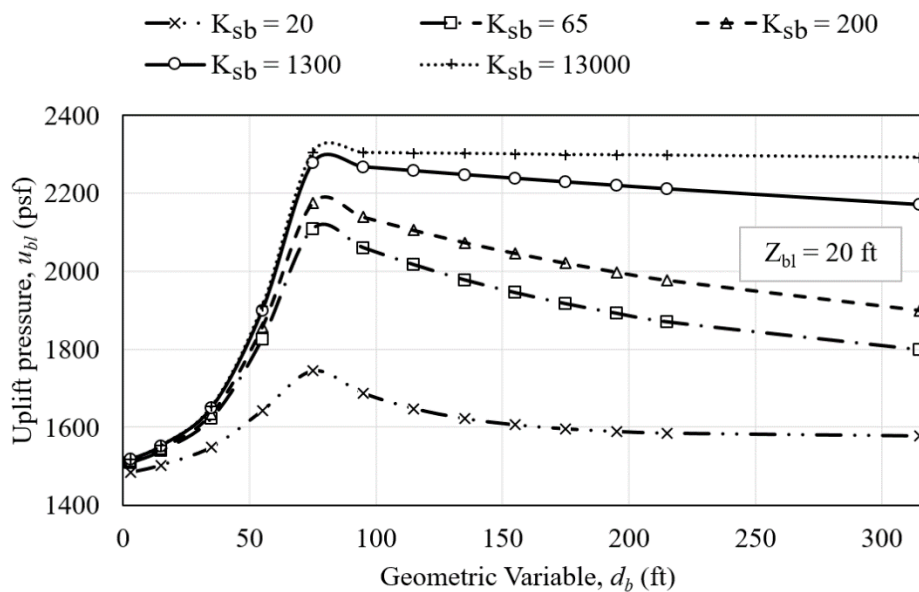


Figure B.6. Family of curves representing relationship between  $d_b$ ,  $K_{sb}$ , and  $u_{bl}$  for  $K_{hv} = 1.0$  and  $Z_{bl} = 20$  ft for Case 3a.



Table B.10. Fit-equations' coefficients and corresponding goodness of fit for family of curves for the computation of  $u_{bl}$  with respect to  $K_{sb}$  used for Case 3a. These values correspond to Figures B.3 through B.6.

$K_{sb}$	$u_{bl} = a_6*d_b^6 + a_5*d_b^5 + a_4*d_b^4 + a_3*d_b^3 + a_2*d_b^2 + a_1*d_b + a_0$							$R^2$
	$a_6$	$a_5$	$a_4$	$a_3$	$a_2$	$a_1$	$a_0$	
Using $K_{hv} = 1.0, Z_{bl} = 5$ ft								
$3ft \leq d_b \leq 75ft$								
20	-	-	-	1.03E-03	-5.16E-02	1.43E+00	4.16E+02	0.99
65	-	-	4.10E-05	-2.35E-03	6.05E-02	3.48E-01	4.25E+02	0.99
200	-	-	5.18E-05	-3.35E-03	9.44E-02	-6.27E-02	4.28E+02	0.99
1300	-	-	7.15E-05	-5.15E-03	1.51E-01	-6.18E-01	4.30E+02	0.99
13000	-	-	7.80E-05	-5.72E-03	1.67E-01	-7.29E-01	4.31E+02	0.99
$75ft \leq d_b \leq 315ft$								
20	9.08E-12	-1.20E-08	6.63E-06	-1.95E-03	3.27E-01	-2.97E+01	1.70E+03	0.99
65	-4.27E-05	3.33E-02	-9.06E+00	1.60E+03	-	-	-	0.99
200	-2.61E-05	2.21E-02	-6.88E+00	1.58E+03	-	-	-	0.99
1300	-1.78E-06	2.58E-03	-1.74E+00	1.44E+03	-	-	-	0.99
13000	-4.15E-08	6.09E-05	-1.74E-01	1.38E+03	-	-	-	0.99
Using $K_{hv} = 1.0, Z_{bl} = 10$ ft								
$3ft \leq d_b \leq 75ft$								
20	-	-	-	3.79E-04	1.17E-02	5.76E-01	7.94E+02	0.99
65	-	-	-	1.83E-03	-4.38E-02	1.66E+00	8.05E+02	0.99
200	-	-	-	2.20E-03	-6.30E-02	2.03E+00	8.06E+02	0.99
1300	-	-	-	2.83E-03	-9.90E-02	2.71E+00	8.06E+02	0.99
13000	-	-	-	3.04E-03	-1.12E-01	2.97E+00	8.06E+02	0.99
$75ft \leq d_b \leq 315ft$								
20	-8.18E-13	-3.42E-10	1.01E-06	-5.52E-04	1.37E-01	-1.69E+01	1.76E+03	0.99
65	-2.12E-05	1.86E-02	-5.98E+00	1.81E+03	-	-	-	0.99
200	-1.07E-05	1.07E-02	-4.18E+00	1.79E+03	-	-	-	0.99
1300	-2.79E-07	8.12E-04	-9.25E-01	1.71E+03	-	-	-	0.99
13000	-1.25E-08	1.93E-05	-9.41E-02	1.69E+03	-	-	-	0.99

$K_{sb}$	$u_{bl} = a_6*d_b^6 + a_5*d_b^5 + a_4*d_b^4 + a_3*d_b^3 + a_2*d_b^2 + a_1*d_b + a_0$							$R^2$
	$a_6$	$a_5$	$a_4$	$a_3$	$a_2$	$a_1$	$a_0$	
Using $K_{hv} = 1.0$ , $Z_{bl} = 15$ ft								
$3\text{ft} \leq d_b \leq 75\text{ft}$								
20	-	-	-	2.46E-06	4.46E-02	2.25E-01	1.15E+03	0.99
65	-	-	-	7.30E-04	5.24E-02	2.60E-01	1.17E+03	0.99
200	-	-	-	9.61E-04	4.43E-02	4.57E-01	1.17E+03	0.99
1300	-	-	-	1.35E-03	2.94E-02	7.67E-01	1.17E+03	0.99
13000	-	-	-	1.47E-03	2.34E-02	9.04E-01	1.17E+03	0.99
$75\text{ft} \leq d_b \leq 315\text{ft}$								
20	3.61E-13	-1.25E-09	1.18E-06	-5.17E-04	1.21E-01	-1.50E+01	2.04E+03	0.99
65	-1.25E-05	1.23E-02	-4.57E+00	2.07E+03	-	-	-	0.99
200	-5.15E-06	6.35E-03	-3.06E+00	2.05E+03	-	-	-	0.99
1300	3.41E-07	2.01E-04	-6.35E-01	2.01E+03	-	-	-	0.99
13000	2.27E-08	-5.16E-06	-6.70E-02	2.00E+03	-	-	-	0.99
Using $K_{hv} = 1.0$ , $Z_{bl} = 20$ ft								
$3\text{ft} \leq d_b \leq 75\text{ft}$								
20	-	-	-	-2.39E-04	6.39E-02	1.77E-02	1.49E+03	0.99
65	-	-	-	2.18E-04	8.95E-02	5.13E-02	1.51E+03	0.99
200	-	-	-	3.55E-04	8.99E-02	9.33E-02	1.51E+03	0.99
1300	-	-	-	6.30E-04	8.39E-02	2.98E-01	1.52E+03	0.99
13000	-	-	-	7.13E-04	8.16E-02	3.56E-01	1.52E+03	0.99
$75\text{ft} \leq d_b \leq 315\text{ft}$								
20	-7.95E-12	7.99E-09	-3.00E-06	4 + 4.727810845E-04	-8.29E-03	-6.18E+00	2.13E+03	0.99
65	-1.01E-05	1.02E-02	-3.98E+00	2.35E+03	-	-	-	0.99
200	-4.07E-06	5.14E-03	-2.63E+00	2.35E+03	-	-	-	0.99
1300	4.43E-08	2.67E-04	-5.56E-01	2.32E+03	-	-	-	0.99
13000	-5.11E-09	2.22E-05	-6.38E-02	2.31E+03	-	-	-	0.99

Table B.11. FOSM calculation for Case 3b as depicted in Figure 3.5 in Chapter 3.

Supporting data for Table 3.2.

Input Variables	MLV	$\sigma$	COV
Blanket thickness ( $Z_{bl}$ )	12.5	5	40%
Length of foundation and top stratum beyond landside levee toe ( $L_3$ )	1.0E+02	5.0E+01	50%
Vertical permeability of top stratum (blanket) ( $K_b$ )	1.0E-06	9.0E-07	90%
Horizontal permeability of pervious substratum (sand) ( $K_f$ )	1.0E-03	9.0E-04	90%
Unit weight of top stratum material ( $\gamma_{blkt}$ )	120	5	4%

## FOSM calculations

Variable	Values	F.S.	$\Delta F$
Blanket thickness ( $Z_{bl}$ ) (ft)			
	MLV + $\sigma$	18	F1+ 1.901
	MLV - $\sigma$	8	F1+ 1.875
			0.027
Length of foundation and top stratum beyond landside levee toe ( $L_3$ ) (ft)			
	MLV + $\sigma$	215	F2+ 1.897
	MLV - $\sigma$	115	F2+ 1.888
			0.008
Unit weight of top stratum material ( $\gamma_{blkt}$ ) (lb/ft <sup>3</sup> )			
	MLV + $\sigma$	1.3E+02	F3+ 1.972
	MLV - $\sigma$	1.2E+02	F3+ 1.814
			0.158
Vertical permeability of blanket ( $K_b$ ) (ft/s)			
	MLV + $\sigma$	1.9E-06	F4+ 1.894
	MLV - $\sigma$	1.0E-07	F4+ 1.892
			0.002
Horizontal permeability of sand ( $K_f$ ) (ft/s)			
	MLV + $\sigma$	1.9E-03	F5+ 1.893
	MLV - $\sigma$	1.0E-04	F5+ 1.899
			-0.006
With all variables assigned their most likely values		F.S. =	0.97

$$\sigma_{FS} = 0.080$$

$$COV_{FS} = 8\%$$

$$\beta = -0.407$$

$$P_{up} = 65.80\%$$

Table B.12. Uplift pressure at the base of the blanket (above seepage block) ( $u_{bl}$ ) as a function of  $d_b$ ,  $K_{sb}$ ,  $Z_{bl}$  and  $K_{hv} = 0.10$  used for Case 3b as depicted in Figure 3.5 in Chapter 3. These values correspond to Figure B.7 through B.10

$d_b$ (ft)	$u_{bl}$				
	$K_{sb}$				
	20	65	200	1300	13000
Using $K_{hv} = 0.10$ , $Z_{bl} = 5$ ft					
3	470.640	513.552	518.232	524.584	526.325
15	482.321	541.944	549.182	559.341	562.155
35	504.080	601.455	615.227	635.482	641.347
55	545.002	766.210	804.960	865.613	883.771
75	546.393	1013.376	1120.954	1305.720	1365.312
95	522.413	943.301	1059.677	1283.318	1362.566
115	513.059	893.818	1012.315	1263.101	1359.946
135	507.799	855.254	972.878	1243.819	1357.325
155	504.648	826.114	941.242	1226.410	1354.891
175	502.595	802.277	914.410	1209.936	1352.458
195	501.203	783.058	891.322	1194.149	1349.962
215	500.236	767.333	871.416	1178.986	1347.528
315	498.320	722.779	808.080	1116.086	1335.797
Using $K_{hv} = 0.10$ , $Z_{bl} = 10$ ft					
3	867.610	943.738	953.160	965.765	969.010
15	881.962	975.562	987.917	1005.014	1009.445
35	911.165	1052.875	1074.403	1105.603	1113.965
55	954.283	1222.042	1269.091	1340.789	1360.757
75	944.674	1393.891	1486.805	1636.066	1679.496
95	913.286	1341.850	1444.997	1623.086	1677.998
115	898.310	1300.104	1409.179	1610.794	1676.563
135	889.699	1266.283	1378.478	1599.250	1675.128
155	884.333	1238.266	1351.709	1588.267	1673.755
175	880.714	1214.429	1327.747	1577.597	1672.445
195	878.218	1193.962	1306.406	1567.238	1671.072
215	876.470	1176.427	1287.250	1557.254	1669.699
315	872.914	1119.394	1218.797	1512.451	1663.022

$d_b$ (ft)	$u_{bl}$				
	$K_{sb}$				
	20	65	200	1300	13000
Using $K_{hv} = 0.10$ , $Z_{bl} = 15$ ft					
3	1231.776	1329.245	1341.288	1357.262	1361.194
15	1250.808	1369.056	1384.906	1406.496	1411.800
35	1284.130	1454.357	1480.502	1517.693	1527.302
55	1324.939	1610.731	1660.901	1735.282	1755.250
75	1309.339	1738.838	1823.952	1955.741	1992.370
95	1274.645	1695.283	1790.318	1946.069	1991.309
115	1256.736	1659.154	1760.866	1936.896	1990.248
135	1245.504	1628.203	1734.283	1927.910	1989.187
155	1238.266	1601.496	1710.509	1919.362	1988.189
175	1233.336	1577.971	1688.856	1910.938	1987.128
195	1229.904	1557.379	1669.200	1902.763	1986.130
215	1227.470	1539.408	1651.166	1894.776	1985.131
315	1222.416	1478.942	1583.338	1858.272	1980.139
Using $K_{hv} = 0.10$ , $Z_{bl} = 20$ ft					
3	1579.157	1687.982	1701.710	1719.931	1724.486
15	1602.557	1736.155	1754.438	1779.211	1785.389
35	1638.998	1827.134	1856.525	1897.834	1908.442
55	1676.126	1967.909	2019.264	2094.269	2114.112
75	1657.219	2069.496	2149.805	2271.734	2304.869
95	1620.778	2030.246	2120.227	2263.560	2303.933
115	1600.373	1996.987	2093.770	2255.698	2303.059
135	1587.581	1967.909	2069.746	2248.022	2302.186
155	1578.970	1942.574	2047.906	2240.659	2301.312
175	1572.979	1919.611	2027.813	2233.421	2300.438
195	1568.736	1899.518	2009.342	2226.370	2299.565
215	1565.741	1881.922	1992.432	2219.443	2298.754
315	1559.438	1819.646	1925.789	2187.245	2294.510

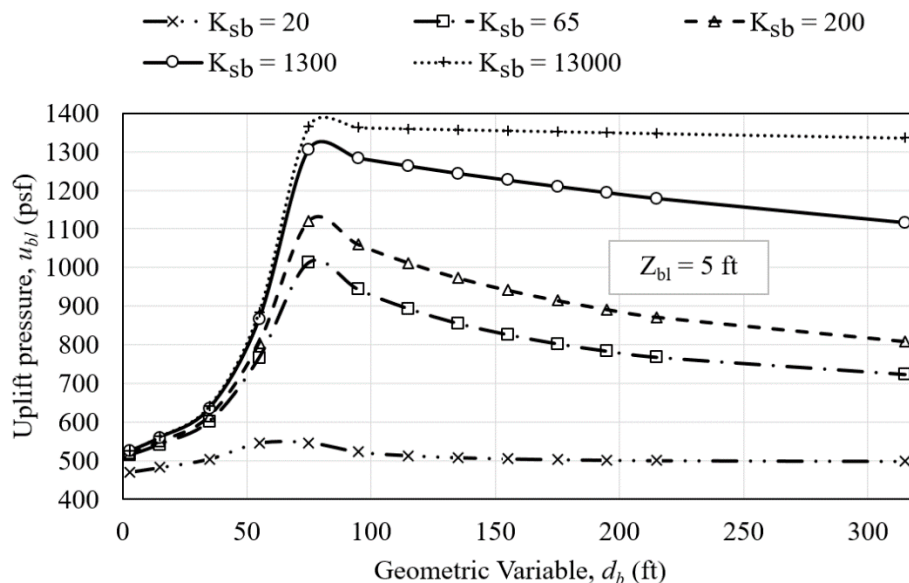


Figure B.7. Family of curves representing relationship between  $d_b$ ,  $K_{sb}$ , and  $u_{bl}$  for  $K_{hv} = 0.10$  and  $Z_{bl} = 5$  ft for Case 3b.

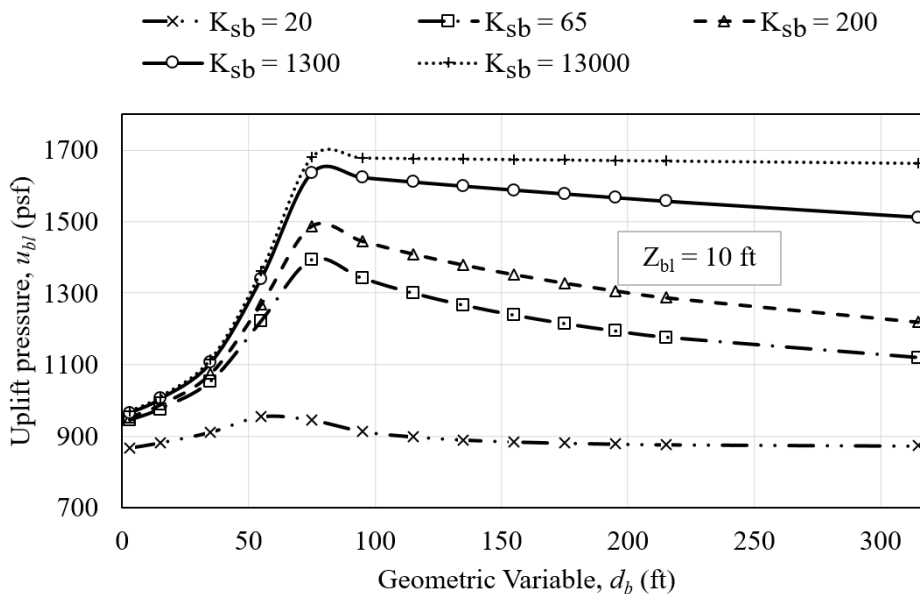


Figure B.8. Family of curves representing relationship between  $d_b$ ,  $K_{sb}$ , and  $u_{bl}$  for  $K_{hv} = 0.10$  and  $Z_{bl} = 10$  ft for Case 3b.

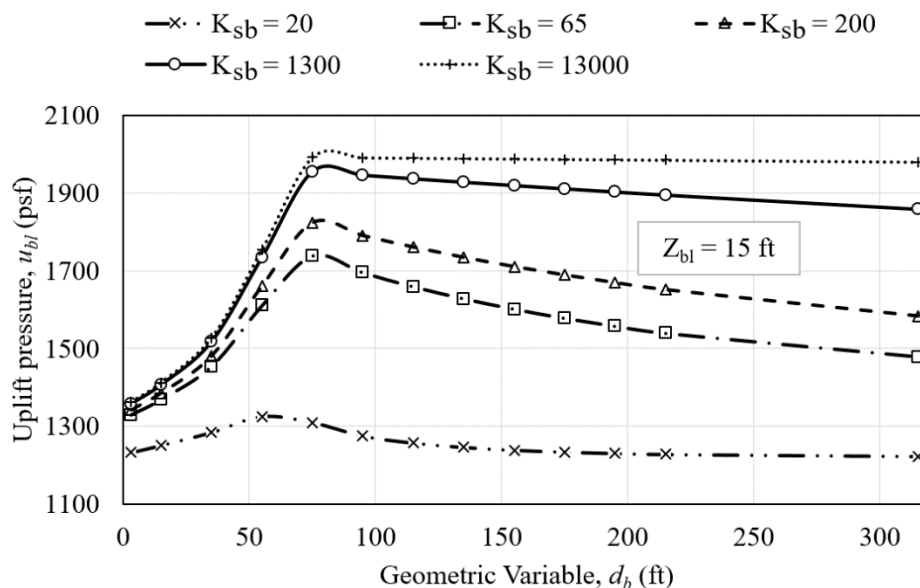


Figure B.9. Family of curves representing relationship between  $d_b$ ,  $K_{sb}$ , and  $u_{bl}$  for  $K_{hv} = 0.10$  and  $Z_{bl} = 15$  ft for Case 3b.

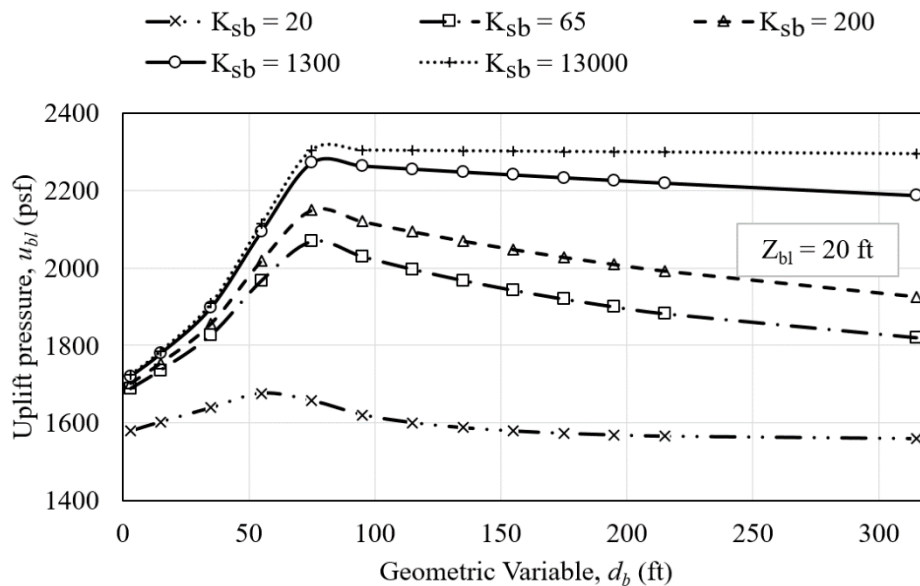


Figure B.10. Family of curves representing relationship between  $d_b$ ,  $K_{sb}$ , and  $u_{bl}$  for  $K_{hv} = 0.10$  and  $Z_{bl} = 20$  ft for Case 3b.

Table B.13. Fit-equations' coefficients and corresponding goodness of fit for family of curves for the computation of  $u_{bl}$  with respect to  $K_{sb}$  used for Case 3b. These values correspond to Figures B.7 through B.10.

$K_{sb}$	$u_{bl} = a_3*d_b^3 + a_2*d_b^2 + a_1*d_b + a_0$				$R^2$
	$a_3$	$a_2$	$a_1$	$a_0$	
Using $K_{hv} = 0.10$ , $Z_{bl} = 5$ ft					
$3\text{ft} \leq d_b \leq 75\text{ft}$					
20	-6.16E-04	6.69E-02	-5.73E-01	4.74E+02	0.99
65	5.17E-04	4.18E-02	6.29E-01	5.14E+02	0.99
200	9.88E-04	1.74E-02	1.20E+00	5.17E+02	0.99
1300	1.91E-03	-3.52E-02	2.36E+00	5.20E+02	0.99
13000	2.24E-03	-5.50E-02	2.79E+00	5.20E+02	0.99
$75\text{ft} \leq d_b \leq 315\text{ft}$					
20	-1.63E-05	1.09E-02	-2.35E+00	6.65E+02	0.99
65	-3.20E-05	2.45E-02	-6.66E+00	1.39E+03	0.99
200	-2.17E-05	1.77E-02	-5.42E+00	1.44E+03	0.99
1300	-2.34E-06	2.54E-03	-1.48E+00	1.40E+03	0.99
13000	-1.64E-07	1.36E-04	-1.55E-01	1.38E+03	0.99
Using $K_{hv} = 0.10$ , $Z_{bl} = 10$ ft					
$3\text{ft} \leq d_b \leq 75\text{ft}$					
20	-8.00E-04	8.04E-02	-5.26E-01	8.70E+02	0.99
65	-6.03E-04	1.33E-01	-6.41E-01	9.48E+02	0.99
200	-4.52E-04	1.35E-01	-5.35E-01	9.57E+02	0.99
1300	-1.49E-04	1.34E-01	-2.83E-01	9.69E+02	0.99
13000	-4.75E-05	1.32E-01	-1.96E-01	9.73E+02	0.99
$75\text{ft} \leq d_b \leq 315\text{ft}$					
20	-2.13E-05	1.45E-02	-3.20E+00	1.11E+03	0.99
65	-1.78E-05	1.47E-02	-4.60E+00	1.66E+03	0.99
200	-9.61E-06	8.83E-03	-3.32E+00	1.69E+03	0.99
1300	-8.99E-07	1.01E-03	-7.93E-01	1.69E+03	0.99
13000	-1.20E-07	8.35E-05	-8.58E-02	1.69E+03	0.99



$K_{sb}$	$u_{bl} = a_3*d_b^3 + a_2*d_b^2 + a_1*d_b + a_0$				$R^2$
	$a_3$	$a_2$	$a_1$	$a_0$	
Using $K_{hv} = 0.10$ , $Z_{bl} = 15$ ft					
$3\text{ft} \leq d_b \leq 75\text{ft}$					
20	-7.81E-04	7.17E-02	4.76E-02	1.23E+03	0.99
65	-8.63E-04	1.36E-01	8.31E-02	1.33E+03	0.99
200	-8.20E-04	1.45E-01	1.40E-01	1.34E+03	0.99
1300	-7.13E-04	1.56E-01	2.67E-01	1.36E+03	0.99
13000	-6.78E-04	1.59E-01	2.95E-01	1.36E+03	0.99
$75\text{ft} \leq d_b \leq 315\text{ft}$					
20	-2.27E-05	1.57E-02	-3.55E+00	1.49E+03	0.99
65	-1.06E-05	9.73E-03	-3.52E+00	1.95E+03	0.99
200	-5.36E-06	5.52E-03	-2.47E+00	1.98E+03	0.99
1300	-3.17E-07	4.79E-04	-5.52E-01	1.99E+03	0.99
13000	-3.21E-08	2.75E-05	-5.76E-02	2.00E+03	0.99
Using $K_{hv} = 0.10$ , $Z_{bl} = 20$ ft					
$3\text{ft} \leq d_b \leq 75\text{ft}$					
20	-7.02E-04	5.74E-02	7.06E-01	1.58E+03	0.99
65	-8.27E-04	1.12E-01	1.35E+00	1.69E+03	0.99
200	-8.19E-04	1.22E-01	1.48E+00	1.70E+03	0.99
1300	-7.79E-04	1.35E-01	1.68E+00	1.72E+03	0.99
13000	-7.64E-04	1.38E-01	1.73E+00	1.72E+03	0.99
$75\text{ft} \leq d_b \leq 315\text{ft}$					
20	-2.34E-05	1.63E-02	-3.76E+00	1.85E+03	0.99
65	-8.12E-06	7.86E-03	-3.06E+00	2.26E+03	0.99
200	-4.10E-06	4.36E-03	-2.11E+00	2.28E+03	0.99
1300	-3.01E-07	3.93E-04	-4.67E-01	2.30E+03	0.99
13000	-3.93E-08	2.98E-05	-4.97E-02	2.31E+03	0.99

Table B.14. FOSM calculation for Cases 4a and 4b as depicted in Figures 3.6 and 3.7, respectively, in Chapter 3. Supporting data for Table 3.2.

Input Variables	MLV	$\sigma$	COV
Blanket thickness ( $Z_{bl}$ )	12.5	5	40%
Length of foundation and top stratum beyond landside levee toe ( $L_3$ )	1.2E+02	5.0E+01	42%
Unit weight of top stratum material ( $\gamma_{bikt}$ )	1.2E+02	5.0E+00	4%
Vertical permeability of top stratum (blanket) ( $K_b$ )	1.0E-06	9.0E-07	90%
Horizontal permeability of pervious substratum (sand) ( $K_f$ )	0.001	0.0009	90%

#### FOSM calculations

Variable	Values	F.S.	$\Delta F$
Blanket thickness ( $Z_{bl}$ ) (ft)			
	MLV + $\sigma$	18	F1+ 1.313
	MLV - $\sigma$	8	F1+ 0.925
			0.388
Length of foundation and top stratum beyond landside levee toe ( $L_3$ ) (ft)			
	MLV + $\sigma$	170	F2+ 1.090
	MLV - $\sigma$	70	F2+ 1.304
			-0.214
Unit weight of top stratum material ( $\gamma_{bikt}$ ) (lb/ft <sup>3</sup> )			
	MLV + $\sigma$	1.3E+02	F3+ 1.214
	MLV - $\sigma$	1.2E+02	F3+ 1.117
			0.097
Vertical permeability of blanket ( $K_b$ ) (ft/s)			
	MLV + $\sigma$	1.9E-06	F4+ 1.168
	MLV - $\sigma$	1.0E-07	F4+ 1.164
			0.004
Horizontal permeability of sand ( $K_f$ ) (ft/s)			
	MLV + $\sigma$	1.9E-03	F5+ 1.165
	MLV - $\sigma$	1.0E-04	F5+ 1.185
			-0.021
With all variables assigned their most likely values		F.S. =	1.17

$$\sigma_{FS} = 0.227$$

$$COV_{FS} = 19\%$$

$$\beta = 0.730$$

$$P_{up} = 23.26\%$$

Table B.15. Uplift pressure at the base of the blanket (above seepage block) ( $u_{bl}$ ) as a function of  $d_e$ ,  $K_{sb}$ ,  $Z_{bl}$  and  $K_{hv} = 1.0$  used for Case 4a as depicted in Figure 3.6 in Chapter 3. These values correspond to Figure B.11 through B.14

$d_e$ (ft)	$u_{bl}$				
	$K_{sb}$				
	20	65	200	1300	13000
Using $K_{hv} = 1.0$ , $Z_{bl} = 5$ ft					
65	386.568	381.108	380.796	380.478	380.415
85	502.726	546.686	549.744	552.827	553.457
105	529.795	617.361	624.963	623.986	634.733
125	541.108	666.931	679.723	693.888	696.883
145	546.630	703.934	722.280	743.184	747.739
165	549.457	732.701	756.725	785.117	791.357
185	550.917	754.915	784.618	820.622	828.797
205	551.685	772.512	807.706	851.635	861.869
225	552.084	786.490	826.675	878.779	891.134
245	552.296	797.222	842.150	902.304	916.906
265	552.402	805.646	855.067	923.140	940.056
365	552.521	827.486	893.318	997.714	1026.792
Using $K_{hv} = 1.0$ , $Z_{bl} = 10$ ft					
65	718.786	711.797	711.422	710.986	710.923
85	844.022	870.230	871.853	873.475	873.787
105	882.211	943.114	947.482	951.974	952.910
125	902.554	996.590	1004.203	1012.315	1014.000
145	914.222	1038.710	1049.942	1062.173	1064.731
165	921.086	1072.406	1087.507	1104.230	1107.787
185	925.142	1099.925	1119.082	1140.672	1145.352
205	927.576	1122.451	1145.789	1172.371	1178.174
225	929.011	1141.324	1168.315	1200.139	1207.190
245	929.885	1156.397	1187.410	1224.475	1232.837
265	930.384	1169.189	1204.008	1246.502	1256.174
365	931.070	1206.566	1257.422	1326.125	1342.910

$d_e$ (ft)	$u_{bl}$				
	$K_{sb}$				
	20	65	200	1300	13000
Using $K_{hv} = 1.0$ , $Z_{bl} = 15$ ft					
65	1046.323	1037.400	1036.963	1036.464	1036.339
85	1172.995	1191.341	1192.402	1193.462	1193.650
105	1216.675	1264.286	1267.531	1270.776	1271.462
125	1241.635	1318.450	1324.190	1330.181	1331.429
145	1257.235	1362.254	1370.866	1380.038	1381.973
165	1267.032	1398.197	1409.928	1422.595	1425.216
185	1273.147	1427.650	1442.501	1458.912	1462.344
205	1277.078	1452.173	1470.456	1490.798	1495.166
225	1279.512	1472.702	1494.293	1518.754	1524.058
245	1281.072	1489.925	1514.885	1543.526	1549.766
265	1282.070	1504.402	1532.669	1565.429	1572.667
365	1283.568	1550.016	1592.573	1646.549	1659.154
Using $K_{hv} = 1.0$ , $Z_{bl} = 20$ ft					
65	1372.987	1362.566	1362.005	1361.443	1361.318
85	1496.539	1512.389	1513.262	1514.198	1514.386
105	1543.464	1583.837	1586.458	1589.141	1589.702
125	1571.294	1638.624	1643.429	1648.483	1649.482
145	1589.203	1682.990	1690.291	1698.029	1699.589
165	1600.872	1719.744	1729.790	1740.461	1742.707
185	1608.485	1750.320	1763.174	1777.027	1779.960
205	1613.414	1775.842	1791.566	1808.914	1812.533
225	1616.659	1797.432	1816.152	1837.056	1841.486
245	1618.781	1815.528	1837.243	1861.766	1867.070
265	1620.154	1831.128	1855.776	1883.981	1890.158
365	1622.400	1880.362	1918.550	1965.163	1975.834

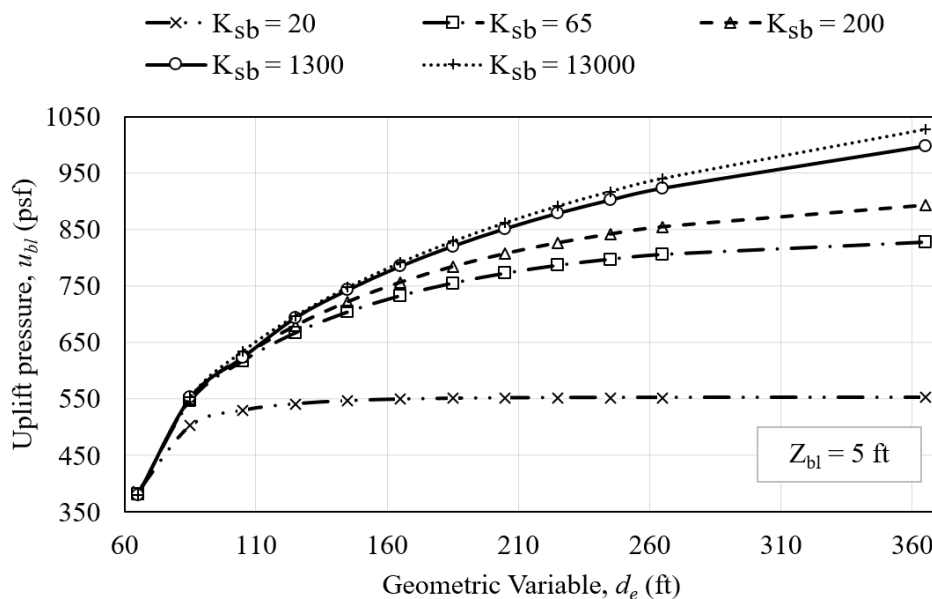


Figure B.11. Family of curves representing relationship between  $d_{be}$ ,  $K_{sb}$ , and  $u_{bl}$  for  $K_{hv} = 1.0$  and  $Z_{bl} = 5$  ft for Case 4a.

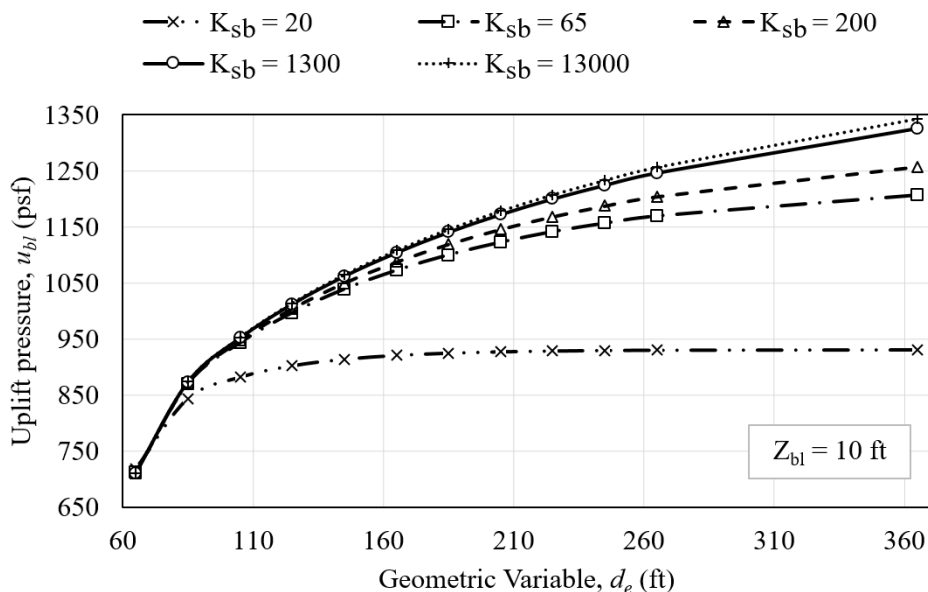


Figure B.12. Family of curves representing relationship between  $d_e$ ,  $K_{sb}$ , and  $u_{bl}$  for  $K_{hv} = 1.0$  and  $Z_{bl} = 10$  ft for Case 4a.

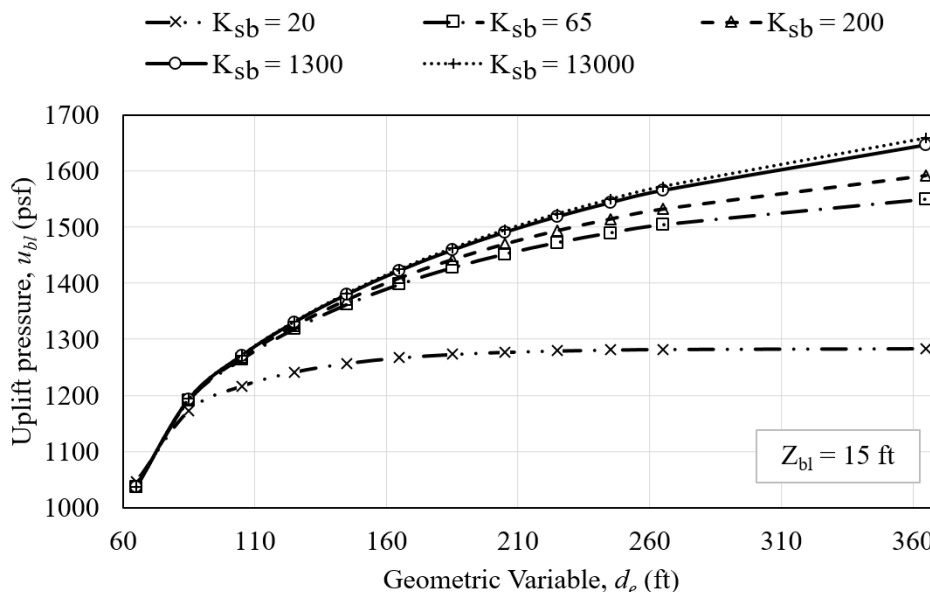


Figure B.13. Family of curves representing relationship between  $d_e$ ,  $K_{sb}$ , and  $u_{bl}$  for  $K_{hv} = 1.0$  and  $Z_{bl} = 15$  ft for Case 4a.

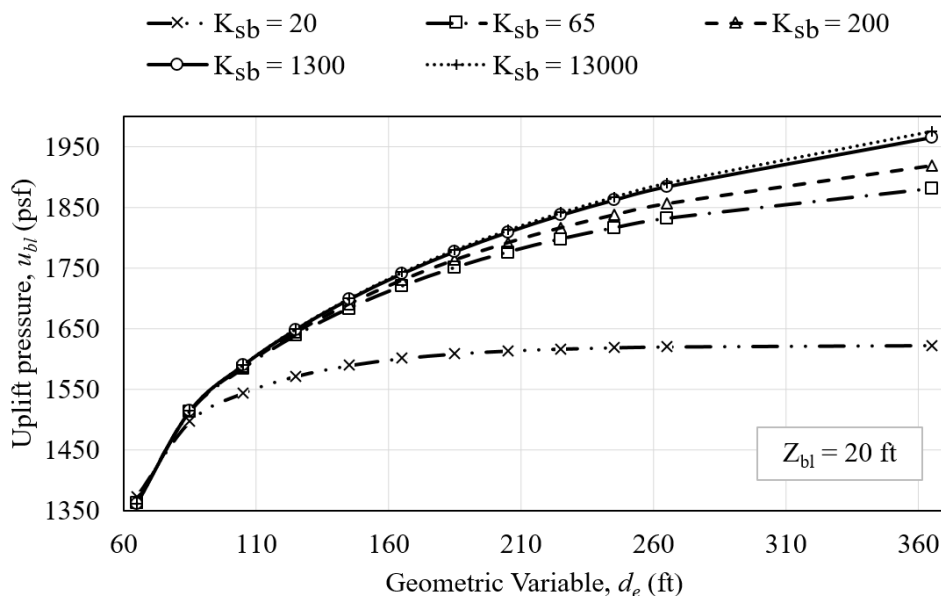


Figure B.14. Family of curves representing relationship between  $d_e$ ,  $K_{sb}$ , and  $u_{bl}$  for  $K_{hv} = 1.0$  and  $Z_{bl} = 20$  ft for Case 4a.

Table B.16. Fit-equations' coefficients and corresponding goodness of fit for family of curves for the computation of  $u_{bl}$  with respect to  $K_{sb}$  used for Case 4a. These values correspond to Figures B.11 through B.14.

$K_{sb}$	$u_{bl} = a_6*d_e^6 + a_5*d_e^5 + a_4*d_e^4 + a_3*d_e^3 + a_2*d_e^2 + a_1*d_e + a_0$							$R^2$
	$a_6$	$a_5$	$a_4$	$a_3$	$a_2$	$a_1$	$a_0$	
Using $K_{hv} = 1.0, Z_{bl} = 5$ ft								
65ft $\leq d_e \leq 265$ ft								
20	-1.26E-10	1.37E-07	-6.06E-05	1.40E-02	-1.78E+00	1.19E+02	-2.72E+03	0.99
65	-1.26E-10	1.36E-07	-6.01E-05	1.38E-02	-1.77E+00	1.21E+02	-2.89E+03	0.99
200	-1.25E-10	1.35E-07	-5.96E-05	1.37E-02	-1.75E+00	1.20E+02	-2.88E+03	0.99
1300	-1.59E-10	1.68E-07	-7.23E-05	1.62E-02	-2.00E+00	1.33E+02	-3.13E+03	0.99
13000	-1.25E-10	1.35E-07	-5.94E-05	1.37E-02	-1.74E+00	1.19E+02	-2.87E+03	0.99
265ft $\leq d_e \leq 365$ ft								
20	-	-	-	-	-	1.19E-03	5.52E+02	0.99
65	-	-	-	-	-	2.18E-01	7.48E+02	0.99
200	-	-	-	-	-	3.83E-01	7.54E+02	0.99
1300	-	-	-	-	-	7.46E-01	7.26E+02	0.99
13000	-	-	-	-	-	8.67E-01	7.10E+02	0.99
Using $K_{hv} = 1.0, Z_{bl} = 10$ ft								
65ft $\leq d_e \leq 265$ ft								
20	-1.17E-10	1.27E-07	-5.59E-05	1.29E-02	-1.65E+00	1.12E+02	-2.25E+03	0.99
65	-1.13E-10	1.23E-07	-5.40E-05	1.24E-02	-1.59E+00	1.09E+02	-2.26E+03	0.99
200	-1.13E-10	1.22E-07	-5.38E-05	1.24E-02	-1.58E+00	1.09E+02	-2.26E+03	0.99
1300	-1.13E-10	1.22E-07	-5.38E-05	1.24E-02	-1.58E+00	1.09E+02	-2.26E+03	0.99
13000	-1.13E-10	1.22E-07	-5.38E-05	1.24E-02	-1.58E+00	1.09E+02	-2.26E+03	0.99
265ft $\leq d_e \leq 365$ ft								
20	-	-	-	-	-	6.86E-03	9.29E+02	0.99
65	-	-	-	-	-	3.74E-01	1.07E+03	0.99
200	-	-	-	-	-	5.34E-01	1.06E+03	0.99
1300	-	-	-	-	-	7.96E-01	1.04E+03	0.99
13000	-	-	-	-	-	8.67E-01	1.03E+03	0.99

$K_{sb}$	$u_{bl} = a_6*d_e^6 + a_5*d_e^5 + a_4*d_e^4 + a_3*d_e^3 + a_2*d_e^2 + a_1*d_e + a_0$							$R^2$
	$a_6$	$a_5$	$a_4$	$a_3$	$a_2$	$a_1$	$a_0$	
Using $K_{hv} = 1.0, Z_{bl} = 15$ ft								
$65\text{ft} \leq d_e \leq 265\text{ft}$								
20	-1.09E-10	1.18E-07	-5.21E-05	1.20E-02	-1.54E+00	1.05E+02	-1.77E+03	0.99
65	-1.10E-10	1.19E-07	-5.25E-05	1.21E-02	-1.53E+00	1.05E+02	-1.83E+03	0.99
200	-1.10E-10	1.19E-07	-5.23E-05	1.20E-02	-1.53E+00	1.05E+02	-1.83E+03	0.99
1300	-1.11E-10	1.19E-07	-5.25E-05	1.21E-02	-1.53E+00	1.05E+02	-1.83E+03	0.99
13000	-1.10E-10	1.19E-07	-5.22E-05	1.20E-02	-1.52E+00	1.05E+02	-1.82E+03	0.99
$265\text{ft} \leq d_e \leq 365\text{ft}$								
20	-	-	-	-	-	1.50E-02	1.28E+03	0.99
65	-	-	-	-	-	4.56E-01	1.38E+03	0.99
200	-	-	-	-	-	5.99E-01	1.37E+03	0.99
1300	-	-	-	-	-	8.11E-01	1.35E+03	0.99
13000	-	-	-	-	-	8.65E-01	1.34E+03	0.99
Using $K_{hv} = 1.0, Z_{bl} = 20$ ft								
$65\text{ft} \leq d_e \leq 265\text{ft}$								
20	-9.60E-11	1.04E-07	-4.61E-05	1.07E-02	-1.38E+00	9.47E+01	-1.19E+03	0.99
65	-1.08E-10	1.17E-07	-5.12E-05	1.18E-02	-1.49E+00	1.02E+02	-1.42E+03	0.99
200	-1.09E-10	1.18E-07	-5.17E-05	1.18E-02	-1.50E+00	1.03E+02	-1.43E+03	0.99
1300	-1.10E-10	1.18E-07	-5.18E-05	1.19E-02	-1.50E+00	1.03E+02	-1.44E+03	0.99
13000	-1.10E-10	1.19E-07	-5.21E-05	1.19E-02	-1.51E+00	1.03E+02	-1.45E+03	0.99
$265\text{ft} \leq d_e \leq 365\text{ft}$								
20	-	-	-	-	-	2.25E-02	1.61E+03	0.99
65	-	-	-	-	-	4.92E-01	1.70E+03	0.99
200	-	-	-	-	-	6.28E-01	1.69E+03	0.99
1300	-	-	-	-	-	8.12E-01	1.67E+03	0.99
13000	-	-	-	-	-	8.57E-01	1.66E+03	0.99



Table B.17. Uplift pressure at the base of the blanket (above seepage block) ( $u_{bl}$ ) as a function of  $d_e$ ,  $K_{sb}$ ,  $Z_{bl}$  and  $K_{hv} = 0.10$  used for Case 4b as depicted in Figure 3.7 in Chapter 3. These values correspond to Figures B.14 through B.17

$d_e$ (ft)	$u_{bl}$				
	$K_{sb}$				
	20	65	200	1300	13000
Using $K_{hv} = 0.10$ , $Z_{bl} = 5$ ft					
65	473.316	462.334	461.248	460.081	459.838
85	480.686	569.743	578.005	587.065	588.981
105	481.971	622.677	641.410	663.562	668.554
125	482.121	651.830	679.349	714.043	722.155
145	482.159	670.862	705.806	752.232	763.464
165	482.177	684.341	725.774	783.370	797.846
185	482.184	694.200	741.125	809.390	827.050
205	482.184	701.626	753.239	831.605	852.384
225	482.190	707.366	763.090	850.699	874.723
245	482.190	711.734	771.014	867.298	894.442
265	482.190	715.104	777.442	881.774	911.976
365	482.190	723.590	795.538	930.322	974.002
Using $K_{hv} = 0.10$ , $Z_{bl} = 10$ ft					
65	838.032	817.440	815.942	814.382	814.070
85	844.709	897.312	900.931	904.738	905.549
105	850.325	958.027	968.386	979.805	982.238
125	851.760	995.904	1012.690	1031.909	1036.090
145	852.134	1021.925	1044.701	1071.658	1077.648
165	852.322	1040.894	1068.974	1103.170	1110.970
185	852.384	1055.683	1088.630	1130.064	1139.674
205	852.384	1067.414	1104.730	1153.152	1164.696
225	852.446	1076.774	1118.208	1173.494	1186.786
245	852.446	1084.325	1129.378	1191.029	1206.130
265	852.446	1090.565	1139.050	1206.878	1223.789
365	852.446	1107.600	1168.066	1260.230	1285.190

$d_e$ (ft)	$u_{bl}$				
	$K_{sb}$				
	20	65	200	1300	13000
Using $K_{hv} = 0.10, Z_{bl} = 15$ ft					
65	1182.917	1157.520	1155.898	1154.213	1153.838
85	1188.658	1221.106	1223.040	1225.099	1225.474
105	1197.394	1283.318	1290.557	1298.357	1299.979
125	1200.202	1323.192	1335.485	1349.088	1351.958
145	1201.075	1351.646	1368.806	1388.213	1392.394
165	1201.512	1372.738	1394.328	1419.350	1424.904
185	1201.637	1389.710	1415.544	1446.182	1453.046
205	1201.762	1403.501	1433.203	1469.333	1477.570
225	1201.824	1414.920	1448.366	1489.925	1499.472
245	1201.886	1424.280	1461.096	1507.834	1518.754
265	1201.886	1432.080	1472.016	1523.746	1536.038
365	1201.949	1454.918	1506.586	1579.219	1597.440
Using $K_{hv} = 0.10, Z_{bl} = 20$ ft					
65	1518.754	1487.678	1485.682	1483.685	1483.310
85	1513.824	1528.051	1528.738	1529.424	1529.549
105	1535.914	1600.061	1604.928	1610.045	1611.106
125	1540.843	1642.181	1651.354	1661.275	1663.397
145	1542.653	1672.632	1685.986	1700.837	1704.019
165	1543.464	1695.408	1712.693	1732.224	1736.467
185	1543.901	1714.003	1735.094	1759.430	1764.734
205	1544.150	1729.291	1753.939	1783.018	1789.445
225	1544.275	1741.958	1770.038	1803.734	1811.285
245	1544.400	1752.691	1783.954	1822.142	1830.816
265	1544.462	1761.677	1795.997	1838.554	1848.350
365	1544.587	1788.821	1834.560	1895.712	1910.563

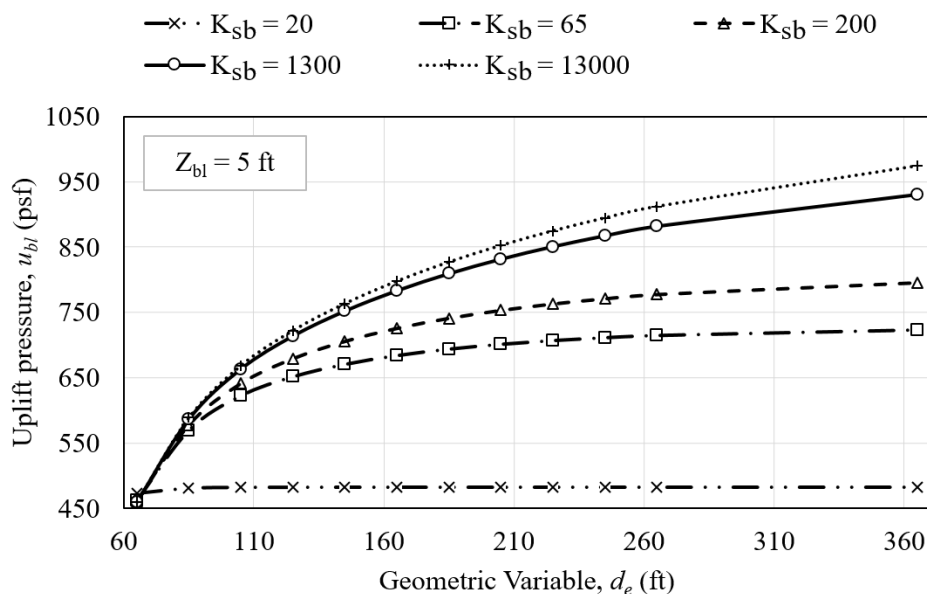


Figure B.15. Family of curves representing relationship between  $d_e$ ,  $K_{sb}$ , and  $u_{bl}$  for  $K_{hv} = 0.10$  and  $Z_{bl} = 5$  ft for Case 4b.

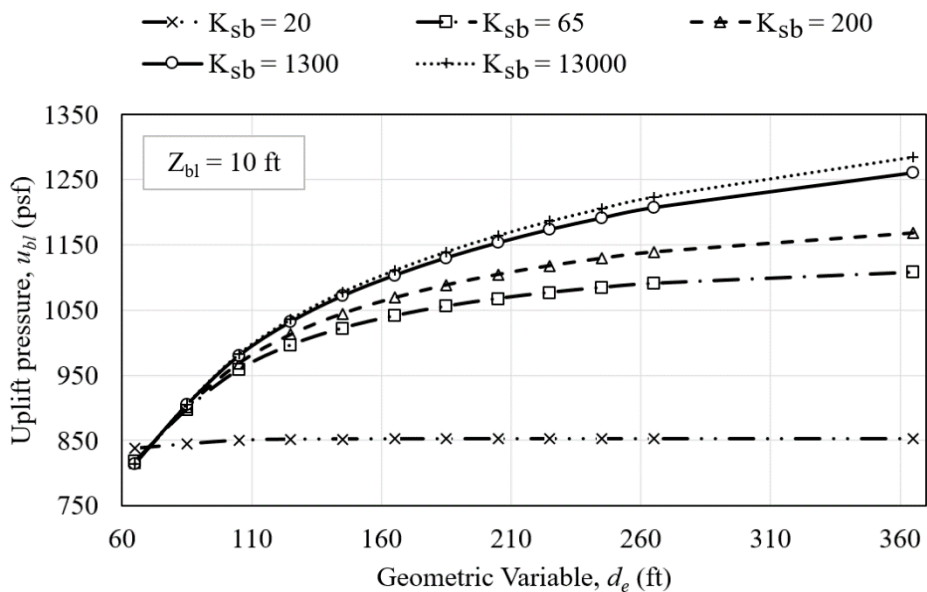


Figure B.16. Family of curves representing relationship between  $d_e$ ,  $K_{sb}$ , and  $u_{bl}$  for  $K_{hv} = 0.10$  and  $Z_{bl} = 10$  ft for Case 4b.

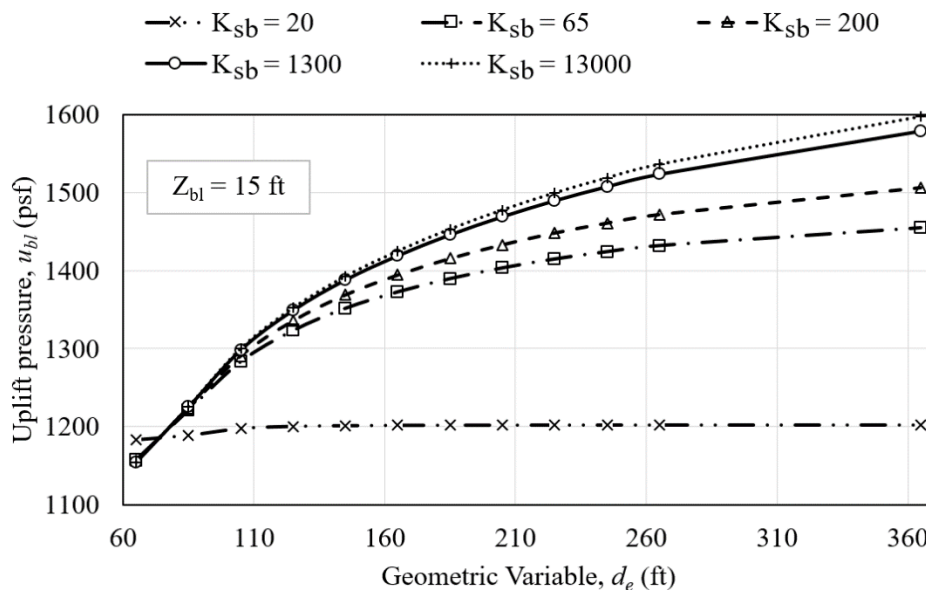


Figure B.17. Family of curves representing relationship between  $d_e$ ,  $K_{sb}$ , and  $u_{bl}$  for  $K_{hv} = 0.10$  and  $Z_{bl} = 15$  ft for Case 4b.

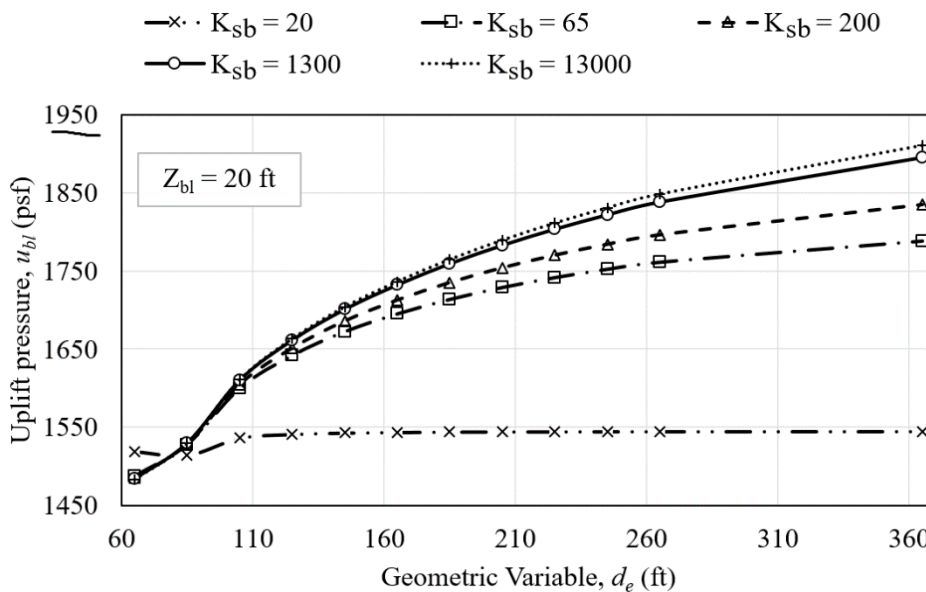


Figure B.18. Family of curves representing relationship between  $d_e$ ,  $K_{sb}$ , and  $u_{bl}$  for  $K_{hv} = 0.10$  and  $Z_{bl} = 20$  ft for Case 4b.

Table B.18. Fit-equations' coefficients and corresponding goodness of fit for family of curves for the computation of  $u_{bl}$  with respect to  $K_{sb}$  used for Case 4b. These values correspond to Figures B.14 through B.17.

$K_{sb}$	$u_{bl} = a_6*d_e^6 + a_5*d_e^5 + a_4*d_e^4 + a_3*d_e^3 + a_2*d_e^2 + a_1*d_e + a_0$							$R^2$
	$a_6$	$a_5$	$a_4$	$a_3$	$a_2$	$a_1$	$a_0$	
Using $K_{hv} = 0.10$ , $Z_{bl} = 5$ ft								
65ft $\leq d_e \leq$ 265ft								
20	-8.81E-12	9.61E-09	-4.28E-06	9.92E-04	-1.26E-01	8.40E+00	2.55E+02	0.99
65	-3.93E-11	4.47E-08	-2.09E-05	5.18E-03	-7.23E-01	5.51E+01	-1.16E+03	0.99
200	-3.36E-11	3.85E-08	-1.83E-05	4.60E-03	-6.55E-01	5.16E+01	-1.11E+03	0.99
1300	-2.54E-11	2.99E-08	-1.46E-05	3.78E-03	-5.58E-01	4.63E+01	-1.01E+03	0.99
13000	-2.41E-11	2.85E-08	-1.39E-05	3.64E-03	-5.39E-01	4.53E+01	-9.85E+02	0.99
265ft $\leq d_e \leq$ 365ft								
20	-	-	-	-	-	4.82E+02	-	0.99
65	-	-	-	-	-	8.49E-02	6.93E+02	0.99
200	-	-	-	-	-	1.81E-01	7.29E+02	0.99
1300	-	-	-	-	-	4.85E-01	7.53E+02	0.99
13000	-	-	-	-	-	6.20E-01	7.48E+02	0.99
Using $K_{hv} = 0.10$ , $Z_{bl} = 10$ ft								
65ft $\leq d_e \leq$ 265ft								
20	9.72E-12	-9.72E-09	3.85E-06	-7.58E-04	7.55E-02	-3.27E+00	8.82E+02	0.99
65	2.85E-11	-2.82E-08	1.09E-05	-2.03E-03	1.68E-01	-1.18E+00	5.79E+02	0.99
200	3.18E-11	-3.19E-08	1.26E-05	-2.41E-03	2.15E-01	-3.85E+00	6.30E+02	0.99
1300	3.61E-11	-3.65E-08	1.46E-05	-2.88E-03	2.73E-01	-7.17E+00	6.97E+02	0.99
13000	3.71E-11	-3.75E-08	1.50E-05	-2.98E-03	2.85E-01	-7.87E+00	7.11E+02	0.99
265ft $\leq d_e \leq$ 365ft								
20	-	-	-	-	-	8.52E+02	-	0.99
65	-	-	-	-	-	1.70E-01	1.05E+03	0.99
200	-	-	-	-	-	2.90E-01	1.06E+03	0.99
1300	-	-	-	-	-	5.34E-01	1.07E+03	0.99
13000	-	-	-	-	-	6.14E-01	1.06E+03	0.99

$K_{sb}$	$u_{bl} = a_6*d_e^6 + a_5*d_e^5 + a_4*d_e^4 + a_3*d_e^3 + a_2*d_e^2 + a_1*d_e + a_0$							$R^2$
	$a_6$	$a_5$	$a_4$	$a_3$	$a_2$	$a_1$	$a_0$	
Using $K_{hv} = 0.10$ , $Z_{bl} = 15$ ft								
$65\text{ft} \leq d_e \leq 265\text{ft}$								
20	2.31E-11	-2.38E-08	9.82E-06	-2.06E-03	2.28E-01	-1.22E+01	1.43E+03	0.99
65	5.99E-11	-6.20E-08	2.57E-05	-5.38E-03	5.83E-01	-2.77E+01	1.58E+03	0.99
200	6.34E-11	-6.57E-08	2.73E-05	-5.76E-03	6.29E-01	-3.04E+01	1.64E+03	0.99
1300	6.70E-11	-6.97E-08	2.91E-05	-6.15E-03	6.78E-01	-3.32E+01	1.69E+03	0.99
13000	6.78E-11	-7.05E-08	2.94E-05	-6.23E-03	6.88E-01	-3.38E+01	1.70E+03	0.99
$265\text{ft} \leq d_e \leq 365\text{ft}$								
20	-	-	-	-	-	6.30E-04	1.20E+03	0.99
65	-	-	-	-	-	2.28E-01	1.37E+03	0.99
200	-	-	-	-	-	3.46E-01	1.38E+03	0.99
1300	-	-	-	-	-	5.55E-01	1.38E+03	0.99
13000	-	-	-	-	-	6.14E-01	1.37E+03	0.99
Using $K_{hv} = 0.10$ , $Z_{bl} = 20$ ft								
$65\text{ft} \leq d_e \leq 265\text{ft}$								
20	9.72E-11	-1.01E-07	4.23E-05	-9.10E-03	1.05E+00	-6.05E+01	2.88E+03	0.99
65	1.40E-10	-1.47E-07	6.18E-05	-1.33E-02	1.53E+00	-8.53E+01	3.28E+03	0.99
200	1.43E-10	-1.49E-07	6.30E-05	-1.36E-02	1.56E+00	-8.74E+01	3.33E+03	0.99
1300	1.46E-10	-1.52E-07	6.43E-05	-1.39E-02	1.60E+00	-8.96E+01	3.37E+03	0.99
13000	1.46E-10	-1.53E-07	6.46E-05	-1.40E-02	1.61E+00	-9.02E+01	3.39E+03	0.99
$265\text{ft} \leq d_e \leq 365\text{ft}$								
20	-	-	-	-	-	1.25E-03	1.54E+03	0.99
65	-	-	-	-	-	2.71E-01	1.69E+03	0.99
200	-	-	-	-	-	3.86E-01	1.69E+03	0.99
1300	-	-	-	-	-	5.72E-01	1.69E+03	0.99
13000	-	-	-	-	-	6.22E-01	1.68E+03	0.99

## APPENDIX C

Appendix C provides supporting data for the parametric analysis presented in Table 4.3 in Chapter 4. Due to the amount of computation and data needed to support each result from Table 4.3, Table 4.3 is presented herein as Table C.1 with the addition of a new column for organizational purposes. A numerical column is added to link the maximum variation in  $h_{\max}$  column (last column) with a corresponding parametric analysis number. Tables C.2 through C.17 present the computation of the parametric analyses and Figures C.1 through C.16 present the plotted results for the corresponding parametric analyses.

Table C.1. Results of parametric analysis to assess the validity of the simplified flow model for crevasse-splay response surface

Parametric analysis	Combined Parameter for Response Surface	Constant Parameters		Varied Parameters		Max. variation in $h_{\max}$ Diff. (m)	
		Dependent	Independent	Dependent	Independent		
1	Transmissivity of Splay, $T_{\text{splay}}$	N/A	$W_s, L_s, W_{ch}, L_{ch}, t_b, K_b$	$K_{sp}, t_s$	$t_{ch}, K_{ch}$	0.24	
2			$W_s, L_s, W_{ch}, L_{ch}$		$K_{ch}, t_{ch}, K_b, t_b$	0.02	
3	Conductance of Blanket, $C_{\text{blanket}}$	$W_s, L_s$	$W_{ch}, L_{ch}, t_s, t_{ch}, K_{sp}$	$K_b, t_b$	$K_{ch}$	0.08	
4		$W_s, L_s$		$K_b, t_b$		0.21	
5		$t_b, L_s$		$K_b, W_s$		0.13	
6		$t_b, W_s$	$W_{ch}, L_{ch}, t_s,$	$t_{ch}, K_{ch}$	$K_b, L_s$	$K_{sp}$	0.26
7		$K_b, L_s$		$t_{ch}, K_{ch}$	$t_b, W_s$		0.07
8		$K_b, W_s$			$t_b, L_s$		0.04
9		$K_b, t_b$			$W_s, L_s$		0.02
10			$W_{ch}, L_{ch}$		$t_{ch}, K_{ch}$		0.15
11			$K_{ch}, L_{ch}$	$W_s, L_s, t_b, K_b$	$t_{ch}, W_{ch}$	$K_{sp}, t_s$	0.17
12	Conductance of Channel, $C_{\text{channel}}$	$K_{ch}, W_{ch}$		$t_{ch}, L_{ch}$		0.49	
13		$t_{ch}, L_{ch}$		$K_{ch}, W_{ch}$		0.08	
14		$t_{ch}, W_{ch}$	$W_s, L_s, t_s, t_b,$	$K_b$	$K_{ch}, L_{ch}$	$K_{sp}$	0.32
15		$K_{ch}, t_{ch}$			$W_{ch}, L_{ch}$		0.32
16		$W_{ch}, L_{ch}$	$W_s, L_s, t_b$	$K_{ch}, t_{ch}$	$K_{sp}, t_s, K_b$	0.02	

Table C.2. Parametric analysis 1 corresponding to the combined parameter  $T_{splay}$ 

$W_s$ (m)	$L_s$ (m)	$L_{ch}$ (m)	$W_{ch}$ (m)	$t_b$ (m)	$K_b$ (cm/s)	$K_f$ (cm/s)	$K_{hv}$
91.4	213.4	29.0	45.7	1.2	3.05E-07	3.05E-04	0.1

		$C_{channel}$ (m <sup>2</sup> /s)				
		1.5E-04	1.5E-05	1.5E-06	1.5E-07	
$L_{ch}$ (m)	$W_{ch}$ (m)	$K_{ch}$ (cm/s)				
29.0	45.7	0.3	3.05E-02	3.05E-03	3.05E-04	3.05E-05
		0.6	1.52E-02	1.52E-03	1.52E-04	1.52E-05
		0.9	1.02E-02	1.02E-03	1.02E-04	1.02E-05
		1.2	7.62E-03	7.62E-04	7.62E-05	7.62E-06
		1.5	6.10E-03	6.10E-04	6.10E-05	6.10E-06
		3.0	3.05E-03	3.05E-04	3.05E-05	3.05E-06

			$C_{channel}$ (m <sup>2</sup> /s)			
			1.5E-04	1.5E-05	1.5E-06	1.5E-07
$K_{sp}$ (cm/s)	$t_s$ (m)	$T_{splay}$ (m <sup>2</sup> /s)	Head at toe at the bottom of the blanket layer (m)			
3.05E-02	0.3	9.3E-05	6.46	4.91	1.73	0.66
1.52E-02	0.6	9.3E-05	6.46	4.89	1.73	0.68
1.02E-02	0.9	9.3E-05	6.46	4.89	1.74	0.70
7.62E-03	1.2	9.3E-05	6.45	4.88	1.75	0.73
6.10E-03	1.5	9.3E-05	6.45	4.87	1.76	0.75
3.05E-03	3.0	9.3E-05	6.44	4.83	1.83	0.90
Maximum variation in $h_{max}$			0.02	0.08	0.10	<b>0.24</b>



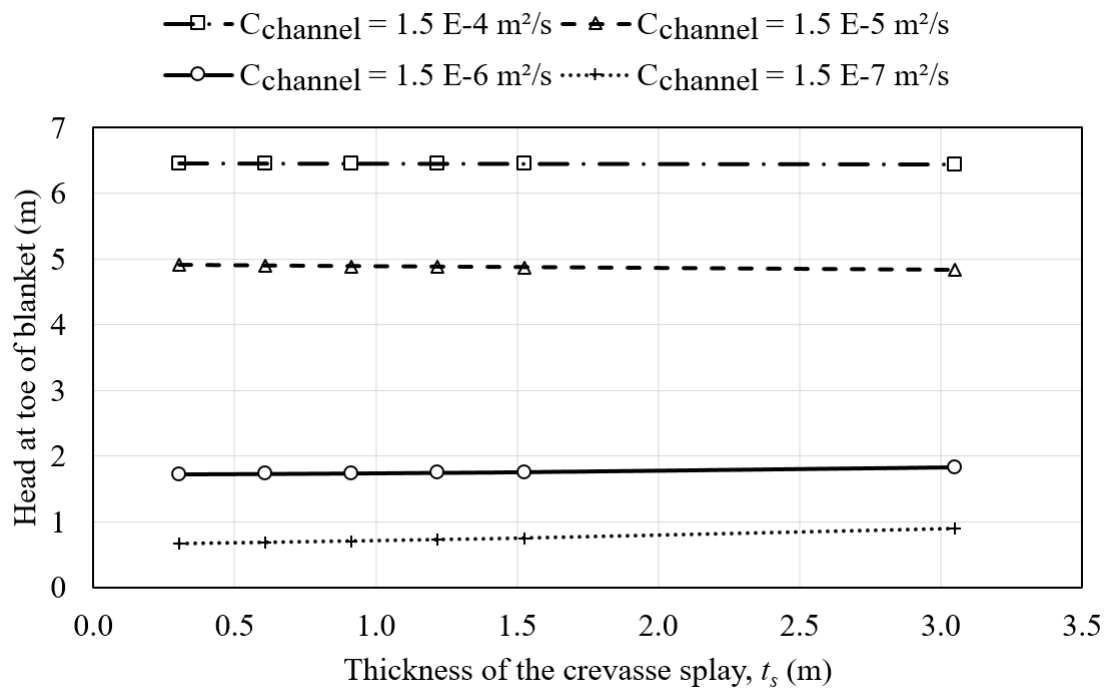


Figure C.1. Results from parametric analysis 1 corresponding to the combined parameter  $T_{splay}$ .

Table C.3. Parametric analysis 2 corresponding to the combined parameter  $T_{splay}$ 

$W_s$ (m)	$L_s$ (m)	$L_{ch}$ (m)	$W_{ch}$ (m)	$K_b$ (cm/s)	$K_f$ (cm/s)	$K_{hv}$
91.4	213.4	29.0	45.7	0.00E+00	3.05E-04	0.1

$K_{ch}$ (cm/s)	$t_{ch}$ (m)	$W_{ch}$ (m)	$L_{ch}$ (m)	$C_{channel}$ (m <sup>2</sup> /s)
3.05E-02	0.3			1.5E-04
1.02E-02	0.9	45.7	29.0	1.5E-04
6.10E-03	1.5			1.5E-04

$K_b$ (cm/s)	$t_b$ (m)	$W_s$ (m)	$L_s$ (m)	$C_{blanket}$ (m <sup>2</sup> /s)
3.05E-07	1.2			4.9E-05
4.57E-07	1.8	91.4	213.4	4.9E-05
6.10E-07	2.4			4.9E-05

		$t_b$ (m)			
		1.2	1.8	2.4	
$K_{sp}$ (cm/s)	$t_s$ (m)	$T_{splay}$ (m <sup>2</sup> /s)	Head at toe at the bottom of the blanket layer (m)		
3.05E-02	0.3	9.3E-05	6.46	6.44	6.43
1.02E-02	0.9	9.3E-05	6.45	6.43	6.41
6.10E-03	1.5	9.3E-05	6.45	6.43	6.41
Maximum variation in $h_{max}$			0.01	0.01	<b>0.02</b>

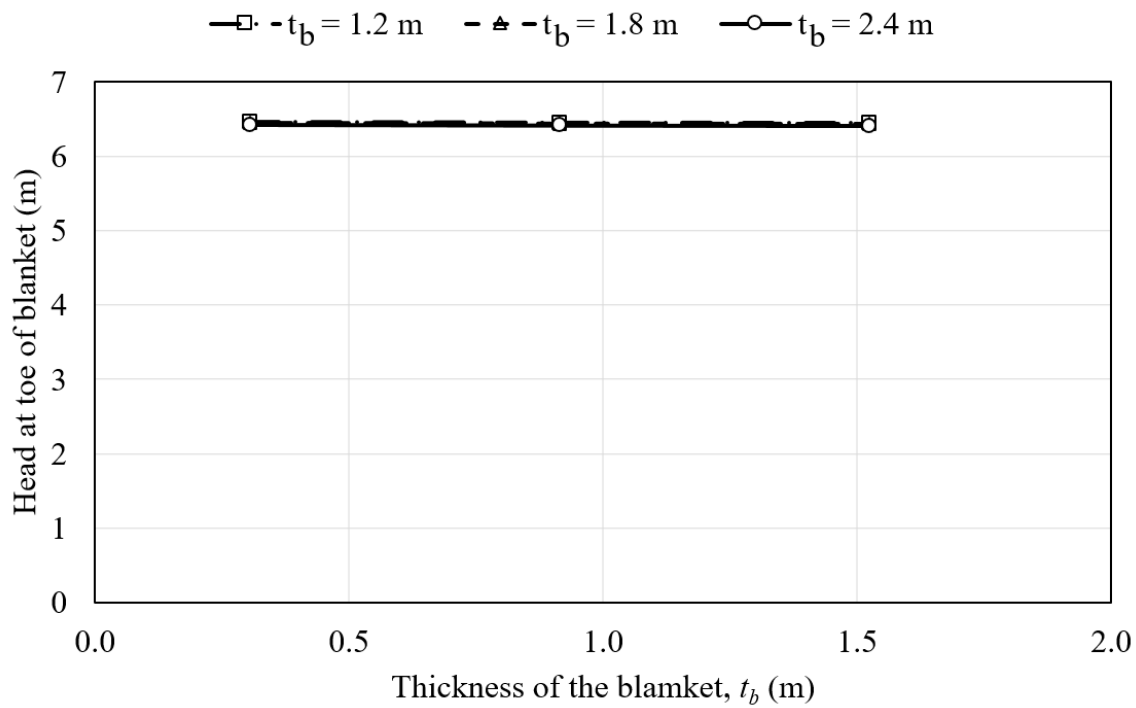


Figure C.2. Results from parametric analysis 2 corresponding to the combined parameter  $T_{splay}$ .

Table C.4. Parametric analysis 3 corresponding to the combined parameter  $C_{blanket}$ 

$L_{ch}$ (m)	$W_{ch}$ (m)	$t_s$ (m)	$t_{ch}$ (m)	$K_{sp}$ (cm/s)	$K_f$ (cm/s)	$K_{hv}$
29.0	45.7	0.9	0.9	3.05E-04	3.05E-04	0.1

					$K_{ch}$ (cm/s)		
					3.0E-01	3.0E-02	3.0E-03
$K_b$ (cm/s)	$t_b$ (m)	$W_s$ (m)	$L_s$ (m)	$C_{blanket}$ (m <sup>2</sup> /s)	Head at toe at the bottom of the blanket layer (m)		
3.05E-07	0.6			9.8E-05	6.53	6.49	6.15
1.52E-06	3.0	91.4	213.4	9.8E-05	6.54	6.50	6.17
3.05E-06	6.1			9.8E-05	6.56	6.52	6.22
Maximum variation in $h_{max}$					0.03	0.03	<b>0.08</b>

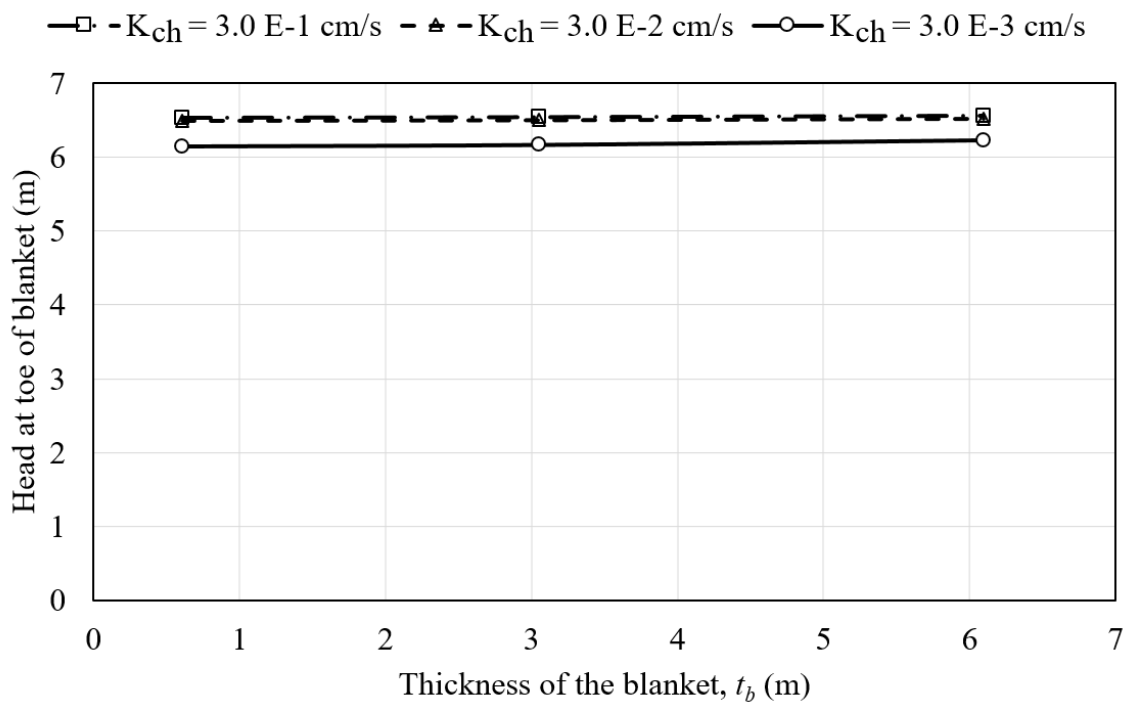
Figure C.3. Results from parametric analysis 3 corresponding to the combined parameter  $C_{blanket}$ .

Table C.5. Parametric analysis 4 corresponding to the combined parameter  $C_{blanket}$ 

$L_{ch}$ (m)	$W_{ch}$ (m)	$t_s$ (m)	$t_{ch}$ (m)	$K_{ch}$ (cm/s)	$K_f$ (cm/s)	$K_{hv}$
29.0	45.7	0.9	0.9	3.05E-03	3.05E-04	0.1

					$K_{sp}$ (cm/s)		
					3.0E-03	3.0E-04	3.0E-05
$K_b$ (cm/s)	$t_b$ (m)	$W_s$ (m)	$L_s$ (m)	$C_{blanket}$ (m <sup>2</sup> /s)	Head at toe at the bottom of the blanket layer (m)		
3.05E-07	0.6			9.8E-05	5.66	6.15	6.16
1.52E-06	3.0	91.4	213.4	9.8E-05	5.54	6.17	6.21
3.05E-06	6.1			9.8E-05	5.45	6.22	6.28
Maximum variation in $h_{max}$					<b>0.21</b>	0.08	0.12

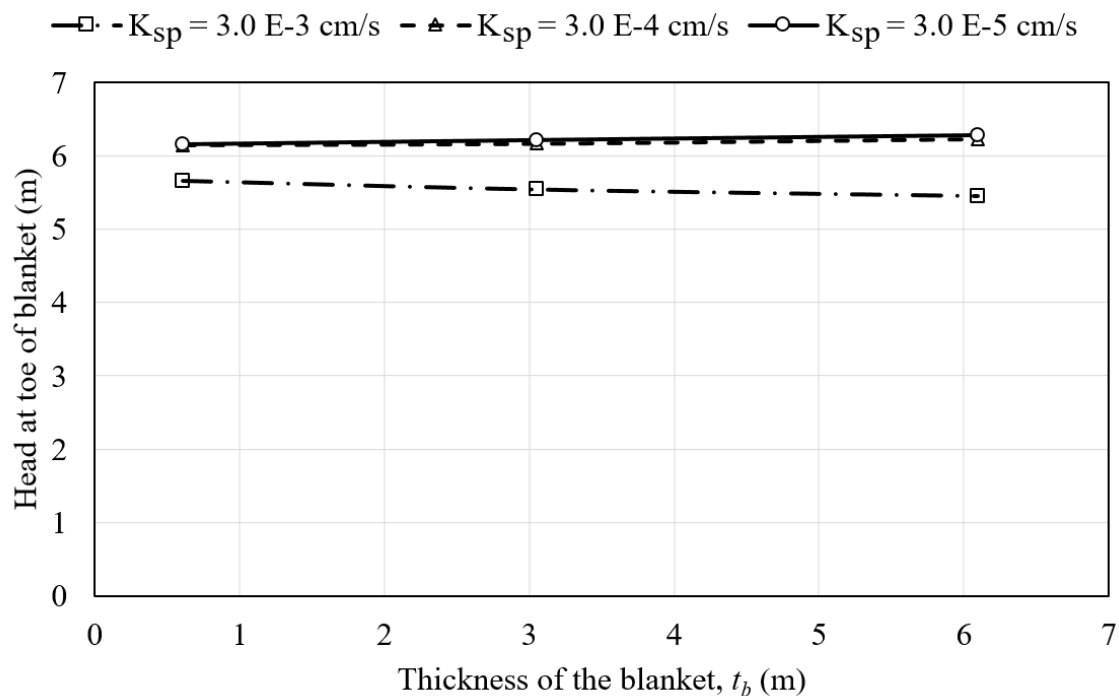
Figure C.4. Results from parametric analysis 4 corresponding to the combined parameter  $C_{blanket}$ .

Table C.6. Parametric analysis 5 corresponding to the combined parameter  $C_{blanket}$ 

$L_{ch}$ (m)	$W_{ch}$ (m)	$t_s$ (m)	$t_{ch}$ (m)	$K_{ch}$ (cm/s)	$K_f$ (cm/s)	$K_{hv}$
29.0	45.7	0.9	0.9	1.68E-02	3.05E-04	0.1

					$K_{sp}$ (cm/s)		
					3.0E-03	3.0E-04	3.0E-05
$K_b$ (cm/s)	$t_b$ (m)	$W_s$ (m)	$L_s$ (m)	$C_{blanket}$ (m <sup>2</sup> /s)	Head at toe at the bottom of the blanket layer (m)		
1.02E-06		45.7		8.1E-05	6.47	6.46	6.15
7.62E-07	1.2	61.0	213.4	8.1E-05	6.48	6.47	6.21
6.10E-07		76.2		8.1E-05	6.48	6.48	6.25
5.08E-07		91.4		8.1E-05	6.47	6.48	6.28
Maximum variation in $h_{max}$					0.01	0.02	<b>0.13</b>

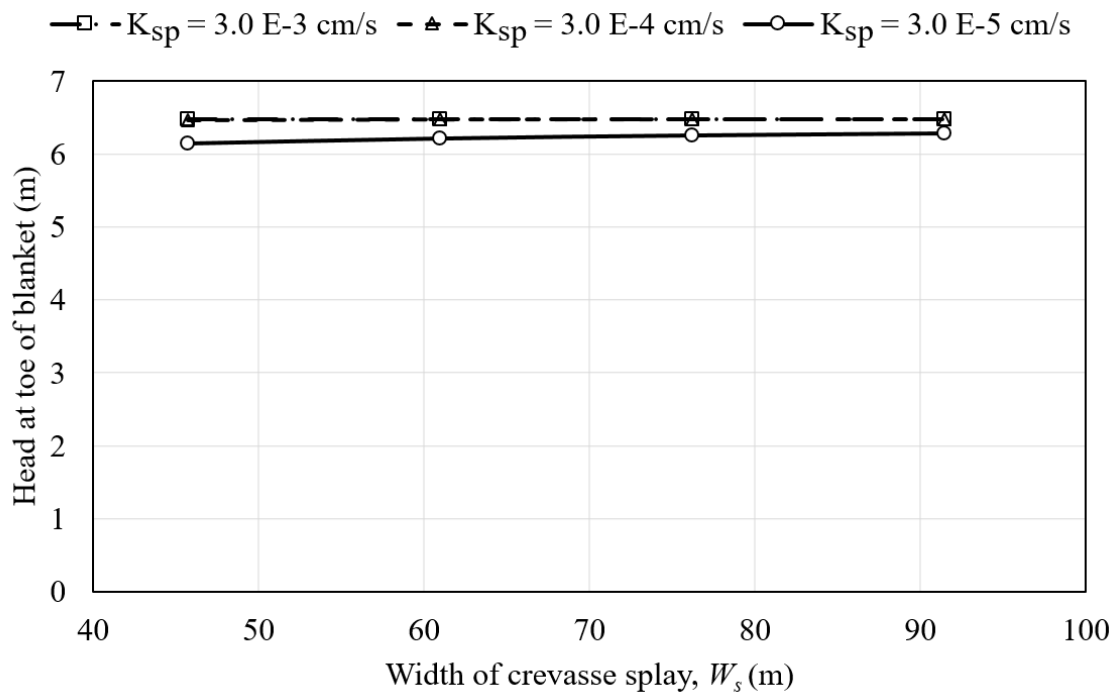
Figure C.5. Results from parametric analysis 5 corresponding to the combined parameter  $C_{blanket}$ .

Table C.7. Parametric analysis 6 corresponding to the combined parameter  $C_{blanket}$ 

$L_{ch}$ (m)	$W_{ch}$ (m)	$t_s$ (m)	$t_{ch}$ (m)	$K_{ch}$ (cm/s)	$K_f$ (cm/s)	$K_{hv}$
29.0	45.7	0.9	0.9	1.68E-02	3.05E-04	0.1

					$K_{sp}$ (cm/s)		
					3.0E-03	3.0E-04	3.0E-05
$K_b$ (cm/s)	$t_b$ (m)	$W_s$ (m)	$L_s$ (m)	$C_{blanket}$ (m <sup>2</sup> /s)	Head at toe at the bottom of the blanket layer (m)		
3.05E-06			213.4	4.9E-04	6.09	6.24	5.79
1.94E-06	1.2	91.4	335.3	4.9E-04	6.18	6.32	5.96
1.42E-06			457.2	4.9E-04	6.24	6.37	6.05
Maximum variation in $h_{max}$					0.16	0.12	<b>0.26</b>

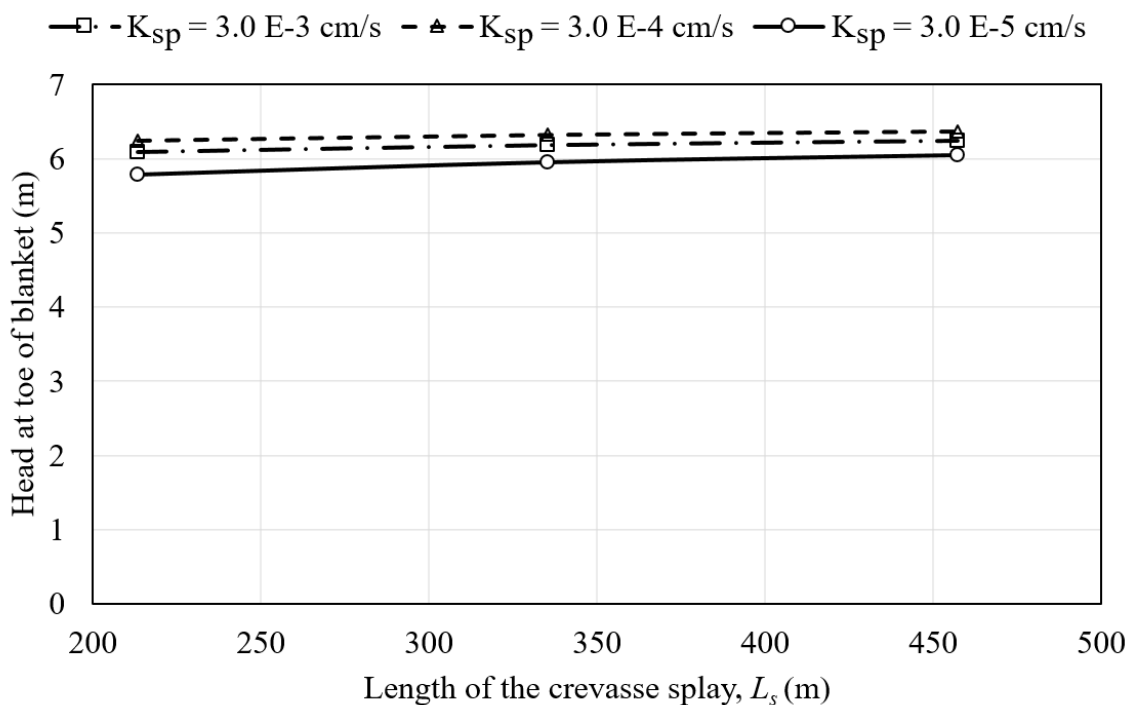
Figure C.6. Results from parametric analysis 6 corresponding to the combined parameter  $C_{blanket}$ .

Table C.8. Parametric analysis 7 corresponding to the combined parameter  $C_{blanket}$ 

$L_{ch}$ (m)	$W_{ch}$ (m)	$t_s$ (m)	$t_{ch}$ (m)	$K_{ch}$ (cm/s)	$K_f$ (cm/s)	$K_{hv}$
29.0	45.7	0.9	0.9	1.68E-02	3.05E-04	0.1

					$K_{sp}$ (cm/s)		
					3.0E-03	3.0E-04	3.0E-05
$K_b$ (cm/s)	$t_b$ (m)	$W_s$ (m)	$L_s$ (m)	$C_{blanket}$ (m <sup>2</sup> /s)	Head at toe at the bottom of the blanket layer (m)		
	1.2	45.7		2.4E-05	6.61	6.57	6.39
3.05E-07	1.8	68.6	213.4	2.4E-05	6.61	6.58	6.43
	2.4	91.4		2.4E-05	6.61	6.57	6.46
Maximum variation in $h_{max}$					0.00	0.01	<b>0.07</b>

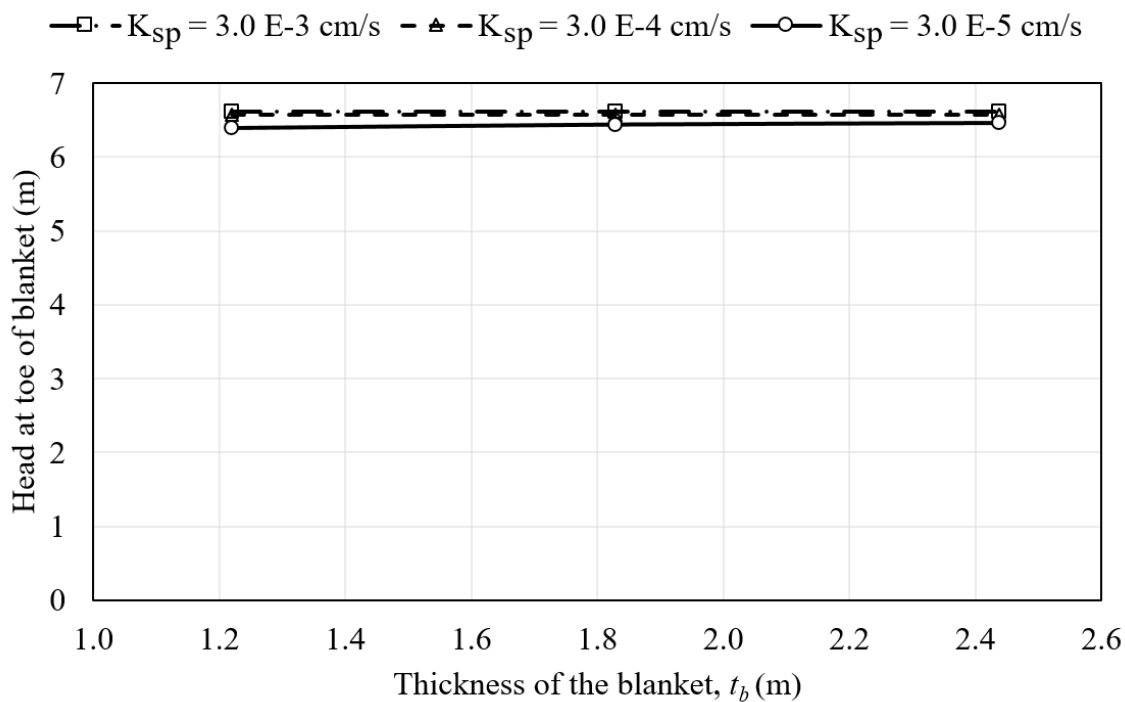
Figure C.7. Results from parametric analysis 7 corresponding to the combined parameter  $C_{blanket}$ .



Table C.9. Parametric analysis 8 corresponding to the combined parameter  $C_{blanket}$ 

$L_{ch}$ (m)	$W_{ch}$ (m)	$t_s$ (m)	$t_{ch}$ (m)	$K_{ch}$ (cm/s)	$K_f$ (cm/s)	$K_{hv}$
29.0	45.7	0.9	0.9	1.68E-02	3.05E-04	0.1

					$K_{sp}$ (cm/s)		
					3.0E-03	3.0E-04	3.0E-05
$K_b$ (cm/s)	$t_b$ (m)	$W_s$ (m)	$L_s$ (m)	$C_{blanket}$ (m <sup>2</sup> /s)	Head at toe at the bottom of the blanket layer (m)		
	1.1		213.4	5.6E-05	6.54	6.52	6.34
3.05E-07	1.2	91.4	243.8	5.6E-05	6.54	6.53	6.36
	1.4		274.3	5.6E-05	6.54	6.53	6.38
Maximum variation in $h_{max}$					0.00	0.02	<b>0.04</b>

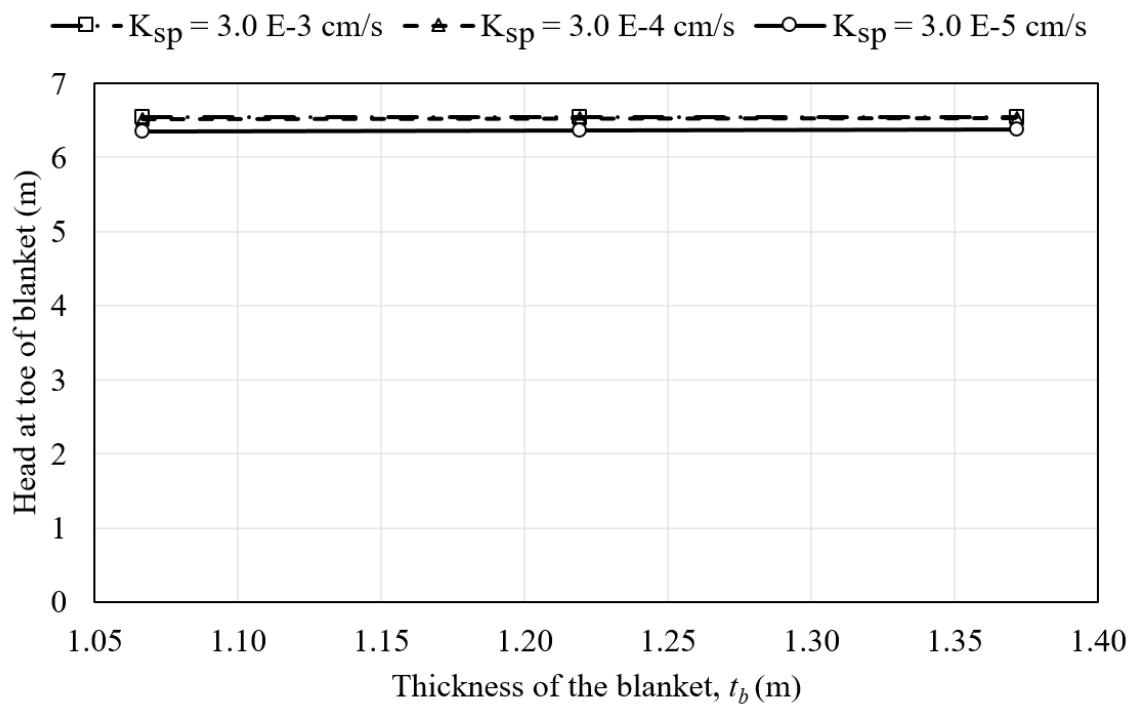
Figure C.8. Results from parametric analysis 8 corresponding to the combined parameter  $C_{blanket}$ .

Table C.10. Parametric analysis 9 corresponding to the combined parameter  $C_{channel}$ 

$L_{ch}$ (m)	$W_{ch}$ (m)	$t_s$ (m)	$t_{ch}$ (m)	$K_{ch}$ (cm/s)	$K_f$ (cm/s)	$K_{hv}$
29.0	45.7	0.0	0.0	1.68E-02	3.05E-04	0.1

					$K_{sp}$ (cm/s)		
					3.0E-03	3.0E-04	3.0E-05
$K_b$ (cm/s)	$t_b$ (m)	$W_s$ (m)	$L_s$ (m)	$C_{blanket}$ (m <sup>2</sup> /s)	Head at toe at the bottom of the blanket layer (m)		
		76.2	213.4	4.1E-05	6.58	6.55	6.38
3.05E-07	1.2	61.0	266.7	4.1E-05	6.58	6.56	6.39
		45.7	355.6	4.1E-05	6.58	6.57	6.40
Maximum variation in $h_{max}$					0.003	<b>0.024</b>	0.020

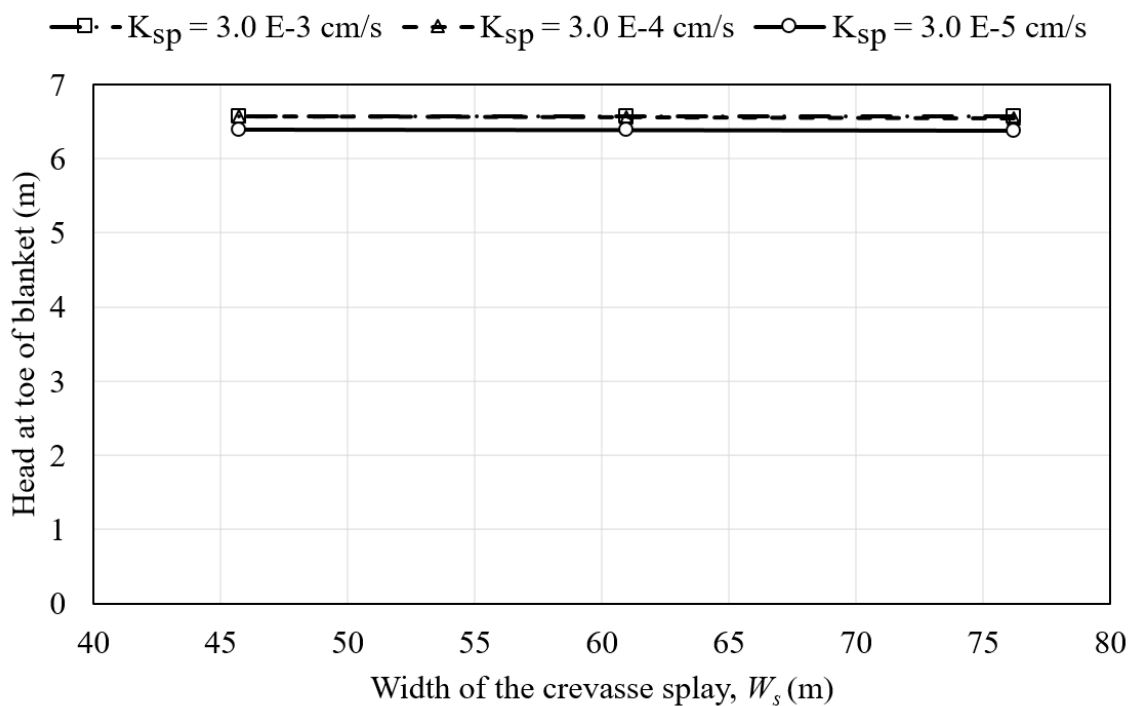
Figure C.9. Results from parametric analysis 9 corresponding to the combined parameter  $C_{channel}$ .

Table C.11. Parametric analysis 10 corresponding to the combined parameter  $C_{channel}$ 

$L_s$ (m)	$W_s$ (m)	$t_b$ (m)	$K_b$ (cm/s)	$K_f$ (cm/s)	$K_{hv}$
213.4	91.4	1.2	3.05E-07	3.05E-04	0.1

$t_s$ (m)	$T_{splay}$ (m <sup>2</sup> /s)			
	9.3E-05	9.3E-07	9.3E-09	9.3E-11
	$K_{sp}$ (cm/s)			
0.3	3.05E-02	3.05E-03	3.05E-04	3.05E-05
0.6	1.52E-02	1.52E-03	1.52E-04	1.52E-05
0.9	1.02E-02	1.02E-03	1.02E-04	1.02E-05
1.2	7.62E-03	7.62E-04	7.62E-05	7.62E-06
1.5	6.10E-03	6.10E-04	6.10E-05	6.10E-06
3.0	3.05E-03	3.05E-04	3.05E-05	3.05E-06

$K_{ch}$ (cm/s)	$t_{ch}$ (m)	$W_{ch}$ (m)	$L_{ch}$ (m)	$C_{channel}$ (m <sup>2</sup> /s)	$T_{splay}$ (m <sup>2</sup> /s)			
					Head at toe at the bottom of the blanket layer (m)			
3.05E-03	0.3	45.7	29.0	1.5E-05	4.90	5.37	6.06	6.09
1.52E-03	0.6			1.5E-05	4.89	5.36	6.05	6.08
1.02E-03	0.9			1.5E-05	4.87	5.35	6.05	6.06
7.62E-04	1.2			1.5E-05	4.87	5.36	6.05	6.05
6.10E-04	1.5			1.5E-05	4.87	5.35	6.05	6.03
3.05E-04	3.0			1.5E-05	4.83	5.34	6.05	5.94
Maximum variation in $h_{max}$					0.07	0.02	0.01	<b>0.15</b>

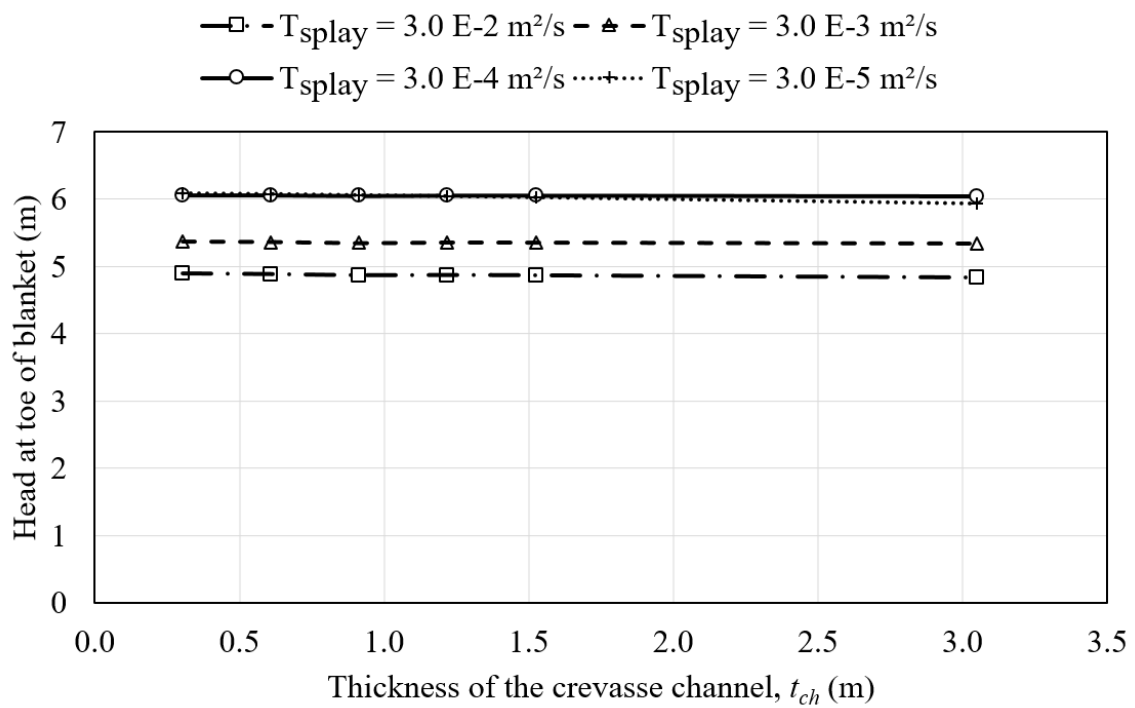


Figure C.10. Results from parametric analysis 10 corresponding to the combined parameter  $C_{channel}$ .

Table C.12. Parametric analysis 11 corresponding to the combined parameter  $C_{channel}$ 

$L_s$ (m)	$W_s$ (m)	$t_b$ (m)	$K_b$ (cm/s)	$K_f$ (cm/s)	$K_{hv}$
213.4	91.4	1.2	3.05E-07	3.05E-04	0.1

$t_s$ (m)	$T_{splay}$ (m <sup>2</sup> /s)			
	9.3E-05	2.3E-07	2.3E-09	2.3E-11
	$K_{sp}$ (cm/s)			
0.6	1.52E-02	1.52E-03	1.52E-04	1.52E-05
1.2	7.62E-03	7.62E-04	7.62E-05	7.62E-06
2.4	3.81E-03	3.81E-04	3.81E-05	3.81E-06

$K_{ch}$ (cm/s)	$t_{ch}$ (m)	$W_{ch}$ (m)	$L_{ch}$ (m)	$C_{channel}$ (m <sup>2</sup> /s)	$T_{splay}$ (m <sup>2</sup> /s)			
					9.3E-05	2.3E-07	2.3E-09	2.3E-11
					Head at toe at the bottom of the blanket layer (m)			
	0.6	91.4		5.9E-05	6.11	6.24	6.39	6.17
3.05E-03	1.2	45.7	29.0	5.9E-05	6.12	6.26	6.38	6.13
	2.4	22.9		5.9E-05	6.10	6.24	6.31	6.00
				Maximum variation in $h_{max}$	0.02	0.03	0.07	<b>0.17</b>

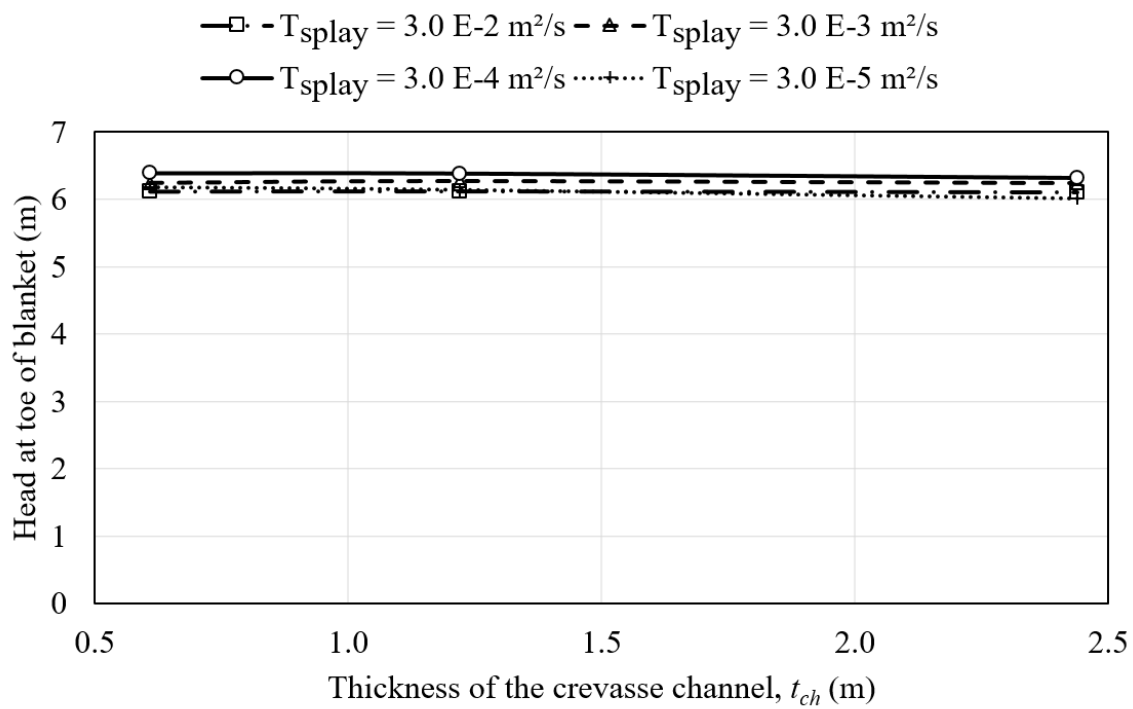


Figure C.11. Results from parametric analysis 11 corresponding to the combined parameter  $C_{channel}$ .

Table C.13. Parametric analysis 12 corresponding to the combined parameter  $C_{channel}$ 

$L_s$ (m)	$W_s$ (m)	$t_b$ (m)	$K_b$ (cm/s)	$K_f$ (cm/s)	$K_{hv}$
213.4	91.4	1.2	3.05E-07	3.05E-04	0.1

$t_s$ (m)	$T_{splay}$ (m <sup>2</sup> /s)			
	9.3E-05	2.3E-07	2.3E-09	2.3E-11
	$K_{sp}$ (cm/s)			
0.6	1.52E-02	1.52E-03	1.52E-04	1.52E-05
0.9	1.02E-02	1.02E-03	1.02E-04	1.02E-05
1.2	7.62E-03	7.62E-04	7.62E-05	7.62E-06

$K_{ch}$ (cm/s)	$t_{ch}$ (m)	$W_{ch}$ (m)	$L_{ch}$ (m)	$C_{channel}$ (m <sup>2</sup> /s)	$T_{splay}$ (m <sup>2</sup> /s)			
					9.3E-05	3.0E-03	3.0E-04	3.0E-05
					Head at toe at the bottom of the blanket layer (m)			
	0.6		29.0	2.9E-05	5.64	5.93	6.27	6.14
3.05E-03	0.9	45.7	43.6	2.9E-05	5.92	6.15	6.49	6.62
	1.2		57.9	2.9E-05	5.95	6.18	6.48	6.60
Maximum variation in $h_{max}$					0.30	0.25	0.22	<b>0.49</b>

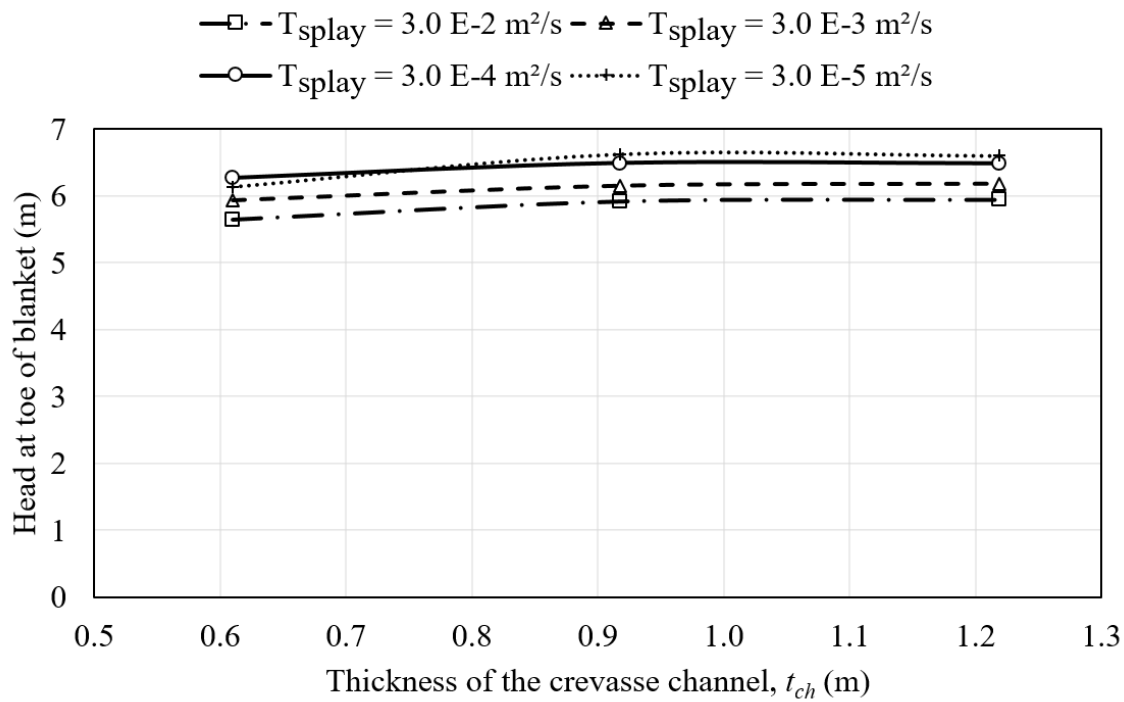


Figure C.12. Results from parametric analysis 12 corresponding to the combined parameter  $C_{channel}$ .



Table C.14. Parametric analysis 13 corresponding to the combined parameter  $C_{channel}$ 

$L_s$ (m)	$W_s$ (m)	$t_b$ (m)	$K_b$ (cm/s)	$K_f$ (cm/s)	$K_{hv}$
213.4	91.4	1.2	3.05E-07	3.05E-04	0.1

$K_{ch}$ (cm/s)	$t_{ch}$ (m)	$W_{ch}$ (m)	$L_{ch}$ (m)	$C_{channel}$ (m <sup>2</sup> /s)	$K_{sp}$ (cm/s)		
					3.0E-03	3.0E-04	3.0E-05
3.05E-03	0.9	22.9	29.0	2.2E-05	5.50	6.02	6.17
2.29E-03		30.5		2.2E-05	5.50	6.03	6.21
1.52E-03		45.7		2.2E-05	5.49	6.02	6.22
1.14E-03		61.0		2.2E-05	5.49	6.02	6.22
9.14E-04		76.2		2.2E-05	5.47	5.99	6.21
7.62E-04		91.4		2.2E-05	5.45	5.95	6.19
Maximum variation in $h_{max}$					0.06	<b>0.08</b>	0.05

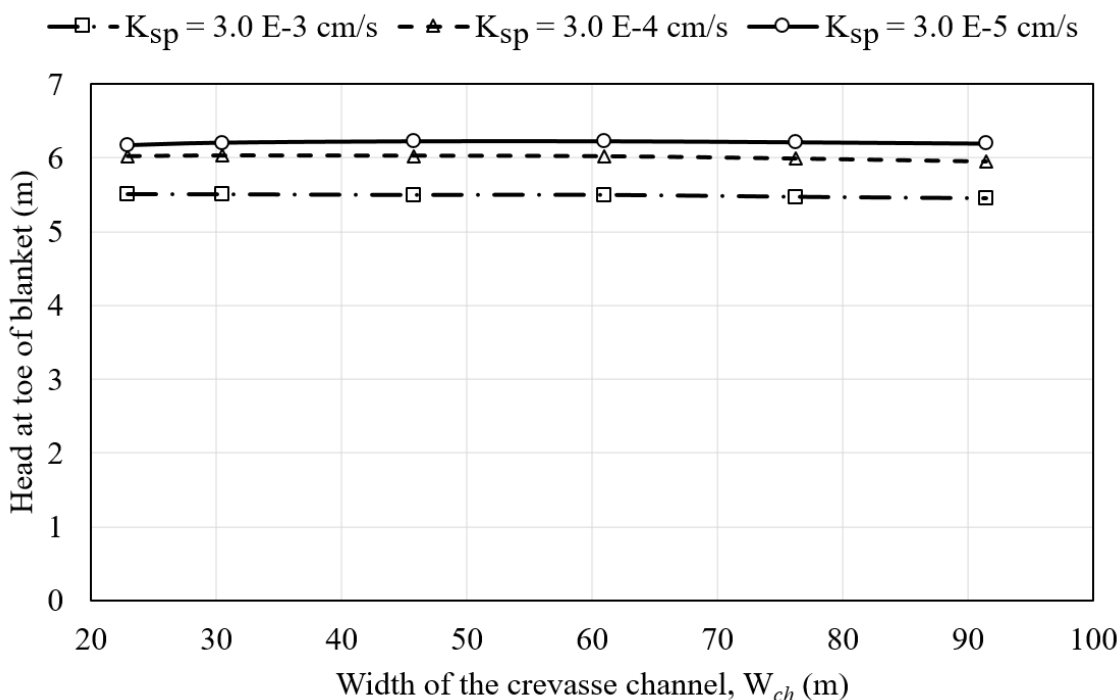
Figure C.13. Results from parametric analysis 13 corresponding to the combined parameter  $C_{channel}$ .

Table C.15. Parametric analysis 14 corresponding to the combined parameter  $C_{channel}$ 

$L_s$ (m)	$W_s$ (m)	$t_b$ (m)	$K_b$ (cm/s)	$K_f$ (cm/s)	$K_{hv}$
213.4	91.4	1.2	3.05E-07	3.05E-04	0.1

$K_{ch}$ (cm/s)	$t_{ch}$ (m)	$W_{ch}$ (m)	$L_{ch}$ (m)	$C_{channel}$ (m <sup>2</sup> /s)	$K_{sp}$ (cm/s)		
					3.0E-03	3.0E-04	3.0E-05
3.05E-03			29.0	4.4E-05	6.03	6.29	6.30
3.21E-03	0.9	45.7	30.5	4.4E-05	6.05	6.41	6.62
3.37E-03			32.0	4.4E-05	6.08	6.41	6.62
Maximum variation in $h_{max}$					0.05	0.13	<b>0.32</b>

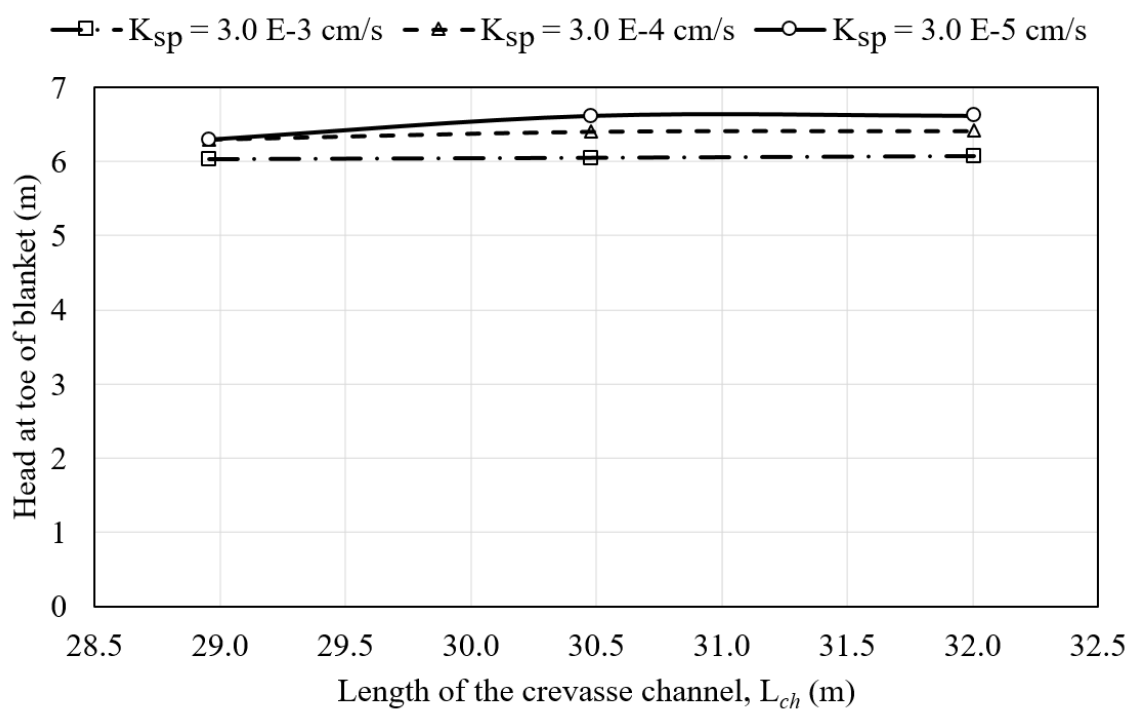
Figure C.14. Results from parametric analysis 14 corresponding to the combined parameter  $C_{channel}$ .

Table C.16. Parametric analysis 15 corresponding to the combined parameter  $C_{channel}$ 

$L_s$ (m)	$W_s$ (m)	$t_b$ (m)	$K_b$ (cm/s)	$K_f$ (cm/s)	$K_{hv}$
213.4	91.4	1.2	3.05E-07	3.05E-04	0.1

$K_{ch}$ (cm/s)	$t_{ch}$ (m)	$W_{ch}$ (m)	$L_{ch}$ (m)	$C_{channel}$ (m <sup>2</sup> /s)	$K_{sp}$ (cm/s)		
					3.0E-03	3.0E-04	3.0E-05
		45.7	29.0	4.4E-05	6.03	6.29	6.30
3.05E-03	0.9	48.1	30.5	4.4E-05	6.05	6.40	6.62
		50.5	32.0	4.4E-05	6.07	6.41	6.62
Maximum variation in $h_{max}$					0.04	0.12	<b>0.32</b>

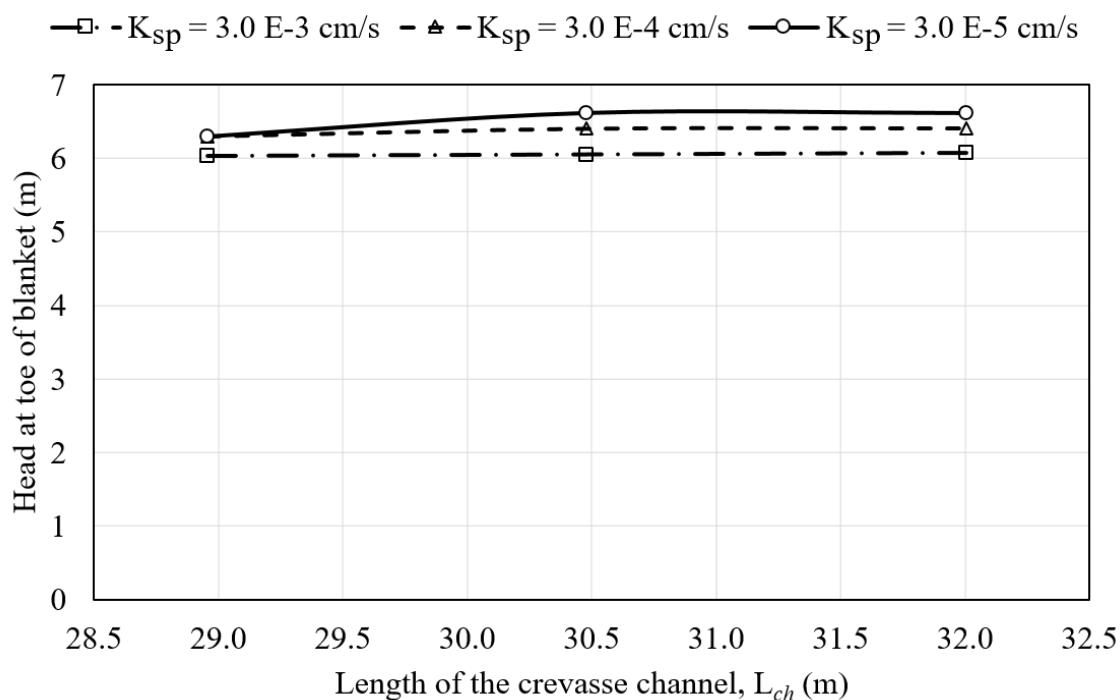
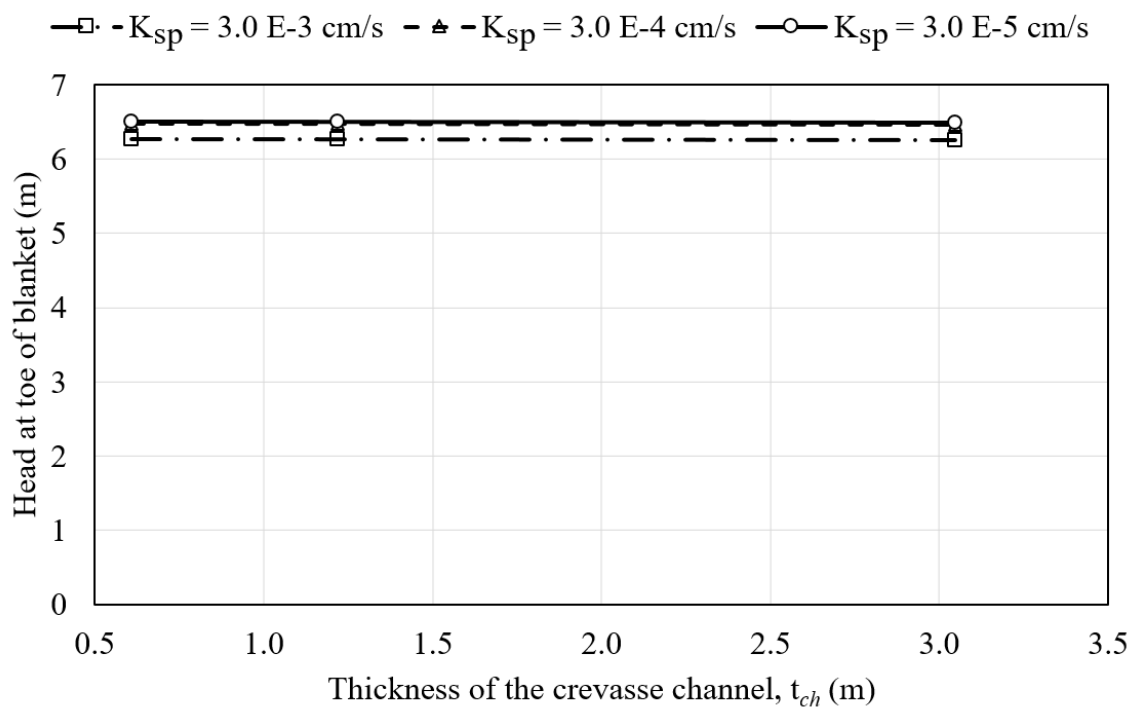
Figure C.15. Results from parametric analysis 15 corresponding to the combined parameter  $C_{channel}$ .

Table C.17. Parametric analysis 16 corresponding to the combined parameter  $C_{channel}$ 

$L_s$ (m)	$W_s$ (m)	$t_b$ (m)	$K_b$ (cm/s)	$K_f$ (cm/s)	$K_{hv}$
213.4	91.4	1.2	3.05E-07	3.05E-04	0.1

$K_{ch}$ (cm/s)	$t_{ch}$ (m)	$W_{ch}$ (m)	$L_{ch}$ (m)	$C_{channel}$ (m <sup>2</sup> /s)	$K_{sp}$ (cm/s)			
					3.0E-06	3.0E-07	3.0E-08	
3.05E-02	0.6			2.9E-04	Head at toe at the bottom of the blanket layer (m)	6.27	6.48	6.50
1.52E-02	1.2	45.7	29.0	2.9E-04	6.27	6.48	6.50	
6.10E-03	3.0			2.9E-04	6.26	6.46	6.49	
Maximum variation in $h_{max}$					0.01	0.02	<b>0.02</b>	

Figure C.16. Results from parametric analysis 16 corresponding to the combined parameter  $C_{channel}$ .

## APPENDIX D

Appendix D provides supporting data for the parametric analysis presented in Table 5.3 in Chapter 5. Due to the amount of computation and data needed to support each result from Table 5.3, Table 5.3 is presented herein as Table D.1 with the addition of a new column for organizational purposes. A numerical column is added to link the maximum variation in resulting head column (last column) with a corresponding parametric analysis number. Tables D.2 through C.23 present the computation of the parametric analyses and Figures D.1 through D.22 present the plotted results for the corresponding parametric analyses. All of the parametric analyses were performed with a constant width of high conductivity channel of 9.1m (30ft).

Table D.1. Results of parametric analysis to assess the validity of the simplified flow model for the high conductivity channel response surface

Parametric analysis	Combined Parameter for RS	Constant Parameters		Varied Parameters		Max. variation in resulting head (m)	
		Dependent	Independent	Dependent	Independent		
1	Tongue effect, $T_{ch}$		$t_b, t_{ch}, RL$		$K_b$	0.00	
2			$t_{ch}, K_b, RL$		$t_b$	0.09	
3		$\alpha$		$t_b, RL$	$K_{ch}, K_f$	$K_b, t_{ch}$	0.00
4				$K_b, RL$		$t_{ch}, t_b$	0.10
5				$t_{ch}, t_b$		$RL, K_b$	0.00
6			$K_{ch}$	$t_b, t_{ch}, RL$	$K_f, \alpha$	$K_b$	0.05
7				$K_{ch}, K_b, t_{ch}, t_b$		$RL$	0.29
8			$K_f$	$t_b, t_{ch}, RL$	$K_{ch}, \alpha$	$K_b$	0.28
9				$t_{ch}, t_b$		$RL, K_b$	0.58
10	Modified leakage factor, $\lambda_m$		$\alpha, RL$		$K_f$	0.00	
11		$t_b, t_{ch}$	$\alpha$	$K_{ch}, K_b$	$RL, K_f$	0.00	
12			$\alpha, RL$		$K_f$	0.02	
13		$t_b, K_b$	$\alpha$	$t_{ch}, K_{ch}$	$RL, K_f$	0.22	
14			$\alpha, RL$		$K_f$	0.02	
15		$t_{ch}, K_b$	$\alpha$	$t_b, K_{ch}$	$RL, K_f$	0.17	
16			$RL, K_f$		$\alpha$	0.04	
17		$t_b, K_{ch}$	$K_f, \alpha$	$t_{ch}, K_b$	$RL$	0.07	
18			$RL, K_f$		$\alpha$	0.02	
19		$t_{ch}, K_{ch}$	$K_f, \alpha$	$t_b, K_b$	$RL$	0.14	
20			$RL, K_f$		$\alpha$	0.03	
21		$K_{ch}, K_b$	$K_f, \alpha$	$t_b, t_{ch}$	$RL$	0.15	
22		$K_f, RL$		$\alpha$	0.03		

Table D.2. Parametric analysis 1 corresponding to the combined parameter  $T_{ch}$ 

$t_b$ (m)		$t_{ch}$ (m)		$RL$ (m)	
3.0		6.1		304.8	

$K_{ch}$ (cm/s)	$\lambda_m$ (m)				
	431	545	562	578	610
	$K_b$ (cm/s)				
3.05E-02	3.05E-06	9.64E-07	3.05E-07	9.64E-08	3.05E-08
2.74E+00	2.74E-04	8.67E-05	2.74E-05	8.67E-06	2.74E-06
2.44E+00	2.44E-04	7.71E-05	2.44E-05	7.71E-06	2.44E-06
2.13E+00	2.13E-04	6.75E-05	2.13E-05	6.75E-06	2.13E-06
1.83E+00	1.83E-04	5.78E-05	1.83E-05	5.78E-06	1.83E-06
1.52E+00	1.52E-04	4.82E-05	1.52E-05	4.82E-06	1.52E-06
1.22E+00	1.22E-04	3.86E-05	1.22E-05	3.86E-06	1.22E-06
9.14E-01	9.14E-05	2.89E-05	9.14E-06	2.89E-06	9.14E-07
6.10E-01	6.10E-05	1.93E-05	6.10E-06	1.93E-06	6.10E-07
3.05E-01	3.05E-05	9.64E-06	3.05E-06	9.64E-07	3.05E-07

$K_{ch}$ (cm/s)	$K_f$ (cm/s)	$\alpha$ (°)	Sin ( $\alpha$ )	$T_{ch}$	$\lambda_m$ (m)				
					431	545	562	578	610
					Head at toe at the bottom of the blanket layer (m)				
3.05E-02	3.05E-04	90	1	100	3.09	3.12	3.12	3.12	3.12
2.74E+00	2.74E-02			100	3.09	3.12	3.12	3.12	3.12
2.44E+00	2.44E-02			100	3.09	3.12	3.12	3.12	3.12
2.13E+00	2.13E-02			100	3.09	3.12	3.12	3.12	3.12
1.83E+00	1.83E-02			100	3.09	3.12	3.12	3.12	3.12
1.52E+00	1.52E-02			100	3.09	3.12	3.12	3.12	3.12
1.22E+00	1.22E-02			100	3.09	3.12	3.12	3.12	3.12
9.14E-01	9.14E-03			100	3.09	3.12	3.12	3.12	3.12
6.10E-01	6.10E-03			100	3.09	3.12	3.12	3.12	3.12
3.05E-01	3.05E-03			100	3.09	3.12	3.12	3.12	3.12
Maximum variation in $h_{max}$					0.00	0.00	0.00	0.00	<b>0.00</b>

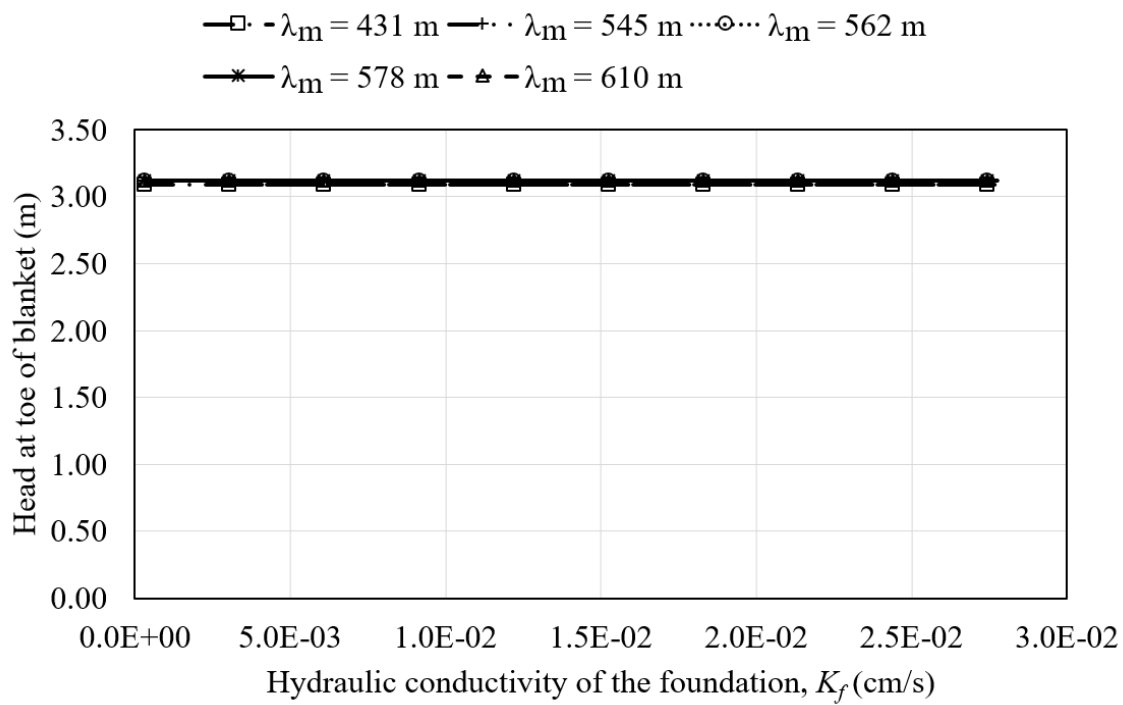


Figure D.1. Results from parametric analysis 1 corresponding to the combined parameter  $T_{ch}$ .



Table D.3. Parametric analysis 2 corresponding to the combined parameter  $T_{ch}$ 

$t_f$ (m)			$t_{ch}$ (m)			$RL$ (m)	
21.3			6.1			152.4	

			$\lambda_m$ (m)				
			528	545	562	578	610
$K_{ch}$ (cm/s)	$t_{ch}$ (m)	$K_b$ (cm/s)	$t_b$ (m)				
3.05E-03			457	488	518	549	610
9.91E-03			141	150	159	169	188
1.68E-02	6.1	3.05E-07	83	89	94	100	111
2.36E-02			59	63	67	71	79
3.05E-02			46	49	52	55	61

					$\lambda_m$ (m)				
					528	545	562	578	610
$K_{ch}$ (cm/s)	$K_f$ (cm/s)	$\alpha$ (°)	$\sin(\alpha)$	$T_{ch}$	Head at toe at the bottom of the blanket layer (m)				
3.05E-03	3.05E-04			7	3.94	3.95	3.95	3.95	3.96
9.91E-03	9.91E-04			7	4.00	4.01	4.01	4.01	4.02
1.68E-02	1.68E-03	45	0.71	7	4.02	4.02	4.04	4.03	4.03
2.36E-02	2.36E-03			7	4.02	4.02	4.03	4.03	4.04
3.05E-02	3.05E-03			7	4.00	4.01	4.02	4.03	4.04
Maximum variation in $h_{max}$					0.08	0.08	<b>0.09</b>	0.08	0.08

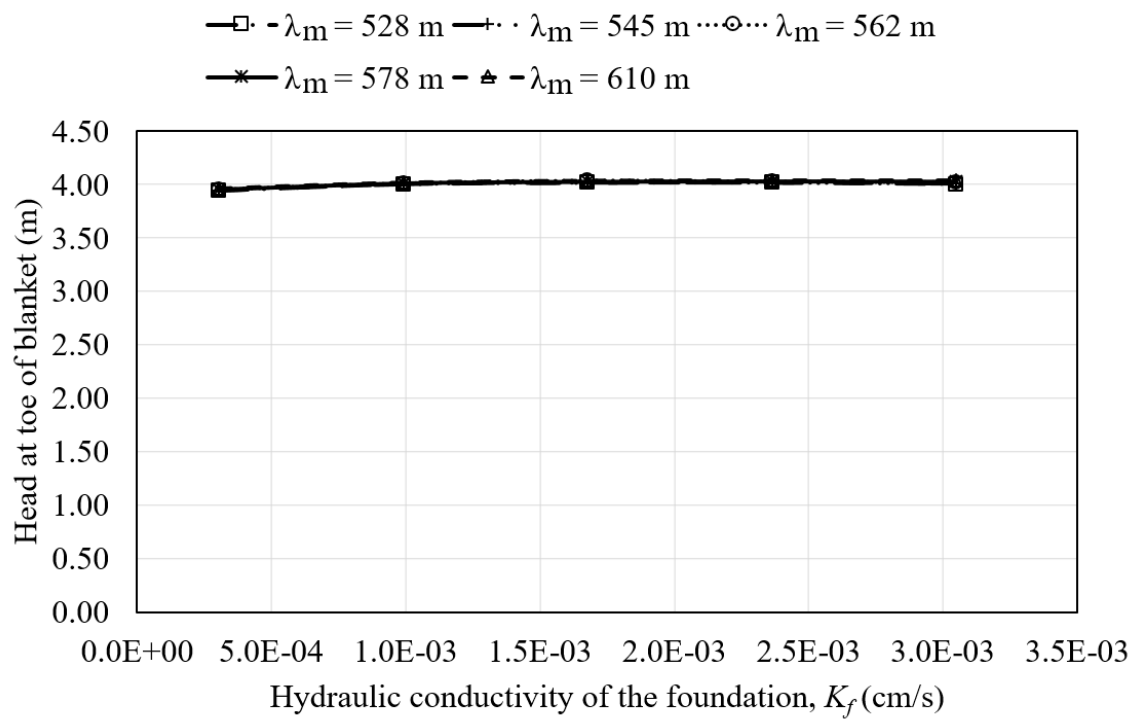


Figure D.2. Results from parametric analysis 2 corresponding to the combined parameter  $T_{ch}$ .

Table D.4. Parametric analysis 3 corresponding to the combined parameter  $T_{ch}$ 

	$t_f$ (m)		$RL$ (m)	
	21.3		152.4	
$\lambda_m$ (m)	682	964	1180	1363
$t_b$ (m)	3.0	3.0	3.0	3.0
$t_{ch}$ (ft)	1.5	3.0	4.6	6.1
$K_b$ (cm/s)	3.05E-07	3.05E-07	3.05E-07	3.05E-07
$K_{ch}$ (cm/s)	3.05E-02	3.05E-02	3.05E-02	3.05E-02
$K_b$ (cm/s)	1.68E-06	1.68E-06	1.68E-06	1.68E-06
$K_{ch}$ (cm/s)	1.68E-01	1.68E-01	1.68E-01	1.68E-01
$K_b$ (cm/s)	3.05E-06	3.05E-06	3.05E-06	3.05E-06
$K_{ch}$ (cm/s)	3.05E-01	3.05E-01	3.05E-01	3.05E-01

						$\lambda_m$ (m)			
						682	964	1180	1363
$K_b$ (cm/s)	$K_{ch}$ (cm/s)	$K_f$ (cm/s)	$\alpha$ (°)	Sin ( $\alpha$ )	$T_{ch}$	Head at toe at the bottom of the blanket layer (m)			
3.05E-07	3.05E-02	3.05E-04			71	3.80	3.90	3.96	4.01
1.68E-06	1.68E-01	1.68E-03	45	0.71	71	3.80	3.90	3.96	4.01
3.05E-06	3.05E-01	3.05E-03			71	3.80	3.90	3.96	4.01
Maximum variation in $h_{max}$						0.00	0.00	0.00	<b>0.00</b>

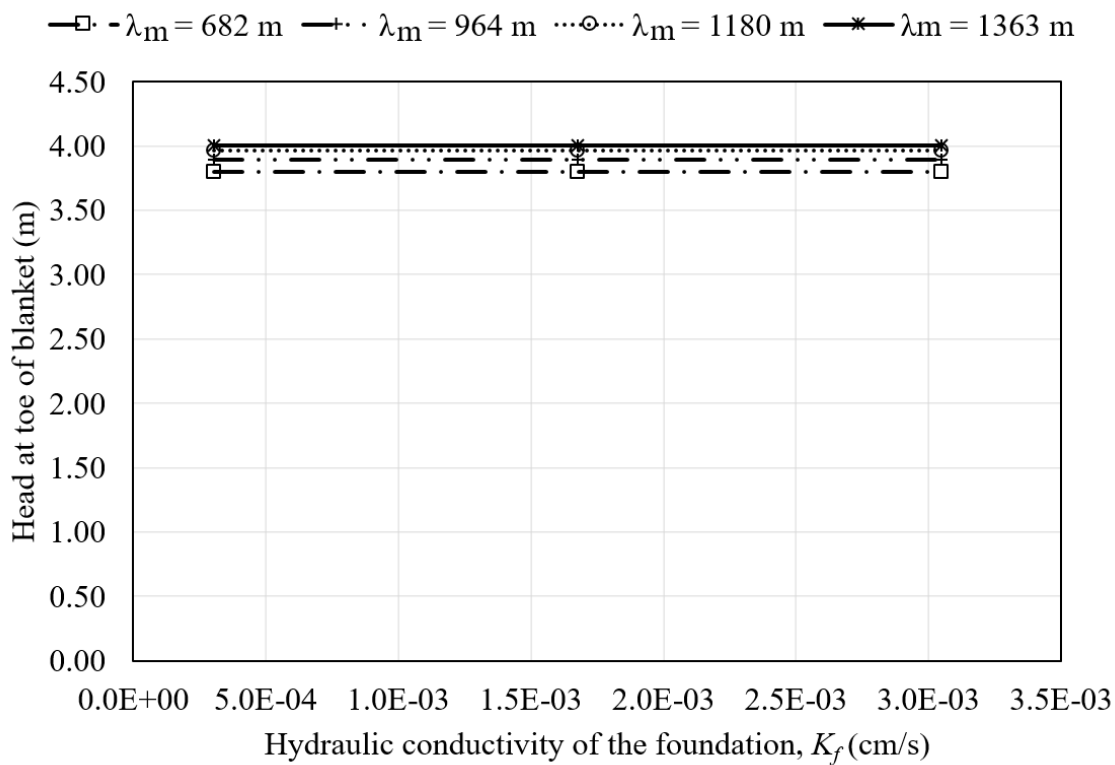


Figure D.3. Results from parametric analysis 3 corresponding to the combined parameter  $T_{ch}$ .

Table D.5. Parametric analysis 4 corresponding to the combined parameter  $T_{ch}$ 

$t_f$ (m)		$RL$ (m)	
30.5		304.8	

			$\lambda_m$ (m)				
			528	472	431	386	305
$K_{ch}$ (cm/s)	$t_{ch}$ (m)	$K_b$ (cm/s)	$t_b$ (m)				
3.05E-03	6.1		457	366	305	244	152
5.42E-03	4.6		343	274	229	183	114
9.64E-03	3.0	3.05E-07	289	231	193	154	96
1.71E-02	2.4		203	163	136	108	68
3.05E-02	1.5		183	146	122	98	61

					$\lambda_m$ (m)				
					528	472	431	386	305
$K_{ch}$ (cm/s)	$K_f$ (cm/s)	$\alpha$ (°)	$\sin(\alpha)$	$T_{ch}$	Head at toe at the bottom of the blanket layer (m)				
3.05E-03	3.05E-04			7	3.89	3.87	3.86	3.84	3.80
5.42E-03	5.42E-04			7	3.91	3.90	3.89	3.87	3.83
9.64E-03	9.64E-04	45	0.71	7	3.93	3.92	3.91	3.90	3.87
1.71E-02	1.71E-03			7	3.95	3.94	3.93	3.92	3.89
3.05E-02	3.05E-03			7	3.95	3.95	3.94	3.93	3.90
Maximum variation in $h_{max}$					0.06	0.08	0.08	0.09	<b>0.10</b>

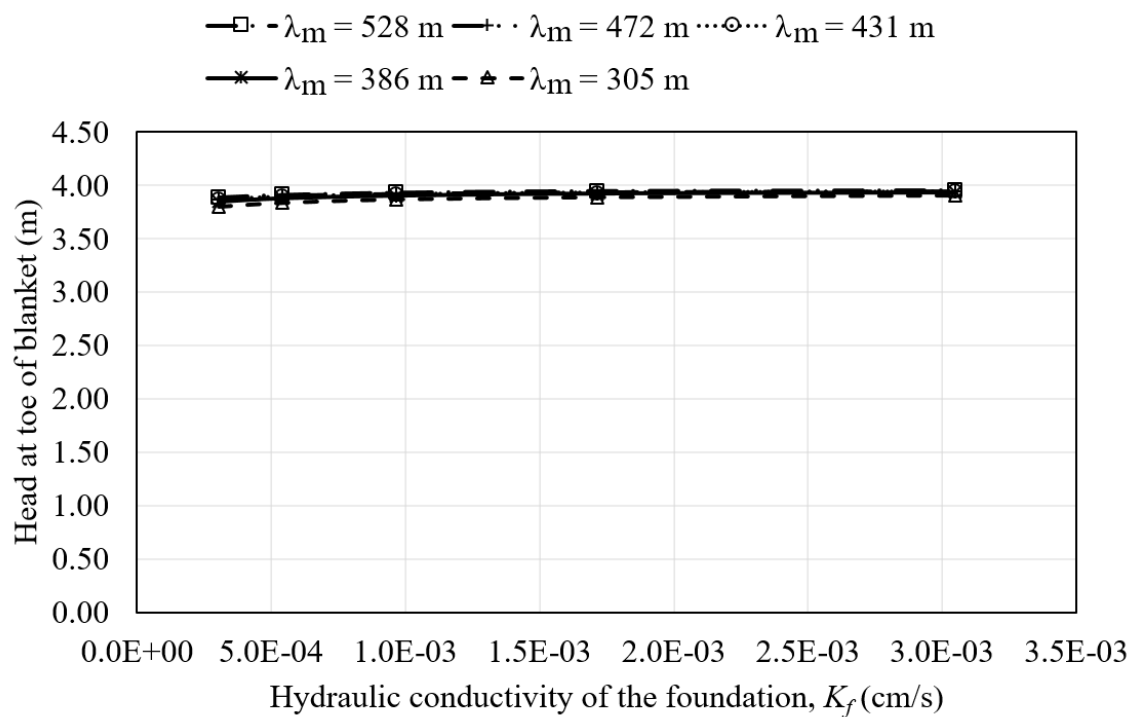


Figure D.4. Results from parametric analysis 4 corresponding to the combined parameter  $T_{ch}$ .



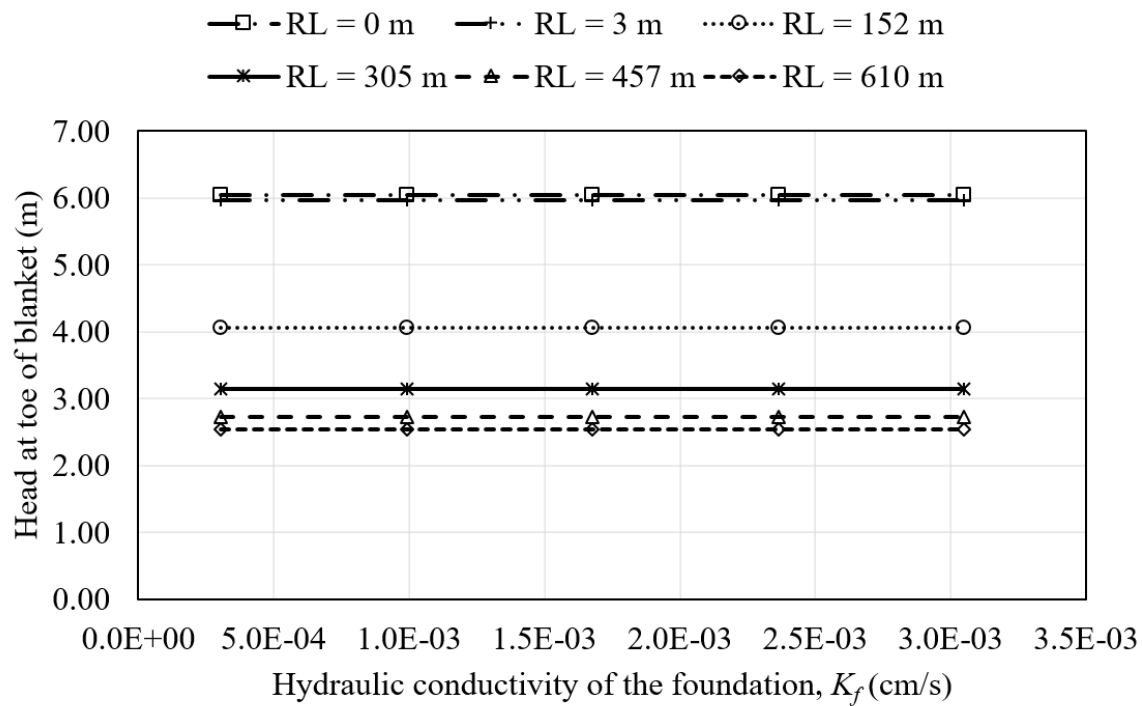


Figure D.5. Results from parametric analysis 5 corresponding to the combined parameter  $T_{ch}$ .



Table D.7. Parametric analysis 6 corresponding to the combined parameter  $T_{ch}$ 

$t_b$ (m)		$t_{ch}$ (m)		$RL$ (m)	
3.0		6.1		304.8	

$\lambda_m$ (m)					
431		767		4311	
$K_{ch}$ (cm/s)			$K_b$ (cm/s)		
3.05E-02	3.05E-06	9.64E-07	3.05E-07	9.64E-08	3.05E-08

					$\lambda_m$ (m)				
					431	767	1363	2424	4311
$K_{ch}$ (cm/s)	$K_f$ (cm/s)	$\alpha$ (°)	Sin ( $\alpha$ )	$T_{ch}$	Head at toe at the bottom of the blanket layer (m)				
	3.05E-03	90	1.00	10	3.07	3.08	3.08	3.08	3.08
	3.00E-03	80	0.98	10	3.08	3.09	3.09	3.09	3.09
3.05E-02	2.64E-03	60	0.87	10	3.10	3.10	3.10	3.10	3.10
	2.16E-03	45	0.71	10	3.11	3.11	3.11	3.11	3.11
	1.52E-03	30	0.50	10	3.11	3.12	3.12	3.12	3.12
	5.29E-04	10	0.17	10	3.12	3.12	3.12	3.12	3.12
Maximum variation in $h_{max}$					0.04	<b>0.05</b>	0.04	0.04	0.04

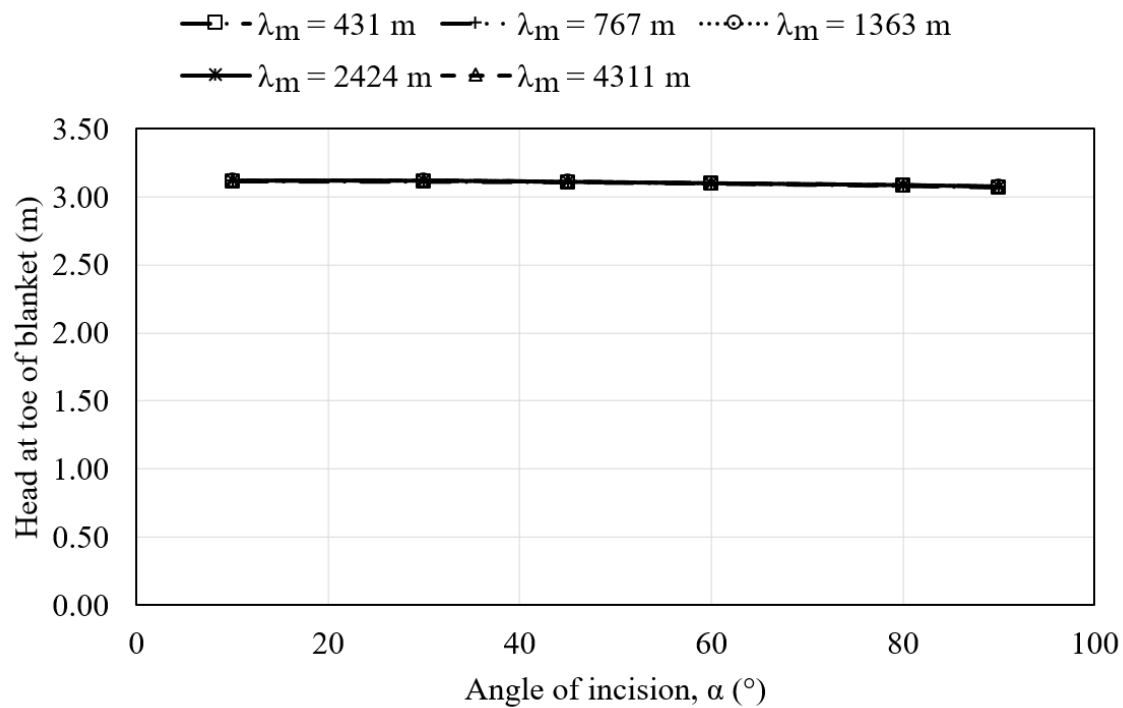


Figure D.6. Results from parametric analysis 6 corresponding to the combined parameter  $T_{ch}$ .

Table D.8. Parametric analysis 7 corresponding to the combined parameter  $T_{ch}$ 

					$t_f$ (m)					
					21.3					
$K_{ch}$ (cm/s)	$K_b$ (cm/s)	$t_{ch}$ (m)	$t_b$ (m)	$\lambda_m$ (m)						
3.05E-02	3.05E-07	6.1	3.0	1363						

					$RL$ (m)					
					0	3	152	305	457	610
$K_{ch}$ (cm/s)	$K_f$ (cm/s)	$\alpha$ (°)	Sin ( $\alpha$ )	$T_{ch}$	Head at toe at the bottom of the blanket layer (m)					
3.05E-02	3.05E-03	90	1.00	10	5.88	5.78	4.04	3.08	2.51	2.14
	3.00E-03	80	0.98	10	5.90	5.80	4.05	3.09	2.52	2.15
	2.64E-03	60	0.87	10	5.94	5.84	4.07	3.12	2.53	2.17
	2.16E-03	45	0.71	10	5.96	5.86	4.08	3.11	2.55	2.20
	1.52E-03	30	0.50	10	5.97	5.85	4.07	3.12	2.58	2.24
	5.29E-04	10	0.17	10	5.86	5.74	3.99	3.12	2.68	2.43
Maximum variation in $h_{max}$					0.11	0.12	0.09	0.04	0.17	<b>0.29</b>

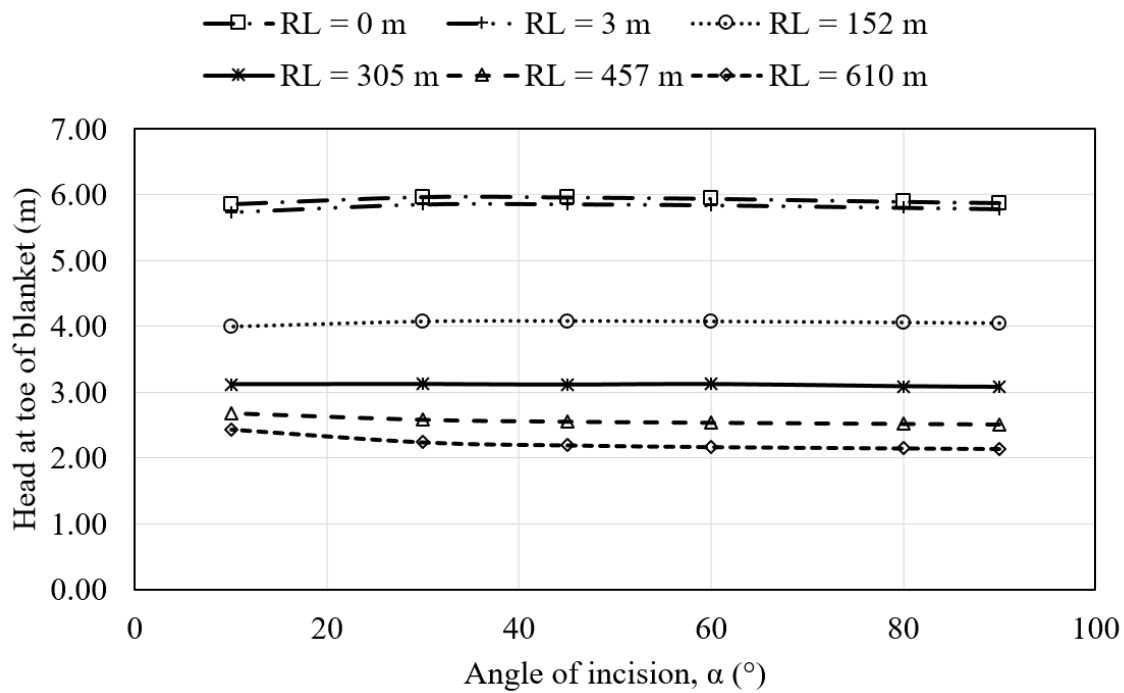


Figure D.7. Results from parametric analysis 7 corresponding to the combined parameter  $T_{ch}$ .

Table D.9. Parametric analysis 8 corresponding to the combined parameter  $T_{ch}$ 

$t_b$ (m)	$t_{ch}$ (m)	$t_f$ (m)	$RL$ (m)		
3.0	6.1	21.3	304.8		

$K_{ch}$ (cm/s)	$\lambda_m$ (m)				
	431	767	1363	2424	4311
	$K_b$ (cm/s)				
3.05E-02	3.05E-06	9.64E-07	3.05E-07	9.64E-08	3.05E-08
3.10E-02	3.10E-06	9.79E-07	3.10E-07	9.79E-08	3.10E-08
3.52E-02	3.52E-06	1.11E-06	3.52E-07	1.11E-07	3.52E-08
4.31E-02	4.31E-06	1.36E-06	4.31E-07	1.36E-07	4.31E-08
6.10E-02	6.10E-06	1.93E-06	6.10E-07	1.93E-07	6.10E-08
1.76E-01	1.76E-05	5.55E-06	1.76E-06	5.55E-07	1.76E-07

$K_{ch}$ (cm/s)	$K_f$ (cm/s)	$\alpha$ (°)	Sin ( $\alpha$ )	$T_{ch}$	$\lambda_m$ (m)				
					431	767	1363	2424	4311
					Head at toe at the bottom of the blanket layer (m)				
3.05E-02	3.05E-04	90	1.00	100	3.09	3.12	3.12	3.12	3.12
3.10E-02		80	0.98	100	3.10	3.13	3.13	3.13	3.13
3.52E-02		60	0.87	100	3.12	3.15	3.15	3.14	3.14
4.31E-02		45	0.71	100	3.11	3.15	3.15	3.15	3.14
6.10E-02		30	0.50	100	3.08	3.15	3.16	3.15	3.14
1.76E-01		10	0.17	100	2.84	3.03	3.13	3.14	3.13
Maximum variation in $h_{max}$					<b>0.28</b>	0.12	0.03	0.03	0.03

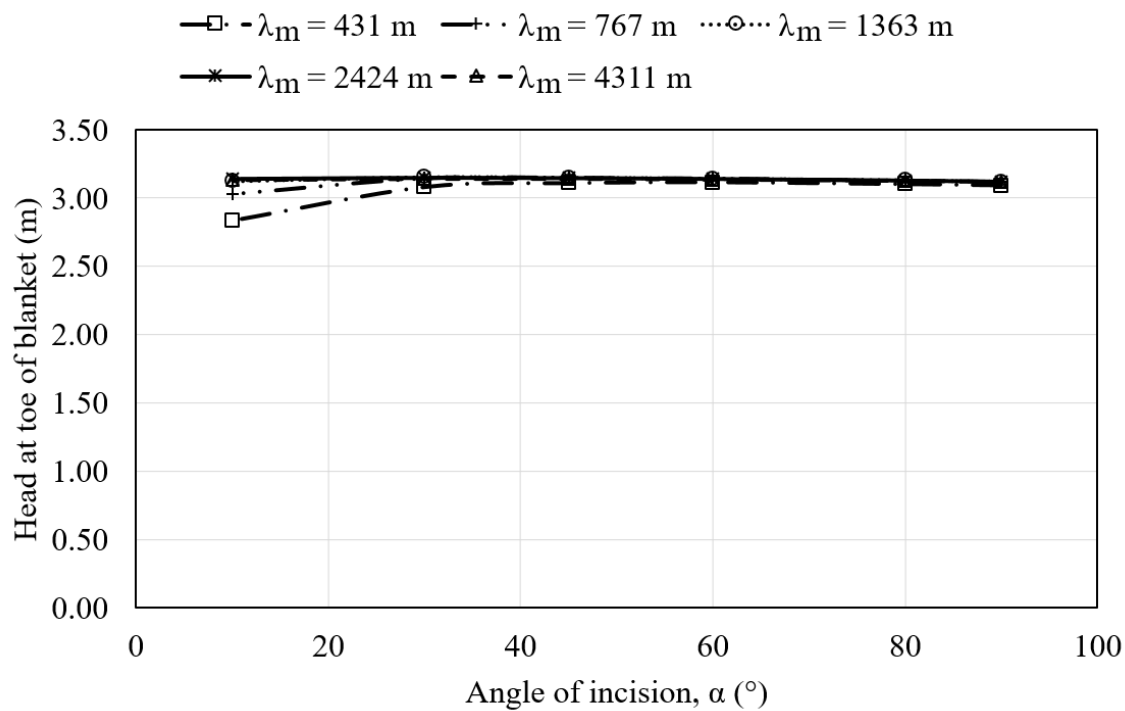


Figure D.8. Results from parametric analysis 8 corresponding to the combined parameter  $T_{ch}$ .

Table D.10. Parametric analysis 9 corresponding to the combined parameter  $T_{ch}$ 

					$t_f$ (m)					
					21.3					
$K_{ch}$ (cm/s)	$K_b$ (cm/s)	$t_{ch}$ (m)	$t_b$ (m)	$\lambda_m$ (m)						
3.05E-02	3.05E-07			1363						
3.10E-02	3.10E-07			1363						
3.52E-02	3.52E-07			1363						
4.31E-02	4.31E-07	6.1	3.0	1363						
6.10E-02	6.10E-07			1363						
1.76E-01	1.76E-06			1363						

					$RL$ (m)					
					0	3	152	305	457	610
$K_{ch}$ (cm/s)	$K_f$ (cm/s)	$\alpha$ (°)	$\sin(\alpha)$	$T_{ch}$	Head at toe at the bottom of the blanket layer (m)					
3.05E-02		90	1.00	100	5.98	5.91	4.07	3.12	2.67	2.47
3.10E-02		80	0.98	100	6.00	5.93	4.07	3.13	2.68	2.46
3.52E-02	3.05E-04	60	0.87	100	6.04	5.96	4.08	3.17	2.72	2.52
4.31E-02		45	0.71	100	6.05	5.97	4.05	3.15	2.77	2.61
6.10E-02		30	0.50	100	6.04	5.96	3.97	3.16	2.86	2.75
1.76E-01		10	0.17	100	5.76	5.64	3.55	3.13	3.05	3.04
Maximum variation in $h_{max}$					0.29	0.34	0.52	0.05	0.38	<b>0.58</b>

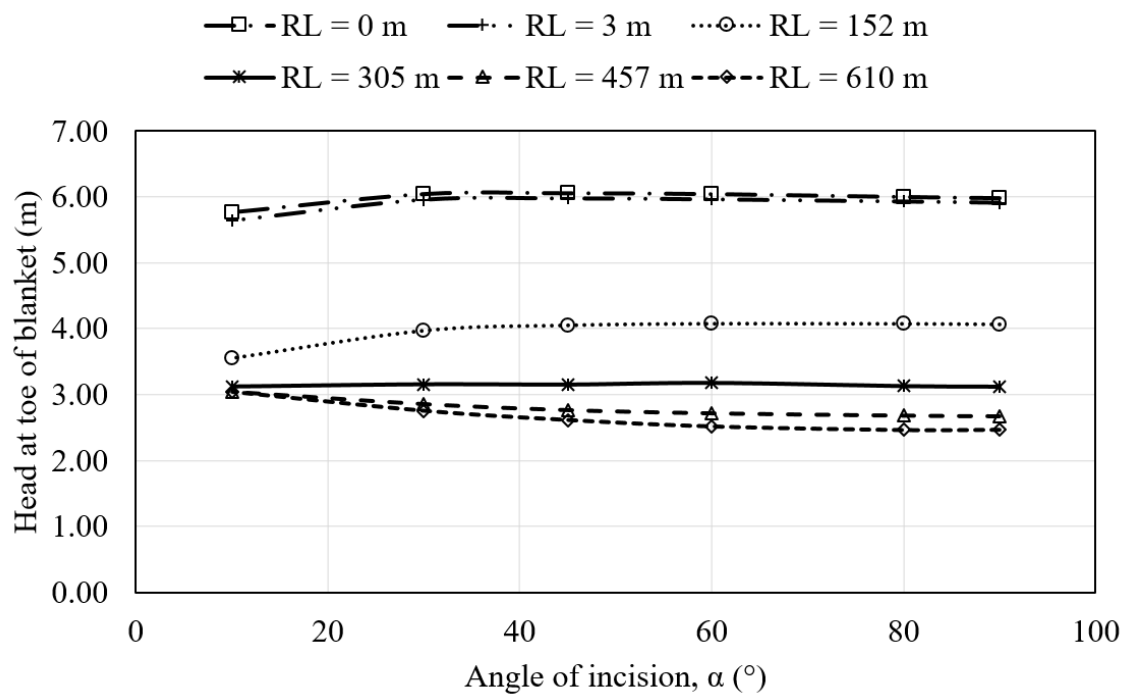


Figure D.9. Results from parametric analysis 9 corresponding to the combined parameter  $T_{ch}$ .



Table D.11. Parametric analysis 10 corresponding to the combined parameter  $\lambda_m$ 

$t_f$ (m)			$RL$ (m)				
21.3			304.8				
			$T_{ch}$				
			1	2	7	22	71
$K_{ch}$ (cm/s)	$\alpha$ (°)	Sin ( $\alpha$ )	$K_f$ (cm/s)				
3.05E-02			3.05E-02	9.64E-03	3.05E-03	9.64E-04	3.05E-04
2.36E-02			2.36E-02	7.47E-03	2.36E-03	7.47E-04	2.36E-04
1.68E-02	45	0.71	1.68E-02	5.30E-03	1.68E-03	5.30E-04	1.68E-04
9.91E-03			9.91E-03	3.13E-03	9.91E-04	3.13E-04	9.91E-05
3.05E-03			3.05E-03	9.64E-04	3.05E-04	9.64E-05	3.05E-05

					$T_{ch}$				
					1	2	7	22	71
$t_b$ (m)	$t_{ch}$ (m)	$K_{ch}$ (cm/s)	$K_b$ (cm/s)	$\lambda_m$ (m)	Head at toe at the bottom of the blanket layer (m)				
		3.05E-02	3.05E-06	431	3.10	3.10	3.11	3.11	3.11
		2.36E-02	2.36E-06	431	3.10	3.10	3.11	3.11	3.11
3.0	6.1	1.68E-02	1.68E-06	431	3.10	3.10	3.11	3.11	3.11
		9.91E-03	9.91E-07	431	3.10	3.10	3.11	3.11	3.11
		3.05E-03	3.05E-07	431	3.10	3.10	3.11	3.11	3.11
Maximum variation in $h_{max}$					0.00	0.00	0.00	0.00	<b>0.00</b>

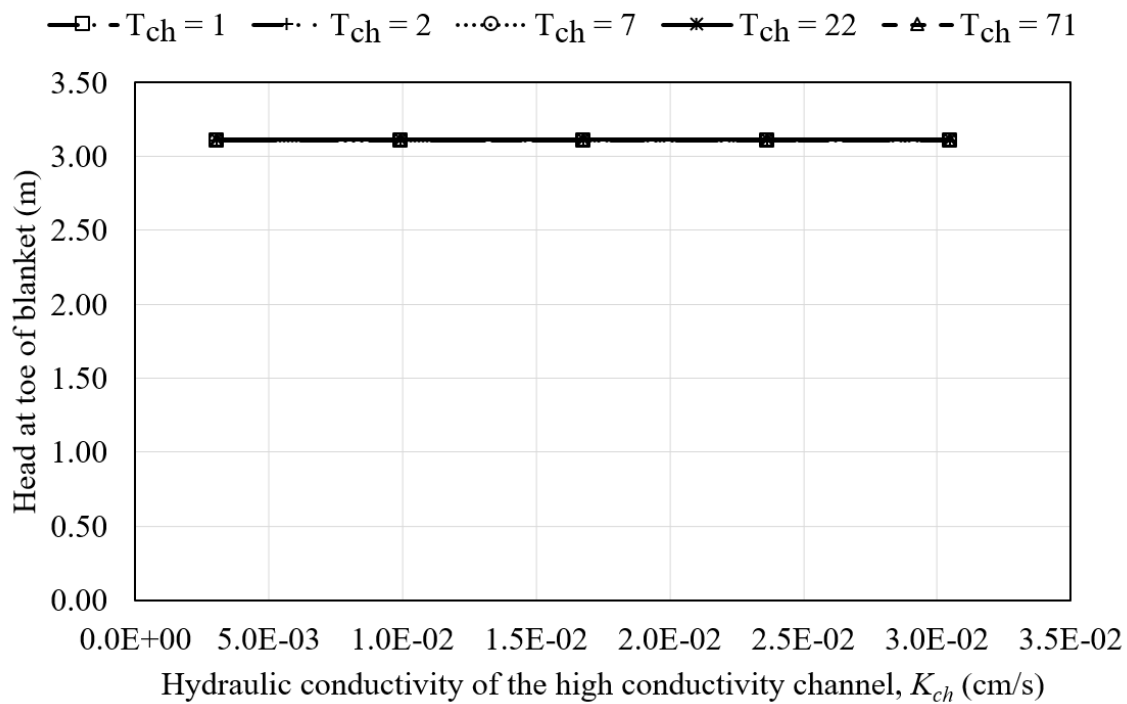


Figure D.10. Results from parametric analysis 10 corresponding to the combined parameter  $\lambda_m$ .



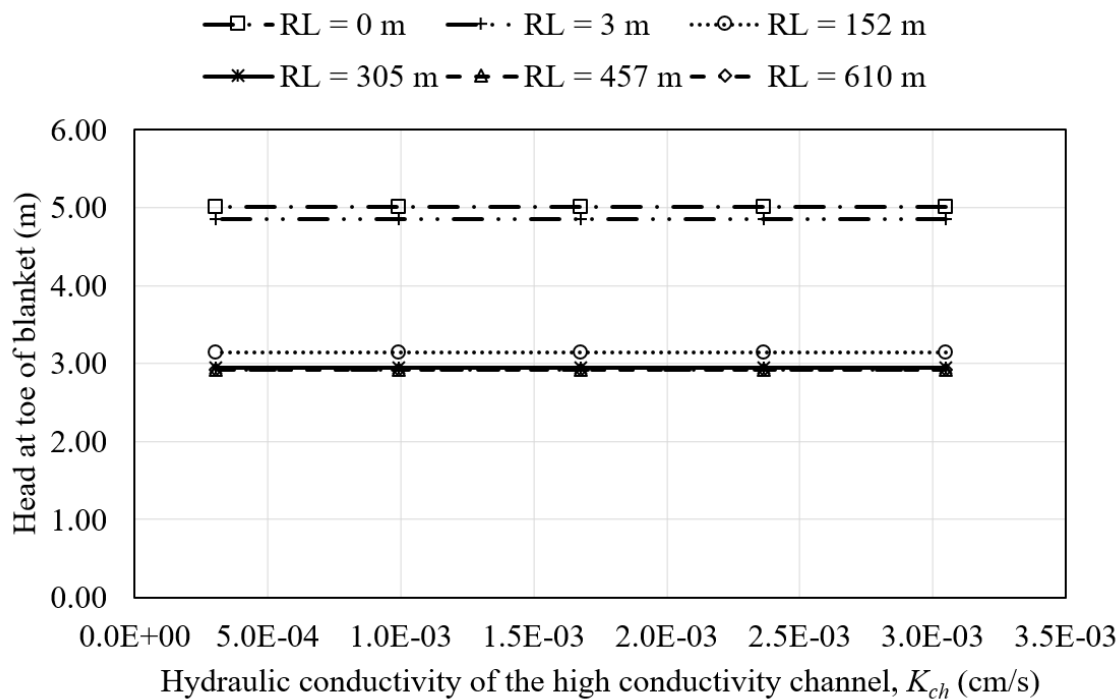


Figure D.11. Results from parametric analysis 11 corresponding to the combined parameter  $\lambda_m$ .

Table D.13. Parametric analysis 12 corresponding to the combined parameter  $\lambda_m$ 

$t_f$ (m)			$RL$ (m)				
21.3			304.8				

$K_{ch}$ (cm/s)	$\alpha$ (°)	Sin ( $\alpha$ )	$T_{ch}$				
			1	2	7	22	71
			$K_f$ (cm/s)				
3.05E-02			3.05E-02	9.64E-03	3.05E-03	9.64E-04	3.05E-04
2.03E-02			2.03E-02	6.43E-03	2.03E-03	6.43E-04	2.03E-04
1.52E-02	45	0.71	1.52E-02	4.82E-03	1.52E-03	4.82E-04	1.52E-04
1.02E-02			1.02E-02	3.21E-03	1.02E-03	3.21E-04	1.02E-04
7.62E-03			7.62E-03	2.41E-03	7.62E-04	2.41E-04	7.62E-05

$t_b$ (m)	$t_{ch}$ (m)	$K_{ch}$ (cm/s)	$K_b$ (cm/s)	$\lambda_m$ (m)	$T_{ch}$				
					1	2	7	22	71
					Head at toe at the bottom of the blanket layer (m)				
	1.5	3.05E-02		682	3.10	3.10	3.10	3.11	3.12
	2.3	2.03E-02		682	3.10	3.10	3.11	3.11	3.13
3.0	3.0	1.52E-02	3.05E-07	682	3.10	3.10	3.11	3.11	3.13
	4.6	1.02E-02		682	3.11	3.11	3.11	3.12	3.14
	6.1	7.62E-03		682	3.11	3.11	3.11	3.12	3.14
Maximum variation in $h_{\max}$					0.01	0.01	0.01	0.01	<b>0.02</b>

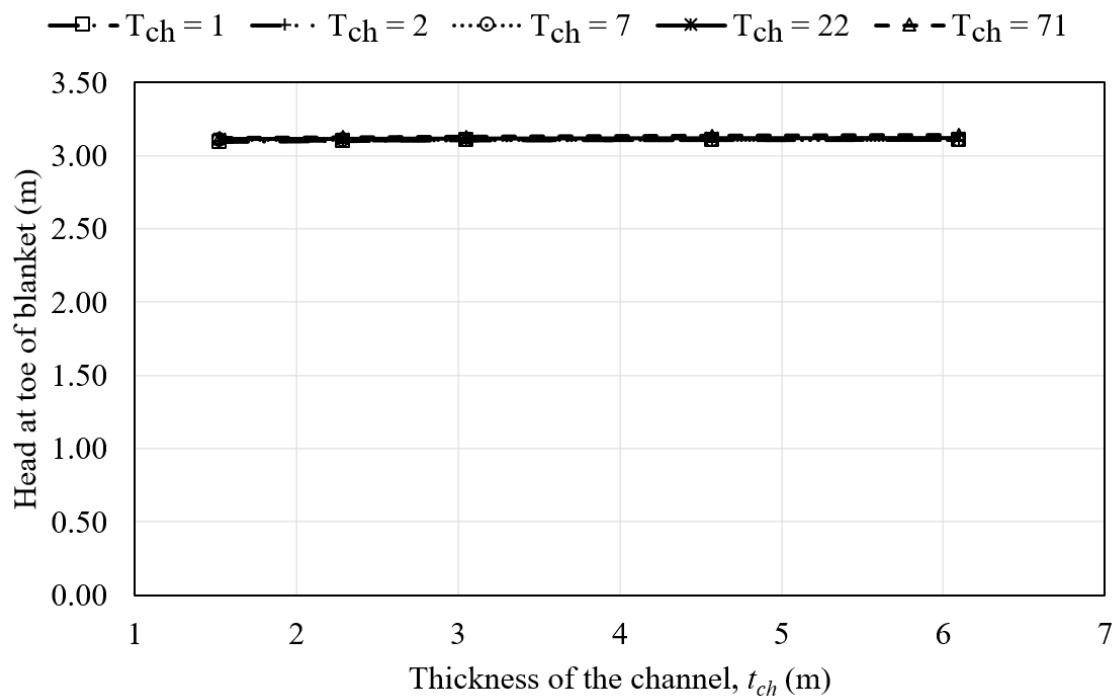


Figure D.12. Results from parametric analysis 12 corresponding to the combined parameter  $\lambda_m$ .

Table D.14. Parametric analysis 13 corresponding to the combined parameter  $\lambda_m$ 

$t_f$ (m)					
24.4					
$K_{ch}$ (cm/s)	$K_f$ (cm/s)	$\alpha$ (°)	Sin ( $\alpha$ )	$T_{ch}$	
3.05E-04	3.05E-03			7	
2.03E-04	2.03E-03			7	
1.52E-04	1.52E-03	45	0.71	7	
1.02E-04	1.02E-03			7	
8.71E-05	8.71E-04			7	

					$RL$ (m)					
					0	3	152	305	457	610
$t_b$ (m)	$t_{ch}$ (m)	$K_{ch}$ (cm/s)	$K_b$ (cm/s)	$\lambda_m$ (m)	Head at toe at the bottom of the blanket layer (m)					
3.0	1.5	3.05E-03	3.05E-07	216	5.57	5.43	3.75	3.08	2.82	2.72
	2.3	2.03E-03		216	5.54	5.40	3.69	3.08	2.87	2.80
	3.0	1.52E-03		216	5.52	5.38	3.65	3.07	2.89	2.83
	4.6	1.02E-03		216	5.50	5.35	3.58	3.06	2.92	2.88
	5.3	8.71E-04		216	5.48	5.35	3.56	3.06	2.92	2.89
	6.1	7.62E-04		216	5.48	5.34	3.54	3.05	2.93	2.89
Maximum variation in $h_{\max}$					0.09	0.09	<b>0.22</b>	0.03	0.10	0.17

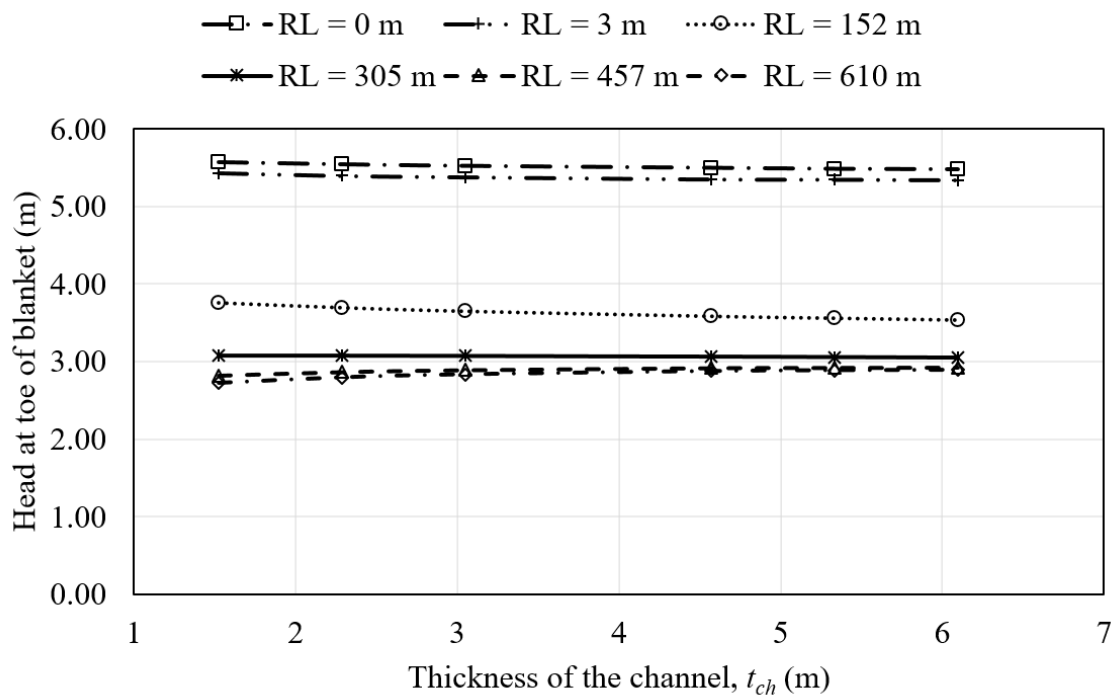


Figure D.13. Results from parametric analysis 13 corresponding to the combined parameter  $\lambda_m$ .



Table D.15. Parametric analysis 14 corresponding to the combined parameter  $\lambda_m$ 

$t_f$ (m)		$RL$ (m)	
21.3		304.8	

$K_{ch}$ (cm/s)	$\alpha$ (°)	Sin ( $\alpha$ )	$T_{ch}$				
			1	2	7	22	71
			$K_f$ (cm/s)				
3.05E-02			3.05E-02	9.64E-03	3.05E-03	9.64E-04	3.05E-04
1.71E-02			1.71E-02	5.42E-03	1.71E-03	5.42E-04	1.71E-04
9.64E-03	45	0.71	9.64E-03	3.05E-03	9.64E-04	3.05E-04	9.64E-05
5.42E-03			5.42E-03	1.71E-03	5.42E-04	1.71E-04	5.42E-05
3.05E-03			3.05E-03	9.64E-04	3.05E-04	9.64E-05	3.05E-05

$t_b$ (m)	$t_{ch}$ (m)	$K_{ch}$ (cm/s)	$K_b$ (cm/s)	$\lambda_m$ (m)	$T_{ch}$				
					1	2	7	22	71
					Head at toe at the bottom of the blanket layer (m)				
0.6		3.05E-02		610	3.10	3.10	3.10	3.10	3.12
1.1		1.71E-02		610	3.10	3.10	3.10	3.11	3.13
1.9	6.1	9.64E-03	3.05E-07	610	3.10	3.10	3.11	3.12	3.14
3.4		5.42E-03		610	3.11	3.11	3.11	3.12	3.14
6.1		3.05E-03		610	3.11	3.11	3.11	3.12	3.13
Maximum variation in $h_{max}$					0.01	0.01	0.01	0.02	<b>0.02</b>

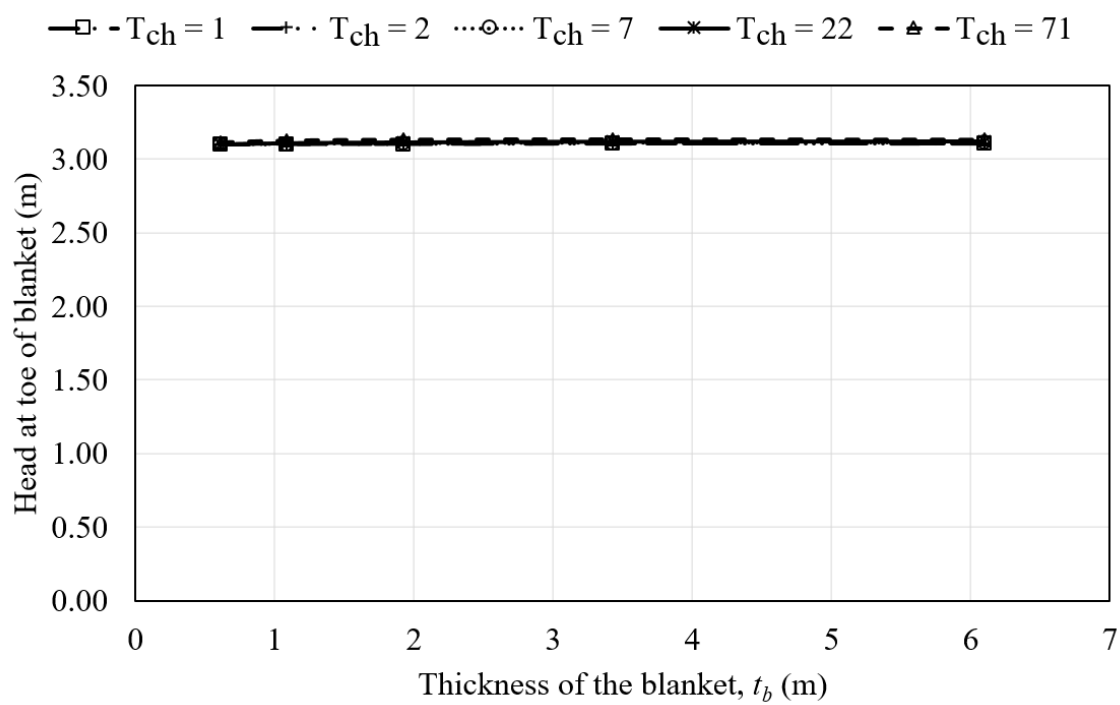


Figure D.14. Results from parametric analysis 14 corresponding to the combined parameter  $\lambda_m$ .

Table D.16. Parametric analysis 15 corresponding to the combined parameter  $\lambda_m$ 

					$t_f$ (m)					
					24.4					
$K_{ch}$ (cm/s)	$K_f$ (cm/s)	$\alpha$ (°)	Sin ( $\alpha$ )	$T_{ch}$						
3.05E-04	3.05E-02			71						
3.91E-04	3.91E-02			71						
5.62E-04	5.62E-02	45	0.71	71						
8.19E-04	8.19E-02			71						
1.16E-03	1.16E-01			71						
					$RL$ (m)					
					0	3	152	305	457	610
$t_b$ (m)	$t_{ch}$ (m)	$K_{ch}$ (cm/s)	$K_b$ (cm/s)	$\lambda_m$ (m)	Head at toe at the bottom of the blanket layer (m)					
6.1		3.05E-02		1363	5.99	5.89	3.99	3.12	2.71	2.53
4.8		3.91E-02		1363	5.99	5.90	4.00	3.11	2.70	2.51
3.3	3.0	5.62E-02	3.05E-07	1363	5.99	5.90	4.01	3.11	2.67	2.47
2.3		8.19E-02		1363	6.00	5.91	4.03	3.11	2.65	2.43
1.6		1.16E-01		1363	6.00	5.91	4.04	3.11	2.63	2.39
1.2		1.50E-01		1363	6.01	5.92	4.05	3.11	2.61	2.36
Maximum variation in $h_{max}$					0.02	0.03	0.05	0.01	0.10	<b>0.17</b>

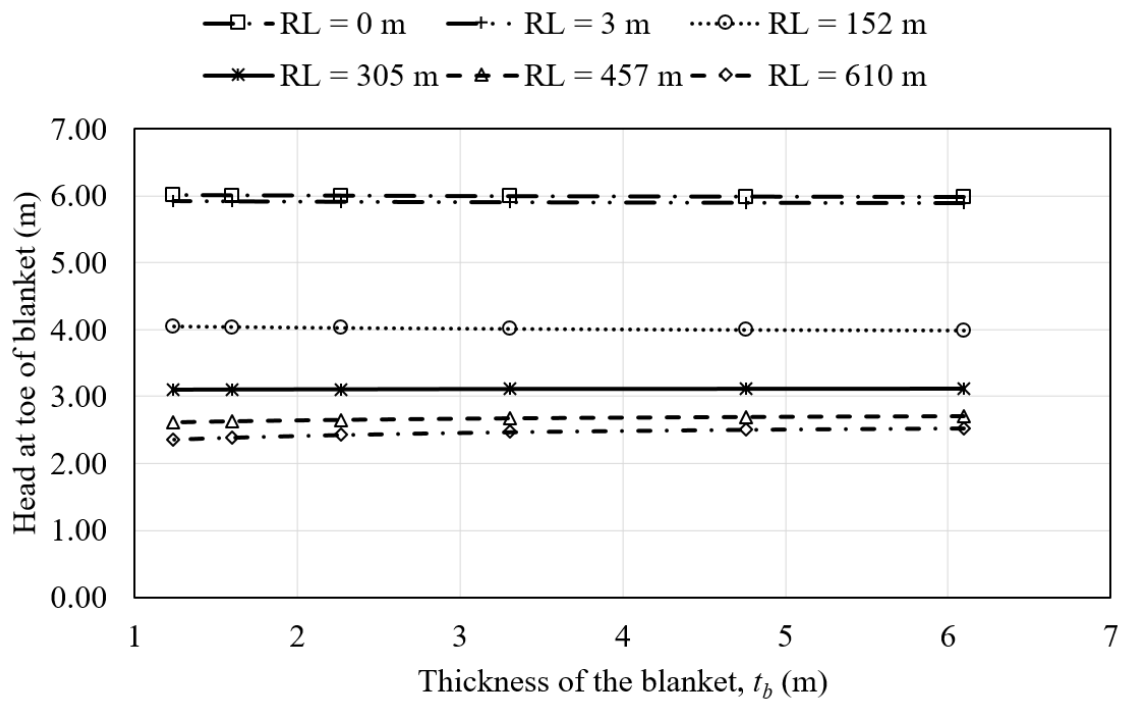


Figure D.15. Results from parametric analysis 15 corresponding to the combined parameter  $\lambda_m$ .

Table D.17. Parametric analysis 16 corresponding to the combined parameter  $\lambda_m$ 

$t_f$ (m)		$RL$ (m)								
21.3		304.8								
		$K_f$ (cm/s)		3.05E-04						
		$K_{ch}$ (cm/s)		3.05E-02						
		$\alpha$ (°)		90	80	60	45	30	10	
		Sin ( $\alpha$ )		1.00	0.98	0.87	0.71	0.50	0.17	
		$T_{ch}$		100	98	87	71	50	17	
$t_b$ (m)	$t_{ch}$ (m)	$K_{ch}$ (cm/s)	$K_b$ (cm/s)	$\lambda_m$ (m)	Head at toe at the bottom of the blanket layer (m)					
	1.5		3.05E-07	682	3.09	3.10	3.12	3.12	3.13	3.12
	3.0		6.10E-07	682	3.11	3.11	3.13	3.13	3.13	3.11
3.0	4.6	3.05E-02	9.14E-07	682	3.11	3.12	3.14	3.14	3.13	3.10
	5.5		1.10E-06	682	3.12	3.13	3.14	3.14	3.13	3.09
	6.1		1.22E-06	682	3.12	3.13	3.14	3.14	3.14	3.09
Maximum variation in $h_{\max}$					0.03	0.03	0.03	0.02	<b>0.01</b>	<b>0.04</b>

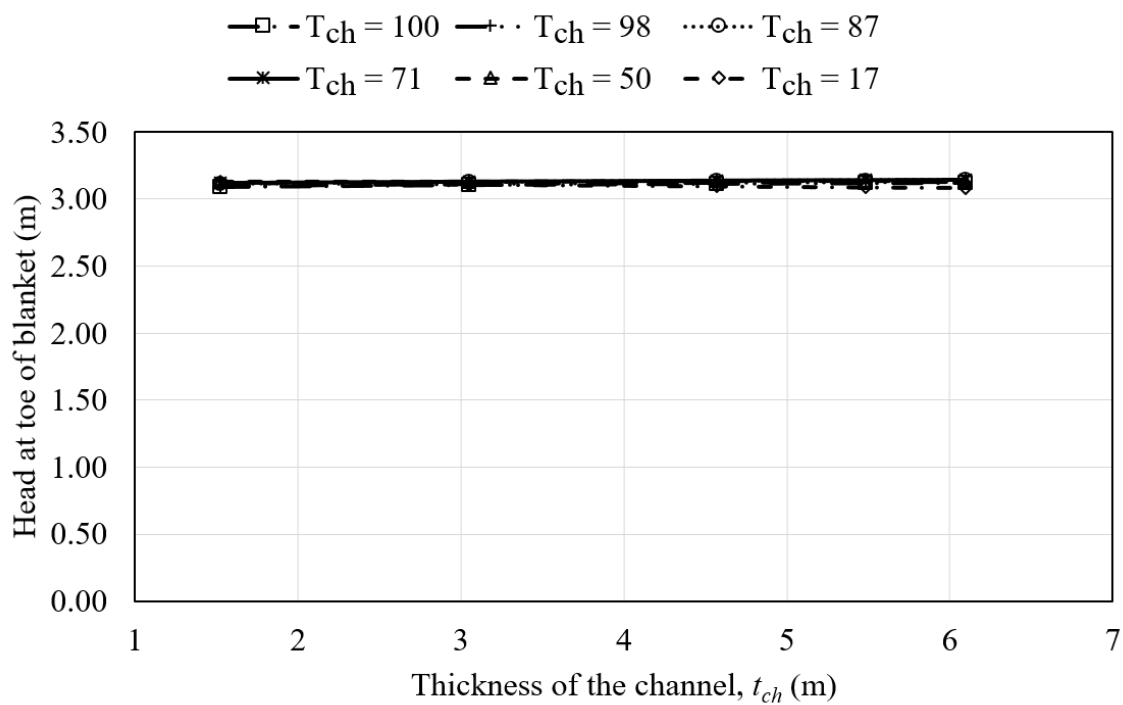


Figure D.16. Results from parametric analysis 16 corresponding to the combined parameter  $\lambda_m$ .

Table D.18. Parametric analysis 17 corresponding to the combined parameter  $\lambda_m$ 

$t_f$ (m)										
24.4										
$K_{ch}$ (cm/s)		$K_f$ (cm/s)		$\alpha$ (°)		Sin ( $\alpha$ )		$T_{ch}$		
1.00E-03		1.00E-05		45		0.71		71		
$RL$ (m)										
					0	3	152	305	457	610
$t_b$ (m)	$t_{ch}$ (m)	$K_{ch}$ (cm/s)	$K_b$ (cm/s)	$\lambda_m$ (m)	Head at toe at the bottom of the blanket layer (m)					
3.0	1.5	3.05E-02	3.05E-06	216	5.07	4.94	3.11	2.98	2.98	2.98
	2.3		4.57E-06	216	5.06	4.94	3.07	2.97	2.98	2.98
	3.0		6.10E-06	216	5.08	4.95	3.06	2.97	2.97	2.98
	4.6		9.14E-06	216	5.12	4.98	3.05	2.96	2.97	2.98
	5.3		1.07E-05	216	5.12	5.00	3.06	2.96	2.97	2.97
	6.1		1.22E-05	216	5.14	5.01	3.06	2.96	2.97	2.98
Maximum variation in $h_{max}$					<b>0.07</b>	0.07	0.05	0.03	0.01	0.01

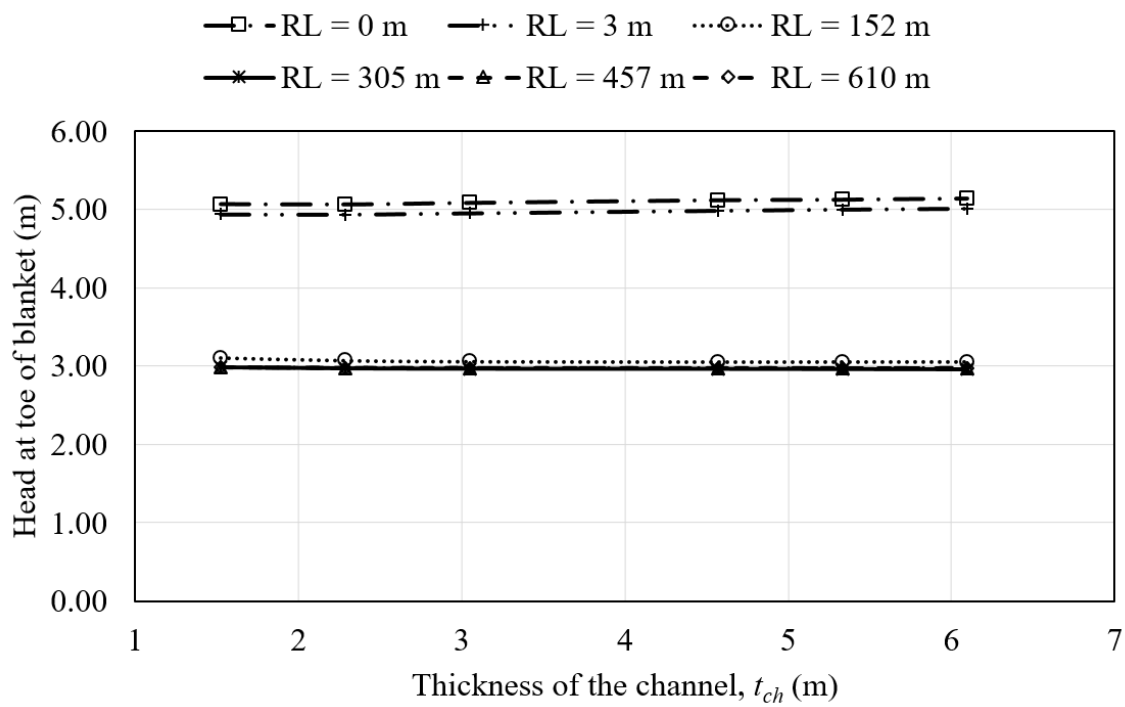


Figure D.17. Results from parametric analysis 17 corresponding to the combined parameter  $\lambda_m$ .



Table D.19. Parametric analysis 18 corresponding to the combined parameter  $\lambda_m$ 

$t_f$ (m)		$RL$ (m)								
21.3		304.8								
		$K_f$ (cm/s)		3.05E-04						
		$K_{ch}$ (cm/s)		3.05E-02						
		$\alpha$ (°)	90	80	60	45	30	10		
		Sin ( $\alpha$ )	1.00	0.98	0.87	0.71	0.50	0.17		
		$T_{ch}$	100	98	87	71	50	17		
$t_b$ (m)	$t_{ch}$ (m)	$K_{ch}$ (cm/s)	$K_b$ (cm/s)	$\lambda_m$ (m)	Head at toe at the bottom of the blanket layer (m)					
1.5			3.05E-07	964	3.13	3.13	3.14	3.14	3.14	3.10
2.4			4.88E-07	964	3.12	3.13	3.14	3.14	3.14	3.11
3.4	6.1	3.05E-02	6.71E-07	964	3.12	3.13	3.14	3.14	3.14	3.11
4.3			8.53E-07	964	3.12	3.13	3.14	3.14	3.14	3.11
5.2			1.04E-06	964	3.11	3.12	3.14	3.14	3.14	3.14
6.1			1.22E-06	964	3.11	3.11	3.13	3.13	3.13	3.11
Maximum variation in $h_{\max}$					<b>0.02</b>	0.02	0.02	0.01	0.01	0.01

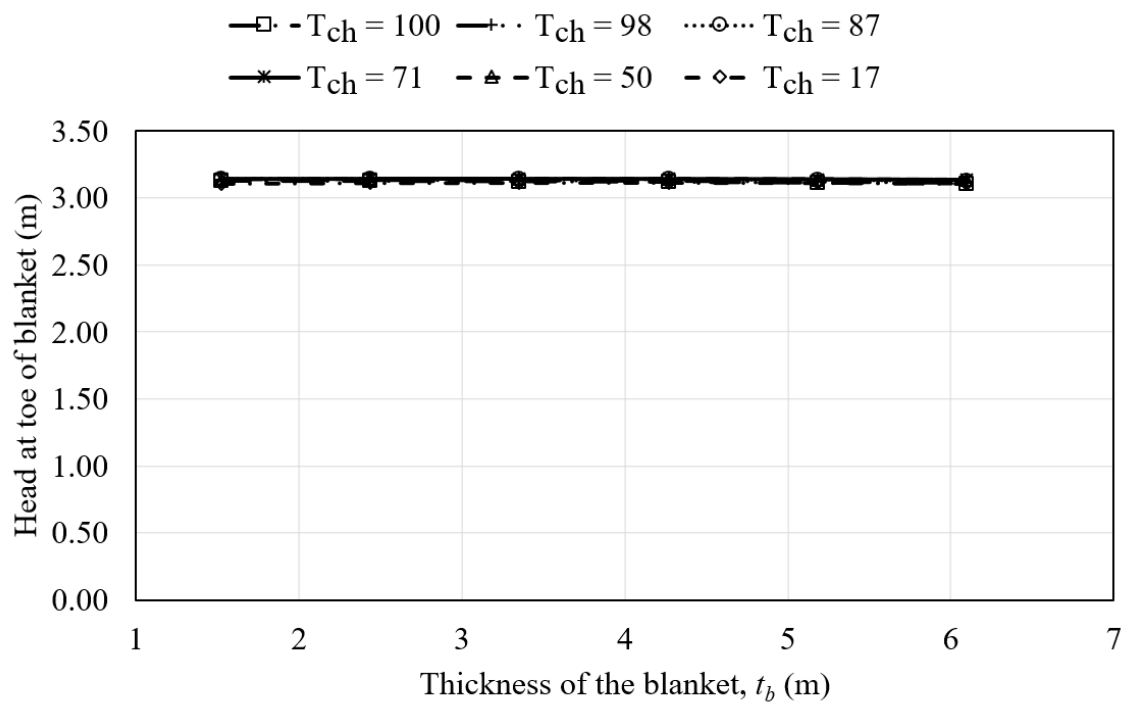


Figure D.18. Results from parametric analysis 18 corresponding to the combined parameter  $\lambda_m$ .

Table D.20. Parametric analysis 19 corresponding to the combined parameter  $\lambda_m$ 

$t_f$ (m)										
24.4										
$K_{ch}$ (cm/s)		$K_f$ (cm/s)		$\alpha$ (°)		Sin ( $\alpha$ )		$T_{ch}$		
1.00E-03		1.00E-05		45		0.71		71		
$RL$ (m)										
					0	3	152	305	457	610
$t_b$ (m)	$t_{ch}$ (m)	$K_{ch}$ (cm/s)	$K_b$ (cm/s)	$\lambda_m$ (m)	Head at toe at the bottom of the blanket layer (m)					
1.5			3.05E-07	682	5.90	5.80	3.86	3.12	2.84	2.90
2.4			4.88E-07	682	5.88	5.78	3.81	3.12	2.89	2.82
3.4	3.0	3.05E-02	6.71E-07	682	5.86	5.76	3.78	3.15	2.92	2.86
4.3			8.53E-07	682	5.85	5.74	3.76	3.12	2.94	2.88
5.2			1.04E-06	682	5.84	5.73	3.74	3.12	2.95	2.90
6.1			1.22E-06	682	5.83	5.73	3.71	3.12	2.96	2.91
Maximum variation in $h_{max}$					0.07	0.08	<b>0.14</b>	0.04	0.12	0.10

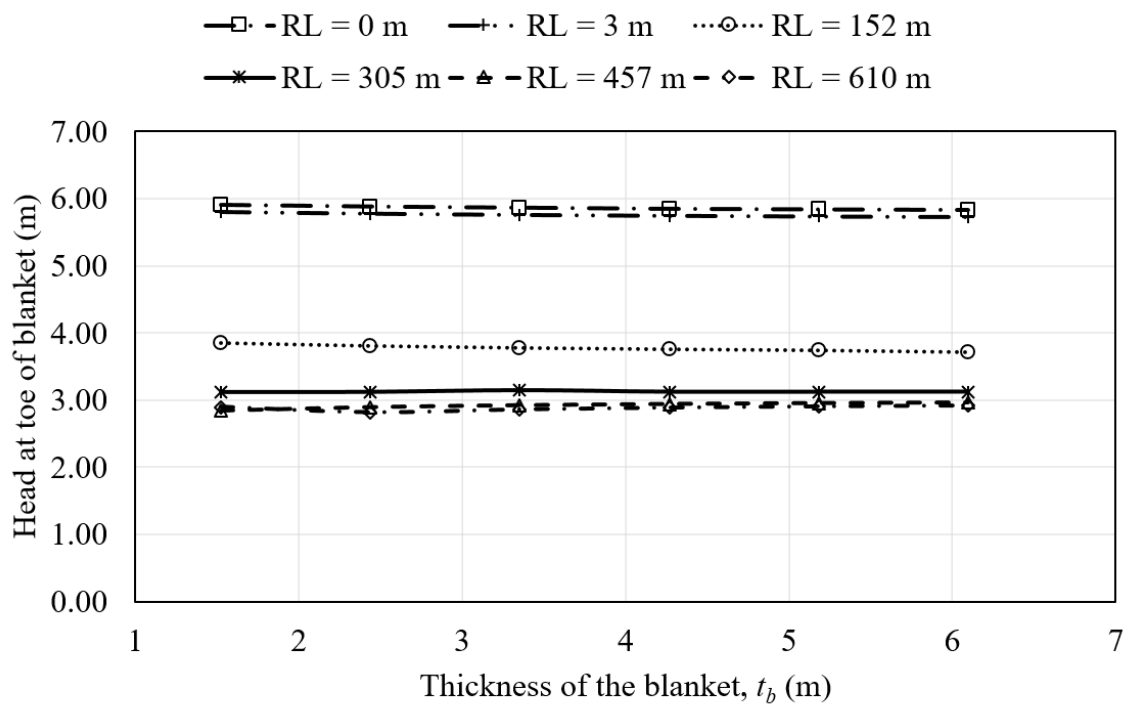


Figure D.19. Results from parametric analysis 19 corresponding to the combined parameter  $\lambda_m$ .

Table D.21. Parametric analysis 20 corresponding to the combined parameter  $\lambda_m$ 

$t_f$ (m)		$RL$ (m)								
21.3		304.8								
		$K_f$ (cm/s)		3.05E-04						
		$K_{ch}$ (cm/s)		3.05E-02						
		$\alpha$ (°)	90	80	60	45	30	10		
		Sin ( $\alpha$ )	1.00	0.98	0.87	0.71	0.50	0.17		
		$T_{ch}$	100	98	87	71	50	17		
$t_b$ (m)	$t_{ch}$ (m)	$K_{ch}$ (cm/s)	$K_b$ (cm/s)	$\lambda_m$ (m)	Head at toe at the bottom of the blanket layer (m)					
1.5	6.1	3.05E-02	3.05E-07	964	3.12	3.13	3.14	3.14	3.13	3.10
1.7	5.5			964	3.12	3.13	3.14	3.14	3.13	3.11
2.0	4.6			964	3.11	3.12	3.13	3.14	3.13	3.11
2.5	3.7			964	3.11	3.12	3.13	3.13	3.13	3.12
3.0	3.0			964	3.11	3.12	3.13	3.13	3.13	3.12
6.1	1.5			964	3.09	3.10	3.12	3.12	3.13	3.13
Maximum variation in $h_{max}$					<b>0.03</b>	0.03	0.02	0.02	0.01	0.02

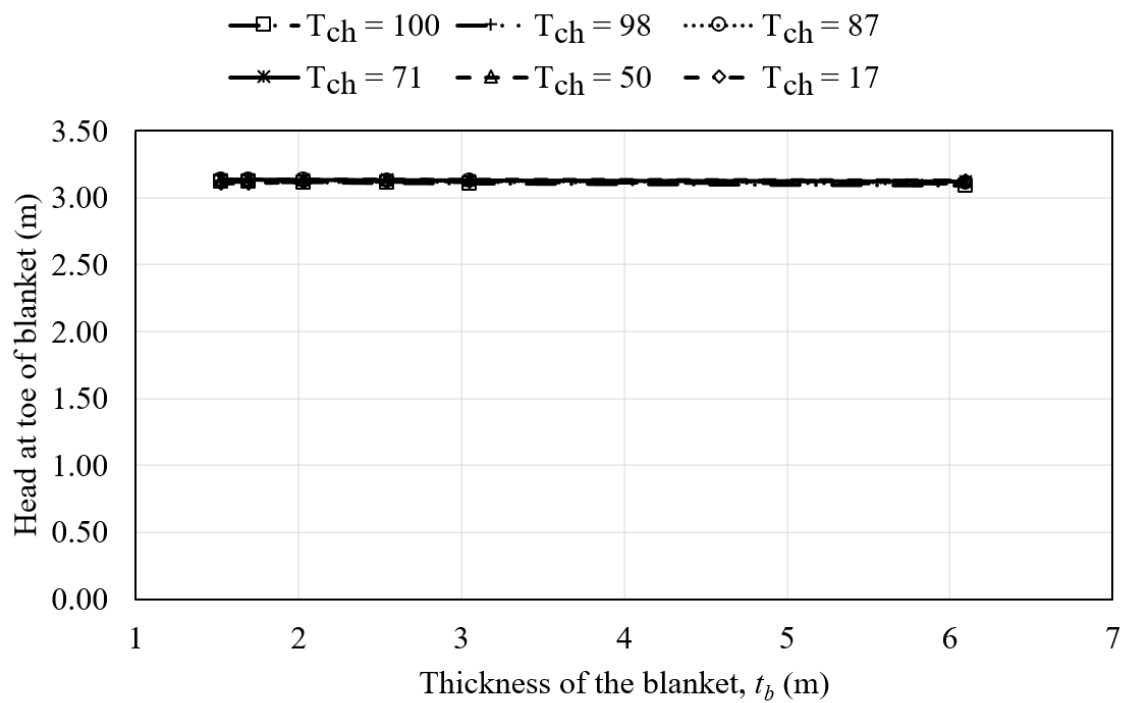


Figure D.20. Results from parametric analysis 20 corresponding to the combined parameter  $\lambda_m$ .

Table D.22. Parametric analysis 21 corresponding to the combined parameter  $\lambda_m$ 

$t_f$ (m)										
27.4										
$K_{ch}$ (cm/s)	$K_f$ (cm/s)	$\alpha$ (°)	Sin ( $\alpha$ )	$T_{ch}$						
1.00E-03	1.00E-05	45	0.71	71						
$RL$ (m)										
					0	3	152	305	457	610
$t_b$ (m)	$t_{ch}$ (m)	$K_{ch}$ (cm/s)	$K_b$ (cm/s)	$\lambda_m$ (m)	Head at toe at the bottom of the blanket layer (m)					
0.6	6.1			610	5.91	5.84	3.87	3.09	2.79	2.67
0.7	5.5			610	5.91	5.84	3.87	3.10	2.80	2.67
0.8	4.6	3.05E-02	3.05E-07	610	5.91	5.82	3.86	3.10	2.80	2.69
1.0	3.7			610	5.89	5.79	3.84	3.10	2.82	2.71
1.2	3.0			610	5.87	5.77	3.82	3.10	2.83	2.73
2.4	1.5			610	5.80	5.69	3.79	3.10	2.84	2.75
Maximum variation in $h_{max}$					0.11	<b>0.15</b>	0.08	0.01	0.05	0.08

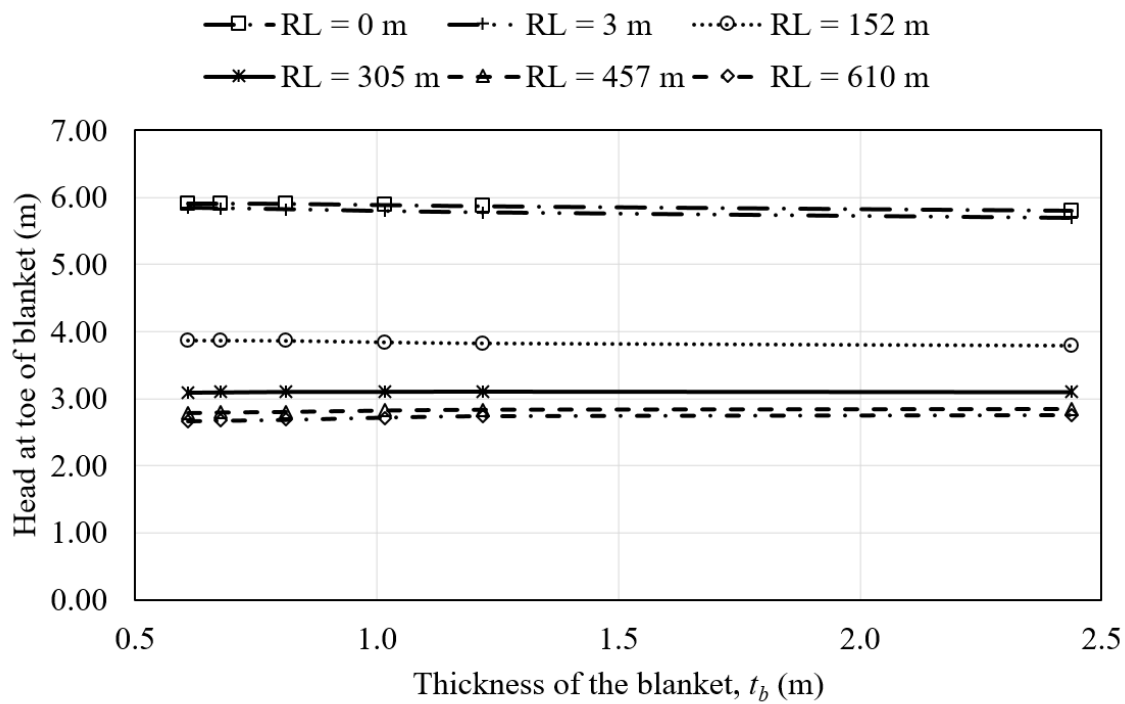


Figure D.21. Results from parametric analysis 21 corresponding to the combined parameter  $\lambda_m$ .



Table D.23. Parametric analysis 22 corresponding to the combined parameter  $\lambda_m$ 

$t_f$ (m)		$RL$ (m)								
21.3		304.8								
		$K_f$ (cm/s)		3.05E-04						
		$K_{ch}$ (cm/s)		3.05E-02						
		$\alpha$ (°)		90	80	60	45	30	10	
		Sin ( $\alpha$ )		1.00	0.98	0.87	0.71	0.50	0.17	
		$T_{ch}$		100	98	87	71	50	17	
$t_b$ (m)	$t_{ch}$ (m)	$K_{ch}$ (cm/s)	$K_b$ (cm/s)	$\lambda_m$ (m)	Head at toe at the bottom of the blanket layer (m)					
1.5	6.1	3.05E-02	3.05E-07	964	3.12	3.13	3.14	3.14	3.13	3.10
1.7	5.5			964	3.12	3.13	3.14	3.14	3.13	3.11
2.0	4.6			964	3.11	3.12	3.13	3.14	3.13	3.11
2.5	3.7			964	3.11	3.12	3.13	3.13	3.13	3.12
3.0	3.0			964	3.11	3.12	3.13	3.13	3.13	3.12
6.1	1.5			964	3.09	3.10	3.12	3.12	3.13	3.13
Maximum variation in $h_{max}$					<b>0.03</b>	0.03	0.02	0.02	0.01	0.02

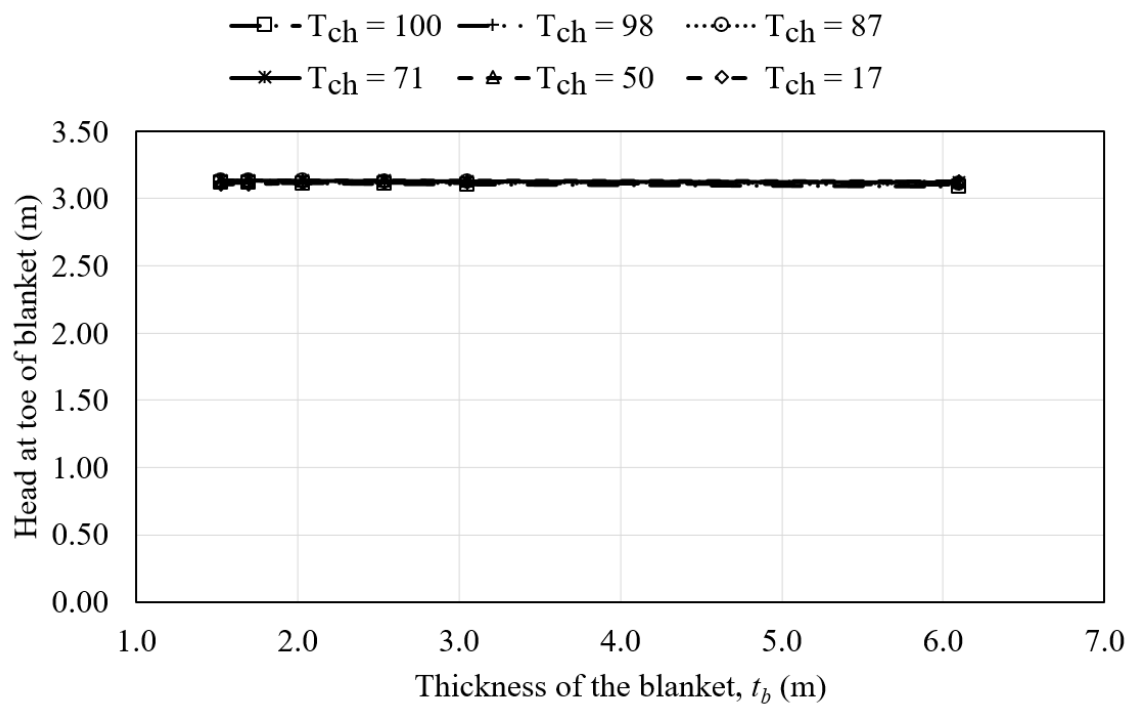


Figure D.22. Results from parametric analysis 22 corresponding to the combined parameter  $\lambda_m$ .

## APPENDIX E

Appendix E provides additional data corresponding to the research performed as part of Chapter 6. The figures and tables presented herein are not part of the research case study presented in Chapter 6 but they do correspond to the additional curvature models that were performed as a comparison with Benjasupattananan (2013) method as presented in Chapter 6. These models can be used to assess the underseepage reliability in high-conductivity channel that correspond or are in between a  $Dc = 30^\circ$  and a  $Dc = 60^\circ$ .

Figure E.1 presents the curvature-channel model used for a  $Dc = 30^\circ$  with a high conductivity channel with  $\alpha = 45^\circ$ ; the corresponding parameters and results for the curvature model are presented as Table E.1 and Figure E.2. Figure E.3 presents the curvature-channel model used for a  $Dc = 30^\circ$  with a high conductivity channel with  $\alpha = 90^\circ$ ; the corresponding parameters and results for the curvature model are presented as Table E.2 and Figure E.4. Figure E.5 presents the curvature-channel model used for a  $Dc = 60^\circ$  with a high conductivity channel with  $\alpha = 45^\circ$ ; the corresponding parameters and results for the curvature model are presented as Table E.3 and Figure E.6. Figure E.7 presents the curvature-channel model used for a  $Dc = 60^\circ$  with a high conductivity channel with  $\alpha = 90^\circ$ ; the corresponding parameters and results for the curvature model are presented as Table E.4 and Figure E.8.

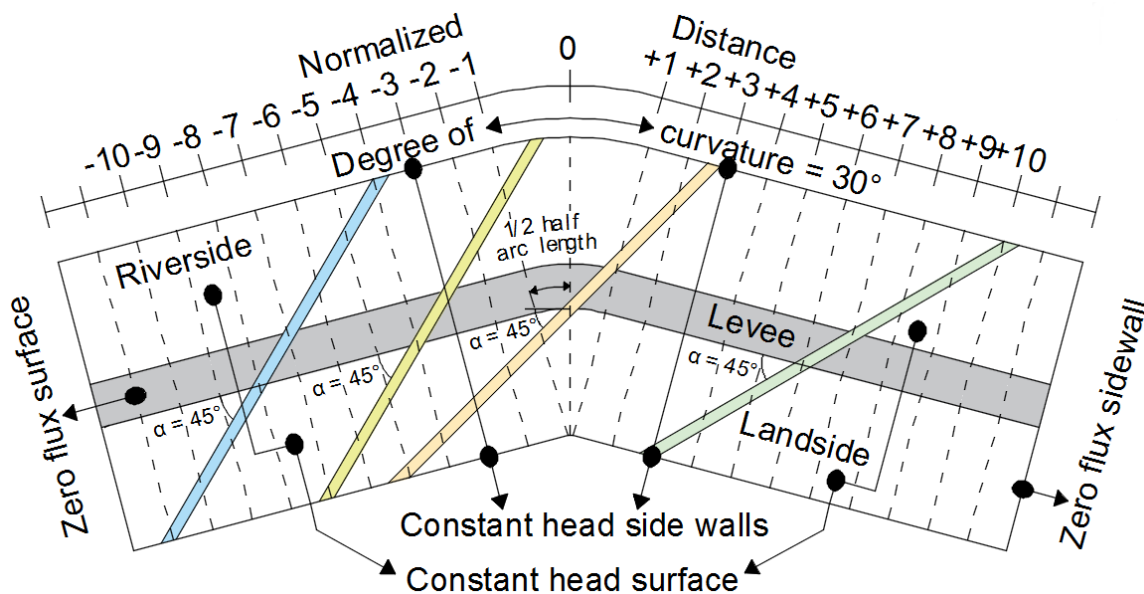


Figure E.1. Schematic top view of the curvature model used for  $D_c = 30^\circ$  and  $\alpha = 45^\circ$  showing channel features at  $ND = -8, -4, 0, +6$ .

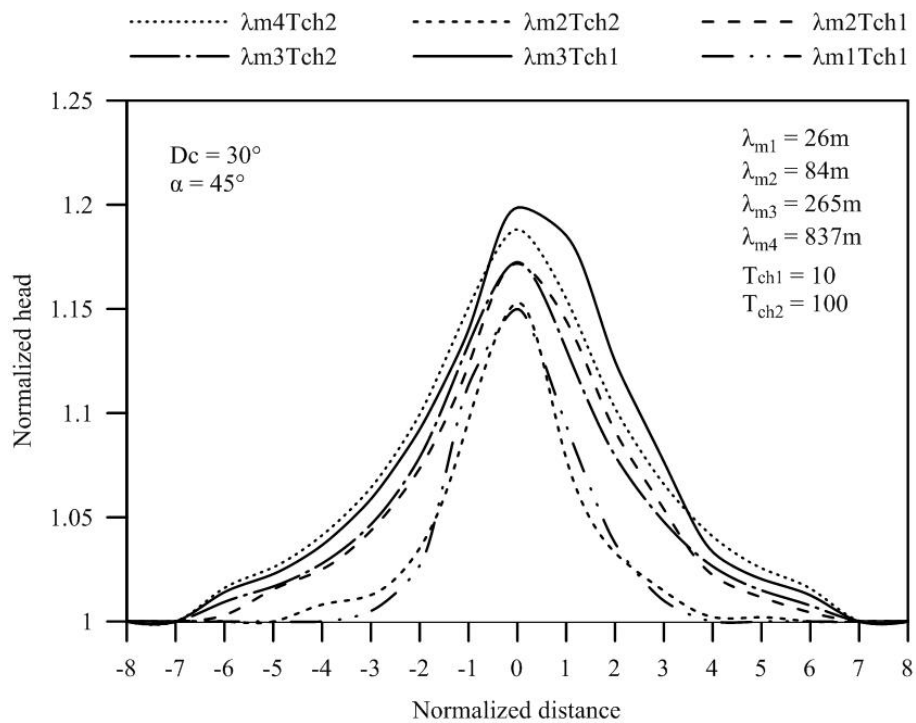


Figure E.2. Results for the curvature model with  $D_c = 30^\circ$  and  $\alpha = 45^\circ$ .

Table E.1. Parameters and results for the curvature model with  $D_c = 30^\circ$  and  $\alpha = 45^\circ$ 

Curvature multiplier for $D_c = 30^\circ$ with $\alpha = 45^\circ$						
$K_f = 1E-05$ m/s, $t_b = 2$ m, $t_{ch} = 3.5$ m, $t_f = 32$ m, $w_{ch} = 10$ m, $RL = 200$ m						
Stage	$\lambda_{m_1} T_{ch_1}$	$\lambda_{m_2} T_{ch_1}$	$\lambda_{m_3} T_{ch_1}$	$\lambda_{m_2} T_{ch_2}$	$\lambda_{m_3} T_{ch_2}$	$\lambda_{m_4} T_{ch_2}$
$K_b$ (m/s)	1.00E-06	1.00E-07	1.00E-08	1.00E-06	1.00E-07	1.00E-08
$K_{ch}$ (m/s)	1.00E-04	1.00E-04	1.00E-04	1.00E-03	1.00E-03	1.00E-03
$\lambda_m$ (m)	26.5	83.7	264.6	83.7	264.6	836.7
$T_{ch}$	10	10	10	100	100	100
$\lambda$ (m)	25.3	80.0	253.0	25.3	80.0	253.0
Normalized distance	Head at top of channel (m)					
-8	1	1	1	1	1	1
-7	1	1	1	1	1	1
-6	1	1	1	1	1	1
-5	1	1	1	1	1	1
-4	1	1	1	1	1	1
-3	1.01	1.04	1.06	1.01	1.05	1.06
-2	1.03	1.07	1.09	1.04	1.08	1.10
-1	1.11	1.12	1.14	1.10	1.13	1.15
0	1.15	1.17	1.20	1.15	1.17	1.19
1	1.09	1.14	1.19	1.08	1.13	1.16
2	1.04	1.09	1.12	1.03	1.08	1.10
3	1.01	1.05	1.08	1.01	1.05	1.07
4	1	1	1	1	1	1
5	1	1	1	1	1	1
6	1	1	1	1	1	1
7	1	1	1	1	1	1
8	1	1	1	1	1	1

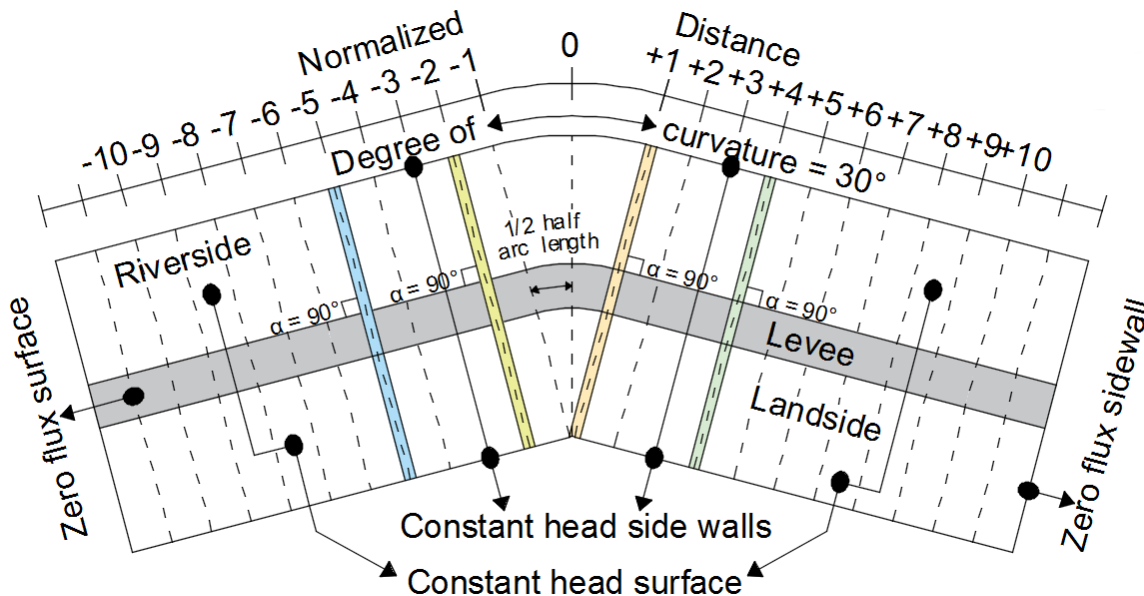


Figure E.3. Schematic top view of the curvature model used for  $D_c = 30^\circ$  and  $\alpha = 90^\circ$  showing channel features at  $ND = -5, -2, +1 +4$ .

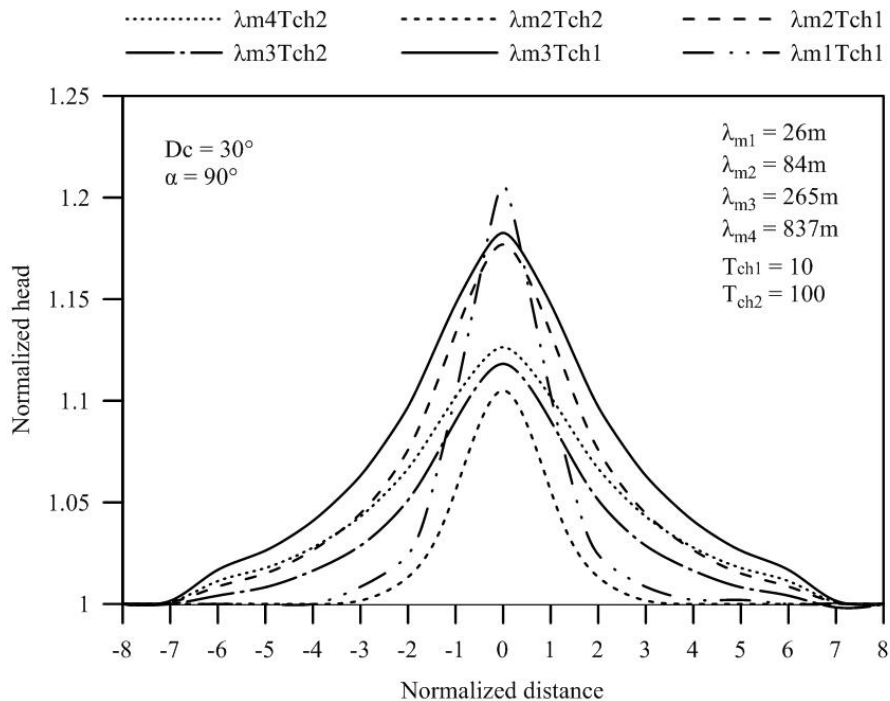


Figure E.4. Results for the curvature model with  $D_c = 30^\circ$  and  $\alpha = 90^\circ$ .

Table E.2. Parameters and results for the curvature model with  $Dc = 30^\circ$  and  $\alpha = 90^\circ$ 

Curvature multiplier for $Dc = 30^\circ$ with $\alpha = 90^\circ$						
$K_f = 1E-05$ m/s, $t_b = 2$ m, $t_{ch} = 3.5$ m, $t_f = 32$ m, $w_{ch} = 10$ m, $RL = 200$ m						
Stage	$\lambda_{m1}T_{ch1}$	$\lambda_{m2}T_{ch1}$	$\lambda_{m3}T_{ch1}$	$\lambda_{m2}T_{ch2}$	$\lambda_{m3}T_{ch2}$	$\lambda_{m4}T_{ch2}$
$K_b$ (m/s)	1.00E-06	1.00E-07	1.00E-08	1.00E-06	1.00E-07	1.00E-08
$K_{ch}$ (m/s)	1.00E-04	1.00E-04	1.00E-04	1.00E-03	1.00E-03	1.00E-03
$\lambda_m$ (m)	26.5	83.7	264.6	83.7	264.6	836.7
$T_{ch}$	10	10	10	100	100	100
$\lambda$ (m)	25.3	80.0	253.0	25.3	80.0	253.0
Normalized distance	Head at top of channel (m)					
-8	1	1	1	1	1	1
-7	1	1	1	1	1	1
-6	1	1	1	1	1	1
-5	1	1	1	1	1	1
-4	1	1	1	1	1	1
-3	1	1	1.1	1	1	1
-2	1.02	1.08	1.10	1.01	1.05	1.07
-1	1.10	1.13	1.15	1.06	1.09	1.10
0	1.21	1.18	1.18	1.11	1.12	1.13
1	1.10	1.13	1.15	1.06	1.09	1.10
2	1.02	1.08	1.10	1.01	1.05	1.07
3	1	1	1.1	1	1	1
4	1	1	1	1	1	1
5	1	1	1	1	1	1
6	1	1	1	1	1	1
7	1	1	1	1	1	1
8	1	1	1	1	1	1

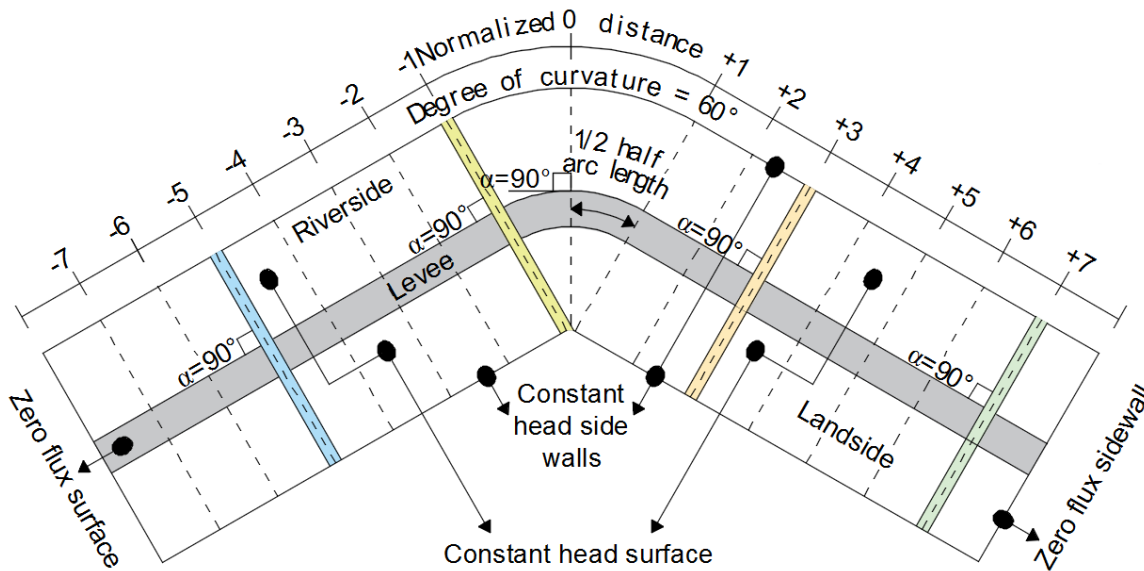


Figure E.5. Schematic top view of the curvature model used for  $D_c = 60^\circ$  and  $\alpha = 45^\circ$  showing channel features at  $ND = -5, -1, +3 +7$ .

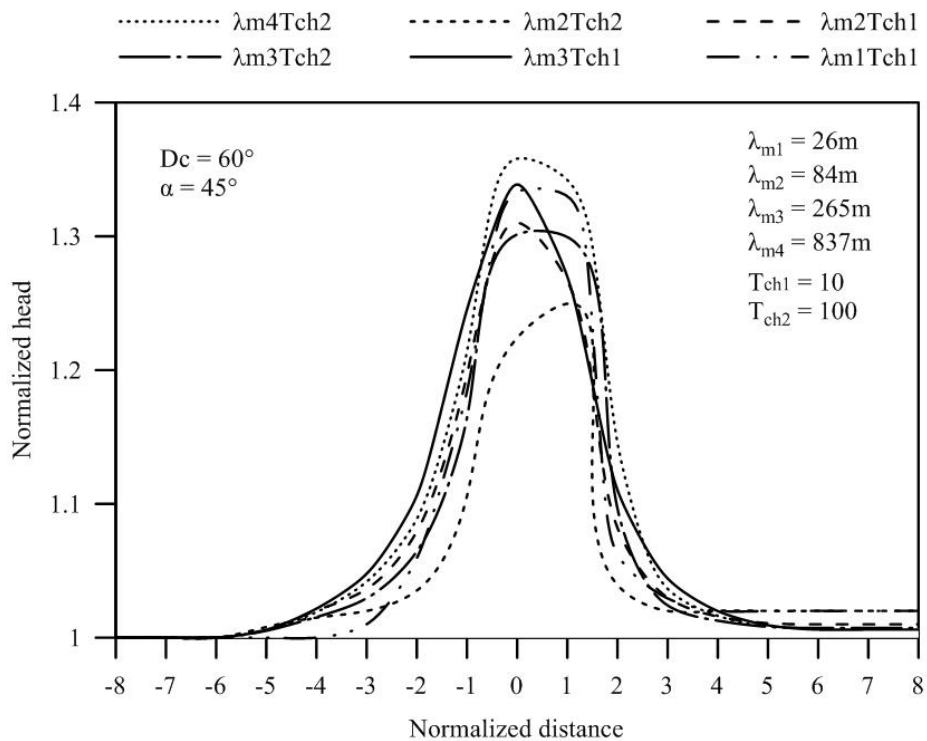


Figure E.6. Results for the curvature model with  $D_c = 60^\circ$  and  $\alpha = 45^\circ$ .



Table E.3. Parameters and results for the curvature model with  $Dc = 60^\circ$  and  $\alpha = 45^\circ$ 

Curvature multiplier for $Dc = 60^\circ$ with $\alpha = 45^\circ$						
$K_f = 1E-05$ m/s, $t_b = 2$ m, $t_{ch} = 3.5$ m, $t_f = 32$ m, $w_{ch} = 10$ m, $RL = 200$ m						
Stage	$\lambda_{m_1} T_{ch_1}$	$\lambda_{m_2} T_{ch_1}$	$\lambda_{m_3} T_{ch_1}$	$\lambda_{m_2} T_{ch_2}$	$\lambda_{m_3} T_{ch_2}$	$\lambda_{m_4} T_{ch_2}$
$K_b$ (m/s)	1.00E-06	1.00E-07	1.00E-08	1.00E-06	1.00E-07	1.00E-08
$K_{ch}$ (m/s)	1.00E-04	1.00E-04	1.00E-04	1.00E-03	1.00E-03	1.00E-03
$\lambda_m$ (m)	26.5	83.7	264.6	83.7	264.6	836.7
$T_{ch}$	10	10	10	100	100	100
$\lambda$ (m)	25.3	80.0	253.0	25.3	80.0	253.0
Normalized distance	Head at top of channel (m)					
-8	1	1	1	1	1	1
-7	1	1	1	1	1	1
-6	1	1	1	1	1	1
-5	1	1	1	1	1	1
-4	1	1	1	1.02	1	1
-3	1.01	1.04	1.05	1.02	1.03	1.04
-2	1.06	1.08	1.11	1.04	1.06	1.09
-1	1.18	1.20	1.25	1.11	1.16	1.21
0	1.33	1.31	1.34	1.22	1.30	1.36
1	1.33	1.27	1.27	1.25	1.30	1.34
2	1.06	1.08	1.11	1.04	1.10	1.15
3	1.03	1.03	1.04	1.02	1.02	1.04
4	1.02	1.02	1.02	1.02	1.01	1.02
5	1.02	1.01	1.01	1.02	1.01	1.01
6	1.02	1.01	1.01	1.02	1.01	1.00
7	1.02	1.01	1.01	1.02	1.01	1.00
8	1	1.01	1.01	1.02	1.01	1.00

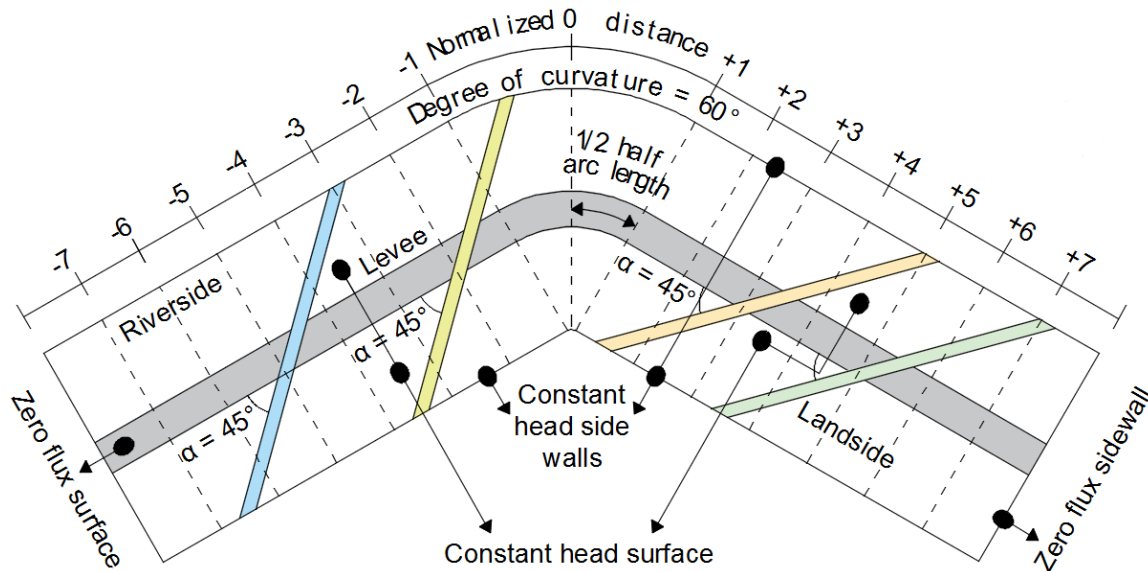


Figure E.7. Schematic top view of the curvature model used for  $D_c = 60^\circ$  and  $\alpha = 90^\circ$  showing channel features at  $ND = -5, -2, +3 +5$ .

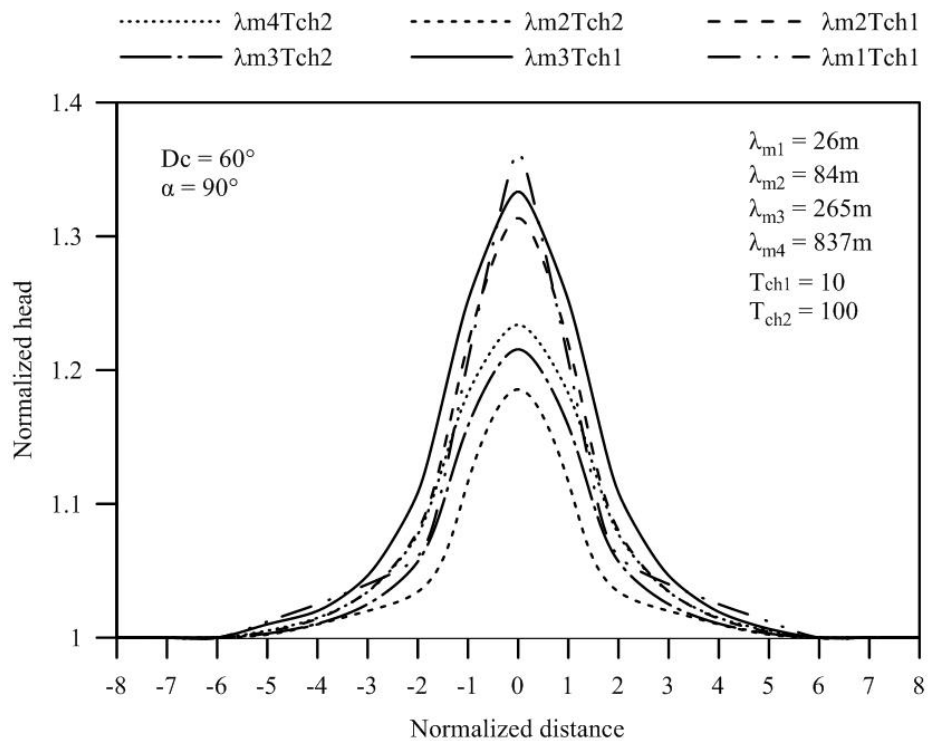


Figure E.8. Results for the curvature model with  $D_c = 60^\circ$  and  $\alpha = 90^\circ$ .

Table E.4. Parameters and results for the curvature model with  $Dc = 60^\circ$  and  $\alpha = 90^\circ$ 

Curvature multiplier for $Dc = 60^\circ$ with $\alpha = 90^\circ$						
$K_f = 1E-05$ m/s, $t_b = 2$ m, $t_{ch} = 3.5$ m, $t_f = 32$ m, $w_{ch} = 10$ m, $RL = 200$ m						
Stage	$\lambda_{m1}T_{ch1}$	$\lambda_{m2}T_{ch1}$	$\lambda_{m3}T_{ch1}$	$\lambda_{m2}T_{ch2}$	$\lambda_{m3}T_{ch2}$	$\lambda_{m4}T_{ch2}$
$K_b$ (m/s)	1.00E-06	1.00E-07	1.00E-08	1.00E-06	1.00E-07	1.00E-08
$K_{ch}$ (m/s)	1.00E-04	1.00E-04	1.00E-04	1.00E-03	1.00E-03	1.00E-03
$\lambda_m$ (m)	26.5	83.7	264.6	83.7	264.6	836.7
$T_{ch}$	10	10	10	100	100	100
$\lambda$ (m)	25.3	80.0	253.0	25.3	80.0	253.0
Normalized distance	Head at top of channel (m)					
-8	1	1	1	1	1	1
-7	1	1	1	1	1	1
-6	1	1	1	1	1	1
-5	1	1	1	1	1	1
-4	1.03	1.01	1.02	1.01	1.01	1.01
-3	1.04	1.03	1.05	1.02	1.03	1.03
-2	1.06	1.08	1.11	1.03	1.06	1.08
-1	1.21	1.22	1.25	1.12	1.16	1.18
0	1.36	1.31	1.33	1.19	1.22	1.23
1	1.21	1.22	1.25	1.12	1.16	1.18
2	1.06	1.08	1.11	1.03	1.06	1.08
3	1.04	1.03	1.05	1.02	1.03	1.03
4	1.03	1.01	1.02	1.01	1.01	1.01
5	1	1	1	1	1	1
6	1	1	1	1	1	1
7	1	1	1	1	1	1
8	1	1	1	1	1	1

## CURRICULUM VITAE

## LOURDES POLANCO BOULWARE

Graduate Research Assistant, Civil and Environmental Engineering  
 Utah State University, 4110 Old Main Hill, Logan UT 84321-4110  
 Email: lourdes.polanco@aggiemail.usu.edu, lourdespolanco@gmail.com

---

EDUCATION

- Ph. D. Civil and Environmental Engineering May 2017  
 Utah State University, Logan, UT GPA 3.78  
*Dissertation:* Reliability Underseepage Failure Assessment of Levees Incorporating  
 Geomorphic Features and Length Effects
  - M. S. Civil and Environmental Engineering December 2009  
 Utah State University, Logan, UT GPA 3.84  
*Thesis:* Reliability-Based Underseepage Analysis in Levees Using Monte Carlo  
 Simulation
  - B. S. Civil Engineering May 2005  
 INTEC, Santo Domingo, D.R. GPA 3.34
- 

EMPLOYMENT*Utah State University*

Graduate Research Assistant September 2008 – Present

- Performed extensive research on levee underseepage reliability by comparing current USACE methods with a developed response surface Monte Carlo (RSMC) simulation method with the purpose of predicting the likelihood behavior of the most significant parameters in the analysis and illustrating the advantages of the developed RSMC; providing a more reliable method to calculating levee underseepage resiliency to failure.
- Developed RSMC methodology by means of finite element analyses (using programs Slide and SVFlux) and the computer program @Risk allowing the integration of complex geologic levee underseepage analysis and a more flexible probabilistic scenario validating novel methodology.

- Incorporated geomorphic features into levee underseepage analysis by means of geologic maps, borings and historical photographs; utilizing available data and statistical estimation when needed.
- Published in credited journals and conferences (see list below)

CEE Instructor

Summer 2012

- Planned and lectured an ‘Introduction to Civil Engineering’ summer class for international students attending a Summer English Immersion program at Utah State University (USU).
- Each class was an introduction to one branch of civil engineering with the aid of power point slides and activities in class or out in the field.
- Speaker guests (USU professors) attended with the purpose of providing a broader scope of each branch of civil engineering and as an opportunity for students to interact with specialist in the respective field.

*Dominican Republic*

Project Management Engineer

June 2006 – July 2007

COHECA and Deconalva (Companies specializing in tourist area construction)

- Developed bids together with several departments (architectural, sales, budget, law) to fulfill the needs of the projects
- Supervised the progression of projects by overlooking cost estimates and monitoring planned versus actual schedule for work completion
- Represented the company in meetings with clients, briefed on the progress of the projects and acted as a spanish to english translator when needed
- Translated documents and manuscripts of meetings that were relevant between clients and contractors for record keeping

Civil Engineer

November 2005 – May 2006

Tecnoproyectos (Company specializing in consulting engineering)

- Assisted with geotechnical surveying as a part of a geotechnical investigation for the channeling and rehabilitation of a river section that was causing instability of slopes due to migration
- Supported audits conducted on governmental projects as part of a presidential transition program by examining reports, leading field investigations to compare filed data, arranging meetings with contractors and serving as a witness of the audit report
- Drafted cut and fill highway sections consulted for reconstruction

AutoCad Assistant

August 2002 – April 2005

- Assisted students in AutoCAD courses in the Instituto Tecnologico de Santo Domingo (INTEC) by providing one-on-one support during class
-

### SELECTED PUBLICATIONS AND PRESENTATIONS

The following are selected from a total of 3 Journal Publications and 10 Conference Proceedings:

- Polanco-Boulware, L. and Rice, J. D. (2016). “Reliability-based three-dimensional assesment of internal erosion potential due to crevasses splays.” *Journal of Geotechnical and Geoenvironmental Engineering*, 10.1061/(ASCE)GT.1943-5606.0001596
- Polanco-Boulware, L. and Rice, J. (2015). Modeling Geomorphic Features in Levee Reliability Analyses. Submitted for Proceedings of 5th International Symposium on Geotechnical Safety and Risk (ISGSR). Rotterdam, Netherlands, October 2015
- Rice, J. and Polanco-Boulware, L. (2015). Modeling Geomorphic Features in Levee Reliability Analyses. Submitted for Proceedings of United States Society on Dams (USSD) Annual Conference, 2015. Louisville, KY.
- Polanco, L. and Rice, J. D. (2014). A reliability-based evaluation of the effects of geometry on levee underseepage potential. *Springer: Geotechnical and Geological Engineering*, 32 (4), 807-820. DOI 10.1007/s10706-014-9759-2
- Polanco, L. and Rice, J. D. (2014). A reliability-based evaluation of the effects of geometry on levee underseepage potential. Proceedings of 2014 ASCE GeoCongress Conference. Atlanta, Georgia February 23-26, 2014.
- Polanco, L. and Rice, J. D. (2013). The effects of geometry in levee underseepage reliability. Proceedings of Dam Safety 2013: Annual Conference of the Association of State Dam Safety Officials (ASDSO), Providence, RI, September 8-13, 2013, Published on CD-ROM. Student Paper Competition.
- Rice, J. D. and Polanco, L. (2012). Reliability-based underseepage analysis in levees using a response surface–Monte Carlo simulation method. *Journal of Geotechnical and Geoenvironmental Engineering*, ASCE, 138 (7), 821-830.

### AWARDS AND FELLOWSHIPS

- United States Society on Dams (USSD) Scholarship Recipient, 2015
- Successful NSF Grant Proposal, \$204,000, 2014 – Assisted with proposal writing and preparation
- Winner of Student Paper Competition, Association of State Dam Safety Officials Conference, 2010, 2013, 2015
- Marriner S. Eccles Foundation Grant, 2012 – Assisted with proposal writing
- 3rd Place Student Poster Competition, GeoFlorida Conference, 2010
- 1st Place Engineering Presentation, 13th Annual Intermountain Graduate Research Symposium, 2010

PROFESIONAL AND HONOR SOCIETIES

- United States Society on Dams (USSD) 2015 - present
  - CEE Engineering Council Representative (USU) Fall 2014-Spring 2015
  - Association of State Dam Safety (ASDSO) 2010 – present
  - National Society of Collegiate Scholars (NSCS) 2010 – present
  - Golden Key International Academic Honor Society 2009 – present
  - American Society of Civil Engineers (ASCE) 2008 – present
  - International Exchange Student Program, Rotary International 2000 – 2001
-

**SKILLS**

- Computer Programs: Rocscience Slide, @Risk, ArcGIS, SVFlux, LPile, WEAP, Autocad, MS Word, MS Excel, MS PowerPoint
- Total Verbal and Written Fluency: Spanish, English
- Partial Verbal and Written Fluency: Italian, French



## PERMISSIONS

2/17/2017

Rightslink® by Copyright Clearance Center



RightsLink®

Home

Account  
Info

Help



**Title:** Reliability-Based Underseepage  
Analysis in Levees Using a  
Response Surface–Monte Carlo  
Simulation Method

Logged in as:  
Lourdes Boulware  
Account #:  
3001114364

**Author:** John D. Rice, Lourdes Polanco

LOGOUT

**Publication:** Journal of Geotechnical and  
Geoenvironmental Engineering

**Publisher:** American Society of Civil  
Engineers

**Date:** 07/01/2012

Copyright © 2012, ASCE. All rights reserved.

**Permissions Request**

As an author of an ASCE journal article, you are permitted to reuse the accepted manuscript version of your article for your thesis or dissertation.

BACK

CLOSE WINDOW

Copyright © 2017 [Copyright Clearance Center, Inc.](#) All Rights Reserved. [Privacy statement](#), [Terms and Conditions](#).  
Comments? We would like to hear from you, E-mail us at [customercare@copyright.com](mailto:customercare@copyright.com)

**SPRINGER LICENSE  
TERMS AND CONDITIONS**

Feb 17, 2017

This Agreement between Lourdes Boulware ("You") and Springer ("Springer") consists of your license details and the terms and conditions provided by Springer and Copyright Clearance Center.

License Number	4051400310149
License date	Feb 17, 2017
Licensed Content Publisher	Springer
Licensed Content Publication	Geotechnical and Geological Engineering
Licensed Content Title	A Reliability-Based Evaluation of the Effects of Geometry on Levee Underseepage Potential
Licensed Content Author	Lourdes Polanco
Licensed Content Date	Jan 1, 2014
Licensed Content Volume	32
Licensed Content Issue	4
Type of Use	Thesis/Dissertation
Portion	Full text
Number of copies	4
Author of this Springer article	Yes and you are a contributor of the new work
Order reference number	
Title of your thesis / dissertation	Reliability underseepage assessment of levees incorporating geomorphic features and length effects
Expected completion date	Apr 2017
Estimated size(pages)	200
Requestor Location	Lourdes Boulware 47 E 300 S  HYRUM, UT 84319 United States Attn: Lourdes Boulware

10/30/2017

Rightslink® by Copyright Clearance Center



RightsLink®

Home

Create  
Account

Help



**Title:** Reliability-Based Three-Dimensional Assessment of Internal Erosion Potential due to Crevasse Splays

**Author:** Lourdes Polanco-Boulware, John D. Rice

**Publication:** Journal of Geotechnical and Geoenvironmental Engineering

**Publisher:** American Society of Civil Engineers

**Date:** 10/27/2016

Copyright © 2016, ASCE. All rights reserved.

LOGIN

If you're a **copyright.com user**, you can login to RightsLink using your copyright.com credentials. Already a **RightsLink user** or want to [learn more?](#)

### Permissions Request

As an author of an ASCE journal article, you are permitted to reuse the accepted manuscript version of your article for your thesis or dissertation.

BACK

CLOSE WINDOW

Copyright © 2017 [Copyright Clearance Center, Inc.](#) All Rights Reserved. [Privacy statement.](#) [Terms and Conditions.](#)  
Comments? We would like to hear from you. E-mail us at [customercare@copyright.com](mailto:customercare@copyright.com)